Water Disinfection Studies using Hybrid Process of Photocatalysis and Photo-Fenton in Fixed Mode

A Thesis

Submitted in Fulfillment of the Requirements for the award of

the degree of

DOCTOR OF PHILOSOPHY

In

ENVIRONMENTAL SCIENCE & TECHNOLOGY

By:

Ina Thakur

(Regd. No. 901714001)

School of Energy and Environment

Thapar Institute of Engineering and Technology
(Deemed to be University)
Patiala -147004, Punjab, India

July, 2022

Candidate's declaration

I hereby certify that the work which is being presented in the thesis entitled "**Water Disinfection Studies using Hybrid Process of Photocatalysis and Photo-Fenton in Fixed Mode"** in fulfillment of the requirements for the award of the degree of Doctor of Philosophy and submitted to the School of Energy and Environment, Thapar Institute of Engineering and Technology, Patiala, India is an authentic record of my work carried out during a period from July 2017 to December 2021 under the supervision of Dr. AnoopVerma, Associate Professor, School of Energy and Environment, TIET, Patiala and Dr. Banu Örmeci, Professor, Jarislowsky Chair in Water & Global Health, Dept. of Civil & Environmental Engg. Carleton University, Canada

The matter presented in the thesis has not been submitted in parts or full to any other institute for the award of any other degree in any other university or institute.

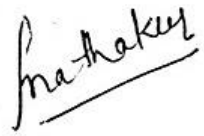

Ina Thakur
(901714001)

Certificate

This is to certify that the thesis entitled "**Water Disinfection Studies using Hybrid Process of Photocatalysis and Photo-Fenton in Fixed Mode"** that is being submitted by Ina Thakur, in the fulfillment for the award of Ph.D. in the School of Energy and Environment, Thapar Institute of Engineering and Technology (Deemed to be University), Patiala, India, for the award of the degree of **' Doctor of Philosophy '** is a record of bonafide research work carried out by her under our guidance and supervision and has fulfilled the requirements for the submission of this thesis, which to our knowledge has reached the requisite standard.

The results embodied in this thesis have not been submitted to any other University or Institute for the award of any degree or diploma.

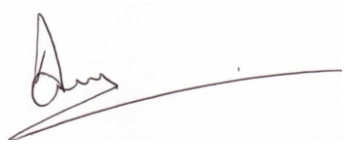

Dr. Anoop Verma
Associate Professor
School of Energy and Environment
Thapar Instt. of Engg. &Technology
Patiala, India

Dr. Banu Örmeci
Professor
Jarislowsky Chair in Water & Global Health
Dept. of Civil & Environmental Engg.
Carleton University, Canada

Acknowledgment

In the beginning, I would like to acknowledge my indebtedness to my supervisors Dr. Anoop Verma, Associate professor, TIET, Patiala, India, and Dr. Banu Örmeci, Professor, Carleton University, Ottawa, Canada to guide me well throughout the research work, from selecting the title to finding the results. Their immense knowledge, motivation, and patience have given me more power and spirit to excel in research writing. Conducting the academic study regarding such a complex topic couldn't be as simple as they made this for me. They are my mentor and a better advisor for my doctorate study beyond the imagination.

I would like to extend my thanks to Dr. Amit Dhir, the Ex-Head of School of Energy and Environment, Professor N. Tejoprakash, Associate Professor, Dr. Anita Rajor, of School of Energy and Environment, TIET for providing me an opportunity to join this esteemed institution, and who gave access to the laboratory and research facilities. Without their precious support, it would not be possible to conduct this research. I owe a deep sense of gratitude to Senior Professor R. Siddique, Dean, Research and Sponsored Projects, TIET University, Patiala, India, for his valuable guidance. You provided me with the tools that I needed to choose the right direction and complete my research work.

I express my deepest gratitude to my doctoral committee members Dr. N. Tejo Prakash, Dr. S. Barman, and Dr. Amit Dhir for their constant encouragement, insightful comments, and keen interest in me at every stage of my research work. I would also like to thank the staff of the Department of Biotechnology and I am also thankful to Mr. Suhail and Mr. Gurpreet Singh from the School of Energy and Environment for their constant cooperation and kind help throughout my Ph.D. work. This research work would have not been completed without the help received from SAI Labs, Patiala.

My heartfelt thanks to my seniors Dr. Palak Bansal, Dr. Jayishnu Singla, Dr. Steffi Talwar, Dr. Pali Rosha for their support and guidance. I would also like to thank my colleagues Prabhdeep Kaur, Sanjoy Gorai, Himanshu Sharma, and Bimalpreet Singh for their cheerful discussion and help. I will cherish all the warmth shown by them.

I would always remember my fellow labmates Sonali, Shelly Tiwari, Gursimranjot Singh for the fun time we spent together, the sleepless nights that gave us the courage to complete tasks before deadlines, and for stimulating the discussions.

Life is definitely not always easy and there always seem to be curveballs coming from every direction. I have a mentor, someone that I can look up to, and someone that always pushes me to learn and grow from mistakes that are made every day. Dr. Saurabh Rawat, the man who also supported me well throughout the entire research program. His immense support actually guided me to rectify numerous things that could have created major challenges in the research. I would never have been able to get as far as I have without your constant support and always pushing me to challenge myself.

In the end, I am grateful to my parents, siblings, friends, and acquaintances who remembered me in their prayers for the ultimate success. I consider myself nothing without them. They gave me enough moral support, encouragement, and motivation to accomplish my personal goals. My two lifelines (parents) have always supported me financially so that I only pay attention to my studies and achieve my objective without any obstacles on the way.

Above all, I owe it all to Almighty God for granting me the wisdom, health, and strength to undertake this research task and enabling me to its completion.

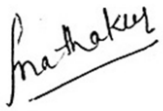

Ina Thakur

(901714001)

Abstract

Contamination of water resources by pathogenic bacteria and associated diseases is a major source of concern for water quality worldwide. Contamination by pathogens is a severe problem that affects all kinds of water bodies, making its identification and understanding important. Advanced oxidation processes (AOPs) such as photo-Fenton and TiO_2 photocatalysis have achieved promising applications for the disinfection of wastewater. Yet, both of them have a few limitations such as prolonged treatment time, catalyst separation, electron-hole recombination, iron sludge formation, and higher H_2O_2 dose which have hindered their effective implementation at the field scale.

Therefore, considerable attention has been paid in the present work to explore the practical applications of AOPs by resolving almost all of the issues raised by these individual processes (photocatalysis or photo-Fenton). Attempts were made to combine these two processes within the same treatment unit for the increased disinfection of targeted bacteria, i.e., *E. coli*. This hybrid technique effectively covers the shortcomings of both technologies (photocatalysis + photo-Fenton) due to the presence of a higher amount of OH^o.

To execute the hybrid process, a low-cost and visibly active Fe−TiO_2 composite was fabricated using industrial waste materials such as foundry sand (FS) and fly ash (FA) (iron source) mixed with clay in the ratio of 2:1:1. A thin film of TiO_2 was coated on spherical composite beads leading to photocatalysis and iron leaching from the composite, leading to photo-Fenton thus incorporating a hybrid effect in one system.

For the lab-scale trials inactivation of *E. coli* was carried out under artificial UV light. Operating parameters such as UV light intensity, size of beads, the addition of oxidant, change in pH, and area/volume ratio of the reactor was optimized for the inactivation of *E. coli*. In the hybrid process, 6.2 *E. coli* log reduction was observed in 90 min of reaction time. An increase of 26 % of synergy with the hybrid process was obtained in comparison to photocatalysis and photo-Fenton alone. The kinetic parameters such as k of log-linear and δ of double Weibull for fitting the *E. coli* inactivation results were used for comparing the different techniques and found that the hybrid-technique in fixed mode ($k = 0.16\ min^{-1}$, $\delta_1 = 8.63$ min, $\delta_2 = 27.7$ min) proved to be significantly faster in comparison to other techniques; TiO_2 assisted photocatalysis ($k = 0.6\ min^{-1}$; $\delta_1 = 23.1$ min, $\delta_2 = 76$ min); photo-Fenton ($k = 0.07\ min^{-1}$; $\delta_1 = 17.66$ min, $\delta_2 = 33.53$ min; H_2O_2 with UV ($k = 0.04\ min^{-1}$; $\delta_1 = 34.05$ min, δ_2

= 100.95 min) and Only UV(k = 0.03 min^{-1}; δ_1 = 51.91 min, δ_2 = 207.73 min). Thus the obtained results present a promising potential of the hybrid technology for the treatment of *E. coli* in water. The beads were proved to be durable for more than 50 recycles for the inactivation of *E. coli*. To confirm the presence of TiO_2, morphological analysis and elemental composition for fresh as well as recycled composite beads were done using SEM and EDS respectively. The activity of the catalyst and the presence of Fe was also checked by using XRD, FTIR, and DRS analysis.

To promote the applicability of AOPs at the field scale in near future, it is mandatory to execute the scale-up trails of lab-scale results. The established in-situ hybrid effect in the present study using composite beads was scaled up for the disinfection of *E. coli* with the development of pilot-scale reactors. The pilot-scale reactors taken into consideration for the present study were UV-assisted re-circulation type fixed-bed glass reactor and solar once through cascade reactor with a total working volume of 2 L and 6 L, respectively. The detailed cost of the process has been evaluated using each type of reactor.

The first reactor that was studied is the continuous recirculating flatbed reactor. The performance of the hybrid process (Fe-TiO_2) was evaluated in terms of reaction rate constant, and some other operating parameters. This hybrid process showed a significant increase in reaction rate constant (0.065 min^{-1}) compared to photo-Fenton (0.029 min^{-1}) and photocatalysis (0.025 min^{-1}) in 150 min of treatment time. The P-value was less than 0.0001 and the F-value was greater than 5 for each process. Response surface methodology (RSM) with box Behnken design (BBD) has been employed for the optimization of different parameters. The optimized values of the operating parameters were found to be 3.5, 62 mg L^{-1}, 106 mL min^{-1} for the reaction pH, H_2O_2 concentration, and flow rate, respectively. With these optimum conditions, a percentage reduction of *E. coli* of 93% was observed. The synergistic effect of the hybrid process over photocatalysis was observed to be 61 % and over photo-Fenton was 55 %. The overall synergy of the hybrid process came out to be 17 %. Various characterizations (SEM−EDX, UV-DRS, FTIR, and XRD) confirmed the longevity and the stability of the Fe−TiO_2 composite even after 50 cycles. The total cost of killing *E. coli* in the solution was US $0.16 per liter, showing the potential for commercial application.

A pilot-scale fixed-bed continuous once-through reactor was used to study the inactivation of *E. coli*. The reactor approached the plug flow condition in 45 min of retention time (Ţ) and a 100% inactivation of *E. coli* cells was observed with an H_2O_2 dose of 50 mg L^{-1}, 100%

surface area covered, 6 L h^{-1} of flow rate, and three reactors in series. Furthermore, these Fe-TiO_2 composites showed exceptional durability even after 100 recycles which further claims the novelty of this technology. The total operating cost for treating water came out to be 0.00827 US$ for one reaction per cycle. No regrowth of bacterial cells in the solution even after 48 h of treatment, clearly indicated the commercial viability of the present reactor system. The cell wall damage was confirmed by the increase in the K^+ concentration at regular intervals. Also, the total cost of the process assessed in this study is substantially lower than other AOPs-related studies found in the literature. Therefore, the current fixed-bed once-through reactor under sunlight integrating into situ hybrid effects with demonstrated validity of theoretical prediction might be efficiently used at a large scale to handle the wastewater in lesser time.

Further, for the authentication of the results of the hybrid effect, the study has been extended to the real secondary treated municipal wastewater. The study was conducted in batch mode and then was implemented in continuous once-through mode. In the batch scale study, 100% inactivation of bacteria with optimized parameters such as 0.9 g L^{-1} of H_2O_2 dose, 5.5 pH, and 100 % surface area covered with the catalyst in 60 min of treatment time was observed. 54 % and 40% reduction in BOD and COD respectively was also observed in 60 min. The scale-up trials using the in-situ hybrid process for the treatment of actual municipal wastewater were executed in a pilot-scale solar once-through cascade reactor system and 4.5 log reduction of bacteria was observed in 45 min of treatment time. Recycling and reuse of the catalyst validated the economic feasibility of the process.

List of Tables

Table 1. 1 Different technologies for wastewater treatments 2

Table 2. 1 Summary of articles on TiO_2-based photocatalytic disinfection of wastewater.....22
Table 2. 2 Summary of articles on photo-Fenton disinfection of wastewater 27
Table 2. 3 Summary of articles on water disinfection by photo-Fenton and photocatalysis carried out at the solar pilot plant 37

Table 3. 1 Concentration of iron species leaching out of fresh composite beads.....52
Table 3. 2 Level of the factors tested in the Box−Behnken experimental design 62

Table 4. 1 Statistical analysis for inactivation of *E. coli* using photocatalysis, photo-Fenton, and hybrid process. 67
Table 4. 2 First order rate constant (k) values for inactivation of *E. coli* K12 using different processes 70
Table 4. 3 Kinetic parameters of mathematical models used in the inactivation of *E. coli* by UV treatment.....88
Table 4. 4 Kinetic parameters of mathematical models used in the inactivation of *E. coli* by H_2O_2/UV treatment 90
Table 4. 5 Kinetic parameters of mathematical models used in the inactivation of *E. coli* by TiO_2-photocatalysis treatment. 92
Table 4. 6 Kinetic parameters of mathematical models used in the inactivation of *E. coli* by photo-Fenton treatment.....94
Table 4. 7 Kinetic parameters of mathematical models used in the inactivation of *E. coli* by hybrid treatment.....97
Table 4. 8 Levels of the factors tested in the Box−Behnken experimental design.....103
Table 4. 9 Full Factorial BBD matrix with 4 independent variables.....103
Table 4. 10 Analysis of variance for the response rate of *E. coli* elimination.....105
Table 4. 11 Concentration of iron species leaching out of fresh composite beads.....108
Table 4. 12 Concentration of iron species leaching out of recycled composite beads 108
Table 4. 13 Reaction rate constant (k) of different processes for *E. Coli* inactivation in the present study 114

Table 4. 14 Tentative cost evaluation of the treatment technique 114
Table 4. 15 Concentration of Iron species leaching out of fresh composite beads in each reactor 127
Table 4. 16 Concentration of Iron species leaching out of recycled composite beads in each reactor 127
Table 4. 17 Photoreactivation of *E. coli* under natural solar light and dark conditions, in solar light, inactivated water.....135
Table 4. 18 Cost analysis for the complete hybrid-process and scale-up study 136
Table 4. 19 Physico-chemical analysis of municipal wastewater.....138
Table 4. 20 Concentration of Iron species leaching out of composite beads at pH 4.5.....142
Table 4. 21 Concentration of Iron species leaching out of composite beads at pH 5.5.....142
Table 4. 22 Concentration of Iron species leaching out of composite beads at pH 6.5.....142
Table 4. 23 Kinetic analysis of the hybrid process using different models 146
Table 4. 24 Kinetic analysis of the photo-Fenton process using different models.....147
Table 4. 25 Kinetic analysis of the TiO_2-photocatalytic process using different models.....147
Table 4. 26 Synergy of hybrid-process over the individual process and combined process .152

List of Figures

Figure 1. 1 Different categories of Advanced oxidation process.....5
Figure 1. 2 Mechanism of the in-situ hybrid process for water disinfection 11
Figure 1. 3 Graphical representation of the hybrid process 13
Figure 1. 4 Structure of Escherichia coli (*E. coli*) 14
Figure 1. 5 Structure of Gram-negative bacteria 15

Figure 2. 1 Source of microorganisms present in the water resources (Ji et al., 2021) 18
Figure 2. 2 Solar CPC pilot-scale reactor (a) Recirculating (b) Non-recirculating for water disinfection studies (Giannakis et al., 2016b).....34

Figure 3. 1 SEM-EDS image of (a) Fly ash and (b) Foundry sand 51
Figure 3. 2 Actual images of (a) blank and (b) TiO_2 immobilized composite beads 51
Figure 3. 3 Elemental mapping of Fe-TiO_2 composite.....52
Figure 3. 4 SEM image showing thickness of TiO_2 coating (Average thickness 71 µm) over composite beads.....52
Figure 3. 5 (a) Line diagram and (b) actual image of the lab-scale experimental set-up 56
Figure 3. 6 Schematic diagram of recirculating glass reactor.....57
Figure 3. 7 Line diagram and actual image of the once-through pilot-scale reactor 59
Figure 3. 8 Box–Behnken design for a three-factor experiment (Kandananond, 2010).....61

Figure 4. 1 The structure of results and discussion.....67
Figure 4. 2 (a) Photoreduction of Fe^{3+} to Fe^{2+} using e^-_{CB} (b) Photoreduction of Fe^{3+} to Fe^{2+} using photo-Fenton process (c) OH^o spectra using a fluorescence spectrophotometer 71
Figure 4. 3 Inactivation of *E. coli* with and without Fe and H_2O_2 in the dark.....72
Figure 4. 4 Inactivation of *E. coli* in different conditions.....75
Figure 4. 5 (a) Effect of H_2O_2 dosage on inactivation of *E.coli* and (b) first-order rate constant at different H_2O_2 dosage 76
Figure 4. 6 (a) Effect of variation of pH on inactivation of *E.coli* and (b) First-order rate constant at different pH.....77

Figure 4. 7 (a) Effect of UV intensity on inactivation of *E.coli* and (b) first-order rate constant at different UV intensities (c) Photo luminance spectra of OH^o at different intensities 78
Figure 4. 8 (a) Effect of bead size on inactivation of *E.coli* and (b) first-order rate constant at different bead sizes 79
Figure 4. 9 (a) Effect of the area to volume ratio on inactivation of *E.coli* and (b) first-order rate constant at the different area to volume ratio.....80
Figure 4. 10 SEM and EDS images of freshly coated, and recycled composite bead 81
Figure 4. 11 XRD pattern of freshly coated and recycled composite bead 82
Figure 4. 12 UV-DRS images of freshly coated, and recycled composite bead.....83
Figure 4. 13 FTIR pattern of freshly coated and recycled composite bead 84
Figure 4. 14 Recyclability studies of composite beads.....85
Figure 4. 15 Concentration of leached iron from fresh and recycled beads 86
Figure 4. 16 Inactivation of *E. coli* at different conditions.....87
Figure 4. 17 Fitting of mathematical models to the inactivation curve of *E.coli* through the UV irradiation treatment. 89
Figure 4. 18 Fitting of mathematical models to the inactivation curve of *E.coli* through the UV/H_2O_2 91
Figure 4. 19 Fitting of mathematical models to the inactivation curve of *E.coli* through the TiO_2-photocatalysis treatment. 93
Figure 4. 20 Fitting of mathematical models to the inactivation curve of *E.coli* through the photo-Fenton treatment. 95
Figure 4. 21 Iron concentration present in the hybrid process.....97
Figure 4. 22 Fitting of mathematical models to the inactivation curve of *E.coli* through the hybrid process. 98
Figure 4. 23 Schematic diagram of *E. coli* inactivation in the recirculating reactor 100
Figure 4. 24 (a) *E. coli* inactivation with and without iron and oxidant dose in the dark (b) *E. coli* inactivation with various technologies.....101
Figure 4. 25 A plot of normal probability vs. internally studentized residuals of the response 103
Figure 4. 26 % reduction of *E. coli* 3D response surface graph (a) % reduction 3D diagram of H_2O_2 Dose with time (b) % reduction 3D diagram of pH with time (c) % reduction 3D diagram of flow-rate w.r.t time (d) % reduction 3D diagram of flow-rate with H_2O_2 107
Figure 4. 27 Recyclability study of composite beads for *E.coli* inactivation 109
Figure 4. 28 SEM/EDS images of fresh as well as recycled composite beads.....110

Figure 4. 29 FTIR image of fresh and recycled composite beads 111
Figure 4. 30 UV-DRS analysis of fresh and recycled composite beads 112
Figure 4. 31 XRD pattern of fresh and recycled composite beads 113
Figure 4. 32 RTD curve attained from the experimental analysis of the three reactors in series along with axial dispersion of fitted model.....118
Figure 4. 33 Preliminary experiments of *E. coli* inactivation 120
Figure 4. 34 Change in the concentration of *E. coli* with (a) variation in the number of reactors (b) crosssection of number of baffles in a reactor (c) variation in the number of baffles.....122
Figure 4. 35 Change in the concentration of *E. coli* with (a) variation in the flow rate of the reactor (b) variation in the % of surface area covered (c) variation in the concentration of H_2O_2 124
Figure 4. 36 Trapping study of different reactive oxygen species.....126
Figure 4. 37 Reusability/durability study of Fe-TiO_2 composite used for *E. coli* inactivation 128
Figure 4. 38 SEM/EDS images of fresh and recycled composite beads.....129
Figure 4. 39 XRD patterns of freshly coated and recycled beads.....130
Figure 4. 40 UV-visible DRS patterns of freshly coated and recycled beads.....131
Figure 4. 41 FTIR analysis of freshly coated and recycled beads 132
Figure 4. 42 HRTEM images of fresh and recycled composite.....132
Figure 4. 43 (a) FESEM image of *E.coli* before treatment (b) FESEM image of inactivated *E. coli* after treatment 133
Figure 4. 44 Leakage of potassium ion from the cell damage (a) in controlled condition (without treatment) (b) after treatment 134
Figure 4. 45 Preliminary analysis of bacterial inactivation 139
Figure 4. 46 Effect of variation of percentage surface area covered on bacterial inactivation 140
Figure 4. 47 Effect of variation of pH on bacterial inactivation.....141
Figure 4. 48 Effect of variation of H_2O_2 doze on bacterial inactivation.....144
Figure 4. 49 Fitting mathematical models to the photocatalysis, photo-Fenton, and hybrid-process inactivation curves of bacteria 145
Figure 4. 50 Photo luminance spectra of OH^oat different processes 146
Figure 4. 51 Treatment of wastewater effluent using Fe-TiO_2 composite (a) BOD removal (b) COD removal (c) Total phosphorous removal (d) Nitrate removal.....148

Figure 4. 52 Change in the concentration of *E. coli* with (a) variation in the number of reactors (b) variation in the concentration of H_2O_2 doze.....150
Figure 4. 53 The durability of Fe-TiO_2 composite beads 151

Contents

Candidate's declaration i

Certificate ii

Acknowledgment iii

Abstract v

List of Tables viii

List of Figures x

Introduction 1

1.1 General Background 1

1.2 An overview of advanced oxidation processes for water disinfection 4

1.3 Application of heterogeneous photocatalysis for water disinfection 5

1.4 Application of homogeneous photocatalysis for water disinfection 7

1.5 Application of pilot-scale fixed bed photocatalytic reactors 8

1.6 The hybrid concept of advanced oxidation Processes 9

1.7 Selected microorganism 14

1.8 Aim of the proposed study 15

1.9 Thesis organization 16

Literature Review 17

2.1 Overview 17

2.2 Assets and liabilities of advanced oxidation process (AOPs) for water disinfection 18

2.2.1 Application of TiO_2 photocatalysis for water disinfection 19

2.2.2 Mechanism of the killing of bacteria using TiO_2 photocatalysis 21

2.2.3 Application of photo-Fenton Process for water disinfection 25

2.2.4 Mechanism of the killing of bacteria using Photo-Fenton process 26

2.2.5 Advances in fixed bed photocatalysis for water disinfection 29

2.2.6 Modification of TiO_2 photocatalyisis 31

2.2.7 Pilot-scale applications of AOPs for water disinfection 33

2.2.8 Real-life applications of photocatalytic reactor 39
2.2.9 Disinfection kinetic models 39
2.2.10 Hybrid effect of TiO_2 photocatalysis and photo-Fenton 43
2.3 Summary 44
2.4 Lacunae 45
2.5 Objectives of the study 46
Materials and Methods 47
3.1 General 47
3.2 Microbial preparation and enumeration protocol 47
3.3 Chemicals and reagents 48
3.4 Analytical method 49
3.5 Fabrication of composite beads and TiO_2 immobilization 49
3.5.1 Fabrication of blank beads 49
3.5.2 Fabrication of clay beads for photocatalysis 50
3.5.3. Fabrication of Fe-TiO_2 composite beads 50
3.5.4 Iron leaching from composite beads 52
3.6 Characteristic analysis of the composite 53
3.7 Photo-disinfection kinetics 53
3.8 Synergistic studies 54
3.9 Statistical analysis 54
3.10 Experimental set-up and procedure for hybrid effect studies for lab-scale reactor 55
3.11 Pilot-scale recirculating fixed bed reactor 56
3.12 Pilot-scale solar fixed-bed once-through reactor 57
3.13 Experimental design and analysis 59
3.13.1 Box-Behnken design 60
3.14 Mathematical models in *E. coli* inactivation 62
3.14.1 The log-linear model 62

3.14.2 The Weibull model 63
3.14.3 Double Weibull model 63
3.14.4 Biphasic model 64
Results and Discussion 65
4. General 65
4.1 Section A (In-situ hybrid process at lab scale batch reactor) 67
4.2 Tentative mechanism of hybrid process 68
4.3 Preliminary studies using UV batch reactor 71
4.3.1 Effect of hydrogen peroxide concentration 75
4.3.2 Effect of pH 76
4.3.3 Effect of UV intensity 77
4.3.4 Effect of bead size 78
4.3.5 Effect of the area to volume ratio (A/V) 79
4.3.6 Characterization of composite beads 80
4.3.6.1 SEM/ EDS analysis 80
4.3.6.2 XRD analysis 81
4.3.6.3 UV-visible DRS analysis 82
4.3.6.4 FTIR analysis 83
4.3.7 Durability studies 85
4.4 Mathematical modeling of *E. coli* inactivation in water using Fe-TiO_2 composite in a fixed bed reactor 86
4.4.1 Mathematical models used in *E. coli* inactivation 87
4.4.1.1 UV assisted study 88
4.4.1.2 TiO_2 assisted photocatalysis in fixed mode 91
4.4.1.3 Photo-Fenton in fixed mode 93
4.4.1.4 Hybrid technique in fixed mode 95
4.5 Section B (Scale-up studies using Fe-TiO_2 composite beads) 98

4.5.1 Fe-TiO_2 composite mediated hybrid effect for the inactivation of *E. coli* using a continuous flow recirculation reactor 99
4.5.1.1 Preliminary study and efficacy of the hybrid process 100
4.5.1.2 Development and evaluation of predicted study 102
4.5.1.3 Optimization of different parameters 106
4.5.2 Extended durability study 108
4.5.3 Characterization of Fe-TiO_2 composite 110
4.5.3.1 SEM-EDS analysis 110
4.5.3.2 FTIR analysis 111
4.5.3.3 UV-DRS analysis 112
4.5.3.4 XRD analysis 112
4.5.4 Kinetic analysis of the hybrid process 113
4.5.5 Cost analysis of the lab-scale in-situ hybrid-process 114
4.6 Once-through fixed-bed cascade reactor (Plug-flow approach) 116
4.6.1 The prominence of the hybrid effect in a cascade reactor 116
4.6.2 Experimental Studies 117
4.6.2.1 Retention time distribution (RTD) and plug flow study 117
4.6.2.2 Dark and controlled experiments 118
4.6.3 Reactor optimization 120
4.6.3.1 Effect of number of reactors 120
4.6.3.2 Effect of number of baffles 121
4.6.3.3 Effect of the flow rate 122
4.6.3.4 Effect of surface area covered 123
4.6.3.5 Effect of H_2O_2 concentration 123
4.6.3.6 Role of various reactive species on *E. coli* inactivation 125
4.6.4 Extended reusability study of the Fe-TiO_2 catalyst 126
4.6.5 Characterization 128

4.6.5.1 SEM-EDS analysis....128
4.6.5.2 XRD analysis....129
4.6.5.3 UV-Vis absorption spectra....130
4.6.5.4 FT-IR analysis....131
4.6.5.4 HRTEM analysis....132
4.6.5.5 Field emission scanning electron microscopy (FESEM) for *E. coli* morphology and K^+ leakage....133
4.6.5.6 Photo-reactivation of *E. coli*....134
4.6.6 Scale-up studies and cost analysis....135
4.7 Section C (Disinfection of real secondary treated municipal wastewater effluent (MWWT))....137
4.7.1 Applications of the in-situ hybrid process for the disinfection of real MWWT....137
4.7.2 Prominence of hybrid process....138
4.7.3 Parametric optimization....139
4.7.3.1 Effect of surface area covered....139
4.7.3.2 Effect of pH change....140
4.7.3.3 Effect of H_2O_2 concentration....143
4.7.4 Kinetic analysis....144
4.7.5 Degradation of organic compounds....148
4.7.6 Durability studies....150
4.8 Synergistic studies....151
Conclusions and Recommendations....153
5.1 Conclusions....153
5.1.1 Inactivation of *E. coli* under UV and solar irradiation (Batch scale reactor)....153
5.1.2 Inactivation of *E. coli* using recirculation type fixed bed reactor (scale-up study)....154
5.1.3 Inactivation of *E. coli* using once-through fixed bed reactor (scale-up study)....154

5.1.4 Inactivation of bacteria present in secondary treated municipal wastewater (At lab-scale and scale-up reactor).....155

5.1.5 Durability studies of the composite beads.....155

5.2 Recommendations.....156

References.....157

Chapter 1

Introduction

1.1 General Background

Contamination of water resources by pathogenic bacteria and associated diseases is a major source of concern for water quality worldwide. Contamination by pathogens is a severe problem that affects all kinds of water bodies, making its identification and understanding important (Dressing and Meals, 2010). Water contamination occurs as a result of point sources of treated and untreated sewage, as well as non-point sources. Non-point sources, such as runoff from naturally vegetated regions, and runoff from commercial or industrial areas contaminate surface waters with pathogens. Additionally, other sources, such as faulty or improperly placed municipal sewage treatment systems, can contribute considerable amounts of microorganisms (Howe et al., 2002; Leight et al., 2018).

These municipal wastewaters are found to be contaminated with viruses, bacteria, and other microscopic organisms, which are all potentially pathogenic to humans (Giannakis et al., 2016c). Regardless of how well a municipal wastewater treatment system handles secondary treated effluent, the effluent nevertheless contains a minimum of tens of thousands of fecal coliforms per 100 mL. The discharge of municipal waste effluent into the river and other water bodies increases the transmission of contagious bacterial strains such as *E. coli*, *Shigella spp.*, *Salmonella spp.*, *C. jejuni*, *Vibrio cholera*, etc (Santhiya et al., 2011). Polluted effluent discharge often contaminates sea life, especially prawns, fish, and cockles; as a result, people who consume contaminated seafood could become gravely ill (Al-Gheethi et al., 2018).

According to the United Nations Children's Fund (UNICEF, 2014), every day more than 700 children under the age group of 1-5 die worldwide, due to the lack of sanitation and contamination of drinking water (UNICEF, 2014). The traditional practices opted by the developing countries involve dumping treated municipal wastewater into natural water, taking advantage of water bodies' self-purification ability for the further treatment of treated municipal wastewater (United Nations, 2014). However, due to the increased odors generated and the amount of waste involved, as well as health risks, these activities are becoming inappropriate. Extremely high levels of organic compounds can reduce dissolved oxygen

resources in natural waters, resulting in rapid bacterial growth (Heritage et al., 1997). Problems are more severe in developing countries like India, where population explosion and poor sanitation led to the contamination of ground and surface water. In India, only 4 % of natural drinking water resources exist, and their quality and quantity are rapidly declining (Dalin et al., 2015). As a result, furthermore effective treatment to eliminate or inactivate microorganisms is frequently required to meet the standards established by national or international agencies.

When considering available technologies for water and wastewater treatment, the most prevalent approaches are listed in Table 1.1. Out of these technologies, chemical disinfection, typically with chlorine or other disinfectants such as peracetic acid (PAA), and ozone or other chemicals or their mixtures, is one of the most frequent techniques of microorganism elimination. While these techniques are extremely effective, their use is restricted due to safety concerns or the creation of toxic disinfection byproducts (DBPs) (Lu et al., 2009). Additionally, while this method eliminates a considerable number of water-borne infections worldwide, the cost of chemical disinfection in many areas of underdeveloped nations must be questioned. As a result, research has shifted to more affordable yet ecologically friendly options.

Table 1. 1 Different technologies for wastewater treatments

S. No.	Technologies	Characteristics
1.	Membranes (Daels et al., 2011)	Physical barrier based on the principle of size exclusion, which is frequently connected with excessive energy usage (when pressure is the driving force). The efficacy of the membrane is strongly reliant on the type of material used.
2.	Adsorption (Hussain et al., 2014)	It is a mass transfer process commonly implemented for the removal of non-degradable compounds. without being degraded. The efficacy is limited by the amount of surface area available and there is a deficiency in selectivity.
3.	Biological Treatments (Miranda-Ríos et al., 2011)	Treatment of wastewater using living organisms. While generally safe and inexpensive, the drawback is the high volume of sludge produced in comparison to

		the amount of wastewater treated.
4.	Chemical oxidation (Megahed et al., 2018)	An oxidizing agent such as ozone, chlorine modifies the molecular structure of pollutants. Additional risks to human health may result from the formation of carcinogenic and mutagenic by-products.
5.	Disinfection (Wirtanen and Salo, 2003)	Inactivation of microorganisms present in water using chemical disinfectants such as chlorine, hydrogen peroxide, Peracetic acid, etc). but these chemicals are highly unstable, corrosive, and have toxic byproducts.

In this context, UV disinfection has been widely investigated throughout the years as an environmentally acceptable sanitizing approach. The use of different UV lights induces considerable changes in the genetic structure of microbes (Hijnen et al., 2006). Solar light, on the other hand, has exhibited disinfectant properties as a result of the UVA and UVB wavelengths' action mechanism. It has been extensively employed in poorer or developing nations for drinking water treatment (McGuigan et al., 2012), as well as its application in treating wastewater has also been researched in tropical latitudes such as Asia, Africa, Australia, etc (Von Sperling, 2005). The abovementioned regions have a greater amount of sunny days annually, making them suitable locations for such pursuits.

However, both UV and solar UV disinfection have a drawback: unlike chemical techniques of wastewater disinfection, they lack residual activity, which means that once the exposure is complete, no disinfection will occur (Núñez-Núñez et al., 2020). Numerous microbes (e.g. viruses, spores, bacteria) have exhibited the ability to repair injury to their cells via a variety of methods following UV exposure. This is referred to as reactivation of cell DNA, and it results in population regrowth. The two primary methods are light-mediated and dark processes, specifically photoreactivation and dark repair. The distinction is in the mechanism in which the enzyme responsible for lesions repair is activated.

As a result, it is reasonable to conclude that typical/conventional disinfection technologies are inefficient in one or another way. Due to the limitations of conventional disinfection technologies, scientists have focused their efforts on improved oxidation methods. The past literature has reported the efficacy of advanced technologies in the disinfection of microorganisms (Carré et al., 2014; Giannakis et al., 2018c; Ndounla et al.,

2014) through microfiltration (Daels et al., 2011), advanced oxidation processes (AOPs) (Mishra et al., 2017), and electro-dialysis (Deng et al., 2015). Taking into consideration all the benefits offered by the aforementioned modern technologies, the AOPs on a broader spectrum offers credible solutions in the field of water disinfection.

1.2 An overview of advanced oxidation processes for water disinfection

The literature has established AOPs as potential solutions for disinfecting a variety of microorganisms found in water/wastewater (Jia et al., 2016; Lv et al., 2019; Núñez-Núñez et al., 2020; Ortega-Liébana et al., 2012; Valero et al., 2017). This AOP consists of homogeneous and heterogeneous photocatalysis for the degradation and disinfection of water/wastewater.

The homogeneous photo-Fenton process is one of the most widely used photo-assisted AOPs for the treatment of wastewater containing organic contaminants (Singh and Garg, 2019; Tsoumachidou et al., 2017). Additionally, this appears to be the most suitable sunlight-driven AOP, as soluble iron-hydroxyl and primarily iron-organic acid complexes absorb not just ultraviolet light but also a considerable portion of the visible light spectrum (Malato et al., 2009).

On the other hand, heterogeneous photocatalysis is a typical AOP that has been extensively explored for the removal of different contaminants from aqueous solutions during the last decades (Antonopoulou et al., 2021; Antonopoulou and Konstantinou, 2016; Konstas et al., 2019). This process entails accelerating contaminant removal (in an aqueous phase) in the presence of a semiconductor present in a solid phase activated by a specific wavelength of light. By and large, heterogeneous photocatalysis can result in the formation of highly reactive species.

AOPs are photochemical oxidation processes that comprise a variety of technologies such as photolysis (Nyangaresi et al., 2019), photocatalysis (Carré et al., 2014; Song et al., 2016), photo-Fenton (Ortega-Gómez et al., 2013; Valero et al., 2017), Fenton (Rodríguez-Chueca et al., 2014a), ozonation (Xi et al., 2017), sono-photocatalysis (Zhang et al., 2017), Electro-oxidation (P. Kaur et al., 2018) and cavitation (Dong and Qin, 2018) as shown in Figure 1.1. Among these AOPs, semiconductor-based photocatalysis using titanium oxide (TiO_2) (Venieri et al., 2017), zinc oxide (ZnO) (Nair et al., 2020), tungsten oxide (WO_3) (Barreca et al., 2016), nickel oxide (NiO) (Duraisamy et al., 2018), reduced graphene oxide (r-GO)

(Gomez-Ruiz et al., 2018)has received considerable attention during the last two decades. Out of these, TiO_2 has been used extensively for disinfection investigation due to the following reasons: 1) low toxicity; 2) eco-friendly; 3) cost-effectiveness; 4) easy modification by doping; 5) potential to expand its use without sacrificing its photocatalytic activity significantly (De Vietro et al., 2019; Rincón and Pulgarin, 2006).

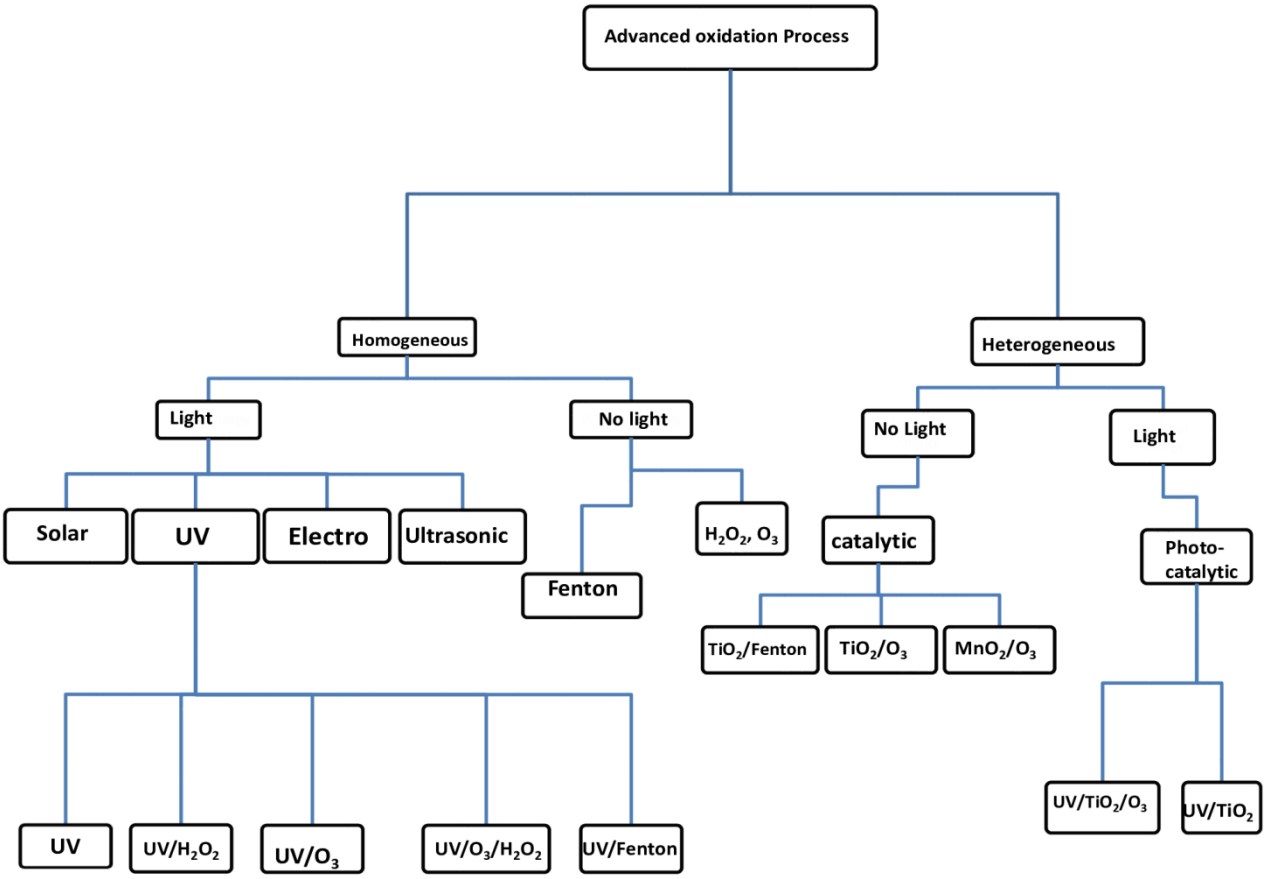

Figure 1. 1 Different categories of Advanced oxidation process

1.3 Application of heterogeneous photocatalysis for water disinfection

Photocatalysis with heterogeneous catalysts, particularly TiO_2, is a commonly used method for the treatment of wastewater. This technology has demonstrated tremendous potential for removing microorganisms from secondary or tertiary treated municipal wastewater (T. Kaur et al., 2018; Yu et al., 2016), pollutants from various industries, including textiles, pulp, and paper (Gümüş and Akbal, 2011; Priya et al., 2015), hospital effluents (Chinnaiyan et al., 2019), and synthetic wastewater comprising pesticides, phenols, and surfactants (Ahmed et al., 2011). In the literature, work on heterogeneous photocatalysis has been published utilizing both a slurry and an immobilized technique.

Heterogeneous photocatalysis occurs on the surface of the solid semiconductor, which absorbs light and serves as active site for reactant adsorption. The fundamental reactions in photocatalysis involving semiconductors are oxidation and reduction reactions comprising of electron-hole transport from the photoexcited semiconductor. The following Equations (1.1-1.5) provide additional insight into the reaction mechanism.

$$TiO_2 + hv(UV) \rightarrow e^-_{(CB)} + h^+_{(VB)} \quad (1.1)$$

$$h^+_{(VB)} + H_2O \rightarrow H^+ + OH^\circ \quad (1.2)$$

$$h^+_{(VB)} + OH^- \rightarrow OH^\circ \quad (1.3)$$

$$E.coli + OH^\circ \rightarrow inactivation\ of\ E.coli \quad (1.4)$$

$$e^-_{(CB)} + O_2 \rightarrow O_2^\circ \quad (1.5)$$

The photocatalytic enhancement of water disinfection has been demonstrated successfully on numerous occasions by photo-exciting TiO_2 nanoparticles (suspended or immobilized) against a diverse array of model water pathogens, including bacteria, viruses, spores fungi, and parasites (Dunlop et al., 2008; Philippe et al., 2016; Sunnotel et al., 2010). Due to the high disinfection/degradation efficacy, the utilization of TiO_2 in suspended form has garnered considerable interest. Suspended finely powdered catalyst particles in solution give enough surface area without requiring any mass transfer. However, the low light absorption capacity and rapid charge carrier recombination will always be a problem.

New routes are being investigated continuously to increase the efficacy of heterogeneous photocatalysis while mitigating the risks associated with this process. Any photocatalytic catalyst performance is generally determined by several criteria, including its size, shape, pore structure, exposed surface area, and crystalline phase (Nakata and Fujishima, 2012). Numerous TiO_2 nanostructures of various shapes have been reported and published in the literature, including spheres (Cunha et al., 2018), nanorods (Ray et al., 2018), fibers (Lin et al., 2013), tubes (Liu et al., 2018) tetc.

To increase the efficacy of photocatalysis doping of metal and non-metal over TiO_2 was also reported in the literature (Dozzi and Selli, 2013; Pelaez et al., 2012). The process of

doped TiO_2 photocatalysis is nearly identical to the mechanism of undoped TiO_2 photocatalysis. The main difference between doped TiO_2 photocatalysis and undoped TiO_2 photocatalysis is the formation of a new energy level in the TiO_2 structure due to the dopant's presence. Doping of non-metal in TiO_2 leads to the formation of s/p states just over the valence band maximum (VBM), which results in the reduction of bandwidth by <1 eV. However, in the case of metal mono-doping (n-type: V, Cr, Mn, and so forth), limited states are created generally underneath the conduction band (CB) and the relative overlapping successfully decreases the bandwidth and makes the catalyst visibly active.

Although the significant outcome in photocatalytic activity even in the visible range is being achieved by modifying TiO_2, field-scale implications of such modified catalysts are still to be investigated. Indeed, the majority of research on these modified catalysts is conducted in suspension mode, posing the significant difficulty of catalyst separation post-treatment. Additionally, the low recyclability of the catalyst in slurry photocatalysis makes the process expensive. As a result, these processes pose challenges during scaling up.

1.4 Application of homogeneous photocatalysis for water disinfection

Some of the disadvantages of TiO_2 photocatalysis, such as mass transfer issues, have been addressed by homogeneous photocatalysis, more precisely photo-Fenton. The photo-Fenton process generates OH^o in the presence of light via the catalytic activity of Fe^{2+} and H_2O_2. Equations can be used to deduce the mechanism of the photo-Fenton reaction (1.6-1.8).

$$Fe^{2+} + H_2O_2 \rightarrow Fe^{3+} + OH^{\circ} + OH^{-} \quad (1.6)$$

$$OH^{\circ} + Fe^{2+} \rightarrow Fe^{3+} + OH^{-} \quad (1.7)$$

$$Fe^{3+} + H_2O + hv \rightarrow Fe^{2+} + OH^{\circ} + H^{+} \quad (1.8)$$

Scientists have conducted extensive research in this field since there is a reasonable prospect of reducing treatment time due to the process's low mass transfer impacts. The photo-Fenton treatment method has been widely employed to eliminate various pathogenic contaminants found in water (Moncayo-Lasso et al., 2009; Ortega-Gómez et al., 2013; Ortega-Liébana et al., 2012; Rodríguez-Chueca et al., 2014b). Only a few studies on the photo-Fenton method have reported on scale-up attempts for wastewater treatment.

Nonetheless, the process's utility on a large scale remains debatable. Indeed, the process's primary disadvantages are the massive amount of iron sludge generated and the high dose of H_2O_2. Additionally, this process has lower photon consumption efficacy which limits its commercial use.

1.5 Application of pilot-scale fixed bed photocatalytic reactors

Effective implementation of AOPs for wastewater treatment is necessary for commercial-scale applications. The conventional reactor scale-up is comparatively more simple than the scaling up of solar reactors. Besides, the problems connected to the typical reactor system, catalyst contact, mixing, flow patterns, temperature control, and mass transfer can create hurdles in the prospective scale-up. For stable dispersion of the sunlight inside the reactor and optimizing the exposed surface area of the reactor, axial and radial scale-up is also regarded as vital characteristics. Numerous investigations are focused on the scale-up process employing TiO_2, notably in suspension form, including annular photoreactor, photocatalytic Taylor vortex reactor, parabolic trough collectors (PTCs), and compound parabolic collectors (CPCs).

Numerous pilot-scale setups of photoreactors for photocatalytic removal of contaminants have been reported. These include concentrating falling film reactors (Shephard et al., 2002), parabolic trough collectors (PTCs) (Dixit et al., 2016), shallow pond reactors (Mozia et al., 2012), compound parabolic collectors (CPCs) (Alrousan et al., 2012; Sordo et al., 2010), tubular reactors (Saran et al., 2019, 2018), falling film photoreactor (Saran et al., 2017), slurry bubble column reactor (Akach et al., 2020), thin-film reactor (Khan et al., 2012), and flat packed-bed reactors (Borges et al., 2017). The field-scale application of fixed bed catalysis has not achieved much appeal. This might be owing to the stability and durability of the supports and catalyst. Another obstacle is mass transfer limitation and increases in treatment time which poses a barrier to the scaling up of the process. An increase in treatment time and more consumption of energy result in a higher treatment cost.

In the large-scale application of the systems, several aspects, such as the overall process's cost-effectiveness, are taken into account. The most preferred reactors for real-life applications are fixed bed reactors with catalysts immobilized on the support. Several supports for catalyst immobilization have been explored, including polystyrene beads (Nair and Shetty Kodialbail, 2020), silica gel beads (Fueda et al., 2006), Pebbles (Rao and Chaturvedi, 2007), glass plates (Zacarías et al., 2012), glass spheres (Ratova et al., 2018), and

zeolite (Reddy et al., 2008), etc. Although various studies on supported catalysts have been published in the literature, the technology has still not been successfully implemented at the field scale to date. The durability and stability of supported catalysts have not been adequately examined in any of the research provided. While the process is more effective and commercially viable, selecting inert and solid materials for catalyst immobilization has long been a challenge for AOP researchers. Additionally, the mass transfer constraints and treatment time associated with fixed-mode catalysis continue to be a disadvantage for commercial applications.

1.6 The hybrid concept of advanced oxidation Processes

With the ongoing growth of combinatorial hybrid systems, extensive research has demonstrated that combining two or more technologies such as photocatalysis-biodegradation (Collivignarelli et al., 2020), photo-Fenton-biological oxidation (Changotra et al., 2019; Pariente et al., 2008), photo-Fenton-coagulation, and flocculation (GilPavas et al., 2017), electro-oxidation (Collivignarelli et al., 2020), photocatalytic-ozonation (Mecha et al., 2017; Yuan et al., 2018) and ultrasonic-photocatalysis (Hu et al., 2017), is an efficient approach for significantly increasing pollutant removal efficacy. In comparison to conventional isolated AOPs, hybrid systems have been shown to offer higher oxidation rates, faster kinetic rates, comparatively short mass transfer operation times, and are simpler to operate.

However, the sludge formation associated with the photo-Fenton process due to the use of iron as a catalyst is of major concern. Simultaneously, with photocatalytic-ozonation, the ozone disintegrates rapidly into oxygen complicating residual removal methods. Also, the relatively expensive cost of the system maintenance, as well as the significant energy consumption associated with the operation process, restrict the development of large-scale applications.

Considering various shortcomings of other coupled processes, the coupling of two techniques, i.e., photocatalysis and photo-Fenton, can reasonably solve the hindrances offered by these processes when operated separately (Bansal & Verma, 2017b). The combined solar-powered AOPs possess a promising application in the treatment of wastewater, i.e., the capability to disinfect various microorganisms, maintaining low cost, and providing a boon for wastewater treatment. The major challenge of this hybrid process is that both mechanisms (photocatalysis and photo-Fenton) should take place without hindering the other process. The hybrid process has excellent disinfection efficacy but has not been explored well yet. The

cost of the process and utilization of higher oxidant dozes can be reduced if the two different processes (photo-Fenton and photocatalysis) are coupled together in one system, consequently increasing the disinfection.

To enhance the disinfection efficacy of the system, few studies have suggested the basic idea of the hybrid effect of photo-Fenton and photocatalysis (Bansal and Verma, 2018a). The generation of a significant amount of OH^o has improved disinfection efficacy. The primary mechanism of the hybrid process involves the reaction of both, TiO_2 particles and iron oxides simultaneously. The TiO_2 particles, when exposed to light, lead to the photoexcitation of electrons to the conduction band leading to the formation of electron and hole pairs (Yu et al., 2013). For the photo-Fenton reactions to initiate, Fe^{2+} reacts with H_2O_2 and converts into Fe^{3+} (Ruales-Lonfat et al., 2015). The electron from the photocatalysis, which poses the recombination problem, reacts with the Fe^{3+} and converts into Fe^{2+}. When Fe^{3+} ions come into contact with TiO_2, some Ti^{5+} species are replaced due to the weakening of the metal-oxygen bond and the imbalance of the charge. This further leads to the formation of Ti^{3+} species and the vacancies of oxygen which act as the reactive species for disinfection (Zhang et al., 2019). This leads to the electron-hole pair being separated, thus helping in the oxidation of pollutants (Kim et al., 2012). This will contribute to more OH^o production and thus favor the overall process. The existence of Fe^{2+} and Ti^{3+} leads to the synergistic effect enhancing the oxidation and reduction, thus leading to the increased treatment of wastewater (Rincón and Pulgarin, 2007).

The present study emphasizes the novel concept of coupling two processes, i.e., photocatalysis and photo-Fenton, in fixed mode and both the processes taking place simultaneously. In this study, the inexpensive inert composite was fabricated by mixing waste material such as foundry sand (FS) and fly ash (FA) with clay. These waste materials are good sources of iron oxides. This composite after fabrication is coated with TiO_2. The surface-active TiO_2 layer contributes to photocatalysis, whereas iron lixiviation under acidic conditions from the support leads to photo-Fenton in the presence of H_2O_2 (Bansal and Verma, 2017a). This process also resolves the issue of e^-h^+ recombination in TiO_2 photocatalysis. As the e^- in the conduction band (e^-_{CB}) generating during TiO_2 photocatalysis reacts with the Fe^{3+} ions and converts into Fe^{2+} (Bansal and Verma, 2018b) as shown in Figure 1.2. Now, this Fe^{2+} ion again reacts with H_2O_2 leading to the photo-Fenton process. Thus depicting a hybrid effect in the system. The whole mechanism is explained in Equations (1.9-1.16).

$$TiO_2 + uv \text{ irradiation} \rightarrow e^-_{TiO_2(CB)} + h^+_{TiO_2(VB)} \quad 1.9$$

$$e^-_{TiO_2(CB)} + O_2 \rightarrow O_2^- \quad 1.10$$

$$h^+_{TiO_2(VB)} + H_2O \rightarrow OH^o + H^+ \quad 1.11$$

$$Fe^{2+}_{(leached)} + H_2O_2 \rightarrow Fe^{3+}_{(leached)} + OH^o + OH^- \quad 1.12$$

$$Fe^{3+}_{(leached)} + H_2O_2 \rightarrow Fe^{2+}_{(leached)} + H_3O^+ + HO_2^- \quad 1.13$$

$$Fe^{3+}_{(leached)} + H_2O \xrightarrow{uv} Fe^{2+}_{(leached)} + OH^o + H^+ \quad 1.14$$

$$Fe^{3+}_{(leached)} + e^-_{(TiO_2)} + H_2O \rightarrow Fe^{2+}_{(leached)} + OH^o + H^+ \quad 1.15$$

$$e^-_{(TiO_2)} + H_2O_2 \rightarrow OH^o + OH^- \quad 1.16$$

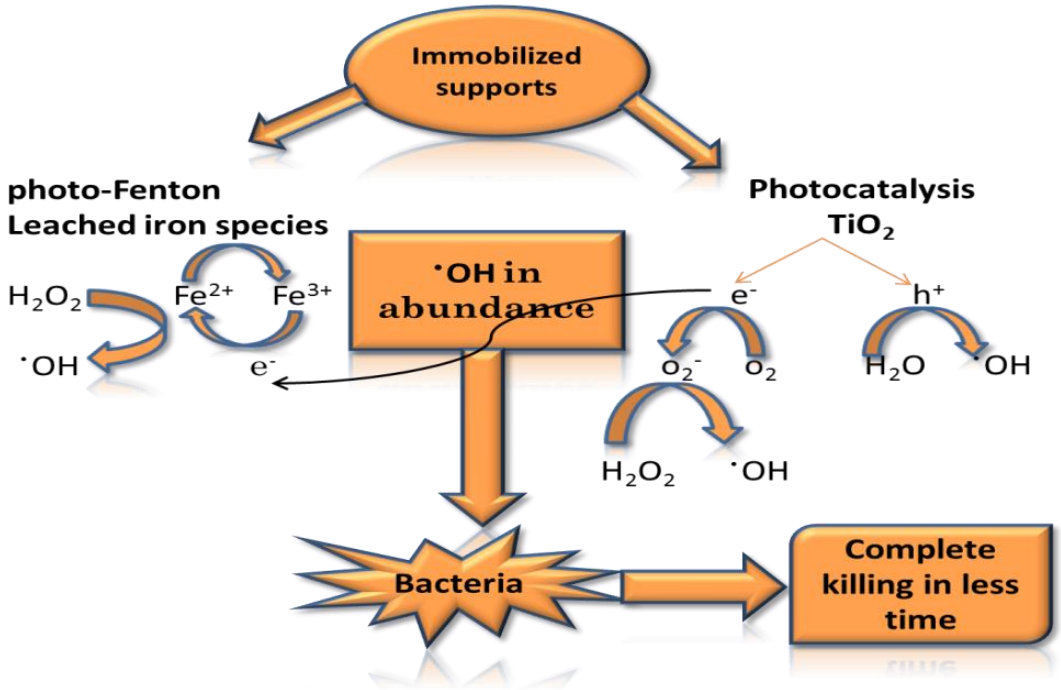

Figure 1. 2 Mechanism of the in-situ hybrid process for water disinfection

One of the novelties of this technology is that unlike other studies mentioned in the literature (Ren et al., 2020; Wang et al., 2021) this study has a natural dopant. The iron present in waste materials, that is used for the fabrication of composite beads (for the photo-Fenton process), acts as a natural dopant. The iron intact on the surface of the composite reacts with coated TiO_2 to form some complexes such as iron titanium oxide as shown in Equation (1.17) (validated using XRD analysis in chapter 4) that reduces the bandgap of the catalyst with time making it active in the visible region also. This hypothesis was further confirmed through UV-visible absorption spectroscopy as explained in chapter 4 (Results and discussion). Thus making this technology cost-effective as no investments were made for the doping of the catalyst.

$$TiO_{2(surface\ coated)} + Iron_{(Trapped\ on\ the\ composite\ surface)} \rightarrow ITO_{(iron\ titaniumoxide)} \quad 1.17$$

Another major component of this technology is that one process is supporting the other by suppressing each other's drawbacks. This hybrid process increases the efficacy of the reaction by increasing the rate of reaction, which in turn improves the disinfection performance of the process. Moreover, systematic lixiviation of the iron from the inert beads (required for the photo-Fenton process) does not lead to the formation of iron sludge. Also, the utilization of FS along with FA increases the compressive strength and binding capacity of supports apart from augmenting the concentration of iron (Naik et al., 2012). Same time the use of waste materials confirms the cost-effectiveness of the process. With the advantage of no sludge formation and continuous availability of OH^o, the hybrid process has depicted satisfactory results in terms of efficacy and synergy as explained in chapter 4 (Results and discussion). The performance of the purposed in-situ hybrid process is assessed in terms of increasing efficacy via reducing treatment time.

A graphical representation of the photocatalytic performance of this hybrid process is given in Figure 1.3.

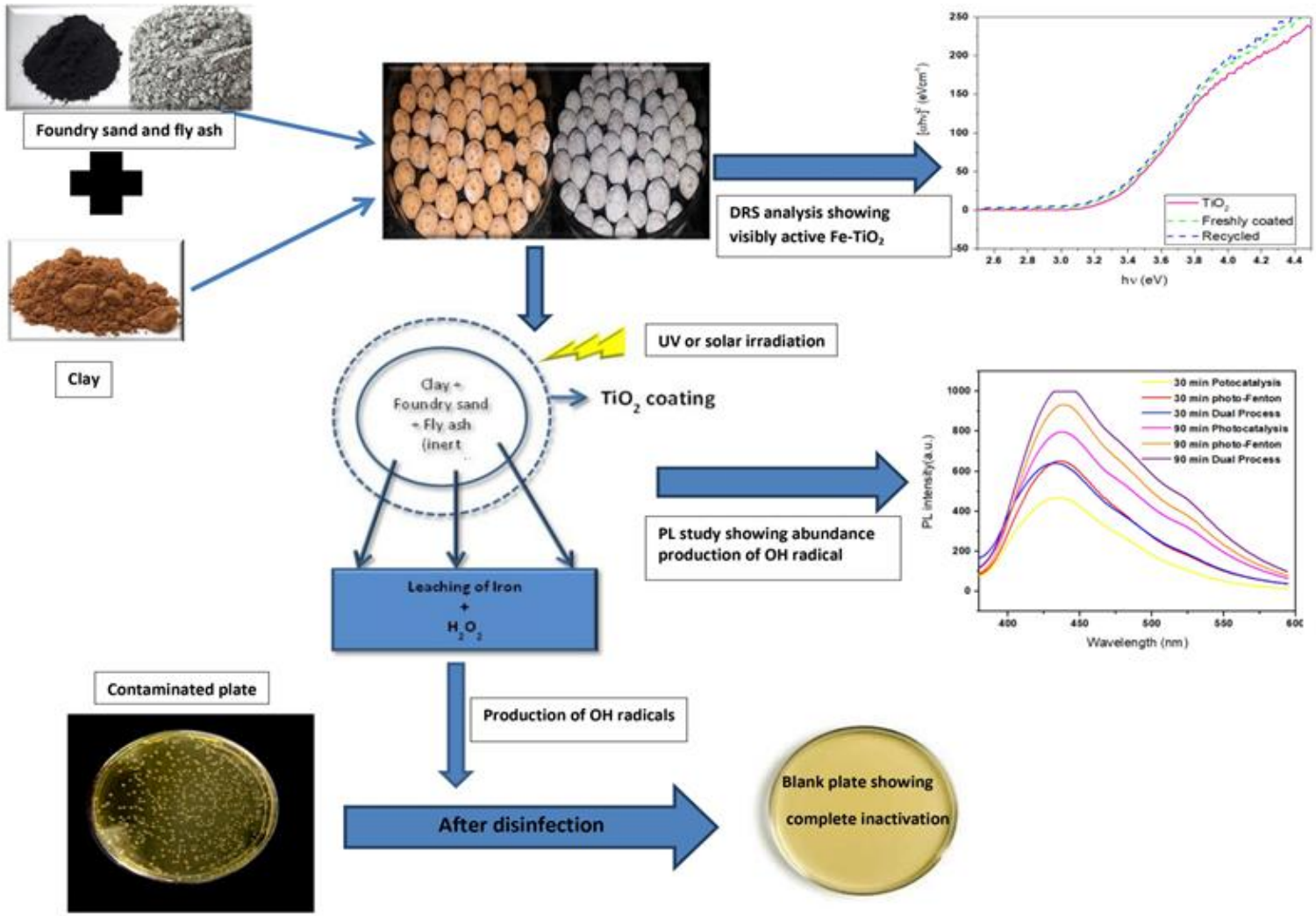

Figure 1. 3 Graphical representation of the hybrid process

1.7 Selected microorganism

In the present study, *Escherichia coli* (*E. coli*) was used to study the disinfectant efficacy of the Fe-TiO_2 composite. *E. coli* is the most researched bacteria in genetics at the moment; it lives in the human intestine and, if detected, suggests upstream fecal contamination of water. Although some researchers have questioned its appropriateness as a fecal indicator bacterium, compelling evidence supports its use in such research (Berney et al. 2006; Sciacca et al. 2011). More precisely, the *E. coli* K-12 strain was used in this study and its structure is shown in Figure 1.4. The particular strain is non-pathogenic and it is a reliable indicator of bacteria that have already been employed in a large number of disinfection studies because of its close resemblance to the wild Gram-negative type (Spuhler et al., 2010) as shown in Figure 1.5. Its ease of growing in the laboratory has proven it as an essential tool in related research. However, its response may vary significantly between strains.

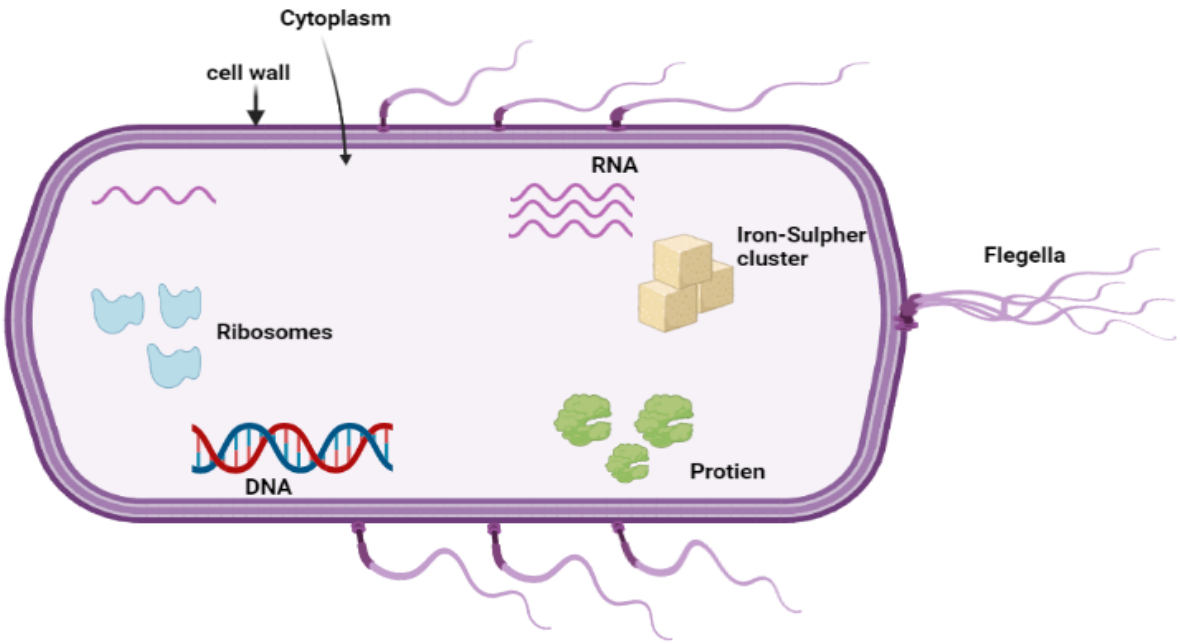

Figure 1. 4 Structure of Escherichia coli (*E. coli*)

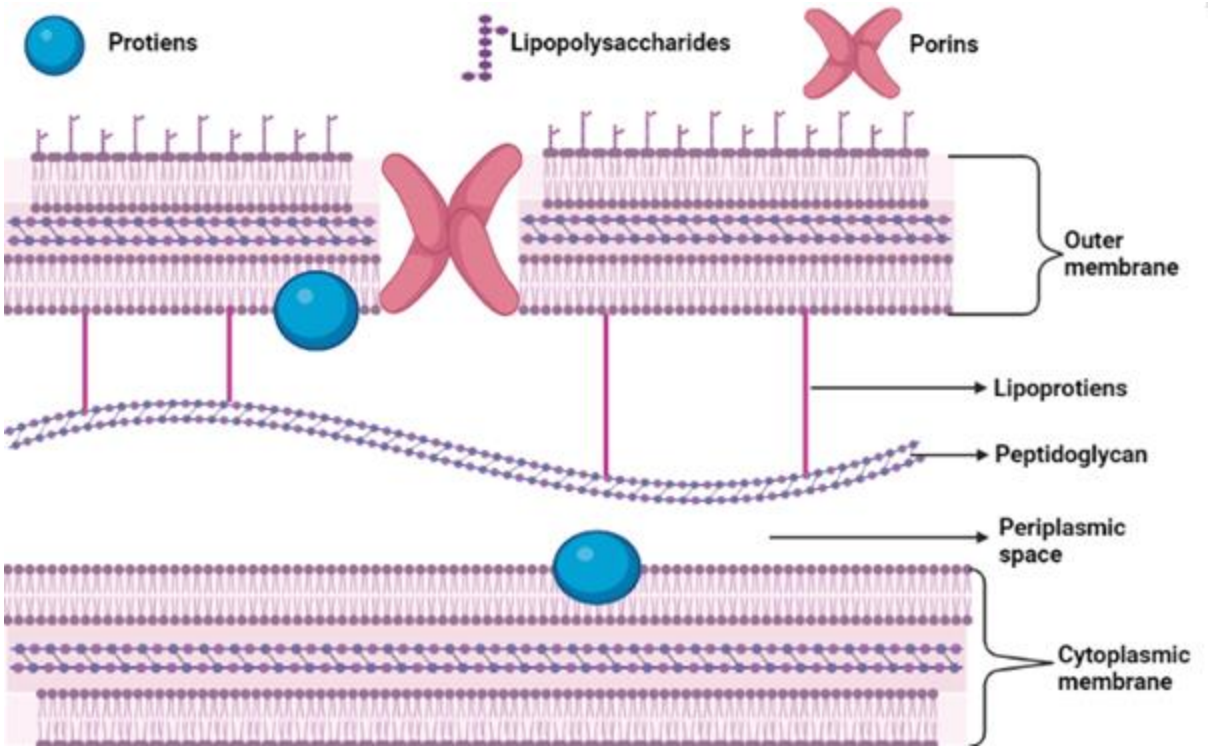

Figure 1. 5 Structure of Gram-negative bacteria

1.8 Aim of the proposed study

The main aim of the present research was to develop novel support incorporating in-situ hybrid effects (photocatalysis and photo-Fenton) for the disinfection of wastewaters. The study has been divided into different development stages comprising:

1. The synthesis and composition of the novel composite support material and utilizing them for the disinfection study of *E. coli* at lab-scale using in-situ hybrid effect.

2. The studies of the inactivation of *E.coli* at a pilot scale, i.e., scale-up of the process. Assessment of the reactors in the series model for the plug flow approach. Various process parameters were optimized by utilizing the appropriate catalyst based on inertness, cost, and, most crucial factor recyclability.

3. For substantiating the novelty of the process, the treatment of secondary treated municipal wastewater using composite beads under solar light was also studied.

1.9 Thesis organization

The first chapter of the thesis provides a brief introduction to the concept of the two advanced oxidation processes (i.e TiO_2-photocatalysis and photo-Fenton) and their application in pilot-scale reactors. This section also discusses the hybrid effect of the above-mentioned technologies in fixed-bed for water disinfection.

The second chapter deals with the review of available literature on analytical and experimental studies. The objective of the present study is also mentioned in this chapter.

The third chapter discusses the step-by-step fabrication of spherical composite beads and the coating of TiO_2 catalyst over the surface of the beads. This chapter also deals with the enumeration of microorganisms as well as the set-up of the different reactors under UV and solar irradiation.

The fourth chapter deals with the systematic study of the effects and interactions of the fundamental parameters governing UV and solar disinfection. Firstly the optimization of lab-scale fixed bed reactor under UV light was studied. Then its application in the pilot-scale reactor under solar irradiation was analyzed. The kinetic modeling of three different processes i.e photocatalysis, photo-Fenton, and the hybrid process was also studied for the lab-scale analysis. Then the chapter closes with the evaluation of bacterial regrowth, in both the short and long term.

The fifth chapter deals with the conclusion derived from the investigation made in chapter 4. An overall vision of the effectiveness of this hybrid process on water disinfection is given as final remarks.

Chapter 2

Literature Review

2.1 Overview

The human need for safe drinking water continues to grow, yet global water supplies are limited. To address this imbalance, effective wastewater treatment and reuse are becoming increasingly necessary. Water contamination by microorganisms is usually caused by fecal bacteria associated with humans (water sewage treatment plants), farm animals, or wildlife. The contamination of natural water resources is mostly caused by discharges from municipal wastewater treatment facilities, hospitals, and other industries. The presence of harmful bacteria and viruses in wastewater is a concern to public health and has developed into a significant public health issue. Figure 2.1 shows sources of microorganisms present in the water.

In response to this issue, the most interesting alternatives are reusing municipal wastewater on-site or reusing it for industrial and agricultural purposes after treating it at the treatment plant (Almuktar et al., 2018). Since these wastewaters represent one of the most significant available water resources, their reuse is expected to counteract the increased use of clean water. Recycled wastewaters generally contain pathogens, suspended particles, and soluble recalcitrant organic matter. Their removal from wastewater is very time-consuming and costly (Warren Viessman et al., 2009). The treatment technologies available for removing these contaminants such as adsorption, coagulation, and sedimentation concentrate the contaminants but they remain unaffected and un-"eliminated" or "destroyed." Other conventional water treatment techniques, such as filtration, chemical, and membrane technologies, are expensive to operate and may introduce dangerous secondary contaminants into the ecosystem. *Chlorination* is yet another technology that has been widely utilized for water disinfection (Anastasi et al., 2013; Firoentino et al., 2015). However, the disinfection byproducts formed are carcinogenic and hazardous to human health.

Due to the inability of conventional treatment technologies to effectively disinfect wastewater containing pathogenic bacteria, innovative treatment approaches such as advanced oxidation processes (AOPs) have been widely explored. This chapter discusses the disadvantages and advantages of AOPs (more precisely, homogeneous and heterogeneous

photocatalysis) concerning their commercial uses in wastewater treatment. Numerous alternatives have been considered to avoid the drawbacks of each other. The viability and potential commercialization of different processes in one unit have also been explored. This review is primarily concerned with the application of the advanced oxidation process in water and wastewater treatment.

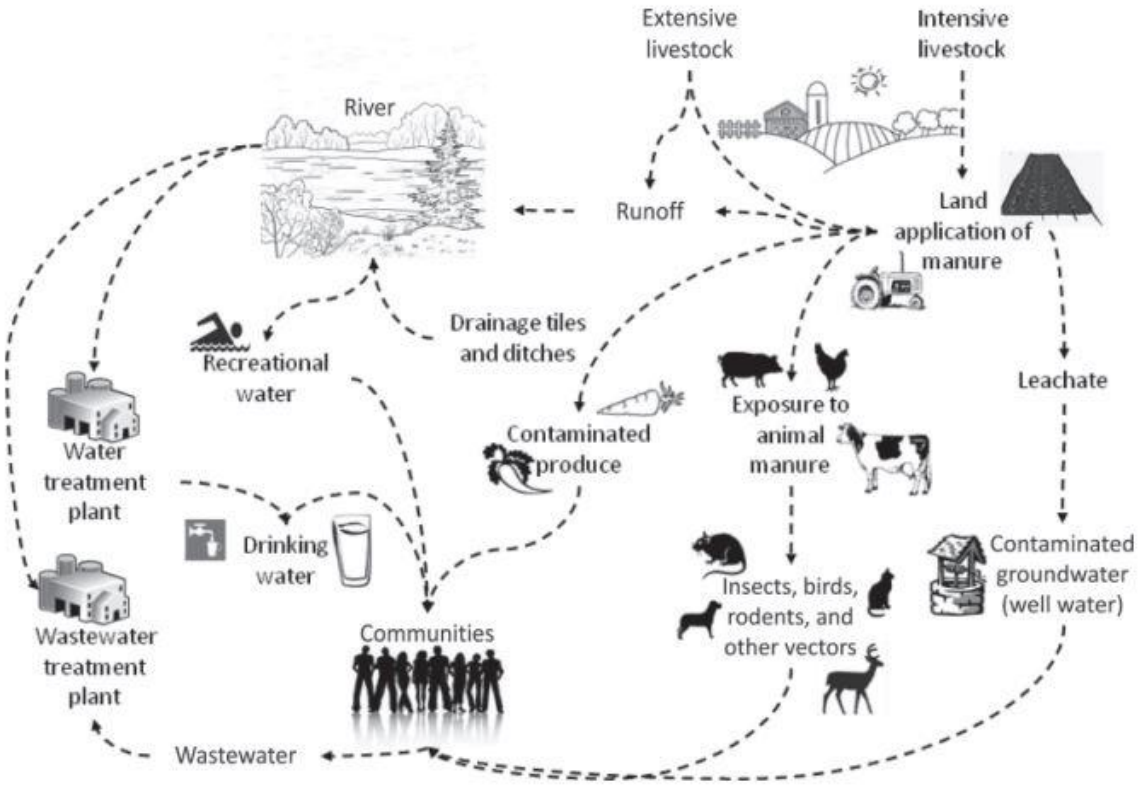

Figure 2. 1 Source of microorganisms present in the water resources (Ji et al., 2021)

2.2 Assets and liabilities of advanced oxidation process (AOPs) for water disinfection

AOP is a well-defined method that involves the production and usage of nonselective strong OH^o that oxidize a large wide variety of organic components found in wastewater. This method has recently been considered as a means of treating new pollutants, particularly pathogenic microorganisms present in water (Giannakis et al., 2018c). AOPs offer a viable technical solution to the challenges associated with traditional water treatment technologies. Such technologies are essential for sustaining and expanding the competence of various commercial sectors globally, including water technology.

The growing interest of both the corporate and academic sectors in AOPs is mirrored in the growing list of papers in several scientific publications devoted to environmental applications. The majority of published works are either on TiO_2 photocatalysis (Carré et al., 2014; Dunlop et al., 2008) or photo-Fenton (García-Fernández et al., 2012; Giannakis, 2018). These approaches have shown effective results in terms of disinfecting a wide range of microorganisms found in water. Both techniques, however, have several drawbacks that hinder their effective execution at the field scale.

2.2.1 Application of TiO_2 photocatalysis for water disinfection

The inactivation of different microorganisms is directly related to the type of technique and their response to it. Advanced oxidation techniques utilizing TiO_2-photocatalysis have garnered considerable attention in this regard. The TiO_2-mediated photocatalysis generates reactive oxygen species (ROS), which are mainly responsible for the disinfectant property, particularly against bacteria. Numerous research has been conducted to characterize a variety of photocatalytic materials useful at disinfecting/inactivating *E. coli*. Over the last few decades, the efficacy of TiO_2-photocatalysis for water disinfection has been widely explored (Acevedo et al., 2012; Chen et al., 2010; Lu et al., 2003). Various physiochemical aspects affect the overall dynamics of the TiO_2-photocatalysis used for water disinfection. These factors include the concentration of the catalyst, it's surface area, crystalline phase (Laxma Reddy et al., 2017; Nakata and Fujishima, 2012), light intensity (Fabbricino and D'Antonio, 2012; Lanao et al., 2012), and presence of oxygen in the solution (Reed, 2004) and initial concentration of bacteria (Gomes et al., 2009; Hallmich and Gehr, 2010).

TiO_2 exists in three major polymorphs: anatase, rutile, and brookite. The majority of research indicates that the photoactivity of anatase is much more efficient than the activity of rutile; the discrepancies are most likely attributable to the degree of electron and hole recombination in the two forms (Miyagi et al., 2004). Yet, it has been demonstrated that combinations of anatase and rutile are much more efficient in the removal of pollutants and killing coliphage MS2 (Sato and Taya, 2006). One commercially viable active TiO_2 is Degussa P25, which comprises around 80% anatase and 20% rutile (Bouanimba et al., 2018). The enhanced activity is often attributed to interactions between the two forms, which result in a decrease in bulk recombination. Brookite has received very little research, although a recent study demonstrated that a blend of brookite and anatase was much more effective than anatase alone (Shah et al., 2008).

Although it was demonstrated that a silver-doped multiphase catalyst enhanced photocatalytic activity, its antibacterial action was not observed (Yu et al., 2005). The demand for UVA irradiation limits the application of photocatalytic disinfection inside. Catalysts that have been modified can narrow the bandgap to the point where visible light initiates photocatalysis. This has been demonstrated for TiO_2 in combination with carbon, nitrogen, and sulfur, metals such as Sn, Pd, and Cu, and dyes, however, the activity is often lower than when activated with UVA (Fujishima and Zhang, 2006). This region is now undergoing extensive research. Matsunaga and coworkers (Tadashi et al., 1985) were the first to demonstrate the antibacterial action of UVA-activated TiO_2. Ever since, publications on the application of photocatalytic activity to destroy bacteria (Rincón and Pulgarin, 2004; Rodríguez-Chueca et al., 2013), protozoa (Pokhum et al. 2017), algae(Hossain et al., 2020; Natarajan et al., 2018), fungus (Mukherjee et al., 2020; Zhang et al., 2020), and viruses (Nakano et al., 2012; Zan et al., 2007), as well as microbial toxins, have been widely reported.

Typically, photocatalytic disinfection and catalyst loading (up to a certain dose) follow a linear relationship with respect to each other (Cho et al., 2004a; Kacem et al., 2014), beyond which efficient light penetration into the solution is impossible, reducing disinfection efficacy (Gaya and Abdullah, 2008). The pH of the wastewater affects the electrostatic charge on the TiO_2 surface, which controls the density of $TiOH_2^+$ groups during photocatalysis. As a result, the activity of TiO_2-photocatalysis to inactivate bacteria and adsorption of bacteria on the surface of the TiO_2 is pH-dependent. Disinfection is 4 to 8 folds higher in oxygenated water than in deoxygenated water (Reed, 2004). Dissolved oxygen (DO) functions as an electron scavenger, generating superoxide radicals ($^{\circ}O_2^-$) that combine with water to generate more OH^o (Collin, 2019).

In the presence of DO in the water sample, the photocatalytic disinfection of *E. coli* is increased due to the formation of more OH^o in comparison to when no oxygen is present (Fernández-Ibáñez et al., 2015). After originally reporting on TiO_2 photocatalytic inactivation in 1985 (Tadashi et al., 1985), the area has seen the publication of over 1000 scientific articles, and some of them are mentioned in Table 2.1. The efficacy of photocatalysis toward microorganisms has been investigated, including bacteria (Carré et al., 2014; Rincón and Pulgarin, 2004), spores (Sunnotel et al., 2010), biofilms (Dunlop et al., 2010), viruses (Nakano et al., 2012), protozoa (Abeledo-Lameiro et al., 2017; Lonnen et al., 2005), fungi (Mitoraj et al., 2007; Rodrigues-Silva et al., 2017), and algae (Gladis and

Schumann, 2011; Ochiai et al., 2010). While all of these described research achieved a reasonable level of disinfection efficacy, certain disadvantages fall into one or another category, limiting their applicability for field-scale applications. Some of the reported shortcomings include the following:

1. The use of artificial UV lights;
2. Catalyst separation;
3. Frequent e^-/h^+ recombination; and
4. High electricity prices and scale-up issues.

2.2.2 Mechanism of the killing of bacteria using TiO_2 photocatalysis

Bacteria have been discovered as an efficient indication of water contamination across all microorganisms. For example, among a diverse group of bacteria, *E. coli* coliform is widely known as a sign of contaminated water, as its existence generally indicates fecal contamination of the water (Mosteo et al., 2020). Numerous research has been conducted to characterize a variety of photocatalytic materials useful at inactivating/disinfecting *E. coli*. Over the last few decades, the efficacy of TiO_2 photocatalysts over bacterial inactivation has been widely explored. OH^o formed on the VB frequently binds to the cell wall of the bacteria, causing cell wall damage via fast potassium ion leakage. Numerous factors affect the production of radicals that enhance bactericidal activity. Even though the OH^o was predicted to play a substantial part in the disinfection mechanism, its exact involvement remains unknown due to its short half-life. But on the other hand, peroxide radicals have a prolonged half-life and may be more powerful than other radicals due to their negative charge. These radicals have a significant effect on the cell wall by degrading the phospholipid membrane. Following the oxidation of the internal coenzyme A. It should be emphasized that the principal disinfection targets for gram-positive and gram-negative bacteria may vary according to their peptidoglycan composition. Additionally, gram-positive bacteria lack an outer membrane. As a result, the disinfection procedure is unique for 2 separate species of bacteria. Nevertheless, both gram-positive and gram-negative bacteria exhibit fast ion leakage, nucleic acid degradation, and lipid peroxidation. This is consistent with the behavior of all other living species, such as plants (Laxma Reddy et al., 2017).

Table 2. 1 Summary of articles on TiO_2-based photocatalytic disinfection of wastewater

Type	Photocatalyst	Concentration	Duration	Efficacy	Reference
E. coli	TiO_2	5 mg	-	64%	(Song et al., 2016)
E. coli	Nanoparticles of Ag@TiO_2	0.4 g/l	-	100%	(Sreeja and Shetty, 2016)
E. coli	2% GO- TiO_2 nano-composites	-	90 min	100%	(Wang et al., 2016)
E. coli	N-TiO_2	(10g/l) N-TiO_2Coationg on glass beads	LED 120 min Sunlight 40 min	-	(Kassahun et al., 2018)
E. coli	Fixed TiO_2	0.3-4g/l	30 min	93%	(Chen et al., 2010)
E. coli	TiO_2	Wall and fixed bed reactor	-	99%	(Rodríguez et al., 2012)
E. coli	TiO_2P25	-	120 min	100%	(Gutiérrez-Alfaro et al., 2015)
E. coli	TiO_2	Coating of TiO_2 over stair type reactor / Coating of TiO_2 over PTC	120 min	28% 75%	(Ahmad et al., 2016)
E. coli	P25 TiO_2 DEGUSSA	Coating of TiO_2	100 min	-	(Marugán et al., 2015)
Hepatitis virus B	TiO_2	The coating on ceramic tiles	240 min	94%	(Zan et al., 2007)
MS2 bacteriophage	TiO_2	binary Mn/Co-doped TiO_2	20 min	99%	(Venieri et al., 2015)
Bacteriophage f2	TiO_2	Cu–TiO_2 nano-fibers	240 min	100%	(Zheng et al., 2017)
E. coli	40% TiO_2 -	binanosheets	240 min	100%	(Jia et al., 2016)

	Bi_2WO_6				
E. coli	TiO_2-Fe_3O_4	hollow spheres	240 min	100%	(Ren et al., 2015)
E. coli	TiO_2–graphene–porphyrin	nanocomposite	440 min	64%	(Rahimi et al., 2015)
E. coli	g-C_3N_4)/TiO_2		180 min	100%	(Li et al., 2015)
E. coli	TiO_2 nanotube	2 g L^{-1}	50 min	95%	(Ng et al., 2010)
E. coli	(Fe, N)-doped TiO_2	-	480 min	94.5%	(He et al., 2009)
S. Aureus Silver-modified	TiO_2/ZnO plasmonic photocatalysts	-	120 min	99.9%	(Tallósy et al., 2014)
P. Aeuroginosa	Ag-doped TiO_2 nanoparticles	-	-	-	(Gupta et al., 2013)
L. monocytogens	Nano-TiO_2	1 g L^{-1}	180 min	-	(Long et al., 2014)
E. coli	TiO_2	Coating on the wall	120 min	100%	(Pablos et al., 2011)
E. coli	P25 TiO_2/rGO composites	-	90 min	95%	(Cruz-Ortiz et al., 2017)
E. coli O157: H7	C_{70}/TiO_2	1 g L^{-1}	120 min	73%	(Ouyang et al., 2016)
M. aeruginosa	g-C_3N_4/TiO_2	2 g L^{-1}	360 min	84%	(Song et al., 2018)
E. coli	g-C_3N_4/TiO_2	0.6 g L^{-1}	180 min	100%	(Li et al., 2015)
E. coli	g-C_3N_4 nanosheet/TiO_2 nanotube on Ti	Not reported	180 min	3.5 log reduction	(Faraji et al., 2018)

	plate				
S. aureus E. coli & E. faecalis P. aeruginosa	TiO_2/graphite	0.1 g L^{-1}	300 min 1440 min 75 min	50% in all bacteria	(Dědková et al., 2015)
E. coli	Pt/TiO_2	1 g L^{-1}	180 min	100%	(Murcia et al., 2017)
E. coli and *S. aureus*	Ag/TiO_2	1 g L^{-1} for *E. coli* 2 g L^{-1} for *S. aureus*	1440 min	100%	(Dong et al., 2019)
E. coli and *total coliform*	TiO_2/SiO_2/Au thin film	8 cm^2 of thin film with 7.5 mm of water level height	30 min for *E. coli* 45 min for coliform	100%	(Levchuk et al., 2018)
E. coli	Ag/TiO_2	0.5 g L^{-1}	300 min	6 log reduction	(Xiang et al., 2012)

2.2.3 Application of photo-Fenton Process for water disinfection

The First study of the photo-Fenton process was established in the 1990s (Zepp et al., 1992) to evaluate the nature and formation efficacy of the transient oxidants generated during the reaction of H_2O_2 and Fe^{2+} at a wide range of pH (3-8). This study provides an essential pathway for environmental oxidation reactions and wastewater treatment. (Cho et al., 2004b) conducted the first attempt to remove microbes using iron compounds, while (Rincón and Pulgarin, 2006) two years later accomplished the first genuine photo-Fenton process for microbial inactivation. The photo-Fenton process's boosting effect on the inactivation of *E. coli* in drinking water was reported for the first time, paving the way for new and relevant studies. After that efficacy of photo-Fenton inactivation of numerous microorganisms has been investigated on fungus (García-Fernández et al., 2012; Polo-López et al., 2014), viruses (Giannakis et al., 2017; Polo et al., 2018), bacteria (Giannakis et al., 2018b; Rommozzi et al., 2020), and spores (Ruiz-Aguirre et al., 2017) and some other related studies are mentioned in Table 2.2. Throughout the last decade, significant efforts have been made to eliminate micro contaminants and microbiological pollutants.

The photo-Fenton reaction is highly dependent on some operating conditions such as microbial population, iron and H_2O_2 concentration, pH, and temperature. (Polo-López et al., 2013) investigated the photo-Fenton system's ability to remove *Phytophthora capsici zoospores* from distilled water, achieving the maximum disinfection rate under 60 min with 10 mg L^{-1} of H_2O_2, 5.0 mg L^{-1} of Fe^{2+} or Fe^{3+} with 2.5 kJ L^{-1} of ultraviolet solar irradiations. Under low iron concentrations < 5.0 mg L^{-1}, the reaction did not produce an excess of OH^o radicals sufficient to inactivate the targeted zoospores. Previously, it was established that the photo-Fenton effect is significantly dependent on the structure of the cell; hence, optimum dozes of iron, H_2O_2, and UV light, as well as exposure times, are target-specific characteristics for each microbe. The best photo-Fenton disinfection of *E. coli* was found with 5 mg L^{-1} of Fe, 20 mg L^{-1} of H_2O_2 at pH 5.0, and light intensity of 500 W m^{-2} (Rodríguez-Chueca et al., 2012). While it has been demonstrated that a homogeneous photo-Fenton method is a realistic approach for disinfection purposes, it does have the following drawbacks:

1. Higher treatment cost;
2. Inadequate regeneration of catalyst;
3. High dose of H_2O_2; and

4. a large volume generation of iron sludge.

2.2.4 Mechanism of the killing of bacteria using the Photo-Fenton process

When iron and H_2O_2 are added to the system it causes two significant alterations in cell inactivation (Giannakis et al., 2016a). The first one is the interaction between iron and H_2O_2 leading to the huge influx of OH^o into the system, which results in bacterial cell oxidation from the outside. The second is the use of cell porins to allow H_2O_2 and ferrous ions to enter the bacterial cell. Since the size of the ferrous ion (<6Å) and the H_2O_2 ion (1.2–1.4 Å) are smaller than the size of bacteria (11 Å), they damage cells from inside after catalases are deactivated. The ferrous ion combines with the reactive oxygen species (ROS) present inside the cell under the influence of UV radiation, causing cell damage.

H_2O_2, on the other hand, causes a reduction in biosynthetic and catabolic activity, resulting in the loss of different ions such as iron from the iron/sulfur cluster and the form of OH^o (Giannakis et al., 2018c). The external cell wall also degrades with the reaction with H_2O_2. This will lead to an increase in the permeability of the cell and a large amount of H_2O_2 will enter the cell, which causes the cell wall to oxidize. It occurs because the oxidative activity of H_2O_2 (0.18) is greater than the membrane's oxidation potential. Outside the cell, H_2O_2 generates ROS by homolysis, and when H_2O_2 combines with iron, it contributes to the bacteria's external oxidation.

Table 2. 2 Summary of articles on photo-Fenton disinfection of wastewater

Types	Operational conditions		Duration	Initial concentration	Final concentration	Reference
E. coli	Fe (mg L^{-1}) 1	H_2O_2 (mg L^{-1}) 10	90 min	10^5CFU mL^{-1}	Total inactivation	(Shekoohiyan et al., 2019)
E. coli	Fe (mg L^{-1}) 1	H_2O_2 (mg L^{-1}) 10	120 min	10^6 CFU mL^{-1}	Total inactivation	(Giannakis et al., 2018c)
E. coli	Fe^{2+} (mg L^{-1}) 0.6	H_2O_2 (mg L^{-1}) 10	120 min	10^6 CFU mL^{-1}	Total inactivation	(Ruales-Lonfat et al., 2015)
E. coli	Fe^{2+} (mg L^{-1}) 0.3	H_2O_2 (mg L^{-1}) 10	360 min	10^7 CFU mL^{-1}	Total inactivation	(Gutiérrez-Zapata et al., 2017)
E. coli	Fe^{2+} (mg L^{-1}) 0.3	H_2O_2 (mg L^{-1}) 20	180 min	10^9 CFU mL^{-1}	Total inactivation	(López et al., 2017)
Enterococcus faecalis	Fe^{2+} (mg L^{-1}) 10	H_2O_2 (mg L^{-1}) 120	120 min	10^6CFU mL^{-1}	Total inactivation	(Ortega-Gómez et al., 2012)
E. coli, f. solani	Fe^{3+} (mg L^{-1}) 5	H_2O_2 (mg L^{-1}) 10	30 min	10^6CFU mL^{-1}	Total inactivation	(García-Fernández et al., 2012)
E. coli DH5α	Fe (mg L^{-1}) 2.8	H_2O_2 (mg L^{-1}) 340	30 min	10^6 CFU mL^{-1}	Total inactivation	(Ahmed et al., 2020)

E. coli k 12	$Fe^{2+ \text{ or } 3+}$ (mg L^{-1}) 5	H_2O_2 (mg L^{-1}) 20	-	10^6 CFU mL^{-1}	2.43 log	(Rodríguez-Chueca et al., 2012)
E. faecalis	Fe^{3+} (mg L^{-1}) 20	H_2O_2 (mg L^{-1}) 50	-	10^6CFU mL^{-1}	Total inactivation	(Ortega-Gómez et al., 2016)
E. coli k12	Fe^{2+} (mg L^{-1}) 0.35	H_2O_2 (mg L^{-1}) 10	30 min	10^6 CFU mL^{-1}	4.6 log	(Alvear-Daza et al., 2018)
E. coli K12 (MG 1655)	Fe^{2+} (mg L^{-1}) 230	H_2O_2 (mg L^{-1}) 10	60 min	10^7 CFU mL^{-1}	Complete Inactivation	(Barreca et al., 2015)
E. coli	Fe^{2+} (mg L^{-1}) 2.5/5/10/20	H_2O_2 (mg L^{-1}) 50	-	10^6 CFU mL^{-1}	-	(Rubio et al., 2013)
E. coli	Fe^{2+} (mg L^{-1}) 20	H_2O_2 (mg L^{-1}) 50	80 min	10^4 CFU mL^{-1}	Complete Inactivation	(Esteban García et al., 2018)
E. coli W1485 (DSMZ 5695)	Fe^{2+} (mg L^{-1}) 1/5	H_2O_2 (mg L^{-1}) 10/50	30 min	10^9 CFU mL^{-1}	Complete Inactivation	(Giannakis et al., 2018a)
E. coli	Fe^{2+} (mg L^{-1}) 2.5-10	H_2O_2 (mg L^{-1}) 5-50	-	10^6 CFU mL^{-1}	Complete Inactivation	(Rodríguez-Chueca et al., 2014b)
E. coli K12 (MG 1655)	Fe^{2+} (mg L^{-1}) 0.6	H_2O_2 (mg L^{-1}) 10	-	10^6 CFU mL^{-1}	-	(Valero et al., 2017)
Bacillus subtilis	-	-	90 min	10^7 CFU mL^{-1}	10^4 log	(Ruiz-Aguirre et al., 2017)

Before executing the photo-Fenton system on a field scale, the aforementioned challenges must be rectified. These consequences can be mitigated somewhat in heterogeneous photo-Fenton processes by fixing the iron inside the catalyst structure, as demonstrated in various investigations. Numerous catalysts, including clays (De León et al., 2008), ferrite (Liu et al., 2012), zeolite (Kasiri et al., 2008), magnetite (Avetta et al., 2015), and minerals, have been used in heterogeneous photo-Fenton reactions. The primary advantage of heterogeneous processes is that they eliminate the problem of iron sludge production that occurs in homogeneous processes. Yet, these techniques result in a slower rate of oxidation than homogeneous processes due to the presence of a lesser amount of iron on the catalyst surface (Punzi et al., 2012).

2.2.5 Advances in fixed bed photocatalysis for water disinfection

Since the discovery of the photocatalytic effect on water splitting using a TiO_2 electrode (Fujishima and Honda, 1972), various studies have been done to generate TiO_2 photocatalysts of various scales, and determine their physical properties, and their photo-oxidation efficacy to the surface-oriented nature of photocatalysis. The TiO_2 catalyst enables a high surface area to volume ratio, further enhancing the efficacy of charge separation and entrapment at the physical surface. The increased oxidation performance of this nanoscale TiO_2 catalyst was stated to be due to its light opacity compared to bulk TiO_2 catalysts. Though these TiO_2 catalysts exhibit significant improvements in physical and chemical properties, the primary issues such as its morphology, and particle size in real-life application remain a problem.

To conquer this issue, specialists have been working in the area of fixed-bed photocatalysis, where the catalyst is being covered/consolidated/trapped on some material and in this way utilized for water disinfection. There are diverse approaches available for the immobilization of photocatalyst films on supporting substrates. To improve the efficacy of water disinfection, TiO_2 has been coated on different support materials like mesh, pills, cylinders, balls, *etc.* It is found from the literature that the TiO_2 in suspended form is much more efficient in killing because of the better contact between catalyst and bacteria. However, the inactivation rate of both fixed bed and suspended reactors is very similar to each other. From these outcomes, it was inferred that the high surface area of TiO_2 is not the main parameter of this design that is in charge of the microorganism's inactivation. However, mechanical and osmotic pressure also plays an important role in the killing of

microorganisms. Recovery of the catalyst in a fixed bed reactor is not required but the life span of the catalyst needs to be considered.

In one of the studies, the catalyst in fixed form was reused ten times and no change in the activity of the catalyst was observed (Sordo et al., 2010). The coating of TiO_2 on the fixed glass surface was done to investigate the inactivation of *E. coli* K-12 (Rincón and Pulgarin, 2003). It was observed from the result that TiO_2-P25 Degussa on the fixed form under UV radiation is more active in the killing of bacteria when compared to immobilized rutile prepared from (nanocrystalline 30 nm) and anatase prepared from acetyl acetonate-isopropoxide ($Ti(acac)_2(iOPr)_2$). In recent years, several different types of supports coated with TiO_2 have been developed for the treatment of wastewater and drinking water. Numerous studies have demonstrated that support improves the surface interaction of catalysts with pollutants. These supports include the immobilization of the catalyst onto mesoporous clay (Mustapha et al., 2020), activated carbon (Yao et al., 2010), fibers (O'Neal Tugaoen et al., 2018), glass plates (Alrousan et al., 2012; Chin et al., 2015), glass rings (Adán et al., 2018), on the membrane (Paredes et al., 2019), cylinders (Acevedo et al., 2012; Sordo et al., 2010), and on the polymers (Coutinho and Gupta, 2009; Kubacka et al., 2009).

Such types of TiO_2 immobilized support materials in photocatalytic disinfection/ degradation processes eliminated the need for a costly post-treatment catalyst separation step. Thus, the process of scaling up may be visualized. However, very few studies have demonstrated that the immobilized catalyst can be utilized for an extended amount of time or that the support material can be used for an extended period. Before considering practical applications of fixed-bed photocatalytic activity, numerous risks associated with the process must be carefully considered, as detailed below:

1. The supported photocatalyst durability;
2. The inertness of the support material;
3. The cost of supports used for catalyst immobilization; and
4. Film diffusion resistance

As a result, there are few investigations on the practical applicability of this technique. Indeed, the film-diffusion resistance associated with the low area/volume ratio of supported catalyst systems has severely limited researchers' ability to develop viable solutions for field-scale operations of fixed-bed processes. This drawback may be overcome with optimal

reactor design, which maximizes catalytic illumination while minimizing mass transfer issues.

2.2.6 Modification of TiO_2 photocatalyisis

To investigate the real-life applications of AOPs, researchers are presently concentrating their efforts on exploiting solar irradiation. Utilizing natural solar light rather than artificial UV lamps in photocatalytic or photo-Fenton techniques is cost-effective and environmentally friendly. Solar light-driven photocatalytic processes are particularly suited for developing countries such as India, which enjoys an abundance of sunlight irradiation across the year.

Due to the solar-induced implementations of photocatalysts, the most difficult challenge is to choose an adequate catalyst/material capable of effectively harvesting solar radiations. Additionally, the catalyst should be resistant to electron-hole recombination. Although TiO_2 has been thoroughly studied for photocatalytic disinfection of a wide variety of microorganisms because of its photostability and low cost, it has several disadvantages, including rapid electron-hole recombination and UV-only absorption. To increase the photocatalytic performance of TiO_2, research is primarily focused on the inhibition of electron-hole recombination and the enhancement of light absorption properties. The physical properties of photocatalysts, such as particle size, crystallinity, morphology, and crystal facets, can be optimized by generating photocurrent and photoluminescence. Additionally, numerous beneficial alterations to the structure of TiO_2 have been documented in the literature to generate highly efficient photocatalysts, either by doping with metals/non-metals or by building nanocomposites.

Numerous ways have been explored to expand the spectral sensitivity of TiO_2 into the visible region and boost its photocatalytic activity. Doping pure TiO_2 with metal/non-metal is one technique to make it visible light sensitive. This technique maximizes the visible portion of the solar spectrum while also ensuring that charge traps separate the electron-hole photo produced. For instance, a TiO_2 shell and Ag core ($Ag@TiO_2$) nanoparticles under UV irradiation have employed the killing of *E. coli* (Sreeja and Shetty, 2016). The results showed that these nanoparticles are highly efficient in killing bacteria present in water both in suspended and immobilized forms. From their results, the author concluded that the $Ag@TiO_2$ nanoparticles are more highly efficient than TiO_2 nanoparticles. Up till now, several studies have been done using *E. coli* as a model microorganism during water

treatment under visible light to estimate the disinfection efficacy of doped catalysts (Gamage et al., 2013; Karunakaran et al., 2013, 2011, 2010; Rizzo et al., 2014; Taylor et al., 2012; Veréb et al., 2013; Vijay et al., 2013; Wong et al., 2006).

Moreover, modifications through the formation of composites are used to check inactivation efficacy. For instance, Bi_2WO_6/TiO_2 composite was used for the sterilization of marine water (Chai et al., 2019). Bi_2WO_6 is a very stable n-type semiconductor that is used as the main photocatalytic material in this experiment. The main advantages of this material are high photochemical stability, lack of toxicity, good activity toward visible light, and low cost. Under sunlight, Bi_2WO_6 produces electrons (e^-) and holes (h^+), which react with water or air to produce strong oxidizing agents (e.g., OH^-, H^+, and O_2). These strong oxidizing radicals can damage the DNA of microorganisms, which causes their death (Giannakopoulou et al., 2016; Shao et al., 2017) and eventually leads to decomposition. But the bandwidth of Bi_2WO_6 is narrow at only about 2.6–2.7 eV, and because of that, the electron-hole pair recombination rate is high. Therefore this material shows less photocatalytic activity in the presence of sunlight, thus limiting its application. To reduce its electron-hole recombination and to increase its photocatalytic activity, a traditional photocatalyst, TiO_2 has a low-cost n-type semiconductor with excellent non-toxicity, high photocatalytic reactivity, and chemical stability is combined with Bi_2WO_6 (Chai et al., 2019).

In another study, a novel and effective two-step *in situ* methodology were introduced for the preparation of TiO_2-Ag composites using different concentration of Ag NPs. The silver precursor is formed in the precipitation reaction and then complete reduction to the Ag NPs was done by atmospheric pressure Dielectric Barrier Discharge cold plasma. The Ag NPs with an average diameter of 3.7 nm and good dispersibility were obtained. From this, it was observed that this technique is more effective in killing gram-negative bacteria than for gram-positive bacteria. This work indicates that the novel two-step method involving a precipitation reaction and atmospheric pressure dielectric barrier discharge (DBD) cold plasma treatment has exceptionally encouraging prospects for utilization of metal nanoparticles and very dispersive upheld metal catalyst. The Composites can be manufactured in a variety of ways. Within 90 min, a TiO_2–graphene oxide (GO) composite (mass ratio 100:2) disinfected *E. coli* at a rate of 99.5%. Additionally, composites created by combining metal and metal oxide (for example, Au/TiO_2 composites) were at least five times more effective than pure TiO_2. Additionally, the disinfecting activity of this composite was seen in both dark and light situations, indicating that metal ions, in addition to the TiO_2

photocatalytic property, play a part in disinfection. Hybrid photocatalysts are composites composed of organic and inorganic substances. Within 180 min, a hybrid photocatalyst based on organic-inorganic graphitic carbon nitride (g-C_3N_4)/TiO_2 was reported to remove 10^7 CFU mL^{-1} of *E. coli* K-12. Although numerous studies on doped or co-doped photocatalysts have been published in recent years, neither research has yet demonstrated field-scale usage of these improved catalysts. Indeed, this research has the following limitations, which hinder its applicability on a large scale:

1. Expensive raw materials were employed in almost all reported investigations to manufacture modified TiO_2; and
2. The majority of reported studies used modified TiO_2 in suspension mode, adding cost for post-treatment catalyst separation.

To fully exploit the benefits of doping or co-doping, the procedure must be economically scaled up.

2.2.7 Pilot-scale applications of AOPs for water disinfection

To increase the AOPs utilization at a large scale in the near future, it is imperative to conduct scale-up trials of lab-scale findings. Effective execution of a field-scale photocatalytic disinfection technique requires a multidisciplinary approach to all operating factors determining the subsequent utilization of light photons within a reactor. There are two types of photocatalytic reactors, the concentrating and non-concentrating types. The concentrating reactors utilize sunlight and are constructed on parabolic trough concentrators (PTC). These reactors solely use direct irradiation and require expensive and difficult-to-maintain solar tracking systems. As a result, these reactors collect a considerable number of photons at all spectra. The non-concentrating reactors are low-cost reactors utilizing both direct and indirect solar light. With specific design changes, photocatalytic reactors have genuinely opened up new pathways for visualizing field-scale applications. Numerous eminent researchers have published in-depth kinetic analyses of reactors based on the fundamental concepts of AOPs. However, it was never apparent whether to use a heterogeneous/homogeneous photo-Fenton technique or a heterogeneous photocatalytic strategy in any of these experiments. The compound parabolic collector (CPC) has received the most attention in the literature for wastewater treatment using photocatalysis or the photo-Fenton process.

To date, one of the most effective options for microbial deactivation by solar AOPs has been the tubular photoreactor combined with a CPC. These are stationary collectors comprised of a cylindrical reactor surrounded by a parabolic reflective surface. The primary advantage of this system is that it successfully exploits the photons coming from the sunlight, as the reflector design redirects the indirect light onto the receiver coil, capturing both direct and indirect solar radiations. Additionally, these reactors operate as static systems; they employ non-imaging concentration optics with diffuse focus; they distribute radiation uniformly into the absorber; and they have a constant concentration factor (CF: 1) for all solar zenith angles within the acceptance angle limit (Malato et al., 2009).

Figure 2.2 depicts the standard CPC pilot-scale reactor for the disinfection of water. CPC reactor lenses are typically made of anodized aluminum due to their high reflectivity in the UV-A and the visible and infrared regions of the solar spectra range. Due to the durable nature of polyethylene and polypropylene, the majority of piping used to link photo-reactor cylinders and tanks may be constructed of durable polypropylene and polyethylene materials (Fendrich et al., 2019). In recirculating reactors, water flows through the tubes to a tank through a centrifugal pump and creates a turbulent environment inside the photoreactor tubes that promotes complete water homogeneity.

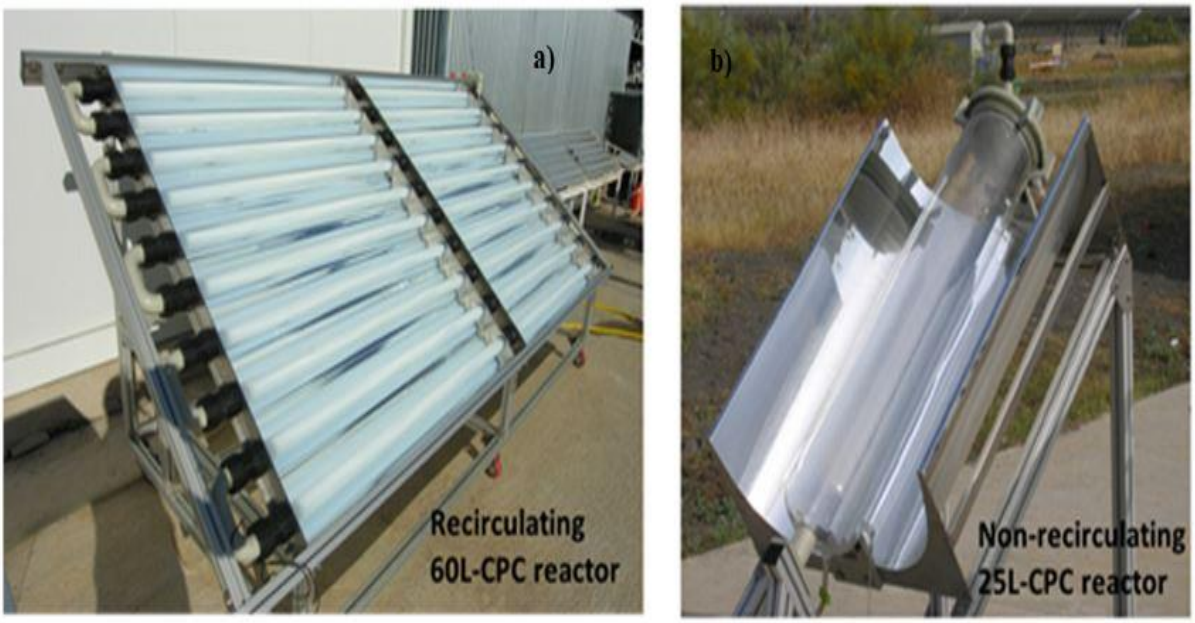

Figure 2. 2 Solar CPC pilot-scale reactor (a) Recirculating (b) Non-recirculating for water disinfection studies (Giannakis et al., 2016b)

These solar CPC reactors have been researched recently for natural water, secondary effluents, and wastewater disinfection using the photo-Fenton process. The very first implementation of CPC reactors using photo-Fenton for disinfection of river water illustrated that adding low concentrations of Fe^{3+} (0.6 mg L^{-1}) and 10 mg L^{-1} H_2O_2 results in a subsequent reduction of total *E. coli* inactivation and TOC (55%) (Moncayo-Lasso et al., 2009). Since 2012, numerous authors have investigated the use of photo-Fenton under solar irradiation to disinfect secondary effluent. Overall, it has been illustrated that low iron concentrations resulted in high inactivation rates of various microorganisms naturally occurring in secondary effluents. In terms of treatment efficacy, the photo-Fenton method was found to be more successful than photocatalysis. Despite this, field-scale applications of either the heterogeneous slurry photocatalysis or homogeneous photo-Fenton process have not been achieved in either of these pilot-scale reactors due to the rise of specific defects inherent in these systems. As previously discussed, the generation of iron sludge, catalyst regeneration issues, and the use of a high dose of oxidant are the major issues that must be addressed in the photo-Fenton process, whereas the catalyst separation and its reusability are the main concerns that must be addressed in slurry photocatalysis, which prevents their use on a large scale in the first place.

On the other hand, TiO_2 photocatalysis is always favored in its fixed state. Additionally, a wide range of research has been published utilizing fixed-bed photocatalysis for wastewater disinfection on a pilot scale. The effectiveness of a thin-film fixed-bed reactor (TFFBR) was investigated for the killing of *Aeromonas hydrophila* at high sunlight intensities (Khan et al., 2012). The researcher provided the concept proof for the significance of photo-catalysis using sunlight in aquaculture systems. The data reveal that higher solar light intensities (600 W m^{-2}) at lower flow rates (4.8 L h^{-1}) offered the optimal circumstances for *Aeromonas -hydrophila* ATCC 35654 inactivation. However, all flow rates and low solar intensity led to decreased total inactivation and increased sub-lethal damage. The utilization of CPC and immobilized titanium dioxide as solar disinfection photocatalysts was also investigated (Alrousan et al., 2012). Solar photocatalytic disinfection of water was carried out employing P25 immobilized on borosilicate glass tubes. Under natural sunlight, the photocatalytic efficacy of immobilized TiO_2 was assessed for inactivating *E. coli* using a 7L-CPC flow reactor. Multiple photoreactor configurations were evaluated: (1) borosilicate glass tubes (1.5 m in length) with a diameter of 50 mm that had been dip-coated with TiO_2, (2) uncoated 50 mm-borosilicate glass tubes, (3) 32 mm-borosilicate glass tube that had been externally dip-coated

with TiO_2 (and then put within the 50 mm glass tube), and (4) uncoated 32 mm-borosilicate glass tube. CPCs were found to enhance solar photocatalytic disinfection. The authors demonstrated that not every combination was effective at inactivating *E. coli*.

The most successful form was the concentric tube arrangement with CPC. (Sordo et al., 2010) investigated the photocatalytic inactivation of *E. coli* using immobilized TiO_2 in two distinct configurations (a wall reactor and a fixed-bed reactor) in a solar 10 L-CPC pilot plant, comparing the usage of a slurry reactor to solar disinfection without a catalyst. TiO_2 was immobilized onto a packing material of 10 mm glass Raschig rings for the fixed-bed reactor. TiO_2 wall reactors were composed of TiO_2 immobilized on a glass tube that was inserted into the photoreactor's axis through tubular support (external diameter of inner tube: 32 mm; inner diameter of outer tube: 46.4 mm). They discovered that slurry TiO_2 had higher efficacy. Finally, it should be noted that no study has ever sought to create an efficient solar photocatalytic disinfection reactor from scratch; instead, research groups have adapted commonly utilized reactors for chemical treatment. In this regard, a chemical engineering approach is required to build a practical reactor for SPC disinfection from the ground up. While existing light modeling and CPC design are essential, disinfection-specific oxygen transfer kinetics, bacteria mass transfer to the catalyst, and catalyst support configuration must be specified. A comprehensive list of publications on photo-Fenton and the TiO_2-photocatalytic process is provided in Table 2.3.

Table 2. 3 Summary of articles on water disinfection by photo-Fenton and photocatalysis carried out at the solar pilot plant

Type of Water	Volume	Type of microorganism	Best operational conditions		Efficiency	Reference
			Fe (mg L^{-1})	**H_2O_2 (mg L^{-1})**		
River water	20 L	*E. coli*	0.6	10	100% inactivation	(Moncayo-Lasso et al., 2009)
2^{ndry} effluents	80 L	Total coliforms	$Fe_2(SO_4)^{3+}$:5.58 + EDDS: 71.5	50	-	(Klamerth et al., 2012)
2^{ndry} effluents	250 L	Enterococci	Fe^{2+}: 5	75	100% inactivation in 180 min	(Michael et al., 2012)
2^{ndry} effluents	10 L	Somatic coliphages, *E. coli*, F-specific RNA Bacteriophages	Fe^{2+} : 10	20	99 % inactivation in 120 min	(Agulló-Barceló et al., 2013)
Synthetic 2^{ndry} effluents	7 L	*E. faecalis*	Fe^{2+} :20	50	99% inactivation in 100 min	(Ortega-Gómez et al., 2013)
Well water	25 L	*Salmonella spp , E. coli*	Fe: 0.01 Fe oxides: 0.23	10	50 %, 80%	(Ndounla and Pulgarin, 2014)
Real & Synthetic 2^{ndry}	20 L	*E. coli, E. faecalis*	Fe^{2+} :10	50	100% inactivation in 240 min	(Rodríguez-Chueca et al., 2014b)

effluents						
2^{ndry} effluents	60 L	*Clostridium sp*	Fe^{2+}:10	140	100% inactivation in 450 min	(Ruiz-Aguirre et al., 2015)
2^{ndry} effluents	7 L	Wild enteric *E. coli*	Fe^{2+}: 20	50	100% inactivation in 60 min	(Ortega-Gómez et al., 2014)
2^{ndry} effluents	60 L	Enterococci	Fe^{3+}: 5.02	160	100% inactivation in 140 min	(Karaolia et al., 2014)
Real and Synthetic 2^{ndry} effluents	60 L	*Fusarium sp*	Fe^{2+}: 5	60	-	(Polo-López et al., 2014)
Real 2^{ndry} effluents	8.5 L	Multidrug resistant *E. coli*	Fe^{2+}: 5.02	10	100% inactivation in 20 min	(Ferro et al., 2015)
Natural alkaline surface water	25 L	Wild total coliforms, *E. coli Salmonella spp.*	Total Fe: 0.10	10	100% inactivation in 120 min	(Ndounla and Pulgarin, 2015)
Distilled water	10 L	*E. coli*	Wall reactor: 32 mm TiO_2 coating Fixed-bed reactor:10mmTiO_2 coating		-	(Sordo et al., 2010)
Reservoir water	7 L	*E.coli*	Glass tubes: 32 mm TiO_2 coating		100% inactivation in 400 min	(Alrousan et al., 2012)
Pond water	10-15 L	Aeromonas hydrophila	TiO_2 coated glass plates		100% inactivation	(Khan et al., 2012)

2.2.8 Real-life applications of photocatalytic reactor

A wide variety of hazardous compounds has been eliminated from water by solar photo-Fenton at pilot-scale CPCs (Malato et al., 2009; Michael et al., 2012; Spasiano et al., 2015). Unfortunately, there is currently no demonstration of solar photo-Fenton plants for wastewater disinfection employed as a tertiary treatment on wide-scale operating CPC reactors. Reduced investment costs are one of the most intriguing strategies for achieving industrial uses for this solar treatment. These methodologies have been discussed previously in the context of photocatalytic (heterogeneous) reactions. A potentially exciting approach is the employment of non-concentrating reactors including, the Double Skin Sheet Reactor (DSSR), Thin Film Fixed Bed Reactor (TFFBR) shallow pond designs, and flat-plate reactors, all of which were researched in the 1990s (Bahnemann, 2004). Unfortunately, these approaches were ruled out because of the low efficacy observed for pollutant rates when compared to those surveyed with CPC reactors operating under identical operating conditions. Nonetheless, these cost-effective alternatives to CPC reactors may be enticing options. This is because fewer OH^{o} is required for effective elimination, requiring less irradiance (fewer photons) (Carra et al., 2014).

Recently, a Raceway Pond Reactor (RPR) was employed to remove micropollutants from secondary effluents by solar photo-Fenton in 240 min using 25 mg L^{-1} Fe and 100 mg L^{-1} H_2O_2) (Carra et al., 2015). This low-cost solar reactor comprises an open reactor with passages for recirculating water, varying the liquid depth, and controlling the flow. Regrettably, no information exists on the use of solar photo-Fenton for water disinfection via RPR. Nonetheless, we believe that additional research on this subject will be conducted in the near future.

2.2.9 Disinfection kinetic models

Kinetic investigations of the photo disinfection rate of water pollution are advantageous for field-scale applications of photoreactors. The adequate use of kinetic models to interpret experimental results helps the latter develop and optimize photoreactor setups with sufficient capacity. This section will address the various kinetics and rate models for photo-disinfection and frequent kinetic modeling misconceptions.

Since the first implementation of semiconductor catalysts for water disinfection (Matsunaga et al., 1985), limited research has been published that extensively examines the kinetics of

photo-disinfection of microbes in water. Given the variability and complexity of the photo-disinfection process, empirical kinetic models seem to be the most frequently used to interpret the data. Equation (2.1) expresses the generic equation for empirical photo-disinfection models under demand-free conditions, often known as the ***Chick-Watson model***. It is believed that a stoichiometric link exists between the number of microbes that need to be disinfected and the number of disinfectant molecules (Bigelow and Esty, 1920).

$$log\frac{A_t}{A_0} = -kCt \rightarrow log\frac{A_t}{A_0} = -k_{ap}t \quad (2.1)$$

where A_0 denotes the initial concentration of microbes and A_t is the concentration of microbes at treatment time t; the disinfectant concentration is denoted by C, and k signifies first-order inactivation rate.

The model can be simplified by integrating the disinfectant concentration at an apparent rate constant (Sun et al., 2007). The ***Hom model*** (Equation 2.2) is a modification of the Chick-Watson model based on empirical evidence. The inactivation kinetics of algal-bacterial systems does not comply with conventional linear kinetic models but rather follow curved kinetics (Rodríguez-Chueca et al., 2016). where k signifies the first-order kinetic rate constant, disinfectant concentration is denoted by C, n is the coefficient of dilution, and m indicates the empirical constant. When the disinfectant concentration is stable, it can be simplified by integrating the microbes population at a pseudo-first-order rate constant. This Hom-model is effective in fitting the disinfection curves with an initial lag (m>1) or with a tailing curve (m<1).

$$log\frac{A_t}{A_0} = -k \times C^n \times t^m \rightarrow log\frac{A_t}{A_0} = -k_{ap} \times t^m \quad (2.2)$$

Marugán et al. described the typical non-linearity observed in the kinetic curve of photo-disinfection when a Degussa P-25 TiO_2 catalyst was used in conjunction with commonly used disinfection models (Marugán et al., 2008). They discovered three distinct inactivation zones in the disinfection profile, namely:

1. a lag or initial smooth decay, labeled as the "shoulder" accompanied by
2. a specific log-linear inactivation region, and ending with
3. a lengthy decreasing process in the last phase of the disinfection labeled as the "tailing"

The presence of a shoulder was explained by the cumulative changes occurring on the cytoplasmic membrane induced by photo disinfection instead of an instantaneous deadly effect (Gyürek and Frinch, 1998). However, the tailing that occurs during photo-disinfection is not understood fully. According to Benabbou et al., the tailing zone was caused by competition for photocatalysis between organic compounds generated by continual cell lyses and the remaining intact cells (Benabbou et al., 2007). Others hypothesized that the tailing deviations from the log-linear decrease were caused by changes in the bacteria sensitive to the disinfectant used (Lambert and Johnston, 2001). Nonetheless, using the Hom model may result in an expensive design for a photo-disinfection system (Gyürek and Frinch, 1998).

Mafart et al. proposed a ***Weibull distribution***-based kinetic model was microbes inactivation. It is a continuous probability distribution created to represent the system behavior with some proportion of the variance (Mafart et al., 2002). At the same time, first-order models suggested that microbes are homogeneous in terms of resistance to the external environment. One of the studies claimed that microbes are heterogeneous in nature and that damage to the cells occurs due to the cell's contact time with external environmental stresses (Mafart et al., 2002). Each cell requires a unique contact time to di and is defined by the Weibull model (Equation 2.3) as follows:

$$log\frac{A_t}{A_0} = -\left(\frac{t}{\delta}\right)^p \tag{2.3}$$

The parameter δ is the time that signifies the first decimal reduction required to perform the first decimal logarithmic reduction in the microbial concentration. The shape of the equation curve is denoted by p. When p>1, the shape of the curve is convex, and when p<1, the shape is concave. when p = 1, the equation follow linear first-order model. There are some modifications done in the Weibull model known as ***Weibull with tailing*** (Mafart et al., 2002). The model is given by Equation (2.4):

$$A = (A_0 - A_{res}) \times 10^{-\left(\frac{t}{\delta}\right)^p} + A_{res} \tag{2.4}$$

where A_{res} denotes the bacterial residual concentration. Finally, when p is in between 0 to 1, the shape of the curve has an inflection point leading to the shoulder effect, and if $A_{res}\neq 0$ tailing phenomena will appear. In the last case, p=1 led to a log-linear reduction. Finally, the ***double Weibull model*** is a modification of the Weibull model presented by (Coroller et al., 2006). It is predicted that the microbes population is divided into two distinct subpopulations

that exhibit varying degrees of resilience to external stressful conditions. It is believed that each subpopulation group's resilience approaches the Weibull distribution. The expression is given as Equation (2.5):

$$A = \frac{A_0}{1 + 10^{\propto}} \times \left(10^{-\left(\frac{1}{\delta_1}\right)^{p_1+\alpha}} + 10^{-\left(\frac{1}{\delta_2}\right)^{p_2}} \right) \tag{2.5}$$

where subscripts 1 and 2 in the δ signify the two subpopulation groups. It is anticipated that subpopulation 1 is more susceptible to stress than subpopulation 2.

Cerf introduced a two-fraction kinetic model in 1977 (Cerf, 1977). This kinetic model is referred to as the ***biphasic model*** (Cerf, 1977). This model presumes that the microbial population is separated into two distinct subpopulations with varying degrees of treatment sensitivity. To develop a modeling approach for disinfection kinetics, both the shoulder and tailing regions must be idealistically rationalized. The occurrence of the shoulder can be explained mechanically by a serial phenomena event or a single strike of multiple targets (Gyürek and Frinch, 1998). The mechanistic assumption views microbial cell damage as gradual rather than instantaneous. This necessitates the denaturant of a significant number of essential molecules before cell inactivation (Gyürek and Frinch, 1998). The cumulative disinfection of a single bacterium could be expressed collectively as a sequence of integer steps (Severin et al., 1984). These disinfection procedures were believed to transfer bacteria from one level to another by a first-order reaction involving the catalyst utilized unless a finite number of deadly events occurred. Microorganisms that acquire fewer fatal steps than the predetermined number are regarded to survive the disinfection operation.

Regarding the tailing region, most have speculated that it was indicated by the accumulation of a thermally resistant microbial subpopulation. Additionally, one of the studies it was proposed that the tailing effect is caused by the inherent distribution of bacterial resistance to the sterilizing procedure, making microbes more resilient, adaptable, and inaccessible to heat treatment (Najm, 2006). Now another study suggested that such tailing is not a regular occurrence during water disinfection (Marugán et al., 2008). Until now, no rational explanation for the occurrence of tailing in the disinfection of water with well-mixed circumstances and an equally resilient cloned microbial population has been proposed. It was believed that tailing could occur only after a sufficient retention time due to a gradual decrease in the rate of total inactivation. The Poisson probability can describe random collisions between the microbes and catalysts, as the number of collisions exceeds

the number of microbiological deaths (Gyürek and Frinch, 1998). Equation (2.6) defines the biphasic model as follows:

$$Log\frac{A_t}{A_0} = Log[P * e^{-k_1 * t} + (1 - P) * e^{-k_2 * t}] \quad (2.6)$$

P denotes the percentage of microorganisms that survive in subpopulation group 1, and (1–P) indicates the fraction of microorganisms that survive in subpopulation group 2. Finally, k_1 represents the kinetic constant of the more susceptible group, and k_2 represents the kinetic constant of the more resistant population. A ***biphasic model with a shoulder*** is a variant of the biphasic model. This model can represent biphasic model curves with a prior shoulder phenomenon (Geeraerd et al., 2005). Equation (2.7) gives the biphasic model with the shoulder:

$$log\frac{A_t}{A_0} =$$

$$\log(fe^{-k_t \times t} \times \frac{e^{k_1 \times S_1}}{1+(e^{k_1 \times S_1}-1)\times e^{-k_1 \times t}} + (1-f) \times e^{-k_2 \times t} \times \left(\frac{e^{k_1 \times S_1}}{1+(e^{k_1 \times S_1}-1)\times e^{-k_1 \times t}}\right)^{\frac{k_1}{k_2}} \quad (2.7)$$

Where A_t denotes the total microbial population, and A_1 and A_2 are the populations of subgroups 1 and 2, respectively. The parameter f is defined as $A_1(0)/A_2(0)$.

2.2.10 Hybrid effect of TiO_2 photocatalysis and photo-Fenton

The growing emphasis on developing environmentally friendly and effective disinfection methods for inactivating all resistant microorganisms from water/wastewater has compelled researchers to examine innovative changes that can be incorporated into advanced wastewater disinfection technologies currently in use. The goal of the investigation in this area is always to reduce inactivation time and optimize the treatment cost of the process. To improve the efficacy of photocatalytic disinfection and decrease the reaction time, extensive attempts have been made and published in the literature to increase the concentration of OH^o present in the photocatalytic process. The addition of reactive oxidants such as ClO_4^-, H_2O_2, IO_4^- has already been shown to increase the rate of the reaction (Bulman et al., 2019).

There are rarely any studies related to the disinfection of *E. coli* with coupled photo-Fenton and TiO_2-photocatalytic processes. This combined system is appropriate for bacterial inactivation as the reaction rate is significantly higher than that of photocatalysis and photo-

Fenton reaction individually. The increased reaction rate would increase the inactivation with a significant reduction in treatment time. This increased treatment efficacy caused by the addition of Fenton reagent to the TiO_2 photocatalytic system can be attributed to the simultaneous generation of sufficient OH^o by both operating processes, i.e., photocatalysis and photo-Fenton.

Additionally, iron inhibits electron-hole recombination in TiO_2, boosting its catalytic performance (Zhu et al., 2004). The integrated technique of photocatalysis and photo-Fenton has exhibited remarkable treatment efficacy by tackling the majority of the issues associated with the individual processes, including electron and hole recombination, mass transfer limitation, and higher treatment time. However, the practicality of this combined approach for field-scale applications remains in question for the reasons listed:

1. The majority of studies reported used both catalysts in suspended form, limiting the practical applicability of this technique because of the higher cost of catalyst separation post-treatment;
2. So far, no study has been published in which both catalysts (iron source and TiO_2) have been completely immobilized for the inactivation of bacteria present in water.

Fixed-bed research utilizing cost-efficient and robust catalyst immobilized inert supports and integrating both photocatalysis and photo-Fenton simultaneously may open up new avenues for effective water disinfection. Additionally, these supports in combination with doped catalysts could represent a paradigm shift in the field of AOPs for water treatment by combining modified photocatalysis in addition to photo-Fenton.

2.3 Summary

AOP has shown its higher performance compared to traditional water disinfection methods in terms of disinfecting different types of microorganisms found in water/wastewater. However, the large-scale implications of these methods have not been investigated. Although photocatalysis with suspended TiO_2 demonstrated a relatively high disinfection efficacy, certain operational drawbacks such as post-treatment catalyst separation, the higher cost of catalyst, inefficient usage of the solar radiation, charge carriers recombination, and inefficient catalyst recovery have limited its practical applications. In comparison to photocatalysis, the homogeneous photo-Fenton method has exhibited significantly greater disinfection efficacy of microorganisms. But, the production of iron sludge, difficulties with the regeneration of catalyst, and a higher concentration of H_2O_2 in the homogeneous photo-Fenton process

restrict its use on a broad scale. The heterogeneous photo-Fenton technique eliminated the issue of iron sludge production but at a significant reduction in process efficacy.

Some disadvantages of heterogeneous photocatalysis, such as the high cost of post-treatment catalyst separation, have been overcome by immobilizing the catalyst on inert supports. However, fixed-bed studies impose additional constraints on the process, such as extended disinfection time, mass transfer issues, and low reusability effectiveness of the immobilized catalyst, all of which remain unanswered. Whereas doping the catalyst with metals/non-metals alleviated some of the problems associated with an inefficient use of solar energy and charge carrier recombination, tedious catalyst fabricating techniques involving costly materials remained their primary issue. Additionally, there are few investigations on the immobilization of doped catalysts.

Numerous pilot-scale reactors have been explored in the literature, including those that use homogeneous photo-Fenton, heterogeneous slurry, and fixed-bed photocatalysis. While the compound parabolic collector (CPC) has demonstrated significant potential for the destruction of a wide variety of pathogens, its higher initial cost has prompted AOPs' economic viability concerns. Thus, non-concentrating solar fixed-bed reactors for wastewater treatment are more cost-effective and practicable. However, none of the experiments have confirmed the immobilized catalyst's continued use or activity underflow circumstances. As a result, additional research is required in fixed-bed photocatalytic reactors, specifically on their suitable design changes and parametric optimization.

Very few studies in the literature address the concept of hybrid processes via combining photocatalysis and photo-Fenton. The investigations established a considerable increase in process efficacy by handling most of the concerns associated with discrete operations. Until now, no fixed-bed studies incorporating this dual impact have been discussed. As a result, commercialization of this process has not yet occurred.

2.4 Lacunae

Based on the literature review, the following gaps have been identified:

1. The coupling of two techniques (photo-catalysis and photo-Fenton) i.e. in-situ approach for application toward water/wastewater disinfection needs to be addressed.
2. The concept of in-situ dual effect in fixed bed mode is a new concept and has not been explored in water/wastewater disinfection studies.

3. Durability and stability studies of the catalyst coated on support material for its long use need to be covered.
4. Reactor studies using in-situ fixed-bed mode for the photocatalytic disinfection of water/wastewater to seek the practical applications of the technique have very limited studies to date.
5. Catalyst stability and film intactness in the case of flow reactor need to be studied.

2.5 Objectives of the study

As a result, efforts have been undertaken in this research to mitigate the drawbacks associated with separate AOPs, namely photocatalysis or photo-Fenton, by combining these two processes in a single treatment unit. By running this hybrid process in fixed-mode, the commercial uses of the approach were visualized. In this hybrid technique, low-cost fixed catalysts manufactured from waste materials were combined with TiO_2, including the dual effect (photocatalysis and photo-Fenton). This hybrid process led to a considerable reduction in the time required to treat water containing targeted *E. coli*. The technique's feasibility was established by conducting disinfection experiments in a pilot-scale solar reactor. In this context, the following objectives guided the doctoral research:

1. Batch disinfection studies using fixed bed composite material incorporating *in-situ* dual process (Photo-catalysis and photo-Fenton).
2. Process optimization by varying size of composite, volume-area ratio, amount of catalyst per bead along with durability studies.
3. Development of pilot-scale fixed-bed continuous reactor employing in-situ dual process (Photo-catalysis and Photo-Fenton) for microbial disinfection studies.

Chapter 3

Materials and Methods

3.1 General

The following chapter describes the materials and methods followed to conduct hybrid (Fe-TiO_2) advanced oxidation studies, sample analysis, and characterization of the composite catalytic beads used to disinfect *E. coli* in water. Additionally, the experimental setup for batch and continuous operation was discussed in detail.

3.2 Microbial preparation and enumeration protocol

The bacterial strain used was *E. coli* (wild type K12) and was supplied by MTCC and Gene bank (Microbial Type Culture Collection) from Chandigarh (India). It is non-pathogenic and an indicator bacteria for enteric pathogens. *E. coli* strain was prepared with 20% glycerol and kept at -20 °C in cryo-vials. The colony from the sample strain was streaked on the agar plate to prepare the pre-cultures for every experimental series. Afterward, the plates were incubated at 37 °C in an incubator for 24 h. After incubation, the grown colony was again plated on a new agar plate and again kept for incubation at 37 °C for 24 h. For the experiments, the cell pellet was prepared by picking the colony from the pre-cultures with the help of a loop and inoculated in a 50 mL of sterile borosilicate Erlenmeyer flask having 5 mL of Luria-Bertani (LB) broth. Then the incubation of the flask was done at 37 °C and 180 rpm in an incubating shaker. After 8 h, 1% dilution of bacterial cells was made in a sterilized 250 mL Erlenmeyer flask having 50 mL of already autoclaved LB broth.

To achieve a physiological stationary phase the cells were incubated in aerobic conditions at 37 °C. The bacterial stationary phase of the growth curve was observed at 600 nm. The LB broth having tryptone (10 g), sodium chloride (10 g), and yeast extract (5 g) in 1L of distilled water was sterilized by autoclaving at 121°C for 20 min. The bacterial cells were harvested by centrifuging for 15 min at 4 °C and 5000 rpm. The obtained bacterial pellet was washed with 0.8 % NaCl saline solution (3 times washing). The final bacterial pellet was obtained and then re-suspended in the saline solution having 50 mL of the initial volume. This method resulted in approximately 10^9 colony-forming units per milliliter (CFU mL^{-1}) of cell density. The bacterial solution (*E.coli*) was diluted in the sterilized distilled water and obtained a cell

density of 10^6 CFU mL^{-1}. This cell density was then used in all the experiments done in this study.

The concentration of the *E. coli* present in the water sample (CFU mL^{-1}) was calculated by plating on agar plates. During the experiments, a 1mL sample was withdrawn, stored at 4 °C, and immediately plated on the agar plate using the standard plate count method. After plating, the plates were kept for incubation overnight at 37 °C and the counting of the colonies on the plates was done manually. Moreover, the plating was done by spreading 0.1 mL of the *E. coli* sample on Petri dishes. To achieve the desired concentration of *E.coli*, serial dilutions were made for each water sample. The data points presented are the average of three replicates and the error bars represent the standard deviation from the mean.

3.3 Chemicals and reagents

TiO_2 (Titanium dioxide) catalyst having 70% and 30% anatase and rutile phase respectively, with bet surface area of 50 m^2 g^{-1} and 30 nm of particle size was purchased from Evonik industries, India and was used as a photocatalyst. Clay, foundry sand (FS), and fly ash (FA) were collected from local industry, Patiala, Punjab, India and were used to prepare spherical beads that act as an iron source in this study. 30 % w/v of hydrogen peroxide (H_2O_2) was used as an oxidant and was purchased from Ranbaxy, India. To maintain the acidic pH conditions of the treatment reaction, acetate buffer was used (made from >99.5 % acetic acid, and 98.5 % sodium acetate) which was purchased from Loba Chemie Pvt Ltd, Maharashtra, India.

Luria Bertani (LB) (10 g BactoTM Tryptone, 5 g Yeast extract, 10 g NaCl, per liter), Miller Agar-Agar, Type I, for cell growth, were purchased from HiMedia Laboratories, Mumbai (India). Washing and re-suspension of *E. coli* were done in heat sterilized isotonic saline solution, using 99.5 % of sodium chloride (NaCl), and was purchased from SD Fines Chemicals Ltd, India.

For iron estimation, hydroxylamine hydrochloride, and ammonium acetate. 1, 0-phenonthralein monohydrate, concentrated hydrochloric acid (HCl), ferrous ammonium sulfate, and potassium permanganate was used. For the estimation of hydroxyl radical (OH^o), Terephthalic acid (TPA) with (>98% purity) of AR grade was used in photocatalytic disinfection were obtained from Merck (U.S.). Potassium dichromate ($K_2Cr_2O_7$) and concentrated sulphuric acid (H_2SO_4) of analytical grade (AR), used during chemical oxygen

demand (COD) estimation were obtained from SD Fine Chemicals Ltd. (India). The reagents including calcium chloride ($CaCl_2$), phosphate buffer, ferric chloride ($FeCl_3$), sodium hydroxide (NaOH), and magnesium sulfate ($MgSO_4$) of AR grade were used for the determination of biochemical oxygen demand (BOD) and were also purchased from SD Fine Chemicals Ltd. (India). For nitrate determination, hydrochloric acid of analytical grade (AR) was used. Stannous chloride ($SnCl_2$) and ammonium molybdate $(NH_4)_2MoO_4$ obtained from Loba Chemie Ltd were used for the phosphate determination. All these chemicals were of analytical grade (AR) and were procured from Loba Chemie Pvt. Ltd. (India).

Methylene blue used as a tracer for PFR studies was purchased from Loba Chemie Pvt Ltd, Maharashtra (India). BQ (1,4-benzoquinone), TEOA (triethanolamine), and IPA (isopropanol) were used as a special scavenger of superoxide radical (O_2^{o-}), hole (h^+), and hydroxyl radical (HO^o) species and were purchased from TCI Chemicals, India. All the solutions were prepared from double-distilled water.

3.4 Analytical method

The Physico-chemical analysis of wastewater was conducted using Standard APHA methods (APHA et al., 2017). Nitrate ions (APHA, 2017: Sec. 4500-NO_3), phosphate ions by stannous chloride method (APHA, 2017: Sec 4500 (P.D)), Biochemical oxygen demand (BOD) (APHA, 2017), Chemical oxygen demand (COD ((APHA, 2017: Sec. 5220 (B)), and for iron estimation ((APHA 2017: Sec. 3111(B)). The generation of OH^o was confirmed by photo-Luminance spectrophotometry (LS-45, Perkin Elmer) by the formation of a fluorescent compound (2-hydroxy terephthalic acid).

3.5 Fabrication of composite beads and TiO_2 immobilization

3.5.1 Fabrication of blank beads

For the fabrication of blank spherical beads, FS and FA were mixed with clay in the ratio of 2:1:1 respectively then dried at room temperature. This ratio proved to be very efficient in terms of improving the strength of the composite as reported in our previous study (Bansal and Verma, 2017a). The clay used in the fabrication of beads is acting as a binding material. The characterization of FS and FA is given in Figure 3.1. The size of the beads was measured by gauging them from four different directions with a vernier caliper. These beads were heated at 800 °C for 1.5–2.0 h and subsequently cured for 48 h in water. This improves the support durability and strength (Amadi and Osu, 2018). These beads without TiO_2 coating are

labeled as blank beads. Before using these beads the working solution was made acidic in nature. This acidic condition helps in iron lixiviation from the beads and shows the presence of Fe^{2+} and Fe^{3+} ions in the solution. Then these beads were used to study the effect of the Fenton and photo-Fenton process on water disinfection.

3.5.2 Fabrication of clay beads for photocatalysis

Clay beads were made without adding any FS and FA and were heated at 800 °C for 1.5-2.0 h. Then, 1% (w/v) TiO_2 catalyst coating was done over these beads using the dip-coating technique (Bansal and Verma, 2017b). Before the coating, sonication of the TiO_2 mixture was done to disperse the TiO_2 particles uniformly. To ensure sufficient coverage of the beads, their surface was coated 2 times with the TiO_2 solution. After drying the beads at room temperature, they were muffled at 350 °C for 1.5 h to ensure optimal adhesion of the TiO_2 to the composite beads' surface. Following that, the beads were washed with distilled water to remove any loosely bound TiO_2 and oven-dried at 100 °C.

3.5.3. Fabrication of Fe-TiO_2 composite beads

For the fabrication of composite beads, the blank beads as mentioned in subsection 3.5.1 were coated with 1% (w/v) sonicated TiO_2. The TiO_2 solution was coated two times for the sufficient coverage of beads with the catalyst. After drying the beads at room temperature, they were muffled at 350 °C for 1.5 h. The images of blank and TiO_2 coated beads are shown in Figure 3.2 (a-b) respectively. Elemental mapping as shown in Figure 3.3 confirms the presence of iron and TiO_2 in composite beads. Using a scanning electron microscopy (SEM) study, the TiO_2 coating was found to be 71 µm thick over the support as shown in Figure 3.4. Following TiO_2 immobilization, the supports were called 'composite' to indicate that they contained both catalysts (iron (FS and FA) and TiO_2). The fixed mode hybrid effect was then investigated using these Fe-TiO_2 composite beads.

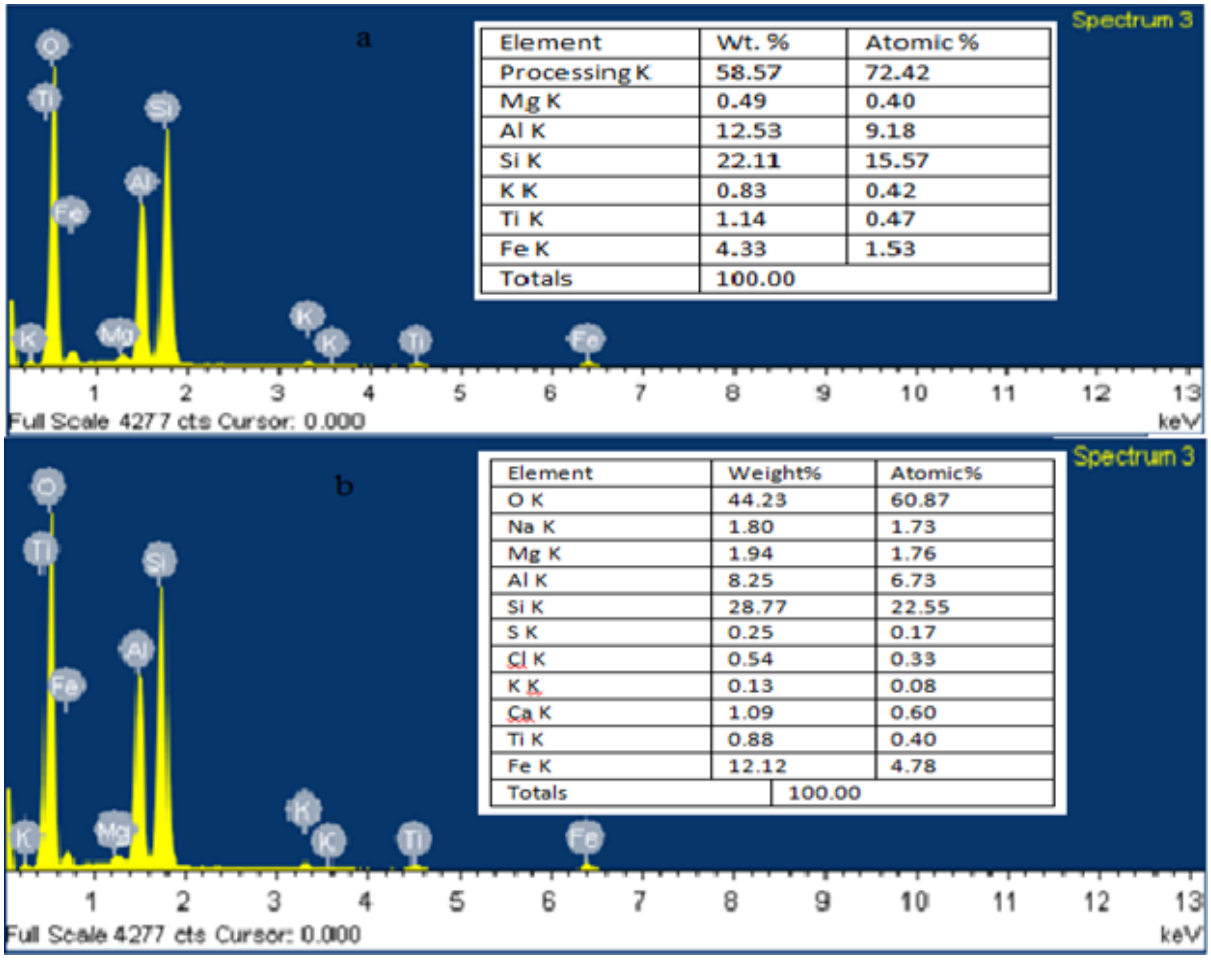

Figure 3. 1 SEM-EDS image of (a) Fly ash and (b) Foundry sand

Figure 3. 2 Actual images of (a) blank and (b) TiO_2 immobilized composite beads

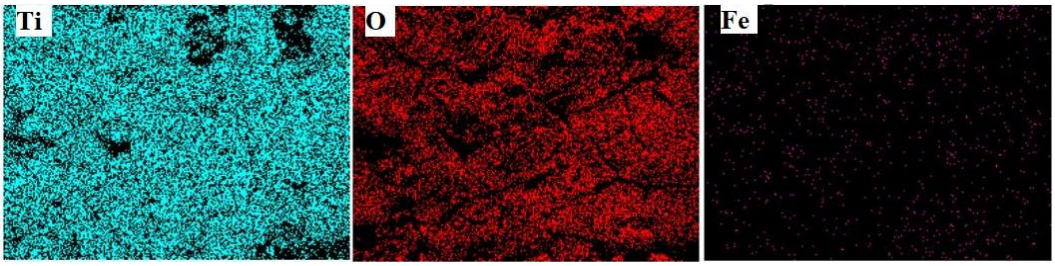

Figure 3. 3 Elemental mapping of Fe-TiO_2 composite

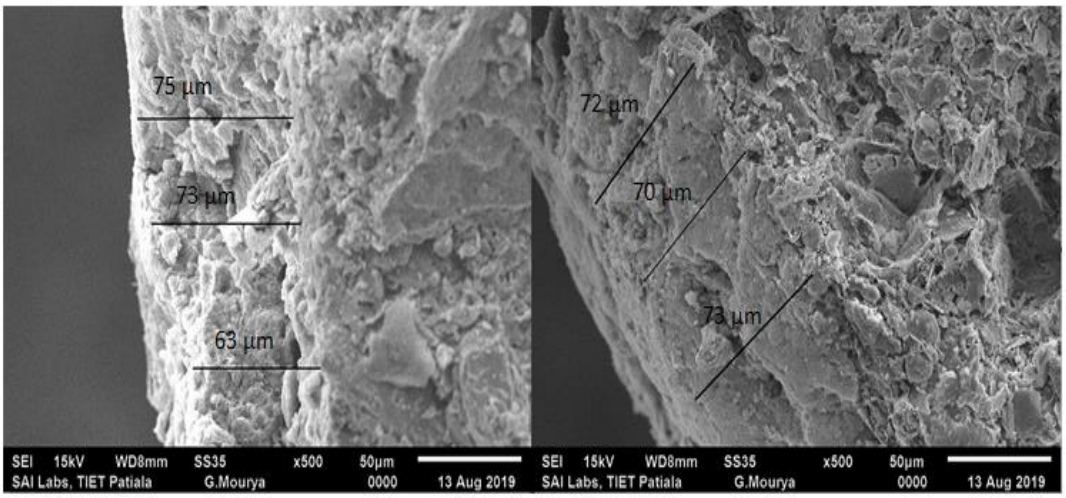

Figure 3. 4 SEM image showing thickness of TiO_2 coating (Average thickness 71 µm) over composite beads

3.5.4 Iron leaching from composite beads

The current study is attributed to the dual in-situ effect of the active TiO_2 layer (leading to photocatalysis) as mentioned in the previous section and leached iron from the beads (leading to photo-Fenton). Therefore to study the leaching of iron from the beads into the solution, the ferric and ferrous ions concentrations were determined at regular intervals time (Table 3.1) (APHA, 2017).

Table 3. 1 Concentration of iron species leaching out of fresh composite beads

Time (min)	Ferric (µg L^{-1})	Ferrous ion (µg L^{-1})	Total iron (µg L^{-1})
20	40	41.15	81.15
40	41.92	46.92	85
60	44.23	51.54	90.38
90	36.54	56.54	90.38
120	37.69	61.92	92.69

3.6 Characteristic analysis of the composite

In this study of the hybrid process, the spherical Fe-TiO_2 beads were analyzed to confirm the presence of both iron and TiO_2 in one system using different techniques such as UV-DRS, XRD, FT-IR, SEM-EDS, FE-SEM, and HRTEM. The chemical composition, morphology, and uniformity of the catalyst were determined via a Scanning Electron Microscope (SEM) (JSM-6510LV, JEOL (Japan)) equipped with Energy-dispersive Spectroscopy (EDS) and Energy-Dispersive X-ray Analysis (EDX). An auto fine coater (Model: JEC-3000FC) was used to deposit a platinum layer on the samples. The X-ray diffraction (XRD) using X'Pert high score in the scanning range of 20^o–80^o was used to study the crystallography of the Fe-TiO_2 catalyst with radiation of Copper-Kα at λ=1.5418 Å. The bandgap energy of the catalyst was recorded using UV-vis diffuse reflectance spectrometer (DRS), UV-2600, Shimadzu (Asia Pacific) equipped with $BaSO_4$ as a standard reflectance, and the wavelength was measured in the range of 200-800 nm. For the evaluation of compound bondings, linkages, and functionalized groups, the Fourier TransformInfra-Red Spectrophotometer model RZX (Perkin Elmer) was used with KBr pellets and scanned in the range of 4000 to 200 cm^{-1}. 0.5 mg of synthesized material was mixed with 20 mg of potassium bromide to get the FTIR spectra. To study the lattice spacing of the Fe-TiO_2 composite High-resolution transmission electron microscopy (HRTEM) was done). Field Emission Scanning Electron Microscopy (FESEM) with EDS analysis was also done to study the morphology and chemical properties of the catalyst.

3.7 Photo-disinfection kinetics

For the kinetic study of the hybrid process, a pseudo-first-order model was used. The slope of the natural log (A_t/A_0) and time for inactivation gives the rate constant as shown in Equation (3.1). Where A_0 is the initial concentration of the bacteria at time t=0, A_t is the bacterial concentration at any time "t" and "k" is the pseudo-first-order rate constant (min^{-1}). The notation for initial and final concentration may change from $A_0 \approx C_0$ and from $A_t \approx C_t$ but the definition stayed the same.

$$ln\left(\frac{A_t}{A_0}\right) = kt \tag{3.1}$$

3.8 Synergistic studies

In the present research work, the synergistic effect of the in-situ hybrid process by integrating photocatalysis and photo-Fenton within the same treatment unit was observed over individual processes (photocatalysis or photo-Fenton) for the disinfection of *E. coli* in water. Synergistic effects are meant to be the phenomenon when the disinfection efficacy of the integrated system is more than the sum of individual processes (Bansal et al., 2016). The synergy of one process over the other for the hybrid effect in the present work was calculated and quantified using the value of the first-order rate constant "k" in each case as per the mentioned Equations (3.2-3.4).

The synergy of the hybrid process on the photocatalysis process:

$$Synergy\% = \left\{\left(\frac{k_{hybrid} - k_{photocatalysis}}{k_{hybrid}}\right) \times 100\right\} \tag{3.2}$$

The synergy of the hybrid process on the photo-Fenton process:

$$Synergy\% = \left\{\left(\frac{k_{hybrid} - k_{photoFenton}}{k_{hybrid}}\right) \times 100\right\} \tag{3.3}$$

Overall synergy:

$$Synergy\% = \left\{\left(\frac{k_{hybrid} - \left(k_{photocatalysis} + k_{photoFenton}\right)}{k_{hybrid}}\right) \times 100 \right\} \tag{3.4}$$

3.9 Statistical analysis

The comparison between the efficacy of different processes was evaluated on Origin 2016. Statistical significance of the mean value of the treated samples was determined by one-way ANOVA. The difference between the two processes was considered to be significant if the value of probability (P-value) was found to be less than 0.05 otherwise considered to be as insignificant. All the experiments were performed in triplicates and the results are shown by taking the average of the three samples and the error bars to show the standard deviation.

3.10 Experimental set-up and procedure for hybrid effect studies for lab-scale reactor

Lab-scale photocatalytic experiments were carried out inside a rectangular wooden chamber (1.37 m × 0.9 m ×1.06 m) consisting of seven UV tubes (Philips, 36W, 365nm) and were fixed in parallel on the underside of the chamber's roof. A borosilicate glass reactor 20 cm in diameter and 5.5 cm in height having a volume of 1000 mL was used to carry out the reactions. The reactor was placed under the UV lights on a laboratory jack so that the irradiation intensity could be changed by altering the height of the jack. The average variation of UV radiation ranged between 10 to 24 Wm^{-2} and was measured from the Eppley radiometer (model no. 33013). The working solution contained 250 mL of double distilled water spiked with 10^6 CFU mL^{-1} of *E. coli*. Then this solution was stirred for 20 min for the acclimatization of bacteria and the TiO_2 immobilized composite beads were added to start the experiment. To support the homogeneity of the reaction, aeration (3 L min^{-1}) was provided to the reactor with two spargers that were placed at an equal distance from the center. The line diagram and actual image of the lab-scale reactor are shown in Figure 3.5.

For disinfection studies, 1 mL of sample was taken out after regular intervals from the reactor, and the decrease in the concentration of the *E. coli* was calculated by the plating method. All the borosilicate reactors were washed and autoclaved before each reaction. Optimization of the process was done by varying different parameters such as H_2O_2 dose, pH, bead size, UV intensity, and volume area ratio based on which reaction kinetics were studied. All the experiments were performed in triplicates, and the results are shown by taking the average of the three samples, and the error bars to show standard deviation are reported in the figures. Statistical significance of the mean value of the treated samples was determined by one-way ANOVA. The results were calculated using Equation (3.5), where L_r is the log unit reduction of *E. coli*, A_t is the reduction in *E. coli* at the time "t" and A_0 is the reduction in *E. coli* at t=0:

$$L_r = log\frac{A_t}{A_0} \tag{3.5}$$

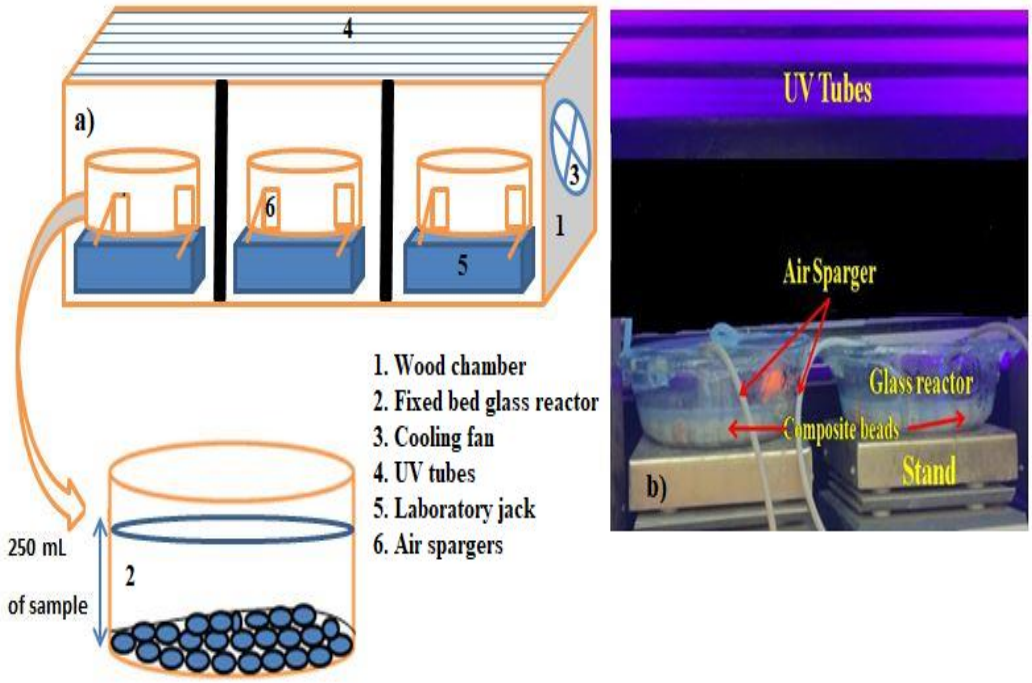

Figure 3. 5 (a) Line diagram and (b) actual image of the lab-scale experimental set-up

3.11 Pilot-scale recirculating fixed bed reactor

A non-concentrating flat-bed reactor made of glass (36 cm × 16 cm × 2.5 cm) was used to disinfect *E. coli* using UV-A irradiation. The reactor included two inlets and two outputs, as well as up to three removable glass baffles (length 6 cm × height 2.5 cm × thickness 0.5 cm) as shown in Figure 3.6. The reactor was meant to treat a total capacity of 2 L and was run in recirculation mode. Aqueous solution contaminated with *E. coli* (2 L) and containing a suitable amount of H_2O_2 was pumped from the wastewater tank through the glass reactor bed at the ideal flow rate, where it came into contact with Fe-TiO_2 composite beads, and then pumped back into the storage tank. Acetate buffer solution was used to preserve the reaction pH. The pH of the process was varied in this investigation within the acidic range (pH = 3-6). Around 1-2 mL of treated solution was collected and evaluated at regular intervals over a period of time. To reduce evaporation losses, the reactor was covered with transparent cling film.

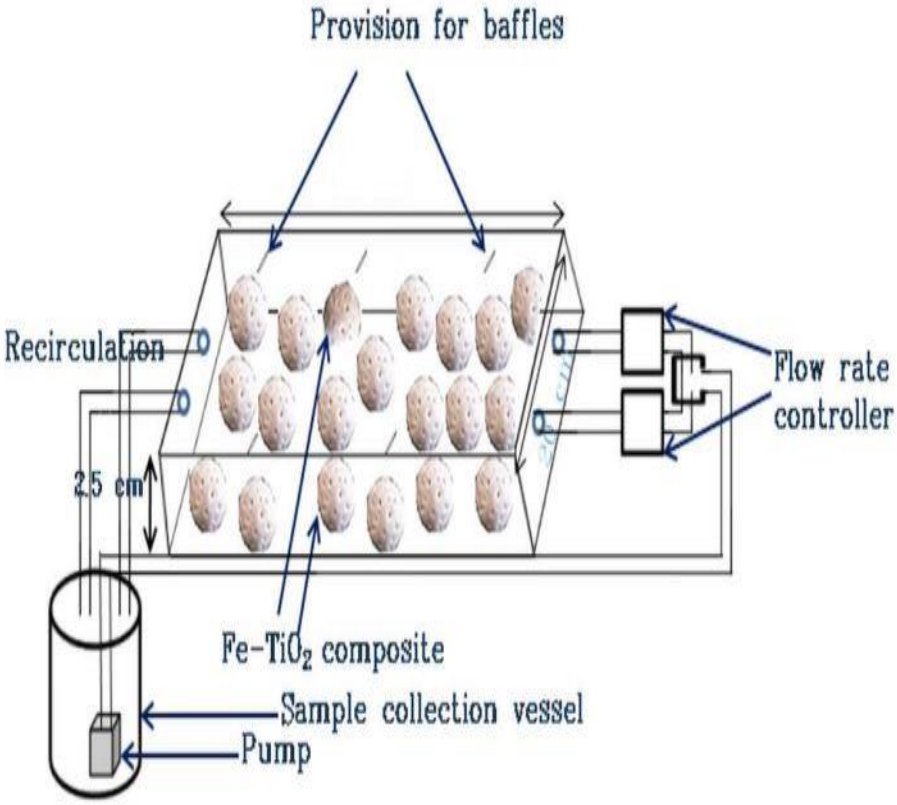

Figure 3. 6 Schematic diagram of recirculating glass reactor

3.12 Pilot-scale solar fixed-bed once-through reactor

For the inactivation of *E. coli*, the current system is comprised of 3 glass reactors connected in series having dimensions of 0.4 m × 0.2 m × 0.025 m each. The surface of the reactor is covered with the appropriate amount of Fe-TiO_2 composite beads and exposed to solar radiation. The complete solar irradiated reactor scheme was operated in once-through mode and connected with a cylindrical tank containing a simulated *E. coli* solution of 6 L. The exit point of the first reactor was attached to the inlet of the first glass reactor and so on to make it once through. An appropriate flow rate was maintained using a peristaltic pump. The schematic diagram of the once-through reactor is shown in Figure 3.7. Before the treatment process started, the *E. coli* solution was kept stirring for 30 min for the cells' acclimatization. The inactivation of *E. coli* tests was carried out at Thapar Institute of Engineering and Technology, Patiala, India, on sunny days of September and October (30.3564° N, 76.3647° E) from 12:00 PM to 2:00 PM. The fixed bed solar reactors were connected in series in such a way that the exit point of the first reactor became the inlet of the other and was placed in the sunlight for the reaction to start. The solar irradiation was monitored using a lux meter, and the values were recorded at regular intervals, from which

the average intensity was calculated and was found to be 590-600 W m^{-2}. The fundamental procedure followed for the experimentation comprises the adjustment of pH as (4-4.5) along with the addition of an appropriate amount of H_2O_2 and with subsequent pumping of the *E.coli* solution to the reactor. The reactor was optimized by optimizing different parameters such as the number of the reactor, number of baffles, H_2O_2, and the surface area covered in terms of the number of beads. After regular intervals, 2 mL of samples were taken out from the inlet and exit from every reactor.

To confirm the hydrodynamic behavior and flow pattern of the once-through reactor, an retention time distribution (RTD) approach was performed. RTD, the hallmark technique for examining the ideal reactor behavior, may also be used to scale up proposals for improved efficacy conditions. For implementing the RTD approach, Exit age distribution (E (t)) was used. The E (t) distribution was calculated using Equation (3.6), and the Peclet number (Pe) was also calculated and mentioned in Equation (3.7):

$$E(t) = \frac{S(t)}{\int S(t)dt} \tag{3.6}$$

where S (t) denotes the tracer's concentration (mg L^{-1}), and t denotes the time (min).

$$Pe = \frac{\vartheta L}{D} \tag{3.7}$$

where ϑ designates the velocity of flow (m s^{-1}), L denotes the characteristics length (m), and D denotes the dispersion coefficient (m^2 s^{-1}).

The experimental and the theoretical retention time ought to have no distinction in the typical working conditions. If the theoretical retention time is less than the actual retention time, then it may be reasoned that either the particles of the tracer might have been held back or the flow rate calculations might be rechecked. Henceforth, for this reason, the dead volume (% Vd) was determined using Equation (3.8).

$$\%Vd = 1 - \frac{T}{t} \times 100 \tag{3.8}$$

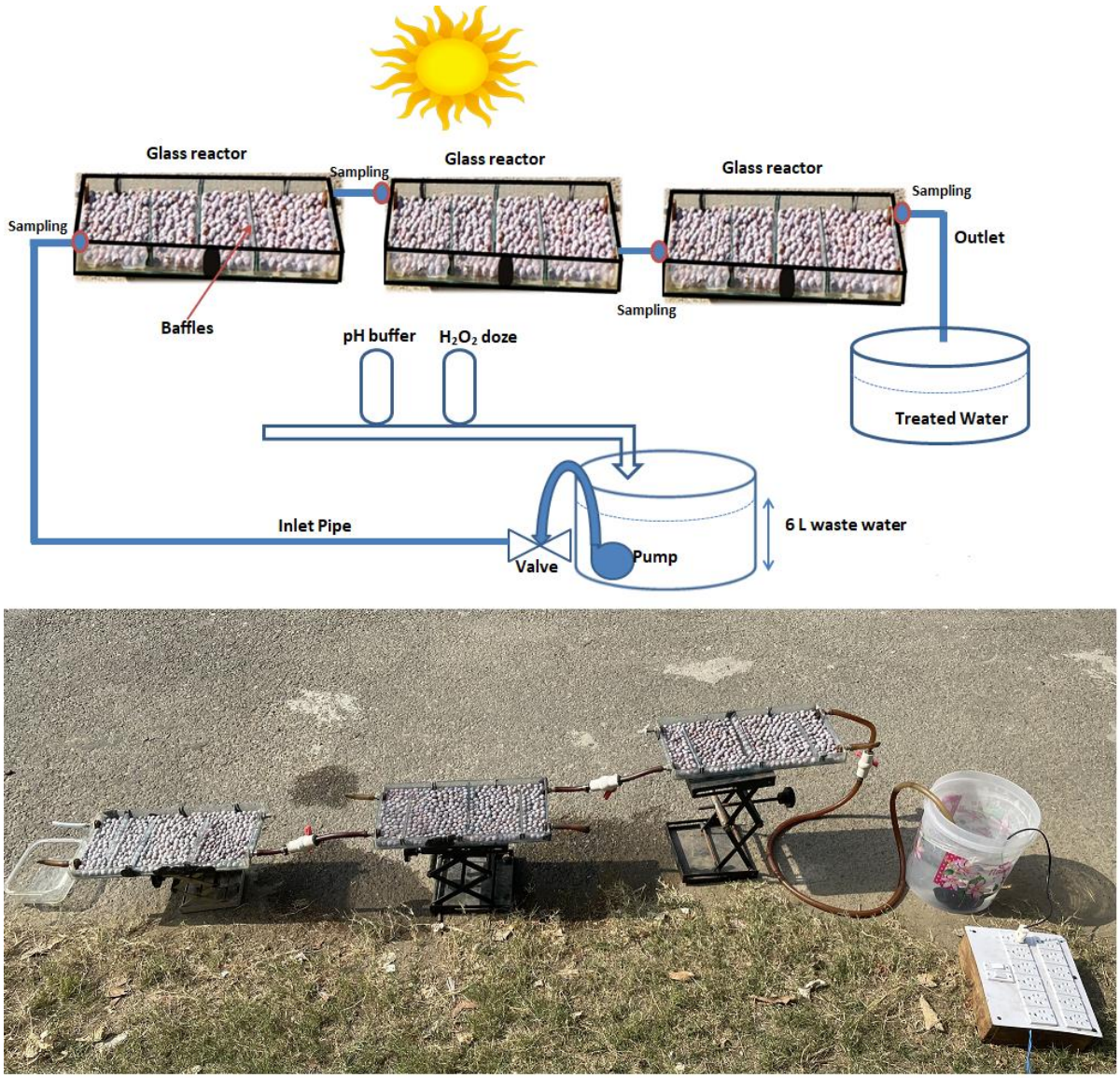

Figure 3. 7 Line diagram and actual image of the once-through pilot-scale reactor

3.13 Experimental design and analysis

For designing the experimental matrix for the Fe-TiO_2 disinfection of *E. coli*, response surface methodology (RSM) was employed. RSM comprises statistical techniques for correlating responses and factors dependent on several process variables for assembling an experimental model (Garai and Kumar, 2013; Yousefzadeh et al., 2018). This technique has many advantages, such as understanding the interactions among different parameters, fast and reliable data accomplishment, and following a significant deduction in experimental runs, cost, and time (Bezerra et al., 2008; Khuri and Mukhopadhyay, 2010). Therefore, RSM has been successfully implemented in the optimization of different parameters for the inactivation of microorganisms (Asadi and Moeinpour, 2019; Feilizadeh et al., 2015a, 2015b; Matin et al.,

2018). The response surface procedure (RSM) is generally utilized numerical and statistical strategy for demonstrating and analyzing a procedure wherein the response of interest is determined by different parameters, and this technique directs to advance the reaction (Braimah et al., 2016; Yousefzadeh et al., 2018). The parameters that influence the procedure are called independent variables, while the responses are called dependent variables (Khuri, 2017). The response variables were fitted by a second-order–nonlinear regression model in the form of a quadratic polynomial equation, represented by Equation (3.9).

$$R = \beta_{\circ} + \sum_{i=1}^{k} \beta_i x_i + \sum_{i=1}^{k} \beta_{ii} x_i^2 + \sum_{i,j=1} \sum_{i<j} \beta_{ij} x_i x_j \ + e \qquad (3.9)$$

Where constant regression coefficients are denoted by β_0, β_i, β_{ii}, and β_{ij}; coded input factors are denoted by x_i and x_j; e is an error function, and R is the response.

The first order, 2k factorial, Plackett–Burman, and simplex designs are frequently utilized. First-order polynomials are less stable and less rotatable in terms of variance prediction and exhibit a lack of fit as a mediating factor between surface curvature and factors. Thus, second-order polynomial studies are required to create a quadratic response surface model to overcome the disadvantages of first-order design and to improve the optimization process. The Box–Behnken design, the Doehlert design, the central composite design, and the three-level factorial design are all examples of second-order symmetrical designs. Among them, the Box–Behnken design was chosen for the current investigation.

3.13.1 Box-Behnken design

George Box and Donald Behnken created the Box-Behnken design in 1960. As illustrated in Figure 3.8 the design offers a three-factorial layout that enables the accurate evaluation of the mathematical model's first and second-order coefficients (Ozgen and Yildiz, 2010). It is a subset of 3 k factorial combinations, making it more convenient and cost-effective, especially when the number of variables is considerable, like in industry research (Khuri and Mukhopadhyay, 2010).

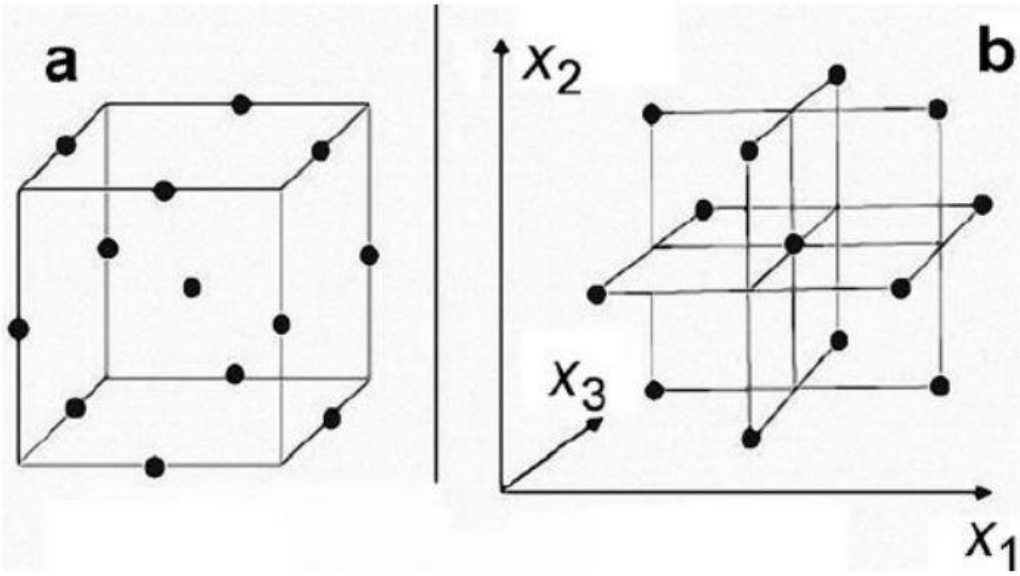

Figure 3. 8 Box–Behnken design for a three-factor experiment (Kandananond, 2010)

Box–Behnken designs (BBD) are a class of rotatable or nearly rotatable designs that are based on the three-level per factor (-1, 0, +1), but avoid corner space by filling it with combinations of the cube's center and extreme levels. Thus, BBD blends fractional factorial and incomplete block designs and excludes extreme vertices to ensure the design's rotatability (Hanrahan and Lu, 2006). The series of experimental trials (N) necessary for process parameter optimization is calculated using the formula provided in Equation (3.10). (Bezerra et al., 2008).

$$N = 2k(k-1) + C_0 \tag{3.10}$$

where the number of factors is denoted by k and the number of replicates for the central points is denoted by C_0.

Thus, Box-Behnken is an altogether effective and efficient design under response surface methodology due to its applications such as (i) model fitness (lack of fit) detection; (ii) sequential designs building; (iii) use of blocks, and (iv) quadratic model parameters estimation (Ferreira et al., 2007).

In this study, Box-Behnken design (BBD) under RSM is used to optimize the process parameters. The statistics Design-Expert 6.0.8 (Stat-Ease Incorporated, East Hennepin Ave, Minneapolis, United States) was used for the experimental design. The RSM helps in the analysis of the experimental data along with the optimization of selected input operational

parameters such as pH (x_1), H_2O_2 dose (mg L^{-1}) (x_2), flow rate (mL min^{-1}) (x_3), and treatment time (min) (x_4). The working range of variables or operating parameters derived from the BBD model is listed in Table 3.2. These variables were coded as follows: low (-1), center (0), and high (+1) levels. The response selected for Fe-TiO_2 treatment of *E. coli* is % Degradation (R). The influence of the operational process parameters on the responses was analyzed from an analysis of variance (ANOVA).

Table 3. 2 Level of the factors tested in the Box−Behnken experimental design

S. No.	Variable	-1	0	-1
1	pH	3	4.5	6
2	H_2O_2 (mg L^{-1})	30	75	120
3	Flow rate (mL min^{-1})	100	250	400
4	Time (min)	30	90	150

3.14 Mathematical models in *E. coli* inactivation

Four different mathematical models (log-linear, Weibull, double Weibull, and Biphasic) for inactivation were used in this study. The kinetic coefficients of these models were obtained by adjusting the experimental results to the corresponding equations by non-linear regression techniques. The fitting of the experimental values was done using Microsoft Excel: Solver and GInaFiT software developed by Geeraerd et al. (2005). R^2 and RMSD were used for the evaluation of the fitting of inactivation results. Also, to get some better information regarding the degree of fit of the models used, the experimental results obtained were compared with results obtained through mathematical models and represented graphically.

3.14.1 The log-linear model

The log-linear model is the moderation of Chick's model. This model is used to govern the relationship between the number of microorganisms inactivated and the number of molecules of disinfectant, as shown in Equation (3.11)

$$log\frac{A_t}{A_0} = -kCt \rightarrow log\frac{A_t}{A_0} = -k_{ap}t \tag{3.11}$$

Where A_0 is the initial and A_t is the final concentration of *E.coli* left after the reaction. k is the first-order rate constant (min^{-1}), C indicates the disinfectant concentration; t is the reaction time. The integration of disinfectant concentration at an apparent rate constant can simplify the model.

3.14.2 The Weibull model

The Weibull model of inactivation is based on continuous probability distribution (Rodríguez-Chueca et al., 2016). This model describes the degree of variability in the behavior of a system. In the case of first-order models, microbial populations are assumed to be homogeneous regarding resistance to external conditions. But the Weibull model describes the microbial population as heterogeneous. Also, the death of the cells depends on the time of exposure of cells to external stress conditions as well as the exposure time required by every cell to die is different. The dispersal resistance to the conditions cells are exposed to is regulated by a Weibull-type distribution. The Weibull model for bacterial inactivation is a cumulative form of asymmetric probability density function for the heat resistance of individual bacterial cells. The Weibull model is given by Equation (3.12).

$$log\frac{A_t}{A_0} = -\left(\frac{t}{\delta}\right)^p \tag{3.12}$$

The first decimal reduction time, i.e., the time required to carry out the first decimal log reduction in the population of the bacterial cycle (e.g., from A_0 to $A_0/10$) is denoted by δ. The shape of the equation is denoted by p. When p>1, convex shape, and when p<1, concave shape. At p = 1, the equation shows a linear first-order model.

3.14.3 Double Weibull model

The double Weibull kinetic model is a moderation of the Weibull model. This model is based on the theory that the resistance to the external stress condition of two different subpopulation groups of microbial populations is at different levels and follows the Weibull distribution as shown in Equation (3.13).

$$A = \frac{A_0}{1+10^{\alpha}} \times \left(10^{-\left(\frac{1}{\delta_1}\right)^{p_1+\alpha}} + 10^{-\left(\frac{1}{\delta_2}\right)^{p_2}}\right) \tag{3.13}$$

where α is the sub-population fraction in the population, subscripts 1 and 2 describe different sub-populations. Also, p indicates the shape parameter, t denotes time, and δ is the first

decimal reduction treatment time. Sub-population 1 shows more sensitivity to stress than sub-population 2($\delta_1 < \delta_2$).

3.14.4 Biphasic model

Cerf introduced a two-fraction kinetic model in 1977(Cerf, 1977). This kinetic model is referred to as the ***biphasic model*** (Cerf, 1977) as shown in Equation (3.14). This model presumes that the microbial population is separated into two distinct subpopulations with varying degrees of treatment sensitivity.

$$log\frac{A_t}{A_0} = Log[P * e^{-k_1 * t} + (1 - P) * e^{-k_2 * t}] \quad (3.14)$$

Chapter 4

Results and Discussion

4. General

This chapter discusses in detail the bacterial disinfection study in simulated and real wastewater. Numerous parameters are analyzed to determine the process's efficacy. Additionally, the oxidation mechanism of *E. coli* following disinfection was examined. Attempts have been made to investigate the effect of two processes operating in a fixed form simultaneously in the same system under artificial UV and natural solar radiations to improve process efficacy and reduce disinfection time.

This approach of the in-situ hybrid effect was fully explained in fixed form for the disinfection of *E. coli* in water using both artificial UV irradiation and natural solar light. The present study attempted to incorporate photocatalysis and photo-Fenton effects simultaneously in one system. This in-situ hybrid method successfully overcomes the disadvantages of photocatalysis and photo-Fenton (electron-hole recombination, iron sludge production, and extended treatment time) when applied individually. The in-situ hybridization process resulted in the abundant generation of OH^{o}. In this context, the results verified the reduction in treatment time using this hybrid technology when compared to the individual processes (photo-Fenton or photocatalysis). Additionally, the use of waste materials such as FA and FS as a substitute for iron defines the process's economic viability.

A detailed study was conducted to determine the effect of a variety of operational parameters, including support material size, catalyst dose, oxidant concentration, etc. Additionally, the selected support material was utilized to immobilize TiO_2 to investigate the combined usage of photocatalysis and photo-Fenton (in-situ hybrid process) for the disinfection of *E. coli* in water. Durability tests were conducted for the immobilized catalyst system to determine the economic viability of the reported approach. The procedure was optimized by adjusting operational parameters, and the study was then modeled kinetically for disinfection purposes. Scaling up this novel in-situ hybrid process was also accomplished through the creation of non-concentrating fixed-bed reactors on a pilot scale. To demonstrate the technique's practical application, pilot-scale reactors such as fixed-bed recirculating glass reactors and solar once-through cascade reactors with in-situ hybrid effects were fabricated

and researched in detail for the disinfection of target contaminants. Finally, the successful treatment of real wastewater utilizing the in-situ hybrid process and highly durable & affordable composite beads demonstrates the technique's field-scale application. The experimental workflow is depicted in a flow chart (Figure 4.1) to provide a visual representation of what and how the research has been described in subsequent sections.

Section A (In-situ hybrid process at lab scale)

- Selection of novel inert support material composed of FA and FS with TiO_2 immobilized on the surface.
- The prominence of the hybrid effect was established by coupling two techniques (photo-Fenton and photocatalysis) within the same system in the fixed-bed mode for the disinfection of *E. coli* in batch mode.
- Various operating parameters including H_2O_2 dose, treatment time, pH of the solution, and Intensity of light were evaluated.
- The synergistic effect of hybrid processes over individual processes was studied.
- Durability studies were conducted in terms of the number of recycles along with the leaching of iron content.

Section B (scale-up studies)

- Scale-up of the in-situ hybrid process was carried out with the development of pilot-scale non-concentrating fixed-bed reactors for the disinfection of *E. coli:* 1) continuous flow recirculation reactor 2) once through the reactor in series
- Various operating parameters evaluated including H_2O_2 dose, treatment time, flow rate, number of reactors were evaluated.
- The synergistic effect of the hybrid processes over the individual processes was studied.
- Durability studies were conducted in terms of a number of recycles along with the leaching of iron content and further reconfirmed using various characterizations including SEM/EDX, XRD, FT-IR, and UV-DRS.

Section C (Treatment of real wastewater)

- The actual viability of implementing the in-situ hybrid process was confirmed by treating the real secondary treated municipal wastewater effluent with the

same catalyst (TiO_2 immobilized composite beads) incorporating the in-situ hybrid effect.

Figure 4. 1 The structure of results and discussion

4.1 Section A (In-situ hybrid process at lab scale batch reactor)

Disinfection of *E. coli* was carried out at a lab scale under artificial UV irradiations using industrial waste material such as FS and FA as an alternative iron source. A borosilicate glass dish of 20 cm in diameter and 5.5 cm in height having a volume of 1000 mL was used as a batch reactor. The reactor was placed under the UV lights on a laboratory jack so that the irradiation intensity could be changed by altering the height of the jack. The average variation of UV radiation ranges between 10 to 24 Wm^{-2} and was measured using a radiometer (Eppley, model no. 33013). The working solution contained 250 mL of double distilled water spiked with 10^6 CFU mL^{-1} of *E. coli*. Then the solution was stirred for 20 min at room temperature for the acclimatization of bacteria and the TiO_2 immobilized composite beads were added to start the experiment.

Optimization of the process was done by varying different parameters such as H_2O_2 dose, pH, bead size, UV intensity, and area-to-volume ratio based on which reaction kinetics were studied. All experiments were performed in triplicates and the results show the average of the three samples and the error bars show the standard deviation in the figures. The statistical significance of the mean value of the treated samples was determined by the one-way ANOVA test. All results were found to be significant as the F-values were greater than 5 and the p-value < 0.05 for all the experiments as shown in Table 4.1. The main emphasis of this research was to study the prominence of Fe-TiO_2 composite for the disinfection of *E.coli* in the fixed mode for which catalyst immobilization materials using clay, FA, and FS were prepared. The disinfection efficacy of *E. coli* was evaluated with the execution of a detailed experimental study under optimized conditions.

Table 4. 1 Statistical analysis for inactivation of *E. coli* using photocatalysis, photo-Fenton, and hybrid process.

S. No.	Process	F-value	P-value
1	Photocatalysis	202.98	2.05×10^{-14}

2	Photo-Fenton	352.82	2.58×10^{-16}
3	Hybrid (photocatalysis+photo-Fenton)	5570	8.11×10^{-23}

4.2 Tentative mechanism of hybrid process

The hybrid process involves the simultaneous occurrence of photocatalysis and the photo-Fenton process in one system. This novel concept of composite beads lixiviates iron in wastewater under acidic conditions, contributing to the photo-Fenton reaction in the presence of H_2O_2 accompanied by TiO_2 photocatalysis. Moreover, systematic lixiviation of iron in the reactor helps in preventing iron sludge formation via photoreduction of Fe^{3+} to Fe^{2+}. The involvement of e^-_{CB} in the photoreduction of Fe^{3+} to Fe^{2+} and utilization of H_2O_2 and UV light for the photoreduction of Fe^{3+} to Fe^{2+}, leading to increased production of OH^{o} (prominence of hybrid effect), can be understood by the following hypothesis: TiO_2 photocatalysis is a well-established technique (Equation 4.1- 4.3) involving the role of e^-_{CB} and h^+_{VB} in the production of oxidative radicals.

At the same time, lixiviation of iron from the catalytic beads after reaction with H_2O_2 resulted in photo-Fenton as shown in Equations (4.4 - 4.6), and showed a reduction of 6.2 log units (combined photocatalysis and photo-Fenton) in 90 min of treatment time as discussed in next section. The hybrid process reduces the e^--h^+ recombination by combining the e^-_{CB} with Fe^{3+} to regenerate Fe^{2+}, as shown in Equation (4.7). Moreover, the presence of H_2O_2 plays a dual role by reacting with the iron (photo-Fenton process, as mentioned above) and with the photocatalysis process, as shown in Equation (4.8). Therefore, this process led to a higher production of OH^{o}.

Now, to verify the existence of a hybrid effect by the proposed mechanism, another set of tests was performed. First, the engagement of e^-_{CB} in the process of Fe^{3+} to Fe^{2+} photoreduction (Equation 4.7) was cross-verified by performing the experiments with different time intervals, as shown in Figure 4.2 (a). Also, the effect of H_2O_2 and UV irradiation on the photoreduction of Fe^{3+} was verified by performing some experiments, as shown in Figure 4.2 (b). An increased concentration of Fe^{2+} was observed, which could be due to the photoreduction of Fe^{3+}. The theory of the extraction of e^-_{CB} from TiO_2 and the use of H_2O_2 for the reduction of Fe^{3+} to Fe^{2+} during the in-situ hybrid process was verified with the excess amount of OH^{o} produced (using the photoluminescence study), which helped in the disinfection of *E.coli* in water, as shown in Figure 4.2 (c).

To quantify and verify the difference in inactivation kinetics between these three different processes (hybrid, photocatalysis, and photo-Fenton), the kinetic rate constants of the inactivation of the three different processes were compared; the results are shown in Table 4.2. The hybrid process showed a log reduction of 6.2 units with a rate constant of 0.15 min^{-1}. On the other hand, photo-Fenton and photocatalysis individually showed a reduction of 3.3 log units with a rate constant of 0.06 min^{-1} and a reduction of 3.2 log units with a rate constant of 0.05 min^{-1}, respectively. The rate constant for the hybrid process was found to be significantly higher than that of the photocatalytic and photo-Fenton processes. This is evident enough to prove the higher production of OH^o in the hybrid process. As expected, the inactivation efficacy of the hybrid effect was about twice that of the photocatalytic and photo-Fenton processes individually. Thus, these results proved the existence of an in situ hybrid effect exhibiting both the active TiO_2 layer (led to photocatalysis) and iron lixiviation from the beads (led to photo-Fenton) with higher production of OH^o. A one-sided ANOVA test was performed to determine the statistical significance of the means of the treated samples and found F values > 5 and a p-value of < 0.0001, making all results significant.

$$TiO_2 + uv \rightarrow TiO_2(e^- + h^+) \quad (4.1)$$

$$e^-_{CB} + O_2 \rightarrow O_2^- \quad (4.2)$$

$$h^+_{(TiO_2)} + H_2O_2 \rightarrow OH^o + H^+ \quad (4.3)$$

$$Fe^{2+}_{(aquous)} + H_2O_2 \rightarrow Fe^{3+}_{(aquous)} + OH^o + OH^- \quad (4.4)$$

$$Fe^{3+}_{(aquous)} + H_2O_2 \rightarrow Fe^{2+}_{(aquous)} + H_3O^+ + HO_2^- \quad (4.5)$$

$$Fe^{3+}_{(aquous)} + H_2O \xrightarrow{uv} Fe^{2+}_{(aquous)} + OH^o + H^+ \quad (4.6)$$

$$Fe^{3+}_{(aquous)} + e^-_{(CB)} + H_2O \rightarrow Fe^{2+}_{(aquous)} + OH^o + H^+ \quad (4.7)$$

$$e^-_{(CB)} + H_2O_2 \rightarrow OH^o + OH^- \quad (4.8)$$

Table 4. 2 First order rate constant (k) values for inactivation of *E. coli* K12 using different processes

Type of process	k value(min^{-1})
Photocatalysis	0.05
Photo-Fenton	0.06
hybrid Process (Photo-Fenton + Photocatalysis)	0.15

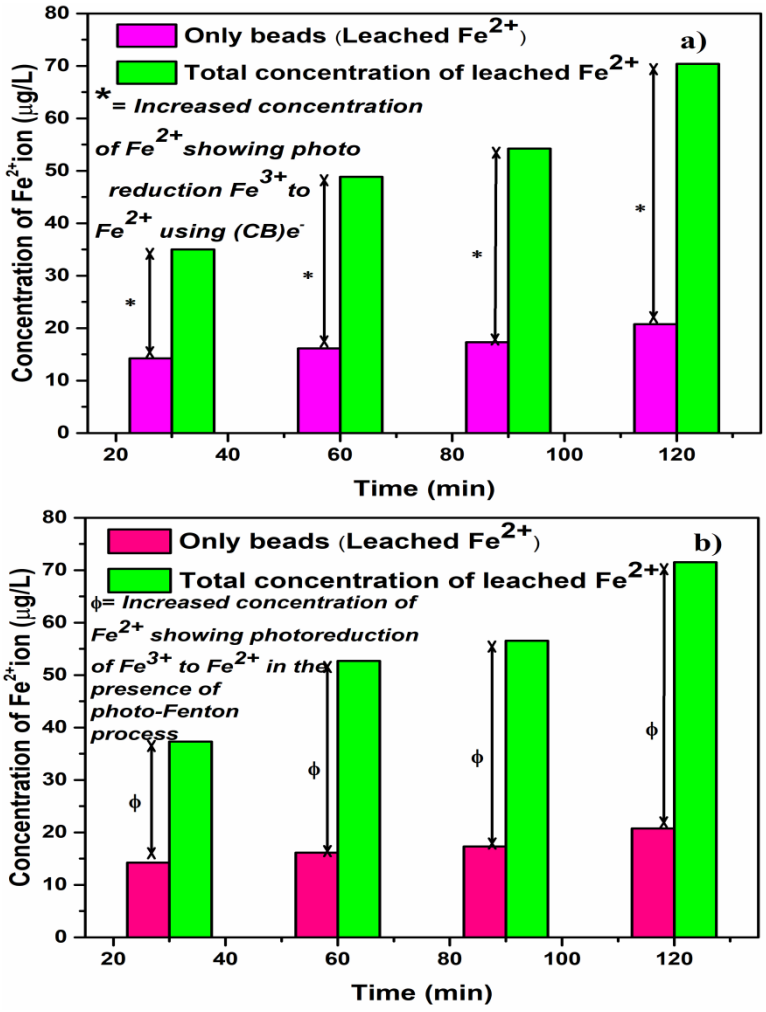

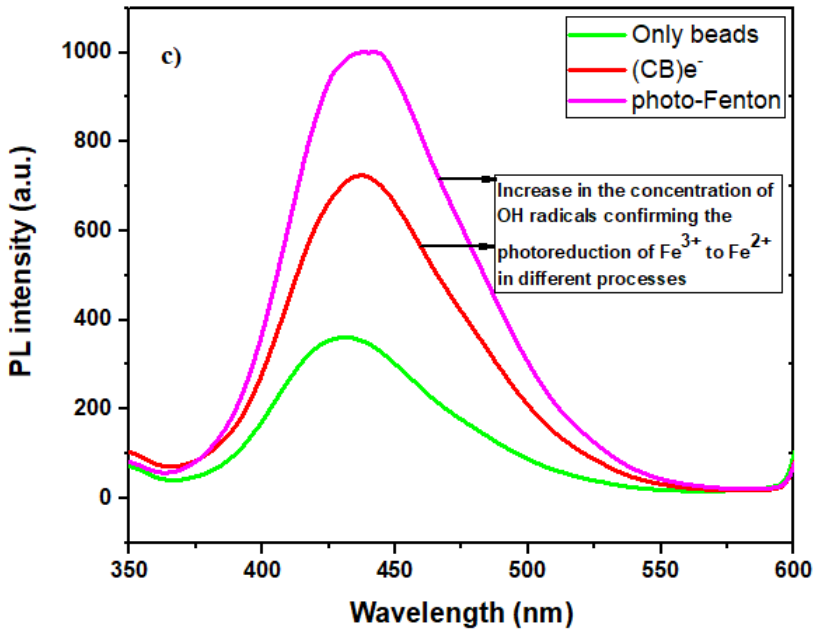

Figure 4. 2 (a) Photoreduction of Fe^{3+} to Fe^{2+} using e^-_{CB} (b) Photoreduction of Fe^{3+} to Fe^{2+} using photo-Fenton process (c) OH^o spectra using a fluorescence spectrophotometer

4.3 Preliminary studies using UV batch reactor

The boundary condition of the experiments was set by performing the experiments in dark without using TiO_2-coated beads. A negligible log reduction of 0.007 in *E. coli* count was observed as shown in Figure 4.3. This negligible reduction can be attributed to the fact that the double-distilled water does not affect the viability of the *E. coli* within 2 h of the experiment; any inactivation of the *E. coli* cell might be due to the osmotic pressure and similar results were observed in previous study mention in the literature (Giannakis et al., 2018c) where no change in the cell count was observed in 2 h. Fe leaching from the composite beads made of clay, FS, and FA had very little effect on the viability of *E. coli* as confirmed by results showing 0.05 log unit reduction. This loss in the viability of cells may have been due to the transportation of iron into the periplasm in the form of Fe^{2+} done by non-specific porins present at the outer membrane of the cell, followed by its transportation into the cytoplasm (Lau et al., 2016). This causes a temporary disturbance of Fe^{2+} balance in the cell (Rodríguez-Chueca et al., 2013).

When H_2O_2 was added to the reactor its diffusion through lipids into the cell is possible because of osmotic stress conditions of the cell and also because of its comparable physical properties with H_2O (Bienert et al., 2007). Inside the cell in the cytoplasm, H_2O_2 is scavenged

primarily by some enzymes acting as regulators such as alkyl hydroperoxide reductase, and most probably KatG which regulates the respiratory system of the cell (Imlay, 2013). Likely due to this scavenging effect, the unit log reduction caused by the addition of H_2O_2 was 0.09.

The viability of the *E. coli* in dark conditions was tested at pH 3-4 in the reactor and no significant decrease in the *E. coli* cell count was found as shown in Figure 4.3. The same results were obtained when Rodríguez-Chueca et. al (Rodríguez-Chueca et al., 2014b) studied the cell viability at the acidic condition and negligible reduction was observed.

In the Fenton process, Fe^{2+} and H_2O_2 can be transported into the cell as described above. The inactivation rate of the Fenton reaction is slowed down by the regeneration of Fe^{3+} to Fe^{2+}. The maximum unit log reduction in this experiment was observed as 0.1. Therefore, it is clear from Figure 4.3 that the baseline process is showing negligible bacterial inactivation indicating the potential for improvement for *E. coli* inactivation using hybrid photocatalysis and photo-Fenton processes.

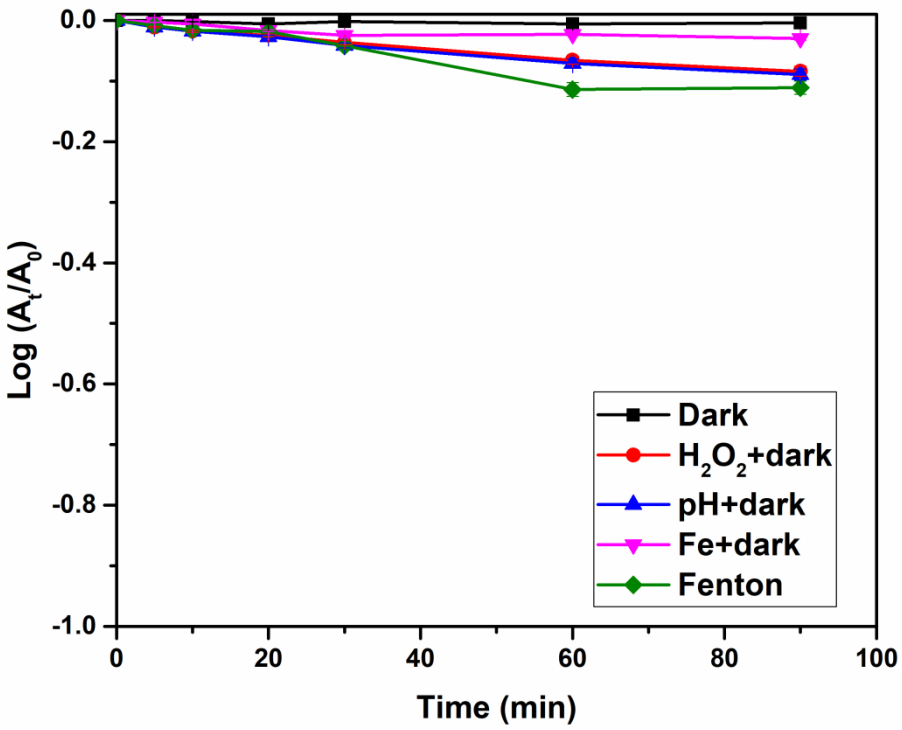

Figure 4. 3 Inactivation of *E. coli* with and without Fe and H_2O_2 in the dark

After analyzing the control experiments, efforts were made to study the disinfection process under UV radiation (average intensity 25 Wm^{-2}) for 90 min, and the results from photo-Fenton, photocatalysis, and hybrid process in water have been presented in Figure 4.4. The experiments were carried out under acidic conditions because iron can only leach from the beads under acidic conditions. This is because the iron in the soil is present in combination with other organic substances and acid helps in breaking the bond between them and helps in extracting the iron from clay called iron leaching (Hseu, 2004). The results showed that UV exposure alone at 365 nm achieved 1.1 log unit reduction. This was attributed to the minimal emission of the energetic portion of the UV spectrum of UV-A light (3.10-3.94 eV), which generally does not cause significant damage to the bacterial cell (Rincón and Pulgarin, 2006). Therefore the other studies emphasize facilitating the UV-A mediated inactivation by some catalyst to attain more cell damage (Chong et al., 2011; Rincón and Pulgarin, 2006).

When radiation falls on the cell, it leads to bacterial inactivation via the inactivation of antioxidant enzymes, such as catalases and peroxidases (Giannakis et al., 2018c). This inactivation of the enzymes leads to the formation of Reactive Oxygen Species (ROS) such as H_2O_2, $^1O_2$, and $O_2^{\circ-}$ (Imlay, 2008). The ROS formed can react with different cell components, such as the reaction of DNA with $^1O_2$, reduction of iron from the [4Fe-4S] clusters, and its reaction such as unregulated H_2O_2, which causes internal photo-Fenton process by the iron inside the cell and the gathered oxidants (Imlay, 2015).

The results for the TiO_2 photocatalysis showed a 3.2 log reduction. The mechanism of the inactivation of cells using TiO_2 photocatalysis has not yet been elucidated. However, several studies have provided different mechanism patterns. The reactive oxygen species (OH^o, HO_2^{-o}, O_2^{-o}) generated on the surface of TiO_2 induce oxidative stress in the bacteria and lead to its inactivation. Several studies reported that the lipid peroxidation reaction in the cell membrane occurs in the presence of TiO_2 which affects the respiratory activity of cells. Other studies proposed that the first step in the photoinactivation of *E. coli* is the damage and disordering of the outer membrane serving as a barrier to the cells (Pigeot-Rémy et al., 2011). The degradation of the outer membrane helps the reactive oxygen species penetrate the cytoplasmic membrane and led to the loss of intracellular substances (Lu et al., 2003). It has been reported that OH^o is highly reactive as compared to the O_2^{-o} but has a short half-life in comparison to O_2^{-o}. Yet, they cannot penetrate the cell membrane to damage DNA because of

their charge (Collin, 2019). Therefore, the TiO_2 photocatalysis interacts immediately with the outer surface of an *E. coli* unless the TiO_2 particle has penetrated the cell.

The addition of H_2O_2 and iron leaching from the beads imposes two important changes in the cell inactivation. First is a massive generation of OH^o into the system (reaction of H_2O_2 and iron), which led to the oxidation of the cells externally (Giannakis et al., 2016a). The second is the penetration of ferrous ions and H_2O_2 into the cell via porins. The size of the Ferrous ion (<6 Å) and H_2O_2 ion (1.2-1.4 Å) is smaller in comparison to the size of bacteria (11 Å), thus destroying cells internally after the deactivation of catalases. As this process is happening in the presence of UV light, ferrous ion reacts with the internal reactive oxygen species (ROS), which results in damage to the cell. Whereas H_2O_2 will cause moderation in biosynthetic and catabolic function, which will further result in loss of iron from the iron/sulfur cluster and generate OH^o (Giannakis et al., 2018c).

This H_2O_2 also affects cells externally via reacting with the cell wall. This increases the permeability of the cell due to the major influx of H_2O_2 leading to the oxidation of the cell wall. It happens because H_2O_2 oxidative activity (0.18 Å) is higher than the oxidation potential of the membrane. The H_2O_2 present outside the cell will generate ROS via homolysis and when H_2O_2 reacts with iron this adds up to the external oxidation of the bacteria. Bacterial inactivation due to the photo-Fenton process is slightly higher than the photocatalysis showing log unit reductions of 3.3 and 3.2 respectively in 120 min of reaction time as shown in Figure 4.4.

In the case of hybrid processes, the production of OH^o is higher as compared to their production in photocatalysis and the photo-Fenton process. This process reduces the electron-hole recombination via the utilization of conduction band e^- to engage with Fe^{3+} for the production of Fe^{2+}, thus leading to the photo-Fenton reaction in a cyclic mode. The hybrid process yielded a maximum 6.2 unit log reduction with a rate constant of 0.15 min^{-1} in 90 min whereas individual processes of photo-Fenton and photocatalysis took 120 min to yield 3.3 log unit reduction with 0.06 min^{-1} of rate constant and 3.2 log unit reduction with 0.05 min^{-1} of rate constant, respectively as shown in Table 4.1.

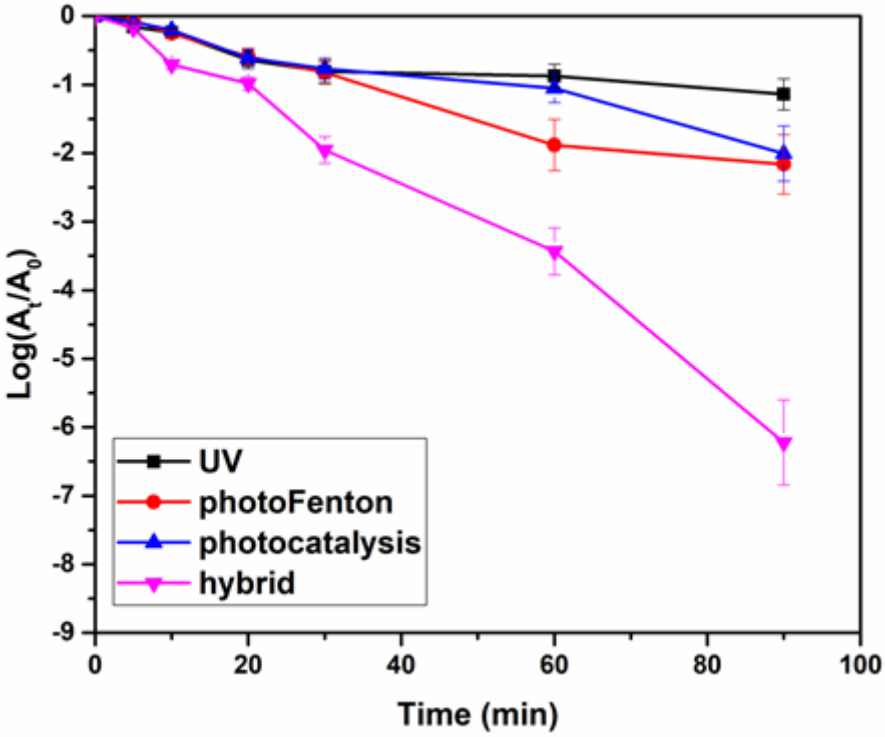

Figure 4. 4 Inactivation of *E. coli* in different conditions

4.3.1 Effect of hydrogen peroxide concentration

Various researchers have reported the effect of H_2O_2 on photo-Fenton and photocatalysis (García-Fernández et al., 2012; Gutiérrez-Zapata et al., 2017; Imlay, 2015; Spuhler et al., 2010; Talwar et al., 2019), as it is a well-established technique to add additional OH^o in the system. However, in this study, the addition of H_2O_2 plays a hybrid role as it is being consumed in both processes simultaneously. In a photocatalytic technique, oxidants are added so that it reacts with the electron in the conduction band and prevents electron-hole recombination, as shown in Equation (4.9). Thus, the optimization of its concentration was an important factor for both of the processes occurring in-situ. This hybrid process also increases the production of oxidizing species and hydroxide radicals. In this study, H_2O_2 concentration was optimized by varying its concentration from 0.12-0.42 g L^{-1}, and the optimum concentration was determined as 0.3 g L^{-1} at pH 4.5. After optimizing the H_2O_2 dose, an inactivation of 4.9 log unit was observed for *E.coli* within 90 min of reaction time, as shown in Figure 4.5 (a). It can be seen in Figure 4.5 (b) that the inactivation rate constant initially increased from 0.102 to 0.126 min^{-1} and started decreasing afterward. This decrease in the inactivation rate was likely due to the scavenging effect of H_2O_2. At high doses, H_2O_2 likely started consuming OH^o, as shown in Equations (4.10) & (4.11)

$$TiO_2(e^-) + H_2O_2 \rightarrow TiO_2 + OH^- + OH^o \quad (4.9)$$

$$H_2O_2 + OH^o \rightarrow HO_2^o + H_2O \quad (4.10)$$

$$HO_2^o + OH^o \rightarrow H_2O + O_2 \quad (4.11)$$

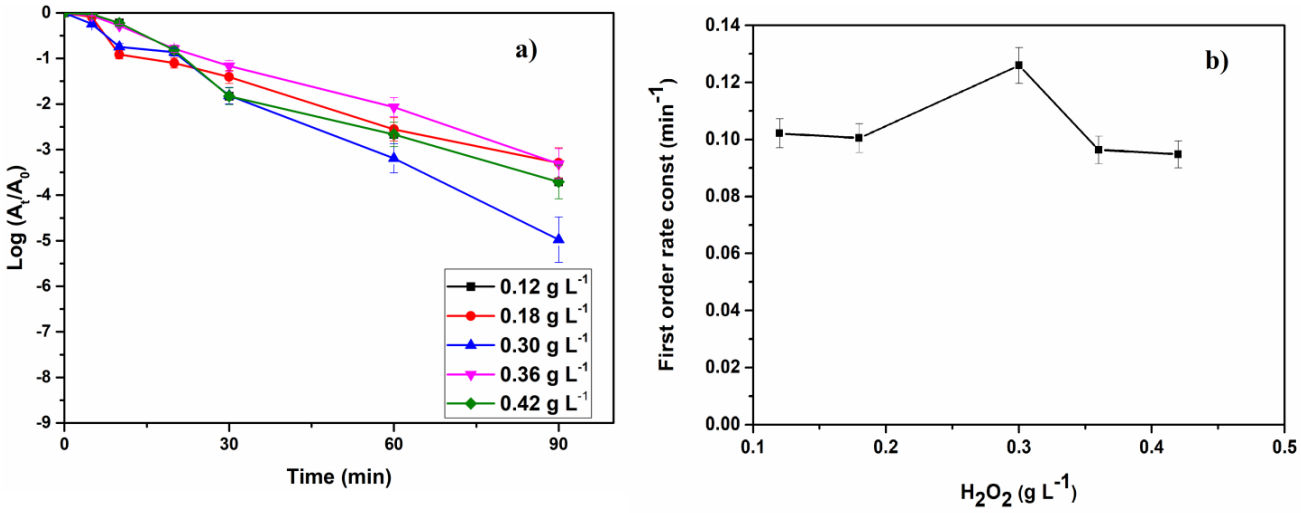

Figure 4. 5 (a) Effect of H_2O_2 dosage on inactivation of *E.coli* and (b) first-order rate constant at different H_2O_2 dosage

4.3.2 Effect of pH

pH plays an important role in the hybrid process as the leaching of iron from composite beads takes place under acidic conditions, and the iron executes the photo-Fenton process in the system. For the optimization of pH, experiments were done at different pH values ranging from 2.5 to 6.5 and at 0.3 g L^{-1} H_2O_2 as shown in Figure 4.6 (a). It was observed that at pH lower than 3.5, the bacterial inactivation rate was lower owing to the scavenging effect of OH^o (Bansal and Verma, 2018b). Subsequently, when pH was increased from 3.5 to 6.5, the rate of inactivation decreased again, as shown in Figure 4.6 (b). This can be due to the precipitation of FeO(OH) complex and hydrolysis of Fe^{3+}, which ultimately decreases the production of OH^o (Bansal and Verma, 2017a). It can be seen from Figure 4.6 (a) that the maximum inactivation of *E.coli* (5.2 log unit reduction) was achieved at pH 3.5 in 90 min, which was used as the optimum pH for the rest of the study. The formation of less active HO_2^- occurs at alkaline pH values. This consequently led to the formation of O_2 and H_2O on

reaction with non-dissociated H_2O_2. Moreover, the above reaction is preferred over a reaction with OH^o. Therefore, it is clear from the results that pH significantly influences the inactivation of *E. coli*.

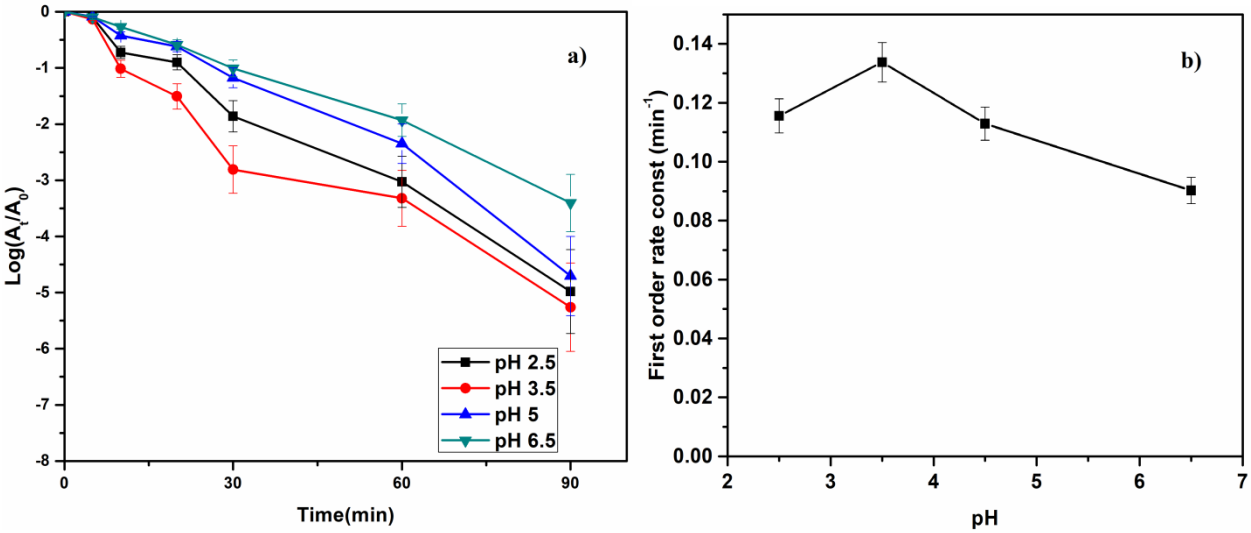

Figure 4. 6 (a) Effect of variation of pH on inactivation of *E.coli* and (b) First-order rate constant at different pH

4.3.3 Effect of UV intensity

In-situ utilization of solar radiation in terms of process feasibility and bacterial inactivation is one of the most important factors for commercial aspects of this technology. As irradiation coming from the sun does not remain constant throughout the day, the effect of UV intensity variation (10 Wm^{-2} to 25 Wm^{-2}) was studied for *E. coli* inactivation. It was observed that the maximum log unit reduction (5.9) was found in 90 min when the intensity of 25 Wm^{-2} was provided to the system (Figure 4.7 a) as higher production of OH^o was observed. This can be attributed to higher absorption of UV intensity by H_2O_2 at a higher intensity (Massoudinejad et al., 2016), which subsequently enhances the OH^o. It can be seen from Figure 4.7 (b) that the rate of inactivation increased from 0.11 min^{-1} to 0.15 min^{-1} with the increase in the intensity. To confirm the prominence of the in-situ hybrid effect, fluorescence spectroscopy was performed for the estimation of OH^o at different intensities as shown in Figure 4.7 (c). The concentration of OH^o increased with an increase in the UV intensity from 10 Wm^{-2} to 25 Wm^{-2}. The results depicted a reasonable log reduction of *E. coli*

at different UV intensities. However, the process can be intensified at lower intensities by effective reactor design and modifications.

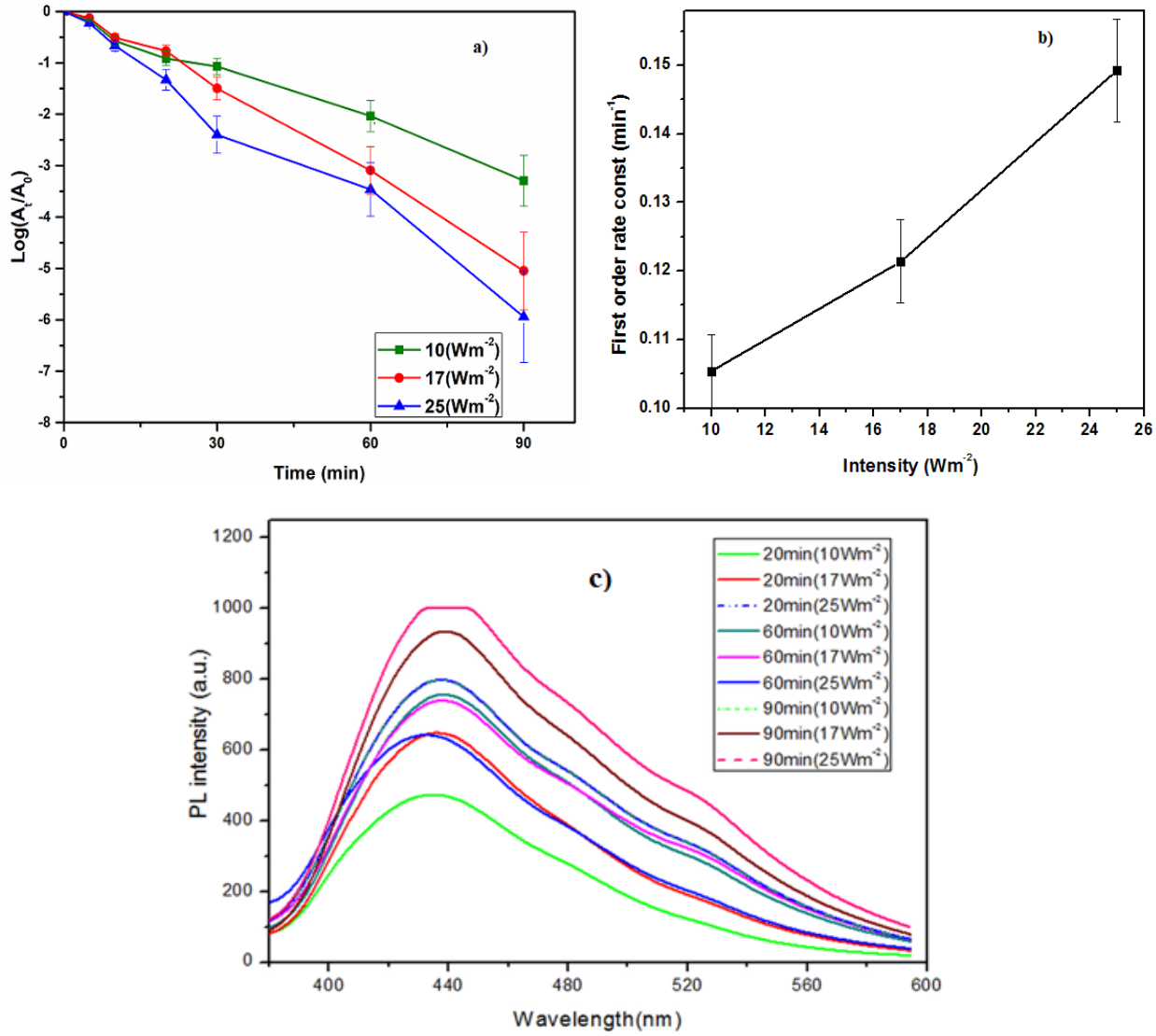

Figure 4. 7 (a) Effect of UV intensity on inactivation of *E.coli* and (b) first-order rate constant at different UV intensities (c) Photo luminance spectra of OH^{o} at different intensities

4.3.4 Effect of bead size

Exposed surface area for the proper illumination of the catalyst is an important operational parameter in fixed-bed studies to provide better contact between the contaminants and the catalyst (Takdastan et al., 2018). For field-scale applications, the type and size of the support material are particularly important for designing the reactor. In this context, the surface area of the composite bead was optimized by varying the size from 10 mm to 20 mm to achieve better inactivation of the *E. coli*.

It was observed from Figure 4.8 (a) that the log unit reduction was maximum (6 logs) when the size of the bead was 10 mm, providing the highest surface area. The log unit reduction of *E. coli* decreased from 6 to 5.3 with the increase in diameter of the beads, and the rate constant "k" also decreased (Figure 4.8 b) with increased bead size owing to the decrease in effective surface area available. Moreover, reducing the size of the composite bead below 10 mm could not help because this size was not able to hold the catalyst film intact. Too small beads would not have enough iron to leach out as FS, and FA concentration would be less. Therefore, 10 mm size was found to be more stable in terms of catalyst activity as well as iron concentration and was subsequently used for all the experiments.

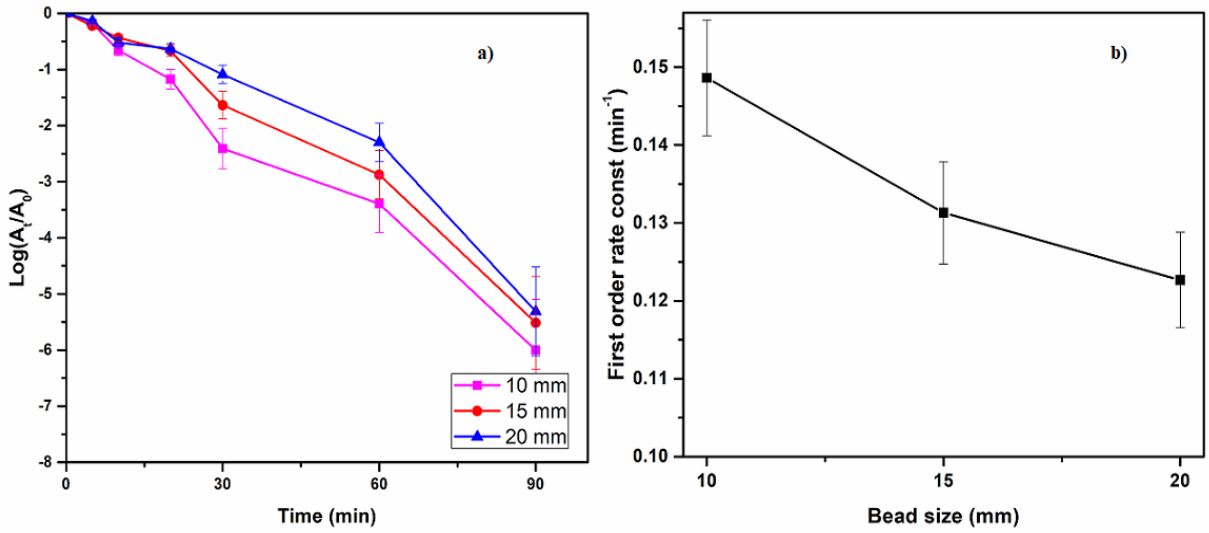

Figure 4. 8 (a) Effect of bead size on inactivation of *E.coli* and (b) first-order rate constant at different bead sizes

4.3.5 Effect of the area to volume ratio (A/V)

The major limitation of AOP in the field-scale application is the depth of the reactor as it hinders the path of solar radiation to reach the solution. For better penetration of light, more exposed area and less depth of reactor are considered appropriate (Verma, A., Prakash, N. T., & Toor, 2016). For this, either area or volume of the reactor can be altered by keeping one of them the same. In this study, the A/V ratio was varied from 0.18 cm^2 mL^{-1} to 0.42 cm^2 mL^{-1} by keeping the area the same and varying the volume of the solution to investigate its effect on the inactivation of bacteria. A significant increase in the log reduction of *E. coli* from 4.9 to 6.2 was observed (Figure 4.9 a) by increasing the A/V ratio. This increased log reduction can also be confirmed in Figure 4.9 (b), showing an increased first-order rate constant 'k' at 0.25 cm^2 mL^{-1}. As the A/V ratio increases (the area is kept the same, volume decreases), the

path length of the photons of light entering the solution increases, therefore, resulting in more OH^o production (Verma, A., Prakash, N. T., & Toor, 2016) and hence, the rate of bacterial inactivation increased. As a result, the optimized result for the A/V ratio was obtained as 0.25 $cm^2\ mL^{-1}$ and showed the maximum *E. coli* inactivation of 6.2 log unit reduction.

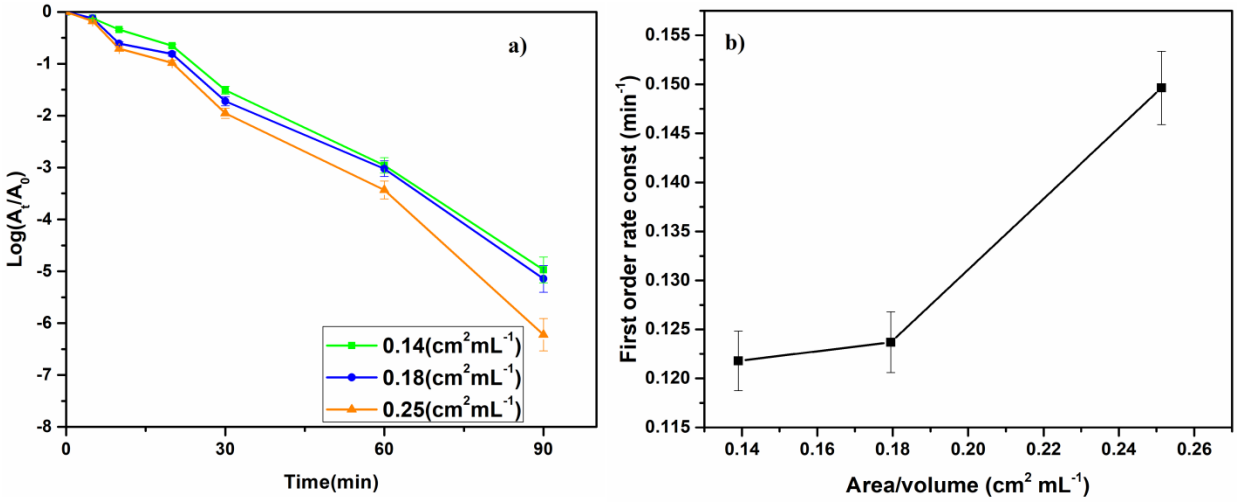

Figure 4. 9 (a) Effect of the area to volume ratio on inactivation of *E.coli* and (b) first-order rate constant at the different area to volume ratio

4.3.6 Characterization of composite beads

As the system executes the hybrid process within the same unit, there is a need to confirm the simultaneous presence of both the components (TiO_2 and iron) leading to photocatalysis and photo-Fenton on the surface of spherical beads for fresh as well as recycled composite beads. For this purpose, characteristic analysis using different technologies such as SEM-EDS, XRD, FTIR, UV-DRS, and HRTEM of fresh and recycled composite beads was done.

4.3.6.1 SEM/ EDS analysis

To analyze the surface morphology as well as the composition of the elements on the composite beads (uncoated, freshly coated, and recycled), scanning electron microscopy (SEM) along with energy dispersive spectroscopy (EDS) was performed and the results are shown in Figure 4.10. The major peaks of Fe, O, and TiO_2 on the EDS image confirm the incorporation of both materials (Fe and TiO_2) in the hybrid process in freshly and recycled beads. The existence of iron can be accredited to the utilization of FA/FS with clay to form composite beads, as no external iron was used for the process. A relatively smooth surface can be seen in the SEM image of freshly as well as recycled (50 times) coated beads. This indicates the presence of the TiO_2 layer and its intactness before and after 50 recycles. Thus,

it can be concluded that Fe-TiO_2 composites can be effectively utilized in in-situ hybrid processes for field-scale applications.

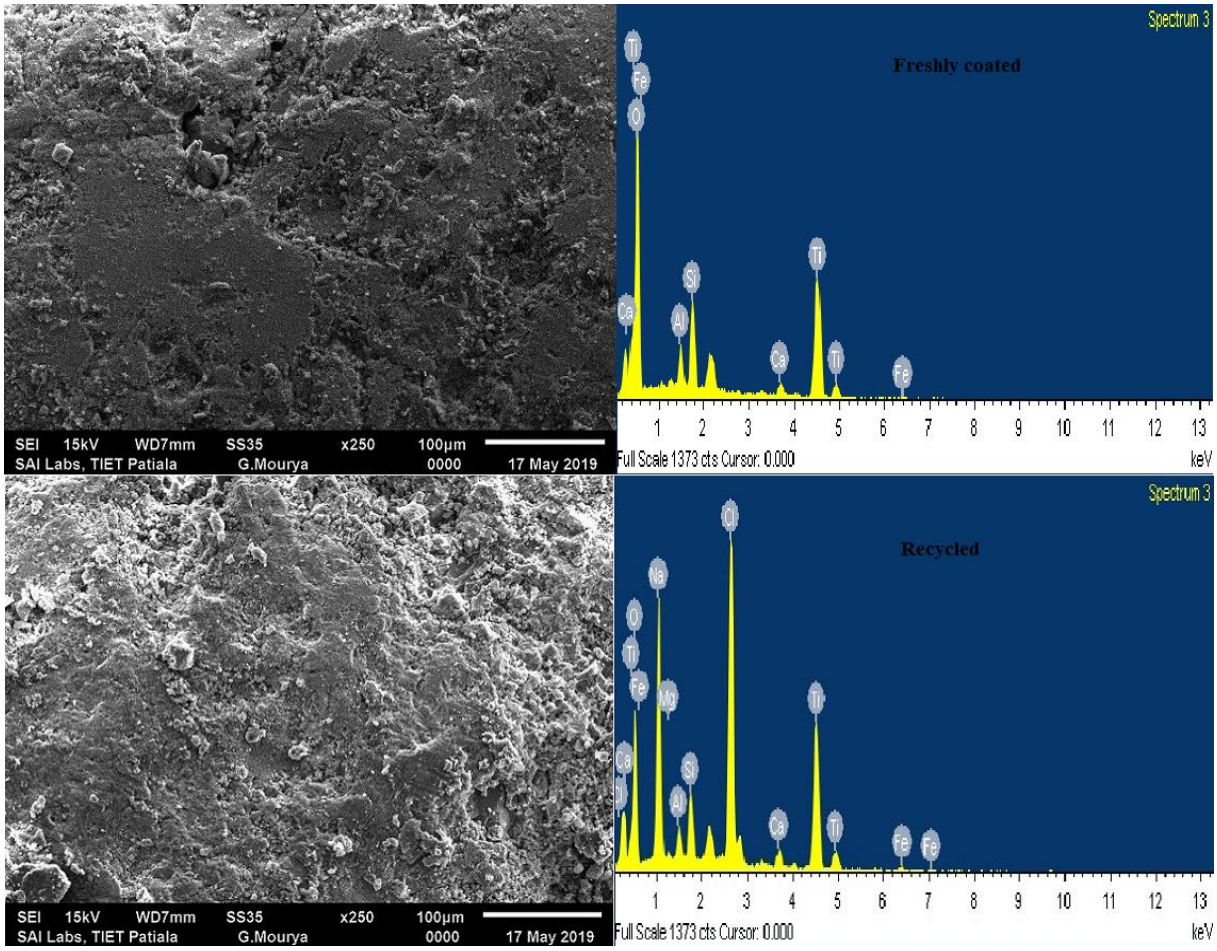

Figure 4. 10 SEM and EDS images of freshly coated, and recycled composite bead

4.3.6.2 XRD analysis

To reaffirm the intactness of crystalline planes of TiO_2 for fresh and recycled beads, the XRD analysis was carried out, and the results are shown in Figure 4.11. The TiO_2-coated composite beads were calcined at 350°C for effective binding of catalyst to surface. For this analysis, TiO_2 particles were scrubbed off from the composite beads and selected for XRD analysis. The diffraction pattern in Figure 4.11 shows the presence of anatase (A) and rutile (R) phases of TiO_2 at 2θ (20^o-80^o) in the fresh and recycled composite bead. The presence of anatase and rutile phase, even after 50 recycles, shows that the TiO_2 over composite beads can be used for practical application. Besides these two phases of TiO_2, the diffraction pattern also shows some other peaks of iron oxide (IO) and titanium iron oxide (TIO), respectively. The presence of iron oxide facilitates the entrapment of photo-excited e^- from TiO_2

photocatalysis for the regeneration of ferrous ions. Also, these IO and ITO (iron titanium oxide) enhance the efficacy of the Fe-TiO_2 catalyst in visible light. This hypothesis was further confirmed through UV-visible absorption spectroscopy, as explained in the next section 4.3.6.3. Thus, both processes of photocatalysis and photo-Fenton occur simultaneously in one unit. Therefore, Fe-TiO_2 composite can be suitably used for hybrid effect studies for numerous cycles without losing the catalyst activity.

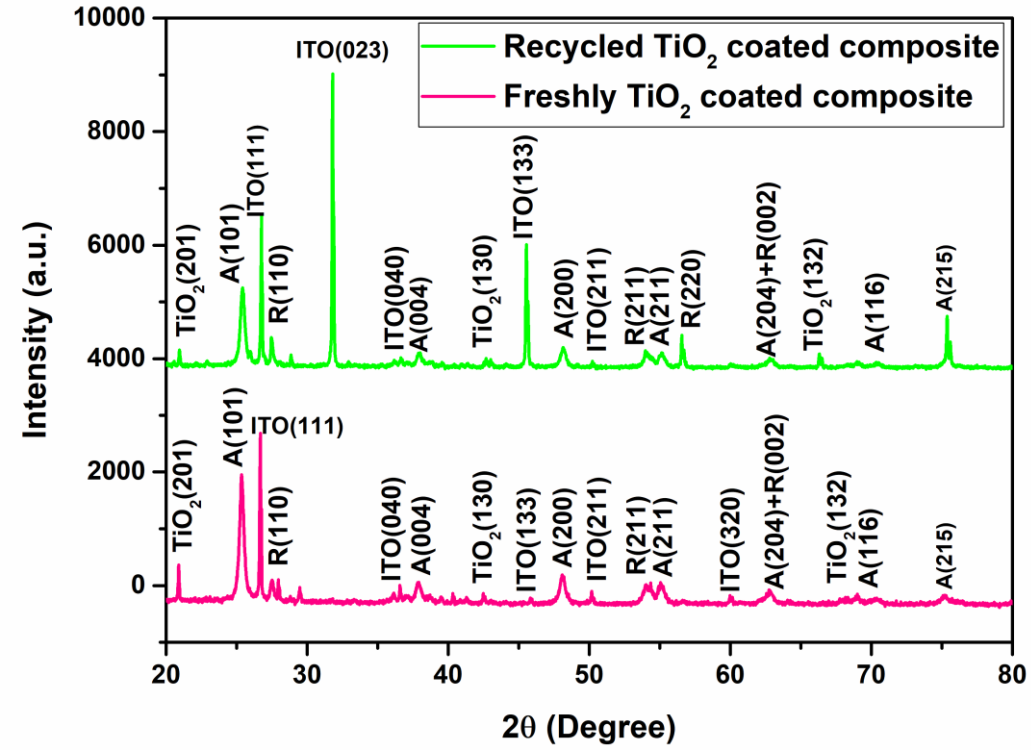

Figure 4. 11 XRD pattern of freshly coated and recycled composite bead

4.3.6.3 UV-visible DRS analysis

The composite beads (fresh and recycled) were analyzed using UV-visible diffuse reflectance spectroscopy (DRS) to confirm the light-absorbing capacity of composite beads in visible spectra. The analysis was carried out under the spectral range of 200-800 nm. It can be seen in Figure 4.12 that the bandgap energy decreases in composite beads thus showing its capability to absorb light in the visible region also as compared to TiO_2. This decrease in the bandgap energy in composite beads may be due to the presence of iron. The absorption wavelength of TiO_2 was 415 nm and extended to 430 nm and 452 nm for fresh and recycled composite beads, respectively as shown in inset (4.12). The energy band gap was calculated using Tauc Equation (4.12) (Tumuluri et al., 2014):

$$(\alpha h\upsilon)^{1/n} = \mathrm{A}\ (h\upsilon - Eg) \quad (4.12)$$

Where E_g is the energy band gap in eV, h is Planck's constant in joule seconds, υ is photon frequency in Hz, A is the proportionality constant. The energy bandgap of TiO_2 was 3.24 eV and reduced to 2.9 eV for fresh and recycled composite beads, respectively.

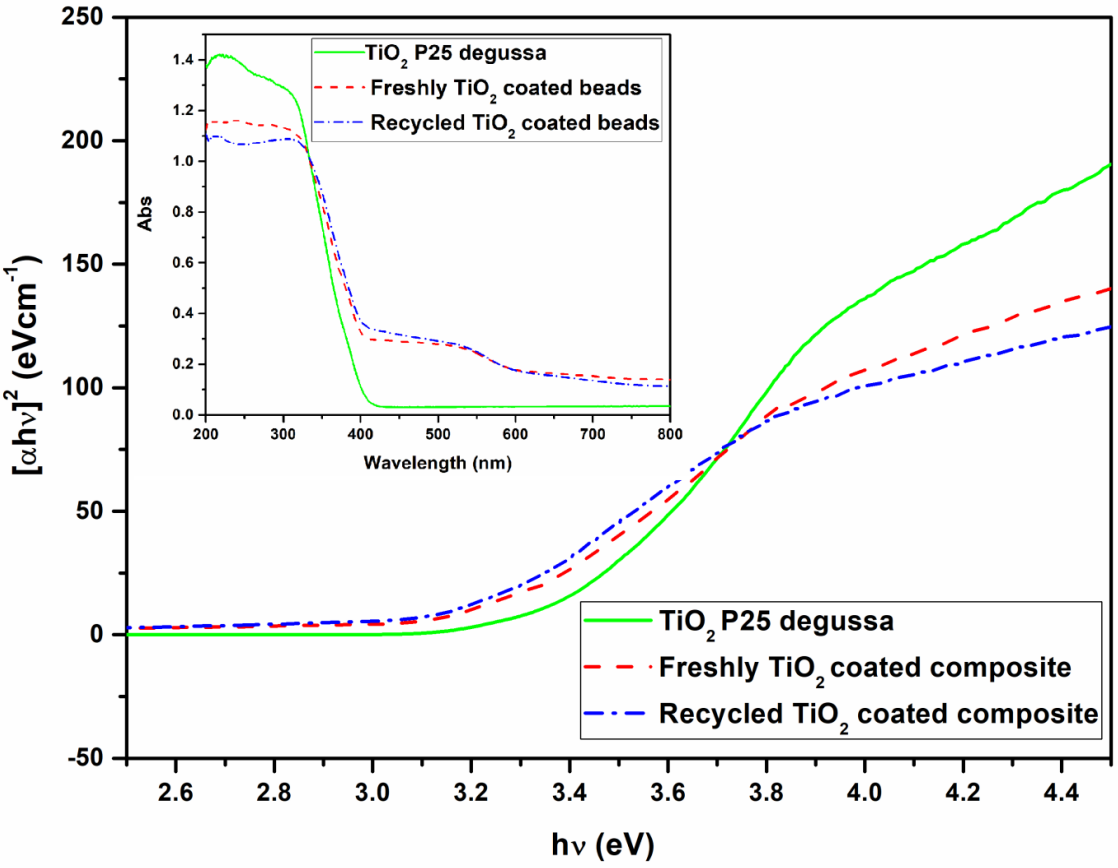

Figure 4. 12 UV-DRS images of freshly coated, and recycled composite bead

4.3.6.4 FTIR analysis

The characteristics and chemical bonds formed in fresh and recycled composite beads were also analyzed by FTIR spectroscopy to confirm the presence of TiO_2 and iron in the system. The infrared spectra of uncoated, fresh, and recycled composite beads are illustrated in Figure 4.13. The presence of H-O-H stretching can be observed between 3441 cm^{-1}-1674.6 cm^{-1} wave number. The peak at 468.9 cm^{-1} in uncoated beads shows the presence of the Si-O-Fe bond (Nayak and Singh, 2007). The occurrence of the peaks between 558 cm^{-1}-794 cm^{-1} wave number in uncoated beads analysis is due to the formation of Si-O vibrations. The occurrence of the peak between 400-1200 cm^{-1} wave number is due to the formation of the

Ti-O-Ti bond in the spectrum of both fresh and recycled composite beads. This also proves the presence of TiO_2 lattice. The anatase phase in the case of fresh and recycled composite beads in the spectrum occurred at 432 $cm^{-1}$and 501.3 cm^{-1}, respectively. This result is in confirmation of an earlier reported study (Ganesh et al., 2013), where the anatase phase occurred between 400-600 cm^{-1} due to the occurrence of Ti-O-Ti vibrations. The peak at 2304 cm^{-1} and at 2323 cm^{-1} in the spectra of fresh and recycled composite beads show the generation of Fe-O-Ti bond, which also confirms the presence of iron in composite beads. Bansal et al. (Bansal and Verma, 2018b) reported similar peaks for the presence of Fe-O-Ti bond in composite beads. Ti-OH bond was observed in Figure 4.13 at 1631cm^{-1} and 1613 cm^{-1} spectrum for the fresh and recycled composite beads, respectively. The presence of the O-H group was also observed at 3247 cm^{-1} and 3374 cm^{-1} for fresh and recycled composite beads because of the stretching vibration as indicated in previous studies (Ganesh et al., 2013; Sayyar et al., 2015).

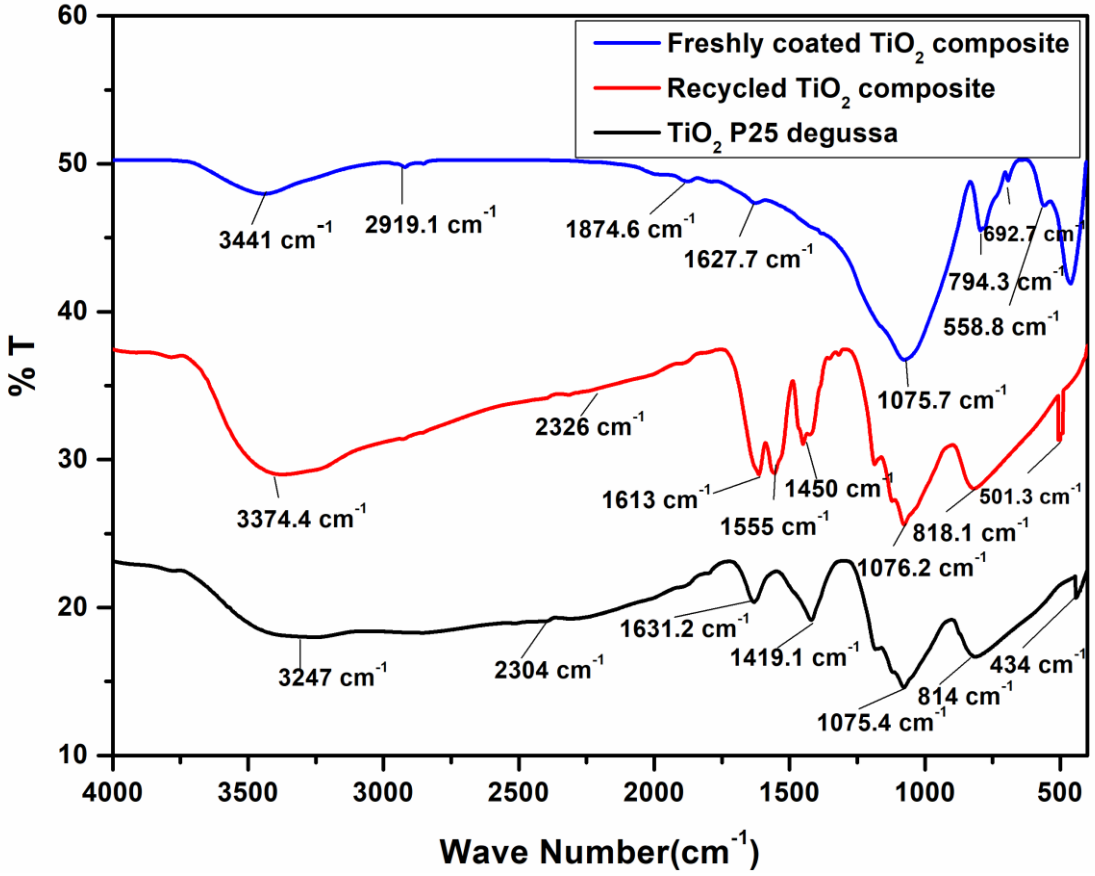

Figure 4. 13 FTIR pattern of freshly coated and recycled composite bead

4.3.7 Durability studies

The biggest challenge in fixed-bed catalytic reactors is the durability/longevity of the catalyst for repeated cycles. For this novel concept, things get more complex as this technology needs to handle two techniques at the same time and in the same place. For this technology to work smoothly, the intactness of the photoactive TiO_2 layer over the surface and incessant iron lixiviating from the Fe-TiO_2 composite plays a very significant role. The support material should be stable enough to keep TiO_2 intact and sustain the iron leaching for the photo-Fenton process. To investigate the durability of the support material, the composite beads were recycled 50 times, as shown in Figure 4.14, and only a 9 % reduction in the activity of the beads was observed. This minute loss can be attributed to the weathering of the catalyst from the composite beads (Talwar et al., 2019). The various characterization techniques discussed above also confirm the stability and durability of the composite beads. There was a significant amount of iron concentration observed before and after the recycling, which contributed to the photo-Fenton process, as shown in Figure 4.15. To further investigate the extent of the durability of the support material and the capacity to execute the in-situ hybrid effect, experiments were performed using composite beads recycled more than 100 times. Significant log reduction (5.04) of *E. coli* was achieved using the same optimized conditions. These findings show the strong potential of this technology for field-scale trials.

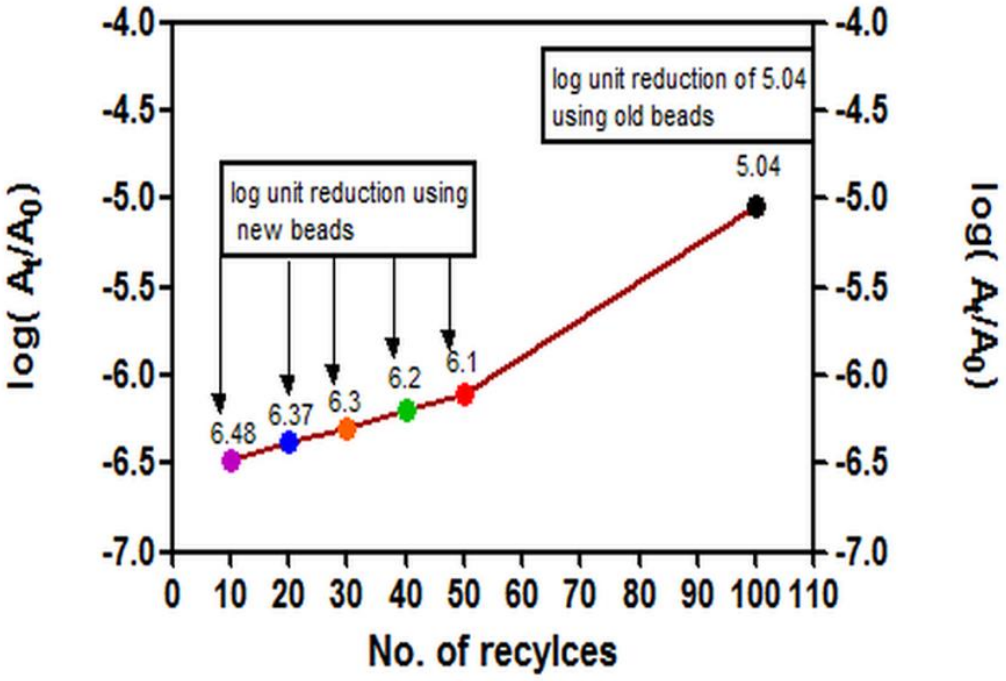

Figure 4. 14 Recyclability studies of composite beads

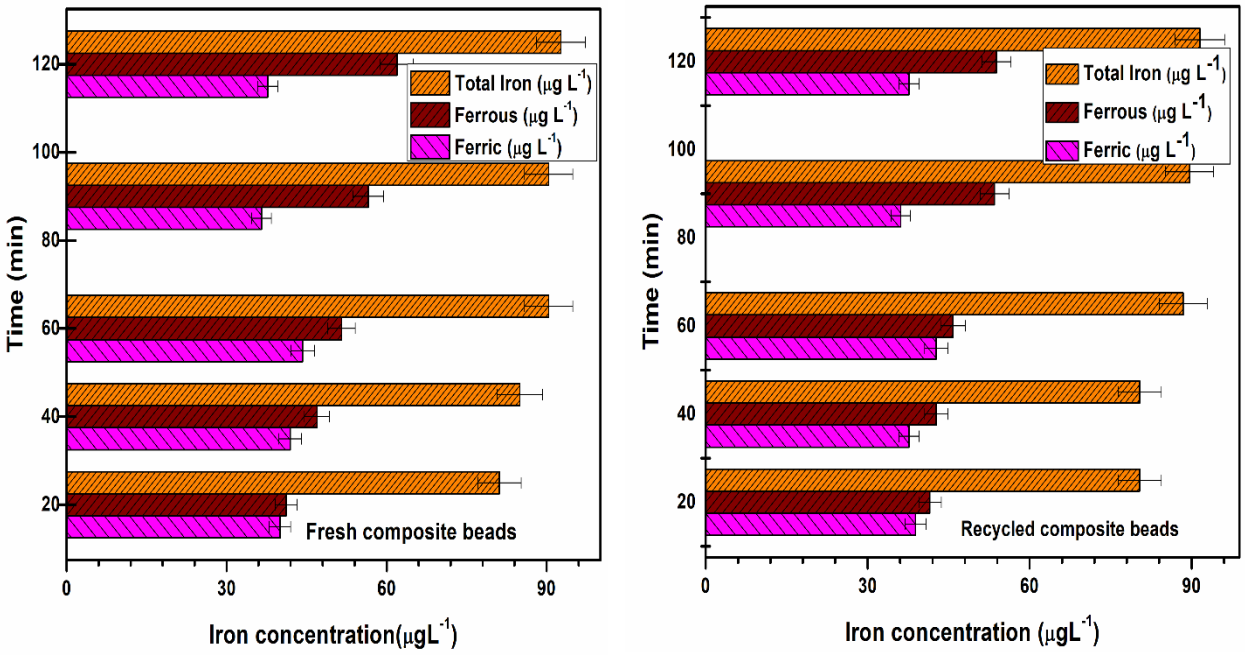

Figure 4. 15 Concentration of leached iron from fresh and recycled beads

4.4 Mathematical modeling of *E. coli* inactivation in water using Fe-TiO_2 composite in a fixed bed reactor

The present study is also followed by the comparison between different kinetic disinfection models and the experimental data associating the results with the key operating parameters affecting the disinfection efficacy of the current system. The results of this study provided useful information using the rate of inactivation, kinetic parameters, and fitting parameters: regression distribution (R^2) and root mean square deviation (RMSD) to comprehend the *E. coli* inactivation mechanisms. The kinetic parameters such as k of log-linear and δ of double Weibull for fitting the *E. coli* inactivation results were used for comparing the different techniques and found that the hybrid-technique in fixed mode (k = 0.16 min^{-1}, δ_1 = 8.63 min, δ_2 = 27.7 min) proved to be significantly faster in comparison to other techniques; TiO_2 assisted photocatalysis (k = 0.6 min^{-1}; δ_1 = 23.1 min, δ_2 = 76 min); photo-Fenton (k = 0.07 min^{-1}; δ_1 = 17.66 min, δ_2 = 33.53 min; H_2O_2 with UV (k = 0.04 min^{-1}; δ_1 = 34.05 min, δ_2 = 100.95 min) and Only UV(k = 0.03 min^{-1}; δ_1 = 51.91 min, δ_2 = 207.73 min. Thus the obtained results present a promising potential of the hybrid technology for the treatment of *E. coli* in water.

4.4.1 Mathematical models used in *E. coli* inactivation

Three different mathematical models (log-linear, Weibull, and double Weibull) for inactivation were used in this study. The kinetic coefficients of these models were obtained by adjusting the experimental results to the corresponding equations by non-linear regression techniques. The fitting of the experimental values was done using Microsoft Excel: Solver and GInaFiT software (Geeraerd et al., 2005) developed by Geeraerd and Van Impe. R^2 and RMSD were used for the evaluation of the fitting of inactivation results. Also, to get some better information regarding the degree of fit of the models used, the experimental results obtained were compared with results obtained through mathematical models and represented graphically.

All the preliminary experiments (dark, Fe+dark, H_2O_2+dark) were carried out to evaluate the effect of individual parameters on the disinfection of model pollutants i.e. *E. coli* (Figure 4.16). Each experiment revealed the negligible reduction of *E. coli* (<1 log) due to the inadequate production of OH^o.

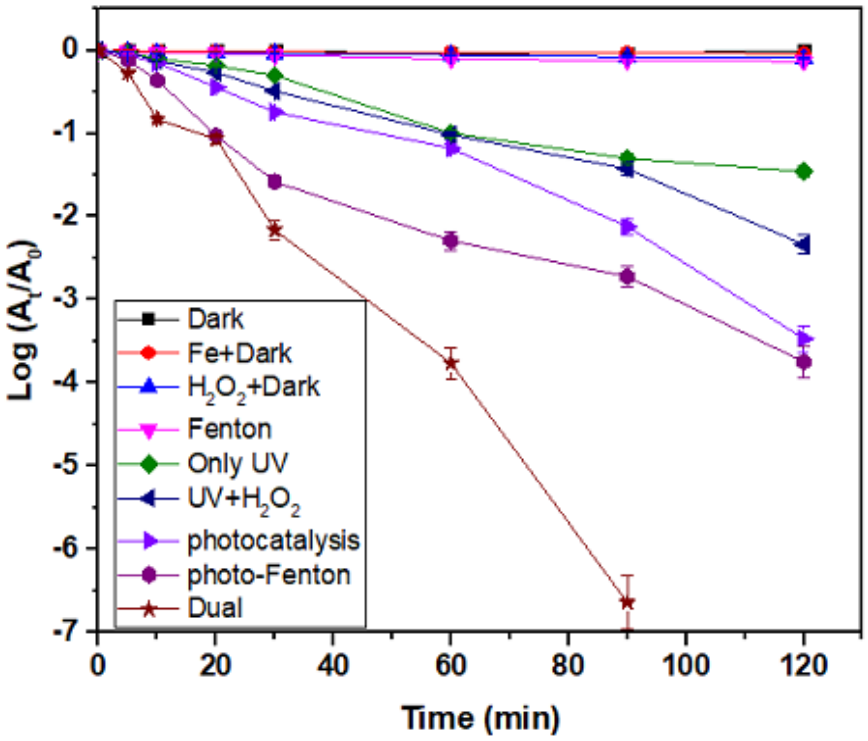

Figure 4. 16 Inactivation of *E. coli* at different conditions

4.4.1.1 UV assisted study

In this study, UV only, UV+H_2O_2, TiO_2-photocatalyst, photo-Fenton, and a combination of the photo-Fenton and TiO_2-photocatalyst in a fixed bed using Fe-TiO_2 composite beads were studied to evaluate and compare the killing efficacy of the system. As clear from Figure 4.16, only UV irradiation and 0.3 g L^{-1} of H_2O_2/UV irradiation experiments showed 1.4 and 2.3 log reduction inactivation of *E. coli,* respectively. It can be seen in Figure 4.17 that all three mathematical models showed good fitting when the only UV treatment for *E.coli* inactivation was applied. Though the double Weibull model showed the best fitting curve for inactivation considering the fitting of the average *E. coli* inactivation results and attaining relatively good R^2 (0.99) and RMSD (0.03) values as given in Table 4.3. Because in the double Weibull model coefficient of determination (R^2) is much closer to 1 as compared to other models that indicate that the regression line completely fits the data. Another reason was RMSD, whose value is much closer to 0 in comparison to the other two models that indicate the perfect fit of estimated values with the real values (Rodríguez-Chueca et al., 2016).

Table 4. 3 Kinetic parameters of mathematical models used in the inactivation of *E. coli* by UV treatment

Treatment	Models	K (min^{-1})	δ_1(min)	δ_2(min)	R^2/RMSD
Assay 1	Log-linear	0.03	-	-	0.961/0.124
	Weibull	-	69.22	-	0.966/0.128
	Double Weibull	-	52.14	232.62	0.999/0.023
Assay 2					
	Log-linear	0.03	-	-	0.971/0.113
	Weibull	-	67.19	-	0.973/0.119
	Double Weibull	-	51.62	187.21	0.998/0.036
Average					
	Log-linear	0.03	-	-	0.966/0.119
	Weibull	-	68.18	-	0.969/0.124
	Double Weibull	-	51.91	207.73	0.998/0.036

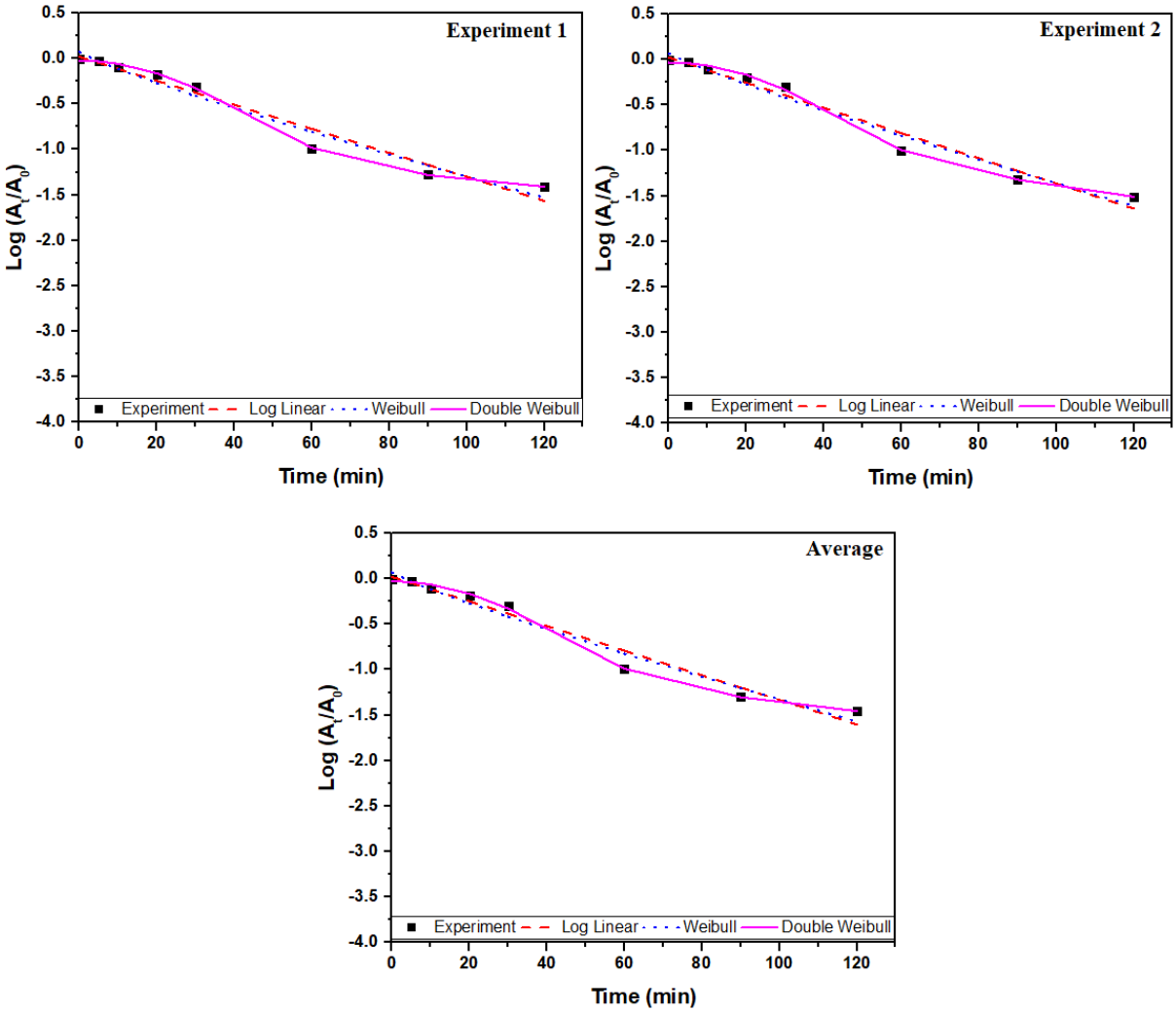

Figure 4. 17 Fitting of mathematical models to the inactivation curve of *E.coli* through the UV irradiation treatment.

In the case of the H_2O_2 with UV light (Figure 4.18), the Weibull and double Weibull model attained the best fit for the average of the *E. coli* inactivation results with R^2 value of 0.99 in both the cases, whereas RMSD is 0.05 for double Weibull and 0.09 for Weibull model. Comparing both the treatment techniques using the inactivation rate constants (k) and the first decimal reduction parameters (δ) showed minute variations among these treatments as observed in Table 4.3 and Table 4.4. By taking into consideration the double Weibull model, the first decimal reduction parameters of the two sub-populations of *E. coli* in the only UV technique were δ_1 = 51.9 min and δ_2 = 207.7 min (Table 4.3), whereas in the H_2O_2 with UV technique, the δ_1 was 34.05 min and δ_2 was 100.95 min as shown in Table 4.4. While comparing the aforementioned techniques through the double Weibull model, the addition of

H_2O_2 with UV is insufficient in improving the *E. coli* inactivation for the selected exposure time in this study. Thus achieving minute change in the rate of reaction and the inactivation level as compared to the only UV technique. Therefore, the results obtained through these techniques are perfectly fitted using the double Weibull model where it is assumed that the two distinct sub-population groups (sub-population 1, which are sensitive cells and inactivates at a short period (δ_1) and Sub-population 2, more resistant and takes more to inactivate (δ_2) are present with different levels of resistance to the disinfection treatment.

Table 4. 4 Kinetic parameters of mathematical models used in the inactivation of *E. coli* by H_2O_2/UV treatment

Treatment	Models	K (min^{-1})	δ_1(min)	δ_2(min)	R^2/RMSD
Assay 1	Log-linear	0.04	-	-	0.985/0.106
	Weibull	-	63.83	-	0.991/0.088
	Double Weibull	-	35.15	104.29	0.998/0.044
Assay 2					
	Log-linear	0.04	-	-	0.985/0.109
	Weibull	-	61.53	-	0.991/0.094
	Double Weibull	-	32.4	96.87	0.997/0.056
Average					
	Log-linear	0.04	-	-	0.985/0.107
	Weibull	-	62.67	-	0.991/0.090
	Double Weibull	-	34.05	100.95	0.997/0.051

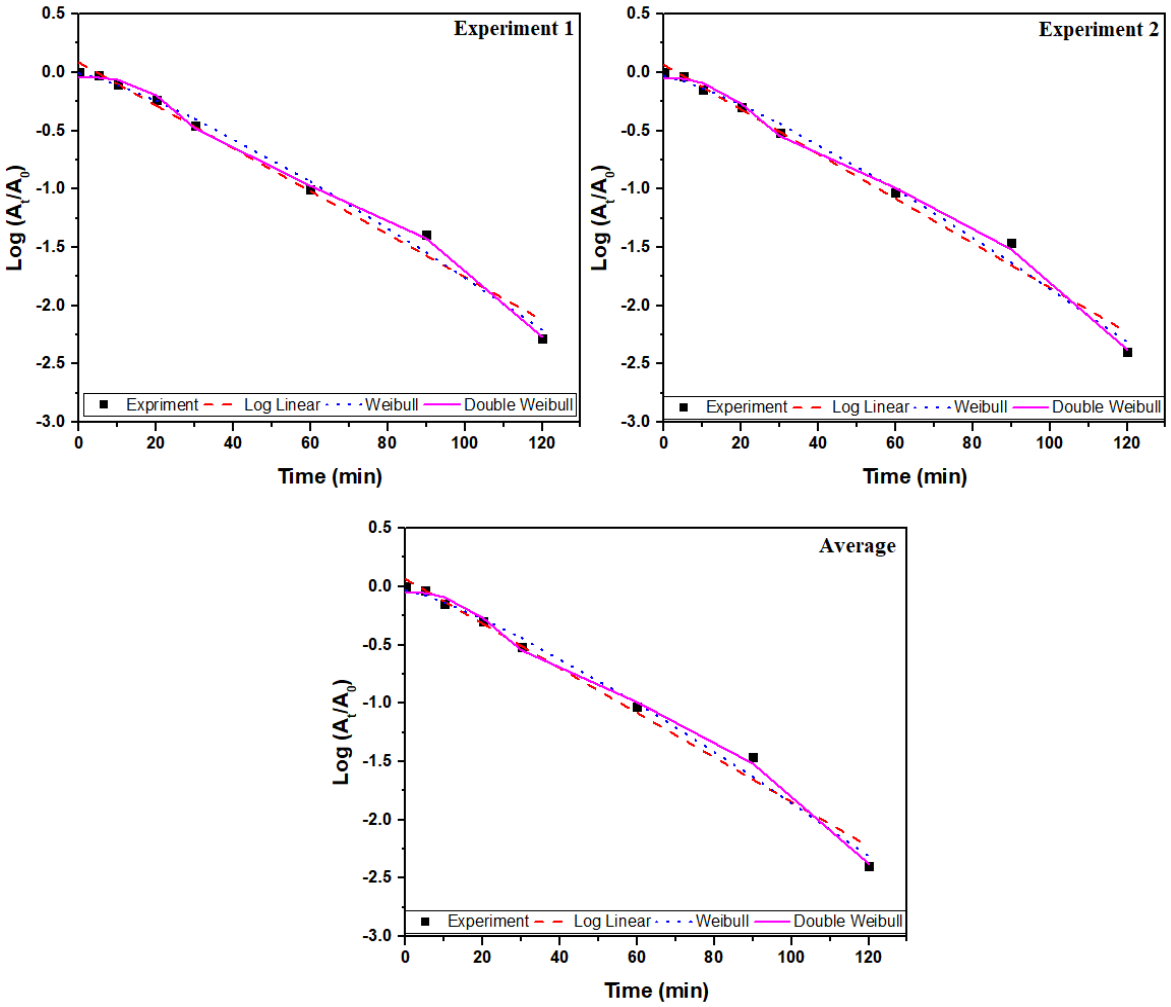

Figure 4. 18 Fitting of mathematical models to the inactivation curve of *E.coli* through the UV/H_2O_2

4.4.1.2 TiO_2 assisted photocatalysis in fixed mode

The TiO_2-photocatalysts coated over clay beads were evaluated for their potential to inactivate the *E. coli* in water under UVA radiation (24 Wm^{-2}) and the results obtained are shown in Figure 4.16. Almost 3.27 log reduction in the *E. coli* population was observed with TiO_2 coated beads upon irradiation for 120 min. These results are consistent with the previous results reported in the literature. For instance, (Adán et al., 2018) studied the *E. coli* inactivation using TiO_2 coated glass raschings and obtained approximately a similar log reduction in 120 min of reaction time. This low inactivation efficacy of the current study might be due to fast e^--h^+ recombination in the semiconductor leading to less production of reactive oxygen species, which ultimately reduces the efficacy of the system (Kang et al., 2019). It can be seen from Figure 4.16 that initially the rate of log reduction is slower and

increases with an increase in the treatment time, thus confirming that the reaction time plays an important role in the bacterial reduction.

It was observed from Figure 4.19 that all the applied mathematical models showed a good fit when TiO_2 assisted photocatalytic technique in a fixed bed was employed. But the perfectly fitted curve was obtained with Weibull and double Weibull distribution models, taking into account the R^2 values (0.99 and 0.98 respectively) and RMSD values (0.02 and 0.1, respectively) as shown in Table 4.5. To understand the influence of different agents on *E.coli* inactivation rate, kinetic modeling is used. Therefore, the k and δ values shown in Table 4.5 in comparison to the values in Table 4.3 (only UV) and Table 4.4 (H_2O_2 with UV) indicate a higher inactivation rate of *E. coli* in the TiO_2 assisted photocatalytic. Therefore, comparing the k and δ values of the average fitted curve obtained by the log-linear and Weibull models showed that the TiO_2 assisted photocatalysis in fixed mode ($k = 0.06\ min^{-1}$; $\delta = 53.32$ min) was significantly faster than the only UV ($k = 0.03\ min^{-1}$; $\delta = 68.13$ min) and H_2O_2 with UV technique ($k = 0.04\ min^{-1}$; $\delta = 62.6$ min).

Table 4. 5 Kinetic parameters of mathematical models used in the inactivation of *E. coli* by TiO_2-photocatalysis treatment.

Treatment	Models	K (min^{-1})	δ_1(min)	δ_2(min)	R^2/RMSD
Assay 1	Log-linear	0.06	-	-	0.968/0.228
	Weibull	-	56.02	-	0.989/0.147
	Double Weibull	-	24.53	78.78	0.999/0.035
Assay 2					
	Log-linear	0.06	-	-	0.977/0.202
	Weibull	-	50.11	-	0.990/0.148
	Double Weibull	-	21.07	72.18	0.998/0.035
Average					
	Log-linear	0.06	-	-	0.973/0.219
	Weibull	-	53.32	-	0.989/0.147
	Double Weibull	-	23.13	76.02	0.999/0.028

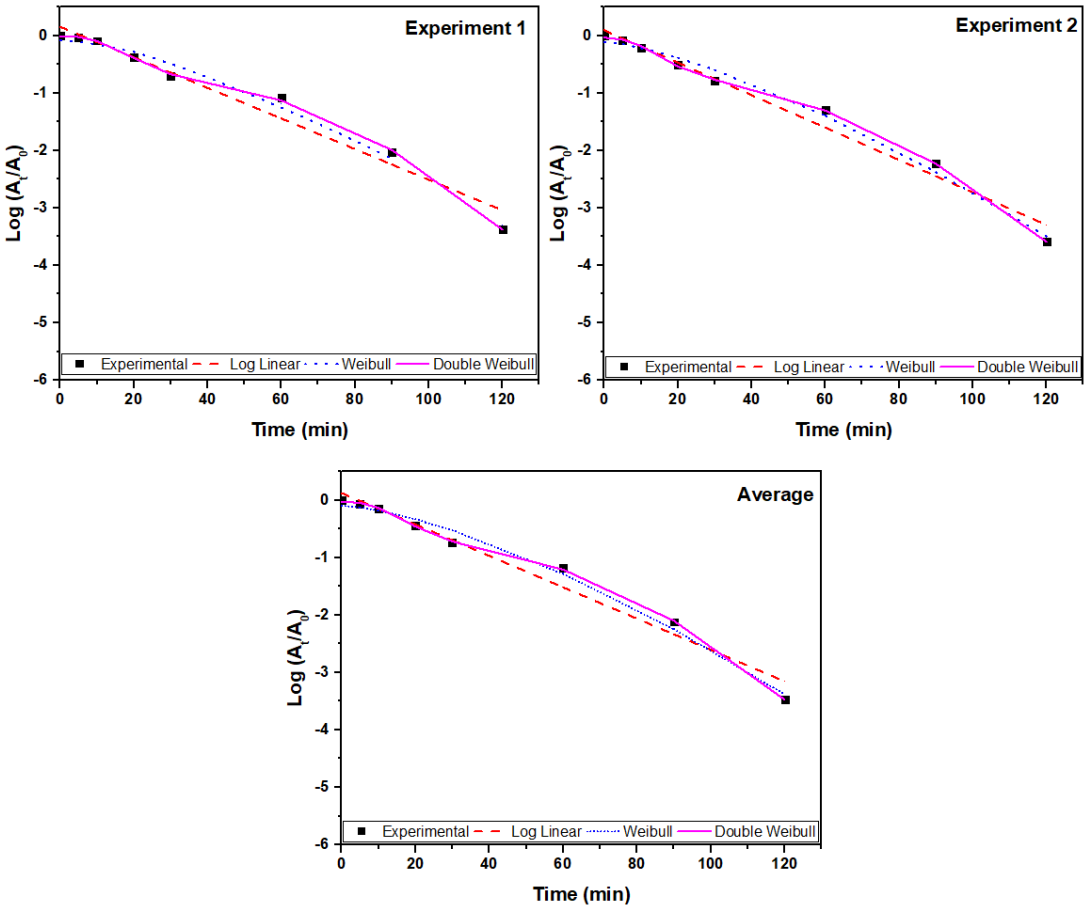

Figure 4. 19 Fitting of mathematical models to the inactivation curve of *E.coli* through the TiO_2-photocatalysis treatment.

4.4.1.3 Photo-Fenton in fixed mode

For executing the fixed bed photo-Fenton technique, the iron was made to leach from the composite beads by maintaining the acidic conditions (pH = 3.5), and Figure 4.16 showed a demonstration of the corresponding inactivation values. Leaching of the iron from the clay always happens in acidic conditions because it helps in tearing the bond of iron with other organic compounds and causes the extraction of iron known as iron leaching (Hseu, 2004). 0.3 g L^{-1} of H_2O_2 concentration (0.25 mL) was added for the photo-Fenton to take place. It was observed that this treatment achieved a 3.79 log reduction in *E. coli* after 120 min of treatment. It was observed from Figure 4.20 that all the applied mathematical models showed a good fit when the photo-Fenton technique in a fixed bed was employed. But the perfectly fitted curve was obtained with Weibull and double Weibull distribution models, taking into account the R^2 values (0.98 for both models) and RMSD values (0.2 for both models). While considering the double Weibull model as shown in Table 4.6, the first decimal reduction

parameters were δ_1 = 17.66 min and δ_2 = 33.53 min of the two sub-populations of *E. coli* inactivation in the photo-Fenton process.

Table 4. 6 Kinetic parameters of mathematical models used in the inactivation of *E. coli* by photo-Fenton treatment

Treatment	Models	K (min^{-1})	δ_1(min)	δ_2(min)	R^2/RMSD
Assay 1	Log-linear	0.07	-	-	0.9606/0.274
	Weibull	-	19.16	-	0.9811/0.203
	Double Weibull	-	18.64	78.06	0.9969/0.094
Assay 2					
	Log-linear	0.08	-	-	0.9618/0.310
	Weibull	-	17.72	-	0.9825/0.23
	Double Weibull	-	19.31	73.65	0.998/0.079
Average					
	Log-linear	0.07	-	-	0.9604/0.29
	Weibull	-	19.07	-	0.9814/0.218
	Double Weibull	-	17.66	33.53	0.9821/0.23

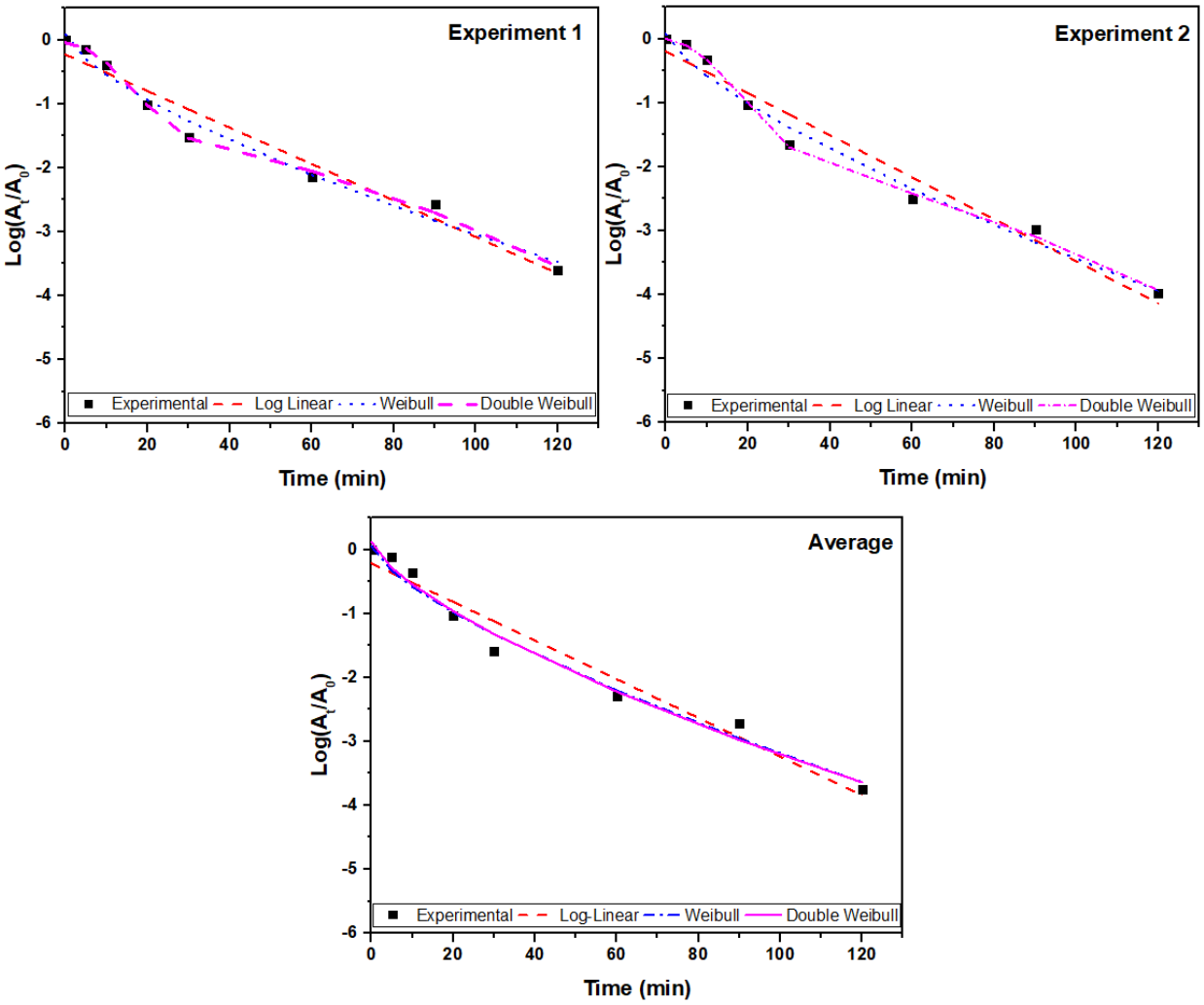

Figure 4. 20 Fitting of mathematical models to the inactivation curve of *E.coli* through the photo-Fenton treatment.

4.4.1.4 Hybrid technique in fixed mode

The in-situ hybrid technique was executed using Fe-TiO_2 composite beads through subsequent leaching of iron and surface-active TiO_2 coating. This process was marked by parallel execution of both processes of photo-Fenton and TiO_2-assisted photocatalysis in a fixed mode. This hybrid technique yielded the highest log reduction of 6.4 as compared to the photo-Fenton and TiO_2-assisted photocatalysis individually, as shown in Figure 4.16. This might be due to its ability to restrict the e^- h^+ recombination occurring in TiO_2 photocatalysis by combining the ferric ion produced from the photo-Fenton technique with e^- present the conduction band of TiO_2 to produce ferrous ions. Hence, this leads to the photo-Fenton process in recurring mode with no sludge formation. The addition of H_2O_2 in the system

played a hybrid role and engaged in reaction with both TiO_2 and iron for the generation of more OH^o in the treatment system. The hybrid mechanism eventually led to an almost double reaction rate in comparison to the photo-Fenton and TiO_2-assisted photocatalysis in fixed mode. The proposed hypothesis has led to the concept of synergy that exists between these three processes. Leaching of the iron in the system in terms of total, ferrous and ferric ion was also determined to confirm the occurrence of the photo-Fenton process. The maximum concentration of total iron, ferric ion, and ferrous ion was found to be (166 μgL^{-1}, 103 μgL^{-1}, and 63 μgL^{-1} respectively) as shown in Figure 4.21. The amount of iron present in the system is less as compared to the other studies (Mosteo et al., 2020; Shekoohiyan et al., 2019), yet have shown better results in less treatment time. A higher concentration of iron in the system only hinders the bacterial inactivation due to light scattering and decreases direct UV-A irradiations. The mechanism of killing *E. coli* will remain the same as discussed above.

The results obtained after inactivating *E. coli* in the hybrid (photo-Fenton + photocatalysis) process in fixed mode, all employed mathematical models showed a good fit as given in Figure 4.22. But, the best-fitted curve was obtained with the Weibull and double Weibull distribution models, considering the R^2 and RMSD values of 0.99 and 0.2 for both the models, respectively. In comparing the k and δ as given in Table 4.7 the rate of *inactivating E. coli* increased in the hybrid process in comparison to the TiO_2 assisted photocatalysis as shown in Table 4.5 and photo-Fenton treatments as shown in Table 4.6. Thus considering the kinetic parameters such as "k" of log-linear and "δ" of double Weibull for fitting the *E. coli* inactivation results and comparing the different techniques showed that the hybrid-technique in fixed mode ($k = 0.16\ min^{-1}$; $\delta_1 = 8.63$ min, $\delta_2 = 27.7$ min) proved to be significantly faster in comparison to other techniques; TiO_2 assisted photocatalysis ($k = 0.6\ min^{-1}$; $\delta_1 = 23.1$ min, $\delta_2 = 76$ min); photo-Fenton ($k = 0.07\ min^{-1}$; $\delta_1 = 17.66$ min, $\delta_2 = 33.53$ min; H_2O_2 with UV ($k = 0.04\ min^{-1}$; $\delta_1 = 34.05$ min, $\delta_2 = 100.95$ min) and Only UV($k = 0.03\ min^{-1}$; $\delta_1 = 51.91$ min, $\delta_2 = 207.73$ min. Thus inactivation efficiency of *E.coli* using different oxidation processes on the bases of the rate constant can be ranked as:

Hybrid > photo-Fenton > photocatalysis > UV+H_2O_2 > UV only

Table 4. 7 Kinetic parameters of mathematical models used in the inactivation of *E. coli* by hybrid treatment

Treatment	Models	K (min^{-1})	δ_1(min)	δ_2(min)	R^2/RMSD
Assay 1	Log-linear	0.17	-	-	0.980/0.299
	Weibull	-	17.90	-	0.992/0.271
	Double Weibull	-	12.75	26.23	0.993/0.279
Assay 2					
	Log-linear	0.16	-	-	0.982/0.295
	Weibull	-	19.48	-	0.981/0.287
	Double Weibull	-	7.35	30.16	0.994/0.23
Average					
	Log-linear	0.16	-	-	0.985/0.287
	Weibull	-	18.56	-	0.991/0.270
	Double Weibull	-	8.63	27.77	0.994/0.257

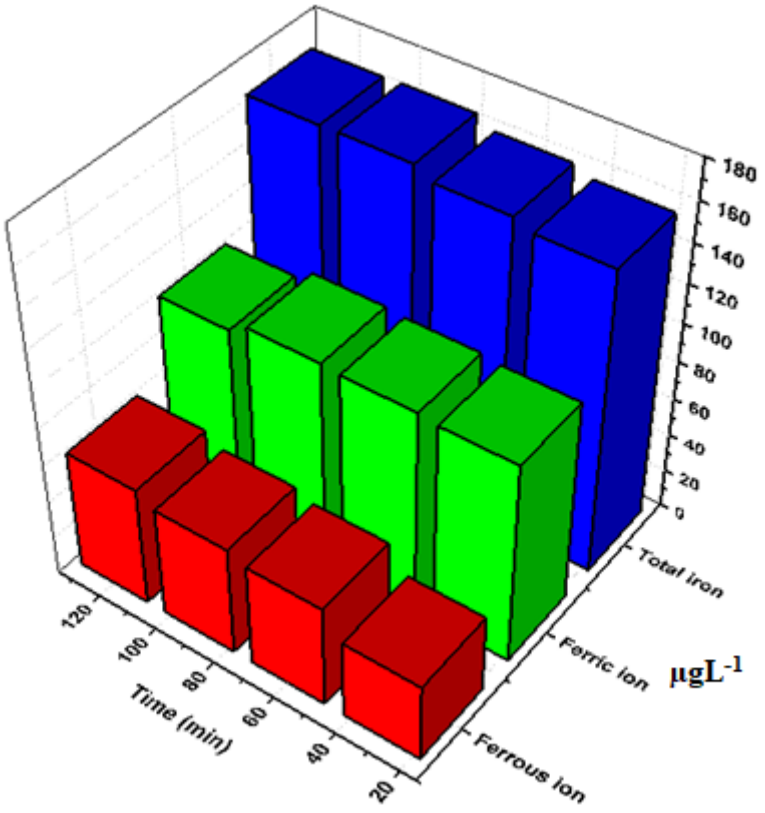

Figure 4. 21 Iron concentration present in the hybrid process

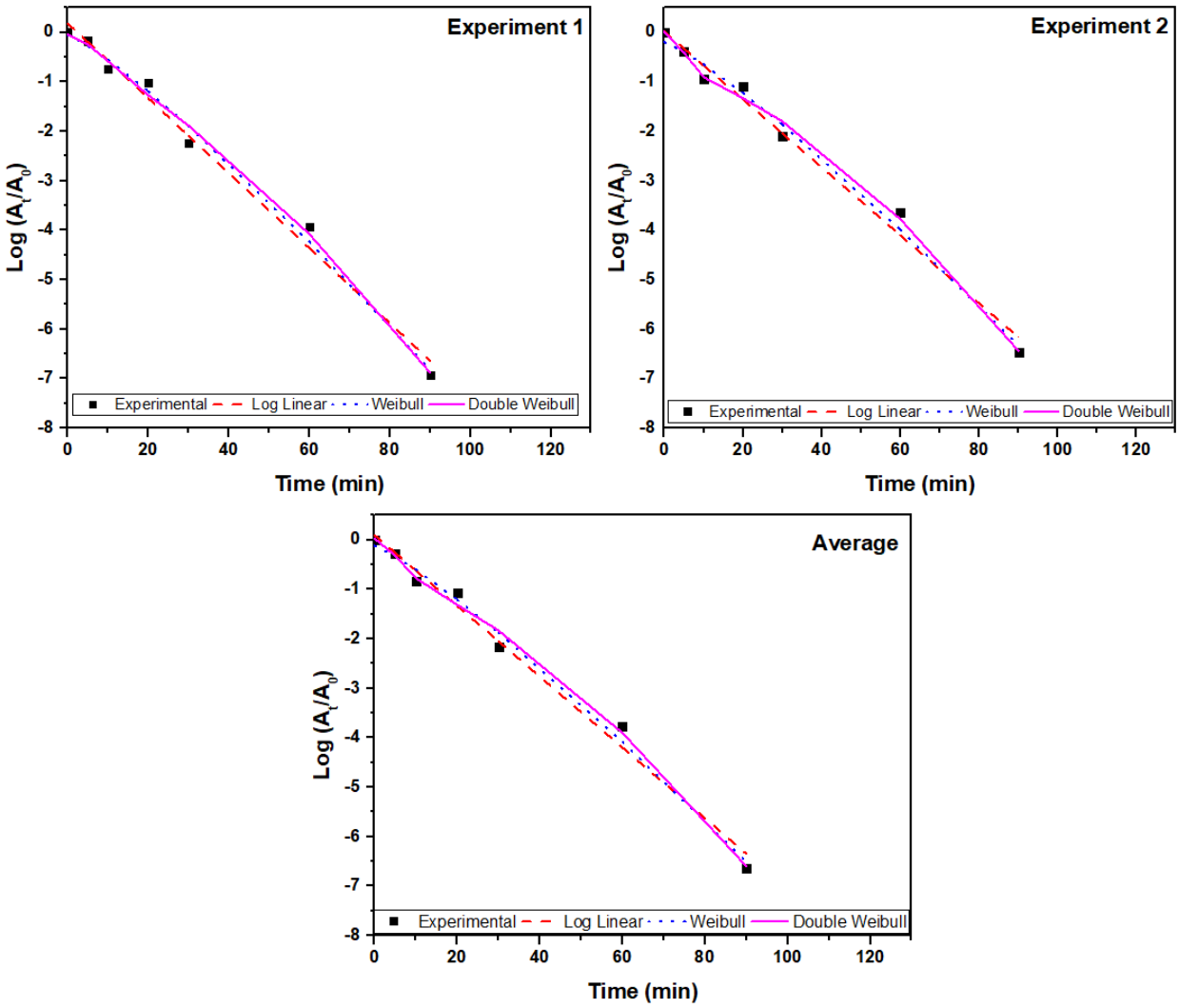

Figure 4. 22 Fitting of mathematical models to the inactivation curve of *E.coli* through the hybrid process.

4.5 Section B (Scale-up studies using Fe-TiO_2 composite beads)

To promote the applicability of AOPs at the field scale in near future, it is mandatory to execute the scale-up trails of lab-scale results. The established in-situ hybrid effect in the present study using composite beads was scaled up for the disinfection of *E. coli* with the development of pilot-scale solar reactors. Fe-TiO_2 composite beads were selected for the scale-up studies especially given their extended recyclability efficacy (> 50 recycles), which has not been achieved with any other type of support reported in the literature. Moreover, the inexpensive nature of these Fe-TiO_2 composite beads would expectedly make the process cost-effective. The pilot-scale reactors taken into consideration for the present study were UV-assisted re-circulation type fixed-bed glass reactor and solar once through cascade

reactor with a total working volume of 2 L and 6 L, respectively. The detailed cost of the process has been evaluated using each type of reactor.

4.5.1 Fe-TiO_2 composite mediated hybrid effect for the inactivation of *E. coli* using a continuous flow recirculation reactor

The feasibility of the in-situ hybrid process employing Fe-TiO_2 composite beads was checked in a pilot-scale solar non-concentrating flat-bed reactor (Figure 4.23) made up of glass with volume handling of 2 L. The in-situ hybrid process was intensified with proper optimization of operating parameters taking *E. coli* as a target pollutant. The performance of the hybrid process (Fe-TiO_2) was evaluated in terms of reaction rate constant, and some other operating parameters. This hybrid process showed a significant increase in reaction rate constant (0.065 min^{-1}) compared to photo-Fenton (0.029 min^{-1}) and photocatalysis (0.025 min^{-1}) in 150 min treatment time. The P-value was less than 0.0001 and the F-value was greater than 5 for each process. The optimized values of the operating parameters were found to be 3.5, 62 mg L^{-1}, 106 mL min^{-1} for the reaction pH, H_2O_2 concentration, and flow rate, respectively. With these optimum conditions, a percentage reduction of *E. coli* of 93% was observed. This significant increase in *E. coli* disinfection in the presence of Fe-TiO_2 composite can indeed be credited to the in-situ hybrid effect caused by the systematic lixiviation of iron from the composite beads in a reactor containing working solution via the composite, which contributes to the photo-Fenton process along with TiO_2-photocatalysis. The synergistic effect of the hybrid process over photocatalysis was observed to be 61 % and over photo-Fenton was 55 %. The overall synergy of the hybrid process came out to be 17 %. The Fe-TiO_2 composites exhibited high stability under continuous flow conditions, demonstrating their long-term durability.

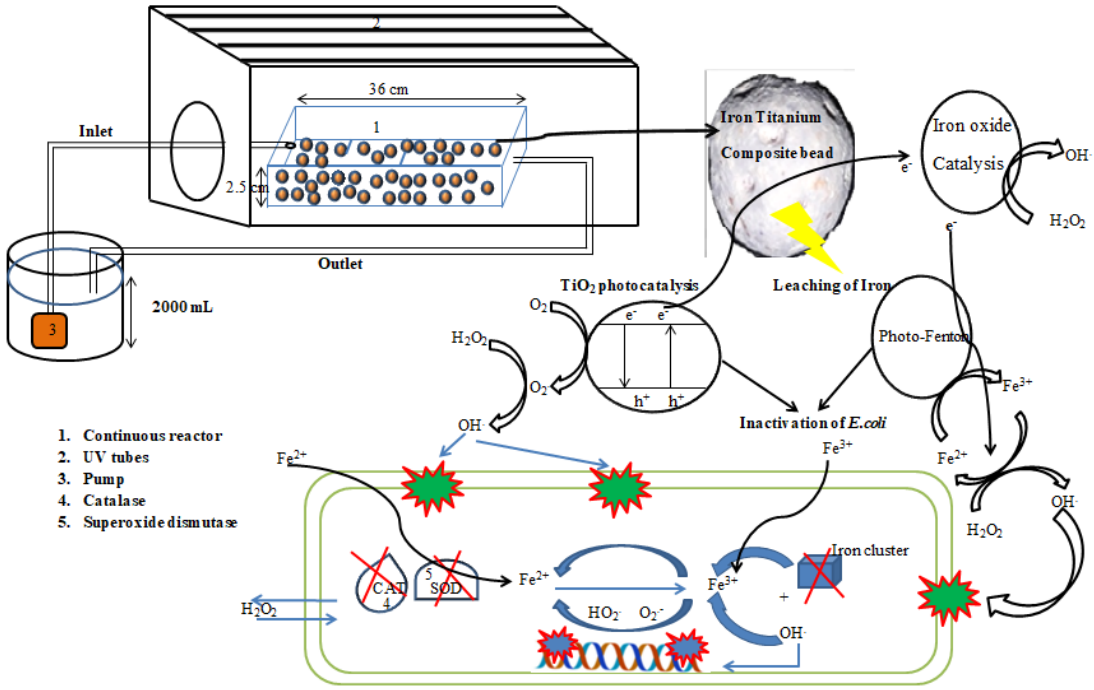

Figure 4. 23 Schematic diagram of *E. coli* inactivation in the recirculating reactor

4.5.1.1 Preliminary study and efficacy of the hybrid process

In order to confirm the efficacy of the hybrid process and to establish the boundary conditions, the preliminary tests were done, the results of which are shown in Figure 4.24 (a). All these preliminary experiments (both in the dark and under UV light) were done using H_2O_2 =100 mg L^{-1}, pH=3-3.5, and flow rate =110 mL min^{-1}. It can be seen from Figure 4.24 (a) that in the dark condition, the *E. coli* concentration (Log C/C_0) showed minimal variation with time for the only dark, Fe + dark, and H_2O_2 + dark conditions. These results were in agreement with the results reported in previous studies (Alrousan et al., 2012; Giannakis et al., 2018c). However, Fenton in dark shows the maximum log reduction of 0.1. Lixiviation of iron from the catalytic beads under acidic conditions in the dark showed a very little effect of 0.038 log units reduction in 150 min. The maximum unit log reduction due to H_2O_2 in the dark is found to be 0.07.

After the baseline was established by preliminary experiments, the experiments were performed under UV light (365 nm) with an average intensity of 25 Wm^{-2} to create a photocatalytic environment. Under the simulated photocatalysis environment, the inactivation of *E. coli* was carried out using TiO_2-coated clay beads. For the photo-Fenton process, the experiments were carried out under acidic conditions since acidic conditions are responsible for the lixiviating of iron from the catalytic beads.

In UV-A treatment without any catalyst for *E. coli* inactivation, it was observed that no reduction (less than 1) in log units of *E. coli* was achieved after 150 min of irradiation, as shown in Figure 4.24 (b). During photocatalysis in a fixed bed, only a 2.2 log unit reduction of *E.coli* was observed as shown in Figure 4.24 (b). The results showed a very low inactivation efficacy of the current system. The photo-Fenton experiments (Figure 4.24 b), consisting of TiO_2 coated composite beads (clay + FA + FS) and 100 mg L^{-1} of H_2O_2, showed a unit log reduction of 2.3 in 150 min. However, in a hybrid process where photo-Fenton and photocatalysis were used simultaneously in one system, it was found that the log unit reduction increased to 4.3. Thus, the inactivation efficacy of *E. coli* with different oxidation processes can be ranked as follows:

hybrid > photo-Fenton > photocatalysis > UV+H_2O_2 > UV only

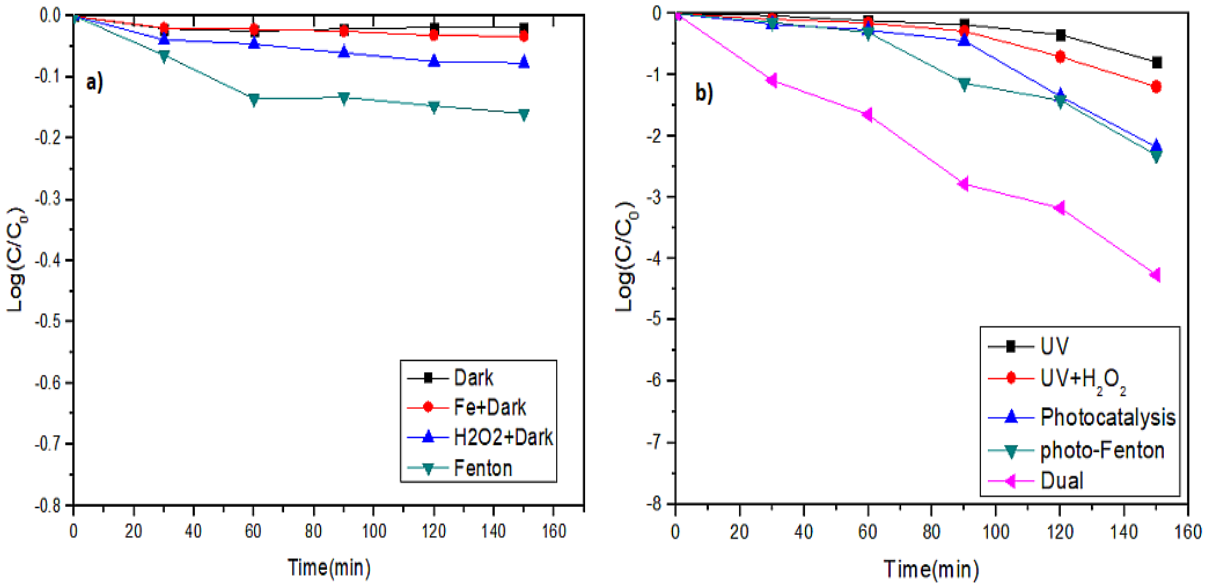

Figure 4. 24 (a) *E. coli* inactivation with and without iron and oxidant dose in the dark (b) *E. coli* inactivation with various technologies

4.5.1.2 Development and evaluation of predicted study

To analyze the photocatalytic disinfection of water, four different operating parameters pH (3-6), H_2O_2 dose (30-120 mg L^{-1}), flow rate (100-400 mL min^{-1}), time (30-150 min) as shown in Table 4.8 were optimized under RSM using Box Behnken Design (BBD). A total of 29 experiments were proposed by BBD and are shown in Table 4.9 with the percentage reduction of *E. coli*. By exploiting the sequential F-test, a quadratic model was proposed. For the response (percentage reduction), it was found that Adequacy Precision is 12.696. Adequacy Precision estimates the signal-to-noise ratio, and a ratio greater than 4 is desirable. Therefore, this model can be used to navigate the design space (Talwar et al., 2018).

The normal probability plot of the internally studentized residuals can be examined to assess the acceptability of the model. It can be seen from (Figure 4.25) that all the residuals are well distributed along the straight lines, indicating that there is no significant departure from the assumptions underlying the analysis (Feilizadeh et al., 2015a). Statistical analysis of the percentage of *E. coli* in water was carried out using ANOVA and the model was found to be significant with an F-value of 11.45. For % reduction of *E. coli*, time was found to be a highly significant variable, and flow rate, time^2, and interaction between time and flow rate were the significant variables as shown in Table 4.10. This method provides a second-order statistical model for *E. coli* inactivation rate in terms of coded factors, as shown in Equation (4.13).

$$\boldsymbol{R} = 95.10 - 2.06x_1 + 1.67x_2 - 4.02x_3 + 15.70x_4 - 0.48x_1^2 + 3.05x_2^2 + 0.33x_3^2 - 12.07x_4^2 - 0.33x_1x_2 + 1.43x_1x_3 + 2.72x_1x_4 - 0.33x_2x_3 - 2.50x_2x_4 + 8.92x_3x_4 \quad (4.13)$$

Where x_1 is pH, x_2 is H_2O_2 dose (mg L^{-1}), x_3 is the flow rate (mL min^{-1}), x_4 is time (min), and R is a percentage reduction of *E. coli* in water. The positive and negative signs before the terms represent the encouraging and opposing effects of the parameters.

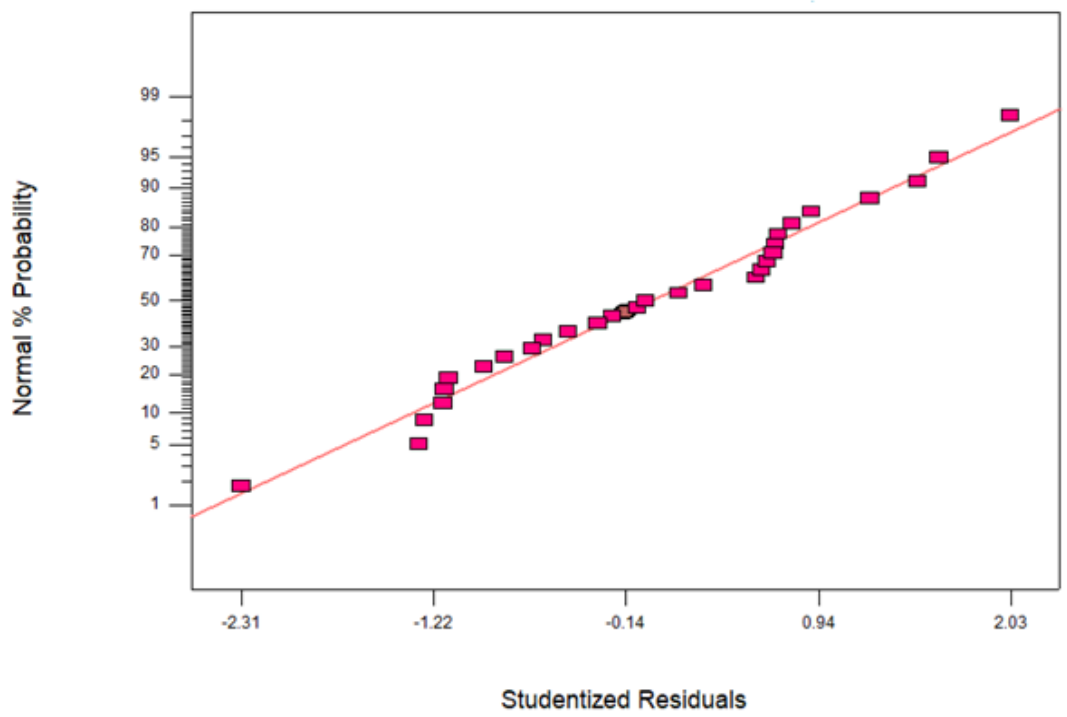

Figure 4. 25 A plot of normal probability vs. internally studentized residuals of the response

Table 4. 8 Levels of the factors tested in the Box−Behnken experimental design

S. No.	Variable	-1	0	-1
1	pH	3	4.5	6
2	H_2O_2 (mg L^{-1})	30	75	120
3	Flow rate (mL min^{-1})	100	250	400
4	Time (min)	30	90	150

Table 4. 9 Full Factorial BBD matrix with 4 independent variables

Experiment No.	x_1 pH	x_2 H_2O_2 (mg L^{-1})	x_3 Flow rate (mL min^{-1})	x_4 Time (min)	R % reduction of *E.coli*
1	3	75	400	90	97.6
2	4.5	75	250	90	98.17
3	3	75	100	90	99.48

4	4.5	30	100	90	96.39
5	3	75	250	150	99.8
6	4.5	120	250	30	81.68
7	4.5	75	250	90	90.10
8	4.5	75	250	90	89.01
9	4.5	30	400	90	95.9
10	4.5	75	400	30	46.6
11	4.5	120	400	90	98.1
12	4.5	75	100	30	82.7
13	6	75	250	150	99.45
14	4.5	75	100	150	99.88
15	4.5	120	250	150	99.88
16	4.5	120	100	90	99.85
17	6	75	250	30	58.07
18	3	120	250	90	99.30
19	4.5	75	250	90	98.1
20	6	120	250	90	95.6
21	6	75	100	90	99.39
22	3	30	250	90	97.27
23	4.5	75	400	150	99.46
24	4.5	30	250	150	99.7
25	4.5	30	250	30	71.49
26	4.5	75	250	90	98.05
27	6	75	400	90	91.8
28	6	30	250	90	93.7
29	3	75	250	30	69.28

Table 4. 10 Analysis of variance for the response rate of *E. coli* elimination

Source	Sum of square	Df	Mean square	F value	P>F	
Model	4762.88	14	340.0	11.45	<0.0001	**Significant**
x_1	51.13	1	51.13	1.72	0.2107	
x_2	33.33	1	33.33	1.12	0.3075	
x_3	194.57	1	194.57	6.55	0.0227	**Significant**
x_4	2956.31	1	2956.31	99.49	<0.0001	**Highly Significant**
x_1^2	0.45	1	0.45	0.015	0.9038	
x_2^2	68.53	1	68.53	2.31	0.1511	
x_3^2	1.91	1	1.91	0.064	0.8035	
x_4^2	912.91	1	912.91	30.72	<0.0001	**significant**
x_1x_2	4.225E-003	1	4.225E-003	1.422E-004	0.9907	
x_1x_2	8.10	1	8.01	0.27	0.6118	
x_1x_4	29.48	1	29.48	0.99	0.3361	
x_2x_3	0.42	1	0.42	0.14	0.9068	
x_2x_4	25.05	1	25.05	0.84	0.3741	
x_3x_4	318.27	1	318.27	10.71	0.0056	**Significant**
Residual	416	14	29.71			
Lack of fit	327.64	10	32.76	1.48	0.3751	**Not Significant**
Pure error	88.36	4	22.09			
Core error	5178.87	28				

4.5.1.3 Optimization of different parameters

The effect of oxidant dose (H_2O_2), pH and flow rate on percentage reduction of *E. coli* as a function of time was studied. The oxidant dose plays an important role in increasing the percent reduction of *E. coli* by adding additional OH^o to the system. However, in the current study, H_2O_2 is consumed simultaneously in both the photocatalytic and photo-Fenton processes by reacting with the e^-_{CB} and preventing e^--h^+ recombination. In this study, the H_2O_2 concentration was varied from 30 to 120 mg L^{-1}. From Figure 4.26 (a), it can be seen that a marginal reduction was observed when the H_2O_2 concentration was less than 75 mg L^{-1}. However, when the H_2O_2 dose was increased from 75-120 mg L^{-1}, a high reduction of *E. coli* was observed with increasing treatment time. In Figure 4.26 (b), it was observed that at the lower H_2O_2 dose (30-75 mg L^{-1}) and pH (4.5), the percentage reduction increased with time.

As the pH increased from 4.5 to 6, the percentage reduction decreased and showed minimal changes in *E. coli* concentration with time. This could be due to the hydrolysis of Fe^{3+} and precipitation of FeO(OH) complex, which eventually decreases the production of $OH^o$and ultimately affects the *E. coli* reduction rate (Bansal and Verma, 2017a). The effect of time and pH on the % reduction of *E.coli* with the change in H_2O_2 dose can be seen in Figure 4.26 (a). With increasing time at lower pH, the % reduction was observed to be high, but when pH increases from 4.5-6; it led to a decrease in the % reduction with time corresponding to a decrease in H_2O_2 dose.

In this study, the flow rate was also varied from 100 to 400 mL min^{-1}. From Figure 4.26 (c), it can be seen that when the flow rate of the reactor was increased from 250 mL min^{-1} to 400 mL min^{-1}, there was less change in the percentage reduction of *E. coli*. This can be attributed to the fact that as the flow rate increases, the contact time of *E. coli* with the catalytic particles decreases. It leaves the reactor without any significant contact with the catalytic particles, thus decreasing the inactivation efficacy. However, when the flow rate was reduced to 100 mL min^{-1}, the percentage reduction of *E. coli* increased with an increase in treatment time. From Figure 4.26 (d), it can be seen that the percentage reduction of *E. coli* was lower when the flow rate was high (400 mL min^{-1}), pH was high (4.5-6) and the oxidant dosage was low (H_2O_2 30-70 mg L^{-1}) than when the flow rate was reduced to 100 mL min^{-1} under the same conditions. With increasing time at low pH (3.5), high H_2O_2 (120 mg L^{-1}), and lower flow rate, the percent reduction of *E. coli* increased. However, the percentage reduction decreased with time when the flow rate of the reactor was increased. In Table 4.9,

as expected, low reduction values (46.6% and 58.0%) were obtained when the flow rate was higher and the contact time was correspondingly lower.

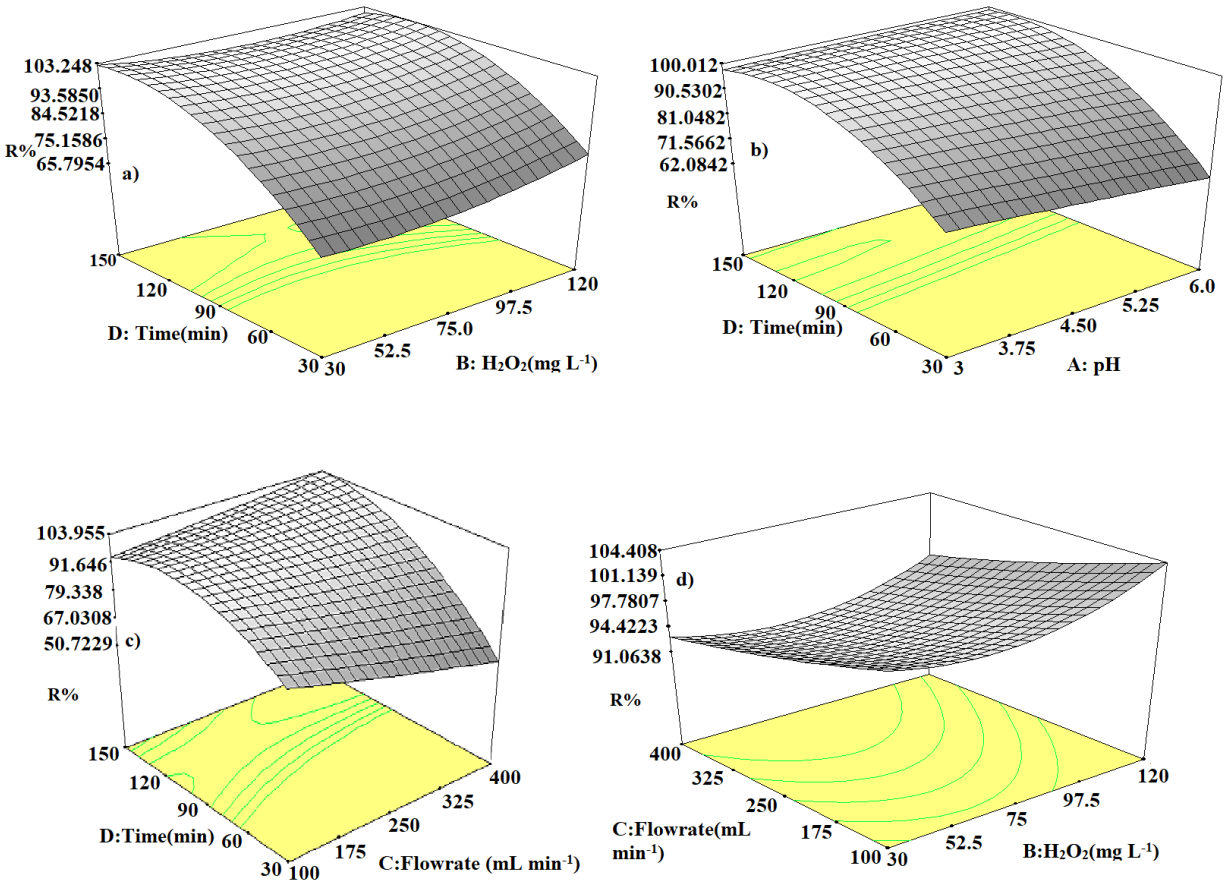

Figure 4. 26 % reduction of *E. coli* 3D response surface graph (a) % reduction 3D diagram of H_2O_2 Dose with time (b) % reduction 3D diagram of pH with time (c) % reduction 3D diagram of flow-rate w.r.t time (d) % reduction 3D diagram of flow-rate with H_2O_2

Based on the proposed model, Design-Expert® software was used for parametric optimization to inactivate *E. coli*. The optimized values of the operating parameters were found to be 3.5, 62 mg L^{-1}, 106 mL min^{-1} and 105 min for the reaction pH, H_2O_2 concentration, flow rate, and reaction time, respectively. With these optimal conditions, the percent reduction of *E. coli* was predicted to be 94.6%. The reason for selecting these particular values coincides with the rationale of minimal use of H_2O_2 dose, lower treatment time, and lower flow rate. To confirm the accuracy of the optimized results, experiments were conducted under the same conditions and a 93% reduction in *E. coli* concentration was observed. This slight change in the percentage reduction of *E. coli* shows good agreement

between predicted and experimental values. It suggests that RSM is a useful tool for optimizing hybrid (photo-Fenton and photocatalysis) disinfection processes. The concentration of iron species leaching out of composite beads from fresh and recycled beads was estimated and listed in Tables 4.11 & 4.12 during the in-situ hybrid process in a recirculating reactor.

Table 4. 11 Concentration of iron species leaching out of fresh composite beads

Time (min)	Concentration (µg L^{-1})		
	Ferrous ions	Ferric ions	Total Iron
30	41.154	36.923	80.769
60	46.154	38.461	84.615
90	50	39.615	89.615
120	55.385	33.846	89.231
150	61.154	30.769	91.923

Table 4. 12 Concentration of iron species leaching out of recycled composite beads

Time (min)	Concentration (µg L^{-1})		
	Ferrous ions	Ferric ions	Total Iron
30	40.769	38.846	79.615
60	41.923	37.692	79.615
90	45	39.615	84.615
120	52.692	33.077	85.769
150	52.692	36.923	89.615

4.5.2 Extended durability study

One of the novel findings of this study is the extended durability of reported Fe-TiO_2 composite beads in terms of exhibiting log term in-situ hybrid effects. Thus to confirm our claim, the parametric optimization studies were performed with Fe-TiO_2 composite beads previously used for at least 50 cycles. In the recycling tests, our reported approach needs to confirm both sustainable leaching of iron as well as stability of TiO_2 coating over the composite. The recyclability efficacy of Fe-TiO_2 composite beads was evaluated in terms of

the disinfection efficacy of *E. coli* with subsequent recycles. These catalytic beads were again reused 50 times and only an 11% decrease in the photoactivity of the catalytic beads was observed, as shown in Figure 4.27. The corresponding lixiviating of iron from the beads was also verified by measuring the concentration of iron in the solution at the beginning and the end of the study, as shown in Tables 4.11 & 4.12. This confirms that a sufficient quantity of catalyst particles was intact to the surface even in the recycled composite beads. It was found that there was sufficient iron concentration in the system before and after recycling to perform the photo-Fenton reaction. The intactness and stability of TiO_2 on the composite beads were also verified by various characterization techniques as described in the next section confirming the presence of photocatalysis in the system.

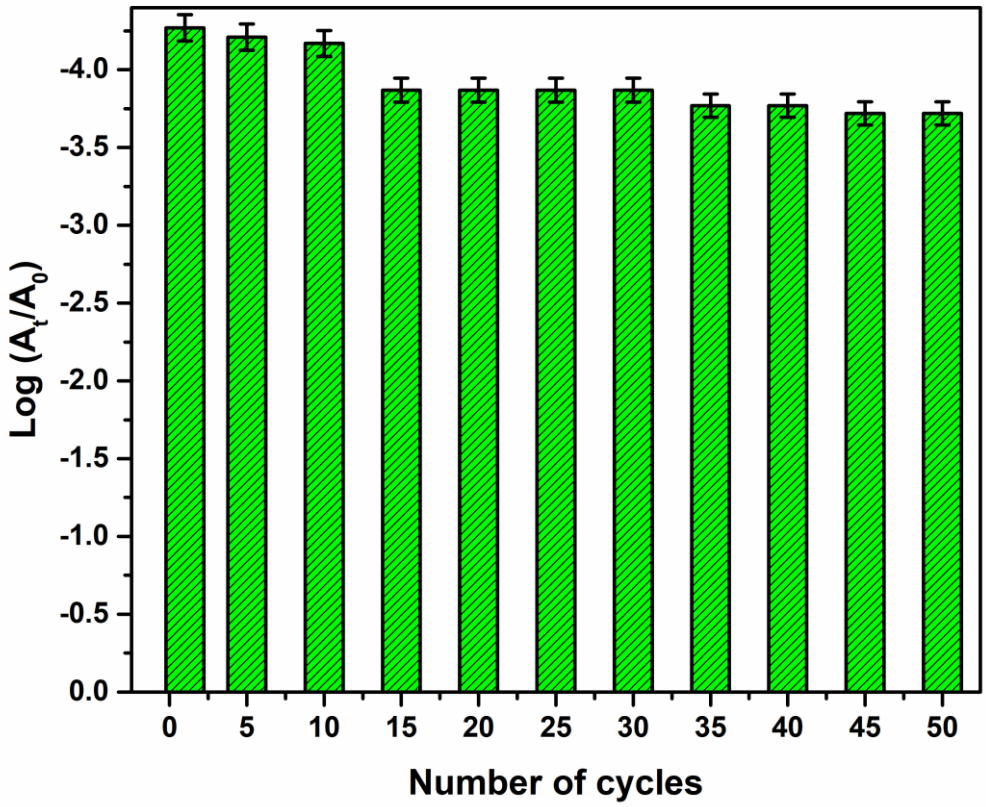

Figure 4. 27 Recyclability study of composite beads for *E.coli* inactivation

4.5.3 Characterization of Fe-TiO_2 composite

The intactness of catalyst particles (TiO_2 and iron) in recycled composite beads (50 recycles) as compared to fresh composite beads was checked through several characterization techniques as discussed below:

4.5.3.1 SEM-EDS analysis

The elemental composition of the composite beads (both freshly coated and recycled) and the surface morphology were determined using energy dispersive spectroscopy (EDS) together with scanning electron microscopy (SEM), as shown in Figure 4.28. The EDS image of the catalyst (fresh beads) and recycled beads showed the prominent peaks of iron (Fe) and titanium oxide (TiO_2); this proves the presence of both iron and TiO_2 as a catalyst in the hybrid technique. The presence of the iron element could be related to the combination of waste FA, FS, and clay that form the composite beads. SEM images for both freshly coated and recycled composite beads showed relatively smooth surfaces, confirming the existence of TiO_2 and its intactness even after recycling.

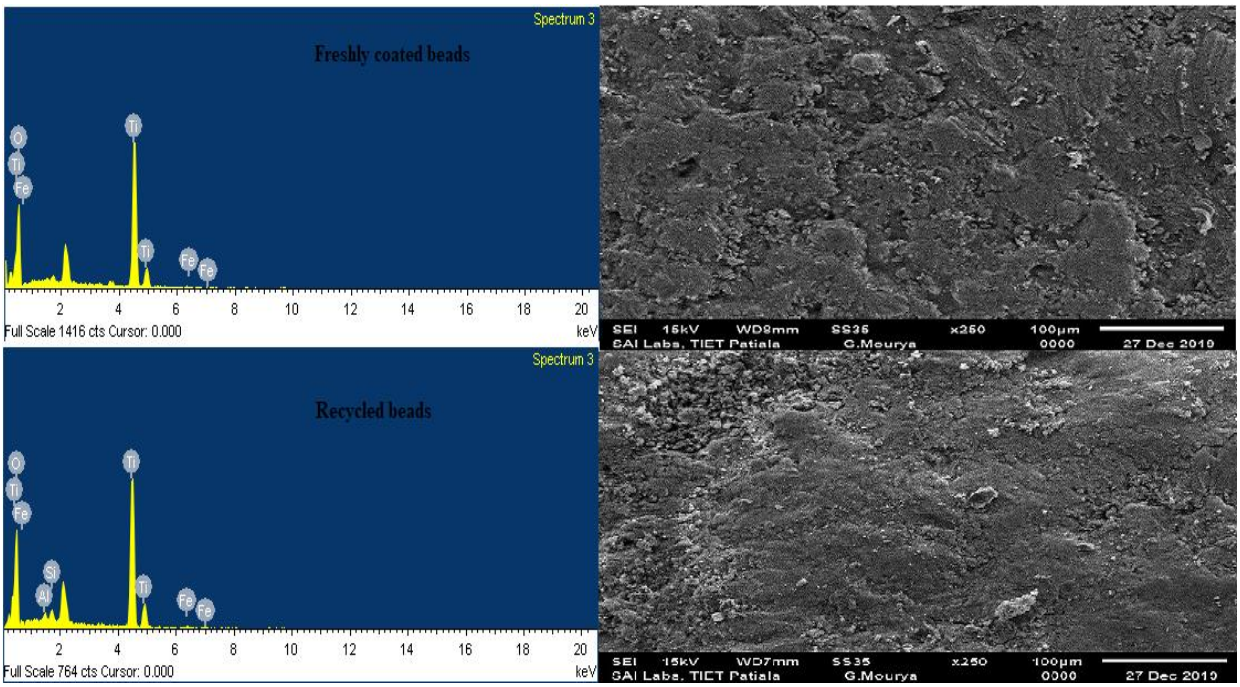

Figure 4. 28 SEM/EDS images of fresh as well as recycled composite beads

4.5.3.2 FTIR analysis

Freshly coated as well as recycled Fe-TiO_2 beads were analyzed by FTIR to determine the chemical bonds formed, as shown in Figure 4.29. The stretching of the H-O-H bond can be seen between the wavenumber of 3418.7 cm^{-1}-1637.7cm^{-1}. The O-H group was found at the wavenumbers of 3418.7 cm^{-1} and 3410.3 cm^{-1} for freshly coated and recycled Fe-TiO_2 beads, and the stretching vibrations are the main reason for the appearance of this group (Sayyar et al., 2015). The Ti-O-Ti bond in the range of 400-1200 cm^{-1} was observed in both freshly coated and recycled Fe-TiO_2 beads, confirming the presence of a TiO_2 lattice. Peaks at 434.8 cm^{-1} and 470 cm^{-1} indicate the anatase phase of freshly coated and recycled Fe-TiO_2 beads, respectively. Similar results were also observed in the previous literature (Bansal and Verma, 2018b), showing the anatase phase in the range of 400-600 cm^{-1} wavenumber due to the presence of vibrations generated by Ti-O-Ti. The Fe-O-Ti bonding was observed at 2000.7 cm^{-1} wavenumbers proving the presence of Fe in the recycled Fe-TiO_2 beads. A similar peak of the Fe-O-Ti bond was also reported by Bansal et al. (Bansal and Verma, 2018b) in the Fe-TiO_2 beads.

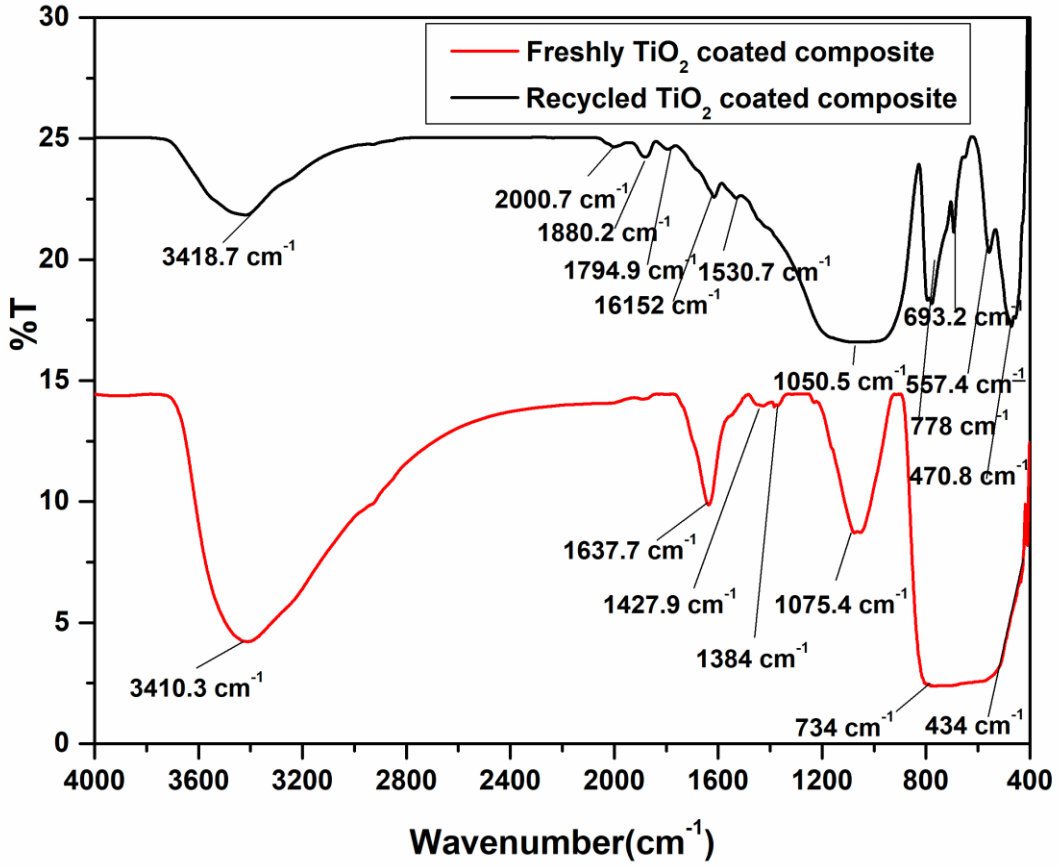

Figure 4. 29 FTIR image of fresh and recycled composite beads

4.5.3.3 UV-DRS analysis

The bandgap energy for the catalytic beads before (fresh beads) and after recycling was scanned in the visible range of 200-800 nm, using $BiSo_4$ as the base compound. A decrease in the bandgap energy of the composite beads compared to TiO_2 was observed, which is due to the presence of iron, as shown in Figure 4.30. This shows the light-absorbing ability of the catalytic beads in the visible region. The absorption range of titanium dioxide was found at 418 nm and then shifted towards 440 nm and 455 nm before (fresh beads) and after recycling the catalytic beads. The energy bandgap of TiO_2 was 3.1 eV and reduced to 2.9 eV for freshly coated and 2.8 eV for recycled composite beads.

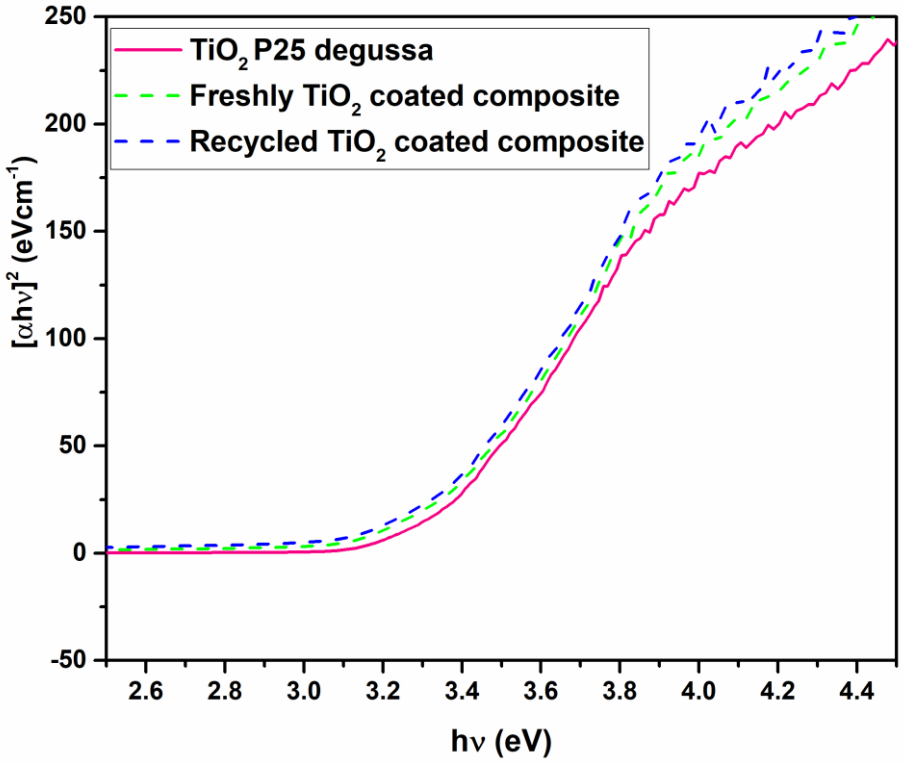

Figure 4. 30 UV-DRS analysis of fresh and recycled composite beads

4.5.3.4 XRD analysis

XRD analysis of the freshly coated as well as the recycled Fe-TiO_2 beads was carried out to confirm the intactness of TiO_2 crystalline planes, as shown in Figure 4.31. The appearance of different phases such as anatase (A) and rutile (R) in freshly coated and recycled Fe-TiO_2 beads proved the intactness of TiO_2 and its activity after 50 cycles. In addition to these two phases of TiO_2, titanium iron oxide (TIO) and iron oxide (IO) also appeared in the diffraction pattern and verified the presence of TiO_2 with Fe in the same unit. In Figure 4.31, iron oxide

peaks are seen to allow the entrapment of photo-excited electrons from the TiO_2 photocatalytic process, regenerating Fe^{2+}. Therefore, both technologies, i.e., photo-Fenton and photocatalysis, occur simultaneously in one unit.

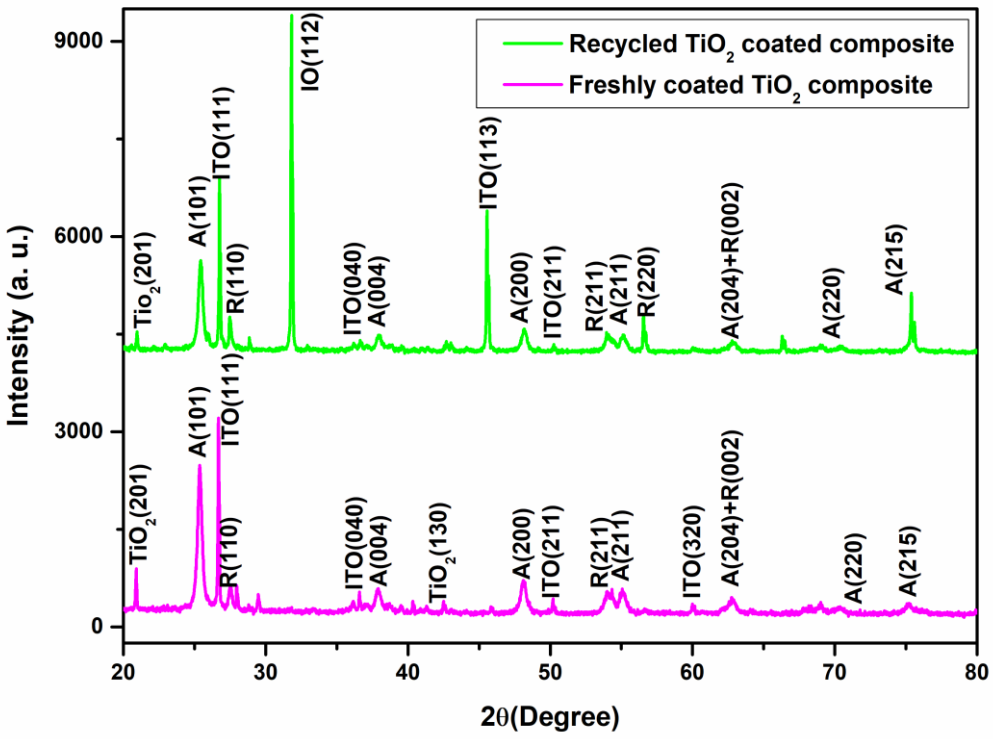

Figure 4. 31 XRD pattern of fresh and recycled composite beads

4.5.4 Kinetic analysis of the hybrid process

The main objective of this part of the study was to determine the catalytic performance of the different processes (photo-Fenton, photocatalysis, and hybrid process) in the fixed form in terms of light inactivation efficacy of *E.coli*. In order to compare the inactivation efficacy of the catalyst used in the three different methods, the reaction rate constants were calculated. The reaction rate constant of each of the processes is shown in Table 4.13. The hybrid process showed a significantly higher rate constant of 0.065 min^{-1} compared to photo-Fenton and photocatalysis with 0.029 min^{-1} and 0.025 min^{-1} rates constant, respectively. This is evident enough to prove the effective performance of the hybrid process compared to others. As expected, the inactivation efficacy of the hybrid effect was about twice that of the individual photocatalytic and photo-Fenton processes. Thus, this fast kinetic rate constant and use of waste iron in the form of foundry sand and fly ash in the present study make Fe-TiO_2 an extremely attractive platform for real-life applications.

Table 4. 13 Reaction rate constant (k) of different processes for *E. Coli* inactivation in the present study

Type of Pollutant	Volume (L)	Initial count (CFU mL^{-1})	Technique	Light source	Wave-length (nm)	Time (min)	Reaction rate constant (min^{-1})	Log Reduction
E. coli k-12	2	10^6	Hybrid process	UV	365	150	0.065	> 4 log
E.coli k-12	2	10^6	Photo-Fenton	UV	365	150	0.029	2.2
E. coli k-12	2	10^6	Photo catalysis	UV	365	150	0.025	2.3

4.5.5 Cost analysis of the lab-scale in-situ hybrid-process

The economic feasibility of the process has to be decided by taking into consideration various expenses such as reagents, catalysts, UV sources, energy consumption, and fabrication of the reactor. The laboratory-scale cost analysis helps to get a rough idea of whether the photocatalytic reactor can be considered for larger-scale applications. Table 4.14 shows the total tentative cost of the treatment technology in the current study. The total cost of the system was evaluated for 50 numbers of recycling. The total tentative cost of treating 2 L of solution in a single run came out to be US $0.327 and US $0.16 per liter. Although there are no related studies to estimate the cost of bacterial deactivation, it still resulted in significantly lower costs than those reported in the literature (Haranaka-Funai et al., 2017) for the degradation of priority pollutants.

Table 4. 14 Tentative cost evaluation of the treatment technique

(a) Preparation of Fe-TiO_2 catalytic material	
Design parameter	**Price**

Price of basic supplies (FS, FA and clay)	= 0.0 $
Electricity consumption while heating the support in muffle at a higher temperature	= 0.75 kWh
Price of electricity in Punjab	= 0.070 $/kWh
Price of electricity consumption	= 0.070 × 0.75 = 0.0525 $/kWh
Price of TiO_2 catalyst used (12 g)	= $ 0.042
Total price of Fe-TiO_2 catalyst	= 0.0525 + 0.042 = $ 0.0945
(b) Oxidant Doze (H_2O_2)	
Total oxidant consumed Cost of oxidant consumed	= 21 mL (for 50 runs) = $ 0.25
(c) Price of energy utilization during treatment	
Total energy consumed to attain 93 % of Efficacy No. of runs Cost of Electricity used by UV tubes Cost of Electricity used by Air spargers The total volume of solution treated Cost/m^3 Energy consumed during pumping of the solution to the reactor Cost for energy consumption Total operating cost	 = 50 = [7×36W×1.5h×$ 0.070/1000]50 = 1.323$/kWh = [2×2.5W×1.5h×$ 0.070/1000]50 = 0.0262 $/kWh = 2L×50 = 100 L = 0.1 m^3 = (a+b)/0.1 = 3.445 $/$m^3$ = 18W×1.5h×50 = 1350 Wh=1.350 kWH = 1.350× 0.070 $ = 0.095$/kWh = $1.35
(d) Assembly of the recirculating reactor	
Total price of reactor comprising pump, pipes and baffles Total price of treatment technique	= 15 $ = c+d = 15+1.35= $16.35

4.6 Once-through fixed-bed cascade reactor (Plug-flow approach)

In recent studies, the development of continuous photocatalytic systems, either continuous stirred type reactor (CSTR) or plug-flow reactor (PFR), has been discussed in view of its field-scale applications related to wastewater treatment (Miyawaki et al., 2016). However, PFR, where there is no axial mixing of the reaction mixture, is always desired as a continuous flow system owing to its high productivity and selectivity (Prokopova and Prokop, 1997). But the concept of PFR visualization in the case of photocatalytic systems has not been investigated widely. Thus, attempts have been made in the present study to approach PFR in a continuous photocatalytic system incorporating an in-situ hybrid effect for the disinfection of *E. coli*. To the best of our knowledge, this is the first ever reported study till date in which pilot-scale once-through cascade reactor system incorporating in-situ hybrid effect for water disinfection has been visualized to approach a PFR.

4.6.1 The prominence of the hybrid effect in a cascade reactor

As in all earlier cases, here also, the prominence of the hybrid effect was established at the pilot scale using a cascade reactor. For this, the cascade reactor system (comprising of 3 packed-bed glass reactors in series) was operated in once-through mode with a total working volume of 6 L. A significant reduction in the treatment time of *E. coli* concentration was observed with 10% synergy of in-situ hybrid-process over individual processes. The implementation of the in-situ hybrid effect in a cascade reactor with three reactors in series helped the reactor approach PFR with 45 min of retention time (τ) and 100% inactivation of *E. coli* concentration was observed with optimized operational parameters. The OH^{o} produced during the process was found to be the main active ROS for the inactivation of *E. coli* confirmed by the trapping study. The cell wall damage was confirmed by the increase in the K^{+} concentration at regular intervals. No regrowth of cells after 24 and 48 h of treatment in the dark was observed in completely inactivated samples. Besides this, the Fe-TiO_2 composite portrayed an exceptional durability/recyclability efficacy (>100 recycles) under continuous flow conditions as confirmed by different characteristics analysis such as SEM/EDS, XRD, DRS, and FTIR. To visualize the practical viability of the proposed high-performance once-through reactor system, the total cost of the treatment process was analyzed in detail in section 4.6.6.

4.6.2 Experimental Studies

To confirm the hydrodynamic behavior and flow pattern of the once-through reactor, an retention time distribution (RTD) approach was performed. Further, to validate the prominence of the hybrid effect, the preliminary studies were executed using all the blank experiments (dark experiment, solar-light, solar-light/H_2O_2, TiO_2-assisted photocatalysis, and photo-Fenton process).

4.6.2.1 Retention time distribution (RTD) and plug flow study

To confirm the hydrodynamic behavior and flow pattern of the once-through reactor, an RTD approach was performed. RTD, the hallmark technique for examining the ideal reactor behavior, may also be used to scale up proposals for improved efficacy conditions. For implementing the RTD approach Exit age distribution (E (t)) was used. The E (t) distribution was calculated using Equation (4.14) and the Peclet number (Pe) was also calculated and mentioned in Equation (4.15):

$$E(t) = \frac{S(t)}{\int S(t)dt} \tag{4.14}$$

where S (t) denotes the tracer's concentration (mg L^{-1}) and t denotes the time (min).

$$Pe = \frac{\vartheta L}{D} \tag{4.15}$$

where ϑ designate the velocity of flow (m s^{-1}), L denotes the characteristics length (m), and D denotes the dispersion coefficient (m^2 s^{-1}).

The experimental and the theoretical retention time ought to have no distinction at the typical working conditions. If the theoretical retention time is less than the actual retention time, then it may be reasoned that either the particles of the tracer might have been held back or the flow rate calculations might be rechecked. Henceforth, for this reason, the dead volume (% Vd) was determined using Equation (4.16).

$$\%Vd = 1 - \frac{T}{t} \times 100 \tag{4.16}$$

Methylene blue was used as a tracer for the RTD study. For modeling, the plug flow reactor model closed to diffusion was used. The average theoretical and actual resident time of 42 min and 45 min respectively was observed which are fairly similar to each other. The dispersion found in Figure 4.32 (retention time distribution curve) is less as the 3 reactors were linked in series with less flow rate (6 L h^{-1}) prompted to the dispersal of the tracer when it moves from one reactor to the next. The estimation of the peclet number (Pe) was acquired as 78 and the dead volume was found to be very less i.e. 0.06, confirming the more contact time of the catalyst with the pollutant. The plug flow approach with the least dispersion is shown by this high Pe number.

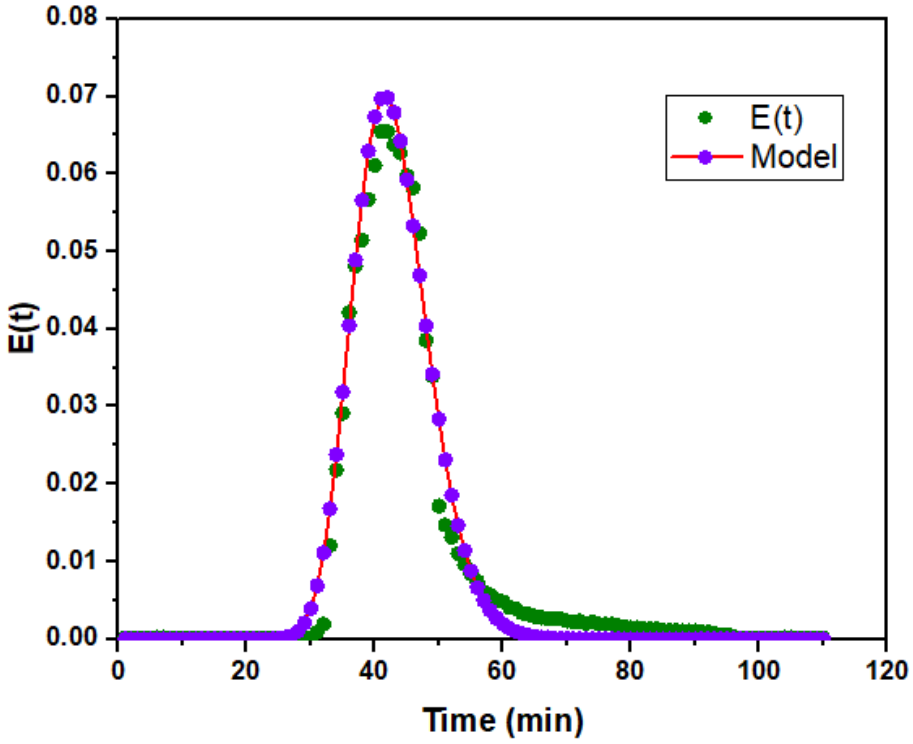

Figure 4. 32 RTD curve attained from the experimental analysis of the three reactors in series along with axial dispersion of fitted model

4.6.2.2 Dark and controlled experiments

The changes that occurred in the concentration of *E. coli* (log CFU mL^{-1}) in dark conditions are discussed in Figure 4.33. No change in the bacterial concentration was found when the experiments were conducted in dark for 2 h without adding any reagents. Similar findings were observed with H_2O_2 as its polarity is the same as that of water which lets its diffusion into the cell and possibly damages the cell via internal Fenton reaction through

oxidative stress, but the presence of catalases (kat) and alkyl hydroperoxide reductase (ahp) in the cytosol of stationary phase and in the growing cells respectively (Seaver et al., 2001) results in the faster decomposition of H_2O_2. In our study, mainly KatE protected the cell against H_2O_2 because the stationary phase cells were used for the entire experiment (Nelson et al., 2018). Previous work, however, showed that the concentration of intracellular H_2O_2 is 20% relative to the external addition (in scavenging-proficient cells) (Seaver and Imlay, 2001a). Hence, under the operating conditions studied, this mode of action is negligible. The viability of the *E. coli* in dark conditions was tested at pH 4-4.5 in the reactor and no significant decrease in the *E. coli* concentration was found, as shown in Figure 4.33. The same results were obtained when (Rodríguez-Chueca et al., 2014b) studied the cell viability at the acidic condition and negligible reduction was observed. Concerning Fe^{2+} leaching, *E. coli* inactivation was close to 0.2 log reduction in 2 h. Therefore, shows no effect on the viability of the cells.

In this study, solar light only, solar/H_2O_2, TiO_2-photocatalyst, and photo-Fenton in the once-through fixed-bed reactor were studied for analyzing and comparing the inactivation efficacy. It was observed from Figure 4.33 that only solar irradiation and solar irradiation with 70 mg L^{-1} of H_2O_2 indicated 1.9 and 2.5 *E. coli* log reduction, respectively. In the TiO_2-photocatalysis, the reaction was carried out with composite beads coated at the neutral condition in the presence of solar light, and approximately 2.9 log reduction was observed on illumination for 2 h.

In the photo-Fenton process, the pH of the reaction was maintained a 4 - 4.5 for the iron lixiviation to start, and correspondingly *E. coli* inactivation was observed as given in Figure 4.33. In acidic conditions, iron lixiviating from clay often occurs because it helps to break the iron bond with other organic compounds and induces iron extraction, known as iron leaching (Hseu, 2004). In this process, 70 mg L^{-1} of H_2O_2 was added for the reaction to start and about 3.9 log reduction in *E. coli* was found in 2h of reaction time.

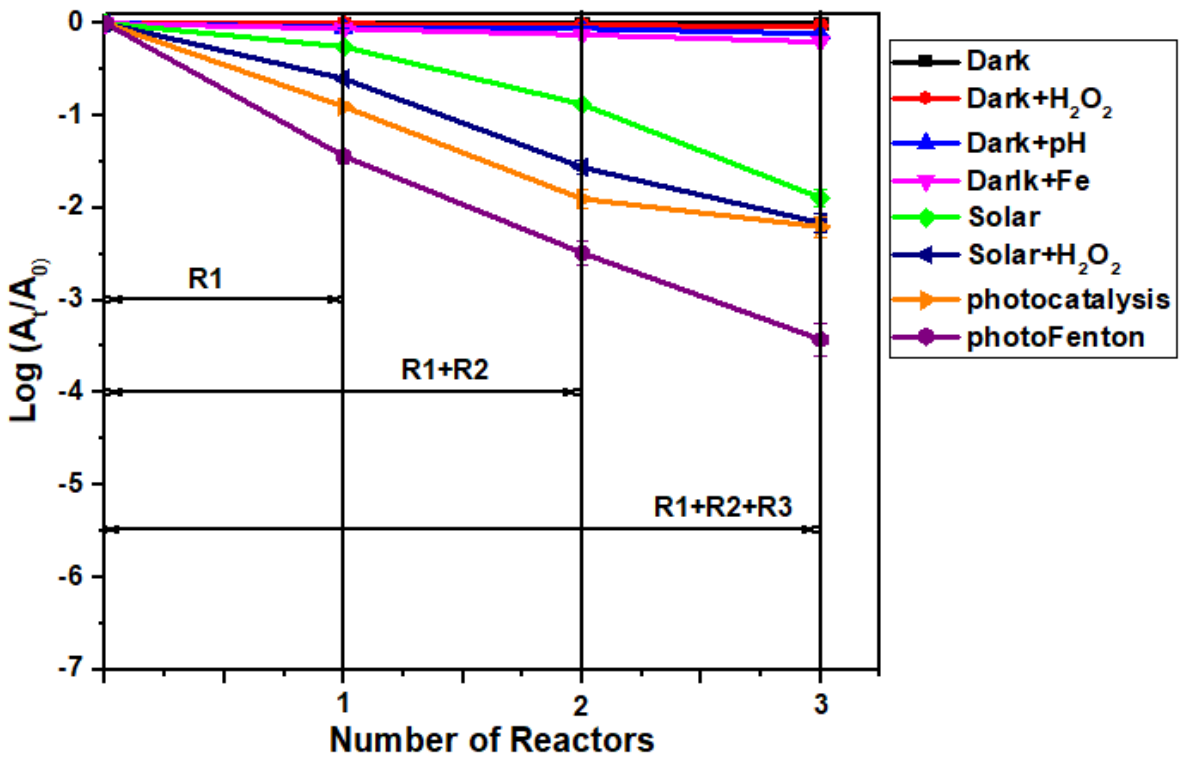

Figure 4. 33 Preliminary experiments of *E. coli* inactivation

4.6.3 Reactor optimization

4.6.3.1 Effect of number of reactors

In addition to raising concerns about the area needed, the number of reactors in a series will affect the conversion rate of any pollutant. To study this, the number of reactors was varied to three (Figure 4.34 a) and the *E. coli* concentration was measured after exiting from each reactor. In this series configuration of three reactors, 6 L of simulated wastewater was treated, with an H_2O_2 concentration of 50 mg L^{-1} and a flow rate of 10 L h^{-1}. To keep the entire experiment economically viable, the treatment of *E. coli* was done under natural solar light. The concentration of *E. coli* was found to decrease with the increasing number of reactors, as shown in Figure 4.34 (a). It was observed that only 0.9 log reduction in *E. coli* after the wastewater exited from the 1st reactor with RTD of approximately 10 min. The entire process was operated at the defined flow rate in once-through mode. It can be seen from Figure 4.34 (a) that there was a further decrease in the concentration of *E. coli* with the increase in the number of reactors in series. After the 2nd reactor, nearly 2.3 log reduction was observed. Also, by adding one more reactor, the efficacy of the treatment reactor was improved with the increase in the log reduction (3.4) of *E. coli*. The number of the reactor

was not increased beyond this point because the decrease in the cell population was not the only aspect in the determination of the optimized number of reactors.

The optimum number of reactors determined is based on the system's maintenance and its control which further depends on the reactor's configuration, nature of pollutant, and conversion factor (Miyawaki et al., 2016). Miyawaki et al. 2016 used slurry bubble column reactors in series for investigating the degradation of cyanide. It was found that for attaining 99 % of degradation, 8 reactors in series were observed to be the optimal number. In these types of reactors, it is not possible to imagine a realistic solution as an enormous loss in energy might occur due to photocatalysis in suspension. In the current study, while the disinfection efficacy of *E.coli* will be further improved by an additional number of reactors (>3), this could make the maintenance and regulation of the system difficult. In this framework, the number of reactors has not been increased further though attempts have been made to boost the disinfection efficacy of *E.coli* by optimizing other operational parameters by selecting 3 as the optimized number of reactors.

4.6.3.2 Effect of number of baffles

The addition of baffles to the reactor is intended to increase the residence time and thus improve the reactor's disinfection performance. In the current study, the number of baffles was varied from 1 to 4, as shown in Figure 4.34 (b). It can be seen from Figure 4.34 (c) that with increasing the baffles from 1 to 3, the log reduction was also increased and reached 3.8 logs. Later, the effectiveness of disinfection began to decrease, which may be accredited to the shading effect of the baffles. The prevalence of the shading effect of baffles caused an ineffective absorption of photons of solar light by the catalyst. A similar pattern was observed in a study done by (Miyawaki et al., 2016) where the decrease in the *E.coli* concentration was reduced with 3 baffles due to the shading effect.

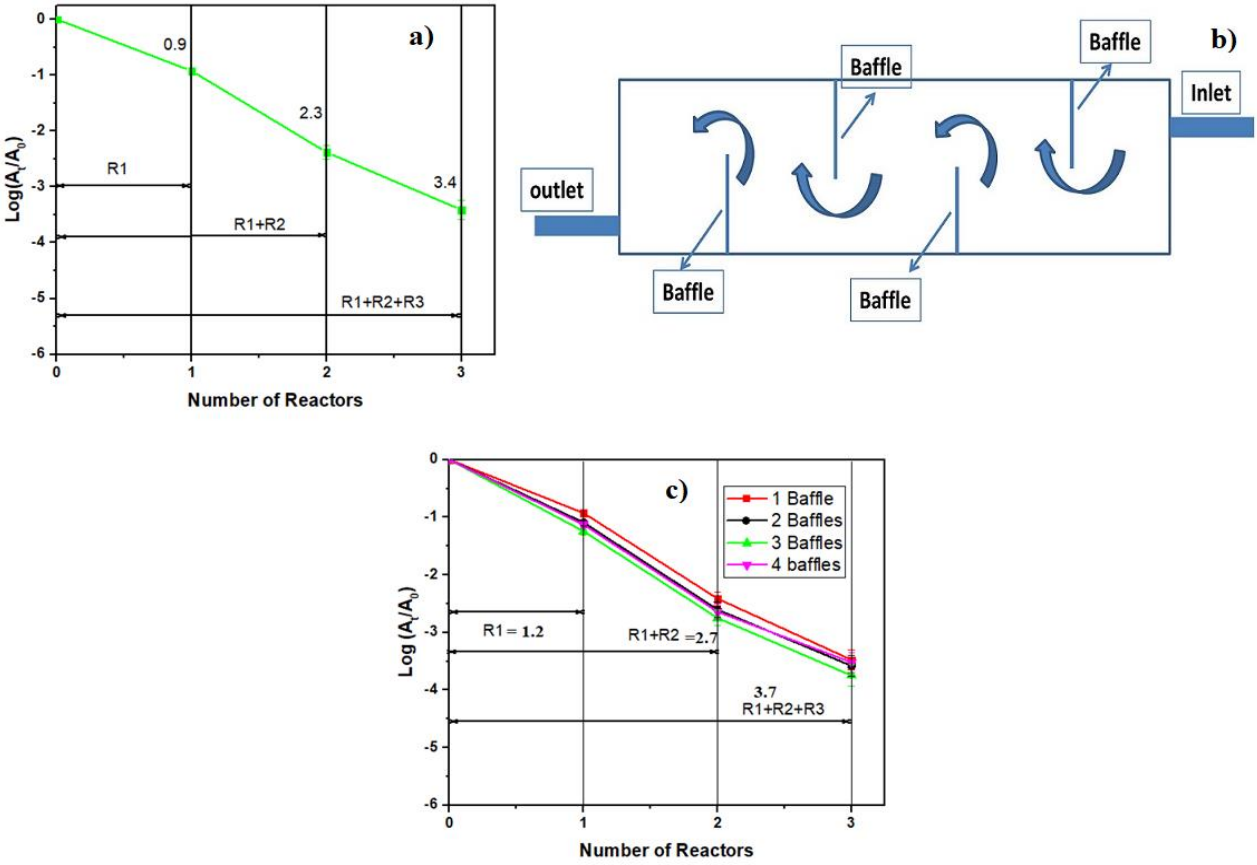

Figure 4. 34 Change in the concentration of *E. coli* with (a) variation in the number of reactors (b) crosssection of number of baffles in a reactor (c) variation in the number of baffles

4.6.3.3 Effect of the flow rate

In the disinfection studies, especially in the plug flow reactor, the flow rate plays a significant role as it determines the retention time of a pollutant in the reactor. With the change in the flow rate, the amount of oxygen, and turbulence level in the system also varies, consequently affecting the disinfection efficacy. In the current work, the flow rate of the reactor was changed from 2 L h^{-1} to 14 L h^{-1} with an H_2O_2 concentration of 50 mg L^{-1} under natural solar irradiation using three glass reactors in series. From Figure 4.35 (a), it was found that the inactivation of *E. coli* in the water started to decrease with an increase in the flow rate from 2 L h^{-1} to 14 L h^{-1}. This might be accredited to less time for the interaction of bacterial cells with the composite material. At a flow rate of 2 L h^{-1}, the reaction time was 1 h 20 min with an overall log reduction of 4.5 at the outlet of the third reactor. The flow rate was not decreased below 2 L h^{-1}. Decreasing the flow rate would have increased the efficacy of the reactor but would hinder its commercial viability by increasing the higher energy

consumption. A similar result was also observed in the flow-through reactor (Wang et al., 2020), where the inactivation of *E. coli* was studied under different flow rates using ultraviolet-C (UV-C) light-emitting diodes (LEDs) and found that the *E. coli* log reduction started to decrease by increasing the flow-rate beyond 2 L h^{-1}. In this study, with the increase in the flow rate to 14 L h^{-1}, a 2.7 log reduction of *E. coli* was found, but the total reaction time was also decreased. Moreover, the log reduction of *E. coli* at 2 L h^{-1} and 6 L h^{-1} was almost the same at the end of the 3rd reactor. Therefore, from an economic point of view, 6 L h^{-1} was preferred as the optimized flow rate for further experimentation.

4.6.3.4 Effect of surface area covered

In the present study, altering the quantity of catalyst-coated beads in proportion to the available surface area enables identifying the influence of surface area covered on bacterial disinfection. This effect is primarily concerned with determining the optimal amount of catalyst required for disinfection in the form of beads. Thus, the study's findings have been expressed as a percentage of the area covered by adjusting the number of beads.

The surface area varied from 50 % to 100 % coverage and an increase in the log reduction of *E. coli* was observed, as shown in Figure 4.35 (b). The increased number of composites increases the amount of catalysts which improves the inactivation rate of *E. coli*. Simultaneously as the water is flowing from one reactor to another, the *E. coli* is coming in contact with the new fixed-bed composite catalyst placed in the reactor, as seen in Figure 4.35 (b), thus increasing the active sites, leading to the production of more OH^o and an increase in the inactivation efficacy. When the % area covered was increased further to 150%, a decrease in the bacterial log reduction was found. This could be because of the excessive iron lixiviation from the composite beads that block the catalyst's active sites, resulting in a decrease in the log reduction. Another reason for the decrease in the log reduction might be the formation of dead zones due to the overlapping of beads which effectively reduces the volume of wastewater to be treated.

4.6.3.5 Effect of H_2O_2 concentration

The addition of H_2O_2 in the hybrid process is utilized simultaneously in both processes for the generation of OH^o. This in-situ hybrid effect improves the reaction rate by using H_2O_2 as an electron acceptor. In this framework, the study was done using visibly active Fe-TiO_2 composite beads at acidic conditions (pH of 4.0-4.5) with varying H_2O_2 concentrations. As

discussed earlier, the reactor was optimized with three glass reactors in series. In this case, the H_2O_2 concentration from 10 to 70 mg L^{-1} was used for the disinfection study. From Figure 4.35 (c) it was found that by increasing the H_2O_2 concentration, the rate of log reduction was increased up to 50 mg L^{-1}. This concentration of H_2O_2 has also shown some effective results (approximately 100% inactivation) in different studies found in the literature (Ortega-Gómez et al., 2014, 2013). Further, with the increase in the concentration up to 70 mg L^{-1}, no change in the concentration of *E. coli* was observed. This could be the scavenging effect of H_2O_2 at a high concentration. Therefore, 50 mg L^{-1} of H_2O_2 concentration was selected as the optimized concentration for the inactivation of *E. coli*, and approximately a 6.2 log reduction was observed.

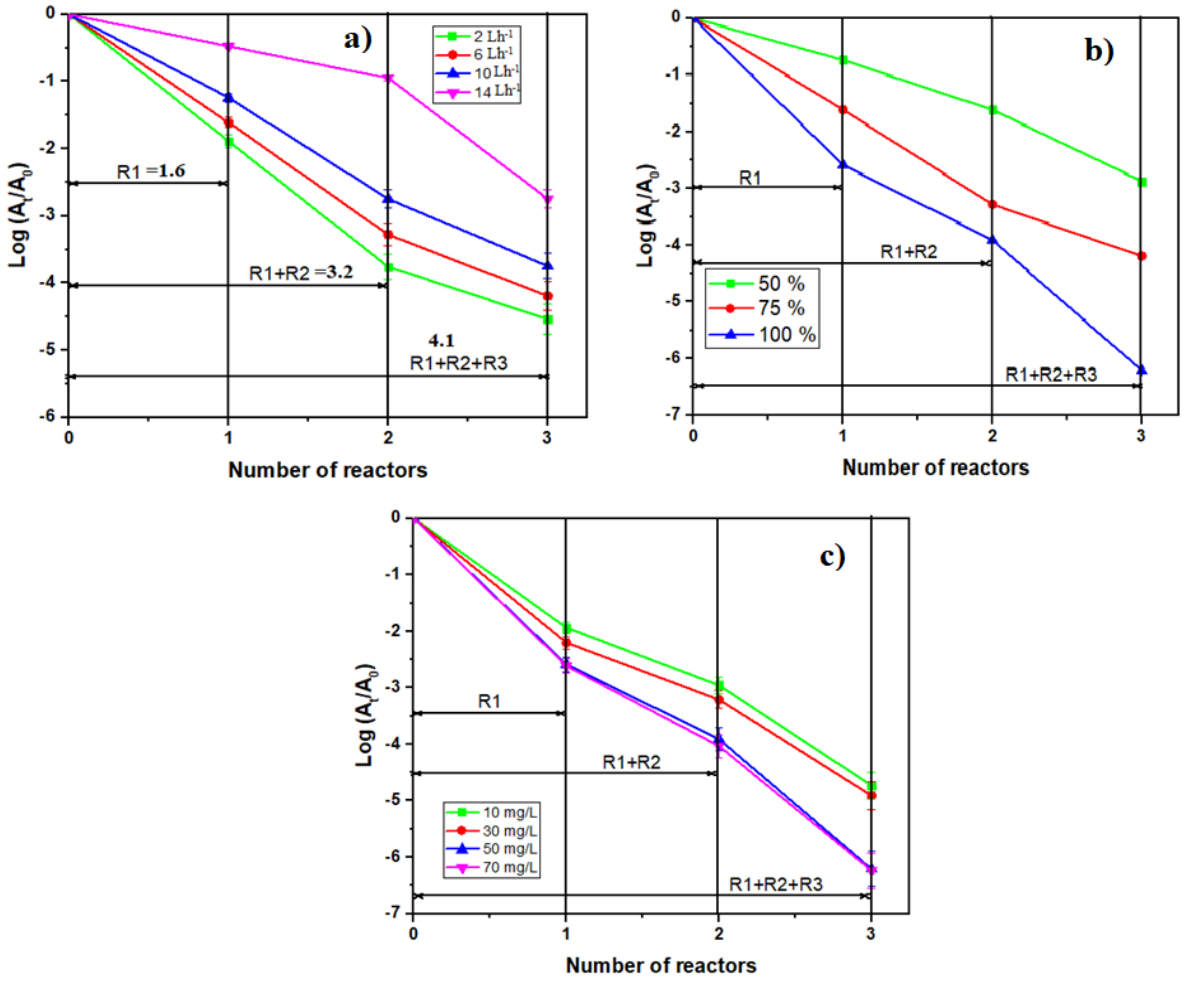

Figure 4. 35 Change in the concentration of *E. coli* with (a) variation in the flow rate of the reactor (b) variation in the % of surface area covered (c) variation in the concentration of H_2O_2

In this study, a 100% reduction in water in 45 min of the treatment time was observed when the 3 reactors in series had a flow rate of 6 L h^{-1}, 100% surface area covered with beads, and 50 mg L^{-1} of H_2O_2 was used. The treatment time of this technology is significantly less as compared to some other studies where approximately similar oxidant doze was used (Ortega-Gómez et al., 2014, 2013) for 100% killing of bacteria. This decrease in the treatment time can be attributed to the hybrid effect of the proposed technology where TiO_2 photocatalysis and photo Fenton process is working simultaneously for the higher production of OH^o. Hence this technology has proved its competence in terms of the effective utilization of waste materials as a promising concept for the wastewater post-treatment that could find successful real-life applications.

4.6.3.6 Role of various reactive species on *E. coli* inactivation

According to earlier research, bacteria are mostly inactivated due to the creation of reactive oxygen species (ROS) by photocatalysts, and the reactive species are created by the separation of electrons and holes. Three major ROS are involved in the photocatalytic disinfection of microorganisms: hole (h^+), superoxide radical, and hydroxyl radical (OH^o) (Wang et al., 2013, 2012; Zhang et al., 2010). Scavengers are an effective approach for assessing the contribution of each reactive species to photocatalytic disinfection (electrification or oxidation) and for elucidating its mechanism. Therefore to determine the main oxidative holes or radicals (i.e., OH^o, O_2^{o-}, and h^+) responsible for solar hybrid disinfection of *E. coli* through Fe-TiO_2 composite, several experiments were carried out at optimum experimental conditions over 60 min reaction employing different quencher compounds like tert-butyl alcohol (TBA) for OH^o, disodium ethylene diamine tetraacetic acid (EDTA) for h^+, and p-benzoquinone (BQ) for O_2^{o-} at a concentration of 0.01 M (Figure 4.36). The results demonstrated a decrease in the log reduction in the presence of all trapping agents, which revealed that all the mentioned oxidative species are responsible for the disinfection of *E.coli*. However, TBA showed a decrease in the log reduction from 6.2 to 5.0, indicating that OH^o is the most prominent agent in the *E. coli* inactivation process. The primary explanation for this pattern is most likely due to the quick separation of photoelectron hole pairs and their reaction with water or O_2 adsorbed on the surface of the material to form active oxidizing compounds with high oxidizing characteristics, which finally kill bacteria.

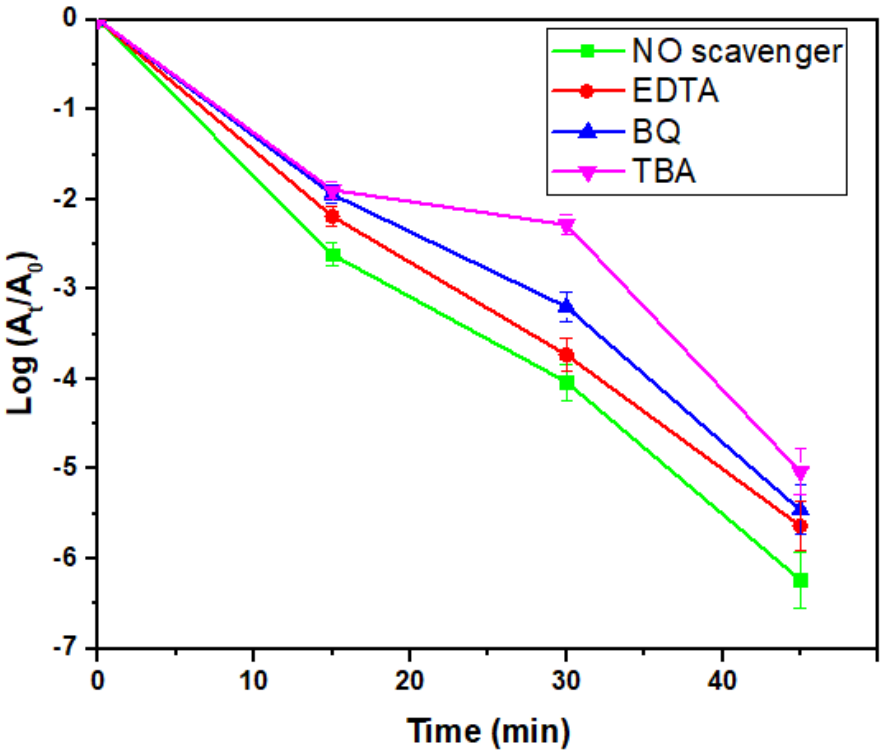

Figure 4. 36 Trapping study of different reactive oxygen species

4.6.4 Extended reusability study of the Fe-TiO_2 catalyst

The durability/ recyclability of the fixed bed catalyst is a critical parameter for the scale-up applications of the technology. Situations became much more challenging in the current research because the process involved combining two different techniques, namely photocatalysis and photo-Fenton, in one system. The most challenging problem was to maintain the recycling and reuse of catalysts even under flow conditions. Because under continuous flow, the coating over the beads might not get stabilized. For the hybrid process, the composite must sustain the TiO_2 layer coated on the bead while maintaining the iron lixiviation from the composite bead.

For this once-through reactor study, already recycled beads for the above-mentioned studies were used to study the parametric optimization of the reactor. For this technology to work smoothly, the intactness of the photoactive TiO_2 layer over the surface and incessant iron lixiviating from the Fe-TiO_2 composite plays a very significant role. In this study, Fe-TiO_2 composite made from FS+FA were recycled for more than 100 cycles without any major reduction in the disinfection of *E. coli*, as shown in Figure 4.37. This confirms that a sufficient quantity of catalyst particles was intact to the surface even in the recycled

composite beads. Even after 100 cycles, the composite beads were found to be capable enough to perform both processes simultaneously in the system, thus further claiming the novelty of the study. The leaching of iron from the composite during the inactivation process was also confirmed by estimating the concentration of total iron in each reactor from fresh and recycled composite beads as depicted in Tables 4.15 & 4.16. To counter-check the efficacy of used composite beads, experiments were executed simultaneously with freshly prepared Fe-TiO_2 composite beads as well. There was about a 5 % reduction in the disinfection efficacy of *E.coli* observed owing to the weathering off loosely bound catalyst particles from the surface of composite beads. None of the studies related to fixed-bed photocatalysis in the literature have ever reported such high recyclability efficacy of the catalyst. The recycled Fe-TiO_2 composite in the present study was characterized through various techniques (Section 4.6.5), which further confirmed the presence of Fe along with TiO_2 even after 100 recycles.

Table 4. 15 Concentration of Iron species leaching out of fresh composite beads in each reactor

Reactors	Concentration (µg L^{-1})		
	Total iron	**Ferrous ion**	**Ferric ion**
1	155	50	105
2	155.385	50.385	105
3	154.615	49.231	105.385

Table 4. 16 Concentration of Iron species leaching out of recycled composite beads in each reactor

Reactors	Concentration (µg L^{-1})		
	Total iron	**Ferrous ion**	**Ferric ion**
1	166.538	50.769	115.769
2	160	52.692	107.308
3	169.615	52.692	116.923

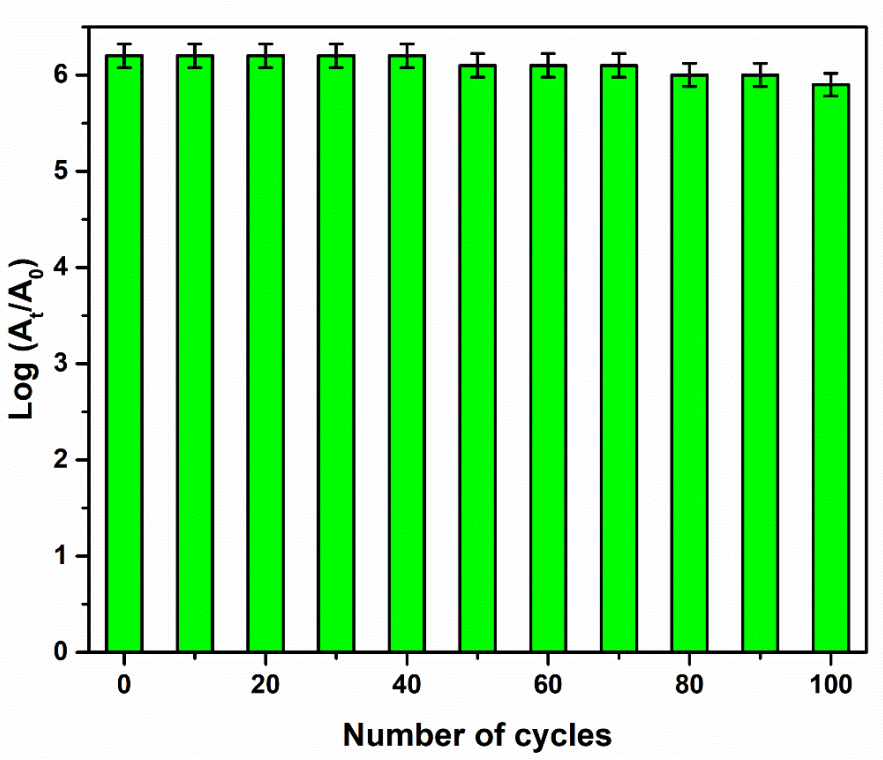

Figure 4. 37 Reusability/durability study of Fe-TiO_2 composite used for *E. coli* inactivation

4.6.5 Characterization

The intactness of catalyst particles (TiO_2 and iron) in recycled composite beads (100 recycles) as compared to fresh composite beads was checked through several characterization techniques as discussed below:

4.6.5.1 SEM-EDS analysis

The morphology and elemental composition of the uncoated and coated Fe-TiO_2 composite were confirmed using SEM-EDS analysis. The SEM image (Figure 4.38) of TiO_2 coated composite beads showed strongly bounded TiO_2 particles on the surface of the composite beads even after recycling. The peaks of Ti, O, and Fe in the EDS spectrum of catalysts (Fresh beads) and recycled beads are in good agreement with the recycled, thus proving the existence of both iron (Fe) as well as TiO_2 catalyst in the hybrid technique.

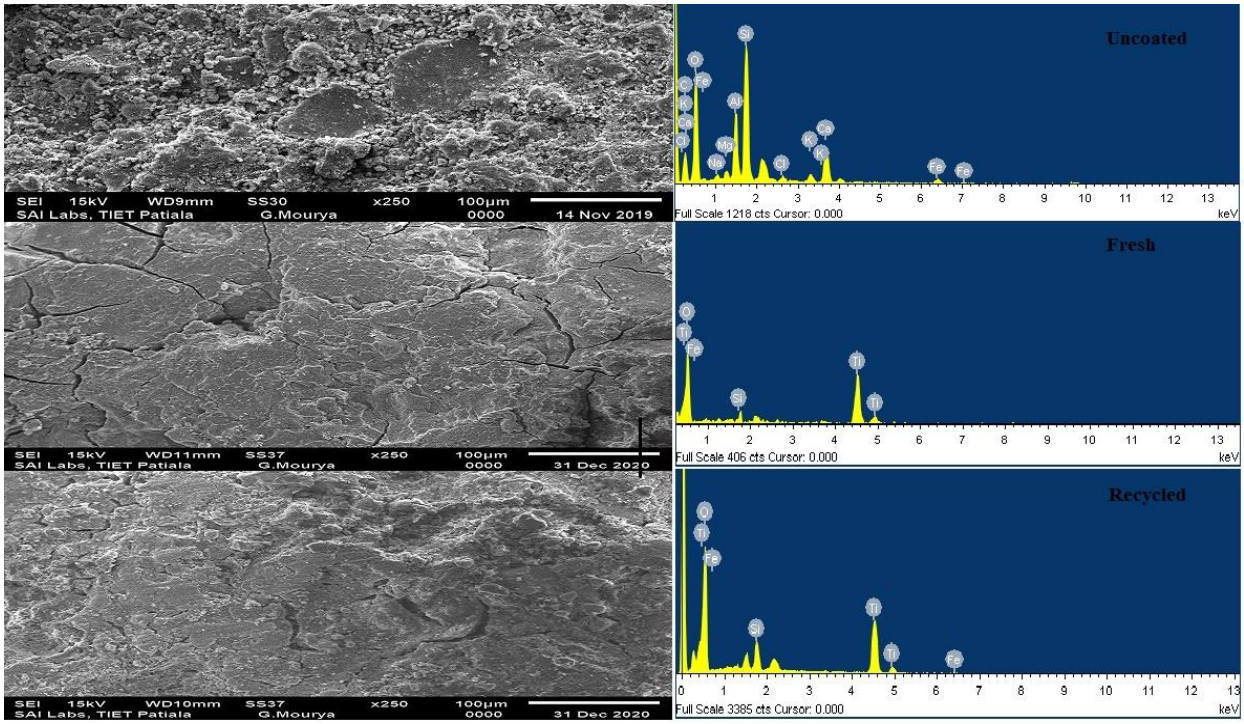

Figure 4. 38 SEM/EDS images of fresh and recycled composite beads

4.6.5.2 XRD analysis

The XRD analysis of the prepared samples was done to see the changes occurring in the crystalline structure and phases of the catalyst after recycling and similar patterns of the XRD spectrum were observed, as shown in Figure 4.39. The anatase phase of the fresh and recycled catalyst was at $2\theta = 25.26^{o}$, 37.79^{o}, 48.04^{o}, 53.9^{o}, 54.9^{o}, and 62.9^{o}, respectively, and the rutile phase of the fresh and recycled catalyst was at $2\theta = 27.552^{o}$, 36.6^{o}, 39.6^{o}, 41.4^{o}, and 55.03^{o} respectively. The anatase phase of the catalyst at different degrees responds to 101, 103, 200, 105, 211, and 204 planes. Similarly, the crystalline planes at 110, 101, 200, 111, and 211 represent the rutile phase. In Figure 4.39, iron oxide (IO) peaks at different planes at 101 and 034 can be seen, which enables the entrapment of photo-excited electrons from the TiO_2 photocatalytic process, which regenerates Fe^{2+}. Therefore, both the technologies, i.e., photo-Fenton and photocatalysis, occur simultaneously in one unit. The presence of these IO and ITO (iron titanium oxide) enhances the efficacy of the Fe-TiO_2 catalyst in visible light. This hypothesis was further confirmed through UV-visible absorption spectroscopy, as explained in the next section 4.6.5.3.

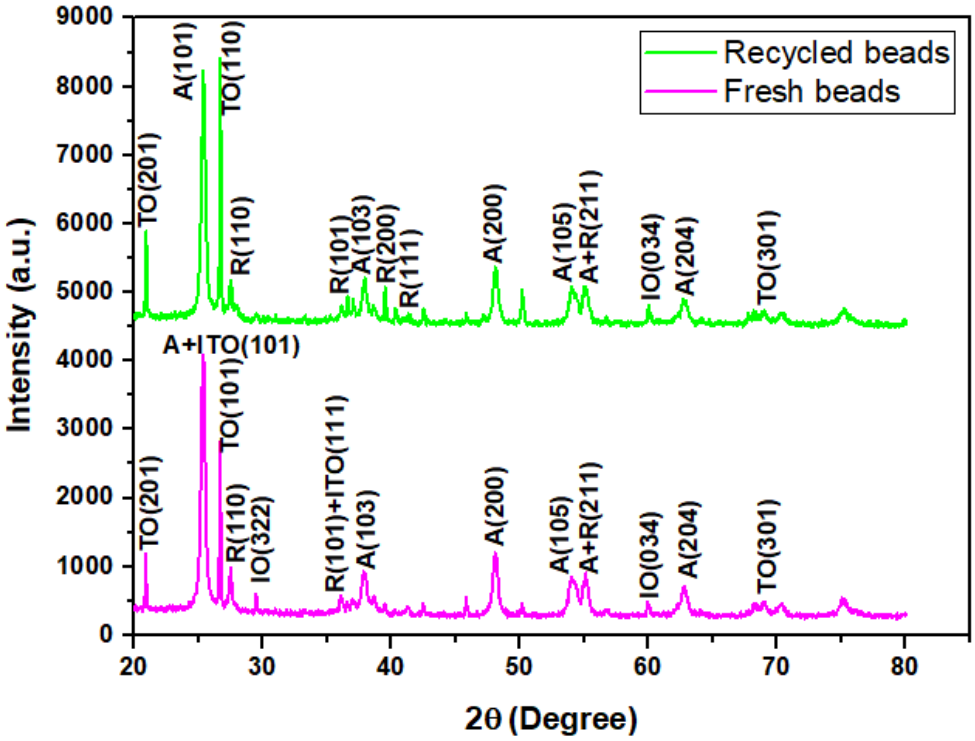

Figure 4. 39 XRD patterns of freshly coated and recycled beads

4.6.5.3 UV-Vis absorption spectra

The bandgap energy of the catalyst was measured in a visual spectrum of 200-800 nm before and after recycling, using $BiSo_4$ as a baseline compound. The introduction of iron resulted in a reduction in composite beads' energy gap compared to TiO_2, as seen in Figure 4.40. It demonstrates the catalytic beads' capacity to absorb light in the visible area. The absorbance range of TiO_2 was determined to be 450 nm and then changed to 470 nm and 490 nm before and following catalytic bead recycling. TiO_2 has a bandgap energy of 3.1 eV, which is lowered to 2.9 eV for newly coated composite and 2.8 eV for recycled composite beads.

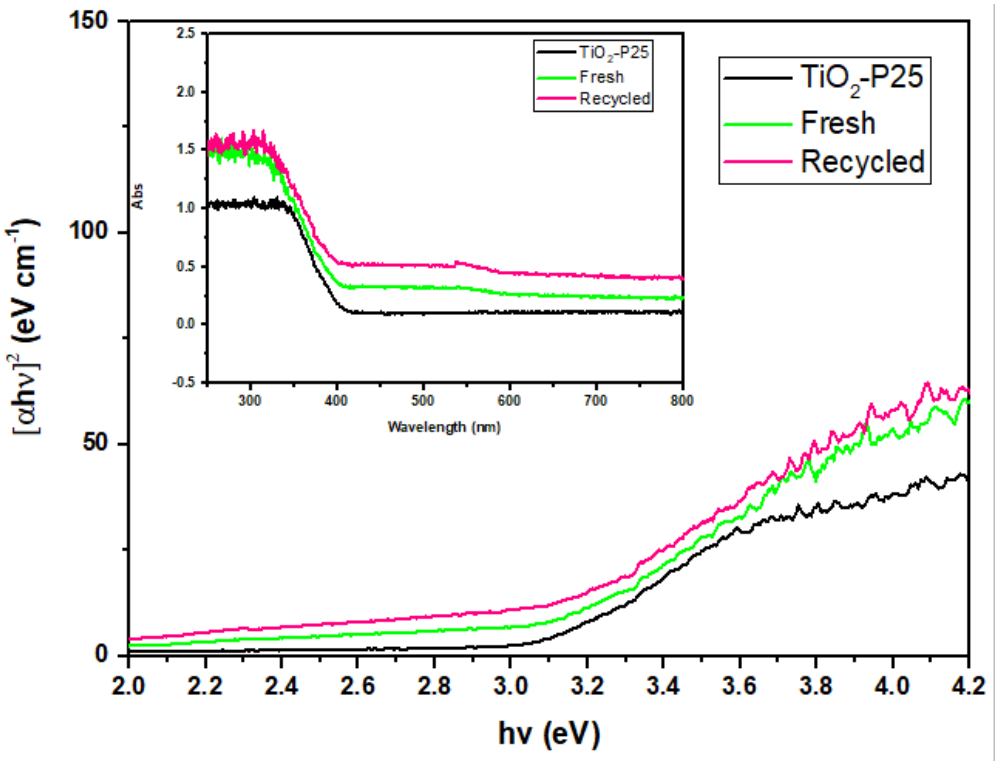

Figure 4. 40 UV-visible DRS patterns of freshly coated and recycled beads

4.6.5.4 FT-IR analysis

Freshly coated as well as recycled Fe-TiO_2 beads were analyzed using FTIR to determine the type of structural unit present in the system, as shown in Figure 4.41. There are four bands present in the system having wavenumbers greater than 1500 cm^{-1}. This is because of the absorption of moisture by the crystalline material resulting in the stretching of the H-O-H bond between the wavenumber of 3398.8 cm^{-1}-1632.2 cm^{-1}. The O-H group was discovered at wavenumbers 3398.8cm^{-1} and 3413.1 cm^{-1} in fresh and recycled Fe-TiO_2 beads, and stretching vibrations are the primary cause of this group's occurrence (Sayyar et al., 2015). In both newly coated and recycled Fe-TiO_2 beads, a Ti-O-Ti bond in the range 400-1200 cm^{-1} was detected, indicating the presence of TiO_2 lattice. The spectra of fresh and recycled Fe-TiO_2 beads revealed the anatase phase at 472.0 cm^{-1} and 479 cm^{-1}, respectively. Similar findings have been obtained previously (Bansal and Verma, 2018b), indicating that the anatase phase exists in the 400–600 cm^{-1} wavenumber range due to the presence of Ti-O-Ti vibrations. The Fe-O-Ti bond was detected at a wavenumber of 2924.9 cm^{-1}, indicating iron in recycled Fe-TiO_2 beads. (Bansal and Verma, 2018b) also observed a comparable peak of the Fe-O-Ti bond in Fe-TiO_2 beads.

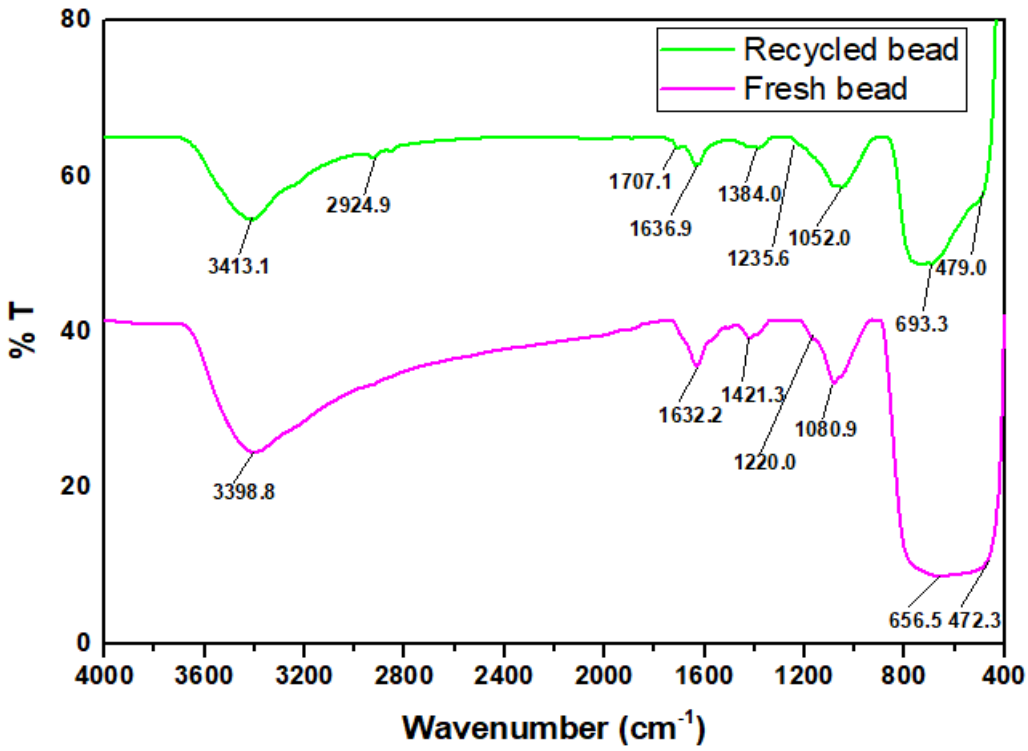

Figure 4. 41 FTIR analysis of freshly coated and recycled beads

4.6.5.4 HRTEM analysis

HRTEM images of fresh and recycled Fe-TiO_2 nanoparticles were analyzed to study their morphology and lattice spacing (Figure 4.42). The lattice stripes of Fe-TiO_2 particles are shown in Figure 4.42, and lattice spacing of 0.35 to 0.36 was observed corresponding to the crystal plane of the TiO_2 anatase (101) phase.

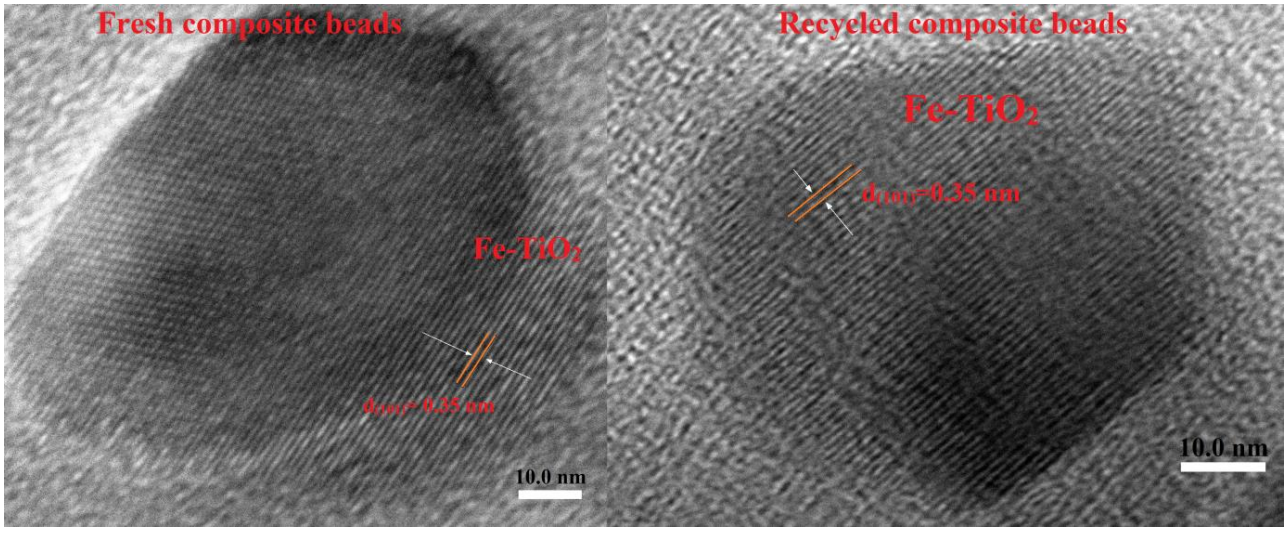

Figure 4. 42 HRTEM images of fresh and recycled composite

4.6.5.5 Field emission scanning electron microscopy (FESEM) for *E. coli* morphology and K^+ leakage

FESEM was used to directly observe the morphological changes in the bacterial cells after being treated with the Fe-TiO_2 catalysts in deionized water Figure 4.43 (a-b) shows a FESEM image of the untreated *E. coli* cells. The cells show uniform electron density, suggesting that they are in a normal condition without environmental disturbance. In contrast, the *E. coli* cells treated with Fe-TiO_2 under the same conditions showed dramatic morphological changes during the process of cell death. For the cells treated in deionized water (shown in Figure 4.43 (a-b), the whole cells completely disappeared, and nothing was observed except for a large number of fibriform cell pieces. The cell pieces observed in Figure 4.43 (b) were possibly due to lysis of the bacterial cells leading to leakage of damaged DNA molecules. This implies that a stronger oxidizing intermediate was formed to destroy the cells more thoroughly.

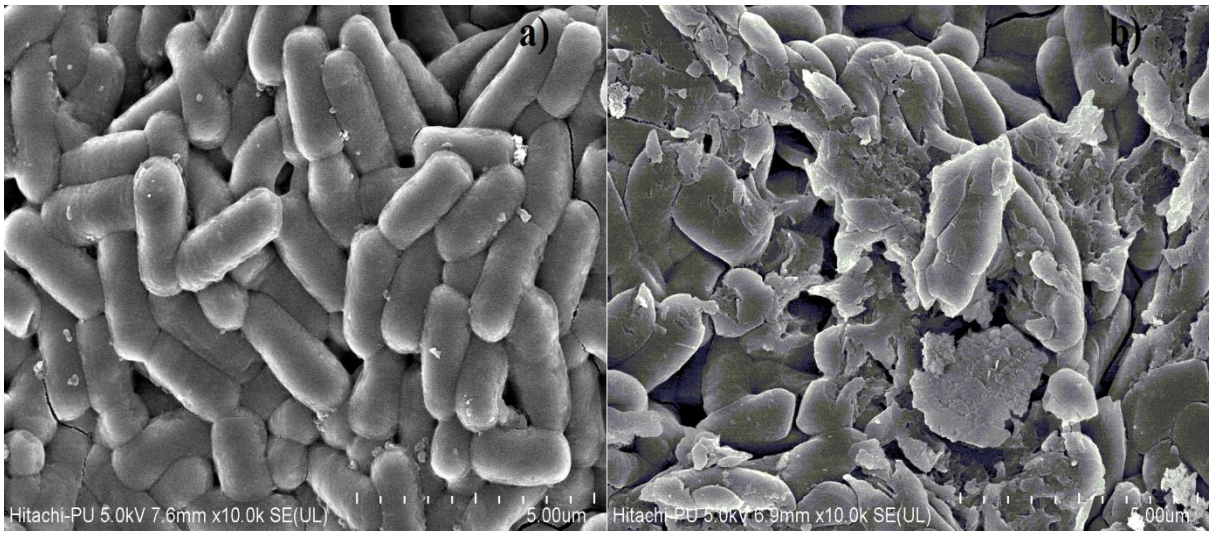

Figure 4. 43 (a) FESEM image of *E.coli* before treatment (b) FESEM image of inactivated *E. coli* after treatment

The outer membrane of *E. coli* is made up of a lipopolysaccharide layer that plays an important role by acting as a barrier to the permeability of the Gram-negative bacteria. K^+ is present in all bacteria (Chang et al., 2008; Hu et al., 2007; Lin et al., 2021) and is required for the proper regulation of protein synthesis and polysome content. As a result, K^+ leakage from *E. coli* was used in this study to better characterize the cell membrane's permeability. The Fe-TiO_2 composite could damage the outer cell wall and the membrane by ROS and could lead

to an increase in the permeability of the cell and subsequent seeping of intracellular substances such as K^+ (Chang et al., 2008; Hu et al., 2007). To see the comparison between treated and non-treated water, K^+ leakage tests of both initial (without treatment) and final (after treatment) were analyzed (shown in Figure 4.44 a-b).

Without the addition of a catalyst, there was nearly no K^+ leakage from *E. coli* cells in the control experiment (some cells may have been injured during the process) (Figure 4.44a), and the concentration of K^+ was relatively stable for 140 min. When Fe-TiO_2 catalyst was used, a gradual increase in the K^+ concentration was observed till 60 min of the treatment and then became steady with an increase in the treatment time. In this hybrid effect study, the K^+ ion instantly leaked out, and the concentration of leaked K^+ increased in parallel with the *E. coli* inactivation with irradiation time. The total K^+ concentration (7 ppm) from the tested *E. coli* was completely released when all the *E. coli* was completely killed at 60 min of irradiation as shown in Figure 4.44 (b). This result suggested that the cell membrane permeability had been disrupted with the inactivation of *E. coli.*

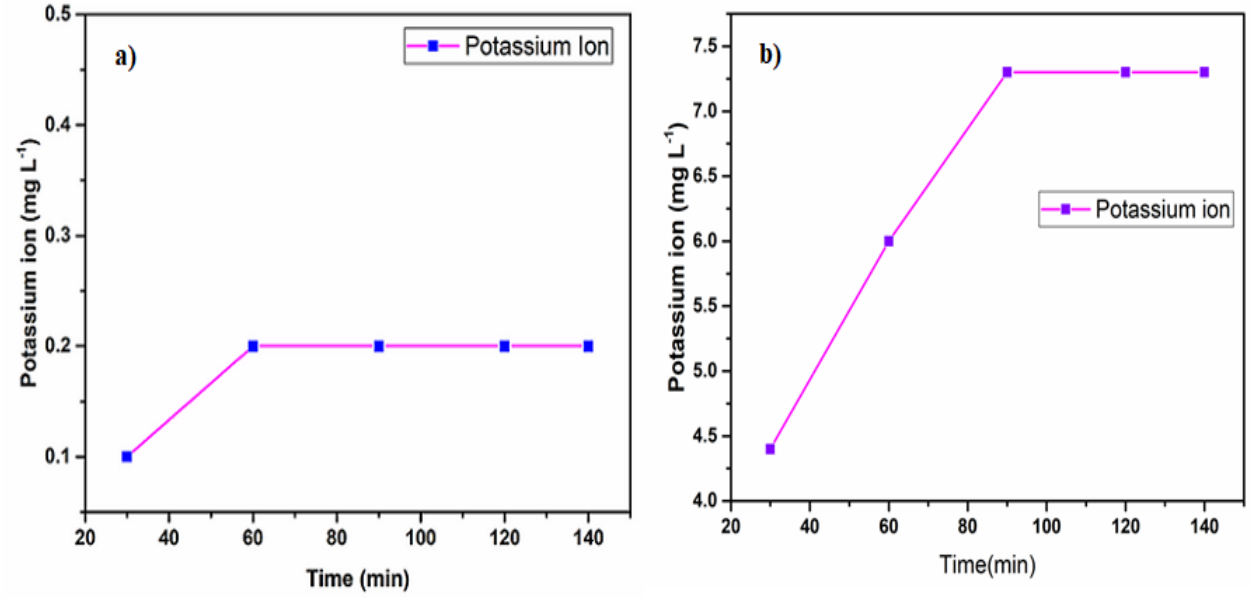

Figure 4. 44 Leakage of potassium ion from the cell damage (a) in controlled condition (without treatment) (b) after treatment

4.6.5.6 Photo-reactivation of *E. coli*

During many deactivation experiments, the bacteria tend to regrow by repairing their damaged DNA in the absence (dark condition) or in the presence (photo-reactivation) of light. Therefore to evaluate bacterial regrowth, samples from the disinfection experiments

(photocatalysis, photo-Fenton, and hybrid process) for which no bacteria were detected after treatment were selected. The reactivation studies of *E. coli* in treated water were done in the dark and natural solar light. The photoreactivation capacity was assessed by taking out 100 mL of the treated water after each experiment. The treated sample was stored in a sterile conical flask and kept at continuous stirring for 3 h, 24 h, and 48 h under dark and natural solar light conditions as shown in Table 4.17. The viability of *E. coli* in the treated sample was analyzed using the same standard method implemented for inactivation experiments

Table 4. 17 Photoreactivation of *E. coli* under natural solar light and dark conditions, in solar light, inactivated water

Technology	***E.coli Concentration***	***Treatment time (min)***	***Treatment***	***E. coli Survival after 3 h inactivation***		***E. coli survival after 24 h of Inactivation***		***E. coli survival after 48 h of Inactivation***	
				light	***dark***	***light***	***dark***	***light***	***dark***
Phtotocataysis	10^6 CFU/mL	120 min	Solar irradiation	Nd*	Nd	Nd	Nd	Nd	Nd
Photo-Fenton	10^6 CFU/mL	100 min	Solar irradiation	Nd	Nd	Nd	Nd	Nd	Nd
Hybrid	10^6 CFU/mL	45 min	Solar irradiation	Nd	Nd	Nd	Nd	Nd	Nd

Nd* = not detectable

4.6.6 Scale-up studies and cost analysis

The scale-up studies are the significant part as they serve the interface between the prototype and the model which is performed using the scale-up factors. The commercial-scale applications of any process would certainly contemplate the economics of the process. The present research emphasizes the estimation of process economics by combining the tentative

cost of raw materials and other process variables. The approximated cost involved in the treatment of wastewater is mentioned in Table 4.18. The anticipated cost can further be changed once the design components of the industrial-scale reactors are taken into consideration. To gauge the treatment cost of a modern scale reactor, let us think about the measure of wastewater being 6,000 L. To assess this, the 0.6 rule was utilized for scaling up(Tribe and Alpine, 1986) and according to Equation (4.17).

$$Cost_B = Cost_A(\frac{Size_B}{Size_A})^N \quad (4.17)$$

The size exponent is denoted by N, the dimensionless size factor is denoted by $Size_A/Size_B$. As discussed, we have considered scaling up the reactor by 6000 times. The values for various N were reported from (Tribe and Alpine, 1986).

The cost analysis showed the total cost of operation to be 0.06 US$ for one reaction per cycle, making it more feasible for the application in the industries, as shown in Table 4.18. The expenditures indicated in the present research are much less than those found in earlier research on AOPs (Ozkal et al., 2016; Vishnuganth et al., 2016). The majority of research has assessed simply the cost of electricity consumed during the reactions or the cost analysis, not taking into account the cost of fabrication of reactor (Haranaka-Funai et al., 2017; Mehrjouei et al., 2014). Due to the remarkable reusability/durability of Fe-TiO_2 composite beads, the total cost of the present technique can be decreased further by using them for multiple cycles. As a result, a cascade reactor system equipped with extremely stable and durable Fe-TiO_2 composite beads would provide a reduced-cost solution for wastewater treatment with a short treatment time.

Table 4. 18 Cost analysis for the complete hybrid-process and scale-up study

Capital Cost	**Energy consumption**
Cost of Reactor fabrication= 14 US$ The cost of fittings and pipings= 5US$ Any pre-treatment required = 3.28US$ The total cost involved in fabrication = 22.28 US$	Cost of energy consumption=0.81 $/kwh
Catalyst and raw material	**Other costs involved**
The cost involved in catalyst	Various costs involving baffles controls = 8

Raw material cost (FS, FA, and clay) = 0US$ Cost of TiO_2 catalyst = 1.152US$gm^{-1} Total Price = 1.2045 US$	US$ Various Contingency cost = 2US$
Cost of oxidant involved H_2O_2 usage= 1.4 mL for 6L For 100 runs= 1.4×100=140 mL The total cost of H_2O_2 used= 1.69 US$	**Total cost** Overall Total cost involved = 36 US$ for 100 recycles and 6 L Treatment cost/ L per cycle = 0.06US$
Scale-up cost analysis (6,000L) Scale-up cost of raw material = 75.99 US$ Scale-up cost of energy comsumption = 51.1 US$ Scale-up cost of oxidant= 106.63 US$ Scale-up cost of reactors fabrication = 1405.8 US$ Other miscellaneous cost and contingency = 630.9 US$ Total cost = 2270.42 US$ (for 100 reactions handling 6,000L Volume) Cost for 1 reaction per cycle = 0.00378 US$	

4.7 Section C (Disinfection of real secondary treated municipal wastewater effluent (MWWT))

4.7.1 Applications of the in-situ hybrid process for the disinfection of real MWWT

Following the demonstration of the in-situ hybrid effect and extensive durability study of Fe-TiO_2 composite beads, the process was extended to the disinfection of real secondary treated municipal wastewater effluent. Table 4.19 lists the key characteristics of the treated wastewater sample. The study's primary goal is to enhance the disinfection of municipal wastewater in a shorter treatment time so that an in-situ hybrid process could be effectively used as a tertiary treatment before it is discharged into the environment.

To improve the efficacy of the hybrid process, different parameters such as pH of the solution, H_2O_2 concentration, and the surface area covered using composite beads were used to optimize the batch reactor under solar irradiation.

Table 4. 19 Physico-chemical analysis of municipal wastewater

Wastewater characteristics	Concentration
pH	7.72
Nitrates	13.63 ± 0.20 mg L^{-1}
Phosphates	4.1 ± 0.3 mg L^{-1}
BOD	118 ± 2.3 mg L^{-1}
COD	200 ± 4.2 mg L^{-1}
Total bacteria count	10^5 CFU mL^{-1}

4.7.2 Prominence of hybrid process

The MWW effluent was subjected to different photo-treatment processes before actually conducting the hybrid effect experiments (coupling of photocatalysis and photo-Fenton). All experiments were performed in natural solar irradiation under acidic conditions. Dark studies (i.e., adsorption) were carried out, which revealed an insignificant reduction in bacterial count in each case. Photolytic studies in the presence of solar light also showed a <1 log reduction after 60 min of reaction time. Thus, it was confirmed that adsorption and photolysis did not impart any significant contribution to the treatment of wastewater.

The TiO_2-photocatalysis reaction was also performed in solar light using composite beads coated with TiO_2 at the neutral state, and after 60 min of illumination, roughly 1 log decrease was detected. In the photo-Fenton process, for the iron lixiviating to begin, the pH of the reaction was kept at 4-4.5, and bacterial inactivation was seen as shown in Figure 4.45. In this method, 0.75 g L^{-1} of H_2O_2 was introduced to initiate the reaction, and after 60 min of reaction time, a 1.2 log decrease was detected. On the other hand, the hybrid process by integrating photocatalysis and photo-Fenton showed a complete reduction of bacteria present in wastewater in 60 min of treatment. Therefore, the prominence of the hybrid effect was established in fixed mode. This dominance of the hybrid process was set by optimizing the following parameters (% surface area covered, pH, and H_2O_2 concentration).

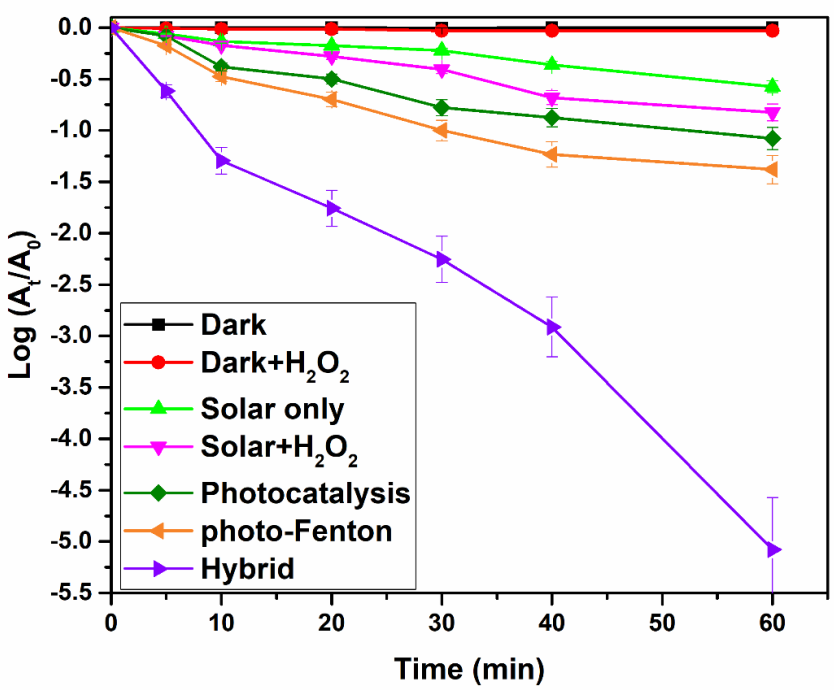

Figure 4. 45 Preliminary analysis of bacterial inactivation

4.7.3 Parametric optimization

4.7.3.1 Effect of surface area covered

The impact of surface area covered for wastewater disinfection was examined in this study by varying the number of composite beads on the surface of the reactor. The optimum number of catalytic beads required for disinfection is investigated in this effect. As a result, the analysis was depicted as a percentage area covered, with a change in the number of beads. As shown in Figure 4.46, increased log reduction was observed when the coverage of the surface of the reactor was changed from 50% to 100%. With an increase in the amount of catalyst, there is an increase in the active sites, resulting in the inactivation efficacy with the production of more OH°. When the coverage of the reactor's surface was further increased to 150%, a decrease in the bacterial log reduction was found. This could be due to excessive iron lixiviation from the beads, which obstruct the active surface area of the catalyst, resulting in a decrease in the log reduction through the formation of dead zones. When the % area covered was increased further to 150%, a decrease in the bacterial log reduction was found. This could be because of the excessive iron lixiviation from the composite beads that block the catalyst's active sites, resulting in a decrease in the log reduction. There might be the formation of dead zones due to the overlapping of beads which effectively reduce the volume of wastewater to be treated.

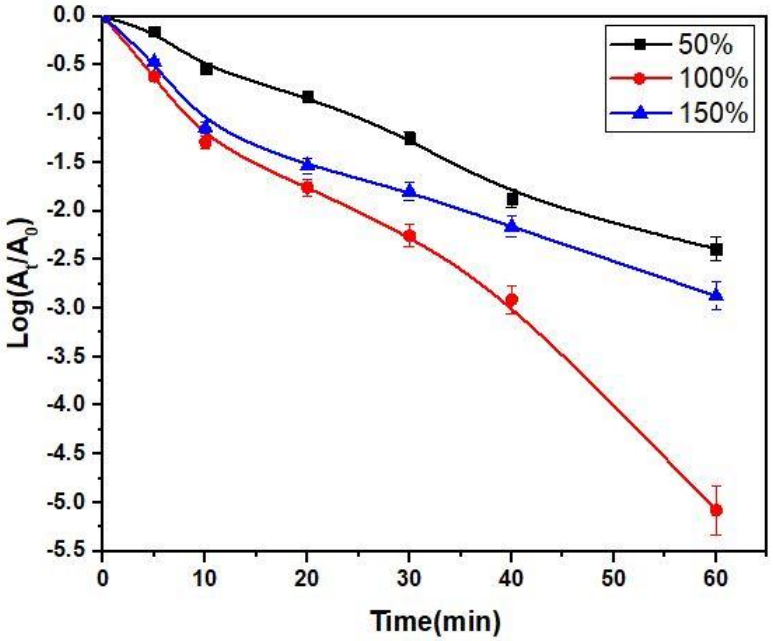

Figure 4. 46 Effect of variation of percentage surface area covered on bacterial inactivation

4.7.3.2 Effect of pH change

pH is a critical parameter in the hybrid process because iron leaches from composite beads under acidic conditions. The iron then performs the photo-Fenton reaction in the system with H_2O_2. To optimize the pH, studies were conducted at various pH values ranging from 4.5 to 6.5, as illustrated in Figure 4.47. The experiment was completed in 60 min with 0.75 g L^{-1} of H_2O_2 concentration. As illustrated in Figure 4.47, maximal bacterial inactivation (5 log units) was achieved in 60 min at pH 4.5. At pH 5.5, a slight drop in log reduction (4.0) was seen after 60 min. The inactivation effectiveness reduces as the pH increases above 5.5 due to the generation of less effective HO_2^- at alkaline conditions. Then its reaction with non-dissociated H_2O_2, O_2, and H_2O are formed, ultimately decreasing the process efficacy as shown in Equation (4.18). Moreover, the formation of OH^o slows down at high pH levels due to the hydrolysis of ferric ions and precipitation of ferric oxyhydroxide complex from the solution, which impacts the generation of OH^o (Herney-Ramirez et al., 2010). As a result of the findings, it is evident that pH has a substantial effect on inactivation.

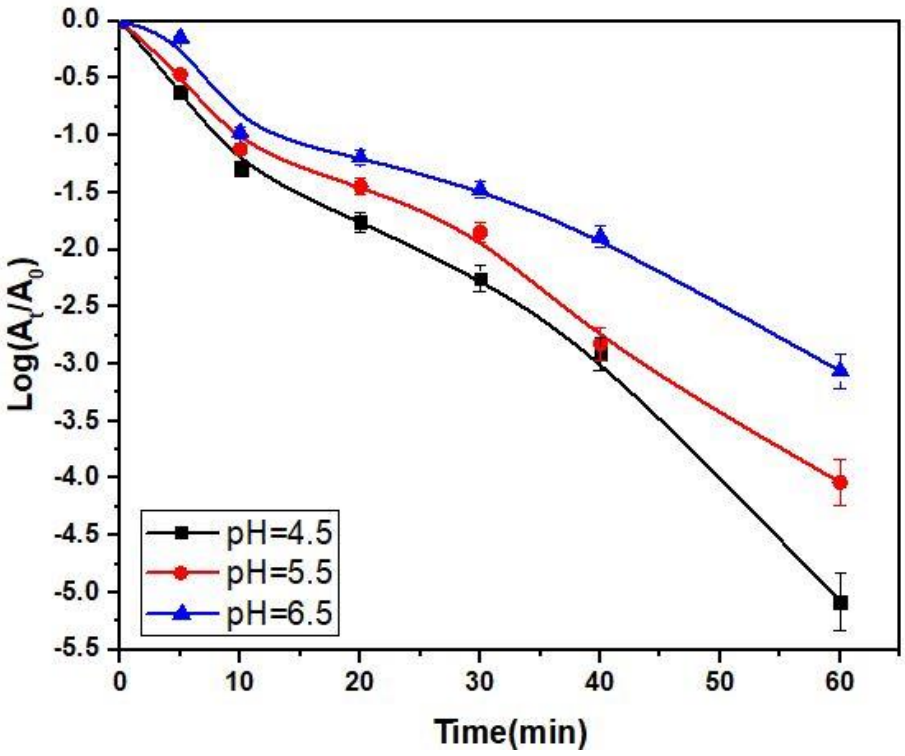

Figure 4. 47 Effect of variation of pH on bacterial inactivation

From the aforementioned results, it was observed that with the increase in the pH, the bacterial log reduction decreases. This is because of the dependency of iron leaching from the composite on the pH of the solution. As the pH of the solution decreases, the lixiviation of iron from the composite increases. In soil, iron is found in association with other components, and acid (pH< 6) aids in disrupting the binding between iron and an organic compound. Thus removing the iron from the clay, is a process known as iron leaching (Hseu, 2004). This was further confirmed by analyzing iron leaching from the Fe-TiO_2 beads under solar light at different time intervals and the results are shown in Table 4.20-4.22. The concentration of iron was found to be increased when pH was decreased from 6.5 to 4.5, subsequently showing an increase in the inactivation efficacy. The pH of the solution was not decreased beyond 4.5 because at lower pH the scavenging effect of OH^o predominates by H^+ (Yadav, 2010), as given in Equation (4.19).

$$H_2O_2 \rightarrow HO_2^- + H^+ + H_2O + O_2 \quad (4.18)$$

$$OH^o + H^+ + e^- \rightarrow H_2O \quad (4.19)$$

Table 4. 20 Concentration of Iron species leaching out of composite beads at pH 4.5

Time (min)	Concentration (µg L^{-1})		
	Ferrous ions	Ferric ions	Total Iron
10	51.54	106.15	157.69
20	53.85	107.69	161.54
30	57.69	108.85	166.54
40	63.08	103.08	166.15
50	68.85	100	168.85

Table 4. 21 Concentration of Iron species leaching out of composite beads at pH 5.5

Time (min)	Concentration (µg L^{-1})		
	Ferrous ions	Ferric ions	Total Iron
10	48.46	78.46	126.92
20	50	92.31	142.31
30	55.77	93.85	149.61
40	61.54	98.08	159.61
50	65	97.31	162.31

Table 4. 22 Concentration of Iron species leaching out of composite beads at pH 6.5

Time (min)	Concentration (µg L^{-1})		
	Ferrous ions	Ferric ions	Total Iron
10	38.46	52.69	91.15
20	39.23	58.85	98.08
30	40	60	100
40	41.15	69.23	110.38
50	41.92	73.46	115.38

4.7.3.3 Effect of H_2O_2 concentration

Numerous studies have investigated the influence of H_2O_2 on photo-Fenton and photocatalysis, as it is a well-established method for increasing the amount of OH^o in the system. In the current case, as discussed earlier, the introduction of H_2O_2 serves a dual purpose because it is used concurrently in both processes, as demonstrated in Equation (4.20-4.22). In a photocatalytic reaction, oxidants are supplied to react with the electron in the conduction band, preventing electron-hole recombination, as mentioned earlier in Equation (4.20). Thus, optimizing its concentration was critical for both in-situ procedures. Additionally, this hybrid process enhances the formation of reactive oxygen species and OH^o. The concentration of H_2O_2 was tuned in this study by adjusting it between 0.3 and 0.9 g L^{-1}, with the best concentration determined to be 0.9 g L^{-1} at pH 5.5. Following dose optimization, complete inactivation of bacteria was seen within 60 min of reaction time having 0.9 g L^{-1} of H_2O_2 as illustrated in Figure 4.48. This is due to the increased availability of H_2O_2 molecules to react with Fe^{2+} ions, increasing the amount of OH^o, as shown in Equation (4.21).

$$TiO_2(e^-) + H_2O_2 \rightarrow TiO_2 + OH^- + OH^o \quad (4.20)$$

$$Fe^{2+}_{(aquous)} + H_2O_2 \rightarrow Fe^{3+}_{(aquous)} + OH^o + OH^- \quad (4.21)$$

$$Fe^{3+}_{(aquous)} + H_2O_2 \rightarrow Fe^{2+}_{(aquous)} + H_3O^+ + HO_2^- \quad (4.22)$$

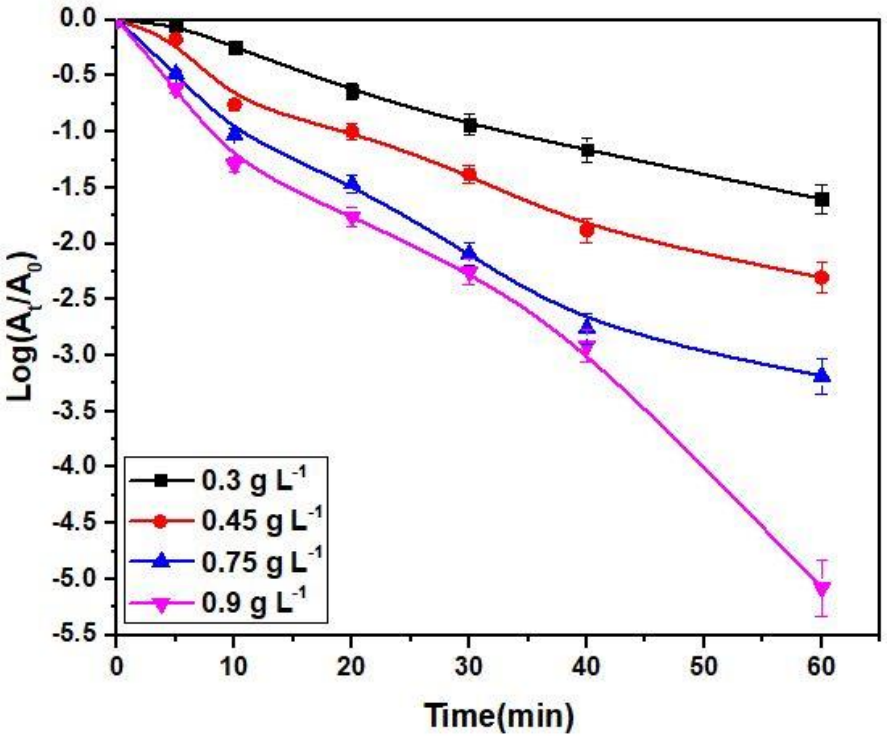

Figure 4. 48 Effect of variation of H_2O_2 doze on bacterial inactivation

4.7.4 Kinetic analysis

A kinetic assessment of the results using five different models such as Log-linear, Weibull, double Weibull, the biphasic, and biphasic shoulder was performed to evaluate and compare the three different processes (hybrid, photo-Fenton, and photocatalysis).

It is critical to establish suitable treatment conditions using a reliable mathematical model that accurately depicts the microbial inactivation kinetics. The parameters R^2 and RMSE were used to ascertain the model's accuracy. The findings of the statistical data of kinetic changes in resistance to treatment for all microorganisms used in this study incorporating various models are summarized in Table 4.22, 4.23 & 4.24. The results obtained following bacterial inactivation in three different fixed-bed processes using solar irradiation demonstrated an excellent fit to the mathematical models used (Figure 4.49). With R^2 values reaching 1 and RMSD values reaching zero, the Weibull and double Weibull distribution model provided the best fit. The δ value parameter in the Weibull model represents the time required for the first decimal reduction of a bacterial colony or the reciprocal of the microbial inactivation rate. That is, the higher the δ value, the slower the process of microorganism inactivation. In this study, values (Table 4.22) for the hybrid process were more significant than those for the other individual processes. The low values

obtained demonstrated the hybrid process's unlimited effectiveness in inactivating bacteria. When the k and values of three different processes were compared as shown in Tables 4.23, 4.24 & 4.25, it was discovered that the hybrid process reduced *E. coli* at a faster rate. Thus, using log-linear and Weibull parameters to fit the *E. coli* inactivation results and comparing the different techniques revealed that the hybrid-technique in fixed mode ($k = 0.08\ min^{-1}$; $\delta = 3.01$ min) was considerably faster than the other technologies: photocatalysis ($k = 0.06\ min^{-1}$; $\delta = 96.48$ min); and photo-Fenton ($k = 0.04\ min^{-1}$; $\delta = 53.9$ min). For further confirmation of the prominence of the hybrid process photoluminescence spectroscopy of three different processes (photo-Fenton, photocatalysis, and hybrid process) was performed as shown in Figure 4.50. Figure 4.50 showed the higher production of OH^{o} in the hybrid process in comparison to the other two processes leading to the complete inactivation of the bacteria present in wastewater.

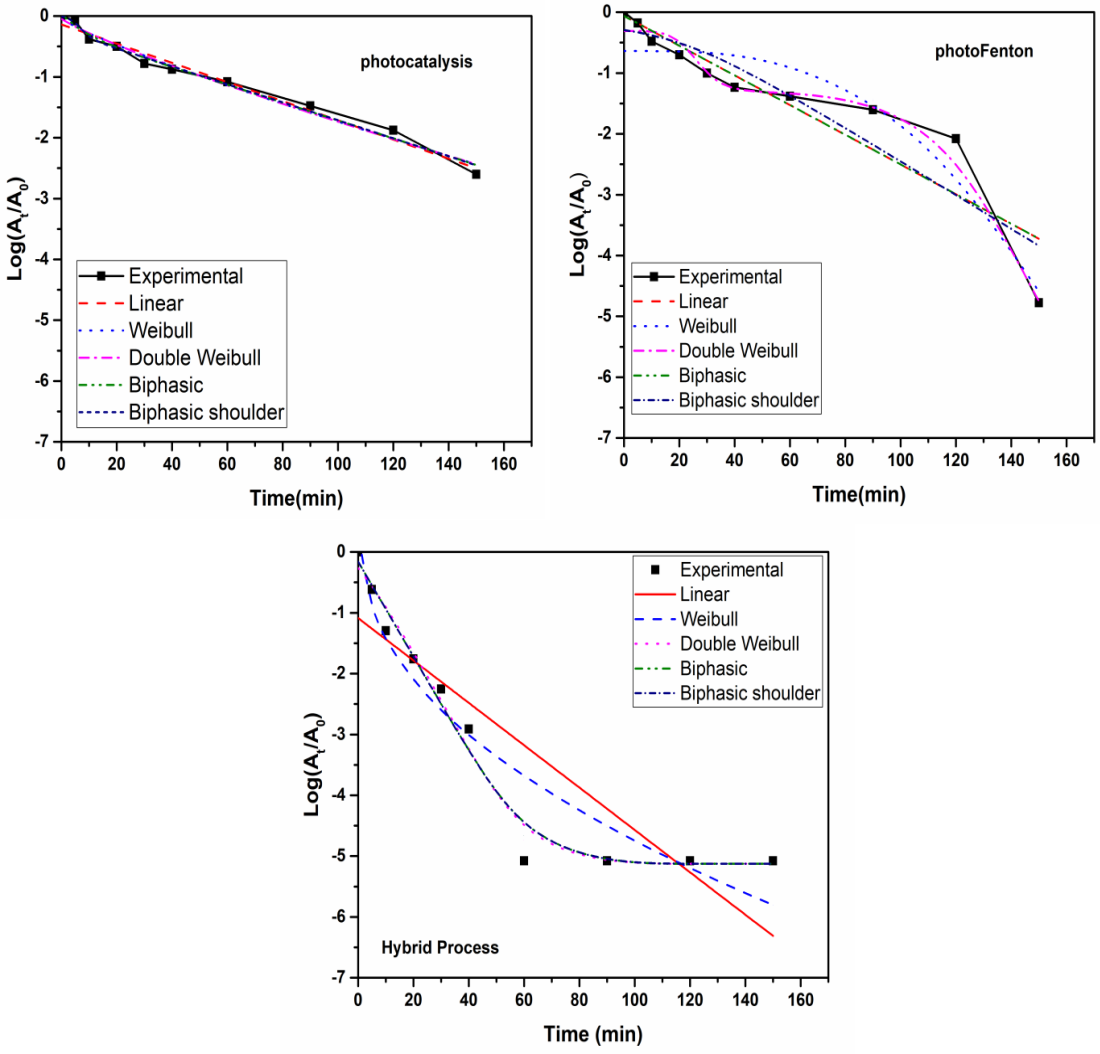

Figure 4. 49 Fitting mathematical models to the photocatalysis, photo-Fenton, and hybrid-process inactivation curves of bacteria

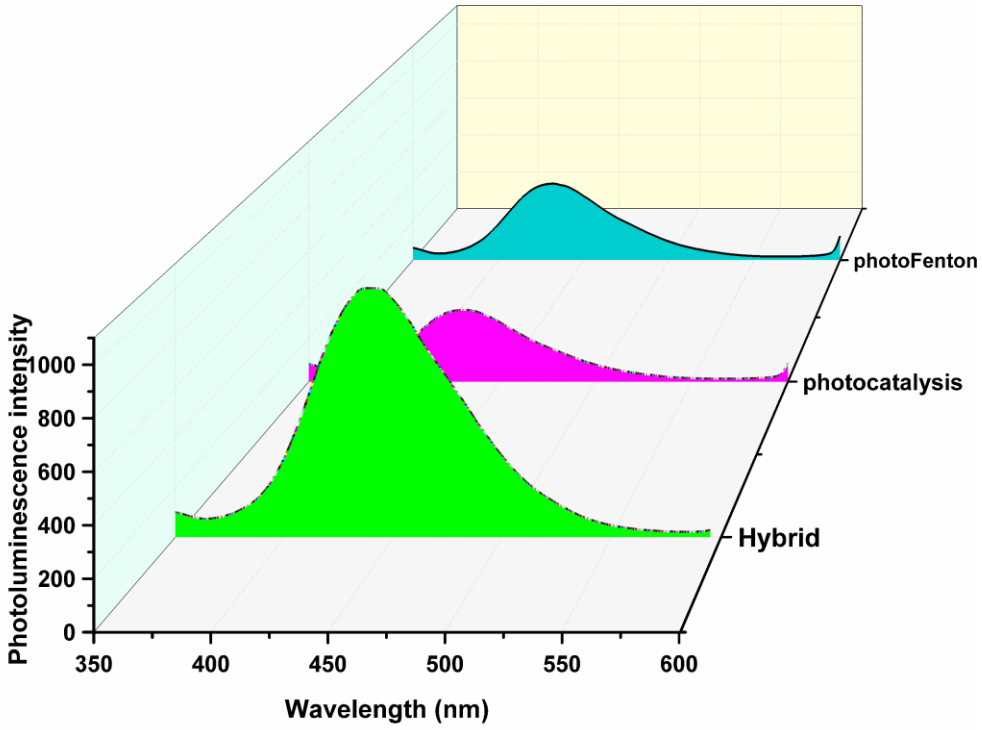

Figure 4. 50 Photo luminance spectra of OH^{o}at different processes

Table 4. 23 Kinetic analysis of the hybrid process using different models

Technology	Different types of models	k (min^{-1})	k_{1max}	k_{2max}	δ_1 (min)	δ_2 (min)	$\frac{R^2}{RMSD}$
Hybrid							
	Log-linear	0.18	-	-	-	-	0.79/0.0.96
	Weibull	-	-	-	3.01	-	0.911/0.464
	Double-Weibull	-			15	62	0.98/0.085
	Biphasic	-	0.18	0	-	-	0.98/0.088
	Biphasic-shoulder	-	0.18	0	-	-	0.98/0.106

Table 4. 24 Kinetic analysis of the photo-Fenton process using different models

Treatment	Models	K (min^{-1})	K_{1max}	K_{2max}	δ_1 (min)	δ_2 (min)	$\frac{R^2}{RMSD}$
photo-Fenton							
	Log-linear	0.06			-	-	0.84/0.31
	Weibull	-			96.48	-	0.90/0.23
	Double Weibull	-			29.7	122.06	0.98/0.047
	Biphasic	-	0.06	0.06	-	-	0.84/0.42
	Biphasic-shoulder	-	0.06	0.06	-	-	0.85/0.49

Table 4. 25 Kinetic analysis of the TiO_2-photocatalytic process using different models

Treatment	Models	K (min^{-1})	K_{1max}	K_{2max}	δ_1 (min)	δ_2 (min)	$\frac{R^2}{RMSD}$
photocatalysis							
	Log-linear	0.04			-	-	0.98/0.015
	Weibull	-			53.9	-	0.98/0.0153
	Double Weibull	-	-	-	53.91	53.91	0.98/0.0178
	Biphasic	-	0.83	0.03	-	-	0.98/0.0127
	Biphasic-shoulder	-	1.22	0.03	-	-	0.99/0.0126

4.7.5 Degradation of organic compounds

When it comes to wastewater treatment, it becomes vital to analyze the process's overall performance. As a result, the elimination of chemical oxygen demand (COD), biochemical oxygen demand (BOD), nitrate (NO_3^-), and Total phosphorous was detected throughout the treatment process using the hybrid process at its optimized conditions (H_2O_2 = 0.9 g L^{-1}, pH = 5.5, the surface area covered = 100%) (Figure 4.51 a-d).

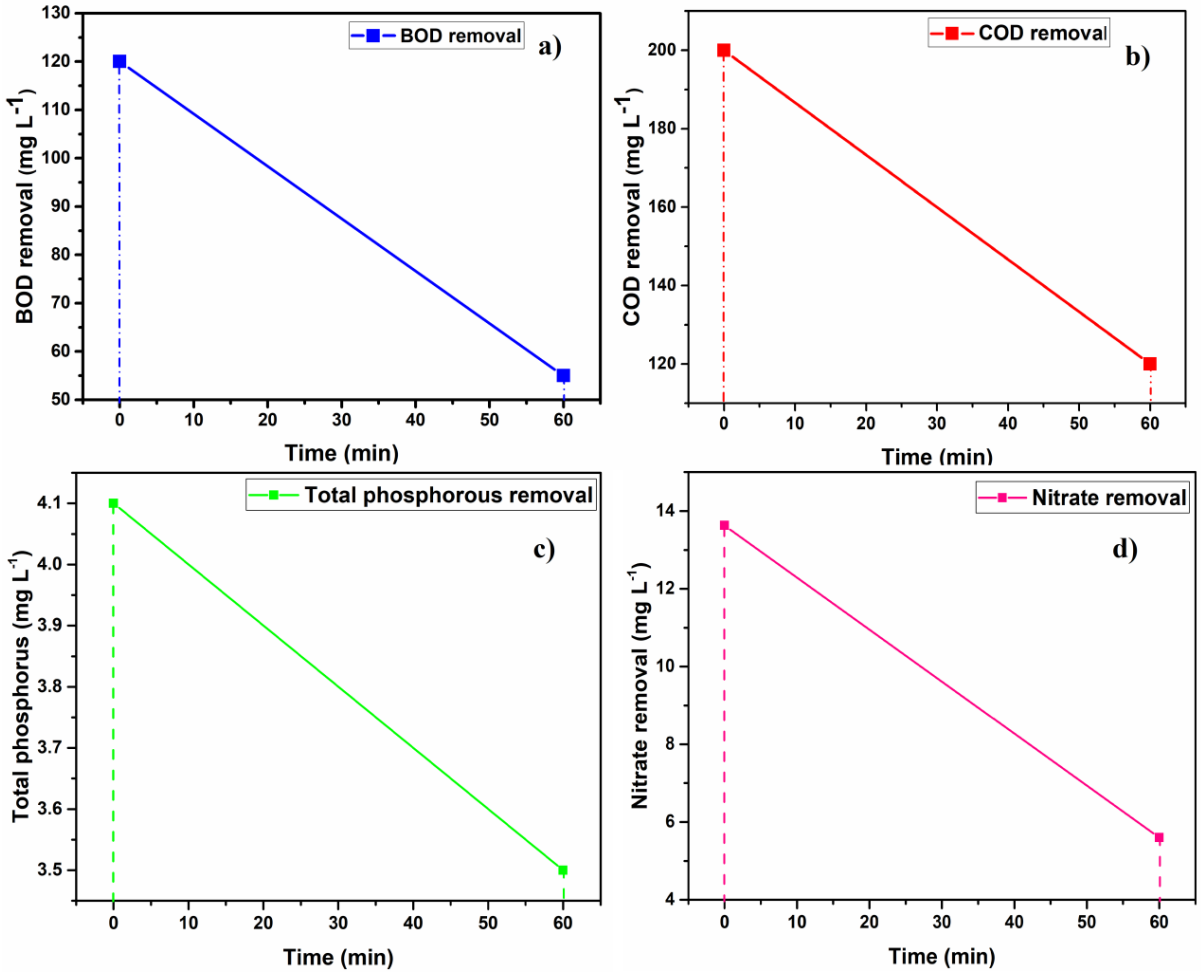

Figure 4. 51 Treatment of wastewater effluent using Fe-TiO_2 composite (a) BOD removal (b) COD removal (c) Total phosphorous removal (d) Nitrate removal

In the present work, the concentration of nitrate and phosphates ions decreased from 13.3 mg L^{-1} to 5.6 mg L^{-1} and 4.1 mg L^{-1} to 3.5 mg L^{-1} respectively in 60 min of treatment time. There was almost a 40% and 54% reduction in both COD and BOD, respectively, after 60 min of treatment. This significant decline in COD and BOD was credited to the leached iron enabling photo-Fenton reaction in conjunction with the intact TiO_2 layer, facilitating

photocatalysis. Additionally, when the entire bottom surface area of the batch reactor was covered entirely with beads, the exposed active sites of the catalyst were maximized and were freely available for effective binding with the pollutant, resulting in the removal of pollutants present in the wastewater.

The scale-up trials using the in-situ hybrid process for the treatment of actual municipal wastewater were executed in a pilot-scale solar once-through cascade reactor system with total volume handling of 5 L. As shown in Figure 4.52 (a&b), the reactor was optimized by varying the flow rate (3 L h^{-1} to 20 L h^{-1}), and H_2O_2 concentration (0.45 to 0.9 g L^{-1}) with 100 % surface area of the reactor covered with composite beads. At a flow rate of 3 L h^{-1} with optimized H_2O_2 doze i.e., 0.9 g L^{-1}, the reaction time was 1 h 20 min with an overall log reduction of 4.5 at the outlet of the third reactor. With a further increase in the flow rate to 8 L h^{-1}, a similar bacterial log reduction (4.1 logs) was observed with the decrease in the treatment time (45 min). Therefore, from an economic point of view, 8 L h^{-1} was preferred as the optimized flow rate for further experimentation. This reactor system using Fe-TiO_2 composite beads incorporating an in-situ hybrid effect gave promising results in context to the treatment of effluent. The solution, after retaining for almost 15 min, in a reactor came into contact with a fresh batch of composite beads in the successive reactor. All active sites of catalyst were freely available to make contact with the pollutant in case of a fresh batch of composite beads, which intensified the process efficacy.

While in the case of a lab-scale batch reactor, the solution remained in contact with the same composite beads during the whole reaction period with a possibility of blocking some of the active sites of the catalyst during the reaction. Therefore the treatment time was found to be high for the batch reactor in comparison to the once-through cascade reactor. Moreover, the simultaneous occurrence of both effects within the same system accelerates the disinfection process in subsequent cascades, which is prominent in our results as 5 L of municipal wastewater was treated in 45 min. Thus, such promising results at the pilot scale for the treatment of real effluent under natural solar irradiations further confirmed the field-scale applications of the fixed-bed in-situ dual process using Fe-TiO_2 composite beads.

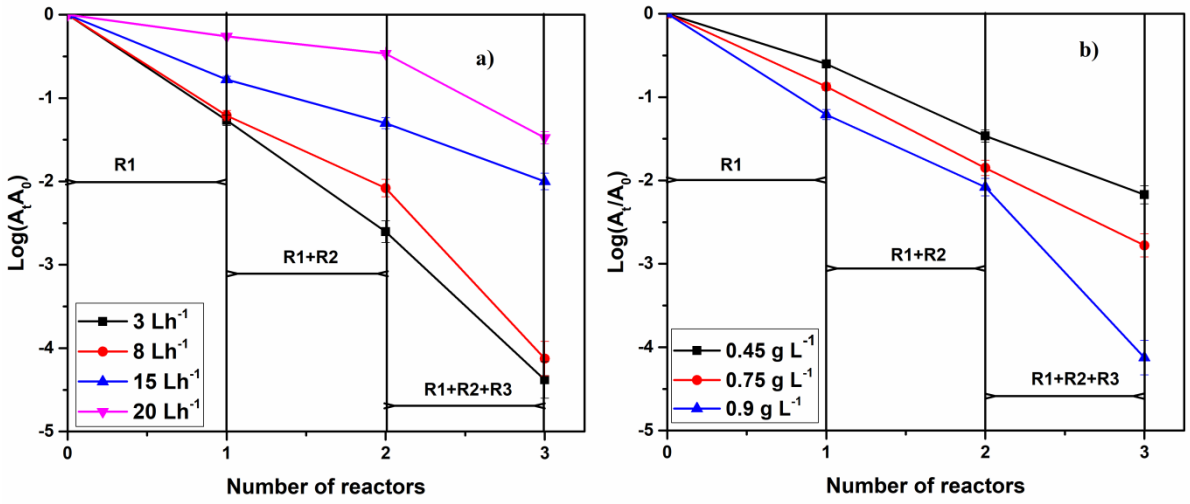

Figure 4. 52 Change in the concentration of *E. coli* with (a) variation in the number of reactors (b) variation in the concentration of H_2O_2 doze

4.7.6 Durability studies

The durability of the immobilized catalyst with retained activity is a critical challenge while visualizing the proposed concept of the hybrid process on a large scale. The primary objective of this research was to investigate the in-situ hybrid effect in disinfection tests. Thus, the reported investigation should demonstrate both the sustainability of iron leaching and the stability of the TiO_2 coating on the composite beads (Fe-TiO_2) by subsequent recycling experiments. The durability of the composite beads was evaluated in terms of both catalysts remaining intact (i.e., TiO_2 and iron). The durability and activity of catalyst (Fe-TiO_2 composite) were examined through recycling experiments for the disinfection of bacteria present in wastewater. The beads were effectively employed for at least 35 trials without showing any significant decrease in bacterial log reduction activity. After 10 recycles, there was no significant variation in disinfection efficacy between subsequent runs ($P > 0.05$). The catalyst remained intact on the surface and was sufficiently active to exhibit effective disinfection even after 35 cycles of recycling, as shown in Figure 4.53. Effective disinfection by an in-situ hybrid approach utilizing recycled composite beads verifies the systematic leaching of iron from recycled beads, hence contributing to the photo-Fenton reaction occurring concurrently with photocatalysis. Even in recycled composite beads, the presence of iron and TiO_2 can be confirmed using the characterization of composite beads outlined in the preceding sections.

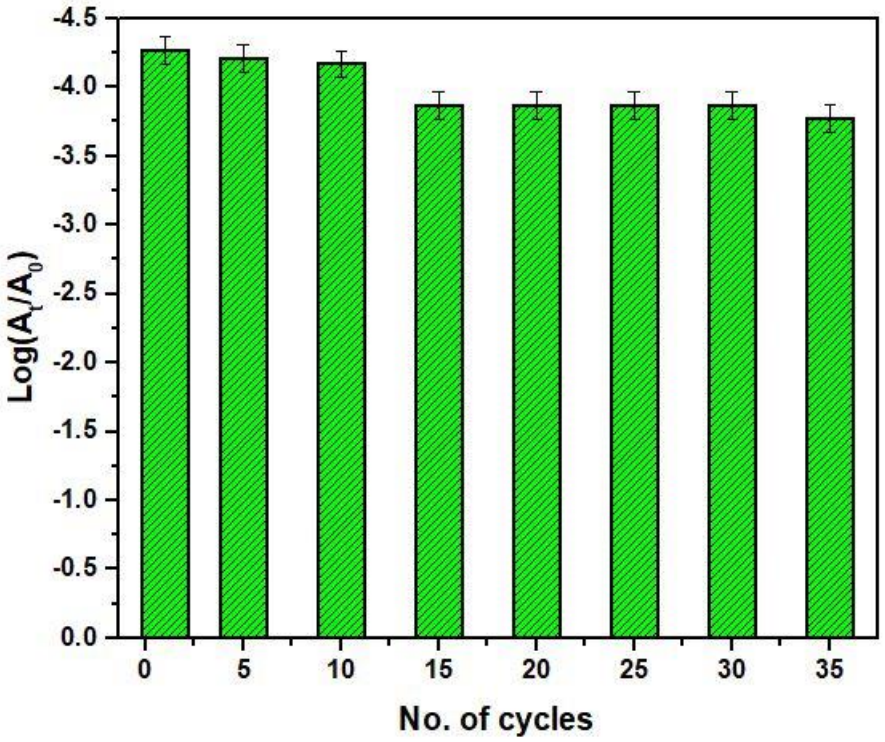

Figure 4. 53 The durability of Fe-TiO_2 composite beads

4.8 Synergistic studies

To investigate the photo-activity of Fe-TiO_2 composite, synergistic studies were performed by three different techniques, which include photocatalysis, photo-Fenton, and hybrid process at optimized conditions. The synergistic studies were performed to check the inactivation efficacy of the hybrid process over the single process as well as some of both processes. In the present work, the synergy of the hybrid process over individual processes has been quantified using the kinetic rate constant obtained through pseudo-first-order reactions. The inactivation experiments of *E. coli* were performed with Fe-TiO_2 composite catalyst in a batch and scale-up reactor under UV and solar light, respectively. Among all the processes, % inactivation of *E. coli* in each study was found maximum in the hybrid process. It was found that the inactivation rate constant obtained under the combined effect of photocatalysis and photo-Fenton (hybrid process) resulted in a reaction rate constant greater than the sum of the reaction rate constants of photocatalysis and photo-Fenton used separately as shown in Table 4.26. Therefore, it concludes that the hybrid process with synergistic results prompts its field-scale applications for water disinfection with a significant decrease in treatment time.

Table 4. 26 Synergy of hybrid-process over the individual process and combined process

Study	**The synergy of the hybrid process on the photocatalysis process**	**The synergy of the hybrid process on the photo-Fenton process**	**Overall Synergy** (The synergy of hybrid-process over both photocatalysis and photo-Fenton process)
Lab Scale batch under UV light	67%	59%	26%
Scale-Up			
Recirculating Reactor using UV light	61%	55%	17%
Once-through Reactor under natural solar radiation	64%	45%	9.8%
Real wastewater			
Batch Reactor under solar radiation	74%	66%	41%

Chapter 5

Conclusions and Recommendations

5.1 Conclusions

The application of a commercially viable catalyst employing an in-situ hybrid process (consisting of photocatalysis and photo-Fenton in one system) in fixed mode has been studied for the inactivation of *E.coli* present in water. This study discusses the potential applications of a low-cost composite composed of foundry sand (FS) and fly ash (FA) for combining hybrid effects. This composite has the intrinsic characteristic of containing iron, which lixiviates in acidic conditions (resulting in photo-Fenton), as well as surface-coated TiO_2, which results in photocatalysis, demonstrating a hybrid effect. The composite support was chosen based upon the strength of beads, intactness of the layer of TiO_2, and continuous lixiviation of iron.

An equilibrium study of this hybrid process was established to ensure that the systematic iron leaching in the system eliminates the formation of iron sludge. This equilibrium study also took into account the reduction of Fe^{3+} to Fe^{2+} by its reaction with $e^-_{(CB)}$ and with H_2O_2 individually under the influence of photons. Thus proving the hypothesis of overcoming the electron-hole recombination and iron sludge formation mentioned in the present research. After confirming the hybrid effect of the system by establishing the equilibrium, the following conclusions based on the experimental results are listed below:

5.1.1 Inactivation of *E. coli* under UV and solar irradiation (Batch scale reactor)

- The Fe-TiO_2 composite was used for carrying out the optimization of the in-situ hybrid process for the disinfection of *E. coli*.
- The optimized conditions obtained for the disinfection of *E. coli* under UV light in fixed bed reactor were UV light intensity = 25 W m^{-2}, size of beads =10 mm, the addition of oxidant = 0.3 g L^{-1}, pH=3.5, and area/volume ratio = 0.18 cm^2 mL^{-1}.
- This optimized condition showed 6.2 log reduction of *E.coli* in 90 min of reaction time.

- An increase of 26 % of synergy with the hybrid-process was obtained in comparison to photocatalysis and photo-Fenton alone.
- In this study, the experiments were also extended in sunlight (UV + visible) at optimum conditions to confirm the viability of the process for real-time application.
- The optimum conditions for this study were the same as for the reaction under UV radiation and complete inactivation was observed in 30 min of reaction time in comparison to the UV light, where the complete reduction was observed in 90 min.

5.1.2 Inactivation of *E. coli* using recirculation type fixed bed reactor (scale-up study)

- Scale-up studies were also conducted with the development of pilot-scale fixed-bed reactors using novel Fe-TiO_2 composite beads incorporating an in-situ hybrid effect.
- Recirculation type fixed-bed glass reactor with volume handling of 2 L was employed for disinfection of *E. coli* using Fe-TiO_2 composite beads under UV irradiations.
- This hybrid process showed a significant increase in reaction rate constant (0.065 min^{-1}) compared to photo-Fenton (0.029 min^{-1}) and photocatalysis (0.025 min^{-1}) in 150 min treatment time.
- The p-value was less than 0.0001, and the F-value was greater than 5 for each process.
- The optimized values of the operating parameters were found to be 3.5, 62 mg L^{-1}, 106 mL min^{-1} for the reaction pH, H_2O_2 concentration, and flow rate, respectively.
- With these optimum conditions, a percentage reduction of *E. coli* of 93% was observed.
- The total cost of treating 2 L of solution in a single run came out to be US $0.32 and US $0.16 per liter.

5.1.3 Inactivation of *E. coli* using once-through fixed bed reactor (scale-up study)

- On the other hand, a once-through fixed-bed cascade reactor with a handling volume of 6 L was employed for the inactivation of *E. coli* using Fe-TiO_2 composite beads under natural solar irradiations.
- This hybrid process showed an aggressive reduction in *E. coli* cell count with 100% inactivation in water within 45 min of the treatment time.
- This effective result was obtained when the 3 reactors in series having a flow rate of 6 L h^{-1}, 100% surface area covered with beads, and 50 mg L^{-1} of H_2O_2 were used.

- The three reactors in series approached the plug flow behavior as confirmed from the Residence time distribution studies with Pecklet number (Pe) of 78 and mean residence time (MRT) of 42 min.
- The total operating cost for treating water came out to be 0.00827 US$ for one reaction per cycle.
- No regrowth of bacterial cells in the solution even after 48 h of treatment clearly indicated the commercial viability of the present reactor system.
- Also, the total cost of the process assessed in this study is substantially lower than other AOPs-related studies found in the literature.

5.1.4 Inactivation of bacteria present in secondary treated municipal wastewater (At lab-scale and scale-up reactor)

- Finally, to confirm the real-time applications of the in-situ hybrid effect, the actual secondary treated municipal wastewater effluent was investigated.
- This hybrid technology showed 100% inactivation of bacteria with optimized parameters such as 0.9 g L^{-1} of H_2O_2 dose, 5.5 pH, and 100 % surface area covered with the catalyst in 60 min of treatment time.
- 54 % and 40% reduction in BOD and COD respectively was also observed in 60 min.
- The kinetic rate constant was found to be 2 times higher in the hybrid process as compared to the individual process.
- For the scaling up of the process, treatment of 5L of wastewater was performed in a once-through reactor with 4.3 bacterial log reduction in 45 min of treatment time.
- Hence, the extended applications of the novel composite for the disinfection of municipal wastewater even at a large scale confirm the commercial-scale viability of the in-situ hybrid effect.

5.1.5 Durability studies of the composite beads

- The Fe-TiO_2 composite portrayed an exceptional extended durability/recyclability efficacy (>200 recycles) under this entire study as confirmed from analysis, including XRD, SEM, EDS FTIR, and DRS.
- Thus the extended durability and stability of the composite further highlight its commercial applications.

5.2 Recommendations

Fixed-bed in-situ dual process using Fe-TiO_2 composite beads has shown its great potential for the disinfection of water/wastewater. The use of waste materials like foundry sand and fly ash as alternative sources of iron has represented an excellent recycling/reuse option for minimizing such hazardous waste from the environment. Thus, future research would aim toward utilizing more waste materials from the environment as either alternative sources of iron or as effective binding materials that can be used to prepare more durable catalyst immobilized supports.

Furthermore, future investigations would emphasize the more techno-economic analysis for establishing large-scale applications of in-situ hybrid processes in the context of wastewater disinfection using more durable and efficient composite materials. The use of the same composite beads with a more efficient reactor design capable of handling large volumes can open up new channels in the field of wastewater treatment with applications of advanced oxidation technology.

With the scale-up studies, the dual effect has shown its credentials for the utilization for the disinfection of real secondary treated municipal wastewater. However real validation requires effective reactor designing with actual field-scale trails

References

1. Abeledo-Lameiro, M.J., Reboredo-Fernández, A., Polo-López, M.I., Fernández-Ibáñez, P., Ares-Mazás, E., Gómez-Couso, H., 2017. Photocatalytic inactivation of the waterborne protozoan parasite Cryptosporidium parvum using TiO2/H2O2 under simulated and natural solar conditions. Catal. Today 280, 132–138. https://doi.org/10.1016/j.cattod.2016.05.046

2. Acevedo, A., Carpio, E.A., Rodríguez, J., Manzano, M.A., 2012. Disinfection of natural water by solar photocatalysis using immobilized TiO 2 devices: Efficiency in eliminating indicator bacteria and operating life of the system. J. Sol. Energy Eng. Trans. ASME 134, 1–10. https://doi.org/10.1115/1.4005338

3. Adán, C., Magnet, A., Fenoy, S., Pablos, C., del Águila, C., Marugán, J., 2018. Concomitant inactivation of Acanthamoeba spp. and Escherichia coli using suspended and immobilized TiO2. Water Res. 144, 512–521. https://doi.org/10.1016/j.watres.2018.07.060

4. Agulló-Barceló, M., Polo-López, M.I., Lucena, F., Jofre, J., Fernández-Ibáñez, P., 2013. Solar Advanced Oxidation Processes as disinfection tertiary treatments for real wastewater: Implications for water reclamation. Appl. Catal. B Environ. 136–137, 341–350. https://doi.org/10.1016/j.apcatb.2013.01.069

5. Ahmad, N., Gondal, M.A., Sheikh, A.K., 2016. Comparative study of different solar-based photo catalytic reactors for disinfection of contaminated water. Desalin. Water Treat. 57, 213–220. https://doi.org/10.1080/19443994.2015.1012340

6. Ahmed, S., Rasul, M.G., Brown, R., Hashib, M.A., 2011. Influence of parameters on the heterogeneous photocatalytic degradation of pesticides and phenolic contaminants in wastewater: A short review. J. Environ. Manage. 92, 311–330. https://doi.org/10.1016/j.jenvman.2010.08.028

7. Ahmed, Y., Lu, J., Yuan, Z., Bond, P.L., Guo, J., 2020. Efficient inactivation of antibiotic resistant bacteria and antibiotic resistance genes by photo-Fenton process under visible LED light and neutral pH. Water Res. 179. https://doi.org/10.1016/j.watres.2020.115878

8. Akach, J., Kabuba, J., Ochieng, A., 2020. Simulation of the light distribution in a solar photocatalytic bubble column reactor using the monte carlo method. Ind. Eng. Chem. Res. 59, 17708–17719. https://doi.org/10.1021/acs.iecr.0c02124

9. Al-Gheethi, A.A., Efaq, A.N., Bala, J.D., Norli, I., Abdel-Monem, M.O., Ab. Kadir, M.O., 2018. Removal of pathogenic bacteria from sewage-treated effluent and biosolids for agricultural purposes. Appl. Water Sci. 8. https://doi.org/10.1007/s13201-018-0698-6

10. Almuktar, S.A.A.A.N., Abed, S.N., Scholz, M., 2018. Wetlands for wastewater treatment and subsequent recycling of treated effluent: a review. Environ. Sci. Pollut. Res. 25, 23595–23623. https://doi.org/https://doi.org/10.1007/s11356-018-2629-3

11. Alrousan, D.M.A., Polo-López, M.I., Dunlop, P.S.M., Fernández-Ibáñez, P., Byrne, J.A., 2012. Solar photocatalytic disinfection of water with immobilised titanium dioxide in re-circulating flow CPC reactors. Appl. Catal. B Environ. 128, 126–134. https://doi.org/10.1016/j.apcatb.2012.07.038

12. Alvear-Daza, J.J., Sanabria, J., Rengifo Herrera, J.A., Gutierrez-Zapata, H.M., 2018. Simultaneous abatement of organics (2,4-dichlorophenoxyacetic acid) and inactivation of resistant wild and laboratory bacteria strains by photo-induced processes in natural groundwater samples. Sol. Energy 171, 761–768. https://doi.org/10.1016/j.solener.2018.07.026

13. Amadi, A.A., Osu, A.S., 2018. Effect of curing time on strength development in black cotton soil – Quarry fines composite stabilized with cement kiln dust (CKD). J. King Saud Univ. - Eng. Sci. 30, 305–312. https://doi.org/10.1016/j.jksues.2016.04.001

14. Anastasi, E.M., Wohlsen, T.D., Stratton, H.M., Katouli, M., 2013. Survival of Escherichia coli in two sewage treatment plants using UV irradiation and chlorination for disinfection. Water Res. 47, 6670–6679. https://doi.org/10.1016/j.watres.2013.09.008

15. Antonopoulou, M., Konstantinou, I., 2016. Photocatalytic degradation and mineralization of tramadol pharmaceutical in aqueous TiO2 suspensions: Evaluation of kinetics, mechanisms and ecotoxicity. Appl. Catal. A Gen. 515, 136–143. https://doi.org/10.1016/j.apcata.2016.02.005

16. Antonopoulou, M., Kosma, C., Albanis, T., Konstantinou, I., 2021. An overview of homogeneous and heterogeneous photocatalysis applications for the removal of pharmaceutical compounds from real or synthetic hospital wastewaters under lab or pilot scale. Sci. Total Environ. 765, 144163. https://doi.org/10.1016/j.scitotenv.2020.144163

17. APHA, AWWA, WEF, 2017. Standard methods: For the examination of water and waste

water, 23rd ed. https://doi.org/https://doi.org/10.2105/SMWW.2882.216

18. Asadi, S., Moeinpour, F., 2019. Inactivation of Escherichia coli in water by silver-coated Ni0.5Zn0.5Fe2O4 magnetic nanocomposite: a Box–Behnken design optimization. Appl. Water Sci. 9, 1–9. https://doi.org/10.1007/s13201-019-0901-4

19. Avetta, P., Pensato, A., Minella, M., Malandrino, M., Maurino, V., Minero, C., Hanna, K., Vione, D., 2015. Activation of persulfate by irradiated magnetite: Implications for the degradation of phenol under heterogeneous photo-fenton-like conditions. Environ. Sci. Technol. 49, 1043–1050. https://doi.org/10.1021/es503741d

20. Bahnemann, D., 2004. Photocatalytic water treatment: Solar energy applications. Sol. Energy 77, 445–459. https://doi.org/10.1016/j.solener.2004.03.031

21. Bansal, P., Verma, A., 2018a. Pilot-scale single-step reactor combining photocatalysis and photo-Fenton aiming at faster removal of Cephalexin. J. Clean. Prod. 195, 540–551. https://doi.org/10.1016/j.jclepro.2018.05.219

22. Bansal, P., Verma, A., 2018b. In-situ dual effect studies using novel Fe-TiO2 composite for the pilot-plant degradation of pentoxifylline. Chem. Eng. J. 332, 682–694. https://doi.org/10.1016/j.cej.2017.09.121

23. Bansal, P., Verma, A., 2017a. Novel Fe-TiO2composite driven dual effect for reduction in treatment time of pentoxifylline: Slurry to immobilized approach. Mater. Des. 125, 135–145. https://doi.org/10.1016/j.matdes.2017.03.083

24. Bansal, P., Verma, A., 2017b. Synergistic effect of dual process (photocatalysis and photo-Fenton) for the degradation of Cephalexin using TiO2 immobilized novel clay beads with waste fly ash/foundry sand. J. Photochem. Photobiol. A Chem. 342, 131–142. https://doi.org/10.1016/j.jphotochem.2017.04.010

25. Bansal, P., Verma, A., Aggarwal, K., Singh, A., Gupta, S., 2016. Investigations on the degradation of an antibiotic Cephalexin using suspended and supported TiO2: Mineralization and durability studies. Can. J. Chem. Eng. 94, 1269–1276. https://doi.org/10.1002/cjce.22512

26. Barreca, D., Carraro, G., Gasparotto, A., Maccato, C., Sada, C., Bontempi, E., Brisotto, M., Pliekhova, O., Štangar, U.L., 2016. Novel two-step vapor-phase synthesis of UV–Vis light active Fe2O3/WO3 nanocomposites for phenol degradation. Environ. Sci. Pollut. Res.

23, 20350–20359. https://doi.org/10.1007/s11356-016-7226-8

27. Barreca, S., Velez Colmenares, J.J., Pace, A., Orecchio, S., Pulgarin, C., 2015. Escherichia coli inactivation by neutral solar heterogeneous photo-Fenton (HPF) over hybrid iron/montmorillonite/alginate beads. J. Environ. Chem. Eng. 3, 317–324. https://doi.org/10.1016/j.jece.2014.10.018

28. Benabbou, A.K., Derriche, Z., Felix, C., Lejeune, P., Guillard, C., 2007. Photocatalytic inactivation of Escherischia coli. Effect of concentration of TiO2 and microorganism, nature, and intensity of UV irradiation. Appl. Catal. B Environ. 76, 257–263. https://doi.org/10.1016/j.apcatb.2007.05.026

29. Berney, M., Weilenmann, H.U., Simonetti, A., Egli, T., 2006. Efficacy of solar disinfection of Escherichia coli, Shigella flexneri, Salmonella Typhimurium and Vibrio cholerae. J. Appl. Microbiol. 101, 828–836. https://doi.org/10.1111/j.1365-2672.2006.02983.x

30. Bezerra, M.A., Santelli, R.E., Oliveira, E.P., Villar, L.S., Escaleira, L.A., 2008. Response surface methodology (RSM) as a tool for optimization in analytical chemistry. Talanta 76, 965–977. https://doi.org/10.1016/j.talanta.2008.05.019

31. Bienert, G.P., Møller, A.L.B., Kristiansen, K.A., Schulz, A., Møller, I.M., Schjoerring, J.K., Jahn, T.P., 2007. Specific aquaporins facilitate the diffusion of hydrogen peroxide across membranes. J. Biol. Chem. 282, 1183–1192. https://doi.org/10.1074/jbc.M603761200

32. Bigelow, W.D., Esty, J.R., 1920. The thermal death point in relation to time of typical thermophilic organisms. J. Infect. Dis. 27, 602–617. https://doi.org/10.1093/infdis/27.6.602

33. Borges, M.E., Sierra, M., Esparza, P., 2017. Solar photocatalysis at semi-pilot scale: wastewater decontamination in a packed-bed photocatalytic reactor system with a visible-solar-light-driven photocatalyst. Clean Technol. Environ. Policy 19, 1239–1245. https://doi.org/10.1007/s10098-016-1312-y

34. Bouanimba, N., Laid, N., Zouaghi, R., Sehili, T., 2018. A comparative study of the activity of TiO2 degussa P25 and millennium PCs in the photocatalytic degradation of bromothymol blue. Int. J. Chem. React. Eng. 16, 1–19. https://doi.org/10.1515/ijcre-2017-0014

35. Braimah, M.N., Anozie, A.N., Odejobi, O.J., 2016. Utilization of Response Surface Methodology (RSM) in the optimization of crude oil refinery. J. Multidiscip. Eng. Sci. Technol. 3, 4361–4369.

36. Bulman, D.M., Mezyk, S.P., Remucal, C.K., 2019. The impact of pH and irradiation wavelength on the production of reactive oxidants during chlorine photolysis. Environ. Sci. Technol. 53, 4450–4459. https://doi.org/10.1021/acs.est.8b07225

37. Carra, I., Santos-Juanes, L., Acién Fernández, F.G., Malato, S., Sánchez Pérez, J.A., 2014. New approach to solar photo-Fenton operation. Raceway ponds as tertiary treatment technology. J. Hazard. Mater. 279, 322–329. https://doi.org/10.1016/j.jhazmat.2014.07.010

38. Carra, I., Sirtori, C., Ponce-Robles, L., Sánchez Pérez, J.A., Malato, S., Agüera, A., 2015. Degradation and monitoring of acetamiprid, thiabendazole and their transformation products in an agro-food industry effluent during solar photo-Fenton treatment in a raceway pond reactor. Chemosphere 130, 73–81. https://doi.org/10.1016/j.chemosphere.2015.03.001

39. Carré, G., Hamon, E., Ennahar, S., Estner, M., Lett, M.C., Horvatovich, P., Gies, J.P., Keller, V., Keller, N., Andre, P., 2014. TiO2 photocatalysis damages lipids and proteins in Escherichia coli. Appl. Environ. Microbiol. 80, 2573–2581. https://doi.org/10.1128/AEM.03995-13

40. Cerf, O., 1977. A review tailing of survival curves of bacterial spores. J. Appl. Bacteriol. 42, 1–19.

41. Chai, Y., Zhou, F., Zhu, Z., 2019. High efficiency and environment-friendly sterilization PEVE coatings modified with Bi2WO6 / TiO2 composites 715, 173–180. https://doi.org/10.1016/j.cplett.2018.11.046

42. Chang, Q., He, H., Ma, Z., 2008. Efficient disinfection of Escherichia coli in water by silver loaded alumina. J. Inorg. Biochem. 102, 1736–1742. https://doi.org/10.1016/j.jinorgbio.2008.05.003

43. Changotra, R., Rajput, H., Dhir, A., 2019. Treatment of real pharmaceutical wastewater using combined approach of Fenton applications and aerobic biological treatment. J. Photochem. Photobiol. A Chem. 376, 175–184. https://doi.org/10.1016/j.jphotochem.2019.02.029

44. Chen, C.Y., Wu, L.C., Chen, H.Y., Chung, Y.C., 2010. Inactivation of staphylococcus aureus and escherichia coli in water using photocatalysis with fixed TiO2. Water. Air. Soil Pollut. 212, 231–238. https://doi.org/10.1007/s11270-010-0335-y

45. Chin, L.Y., Pei, L.Y., Rosli, R. binti, Atni, N.H.B.M., 2015. Immobilization of nano-sized TiO2 on glass plate for the removal of methyl orange and methylene blue, in: Icgsce 2014. pp. 105–113. https://doi.org/10.1007/978-981-287-505-1

46. Chinnaiyan, P., Thampi, S.G., Kumar, M., Balachandran, M., 2019. Photocatalytic degradation of metformin and amoxicillin in synthetic hospital wastewater: effect of classical parameters. Int. J. Environ. Sci. Technol. 16, 5463–5474. https://doi.org/10.1007/s13762-018-1935-0

47. Cho, M., Chung, H., Choi, W., Yoon, J., 2004a. Linear correlation between inactivation of E. coli and OH radical concentration in TiO2 photocatalytic disinfection. Water Res. 38, 1069–1077. https://doi.org/10.1016/j.watres.2003.10.029

48. Cho, M., Lee, Y., Chung, H., Yoon, J., 2004b. Inactivation of Escherichia coli by photochemical reaction of ferrioxalate at slightly acidic and near-neutral pHs. Appl. Environ. Microbiol. 70, 1129–1134. https://doi.org/10.1016/b978-0-12-480560-6.50020-x

49. Chong, M.N., Jin, B., Saint, C.P., 2011. Bacterial inactivation kinetics of a photo-disinfection system using novel titania-impregnated kaolinite photocatalyst. Chem. Eng. J. 171, 16–23. https://doi.org/10.1016/j.cej.2011.03.024

50. Collin, F., 2019. Chemical basis of reactive oxygen species reactivity and involvement in neurodegenerative diseases. Int. J. Mol. Sci. 20. https://doi.org/10.3390/ijms20102407

51. Collivignarelli, M.C., Abbà, A., Carnevale Miino, M., Arab, H., Bestetti, M., Franz, S., 2020. Decolorization and biodegradability of a real pharmaceutical wastewater treated by H2O2-assisted photoelectrocatalysis on TiO2 meshes. J. Hazard. Mater. 387, 121668. https://doi.org/10.1016/j.jhazmat.2019.121668

52. Coroller, L., Leguerinel, I., Mettler, E., Savy, N., Mafart, P., 2006. General model, based on two mixed weibull distributions of bacterial resistance, for describing various shapes of inactivation curves. Appl. Environ. Microbiol. 72, 6493–6502. https://doi.org/10.1128/AEM.00876-06

53. Coutinho, C.A., Gupta, V.K., 2009. Photocatalytic degradation of methyl orange using polymer-titania microcomposites. J. Colloid Interface Sci. https://doi.org/10.1016/j.jcis.2009.02.016

54. Cruz-Ortiz, B.R., Hamilton, J.W.J., Pablos, C., Díaz-Jiménez, L., Cortés-Hernández, D.A., Sharma, P.K., Castro-Alférez, M., Fernández-Ibañez, P., Dunlop, P.S.M., Byrne, J.A., 2017. Mechanism of photocatalytic disinfection using titania-graphene composites under UV and visible irradiation. Chem. Eng. J. 316, 179–186. https://doi.org/10.1016/j.cej.2017.01.094

55. Cunha, D.L., Kuznetsov, A., Achete, C.A., Machado, A.E. da H., Marques, M., 2018. Immobilized TiO2 on glass spheres applied to heterogeneous photocatalysis: Photoactivity, leaching and regeneration process. PeerJ 2018, 1–19. https://doi.org/10.7717/peerj.4464

56. Daels, N., De Vrieze, S., Sampers, I., Decostere, B., Westbroek, P., Dumoulin, A., Dejans, P., De Clerck, K., Van Hulle, S.W.H., 2011. Potential of a functionalised nanofibre microfiltration membrane as an antibacterial water filter. Desalination 275, 285–290. https://doi.org/10.1016/j.desal.2011.03.012

57. Dalin, C., Qiu, H., Hanasaki, N., Mauzerall, D.L., Rodriguez-Iturbe, I., 2015. Balancing water resource conservation and food security in China. Proc. Natl. Acad. Sci. 112, 4588–4593. https://doi.org/10.1073/pnas.1504345112

58. De León, M.A., Castiglioni, J., Bussi, J., Sergio, M., 2008. Catalytic activity of an iron-pillared montmorillonitic clay mineral in heterogeneous photo-Fenton process. Catal. Today 133–135, 600–605. https://doi.org/10.1016/j.cattod.2007.12.130

59. De Vietro, N., Tursi, A., Beneduci, A., Chidichimo, F., Milella, A., Fracassi, F., Chatzisymeon, E., Chidichimo, G., 2019. Photocatalytic inactivation of Escherichia coli bacteria in water using low pressure plasma deposited TiO2 cellulose fabric. Photochem. Photobiol. Sci. 18, 2248–2258. https://doi.org/10.1039/c9pp00050j

60. Dědková, K., Lang, J., Matějová, K., Peikertová, P., Holešinský, J., Vodárek, V., Kukutschová, J., 2015. Nanostructured composite material graphite/TiO2 and its antibacterial activity under visible light irradiation. J. Photochem. Photobiol. B Biol. 149, 265–271. https://doi.org/10.1016/j.jphotobiol.2015.06.018

61. Deng, D., Aouad, W., Braff, W.A., Schlumpberger, S., Suss, M.E., Bazant, M.Z., 2015. Water purification by shock electrodialysis: Deionization, filtration, separation, and

disinfection. Desalination 357, 77–83. https://doi.org/10.1016/j.desal.2014.11.011

62. Dixit, D., Verma, A., Gupta, S., Bansal, P., 2016. Assessment of solar photocatalytic degradation and mineralization of amoxicillin trihydrate (AMT) using slurry and fixed-bed batch reactor: Efficacy of parabolic trough collector. RSC Adv. 6, 36109–36117. https://doi.org/10.1039/c6ra03414d

63. Dong, P., Yang, F., Cheng, X., Huang, Z., Nie, X., Xiao, Y., Zhang, X., 2019. Plasmon enhanced photocatalytic and antimicrobial activities of Ag-TiO 2 nanocomposites under visible light irradiation prepared by DBD cold plasma treatment. Mater. Sci. Eng. C 96, 197–204. https://doi.org/10.1016/j.msec.2018.11.005

64. Dong, Z., Qin, Z., 2018. Experimental Study of Pathogenic Microorganisms Inactivated by Venturi-Type Hydrodynamic Cavitation with Different Throat Lengths. J. Civ. Eng. Forum 4, 209. https://doi.org/10.22146/jcef.38756

65. Dozzi, M.V., Selli, E., 2013. Doping TiO2 with p-block elements : Effects on photocatalytic activity. J. Photochem. Photobiol. C Photochem. Rev. 14, 13–28. https://doi.org/10.1016/j.jphotochemrev.2012.09.002

66. Dressing, S.A., Meals, D.W., 2010. Monitoring and evaluating nonpoint source watershed projects, United States Environmental Protection Agency Office of Water.

67. Dunlop, P.S.M., McMurray, T.A., Hamilton, J.W.J., Byrne, J.A., 2008. Photocatalytic inactivation of Clostridium perfringens spores on TiO2 electrodes. J. Photochem. Photobiol. A Chem. 196, 113–119. https://doi.org/10.1016/j.jphotochem.2007.11.024

68. Dunlop, P.S.M., Sheeran, C.P., Byrne, J.A., McMahon, M.A.S., Boyle, M.A., McGuigan, K.G., 2010. Inactivation of clinically relevant pathogens by photocatalytic coatings. J. Photochem. Photobiol. A Chem. 216, 303–310. https://doi.org/10.1016/j.jphotochem.2010.07.004

69. Duraisamy, N., Kandiah, K., Rajendran, R., Prabhu, S., Ramesh, R., Dhanaraj, G., 2018. Electrochemical and photocatalytic investigation of nickel oxide for energy storage and wastewater treatment. Res. Chem. Intermed. 44, 5653–5667. https://doi.org/10.1007/s11164-018-3446-5

70. Esteban García, B., Rivas, G., Arzate, S., Sánchez Pérez, J.A., 2018. Wild bacteria

inactivation in WWTP secondary effluents by solar photo-fenton at neutral pH in raceway pond reactors. Catal. Today 313, 72–78. https://doi.org/10.1016/j.cattod.2017.10.031

71. Fabbricino, M., D'Antonio, L., 2012. Use of solar radiation for continuous water disinfection in isolated areas. Environ. Technol. 33, 539–544. https://doi.org/10.1080/09593330.2011.584570

72. Faraji, M., Mohaghegh, N., Abedini, A., 2018. Ternary composite of TiO2 nanotubes/Ti plates modified by g-C3N4 and SnO2 with enhanced photocatalytic activity for enhancing antibacterial and photocatalytic activity. J. Photochem. Photobiol. B Biol. 178, 124–132. https://doi.org/10.1016/j.jphotobiol.2017.11.009

73. Feilizadeh, M., Alemzadeh, I., Delparish, A., Estahbanati, M.R.K., Soleimani, M., Jangjou, Y., Vosoughi, A., 2015a. Optimization of operating parameters for efficient photocatalytic inactivation of Escherichia coli based on a statistical design of experiments. Water Sci. Technol. 71, 823–831. https://doi.org/10.2166/wst.2015.013

74. Feilizadeh, M., Mul, G., Vossoughi, M., 2015b. E. coli inactivation by visible light irradiation using a Fe-Cd/TiO2 photocatalyst: Statistical analysis and optimization of operating parameters. Appl. Catal. B Environ. 168–169, 441–447. https://doi.org/10.1016/j.apcatb.2014.12.034

75. Fendrich, M.A., Quaranta, A., Orlandi, M., Bettonte, M., Miotello, A., 2019. Solar concentration for wastewaters remediation: A review of materials and technologies. Appl. Sci. 9, 118. https://doi.org/10.3390/app9010118

76. Fernández-Ibáñez, P., Polo-López, M.I., Malato, S., Wadhwa, S., Hamilton, J.W.J., Dunlop, P.S.M., D'Sa, R., Magee, E., O'Shea, K., Dionysiou, D.D., Byrne, J.A., 2015. Solar photocatalytic disinfection of water using titanium dioxide graphene composites. Chem. Eng. J. 261, 36–44. https://doi.org/10.1016/j.cej.2014.06.089

77. Ferro, G., Fiorentino, A., Alferez, M.C., Polo-López, M.I., Rizzo, L., Fernández-Ibáñez, P., 2015. Urban wastewater disinfection for agricultural reuse: effect of solar driven AOPs in the inactivation of a multidrug resistant E. coli strain. Appl. Catal. B Environ. 178, 65–73. https://doi.org/10.1016/j.apcatb.2014.10.043

78. Firoentino, A., Ferro, G., Alferez Casto, M., Polo-Lopez, M.I., Fernandez-Ibanez, P., Rizza, L., 2015. Inactivation and regrowth of multidrug resistant bacteria in urban wastwater

after disinfection by solar-driven and chlorination processes. J. Photochem. Photobiol. B Biol. 148, 43–50. https://doi.org/https://doi.org/10.1016/j.jphotobiol.2015.03.029

79. Fueda, Y., Suzuki, H., Komiya, Y., Asakura, Y., Shiragami, T., Matsumoto, J., Yokoi, H., Yasuda, M., 2006. Bactericidal effect of silica gel-supported porphyrinatophosphorus(V) catalysts on Escherichia coli under visible-light irradiation. Bull. Chem. Soc. Jpn. 79, 1420–1425. https://doi.org/10.1246/bcsj.79.1420

80. Fujishima, A., Honda, K., 1972. Electrochemical Photolysis of Water at a Semiconductor Electrode. Nature 238, 37–38.

81. Fujishima, A., Zhang, X., 2006. Titanium dioxide photocatalysis: present situation and future approaches. Comptes Rendus Chim. 9, 750–760. https://doi.org/10.1016/j.crci.2005.02.055

82. Gamage, J., Cui, W., Zhang, Z., 2013. Degradative and disinfective properties of carbon-doped anatase – rutile TiO 2 mixtures under visible light irradiation. Catal. Today 207, 191–199. https://doi.org/10.1016/j.cattod.2012.04.015

83. Ganesh, I., Kumar, P., Gupta, A., Sekhar, P., Radha, K., Padmanabham, G., Sundararajan, G., 2013. Preparation and characterization of Fe-doped TiO2 powders for solar light response and photocatalytic applications. Process. Appl. Ceram. 6, 21–36. https://doi.org/10.2298/pac1201021g

84. Garai, D., Kumar, V., 2013. Response surface optimization for xylanase with high volumetric productivity by indigenous alkali tolerant Aspergillus candidus under submerged cultivation. 3 Biotech 3, 127–136. https://doi.org/10.1007/s13205-012-0077-1

85. García-Fernández, I., Polo-López, M.I., Oller, I., Fernández-Ibáñez, P., 2012. Bacteria and fungi inactivation using Fe3+/sunlight, H2O2/sunlight and near neutral photo-Fenton: A comparative study. Appl. Catal. B Environ. 121–122, 20–29. https://doi.org/10.1016/j.apcatb.2012.03.012

86. Gaya, U.I., Abdullah, A.H., 2008. Heterogeneous photocatalytic degradation of organic contaminants over titanium dioxide: A review of fundamentals, progress and problems. J. Photochem. Photobiol. C Photochem. Rev. 9, 1–12. https://doi.org/10.1016/j.jphotochemrev.2007.12.003

87. Geeraerd, A.H., Valdramidis, V.P., Van Impe, J.F., 2005. GInaFiT, a freeware tool to assess non-log-linear microbial survivor curves. Int. J. Food Microbiol. 102, 95–105. https://doi.org/10.1016/j.ijfoodmicro.2004.11.038

88. Giannakis, S., 2018. Analogies and differences among bacterial and viral disinfection by the photo-Fenton process at neutral pH: a mini review. Environ. Sci. Pollut. Res. 25, 27676–27692. https://doi.org/10.1007/s11356-017-0926-x

89. Giannakis, S., Androulaki, B., Comninellis, C., Pulgarin, C., 2018a. Wastewater and urine treatment by UVC-based advanced oxidation processes: Implications from the interactions of bacteria, viruses, and chemical contaminants. Chem. Eng. J. 343, 270–282. https://doi.org/10.1016/j.cej.2018.03.019

90. Giannakis, S., Inmaculada, M., López, P., Spuhler, D., Antonio, J., Pérez, S., Fernández, P., 2016a. Solar disinfection is an augmentable , in situ -generated photo-Fenton reaction - Part 1 : A review of the mechanisms and the fundamental aspects of the process. Appl. Catal. B Environ. 199, 199–223. https://doi.org/10.1016/j.apcatb.2016.06.009

91. Giannakis, S., Le, T.T.M., Entenza, J.M., Pulgarin, C., 2018b. Solar photo-Fenton disinfection of 11 antibiotic-resistant bacteria (ARB) and elimination of representative AR genes. Evidence that antibiotic resistance does not imply resistance to oxidative treatment. Water Res. 143, 334–345. https://doi.org/10.1016/j.watres.2018.06.062

92. Giannakis, S., Liu, S., Carratalà, A., Rtimi, S., Talebi Amiri, M., Bensimon, M., Pulgarin, C., 2017. Iron oxide-mediated semiconductor photocatalysis vs. heterogeneous photo-Fenton treatment of viruses in wastewater. Impact of the oxide particle size. J. Hazard. Mater. 339, 223–231. https://doi.org/10.1016/j.jhazmat.2017.06.037

93. Giannakis, S., López, M.I.P., Spuhler, D., Pérez, J.A.S., Ibáñez, P.F., Pulgarin, C., 2016b. Solar disinfection is an augmentable, in situ-generated photo-Fenton reaction-Part 2: A review of the applications for drinking water and wastewater disinfection. Appl. Catal. B Environ. 198, 431–446. https://doi.org/10.1016/j.apcatb.2016.06.007

94. Giannakis, S., Voumard, M., Grandjean, D., Magnet, A., De Alencastro, L.F., Pulgarin, C., 2016c. Micropollutant degradation, bacterial inactivation and regrowth risk in wastewater effluents: Influence of the secondary (pre)treatment on the efficiency of Advanced Oxidation Processes. Water Res. 102, 505–515. https://doi.org/10.1016/j.watres.2016.06.066

95. Giannakis, S., Voumard, M., Rtimi, S., Pulgarin, C., 2018c. Bacterial disinfection by the photo-Fenton process: Extracellular oxidation or intracellular photo-catalysis? Appl. Catal. B Environ. 227, 285–295. https://doi.org/10.1016/j.apcatb.2018.01.044

96. Giannakopoulou, T., Papailias, I., Todorova, N., Boukos, N., Liu, Y., Yu, J., Trapalis, C., 2016. Tailoring the energy band gap and edges potentials of g-C3N4/TiO2 composite photocatalysts for NOx removal. Chem. Eng. J. 310, 571–580. https://doi.org/10.1016/j.cej.2015.12.102

97. GilPavas, E., Dobrosz-Gómez, I., Gómez-García, M.Á., 2017. Coagulation-flocculation sequential with Fenton or Photo-Fenton processes as an alternative for the industrial textile wastewater treatment. J. Environ. Manage. 191, 189–197. https://doi.org/10.1016/j.jenvman.2017.01.015

98. Gladis, F., Schumann, R., 2011. A suggested standardised method for testing photocatalytic inactivation of aeroterrestrial algal growth on TiO2-coated glass. Int. Biodeterior. Biodegrad. 65, 415–422. https://doi.org/10.1016/j.ibiod.2011.01.005

99. Gomes, A.I., Vilar, V.J.P., Boaventura, R.A.R., 2009. Synthetic and natural waters disinfection using natural solar radiation in a pilot plant with CPCs. Catal. Today 144, 55–61. https://doi.org/10.1016/j.cattod.2008.12.023

100. Gomez-Ruiz, B., Ribao, P., Diban, N., Rivero, M.J., Ortiz, I., Urtiaga, A., 2018. Photocatalytic degradation and mineralization of perfluorooctanoic acid (PFOA) using a composite TiO2 −rGO catalyst. J. Hazard. Mater. 344, 950–957. https://doi.org/10.1016/j.jhazmat.2017.11.048

101. Gümüş, D., Akbal, F., 2011. Photocatalytic degradation of textile dye and wastewater. Water. Air. Soil Pollut. 216, 117–124. https://doi.org/10.1007/s11270-010-0520-z

102. Gupta, K., Singh, R.P., Pandey, Ashutosh, Pandey, Anjana, 2013. Photocatalytic antibacterial performance of TiO2 and Ag-doped TiO2 against S. Aureus. P. Aeruginosa and E. Coli. Beilstein J. Nanotechnol. 4, 345–351. https://doi.org/10.3762/bjnano.4.40

103. Gutiérrez-Alfaro, S., Acevedo, A., Rodríguez, J., Carpio, E., Manzano, M.A., 2015. Solar photocatalytic water disinfection of Escherichia coli , Enterococcus spp . and Clostridium Perfringens using differnt low-cost devices. Soc. Chem. Ind. 91, 2026–2037. https://doi.org/10.1002/jctb.4795

104. Gutiérrez-Zapata, H.M., Alvear-Daza, J.J., Rengifo-Herrera, J.A., Sanabria, J., 2017. Addition of hydrogen peroxide to groundwater with natural iron induces water disinfection by photo-Fenton at circumneutral pH and other photochemical events. Photochem. Photobiol. 93, 1224–1231. https://doi.org/doi.org/10.1111/php.12779

105. Gyürek, L.L., Frinch, G.R., 1998. Modeling water treatment chemical disinfection kinetics. J. Environ. Eng. 124, 783–793. https://doi.org/https://doi.org/10.1061/(ASCE)0733-9372(1998)124:9(783)

106. Hallmich, C., Gehr, R., 2010. Effect of pre- and post-UV disinfection conditions on photoreactivation of fecal coliforms in wastewater effluents. Water Res. 44, 2885–2893. https://doi.org/10.1016/j.watres.2010.02.003

107. Haranaka-Funai, D., Didier, F., Giménez, J., Marco, P., Esplugas, S., Machulek-Junior, A., 2017. Photocatalytic treatment of valproic acid sodium salt with TiO2 in different experimental devices: An economic and energetic comparison. Chem. Eng. J. 327, 656–665. https://doi.org/10.1016/j.cej.2017.06.148

108. He, R.L., Wei, Y., Cao, W. Bin, 2009. Preparation of (Fe, N)-Doped TiO2 powders and their antibacterial activities under visible light irradiation. J. Nanosci. Nanotechnol. 9, 1094–1097. https://doi.org/10.1166/jnn.2009.C095

109. Heritage, J., Evans, E.G.., Killington, R.A., 1997. Introductory Microbiology (Studies in Biology), Cambridge University Press, New Year. https://doi.org/doi.org/10.1002/jobm.3620370313

110. Herney-Ramirez, J., Vicente, M.A., Madeira, L.M., 2010. Heterogeneous photo-Fenton oxidation with pillared clay-based catalysts for wastewater treatment: A review. Appl. Catal. B Environ. 98, 10–26. https://doi.org/10.1016/j.apcatb.2010.05.004

111. Hijnen, W.A.M., Beerendonk, E.F., Medema, G.J., 2006. Inactivation credit of UV radiation for viruses, bacteria and protozoan (oo)cysts in water: A review. Water Res. 40, 3–22. https://doi.org/10.1016/j.watres.2005.10.030

112. Hossain, S. mukit, Park, H., Kang, H.-J., Kim, J.B., Tijing, L., Rhee, I., Jun, Y., Shon, H.K., Kim, J., 2020. Preparation and characterization of photoactive anatase TiO2 from algae bloomed surface water. Catalysts 10. https://doi.org/doi:10.3390/catal10040452

113. Howe, A.D., Forster, S., Morton, S., Marshall, R., Osborn, K.S., Wright, P., Hunter, P.R., 2002. Cryptosporidium oocysts in a water supply associated with a cryptosporidiosis outbreak. Emerg. Infect. Dis. 8, 619–624. https://doi.org/10.3201/eid0806.010271

114. Hseu, Z., 2004. Evaluating heavy metal contents in nine composts using four digestion methods. Bioresour. Technol. 95, 53–59. https://doi.org/10.1016/j.biortech.2004.02.008

115. Hu, C., Guo, J., Qu, J., Hu, X., 2007. Photocatalytic degradation of pathogenic bacteria with AgI/TiO2 under visible light irradiation. Langmuir 23, 4982–4987. https://doi.org/10.1021/la063626x

116. Hu, X., Zhu, Q., Gu, Z., Zhang, N., Liu, N., Stanislaus, M.S., Li, D., Yang, Y., 2017. Wastewater treatment by sonophotocatalysis using PEG modified TiO2 film in a circular Photocatalytic-Ultrasonic system. Ultrason. Sonochem. 36, 301–308. https://doi.org/10.1016/j.ultsonch.2016.12.008

117. Hussain, S.N., De las Heras, N., Asghar, H.M.A., Brown, N.W., Roberts, E.P.L., 2014. Disinfection of water by adsorption combined with electrochemical treatment. Water Res. 54, 170–178. https://doi.org/10.1016/j.watres.2014.01.043

118. Imlay, J.A., 2015. Diagnosing oxidative stress in bacteria: not as easy as you might think. Curr. Opin. Microbiol. 24, 124–131. https://doi.org/10.1016/j.mib.2015.01.004

119. Imlay, J.A., 2013. The molecular mechanisms and physiological consequences of oxidative stress: lessons from a model bacterium. Nat. Rev. Microbiol. 11, 443–54. https://doi.org/10.1038/nrmicro3032

120. Imlay, J.A., 2008. Cellular defenses against superoxide and hydrogen peroxide. Annu. Rev. Biochem. 77, 755–776. https://doi.org/10.1146/annurev.biochem.77.061606.161055

121. Ji, M., Liu, Z., Sun, K., Li, Z., Fan, X., Li, Q., 2021. Bacteriophages in water pollution control: Advantages and limitations. Front. Environ. Sci. Eng. 15. https://doi.org/10.1007/s11783-020-1378-y

122. Jia, Y., Zhan, S., Ma, S., Zhou, Q., 2016. Fabrication of TiO2-Bi2WO6 binanosheet for enhanced solar photocatalytic disinfection of E. coli: Insights on the mechanism. ACS Appl. Mater. Interfaces 8, 6841–6851. https://doi.org/10.1021/acsami.6b00004

123. Kacem, M., Plantard, G., Wery, N., Goetz, V., 2014. Kinetics and efficiency displayed

by supported and suspended TiO2 catalysts applied to the disinfection of Escherichia coli. Chinese J. Catal. 35, 1571–1577. https://doi.org/10.1016/S1872-2067(14)60212-6

124. Kandananond, K., 2010. Using the response surface method to optimize the turning process of AISI 12L14 steel. Adv. Mech. Eng. 2010. https://doi.org/10.1155/2010/362406

125. Kang, X., Liu, S., Dai, Z., He, Y., Song, X., Tan, Z., 2019. Titanium dioxide: From engineering to applications. Catalysts 9, 191. https://doi.org/10.3390/catal9020191

126. Karaolia, P., Michael, I., García-Fernández, I., Agüera, A., Malato, S., Fernández-Ibáñez, P., Fatta-Kassinos, D., 2014. Reduction of clarithromycin and sulfamethoxazole-resistant Enterococcus by pilot-scale solar-driven Fenton oxidation. Sci. Total Environ. 468–469, 19–27. https://doi.org/10.1016/j.scitotenv.2013.08.027

127. Karunakaran, C., Abiramasundari, G., Gomathisankar, P., Manikandan, G., Anandi, V., 2010. Cu-doped TiO 2 nanoparticles for photocatalytic disinfection of bacteria under visible light. J. Colloid Interface Sci. 352, 68–74. https://doi.org/10.1016/j.jcis.2010.08.012

128. Karunakaran, C., Vijayabalan, A., Manikandan, G., 2013. Photocatalytic bacteria inactivation by polyethylene glycol-assisted sol–gel synthesized Cd-doped TiO2 under visible light. Res. Chem. Intermed. 39, 1437–1446. https://doi.org/10.1007/s11164-012-0700-0

129. Karunakaran, C., Vijayabalan, A., Manikandan, G., Gomathisankar, P., 2011. Visible light photocatalytic disinfection of bacteria by Cd – TiO2. Catal. Commun. 12, 826–829. https://doi.org/10.1016/j.catcom.2011.01.017

130. Kasiri, M.B., Aleboyeh, H., Aleboyeh, A., 2008. Degradation of Acid Blue 74 using Fe-ZSM5 zeolite as a heterogeneous photo-Fenton catalyst. Appl. Catal. B Environ. 84, 9–15. https://doi.org/10.1016/j.apcatb.2008.02.024

131. Kassahun, S.K., Kiflie, Z., Shin, D.W., Park, S.S., Chung, Y.R., 2018. Novel multistage fixed-bed photoreactor for bacterial inactivation using N-doped TiO2 nanoparticles under vis-LEDs and sunlight illumination. Nanotechnol. Environ. Eng. 3, 1–11. https://doi.org/10.1007/s41204-017-0032-9

132. Kaur, P., Kushwaha, J.P., Sangal, V.K., 2018. Electrocatalytic oxidative treatment of real textile wastewater in continuous reactor: Degradation pathway and disposability study. J.

Hazard. Mater. 346, 242–252. https://doi.org/10.1016/j.jhazmat.2017.12.044

133. Kaur, T., Sraw, A., Wanchoo, R.K., Toor, A.P., 2018. Solar assisted degradation of carbendazim in water using clay beads immobilized with TiO2 & Fe doped TiO2. Sol. Energy 162, 45–56. https://doi.org/10.1016/j.solener.2017.11.033

134. Khan, S.J., Reed, R.H., Rasul, M.G., 2012. Thin-film fixed-bed reactor for solar photocatalytic inactivation of Aeromonas hydrophila: Influence of water quality. BMC Microbiol. 12. https://doi.org/10.1186/1471-2180-12-285

135. Khuri, A.I., 2017. Response Surface Methodology and Its Applications In Agricultural and Food Sciences. Biometrics Biostat. Int. J. 5, 1–11. https://doi.org/10.15406/bbij.2017.05.00141

136. Khuri, A.I., Mukhopadhyay, S., 2010. Response surface methodology. Wiley Interdiscip. Rev. Comput. Stat. 2, 128–149. https://doi.org/10.1002/wics.73

137. Kim, H.E., Lee, J., Lee, H., Lee, C., 2012. Synergistic effects of TiO2 photocatalysis in combination with Fenton-like reactions on oxidation of organic compounds at circumneutral pH. Appl. Catal. B Environ. 115–116, 219–224. https://doi.org/10.1016/j.apcatb.2011.12.027

138. Klamerth, N., Malato, S., Agüera, A., Fernández-Alba, A., Mailhot, G., 2012. Treatment of municipal wastewater treatment plant effluents with modified photo-fenton as a tertiary treatment for the degradation of micro pollutants and disinfection. Environ. Sci. Technol. 46, 2885–2892. https://doi.org/10.1021/es204112d

139. Konstas, P.S., Kosma, C., Konstantinou, I., Albanis, T., 2019. Photocatalytic treatment of pharmaceuticals in real hospital wastewaters for effluent quality amelioration. Water (Switzerland) 11, 1–17. https://doi.org/10.3390/w11102165

140. Kubacka, A., Ferrer, M., Cerrada, M.L., Serrano, C., Sánchez-Chaves, M., Fernández-García, Marta, de Andrés, A., Riobóo, R.J.J., Fernández-Martín, F., Fernández-García, Marcos, 2009. Boosting TiO2-anatase antimicrobial activity: Polymer-oxide thin films. Appl. Catal. B Environ. 89, 441–447. https://doi.org/10.1016/j.apcatb.2009.01.002

141. Lambert, R.J.W., Johnston, M.D., 2001. The effect of interfering substances on the disinfection process: A mathematical model. J. Appl. Microbiol. 91, 548–555. https://doi.org/10.1046/j.1365-2672.2001.01422.x

142. Lanao, M., Ormad, M.P., Mosteo, R., Ovelleiro, J.L., 2012. Inactivation of Enterococcus sp. by photolysis and TiO2 photocatalysis with H2O2 in natural water. Sol. Energy 86, 619–625. https://doi.org/10.1016/j.solener.2011.11.007

143. Lau, C.K.Y., Krewulak, K.D., Vogel, H.J., 2016. Bacterial ferrous iron transport: The Feo system. FEMS Microbiol. Rev. 40, 273–298. https://doi.org/10.1093/femsre/fuv049

144. Laxma Reddy, P.V., Kavitha, B., Kumar Reddy, P.A., Kim, K.H., 2017. TiO2-based photocatalytic disinfection of microbes in aqueous media: A review. Environ. Res. 154, 296–303. https://doi.org/10.1016/j.envres.2017.01.018

145. Leight, A.K., Crump, B.C., Hood, R.R., 2018. Assessment of fecal indicator bacteria and potential pathogen co-occurrence at a shellfish growing area. Front. Microbiol. 9, 1–13. https://doi.org/10.3389/fmicb.2018.00384

146. Levchuk, I., Kralova, M., Rueda-Márquez, J.J., Moreno-Andrés, J., Gutiérrez-Alfaro, S., Dzik, P., Parola, S., Sillanpää, M., Vahala, R., Manzano, M.A., 2018. Antimicrobial activity of printed composite TiO2/SiO2 and TiO2/SiO2/Au thin films under UVA-LED and natural solar radiation. Appl. Catal. B Environ. 239, 609–618. https://doi.org/10.1016/j.apcatb.2018.08.051

147. Li, G., Nie, X., Chen, J., Jiang, Q., An, T., Wong, P.K., Zhang, H., Zhao, H., Yamashita, H., 2015. Enhanced visible-light-driven photocatalytic inactivation of Escherichia coli using g-C3N4/TiO2 hybrid photocatalyst synthesized using a hydrothermal-calcination approach. Water Res. 86, 17–24. https://doi.org/10.1016/j.watres.2015.05.053

148. Lin, L., Su, Z., Li, Y., Zhang, C., 2021. Comparative performance and mechanism of bacterial inactivation induced by metal-free modified g-C3N4 under visible light: Escherichia coli versus Staphylococcus aureus. Chemosphere 265. https://doi.org/10.1016/j.chemosphere.2020.129060

149. Lin, S., Zhang, X., Sun, Q., Zhou, T., Lu, J., 2013. Fabrication of solar light induced Fe-TiO2 immobilized on glass-fiber and application for phenol photocatalytic degradation. Mater. Res. Bull. 48, 4570–4575. https://doi.org/10.1016/j.materresbull.2013.07.063

150. Liu, D., Mao, Y., Ding, L., 2018. Carbon nanotubes as antimicrobial agents for water disinfection and pathogen control. J. Water Health 16, 171–180. https://doi.org/10.2166/wh.2018.228

151. Liu, S.Q., Feng, L.R., Xu, N., Chen, Z.G., Wang, X.M., 2012. Magnetic nickel ferrite as a heterogeneous photo-Fenton catalyst for the degradation of rhodamine B in the presence of oxalic acid. Chem. Eng. J. 203, 432–439. https://doi.org/10.1016/j.cej.2012.07.071

152. Long, M., Wang, J., Zhuang, H., Zhang, Y., Wu, H., Zhang, J., 2014. Performance and mechanism of standard nano-TiO2 (P-25) in photocatalytic disinfection of foodborne microorganisms - Salmonella typhimurium and listeria monocytogenes. Food Control 39, 68–74. https://doi.org/10.1016/j.foodcont.2013.10.033

153. Lonnen, J., Kilvington, S., Kehoe, S.C., Al-Touati, F., McGuigan, K.G., 2005. Solar and photocatalytic disinfection of protozoan, fungal and bacterial microbes in drinking water. Water Res. 39, 877–883. https://doi.org/10.1016/j.watres.2004.11.023

154. López, A.V., López, K.H., Giannakis, S., Benítez, N., 2017. Effect of reactor material and its reuse on photo-Fenton process efficiency at near-neutral pH: Alterations in E. coli inactivation and resorcinol degradation kinetics in water. J. Photochem. Photobiol. A Chem. 344, 228–237. https://doi.org/10.1016/j.jphotochem.2017.04.019

155. Lu, J., Zhang, T., Ma, J., Chen, Z., 2009. Evaluation of disinfection by-products formation during chlorination and chloramination of dissolved natural organic matter fractions isolated from a filtered river water. J. Hazard. Mater. 162, 140–145. https://doi.org/10.1016/j.jhazmat.2008.05.058

156. Lu, Z.X., Zhou, L., Zhang, Z.L., Shi, W.L., Xie, Z.X., Xie, H.Y., Pang, D.W., Shen, P., 2003. Cell Damage Induced by Photocatalysis of TiO2 Thin Films. Langmuir 19, 8765–8768. https://doi.org/10.1021/la034807r

157. Lv, R., Zou, M., Chantapakul, T., Chen, W., Muhammad, A.I., Zhou, J., Ding, T., Ye, X., Liu, D., 2019. Effect of ultrasonication and thermal and pressure treatments, individually and combined, on inactivation of Bacillus cereus spores. Appl. Microbiol. Biotechnol. 103, 2329–2338. https://doi.org/10.1007/s00253-018-9559-3

158. Mafart, P., Couvert, O., Gaillard, S., Leguerinel, I., 2002. On calculating sterility in thermal preservation methods : Application of the Weibull frequency distribution model. Acta Hortic. 566, 107–114. https://doi.org/10.17660/ActaHortic.2001.566.11

159. Malato, S., Fernández-Ibáñez, P., Maldonado, M.I., Blanco, J., Gernjak, W., 2009. Decontamination and disinfection of water by solar photocatalysis: Recent overview and

trends. Catal. Today 147, 1–59. https://doi.org/10.1016/j.cattod.2009.06.018

160. Marugán, J., van Grieken, R., Pablos, C., Satuf, M.L., Cassano, A.E., Alfano, O.M., 2015. Photocatalytic inactivation of Escherichia coli aqueous suspensions in a fixed-bed reactor. Catal. Today 252, 143–149. https://doi.org/10.1016/j.cattod.2014.10.031

161. Marugán, J., van Grieken, R., Sordo, C., Cruz, C., 2008. Kinetics of the photocatalytic disinfection of Escherichia coli suspensions. Appl. Catal. B Environ. 82, 27–36. https://doi.org/10.1016/j.apcatb.2008.01.002

162. Massoudinejad, M., Golmohammadi, S., Ghaderpoori, M., 2016. Use of ultraviolet and ultraviolet /peroxide hydrogen processes for degradation of humic substances from aqueous solutions 9, 680–688.

163. Matin, A.R., Yousefzadeh, S., Ahmadi, E., Mahvi, A., Alimohammadi, M., Aslani, H., Nabizadeh, R., 2018. A comparative study of the disinfection efficacy of H2O2/ferrate and UV/H2O2/ferrate processes on inactivation of Bacillus subtilis spores by response surface methodology for modeling and optimization. Food Chem. Toxicol. 116, 129–137. https://doi.org/10.1016/j.fct.2018.04.002

164. Matsunaga, T., Tomoda, R., Nakajima, T., Wake, H., 1985. Photoelectrochemical sterilization of microbial cells by semiconductor powders (Sterilization; semiconductor; Saccharomyces cereoisiae; coenzyme A). FEMS Microbiol. Lett. 29, 211–214.

165. McGuigan, K.G., Conroy, R.M., Mosler, H.J., du Preez, M., Ubomba-Jaswa, E., Fernandez-Ibañez, P., 2012. Solar water disinfection (SODIS): A review from bench-top to roof-top. J. Hazard. Mater. 235–236, 29–46. https://doi.org/10.1016/j.jhazmat.2012.07.053

167. Mecha, A.C., Onyango, M.S., Ochieng, A., Momba, M.N.B., 2017. Evaluation of synergy and bacterial regrowth in photocatalytic ozonation disinfection of municipal wastewater. Sci. Total Environ. 601–602, 626–635. https://doi.org/10.1016/j.scitotenv.2017.05.204

168. Megahed, A., Aldridge, B., Lowe, J., 2018. The microbial killing capacity of aqueous and gaseous ozone on different surfaces contaminated with dairy cattle manure. PLoS One 13, 1–22. https://doi.org/10.1371/journal.pone.0196555

169. Mehrjouei, M., Müller, S., Möller, D., 2014. Catalytic and photocatalytic ozonation of

tert-butyl alcohol in water by means of falling film reactor: Kinetic and cost-effectiveness study. Chem. Eng. J. 248, 184–190. https://doi.org/10.1016/j.cej.2014.03.047

170. Michael, I., Hapeshi, E., Michael, C., Varela, A.R., Kyriakou, S., Manaia, C.M., Fatta-Kassinos, D., 2012. Solar photo-Fenton process on the abatement of antibiotics at a pilot scale: Degradation kinetics, ecotoxicity and phytotoxicity assessment and removal of antibiotic resistant enterococci. Water Res. 46, 5621–5634. https://doi.org/10.1016/j.watres.2012.07.049

171. Miranda-Ríos, M., Luna-Pabello, V.M., de Velásquez, M.T.O., Barrera-Godínez, J.A., 2011. Removal of escherichia coli from biological effluents using natural and artificial mineral aggregates. Water SA 37, 213–220. https://doi.org/10.4314/wsa.v37i2.65866

172. Mishra, N.S., Reddy, R., Kuila, A., Rani, A., Mukherjee, A.N., Pichiah, S., 2017. A review on Advanced Oxidation Process for Effective Water Treatment. Curr. world Environ. 12, 470–490. https://doi.org/http://dx.doi.org/10.12944/CWE.12.3.02

173. Mitoraj, D., Jańczyk, A., Strus, M., Kisch, H., Stochel, G., Heczko, P.B., Macyk, W., 2007. Visible light inactivation of bacteria and fungi by modified titanium dioxide. Photochem. Photobiol. Sci. 6, 642–648. https://doi.org/10.1039/b617043a

174. Miyagi, T., Kamei, M., Mitsuhashi, T., Ishigaki, T., Yamazaki, A., 2004. Charge separation at the rutile/anatase interface: A dominant factor of photocatalytic activity. Chem. Phys. Lett. 390, 399–402. https://doi.org/10.1016/j.cplett.2004.04.042

175. Miyawaki, A., Taira, S., Shiraishi, F., 2016. Performance of continuous stirred-tank reactors connected in series as a photocatalytic reactor system. Chem. Eng. J. 286, 594–601. https://doi.org/10.1016/j.cej.2015.11.007

176. Moncayo-Lasso, A., Sanabria, J., Pulgarin, C., Benítez, N., 2009. Simultaneous E. coli inactivation and NOM degradation in river water via photo-Fenton process at natural pH in solar CPC reactor. A new way for enhancing solar disinfection of natural water. Chemosphere 77, 296–300. https://doi.org/10.1016/j.chemosphere.2009.07.007

177. Mosteo, R., Varon Lopez, A., Muzard, D., Benitez, N., Giannakis, S., Pulgarin, C., 2020. Visible light plays a significant role during bacterial inactivation by the photo-fenton process, even at sub-critical light intensities. Water Res. 174, 115636. https://doi.org/10.1016/j.watres.2020.115636

178. Mozia, S., Brozek, P., Przepiórski, J., Tryba, B., Morawski, A.W., 2012. Immobilized TiO2 for phenol degradation in a pilot-scale photocatalytic reactor. J. Nanomater. 2012, 10. https://doi.org/10.1155/2012/949764

179. Mukherjee, K., Acharya, K., Biswas, A., Jana, N.R., 2020. TiO2 nanoparticles Co-doped with nitrogen and fluorine as visible-light-activated antifungal agents. ACS Appl. Nano Mater. 3, 2016–2025. https://doi.org/10.1021/acsanm.0c00108

180. Murcia, J.J., Ávila-Martínez, E.G., Rojas, H., Navío, J.A., Hidalgo, M.C., 2017. Study of the E. coli elimination from urban wastewater over photocatalysts based on metallized TiO2. Appl. Catal. B Environ. 200, 469–476. https://doi.org/10.1016/j.apcatb.2016.07.045

181. Mustapha, S., Ndamitso, M.M., Abdulkareem, A.S., Tijani, J.O., Shuaib, D.T., Ajala, A.O., Mohammed, A.K., 2020. Application of TiO2 and ZnO nanoparticles immobilized on clay in wastewater treatment: a review. Appl. Water Sci. 10, 1–36. https://doi.org/10.1007/s13201-019-1138-y

182. Naik, T.R., Kraus, R.N., Ramme, B.W., Canpolat, F., 2012. Effects of Fly Ash and Foundry Sand on Performance of Architectural Precast Concrete. J. Mater. Civ. Eng. 24, 851–859. https://doi.org/10.1061/(asce)mt.1943-5533.0000432

183. Nair, K.K., Harris, R.A., Viljoen, B., Swart, H.C., Aravind, U.K., Aravindakumar, C.T., 2020. Synthesis of silver incorporated lithium doped zinc oxide nanocomposites for in-vitro biorational evaluation of Candiasis and Cryptococcosis. Appl. Surf. Sci. 506, 144800. https://doi.org/10.1016/j.apsusc.2019.144800

184. Nair, V.R., Shetty Kodialbail, V., 2020. Floating bed reactor for visible light induced photocatalytic degradation of Acid Yellow 17 using polyaniline-TiO2 nanocomposites immobilized on polystyrene cubes. Environ. Sci. Pollut. Res. 27, 14441–14453. https://doi.org/10.1007/s11356-020-07959-2

185. Najm, I., 2006. An alternative interpretation of disinfection kinetics. J. Am. Water Work. Assoc. 98, 93–101. https://doi.org/10.1002/j.1551-8833.2006.tb07781.x

186. Nakano, R., Ishiguro, H., Yao, Y., Kajioka, J., Fujishima, A., Sunada, K., Minoshima, M., Hashimoto, K., Kubota, Y., 2012. Photocatalytic inactivation of influenza virus by titanium dioxide thin film. Photochem. Photobiol. Sci. 11, 1293–1298. https://doi.org/10.1039/c2pp05414k

187. Nakata, K., Fujishima, A., 2012. TiO2 photocatalysis: Design and applications. J. Photochem. Photobiol. C Photochem. Rev. 13, 169–189. https://doi.org/10.1016/j.jphotochemrev.2012.06.001

188. Natarajan, S., Lakshmi, D.S., Thiagarajan, V., Mrudula, P., Chandrasekaran, N., Mukherjee, A., 2018. Antifouling and anti-algal effects of chitosan nanocomposite (TiO2/Ag) and pristine (TiO2 and Ag) films on marine microalgae Dunaliella salina. J. Environ. Chem. Eng. 6, 6870–6880. https://doi.org/10.1016/j.jece.2018.10.050

189. Nayak, P.S., Singh, B.K., 2007. Instrumental characterization of clay by XRF , XRD and FTIR. Bull. Mater. Sci. 30, 235–238. https://doi.org/10.1007/s12034-007-0042-5

190. Ndounla, J., Kenfack, S., Wéthé, J., Pulgarin, C., 2014. Relevant impact of irradiance (vs. dose) and evolution of pH and mineral nitrogen compounds during natural water disinfection by photo-Fenton in a solar CPC reactor. Appl. Catal. B Environ. 148–149, 144–153. https://doi.org/10.1016/j.apcatb.2013.10.048

191. Ndounla, J., Pulgarin, C., 2015. Solar light (hv) and H2O2/hv photo-disinfection of natural alkaline water (pH 8.6) in a compound parabolic collector at different day periods in Sahelian region. Environ. Sci. Pollut. Res. 22, 17082–17094. https://doi.org/10.1007/s11356-015-4784-0

192. Ndounla, J., Pulgarin, C., 2014. Evaluation of the efficiency of the photo Fenton disinfection of natural drinking water source during the rainy season in the Sahelian region. Sci. Total Environ. 493, 229–238. https://doi.org/10.1016/j.scitotenv.2014.05.139

193. Nelson, K.L., Boehm, A.B., Davies-Colley, R.J., Dodd, M.C., Kohn, T., Linden, K.G., Liu, Y., Maraccini, P.A., McNeill, K., Mitch, W.A., Nguyen, T.H., Parker, K.M., Rodriguez, R.A., Sassoubre, L.M., Silverman, A.I., Wigginton, K.R., Zepp, R.G., 2018. Sunlight-mediated inactivation of health-relevant microorganisms in water: a review of mechanisms and modeling approaches. Environ. Sci. Process. Impacts 20, 1089–1122. https://doi.org/10.1039/c8em00047f

194. Ng, J., Zhang, X., Zhang, T., Pan, J.H., Du, J.H.A., Sun, D.D., 2010. Construction of self-organized free-standing TiO2 nanotube arrays for effective disinfection of drinking water. J. Chem. Technol. Biotechnol. 85, 1061–1066. https://doi.org/10.1002/jctb.2395

195. Núñez-Núñez, C.M., Osorio-Revilla, G.I., Villanueva-Fierro, I., Antileo, C., Proal-

Nájera, J.B., 2020. Solar fecal coliform disinfection in a wastewater treatment plant by oxidation processes: Kinetic analysis as a function of solar radiation. Water 12, 1–16. https://doi.org/10.3390/w12030639

196. Nyangaresi, P.O., Qin, Y., Chen, G., Zhang, B., Lu, Y., Shen, L., 2019. Comparison of UV-LED photolytic and UV-LED/TiO2 photocatalytic disinfection for Escherichia coli in water. Catal. Today 335, 200–207. https://doi.org/10.1016/j.cattod.2018.11.015

197. O'Neal Tugaoen, H., Garcia-Segura, S., Hristovski, K., Westerhoff, P., 2018. Compact light-emitting diode optical fiber immobilized TiO2 reactor for photocatalytic water treatment. Sci. Total Environ. 613–614, 1331–1338. https://doi.org/10.1016/j.scitotenv.2017.09.242

198. Ochiai, T., Fukuda, T., Nakata, K., Murakami, T., Tryk, D.A., Koide, Y., Fujishima, A., 2010. Photocatalytic inactivation and removal of algae with TiO2-coated materials. J. Appl. Electrochem. 40, 1737–1742. https://doi.org/10.1007/s10800-010-0133-7

199. Ortega-Gómez, E., Esteban García, B., Ballesteros Martín, M.M., Fernández Ibáñez, P., Sánchez Pérez, J.A., 2014. Inactivation of natural enteric bacteria in real municipal wastewater by solar photo-Fenton at neutral pH. Water Res. 63, 316–324. https://doi.org/10.1016/j.watres.2014.05.034

200. Ortega-Gómez, E., Esteban García, B., Ballesteros Martín, M.M., Fernández Ibáñez, P., Sánchez Pérez, J.A., 2013. Inactivation of Enterococcus faecalis in simulated wastewater treatment plant effluent by solar photo-Fenton at initial neutral pH. Catal. Today 209, 195–200. https://doi.org/10.1016/j.cattod.2013.03.001

201. Ortega-Gómez, E., Fernández-Ibáñez, P., Ballesteros Martín, M.M., Polo-López, M.I., Esteban García, B., Sánchez Pérez, J.A., 2012. Water disinfection using photo-Fenton: Effect of temperature on Enterococcus faecalis survival. Water Res. 46, 6154–6162. https://doi.org/10.1016/j.watres.2012.09.007

202. Ortega-Gómez, E., Martín, M.M.B., García, B.E., Pérez, J.A.S., Ibáñez, P.F., 2016. Wastewater disinfection by neutral pH photo-Fenton: The role of solar radiation intensity. Appl. Catal. B Environ. 181, 1–6. https://doi.org/10.1016/j.apcatb.2015.06.059

203. Ortega-Liébana, M.C., Sánchez-López, E., Hidalgo-Carrillo, J., Marinas, A., Marinas, J.M., Urbano, F.J., 2012. A comparative study of photocatalytic degradation of 3-

chloropyridine under UV and solar light by homogeneous (photo-Fenton) and heterogeneous (TiO 2) photocatalysis. Appl. Catal. B Environ. 127, 316–322. https://doi.org/10.1016/j.apcatb.2012.08.036

204. Ouyang, K., Dai, K., Walker, S.L., Huang, Q., Yin, X., Cai, P., 2016. Efficient photocatalytic disinfection of Escherichia coli O157:H7 using C70-TiO2 hybrid under visible light irradiation. Sci. Rep. 6, 1–8. https://doi.org/10.1038/srep25702

205. Ozkal, C.B., Koruyucu, A., Meric, S., 2016. Heterogeneous photocatalytic degradation, mineralization and detoxification of ampicillin under varying pH and incident photon flux conditions. Desalin. Water Treat. 57, 18391–18397. https://doi.org/10.1080/19443994.2016.1155175

206. Pablos, C., Van Grieken, R., Marugán, J., Moreno, B., 2011. Photocatalytic inactivation of bacteria in a fixed-bed reactor: Mechanistic insights by epifluorescence microscopy. Catal. Today 161, 133–139. https://doi.org/10.1016/j.cattod.2010.10.051

207. Paredes, L., Murgolo, S., Dzinun, H., Dzarfan Othman, M.H., Ismail, A.F., Carballa, M., Mascolo, G., 2019. Application of immobilized TiO2 on PVDF dual layer hollow fibre membrane to improve the photocatalytic removal of pharmaceuticals in different water matrices. Appl. Catal. B Environ. 240, 9–18. https://doi.org/10.1016/j.apcatb.2018.08.067

208. Pariente, M.I., Martínez, F., Melero, J.A., Botas, J.Á., Velegraki, T., Xekoukoulotakis, N.P., Mantzavinos, D., 2008. Heterogeneous photo-Fenton oxidation of benzoic acid in water: Effect of operating conditions, reaction by-products and coupling with biological treatment. Appl. Catal. B Environ. 85, 24–32. https://doi.org/10.1016/j.apcatb.2008.06.019

209. Pelaez, M., Nolan, N.T., Pillai, S.C., Seery, M.K., Falaras, P., Kontos, A.G., Dunlop, P.S.M., Hamilton, J.W.J., Byrne, J.A., O'Shea, K., Entezari, M.H., Dionysiou, D.D., 2012. A review on the visible light active titanium dioxide photocatalysts for environmental applications. Appl. Catal. B Environ. 125, 331–349. https://doi.org/10.1016/j.apcatb.2012.05.036

210. Philippe, K.K., Timmers, R., Van Grieken, R., Marugan, J., 2016. Photocatalytic disinfection and removal of emerging pollutants from effluents of biological wastewater treatments, using a newly developed large-scale solar simulator. Ind. Eng. Chem. Res. 55, 2952–2958. https://doi.org/10.1021/acs.iecr.5b04927

211. Pigeot-Rémy, S., Simonet, F., Errazuriz-Cerda, E., Lazzaroni, J.C., Atlan, D., Guillard, C., 2011. Photocatalysis and disinfection of water: Identification of potential bacterial targets. Appl. Catal. B Environ. 104, 390–398. https://doi.org/10.1016/j.apcatb.2011.03.001

212. Pokhum, C., Viboonratanasri, D., Chawengkijwanich, C., 2017. New insight into the disinfection mechanism of Fusarium monoliforme and Aspergillus niger by TiO2 photocatalyst under low intensity UVA light. J. Photochem. Photobiol. B Biol. 176, 17–24. https://doi.org/10.1016/j.jphotobiol.2017.09.014

213. Polo-López, M.I., Castro-Alférez, M., Oller, I., Fernández-Ibáñez, P., 2014. Assessment of solar photo-Fenton, photocatalysis, and H2O2 for removal of phytopathogen fungi spores in synthetic and real effluents of urban wastewater. Chem. Eng. J. 257, 122–130. https://doi.org/10.1016/j.cej.2014.07.016

214. Polo-López, M.I., Oller, I., Fernández-Ibáñez, P., 2013. Benefits of photo-Fenton at low concentrations for solar disinfection of distilled water. A case study: Phytophthora capsici. Catal. Today 209, 181–187. https://doi.org/10.1016/j.cattod.2012.10.006

215. Polo, D., García-Fernández, I., Fernández-Ibañez, P., Romalde, J.L., 2018. Hepatitis A Virus Disinfection in Water by Solar Photo–Fenton Systems. Food Environ. Virol. 10, 159–166. https://doi.org/10.1007/s12560-018-9339-3

216. Priya, S.S., Deshpande, A., Dwarakanath, R., 2015. Visible light solar photocatalytic degradation of pulp and paper wastewater using dye-sensitised TiO2. IJRET Int. J. Res. Eng. Technol. 04.

217. Prokopova, Z., Prokop, R., 1997. Modelling and simulation of chemical industrial reactors. Curr. Opin. Solid State Mater. Sci. 2, 693–695. https://doi.org/10.1016/S1359-0286(97)80011-3

218. Punzi, M., Mattiasson, B., Jonstrup, M., 2012. Treatment of synthetic textile wastewater by homogeneous and heterogeneous photo-Fenton oxidation. J. Photochem. Photobiol. A Chem. 248, 30–35. https://doi.org/10.1016/j.jphotochem.2012.07.017

219. Rahimi, R., Zargari, S., Yousefi, A., Yaghoubi Berijani, M., Ghaffarinejad, A., Morsali, A., 2015. Visible light photocatalytic disinfection of E. coli with TiO2-graphene nanocomposite sensitized with tetrakis(4-carboxyphenyl)porphyrin. Appl. Surf. Sci. 355, 1098–1106. https://doi.org/10.1016/j.apsusc.2015.07.115

220. Rao, N.N., Chaturvedi, V., 2007. Photoactivity of TiO2-coated pebbles. Ind. Eng. Chem. Res. 46, 4406–4414. https://doi.org/https://doi.org/10.1021/ie0702532

221. Ratova, M., Redfern, J., Verran, J., Kelly, P.J., 2018. Highly efficient photocatalytic bismuth oxide coatings and their antimicrobial properties under visible light irradiation. Appl. Catal. B Environ. 239, 223–232. https://doi.org/10.1016/j.apcatb.2018.08.020

222. Ray, S.K., Pandey, R.P., Jeong, S., Lee, S.W., 2018. Rapid Escherichia coli inactivation in visible light by Fe/Zn-α-NiMoO4 nanorod. J. Photochem. Photobiol. A Chem. 367, 162–170. https://doi.org/10.1016/j.jphotochem.2018.08.031

223. Reddy, M.P., Phil, H.H., Subrahmanyam, M., 2008. Photocatalytic disinfection of Escherichia coli over titanium (IV) oxide supported on Hβ zeolite. Catal. Letters 123, 56–64. https://doi.org/10.1007/s10562-008-9393-9

224. Reed, R.H., 2004. The inactivation of microbes by sunlight: Solar disinfection as a water treatment process. Adv. Appl. Microbiol. 54, 333–365. https://doi.org/10.1016/S0065-2164(04)54012-1

225. Ren, K., Liu, Y., He, X., Li, H., 2015. Suspension plasma spray fabrication of nanocrystalline titania hollow microspheres for photocatalytic applications. J. Therm. Spray Technol. 24, 1213–1220. https://doi.org/10.1007/s11666-015-0296-1

226. Ren, Y., Han, Y., Li, Z., Liu, X., Zhu, S., Liang, Y., Yeung, K.W.K., Wu, S., 2020. Ce and Er Co-doped TiO2 for rapid bacteria- killing using visible light. Bioact. Mater. 5, 201–209. https://doi.org/10.1016/j.bioactmat.2020.02.005

227. Rincón, A., Pulgarin, C., 2004. Effect of pH , inorganic ions , organic matter and H2O2 on E. coli K12 photocatalytic inactivation by TiO2 implications in solar water disinfection 51, 283–302. https://doi.org/10.1016/j.apcatb.2004.03.007

228. Rincón, A.G., Pulgarin, C., 2007. Absence of E. coli regrowth after Fe3+ and TiO2 solar photoassisted disinfection of water in CPC solar photoreactor. Catal. Today 124, 204–214. https://doi.org/10.1016/j.cattod.2007.03.039

229. Rincón, A.G., Pulgarin, C., 2006. Comparative evaluation of Fe3+ and TiO2 photoassisted processes in solar photocatalytic disinfection of water. Appl. Catal. B Environ. 63, 222–231. https://doi.org/10.1016/j.apcatb.2005.10.009

230. Rincón, A.G., Pulgarin, C., 2003. Photocatalytical inactivation of E. coli: Effect of (continuous-intermittent) light intensity and of (suspended-fixed) TiO2 concentration. Appl. Catal. B Environ. 44, 263–284. https://doi.org/10.1016/S0926-3373(03)00076-6

231. Rizzo, L., Sannino, D., Vaiano, V., Sacco, O., Scarpa, A., Pietrogiacomi, D., 2014. Environmental Effect of solar simulated N-doped TiO2 photocatalysis on the inactivation and antibiotic resistance of an E . coli strain in biologically treated urban wastewater. "Applied Catal. B, Environ. 144, 369–378. https://doi.org/10.1016/j.apcatb.2013.07.033

232. Rodrigues-Silva, C., Miranda, S.M., Lopes, F.V.S., Silva, M., Dezotti, M., Silva, A.M.T., Faria, J.L., Boaventura, R.A.R., Vilar, V.J.P., Pinto, E., 2017. Bacteria and fungi inactivation by photocatalysis under UVA irradiation: liquid and gas phase. Environ. Sci. Pollut. Res. 24, 6372–6381. https://doi.org/10.1007/s11356-016-7137-8

233. Rodríguez-Chueca, J., Mediano, A., Ormad, M.P., Mosteo, R., Ovelleiro, J.L., 2014a. Disinfection of wastewater effluents with the Fenton-like process induced by electromagnetic fields. Water Res. 60, 250–258. https://doi.org/10.1016/j.watres.2014.04.040

234. Rodríguez-Chueca, J., Morales, M., Mosteo, R., Ormad, M.P., Ovelleiro, J.L., 2013. Inactivation of Enterococcus faecalis, Pseudomonas aeruginosa and Escherichia coli present in treated urban wastewater by coagulation-flocculation and photo-Fenton processes. Photochem. Photobiol. Sci. 12, 864–871. https://doi.org/10.1039/c3pp25352j

235. Rodríguez-Chueca, J., Mosteo, R., Ormad, M.P., Ovelleiro, J.L., 2012. Factorial experimental design applied to Escherichia coli disinfection by Fenton and photo-Fenton processes. Sol. Energy 86, 3260–3267. https://doi.org/10.1016/j.solener.2012.08.015

236. Rodríguez-Chueca, J., Ormad, M.P., Mosteo, R., Canalis, S., Ovelleiro, J.L., 2016. Escherichia coli inactivation in fresh water through photocatalysis with TiO2-effect of H2O2 on disinfection kinetics. Clean - Soil, Air, Water 44, 515–524. https://doi.org/10.1002/clen.201500083

237. Rodríguez-Chueca, J., Polo-López, M.I., Mosteo, R., Ormad, M.P., Fernández-Ibáñez, P., 2014b. Disinfection of real and simulated urban wastewater effluents using a mild solar photo-Fenton. Appl. Catal. B Environ. 150–151, 619–629. https://doi.org/10.1016/j.apcatb.2013.12.027

238. Rodríguez, E.M., Fernández, G., Alvarez, P.M., Beltrán, F.J., 2012. TiO2 and Fe (III)

photocatalytic ozonation processes of a mixture of emergent contaminants of water. Water Res. 46, 152–166. https://doi.org/10.1016/j.watres.2011.10.038

239. Rommozzi, E., Giannakis, S., Giovannetti, R., Vione, D., Pulgarin, C., 2020. Detrimental vs. beneficial influence of ions during solar (SODIS) and photo-Fenton disinfection of E. coli in water: (Bi)carbonate, chloride, nitrate and nitrite effects. Appl. Catal. B Environ. 270. https://doi.org/10.1016/j.apcatb.2020.118877

240. Ruales-Lonfat, C., Barona, J.F., Sienkiewicz, A., Bensimon, M., Vélez-Colmenares, J., Benítez, N., Pulgarín, C., 2015. Iron oxides semiconductors are efficients for solar water disinfection: A comparison with photo-Fenton processes at neutral pH. Appl. Catal. B Environ. 166–167, 497–508. https://doi.org/10.1016/j.apcatb.2014.12.007

241. Rubio, D., Nebot, E., Casanueva, J.F., Pulgarin, C., 2013. Comparative effect of simulated solar light, UV, UV/H2O2 and photo-Fenton treatment (UV-Vis/H2O2/Fe2+,3+) in the Escherichia coli inactivation in artificial seawater. Water Res. 47, 6367–6379. https://doi.org/10.1016/j.watres.2013.08.006

242. Ruiz-Aguirre, A., Polo-López, M.I., Fernández-Ibáñez, P., Zaragoza, G., 2017. Integration of Membrane Distillation with solar photo-Fenton for purification of water contaminated with Bacillus sp. and Clostridium sp. spores. Sci. Total Environ. 595, 110–118. https://doi.org/10.1016/j.scitotenv.2017.03.238

243. Ruiz-Aguirre, A., Polo-López, M.I., Fernández-Ibáñez, P., Zaragoza, G., 2015. Assessing the validity of solar membrane distillation for disinfection of contaminated water. Desalin. Water Treat. 55, 2792–2799. https://doi.org/10.1080/19443994.2014.946717

244. Santhiya, G., Lakshumanan, C., Selvin, J., Asha, D., 2011. Microbiological analysis of seawater and sediments in urban shorelines: Occurrence of heavy metals resistance bacteria on Chennai beaches, Bay of Bengal. Microchem. J. 99, 197–202. https://doi.org/10.1016/j.microc.2011.05.004

245. Saran, S., Arunkumar, P., Devipriya, S.P., 2018. Disinfection of roof harvested rainwater for potable purpose using pilot-scale solar photocatalytic fixed bed tubular reactor. Water Sci. Technol. Water Supply 18, 49–59. https://doi.org/10.2166/ws.2017.097

246. Saran, S., Arunkumar, P., Manjari, G., Devipriya, S.P., 2019. Reclamation of grey water for non-potable purposes using pilot-scale solar photocatalytic tubular reactors. Environ.

Technol. 40, 3190–3199. https://doi.org/10.1080/09593330.2018.1468486

247. Saran, S., Manjari, G., Arunkumar, P., Devipriya, S.P., 2017. Solar photocatalytic decolorization of synthetic dye solution using pilot scale slurry type falling film reactor. Korean J. Chem. Eng. 34, 2984–2992. https://doi.org/10.1007/s11814-017-0204-0

248. Sato, T., Taya, M., 2006. Enhancement of phage inactivation using photocatalytic titanium dioxide particles with different crystalline structures. Biochem. Eng. J. 28, 303–308. https://doi.org/10.1016/j.bej.2006.01.004

249. Sayyar, Z., Akbar Babaluo, A., Shahrouzi, J.R., 2015. Kinetic study of formic acid degradation by Fe 3+ doped TiO2 self-cleaning nanostructure surfaces prepared by cold spray. Appl. Surf. Sci. 335, 1–10. https://doi.org/10.1016/j.apsusc.2015.01.014

250. Sciacca, F., Rengifo-Herrera, J.A., Wéthé, J., Pulgarin, C., 2011. Solar disinfection of wild Salmonella sp. in natural water with a 18L CPC photoreactor: Detrimental effect of non-sterile storage of treated water. Sol. Energy 85, 1399–1408. https://doi.org/10.1016/j.solener.2011.03.022

251. Seaver, L.C., Imlay, J.A., Loewen, P., 2001. Alkyl hydroperoxide reductase is the primary scavenger of endogenous hydrogen peroxide in Escherichia coli. J. Bacteriol. 183, 7173–7181. https://doi.org/10.1128/JB.183.24.7173

252. Severin, B.F., Suidan, M.T., Engelbrecht, R.S., 1984. Series-Event kinetic model for chemical disinfection. J. Environ. Eng. 110, 430–439. https://doi.org/10.1061/(asce)0733-9372(1984)110:2(430)

253. Shah, R.R., Kaewgun, S., Lee, B.I., Tzeng, T.R.J., 2008. The antibacterial effects of biphasic brookite-anatase titanium dioxide nanoparticles on multiple-drug-resistant Staphylococcus aureus. J. Biomed. Nanotechnol. 4, 339–348. https://doi.org/10.1166/jbn.2008.324

254. Shao, J., Sheng, W., Wang, M., Li, S., Chen, J., Zhang, Y., Cao, S., 2017. Environmental In situ synthesis of carbon-doped TiO 2 single-crystal nanorods with a remarkably photocatalytic efficiency. "Applied Catal. B, Environ. 209, 311–319. https://doi.org/10.1016/j.apcatb.2017.03.008

255. Shekoohiyan, S., Rtimi, S., Moussavi, G., Giannakis, S., Pulgarin, C., 2019. Enhancing

solar disinfection of water in PET bottles by optimized in-situ formation of iron oxide films. From heterogeneous to homogeneous action modes with H2O2 vs. O2 – Part 1: Iron salts as oxide precursors. Chem. Eng. J. 358, 211–224. https://doi.org/10.1016/j.cej.2018.09.219

256. Shephard, G.S., Stockenström, S., De Villiers, D., Engelbrecht, W.J., Wessels, G.F.S., 2002. Degradation of microcystin toxins in a falling film photocatalytic reactor with immobilized titanium dioxide catalyst. Water Res. 36, 140–146. https://doi.org/10.1016/S0043-1354(01)00213-5

257. Singh, S., Garg, A., 2019. Performance of photo-catalytic oxidation for degradation of chlorophenols: Optimization of reaction parameters and quantification of transformed oxidized products. J. Hazard. Mater. 361, 73–84. https://doi.org/10.1016/j.jhazmat.2018.08.055

258. Song, J., Wang, Xuejiang, Ma, J., Wang, Xin, Wang, J., Xia, S., Zhao, J., 2018. Removal of Microcystis aeruginosa and Microcystin-LR using a graphitic-C3N4/TiO2 floating photocatalyst under visible light irradiation. Chem. Eng. J. 348, 380–388. https://doi.org/10.1016/j.cej.2018.04.182

259. Song, M.-S., Vijayarangamuthu, K., Han, E., Jeon, K.-J., Seo, J.-W., 2016. Enhancement of photocatalytic disinfection of surface modified rutile TiO2 nanocatalyst. Korean J. Chem. Eng. 33, 2392–2395. https://doi.org/10.1007/s11814-016-0117-3

260. Sordo, C., Van Grieken, R., Marugán, J., Fernández-Ibáñez, P., 2010. Solar photocatalytic disinfection with immobilised TiO2 at pilot-plant scale. Water Sci. Technol. 61, 507–512. https://doi.org/10.2166/wst.2010.876

261. Spasiano, D., Marotta, R., Malato, S., Fernandez-Ibañez, P., Di Somma, I., 2015. Solar photocatalysis: Materials, reactors, some commercial, and pre-industrialized applications. A comprehensive approach. Appl. Catal. B Environ. 170–171, 90–123. https://doi.org/10.1016/j.apcatb.2014.12.050

262. Spuhler, D., Andrés Rengifo-Herrera, J., Pulgarin, C., 2010. The effect of Fe2+, Fe3+, H2O2 and the photo-Fenton reagent at near neutral pH on the solar disinfection (SODIS) at low temperatures of water containing Escherichia coli K12. Appl. Catal. B Environ. 96, 126–141. https://doi.org/10.1016/j.apcatb.2010.02.010

263. Sreeja, S., Shetty, V., 2016. Microbial disinfection of water with endotoxin degradation

by photocatalysis using Ag@TiO2 core shell nanoparticles. Environ. Sci. Pollut. Res. 18, 18154–64. https://doi.org/10.1007/s11356-016-6841-8

264. Sun, J.H., Sun, S.P., Fan, M.H., Guo, H.Q., Qiao, L.P., Sun, R.X., 2007. A kinetic study on the degradation of p-nitroaniline by Fenton oxidation process. J. Hazard. Mater. 148, 172–177. https://doi.org/10.1016/j.jhazmat.2007.02.022

265. Sunnotel, O., Verdoold, R., Dunlop, P.S.M., Snelling, W.J., Lowery, C.J., Dooley, J.S.G., Moore, J.E., Byrne, J.A., 2010. Photocatalytic inactivation of Cryptosporidium parvum on nanostructured titanium dioxide films. J. Water Health 8, 83–91. https://doi.org/10.2166/wh.2009.204

266. Tadashi, M., Ryozo, T., Toshiaki, N., Hitoshi, W., 1985. Photoelectrochemical sterilization of microbial cells by semiconductor powders. FEMS Microbiol. Lett. 29, 211–214.

267. Takdastan, A., Kakavandi, B., Azizi, M., Golshan, M., 2018. Efficient activation of peroxymonosulfate by using ferroferric oxide supported on carbon/UV/US system: A new approach into catalytic degradation of bisphenol A. Chem. Eng. J. 331, 729–743. https://doi.org/10.1016/j.cej.2017.09.021

268. Tallósy, S.P., Janovák, L., Ménesi, J., Nagy, E., Juhász, Á., Balázs, L., Deme, I., Buzás, N., Dékány, I., 2014. Investigation of the antibacterial effects of silver-modified TiO2 and ZnO plasmonic photocatalysts embedded in polymer thin films. Environ. Sci. Pollut. Res. 21, 11155–11167. https://doi.org/10.1007/s11356-014-2568-6

269. Talwar, S., Sangal, V.K., Verma, A., 2018. Feasibility of using combined TiO2 photocatalysis and RBC process for the treatment of real pharmaceutical wastewater. J. Photochem. Photobiol. A Chem. 353, 263–270. https://doi.org/10.1016/j.jphotochem.2017.11.013

270. Talwar, S., Sangal, V.K., Verma, A.K., 2019. In-situ dual effect of novel Fe-TiO2 composite for the degradation of phenazone. Sep. Purif. Technol. 211, 391–400. https://doi.org/10.1016/j.seppur.2018.10.007

271. Taylor, P., Suri, R.P.S., Thornton, H.M., Muruganandham, M., 2012. Disinfection of water using Pt- and Ag-doped TiO2 photocatalysts. Environ. Technol. 1651–1659. https://doi.org/10.1080/09593330.2011.641590

272. Tribe, M.A., Alpine, R.L.W., 1986. Scale economies and the "0.6 rule." Eng. Costs Prod. Econ. 10, 271–278. https://doi.org/10.1016/0167-188X(86)90053-4

273. Tsoumachidou, S., Velegraki, T., Antoniadis, A., Poulios, I., 2017. Greywater as a sustainable water source: A photocatalytic treatment technology under artificial and solar illumination. J. Environ. Manage. 195, 232–241. https://doi.org/10.1016/j.jenvman.2016.08.025

274. Tumuluri, A., Naidu, K.L., Raju, K.C.J., 2014. Band gap determination using Tauc 's plot for LiNbO3 thin films. Int. J. ChemTech Res. 6, 3353–3356.

275. UNICEF, 2014. Drinking Water and Sanitation.

276. United Nations, 2014. Economic and social commission for Western Asia input to the high-Level political forum on sustainable development and the ECOSOC annual ministerial review, United Nations, Distr. General E/ESCWA/SDPD.

277. Valero, P., Giannakis, S., Mosteo, R., Ormad, M.P., Pulgarin, C., 2017. Comparative effect of growth media on the monitoring of E. coli inactivation and regrowth after solar and photo-Fenton treatment. Chem. Eng. J. 313, 109–120. https://doi.org/10.1016/j.cej.2016.11.126

278. Venieri, D., Gounaki, I., Binas, V., Zachopoulos, A., Kiriakidis, G., Mantzavinos, D., 2015. Inactivation of MS2 coliphage in sewage by solar photocatalysis using metal-doped TiO2. Appl. Catal. B Environ. 178, 54–64. https://doi.org/10.1016/j.apcatb.2014.10.052

279. Venieri, D., Tournas, F., Gounaki, I., Binas, V., Zachopoulos, A., Kiriakidis, G., Mantzavinos, D., 2017. Inactivation of Staphylococcus aureus in water by means of solar photocatalysis using metal doped TiO2 semiconductors. J. Chem. Technol. Biotechnol. 92, 43–51. https://doi.org/10.1002/jctb.5085

280. Veréb, G., Manczinger, L., Bozsó, G., Sienkiewicz, A., Forró, L., Mogyorósi, K., Hernádi, K., Dombi, A., 2013. Environmental comparison of the photocatalytic efficiencies of bare and doped rutile and anatase TiO2 photocatalysts under visible light for phenol degradation and E . coli inactivation. Appl. Catal. B, Environ. 129, 566–574. https://doi.org/10.1016/j.apcatb.2012.09.045

281. Verma, A., Prakash, N. T., & Toor, A.P., 2016. Photocatalytic degradation of herbicide

isoproturon in TiO2 aqueous suspensions: Study of reaction intermediates and degradation pathways. Environ. Prog. Sustain. Energy 33, 1–10. https://doi.org/10.1002/ep

282. Vijay, M., Ramachandran, K., Ananthapadmanabhan, P. V, Nalini, B., Pillai, B.C., Bondioli, F., Manivannan, A., Narendhirakannan, R.T., 2013. Photocatalytic inactivation of Gram-positive and Gram-negative bacteria by reactive plasma processed nanocrystalline TiO 2 powder. Curr. Appl. Phys. 13, 510–516. https://doi.org/10.1016/j.cap.2012.09.014

283. Vishnuganth, M.A., Remya, N., Kumar, M., Selvaraju, N., 2016. Photocatalytic degradation of carbofuran by TiO2-coated activated carbon: Model for kinetic, electrical energy per order and economic analysis. J. Environ. Manage. 181, 201–207. https://doi.org/10.1016/j.jenvman.2016.06.016

284. Von Sperling, M., 2005. Modelling of coliform removal in 186 facultative and maturation ponds around the world. Water Res. 39, 5261–5273. https://doi.org/10.1016/j.watres.2005.10.016

285. Wang, C.P., Chang, C.S., Lin, W.C., 2020. Efficiency improvement of a flow-through water disinfection reactor using UV-C light emitting diodes. J. Water Process Eng. https://doi.org/10.1016/j.jwpe.2020.101819

286. Wang, G., Feng, W., Zeng, X., Wang, Z., Feng, C., Mccarthy, D.T., Deletic, A., Zhang, X., 2016. Highly recoverable TiO2-GO nanocomposites for stormwater disinfection. Water Res. 94, 363–370. https://doi.org/10.1016/j.watres.2016.02.067

287. Wang, W., Yu, J.C., Xia, D., Wong, P.K., Li, Y., 2013. Graphene and g-C3N4 nanosheets cowrapped elemental α-sulfur as a novel metal-free heterojunction photocatalyst for bacterial inactivation under visible-light. Environ. Sci. Technol. 47, 8724–8732. https://doi.org/https://doi.org/10.1021/es4013504

288. Wang, W., Yu, Y., An, T., Li, G., Yip, H.Y., Yu, J.C., Wong, P.K., 2012. Visible-light-driven photocatalytic inactivation of E. coli K-12 by bismuth vanadate nanotubes: Bactericidal performance and mechanism. Environ. Sci. Technol. 46, 4599–4606. https://doi.org/10.1021/es2042977

289. Wang, X.L., Lu, Y., Hua, K., Yang, D., Yang, Y., 2021. Iodine-doped carbon dots with inherent peroxidase catalytic activity for photocatalytic antibacterial and wound disinfection. Anal. Bioanal. Chem. 413, 1373–1382. https://doi.org/10.1007/s00216-020-03100-x

290. Warren Viessman, J., Hammer, M.J., Perez, E.M., Chadik, P.A., 2009. Water Supply and Pollution Control, 7th ed.

291. Wirtanen, G., Salo, S., 2003. Disinfection in food processing - Efficacy testing of disinfectants. Rev. Environ. Sci. Biotechnol. 2, 293–306. https://doi.org/10.1023/B:RESB.0000040471.15700.03

292. Wong, M., Chu, W., Sun, D., Huang, H., Chen, J., Tsai, P., Lin, N., Yu, M., Hsu, S., Wang, S., Chang, H., 2006. Visible-Light-Induced Bactericidal Activity of a Nitrogen-Doped Titanium Photocatalyst against Human Pathogens 72, 6111–6116. https://doi.org/10.1128/AEM.02580-05

293. Xi, J., Zhang, F., Lu, Y., Hu, H.Y., 2017. A novel model simulating reclaimed water disinfection by ozonation. Sep. Purif. Technol. 179, 45–52. https://doi.org/10.1016/j.seppur.2017.01.027

294. Xiang, Q., Yu, J., Jaroniec, M., 2012. Graphene-based semiconductor photocatalysts. Chem. Soc. Rev. 41, 782–796. https://doi.org/10.1039/c1cs15172j

295. Yadav, P., 2010. Titanium Dioxide Mediated Photocatalytic Degradation of Chlorpyrifos in Aqueous Phase. Int. J. Environ. Sci. s 3, 743–755. https://doi.org/10.6088/ijes.2012030132001

296. Yao, S., Li, J., Shi, Z., 2010. Immobilization of TiO2 nanoparticles on activated carbon fiber and its photodegradation performance for organic pollutants. Particuology 8, 272–278. https://doi.org/10.1016/j.partic.2010.03.013

297. Yousefzadeh, S., Matin, A.R., Ahmadi, E., Sabeti, Z., Alimohammadi, M., Aslani, H., Nabizadeh, R., 2018. Response surface methodology as a tool for modeling and optimization of Bacillus subtilis spores inactivation by UV/ nano-Fe0 process for safe water production. Food Chem. Toxicol. 114, 334–345. https://doi.org/10.1016/j.fct.2018.02.045

298. Yu, H., Nie, E., Xu, J., Yan, S., Cooper, W.J., Song, W., 2013. Degradation of Diclofenac by Advanced Oxidation and Reduction Processes: Kinetic Studies, Degradation Pathways and Toxicity Assessments. Water Res. 47, 1909–1918. https://doi.org/10.1016/j.watres.2013.01.016

299. Yu, H., Song, L., Hao, Y., Lu, N., Quan, X., Chen, S., Zhang, Y., Feng, Y., 2016.

Fabrication of pilot-scale photocatalytic disinfection device by installing TiO2 coated helical support into UV annular reactor for strengthening sterilization. Chem. Eng. J. 283, 1506–1513. https://doi.org/10.1016/j.cej.2015.08.042

300. Yu, J., Xiong, J., Cheng, B., Liu, S., 2005. Fabrication and characterization of Ag-TiO2 multiphase nanocomposite thin films with enhanced photocatalytic activity. Appl. Catal. B Environ. 60, 211–221. https://doi.org/10.1016/j.apcatb.2005.03.009

301. Yuan, X., Duan, S., Wu, G., Sun, L., Cao, G., Li, D., Xu, H., Li, Q., Xia, D., 2018. Enhanced catalytic ozonation performance of highly stabilized mesoporous ZnO doped g-C3N4 composite for efficient water decontamination. Appl. Catal. A Gen. 551, 129–138. https://doi.org/10.1016/j.apcata.2017.12.011

302. Zacarías, S.M., Satuf, M.L., Vaccari, M.C., Alfano, O.M., 2012. Efficiency evaluation of different TiO 2 coatings on the photocatalytic inactivation of airborne bacterial spores. Ind. Eng. Chem. Res. 51, 13599–13608. https://doi.org/10.1021/ie3009956

303. Zan, L., Fa, W., Peng, T., Gong, Z. kui, 2007. Photocatalysis effect of nanometer TiO2 and TiO2-coated ceramic plate on Hepatitis B virus. J. Photochem. Photobiol. B Biol. 86, 165–169. https://doi.org/10.1016/j.jphotobiol.2006.09.002

304. Zepp, R.G., Faust, B.C., Jürg, H., 1992. Hydroxyl radical formation in aqueous reactions (pH 3-8) of iron(II) with hydrogen peroxide: The Photo-Fenton reaction. Environ. Sci. Technol. 26, 313–319. https://doi.org/10.1021/es00026a011

305. Zhang, J., Yuan, M., Liu, X., Wang, X., Liu, S., Han, B., Liu, B., Shi, H., 2020. Copper modified Ti3+ self-doped TiO2 photocatalyst for highly efficient photodisinfection of five agricultural pathogenic fungus. Chem. Eng. J. 387, 124171. https://doi.org/10.1016/j.cej.2020.124171

306. Zhang, L., Qi, H., Yan, Z., Gu, Y., Sun, W., Zewde, A.A., 2017. Sonophotocatalytic inactivation of E. coli using ZnO nanofluids and its mechanism. Ultrason. Sonochem. 34, 232–238. https://doi.org/10.1016/j.ultsonch.2016.05.045

307. Zhang, L.S., Wong, K.H., Yip, H.Y., Hu, C., Yu, J.C., Chan, C.Y., Wong, P.K., 2010. Effective photocatalytic disinfection of E. coli K-12 using AgBr-Ag-Bi 2WO6 nanojunction system irradiated by visible light: The role of diffusing hydroxyl radicals. Environ. Sci. Technol. 44, 1392–1398. https://doi.org/10.1021/es903087w

308. Zhang, Y., Hu, Y., Zhao, J., Park, E., Jin, Y., Liu, Q., Zhang, W., 2019. Covalent organic framework-supported Fe-TiO2 nanoparticles as ambient-light-active photocatalysts. J. Mater. Chem. A 7, 16364–16371. https://doi.org/10.1039/c9ta03649k

309. Zheng, X., Shen, Z.P., Cheng, C., Shi, L., Cheng, R., Dong, J., 2017. Electrospinning Cu-TiO2 nanofibers used for photocatalytic disinfection of bacteriophage f2: Preparation, optimization and characterization. RSC Adv. 7, 52172–52179. https://doi.org/10.1039/c7ra07770j

310. Zhu, J., Zheng, W., He, B., Zhang, J., Anpo, M., 2004. Characterization of Fe-TiO2 photocatalysts synthesized by hydrothermal method and their photocatalytic reactivity for photodegradation of XRG dye diluted in water. J. Mol. Catal. A Chem. 216, 35–43. https://doi.org/10.1016/j.molcata.2004.01.008

List of Publications

S.No.	Title of the Paper	Authors	Journal name, vol., Page no., year of publish	Publisher/ISSN/ Impact factor
1.	Inactivation of *E. coli* in water employing Fe-TiO_2 composite incorporating the in-situ dual process of photocatalysis and photo-Fenton in fixed-mode.	Ina Thakur, Banu Örmeci, Aoop Verma	Journal of Water Process Engineering, 33(2020)101085	Elsevier, 2214-7144 IF: 7.34
2.	Mathematical modeling of *E. coli* inactivation in water using Fe-TiO_2 composite in a fixed bed reactor	Ina Thakur, Aoop Verma, Banu Örmeci	Separation and Purification Technology, 260(2021) 118242	Elsevier, 1383-5866 I F: 9.136
3.	Fe-TiO_2 Composite Mediated the Hybrid Effect of Photocatalysis and Photo-Fenton for the Inactivation of Escherichia coli Using a Continuous Flow Recirculation Reactor	Ina Thakur, Aoop Verma, Banu Örmeci	Industrial & Engineering Chemistry Research 60(2021)7558−7571	American Chemical Society, IF: 4.326
4.	Visibly active Fe-TiO_2 composite: A stable and efficient catalyst for the catalytic disinfection of water using a once-through reactor.	Ina Thakur, Aoop Verma, Banu Örmeci	Journal of Environmental Chemical Engineering. 9(2021)10322	Elsevier, 2213-3437 IF: 7.968
5.	Inactivation of bacteria present in secondary municipal wastewater effluent using the hybrid effect of Fe-TiO_2 catalyst	Ina Thakur, Aoop Verma, Banu Örmeci	Journal of Cleaner Production, *352*, 131575.	Elsevier (IF.: 11.072 *Elsevier*)
6.	Applications of waste-derived visibly active Fe-TiO_2 composite incorporating the hybrid process of photocatalysis and photo-Fenton for the inactivation of *E. coli*	I. Thakur, A. Verma, B. Örmeci, V. Sangal	Environmental Science and Pollution Research, 1-13	(IF.: 5.19 *Springer*)

Journal of Water Process Engineering 33 (2020) 101085

Contents lists available at ScienceDirect

Journal of Water Process Engineering

journal homepage: www.elsevier.com/locate/jwpe

Inactivation of *E. coli* in water employing Fe-TiO_2 composite incorporating in-situ dual process of photocatalysis and photo-Fenton in fixed-mode

Ina Thakur[a], Banu Örmeci[b], Anoop verma[a,*]

[a] School of Energy and Environment, Thapar Institute of Engineering and Technology, Patiala, 147004, India
[b] Civil and Environmental Department, Carleton University, Ottawa, ON KIS 5B6, Canada

ARTICLE INFO

Keywords:
Photocatalysis
Photo-Fenton
Fixed-mode
Water
E. coli
Inactivation

ABSTRACT

Applications of Fe-TiO_2 composite incorporating in-situ dual effect of photocatalysis and photo-Fenton process was studied for inactivation of *E. coli* K12 strain. A thin film of TiO_2 was coated on spherical composite beads (leading to photocatalysis) comprising of clay, foundry sand (FS) and fly ash (FA) from which iron leached out (leading to photo-Fenton) thus incorporating dual effect. Operating parameters such as UV light intensity, size of beads, addition of oxidant, buffer, and area/volume ratio of the reactor were optimized for the inactivation of *E. coli*. In dual process, 6.2 *E. coli* log reduction was observed in 90 min of reaction time. An increase of 26 % of synergy with dual process was obtained in comparison to photocatalysis and photo-Fenton alone. The beads were proved to be durable for more than 50 recycles for the inactivation of *E. coli*. To confirm the presence of TiO_2, morphological analysis and elemental composition for fresh as well as recycled composite beads was done using SEM and EDS respectively. The activity of catalyst and presence of Fe was also checked by using XRD, FTIR, and DRS.

1. Introduction

Acceptance of oxidation technologies for water disinfection has been widely declined either due to their high cost (e.g., ozonation) or formation of disinfection byproducts (e.g., chlorination). Problems are more severe in developing countries like India, where population explosion and poor sanitation led to the contamination of ground and surface water. In India, only 4 % of natural drinking water resources exist, and their quality and quantity are rapidly declining [1]. The contaminated water sources pose significant threat to environmental and human health leading to loss of life of more than 800,000 people annually around the world [2–4]. Moreover continual dependence on old conventional treatment techniques has drastically deepened the concern.

The presence of chlorinated disinfection byproduct, which may be carcinogenic to humans [5], has directed scientists to look for alternative techniques for disinfection of water. Previous studies have reported the efficacy of advance technologies towards the treatment of different organic compounds [6–8] and disinfection of microorganisms [9–11] through microfiltration [12], advanced oxidation processes (AOPs) [13], and electro-dialysis [14]. Although these technologies have some successful stories to tell yet utilization of these technologies in field-scale application is very limited. This might be due to the operational as well as technical drawbacks of AOP technologies used while executing their scale-up studies. TiO_2 photocatalysis, for example, has been extensively used to overcome the challenges in energy [15–17] as well as in disinfection of water and wastewater [9,18,19]. This process work on well-established phenomena of the production of oxidative free radicals (OH·) through charge carriers formed by excitation of e^- of the semiconductor and thus leading to redox reactions [20]. Use of this process in suspension as well as fixed form have reported many studies on inactivation of bacteria [21–24]. Owing to its potential for scaled-up, fixed-bed studies used different support materials such as cylinders [25], plate [26], glass-balls [27], polymers [28,29] for disinfection as well as degradation studies. Although very prominent in terms of its efficacy, the major drawbacks include electron hole recombination, separation of catalyst from the solution after the reaction [30], durability of support/catalyst stability, mass transfer limitation, and increase in treatment time. These aforementioned drawbacks question their viability for commercialization and thus limit its applications.

Another important technique, photo-Fenton, has also been well reported in the literature for water disinfection as well as for the degradation of contaminants [11,31–35]. In this homogeneous process, reaction of H_2O_2 with Fe^{2+} in the presence of light and acidic pH generates strong reactive oxygen species such as $OH^{\bullet}$ [32]. High doses

* Corresponding author.
E-mail address: anoop.kumar@thapar.edu (A. verma).

https://doi.org/10.1016/j.jwpe.2019.101085
Received 7 October 2019; Received in revised form 26 November 2019; Accepted 26 November 2019
2214-7144/ © 2019 Elsevier Ltd. All rights reserved.

of H_2O_2 along with formation of iron sludge are the main drawbacks.

There are a lot of studies where iron and TiO_2 was used together to increase the bacterial inactivation rate [36–39]. Zhang et al. [38] reported the Fe^{+3} doped TiO_2 catalyst coated over glass slides to study the inactivation rate of *E. coli* and observed the killing of 95 % of bacteria in 120 min of reaction time. Although this process helps in decreasing electron-hole recombination yet stability of the catalyst is the major concern.

Taking into consideration the advantages and drawbacks of aforementioned systems, the present study proposes the in-situ dual process of photocatalysis and photo-Fenton for the disinfection studies. As per our knowledge this technique has not been reported for bacterial killing yet. The Fe-TiO_2 composite (in the form of spherical beads) made up of clay and waste foundry sand (FS) and fly-ash (FA) is capable of introducing the dual effect in the system. FS, FA being sources of iron, leaches into the solution and thus triggers photo-Fenton reaction in the presence of H_2O_2. This composite retains the surface active TiO_2 layer, which facilitates the photocatalysis. The process is designed in such a way that a drawback of individual process is covered by other process happening in-situ thus providing the synergy to the system. Production of iron waste (foundry sand and fly ash) from industrial processes is increasing rapidly, and every year more than 99 million tons of foundry sand and 365 million tons of fly ash is produced worldwide [40,41]. Utilization of such waste as an absorbent [42] and as a construction material [43] has been reported, but very few studies regarding its utilization in degradation of pollutants present in water [7,8,44,45] have been reported.

The present study successfully assimilated photocatalysis and photo-Fenton into one unit in fixed-mode using industrial waste FS and FA as an iron source and mixing them with clay to form spherical beads. This dual process is likely to increase the production of hydroxyl radical and utilization of iron reduces the electron hole recombination, thus increasing the disinfection efficiency of the system. To the best of our knowledge, this is the first reported study in which both TiO_2 and iron source are completely immobilized to increase the inactivation efficiency of *E. coli* present in water.

2. Materials and method

2.1. Chemicals and reagents

All the chemicals were used as received. TiO_2-P25 Degussa was purchased from Evonik Enterprises, Mumbai (India). The oxidant, 30 % w/v hydrogen peroxide (H_2O_2), was bought from Ranbaxy, India. Clay was procured from a local supplier to prepare the inert support material. Fly ash (FA) and foundry sand (FS) was used as an iron source in photo-Fenton reaction and were provided from a local industry, Patiala, Punjab (India). SEM-EDS for FA and FS were performed to check the iron content and the data are provided in the supplementary file (Fig. S1). Sodium acetate (> 98.5 %) and acetic acid (> 99.5 %) were obtained from Tokyo Chemical Industry (India) to prepare the acetate buffer for pH control. NaCl (99.5 %) was obtained from S.D Fine-Chemical, Ambala, Haryana (India) to provide an isotonic solution for the bacterial cells. Luria Bertani broth and Agar Agar, Type I for bacterial growth were purchased from Himedia Laboratories, Nasik, India. The double-distilled water was used for the preparation of all solutions.

2.2. Preparation of composite beads and immobilization of TiO_2

Clay was used as an inert support material and was mixed with FS and FA in the ratio of 2:1:1 respectively to form spherical beads manually. The size of the bead was measured using screw gauge from at least four different directions to obtain the average size, and subsequently, the beads were grouped in three different sizes of 10 mm, 15 mm, and 20 mm. This procedure was repeated for every composite bead, and accordingly beads of equal diameter were selected. After drying at room temperature, these blank beads were muffled at 800 °C for 2 h followed by immersion in water for curing to increase the strength of the inert material.

The coating of TiO_2 on these beads was executed using the dipping technique as previously described [45]. 1 % solution of TiO_2 (1 g in 100 mL) was prepared using distilled water and sonicated for 20 min. to achieve dispersion of TiO_2 nanoparticles. After that, beads were immersed in the TiO_2 solution for 24 h. and adequate time and shaking were provided for coating the beads with TiO_2. For adequate coverage of the bead surface, at least 2 coatings of TiO_2 were performed. To achieve binding of TiO_2 on the beads, they were muffled for 1.5 h at 350 °C and then cooled at room temperature. This process was repeated after each cycle of coating to fully coat the beads with TiO_2. Afterwards, the coated beads were washed with distilled water to remove the loosely attached TiO_2 and then oven-dried. The average thickness of coating over bead was 71 μm and the SEM image for the same has been provided in supplementary file (Fig. S2).

2.3. Bacterial strain and growth

The *E. coli* strain (wild type K12) was bought from Microbial Type Culture Collection and Gene Bank (MTCC, No. 1302), Chandigarh, India. *E. coli* is a gram-negative bacteria and used as an indicator of fecal pollution in water. For this study, *E. coli* was grown in Miller's Luria Bertani Broth (LB) (Tryptone 10 g L^{-1}, Yeast extract 5 g L^{-1}, Sodium chloride 10 g L^{-1}) in double-distilled water. Bacterial growth phase was monitored at an optical density of 600 nm until the stationary phase was reached. 1 % dilution was done in 50 mL of LB broth followed by overnight incubation of *E.coli* at 37 °C. After the incubation, cells were centrifuged at 4 °C at 5000 rpm for 15 min. The supernatant left after the centrifugation was removed and the bacterial pellet was washed with saline solution (0.8 % of NaCl). Finally, the bacterial pellet was suspended into saline solution (25 mL) to give a final concentration of 10^9 CFU mL^{-1}.

2.4. Bacterial enumeration and sampling

All the working solutions were sterilized using autoclave before use. Bacterial samples in the reactor were continuously aerated using spargers. The flow rate of aeration was 3 L min^{-1}. During each inactivation experiment, 1 mL of sample was recovered from the reactor and stored at 4 °C in 2 mL Eppendorf tubes until the plating of cells was done. Viable cell count was done on Petri plates containing LB and Agar Type 1 using standard plate count method. Serial dilution of the sterile saline solution of 9 ml from 10^{-1} to 10^{-7} was made, and 0.1 mL of sample from the dilution tubes was plated on agar plates. Then the plates were kept in the incubator at 37 °C for 24 h. The inactivation efficiency was shown by log unit reduction of *E. coli* (L_r):

$$Lr = \left(\frac{A_t}{A_0}\right)$$

Where, A_t and A_0 are initial concentration and concentration at a particular treatment time, respectively.

2.5. Characterization

Fresh and recycled spherical beads were characterized to confirm the presence of iron and TiO_2 through different techniques. The surface morphology of TiO_2 coated over the surface of composite beads and the composition of the elements present on the surface of the beads were analyzed by scanning electron microscopy (SEM) model no. JSM-6510LV, JEOL (Japan) and electron-dispersive spectroscopy (EDS), model no. INCAX-act, Oxford instruments (UK), respectively. The band gap energy of TiO_2 was determined between the range of 200–800 nm by the UV–vis diffuse reflectance spectrometer (DRS), UV-2600, Shimadzu (Asia Pacific). The crystalline structure of TiO_2 on the

composite beads was determined by X-Ray diffraction analysis using PANalyticalXpert Pro with Cu Kα wavelength (λ = 1.5405) between the range of 2θ = 20° to 80°. The catalyst over the surface of composite beads was also analyzed by Fourier – transform infrared spectroscopy (FTIR). The infrared spectrum of the powered sample was analyzed in the range of 4000 to 400 cm^{-1}. The generation of $OH^{\cdot}$ due the photocatalysis and photo-Fenton process was analyzed by fluorescence spectrophotometer at 460 nm. In this method, reaction of hydroxyl radical with sodium salts of terephthalic acid produces 2-hydroxy terephthalic acid (fluorescent compound) which can be measured by the fluorescence spectrophotometer to validate the production of hydroxyl radicals.

2.6. Experimental setup

All the experiments were carried out inside a fully-enclosed rectangular wooden chamber (1.37 m × 0.9 m × 1.06 m) consisting of seven UV tubes (Philips, 36 W, 365 nm) and was fixed on the ceiling of the wooden chamber [6]. A borosilicate glass dish of 20 cm of diameter and 5.5 cm of height having a volume of 1000 ml was used as a reactor. The reactor was placed under the UV lights on a laboratory jack so that the irradiation intensity can be changed by altering the height of the jack. The average variation of UV radiation ranges between 10 to 24 Wm^{-2} and was measured using a radiometer (Eppley, model no. 33013). The working solution contained 250 mL of double distilled water spiked with 10^6 CFU mL^{-1} of *E. coli*. Then the solution was stirred for 20 min. at room temperature for the acclimatization of bacteria and the TiO_2 immobilized composite beads were added to start the experiment. To support the homogeneity of the reaction, aeration (3 L min^{-1}) was provided to the reactor with two spargers that were placed at equal distance from the center. Then the dual effect of the process (simultaneous incorporation of photocatalysis and photo-Fenton in one unit) was studied as shown in Fig. 1. For disinfection studies, 1 mL of sample was taken out after regular intervals from the reactor and the decrease in the concentration of the *E. coli* was calculated by plating method. All the borosilicate reactors were washed and autoclaved prior to each reaction. Optimization of the process was done by varying different parameters such as H_2O_2 dose, pH, bead size, UV intensity, volume to area ratio based on which reaction kinetics was studied. All experiments were performed in triplicates and the results show the average of the three samples and the error bars show the standard deviation in the figures. Statistical significance of the mean value of the treated samples was determined by the one-way ANOVA test. All results were found to be significant as the F-values were greater than 5 and p-value < 0.05 for all the experiments as shown in Table 1.

Table 1
Statistical analysis for inactivation of *E. coli* using photocatalysis, photo-Fenton, and dual process.

S. No.	Process	F-value	P-value
1	Photocatalysis	202.98	2.05×10^{-14}
2	Photo-Fenton	352.82	2.58×10^{-16}
3	Dual (Photocatalysis + photo-Fenton) process	5570	8.11×10^{-23}

3. Results and discussion

3.1. Characterization of composite beads

As the system executes the dual process within the same unit, there is a need to confirm both the components leading to photocatalysis and photo-Fenton on the surface of spherical beads for fresh as well as recycled composite beads, characterization using different techniques was done.

3.1.1. SEM/ EDS analysis

To analyze the surface morphology as well as the composition of the elements on the composite beads (uncoated, freshly coated and recycled), scanning electron microscopy (SEM) along with energy dispersive spectroscopy (EDS) was performed and the results are shown in Fig. 2. The major peaks of Fe, O, and TiO_2 on the EDS image confirm the incorporation of both materials (Fe and TiO_2) in the dual process in freshly and recycled beads. The existence of iron can be accredited to the utilization of FA/FS with clay to form composite beads as no

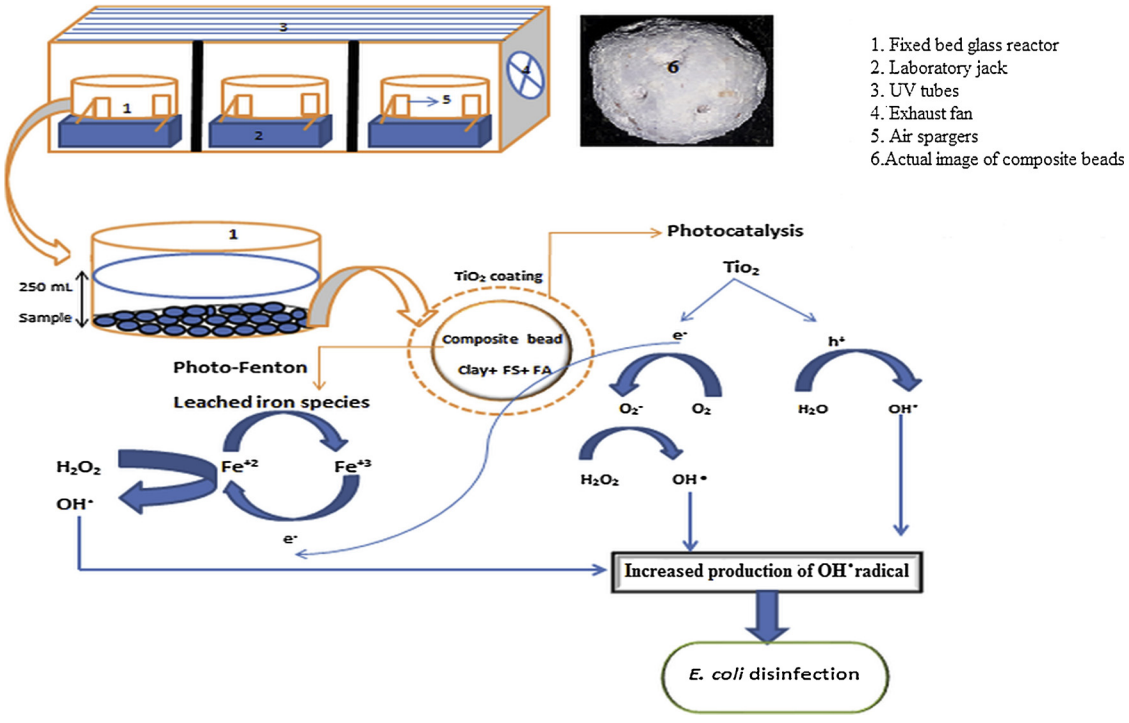

Fig. 1. Dual effect of photocatalysis and photo-Fenton for inactivation of *E. coli*.

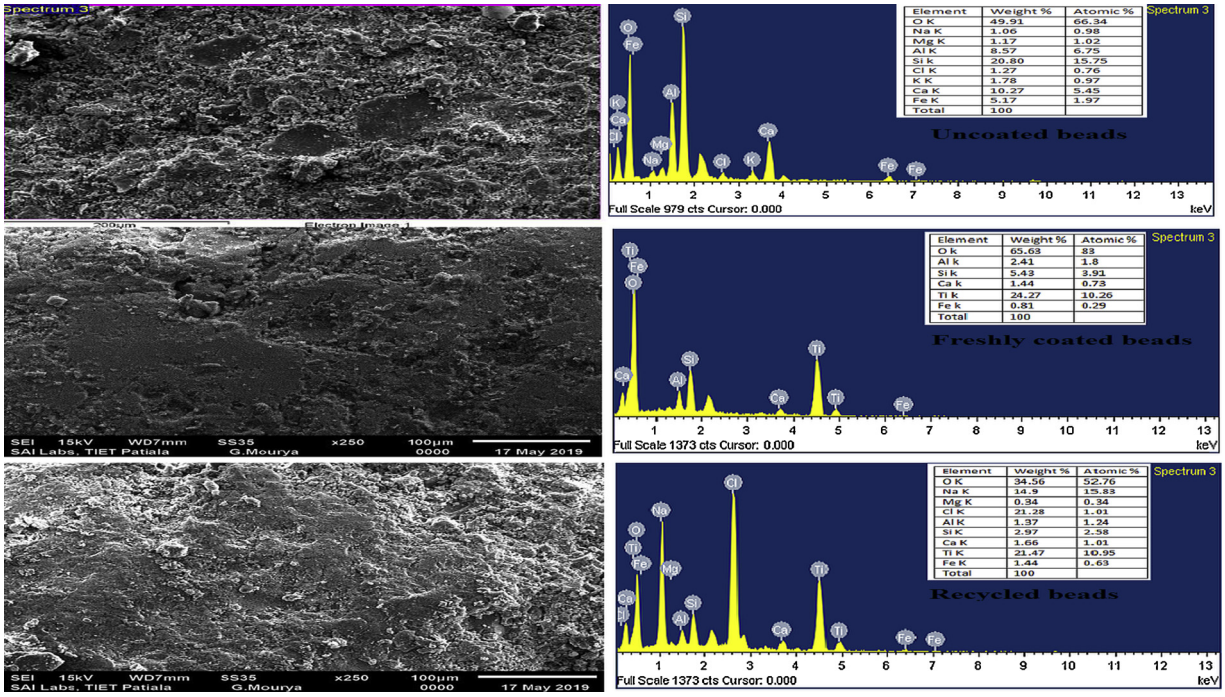

Fig. 2. SEM and EDS images of uncoated, freshly coated and recycled composite bead.

external iron was used for the process. A relatively smooth surface can be seen in the SEM image of freshly as well as recycled (50 times) coated beads. This indicates the presence of TiO_2 layer and its intactness before and after 50 recycles.

3.1.2. UV–vis DRS analysis

The composite beads (fresh and recycled) were analysed using UV–vis diffuse reflectance spectroscopy (DRS) to confirm the light-absorbing capacity of composite beads in visible spectra. The analysis was carried out under the spectral range of 200 − 800 nm. It can be seen in Fig. 3 (a) that the band gap energy decreases in composite beads thus showing its capability to absorb light in the visible region also as compared to TiO_2. This decrease in the band gap energy in composite beads may be due to the presence of iron. The absorption wavelength of TiO_2 was 415 nm and extended to 430 nm and 452 nm for fresh and recycled composite beads, respectively as shown in inset (3a). The energy band gap was calculated using Tauc Eq. (1) [46]:

$$(\alpha h\upsilon)^{\frac{1}{n}} = A\,(h\upsilon - Eg) \tag{1}$$

Where, E_g is energy band gap in eV, h is Planck's constant, υ is photon

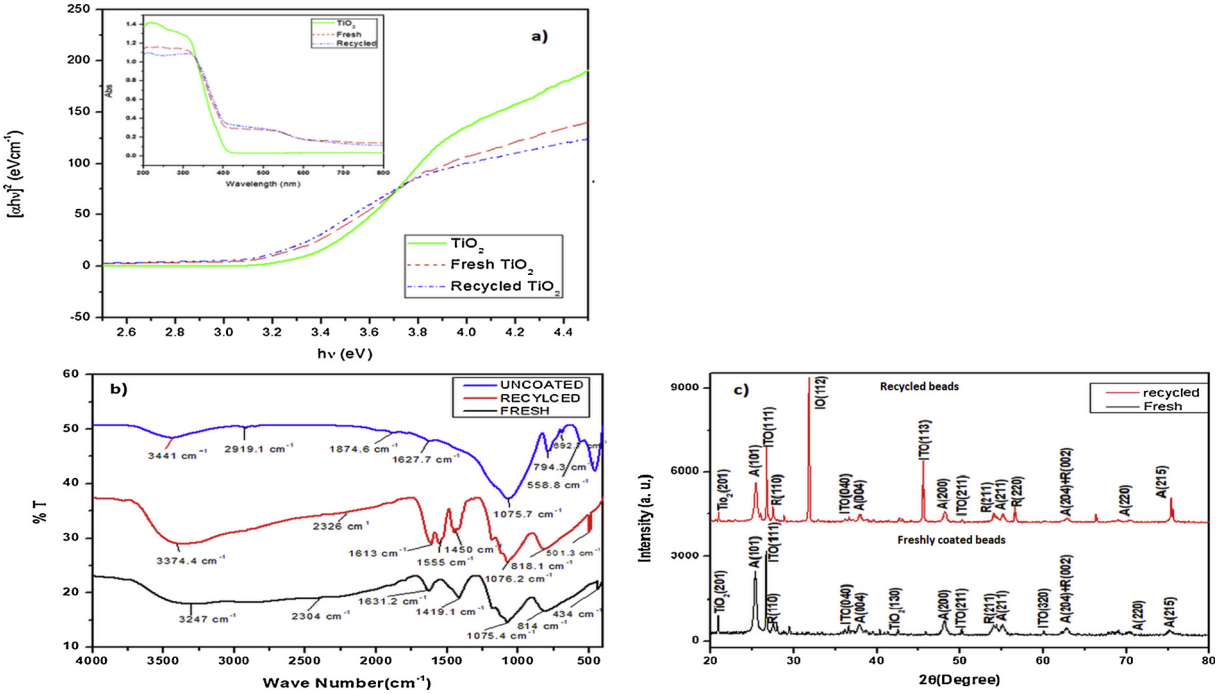

Fig. 3. (a) UV–vis DRS image of fresh and recycled composite bead (b) FTIR image of uncoated, freshly coated and recycled composite bead (c) XRD pattern of freshly coated and recycled composite bead.

frequency in Hz, A is proportionality constant. The energy band gap of TiO_2 was 3.24 eV and reduced to 2.9 eV for fresh and recycled composite beads, respectively.

3.1.3. FTIR analysis

The characteristics and chemical bonds formed in fresh and recycled composite bead were also analyzed by FTIR spectroscopy to confirm the presence of TiO_2 and iron in the system. The infrared spectra of uncoated, fresh and recycled composite beads are illustrated in Fig. 3(b). Presence of H—O—H stretching can be observed between 3441 cm^{-1}-1674.6 cm^{-1} wave number. The peak at 468.9 cm^{-1} in uncoated beads show the presence of Si—O—Fe bond [47]. The occurrence of the peaks between 558 cm^{-1}-794 cm^{-1} wave number in uncoated beads analysis is due the formation of Si-O vibrations. The occurrence of the peak between 400 − 1200 cm^{-1} wave number is due to the formation of Ti—O—Ti bond in the spectrum of both fresh and recycled composite beads. This also proves the presence of TiO_2 lattice. The anatase phase in case of fresh and recycled composite beads in the spectrum occurred at 432 $cm^{-1}$and 501.3 cm^{-1} respectively. This result is in confirmation with an earlier reported study [48], where anatase phase occurred between 400 − 600 cm^{-1} due to the occurrence of Ti—O—Ti vibrations. The peak at 2304 cm^{-1} and at 2323 cm^{-1} in the spectra of fresh and recycled composite beads show the generation of Fe—O—Ti bond which also confirms the presence of iron in composite beads. Bansal et al. [44] reported similar peaks for the presence of Fe—O—Ti bond in composite beads. Ti—OH bond was observed in Fig. 3(b) at 1631 and 1613 cm^{-1} spectrum for the fresh and recycled composite beads, respectively. Presence of O—H group was also observed at 3247 cm^{-1} and 3374 cm^{-1} for fresh and recycled composite beads because of the stretching vibration as indicated in previous studies [48,49].

3.1.4. XRD analysis

To reaffirm the intactness of crystalline planes of TiO_2 for fresh and recycled beads, the XRD analysis was carried out and the results are shown in Fig. 3(c). The TiO_2 coated composite beads were calcined at 350 °C for effective binding of catalyst to surface. For this analysis, TiO_2 particles were scrubbed off from the composite beads and selected to XRD analysis. Diffraction pattern in Fig. 3(c) shows the presence of anatase (A) and rutile (R) phase of TiO_2 in fresh and recycled composite bead. The presence of anatase and rutile phase with respectively even after 50 recycles shows that the TiO_2 over composite beads can be used for practical application. Besides these two phases of TiO_2, diffraction pattern also shows some other peaks of iron oxide (IO) and titanium iron oxide (TIO) respectively. The presence of iron oxide facilitates the entrapment of photo-excited e^- from TiO_2 photocatalysis for the regeneration of ferrous ion Thus, both processes of photocatalysis and photo-Fenton occur simultaneously in one unit.

4. Inactivation studies in fixed-mode using composite beads

4.1. Preliminary results

The boundary condition of the experiments was set by performing the experiments in dark without using TiO_2 coating beads. Negligible log reduction of 0.007 in *E. coli* count was observed as shown in Fig. 4 (a). This negligible reduction can be attributed to the fact that the double-distilled water does not affect the viability of the *E. coli* in 2 h of experiment; any inactivation of the *E. coli* cell might be due the osmotic pressure [10]. Fe leaching from the composite beads made of clay, FS and FA had very little effect on the viability of *E. coli* as confirmed by results showing 0.05 log unit reduction. This loss in the viability of cells may have been due to the transportation of iron into the periplasm in the form of Fe^{2+} done by non-specific porins present at the outer membrane of the cell, followed by its transportation into the cytoplasm [50]. This causes temporary disturbance of Fe^{+2} balance in the cell [51].

When H_2O_2 was added into the reactor its diffusion through lipids into the cell is possible because of osmotic stress conditions of the cell and also because of its comparable physical properties with H_2O [52]. Inside the cell in the cytoplasm, H_2O_2 is scavenged primarily by some enzymes acting as regulators such as alkyl hydroperoxide reductase, and most probably KatG which regulates the respiratory system of the cell [53]. Likely due to this scavenging effect, the unit log reduction caused by the addition of H_2O_2 was 0.09.

In the Fenton process, Fe^{2+} and H_2O_2 can be transported into the cell as described above. The inactivation rate of the Fenton reaction is slowed down by the regeneration of Fe^{3+} to Fe^{2+}. The maximum unit log reduction in this experiment was observed as 0.1. Therefore, it is clear from Fig. 4 (a) that the baseline process is showing negligible bacterial inactivation indicating potential for improvement for *E. coli* inactivation using dual photocatalysis and photo-Fenton processes.

After analyzing the control experiments, efforts were made to study the disinfection process under UV radiation (average intensity 25 Wm^{-2}) for 90 min and the results from photo-Fenton, photocatalysis and dual process in water have been presented in Fig. 4(b). The experiments were carried out under acidic conditions because iron can only leach from the beads under acidic conditions. This is because the iron in the soil is present in combination with other organic substances and acid helps in breaking the bond between them and helps in extracting the iron from clay called as iron leaching [54]. The results showed that UV exposure alone at 365 nm achieved 1.1 log unit reduction. When radiation falls on the cell, it leads to bacterial inactivation via inactivation of antioxidant enzymes, such as the catalases and the peroxidases [10]. This inactivation of the enzymes lead to the formation of Reactive Oxygen Species (ROS) such as H_2O_2, $^1O_2$, and O_2°- [55]. The ROS formed can react with different cell components, such as, reaction of DNA with $^1O_2$, reduction of iron from the [4Fe-4S] clusters and its reaction such as unregulated H_2O_2 which causes internal photo-Fenton process by the iron inside the cell and the gathered oxidants [56].

In the photo-Fenton process, the addition of Fe and H_2O_2 causes production of $OH^{\cdot}$ which starts degrading the cell wall externally. Under UV radiation, the ferric ion (Fe^{3+}) can be reduced to ferrous ion (Fe^{2+}) via ligand to metal charge transfer (LMCT) by the cell wall. Simultaneously, the mechanisms of iron transport as well as the H_2O_2 transport would remain same inside the cell as previously explained. Bacterial inactivation due to photo-Fenton process is slightly higher than the photocatalysis showing log unit reductions of 3.3 and 3.2 respectively in 120 min of reaction time. In the case of dual process, the production of $OH^{\cdot}$ radicals is higher as compared to their production in photocatalysis and photo-Fenton process. This process reduces the electron hole recombination via utilization of conduction band e^- to engage with Fe^{3+} for the production of Fe^{2+} thus leading to the photo-Fenton reaction in cyclic mode. The dual process yielded a maximum 6.2 unit log reduction with a rate constant of 0.15 min^{-1} in 90 min whereas individual processes of photo-Fenton and photocatalysis took 120 min to yield 3.3 log unit reduction with 0.06 min^{-1} of rate constant and 3.2 log unit reduction with 0.05 min^{-1} of rate constant respectively as shown in Fig. 4 (b–c). The occurrence of photocatalysis due to an active layer of TiO_2 was confirmed by SEM-EDS as shown in Fig. 2 (a) and photo-Fenton process was confirmed by determining the leaching of ferrous and ferric ions from freshly coated beads and from the recycled beads at regular time intervals from standard method of APHA [57] as shown in Fig. 5.

4.2. Effect of hydrogen peroxide concentration

Various researchers have reported the effect of H_2O_2 for photo-Fenton and photocatalysis [31,32,45,56,58], as it is a well-established technique to add additional $OH^{\cdot}$ in the system. However, in this study, the addition of H_2O_2 plays a dual role as it is being consumed in both processes simultaneously. In a photocatalytic technique, oxidants are

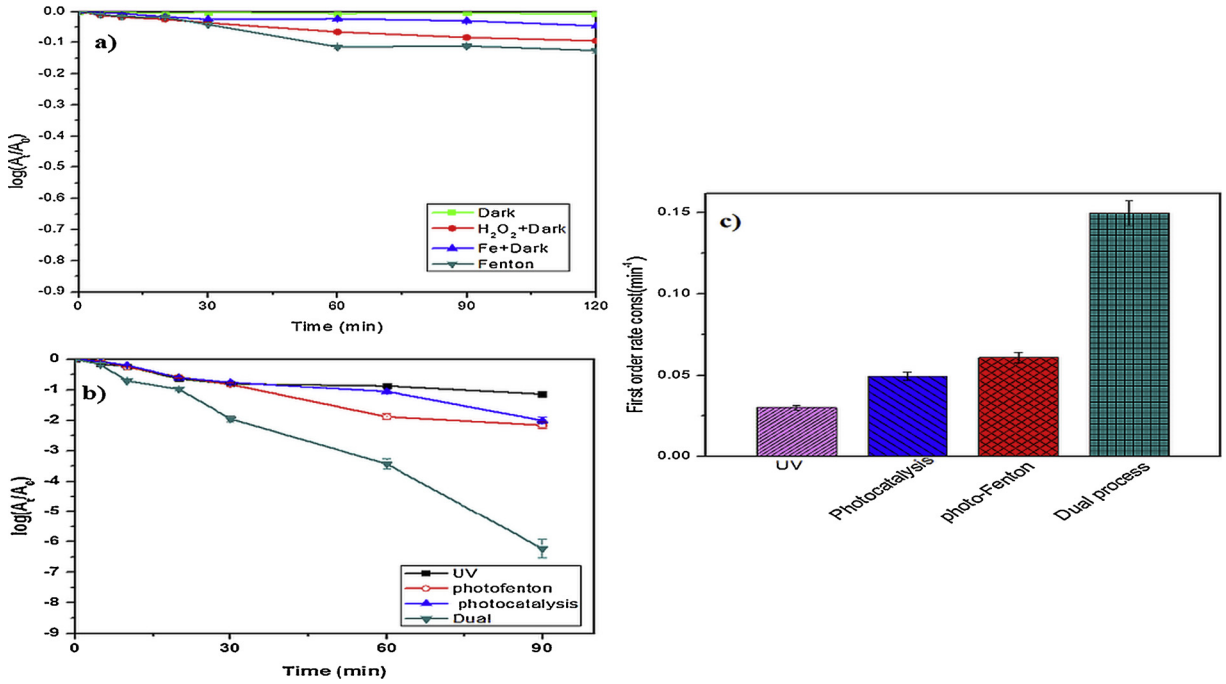

Fig. 4. (a) Inactivation of *E. coli* with and without Fe and H_2O_2 in the dark (b) Inactivation of *E. coli* in different processes (c) First order rate constant for different processes.

added so that it reacts with the electron in the conduction band and prevents electron hole recombination as shown in Eq. (2). Thus, the optimization of its concentration was an important factor for both of the processes occurring in-situ. This dual process also increases the production of oxidizing species and hydroxide radicals. In this study, H_2O_2 concentration was optimized by varying its concentration from 0.12-0.42 g L^{-1} and the optimum concentration was determined as 0.3 g L^{-1} at pH 4.5. After optimizing the H_2O_2 dose, an inactivation of 4.9 log unit was observed for *E.coli* within 90 min of reaction time as shown in Fig. 6 (a). It can be seen in (inset 6 (a)) that the inactivation rate constant initially increased from 0.102 to 0.126 min^{-1} and started decreasing afterwards. This decrease in the inactivation rate was likely due to the scavenging effect of H_2O_2. At high doses, H_2O_2 likely started consuming $OH^{\cdot}$ as shown in Eq. (3) & (4)

$$TiO_2\ (e^-) + H_2O_2 \rightarrow TiO_2 + OH^- + OH^{\cdot} \quad (2)$$

$$H_2O_2 + OH^{\cdot} \rightarrow HO_2^{\cdot} + H_2O \quad (3)$$

$$HO_2^{\cdot} + OH^{\cdot} \rightarrow H_2O + O_2 \quad (4)$$

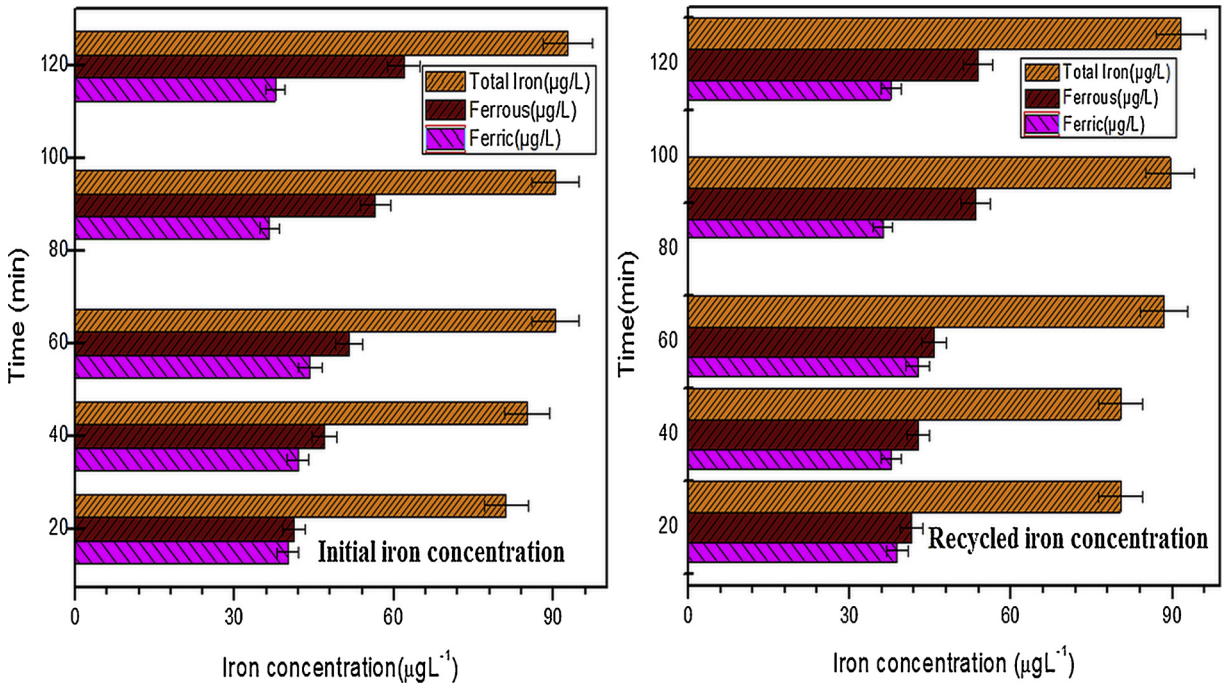

Fig. 5. Total, Ferrous and Ferric iron concentration before and after recycling.

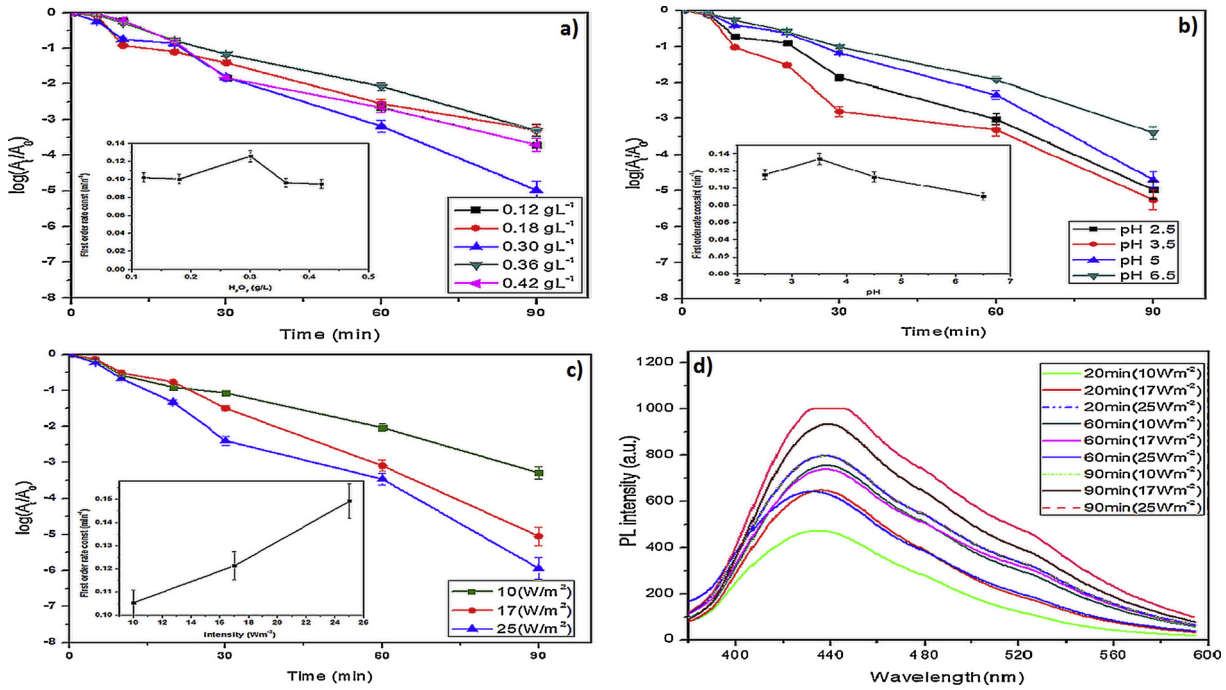

Fig. 6. (a) Effect of H_2O_2 dosage on inactivation of *E.coli* and first order rate constant at different H_2O_2 dosage (inset) (b) Effect of variation of pH on inactivation of *E.coli* and first order rate constant at different pH (c) Effect of UV intensity on inactivation of *E.coli* and first order rate constant at different UV intensities (inset) (d) Photo luminance spectra of H_2O_2 at different intensities.

4.3. Effect of pH

pH plays an important role in the dual process as the leaching of iron from composite beads takes place under acidic conditions and the iron executes photo-Fenton process in the system. For the optimization of pH, experiments were done at different pH values ranging from 2.5–6.5 and at 0.3 g L^{-1} H_2O_2 as shown in Fig. 6(b). It was observed that at pH lower than 3.5, bacterial inactivation rate was lower owing to the scavenging effect of $OH^{\cdot}$ [44]. Subsequently, when pH was increased from 3.5–6.5, the rate of inactivation decreased again as shown in inset 6 (b). This can be due to the precipitation of FeO(OH) complex and hydrolysis of Fe^{3+} which ultimately decreases the production of OH radicals [8]. It can be seen from Fig. 6 (b) that maximum inactivation of *E.coli* (5.2 log unit reduction) was achieved at pH 3.5 in 90 min which was used as the optimum pH for the rest of the study. Formation of less active HO_2- occurs at alkaline pH values. This consequently led to the formation of O_2 and H_2O on reaction with non-dissociated H_2O_2. Moreover, the above reaction is preferred over reaction with $OH^{\cdot}$. Therefore, it is clear from the results that pH significantly influences the inactivation of *E. coli*.

4.4. Effect of UV intensity

In-situ utilization of solar radiation in-terms of process feasibility and bacterial inactivation is one of the most important factors for commercial aspects of this technology. As irradiation coming from the sun does not remain constant throughout the day, the effect of UV intensity variation (10 Wm^{-2} to 25 Wm^{-2}) was studied for *E. coli* inactivation. It was observed that the maximum log unit reduction (5.9) was found in 90 min when the intensity of 25 Wm^{-2} was provided to the system (Fig.6 (c)) owing to the high production of $OH^{\cdot}$. This can be attributed to higher absorption of UV intensity by H_2O_2 at higher intensity [59], which subsequently enhance the $OH^{\cdot}$. It can be seen from inset (c) that the rate of inactivation increased from 0.11 m^{-1} to 0.15 m^{-1} with increase in the intensity. To confirm the prominence of in-situ dual effect, florescence spectroscopy was performed for the estimation of $OH^{\cdot}$ at different intensities as shown in Fig. 6(d). Concentration of $OH^{\cdot}$ increased with increase in the UV intensity from 10 Wm^{-2} to 25 Wm^{-2}. The results depicted reasonable log reduction of *E. coli* at different UV intensities. However, the process can be intensified at lower intensities by effective reactor design and modifications.

4.5. Effect of bead size

Exposed surface area for the proper illumination of the catalyst is an important operational parameter in fixed-bed studies to provide better contact between the contaminants and the catalyst [60]. For field-scale applications, the type and size of the support material is particularly important for designing the reactor. In this context, the surface area of the composite bead was optimized by varying the size from 10 mm to 20 mm to achieve better inactivation of the *E. coli*. The size of the selected beads was varied by altering the diameter using screw gauge as discussed in section 2.2. It was observed from Fig.7 (a) that the log unit reduction was maximum (6 logs) when the size of the bead was 10 mm providing the highest surface area. The log unit reduction of *E. coli* decreased from 6 to 5.3 with increase in diameter of the beads and the rate constant "k" also decreased (inset 7(b)) with increased bead size owing to the decrease in effective surface area available. Moreover, reducing the size of composite bead below 10 mm could not help as this size was not able to hold the catalyst film intact. Too small beads would not have enough iron to leach out as FS, FA concentration would be less. Therefore, 10 mm size was found to be more stable in terms of catalyst activity as well as iron concentration and subsequently used for all the experiments.

4.6. Effect of area to volume ratio (A/V)

The major limitation of AOP in the field-scale application is the depth of the reactor as it hinders the path of solar radiation to reach the solution. For better penetration of light, more exposed area and less depth of reactor is considered appropriate [6]. For this, either area or volume of the reactor can be altered by keeping one of them same. In this study, A/V ratio was varied from 0.18 cm^2 mL^{-1} to 0.42 cm^2 mL^{-1} by keeping the area same and varying the volume of the solution to

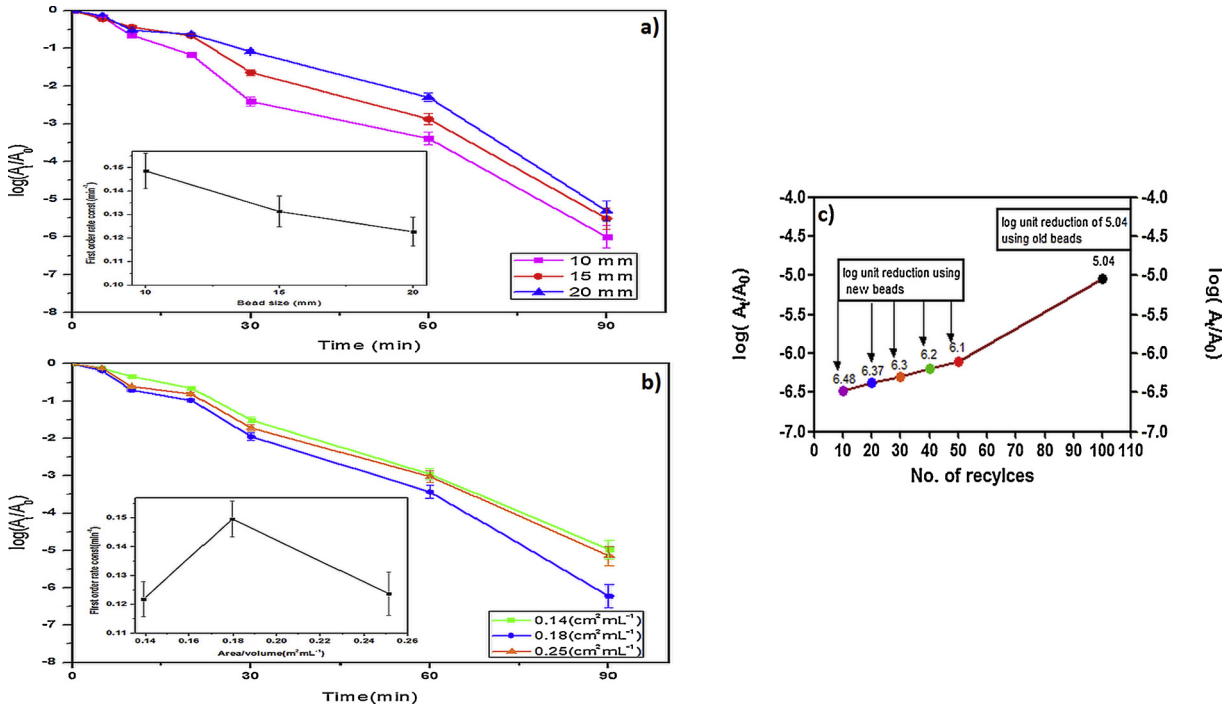

Fig. 7. (a) Effect of bead size on inactivation of *E.coli* and first order rate constant at different bead size (inset) (b) Effect of area to volume ratio on inactivation of *E.coli* and first order rate constant at different area to volume ratio (inset) (c) Recyclability studies of composite beads.

investigate the inactivation of bacteria. A significant increase in the log reduction of *E. coli* from 4.9 to 6.2 was observed (Fig. 7 (b)) by increasing the A/V ratio as the rate constant 'k' increased as demonstrated in the inset 7(b). As the A/V ratio increases (area is kept same, volume decreases), the path length of the photons of light entering the solution increases, therefore, resulting in more $OH^{\cdot}$ radical production [6] and hence, the rate of bacterial inactivation increased. As a result, the optimized result for A/V ratio was obtained as $0.25\,cm^2\,mL^{-1}$, and showed the maximum *E. coli* inactivation of 6.2 log unit reduction.

4.7. Durability studies

Another important parameter is the stability of the support material. The support material should be stable enough to keep TiO_2 intact and sustain the iron leaching for the photo-Fenton process. To investigate the durability of the support material, the composite beads were recycled for 50 times as shown in Fig. 7(c) and only 9 % reduction in the activity of the beads was observed. This minute loss can be attributed to the weathering of the catalyst from the composite beads [45]. The various characterization techniques discussed above also confirms the stability and durability of the composite beads. Further to confirm the simultaneous leaching of the iron from the composite beads into the solution, iron concentration was measured before and after 50 recycles (100 h) of the beads as shown in Fig. 5. There was a significant amount of iron concentration observed before and after the recycling, which contributed to the photo-Fenton process.

For further investigating the extend of the durability of the support material and the capacity to execute the in-situ dual effect, experiments were performed using composite beads recycled for more than 100 times. Significant log reduction (5.04) of *E-coli* was achieved using the same optimized conditions. These findings show the strong potential of this technology for field-scale trials.

4.8. Kinetic study and synergy effect of dual process

For the kinetic study of the dual process, pseudo first-order model was used as shown in Eq. (5). The slope of natural log (A/A_0) and time for inactivation gives the rate constant as shown in Eq. (6). Where A_0 is the initial concentration of the bacteria at time t = 0, A is the bacterial concentration at any time "t" and "k" is the pseudo first-order rate constant (min^{-1}).

$$\frac{dA}{dt} = K_1 C \tag{5}$$

$$ln\left(\frac{A}{A_0}\right) = kt \tag{6}$$

For dual process the value of pseudo first-order constant was higher as compared to the photocatalysis and photo-Fenton process as shown in Table 2.

The dual effect has shown better inactivation efficiency over photocatalysis and photo-Fenton individually. During the inactivation studies of *E. coli*, it was observed that the synergistic effect of dual process over the photo-Fenton was 59 % and on photocatalysis was 67 %. Altogether, the synergy of dual process over both the techniques was observed as 26 % as calculated using the following Eq.s (7–9). All calculations regarding synergy effect are provided in supplementary file (Text S3).

Synergy of dual over photocatalysis

$$\%\ \text{synergy} = 100 \times \{(k_{dual} - k_{photocatalysis})\}/\ k_{dual} \tag{7}$$

Synergy of dual over photoFenton process

$$\%\ \text{synergy} = 100 \times \{(k_{dual} - k_{photoFenton})\}/\ k_{dual} \tag{8}$$

Synergy of dual over both photo Fenton and photocatalysis

Table 2
K values for inactivation of *E. coli* K12 using different processes.

Type of process	K value(min^{-1})
Photocatalysis	0.0494
Photo-Fenton	0.0608
Dual Process (Photo-Fenton + Photocatalysis)	0.1496

$$\% \text{ synergy} = 100 \times \{(k_{dual}-(k_{photoFenton+} k_{photocatalysis}))\}/ k_{dual} \quad (9)$$

Positive synergistic effect of the dual technique over both processes individually as well as combined process indicates the potential of this technology for possible field-scale applications.

In this study, experiment was also extended in sunlight (UV + visible) at optimum conditions to confirm the viability of the process for real time application. The optimum conditions for this study were same as for the reaction under UV radiation and 6.9 log reduction was observed in 30 min of reaction time.

5. Conclusion

The present study was carried out to introduce hybridization of photo-Fenton and photocatalysis process for the inactivation of *E. coli* using waste material such as FA and FS along with TiO_2 in fixed-mode. The results showed that parameters such as the intensity of light, H_2O_2 dose, and pH played a significant role in the inactivation of *E. coli*. Photocatalysis using TiO_2 as a catalyst in the fixed-mode resulted in 3.3 log reduction while photo-Fenton in fixed-mode using FS and FA resulted in 3.2 log reduction after 120 min of reaction. The inactivation time of *E. coli* was reduced to 90 min with increase in the log reduction up to 6.2 when photo-Fenton and photocatalysis processes were incorporated in the same system under UV irradiation. Therefore, this novel dual technique in fixed form proved to be a viable solution to treat contaminated water and wastewater. The beads were recycled for 50 times with 9 % decrease in the inactivation efficiency. Characterization of composite beads was done through SEM/EDS, XRD, FTIR, and DRS analysis which confirmed the stability and effectiveness of the beads after 50 recycles. This is the first study of its kind which is carried out to investigate the inactivation of *E. coli* through the dual process in fixed-mode.

Funding

This research did not receive any specific grant from funding agencies in the public, commercial, or not-for-profit sectors.

All authors have participated in (a) conception and design, or analysis and interpretation of the data; (b) drafting the article or revising it critically for important intellectual content; and (c) approval of the final version.

Declaration of Competing Interest

All authors have participated in (a) conception and design, or analysis and interpretation of the data; (b) drafting the article or revising it critically for important intellectual content; and (c) approval of the final version.

Acknowledgement

Authors would like to thank central instrumentation laboratory and sophisticated analytical instrumentation facility, Punjab university, Chandigarh, India for providing their facilities for the characterization of samples.

Appendix A. Supplementary data

Supplementary material related to this article can be found, in the online version, at doi:https://doi.org/10.1016/j.jwpe.2019.101085.

References

[1] C. Dalin, H. Qiu, N. Hanasaki, D.L. Mauzerall, I. Rodriguez-Iturbe, Balancing water resource conservation and food security in China, Proc. Natl. Acad. Sci. 112 (15) (2015) 4588–4593.
[2] M. Gavrilescu, K. Demnerová, J. Aamand, S. Agathos, F. Fava, Emerging pollutants in the environment: present and future challenges in biomonitoring, ecological risks and bioremediation, N. Biotechnol. 32 (1) (2015) 147–156.
[3] M. Ramkumar, Microbial pollution indicators in the Cauvery river, Southern India," a Sustain, Futur. Earth's Nat. Resour. (July) (2013) p. v.
[4] V.K. Tyagi, A.K. Chopra, A.A. Kazmi, A. Kumar, Alternative microbial indicators of faecal pollution: current perspective, Iran. J. Environ. Health. Sci. Eng. 3 (3) (2006) 205–216.
[5] M. Koivusalo, T. Vartiainen, Drinking water chlorination by-products and Cancer, Rev. Environ. Health 12 (2) (1997) 81–90.
[6] A. Verma, N.T. Prakash, A.P. Toor, Photocatalytic degradation of herbicide isoproturon in TiO2 aqueous suspensions: study of reaction intermediates and degradation pathways, Environ. Prog. Sustain. Energy 33 (00) (2016) 1–10.
[7] P. Bansal, A. Verma, Pilot-scale single-step reactor combining photocatalysis and photo-Fenton aiming at faster removal of Cephalexin, J. Clean. Prod. 195 (2018) 540–551.
[8] P. Bansal, A. Verma, Novel Fe-TiO2composite driven dual effect for reduction in treatment time of pentoxifylline: slurry to immobilized approach, Mater. Des. 125 (2017) 135–145.
[9] G. Carré, et al., TiO2 photocatalysis damages lipids and proteins in Escherichia coli, Appl. Environ. Microbiol. 80 (8) (2014) 2573–2581.
[10] S. Giannakis, M. Voumard, S. Rtimi, C. Pulgarin, Bacterial disinfection by the photo-Fenton process: extracellular oxidation or intracellular photo-catalysis? Appl. Catal. B Environ. 227 (2018) 285–295.
[11] J. Ndounla, S. Kenfack, J. Wéthé, C. Pulgarin, Relevant impact of irradiance (vs. dose) and evolution of pH and mineral nitrogen compounds during natural water disinfection by photo-Fenton in a solar CPC reactor, Appl. Catal. B Environ 148–149 (2014) 144–153.
[12] N. Daels, et al., Potential of a functionalised nanofibre microfiltration membrane as an antibacterial water filter, Desalination 275 (1–3) (2011) 285–290.
[13] N.S. Mishra, R. Reddy, A. Kuila, A reviw on advanced oxidation process for effective water treatment, Curr. World Environ. 12 (3) (2017) 470–490.
[14] D. Deng, W. Aouad, W.A. Braff, S. Schlumpberger, M.E. Suss, M.Z. Bazant, Water purification by shock electrodialysis: deionization, filtration, separation, and disinfection, Desalination 357 (2015) 77–83.
[15] W. Zhou, et al., Well-Ordered Large-pore Mesoporous Anatase TiO 2 With Remarkably High Thermal Stability and Improved Crystallinity: Preparation, Characterization, and Photocatalytic Performance, (2011), pp. 1922–1930.
[16] B. Sun, et al., Synthesis of Particulate Hierarchical Tandem Heterojunctions Toward Optimized Photocatalytic Hydrogen Production vol. 1804282, (2018), pp. 1–8.
[17] W. Zhou, et al., Ordered mesoporous black TiO 2 as highly efficient hydrogen evolution photocatalyst, ACS Publ. (2014) 5–8.
[18] M.-S. Song, K. Vijayarangamuthu, E. Han, K.-J. Jeon, J.-W. Seo, Enhancement of photocatalytic disinfection of surface modified rutile TiO2 nanocatalyst, Korean J. Chem. Eng. 33 (8) (2016) 2392–2395.
[19] F. Achouri, M. BenSaid, L. Bousselmi, S. Corbel, R. Schneider, A. Ghrabi, Comparative study of gram-negative bacteria response to solar photocatalytic inactivation, Environ. Sci. Pollut. Res. (2018) 1–10.
[20] J.-J. Oturan, A. Mehmet, Aaron, Advanced oxidation processes in water / wastewater treatment: principles and applications. A review in water / wastewater treatment : principles, Crit. Rev. Environ. Sci. Technol. 44 (July 2017) (2014) 2577–2641.
[21] M. Lorenzetti, et al., The influence of surface modification on bacterial adhesion to titanium-based substrates, ACS Appl. Mater. Interfaces 7 (3) (2015) 1644–1651.
[22] G. Rao, K.S. Brastad, Q. Zhang, R. Robinson, Z. He, Y. Li, Enhanced disinfection of Escherichia coli and bacteriophage MS2 in water using a copper and silver loaded titanium dioxide nanowire membrane, Front. Environ. Sci. Eng. China 10 (4) (2016).
[23] A. Fiorentino, L. Rizzo, H. Guilloteau, X. Bellanger, C. Merlin, Comparing TiO2 photocatalysis and UV-C radiation for inactivation and mutant formation of Salmonella typhimurium TA102, Environ. Sci. Pollut. Res. 24 (2) (2017) 1871–1879.
[24] P.V. Laxma Reddy, B. Kavitha, P.A. Kumar Reddy, K.H. Kim, TiO2-based photocatalytic disinfection of microbes in aqueous media: a review, Environ. Res. 154 (December 2016) (2017) 296–303.
[25] C. Sordo, R. Van Grieken, J. Marugán, P. Fernández-Ibáñez, Solar photocatalytic disinfection with immobilised TiO2 at pilot-plant scale, Water Sci. Technol. 61 (2) (2010) 507–512.
[26] N. Ahmad, M.A. Gondal, A.K. Sheikh, Comparative study of different solar-based photo catalytic reactors for disinfection of contaminated water, Desalin. Water Treat. 57 (1) (2016) 213–220.
[27] S.K. Kassahun, Z. Kiflie, D.W. Shin, S.S. Park, Y.R. Chung, Novel multistage fixed-bed photoreactor for bacterial inactivation using N-doped TiO2 nanoparticles under vis-LEDs and sunlight illumination, Nanotechnol. Environ. Eng. 3 (1) (2018).
[28] C.A. Coutinho, V.K. Gupta, Photocatalytic degradation of methyl orange using polymer-titania microcomposites, J. Colloid Interface Sci. 333 (2) (2009) 457–464.
[29] A. Kubacka, et al., Boosting TiO2-anatase antimicrobial activity: polymer-oxide thin films, Appl. Catal. B Environ. 89 (3–4) (2009) 441–447.
[30] F. Shiraishi, A. Miyawaki, R. Chand, A mechanism of the photocatalytic decomposition of 2,4-dinitrophenol on TiO2 immobilized on a glass surface, Chem. Eng. J. 262 (2015) 831–838.
[31] I. García-Fernández, M.I. Polo-López, I. Oller, P. Fernández-Ibáñez, Bacteria and fungi inactivation using Fe 3+/sunlight, H 2O 2/sunlight and near neutral photo-Fenton: a comparative study, Appl. Catal. B Environ 121–122 (2012) 20–29.
[32] D. Spuhler, J. Andrés Rengifo-Herrera, C. Pulgarin, The effect of Fe2+, Fe3+, H2O2 and the photo-Fenton reagent at near neutral pH on the solar disinfection (SODIS) at low temperatures of water containing Escherichia coli K12, Appl. Catal.

B Environ. 96 (1–2) (2010) 126–141.
[33] J. Rodríguez-Chueca, M.I. Polo-López, R. Mosteo, M.P. Ormad, P. Fernández-Ibãnez, Applied Catalysis B : environmental Disinfection of real and simulated urban wastewater effluents using a mild solar photo-Fenton, Appl. Catal. B Environ. 151 (2014) 619–629.
[34] E. Ortega-Gómez, M.M. Ballesteros Martín, B. Esteban García, J.A. Sánchez Pérez, P. Fernández Ibáñez, Solar photo-Fenton for water disinfection: an investigation of the competitive role of model organic matter for oxidative species, Appl. Catal. B Environ 148–149 (2014) 484–489.
[35] M.I. Polo-López, M. Castro-Alférez, I. Oller, P. Fernández-Ibáñez, Assessment of solar photo-Fenton, photocatalysis, and H2O2 for removal of phytopathogen fungi spores in synthetic and real effluents of urban wastewater, Chem. Eng. J. 257 (2014) 122–130.
[36] H.M. Yadav, J. Kim, S.H. Pawar, Developments in photocatalytic antibacterial activity of nano TiO 2 : a review, Korean J. Chem. Eng. 33 (7) (2016) 1989–1998.
[37] N. Yeh, Y.C. Lee, C.Y. Chang, T.C. Cheng, Anti- fi sh bacterial pathogen effect of visible light responsive Fe 3 O 4 @ TiO 2 nanoparticles immobilized on glass using TiO 2 sol – gel, Thin Solid Films 549 (2013) 93–97.
[38] W. Zhang, Y. Chen, S. Yu, S. Chen, Y. Yin, Preparation and Antibacterial Behavior of Fe 3 + -Doped Nanostructured TiO 2 Thin Films 516 (2008), pp. 4690–4694.
[39] S.M.H. Al-jawad, A.A. Taha, M.M. Salim, Optik synthesis and characterization of pure and Fe doped TiO 2 thin films for antimicrobial activity, Opt. Int. J. Light Electron. Opt. 142 (2017) 42–53.
[40] D.R. Bhimani, J. Pitroda, J.J. Bhavsar, A study on foundry sand: opportunities for sustainable and economical concrete, Glob. J. Res. Anal. 2 (1) (2014) 60–63.
[41] A. Dwivedi, M.K. Jain, Fly ash – waste management and overview : a Review,", Recent Res. Sci. Technol. 6 (1) (2014) 30–35.
[42] M. Ahmaruzzaman, A review on the utilization of fly ash, Prog. Energy Combust. Sci. 36 (3) (2010) 327–363.
[43] Z.T. Yao, et al., A comprehensive review on the applications of coal fly ash, Earth Sci. Rev. 141 (2015) 105–121.
[44] P. Bansal, A. Verma, In-situ dual effect studies using novel Fe-TiO2 composite for the pilot-plant degradation of pentoxifylline, Chem. Eng. J. 332 (2018) 682–694.
[45] S. Talwar, V.K. Sangal, A.K. Verma, In-situ dual effect of novel Fe-TiO2 composite for the degradation of phenazone, Sep. Purif. Technol. 211 (September) (2019) 391–400 2018.
[46] A. Tumuluri, K.L. Naidu, K.C.J. Raju, Band gap determination using Tauc' s plot for LiNbO 3 thin films, Int. J. Chemtech Res. 6 (6) (2014) 3353–3356.
[47] P.S. Nayak, B.K. Singh, Instrumental characterization of clay by XRF, XRD FTIR 30 (3) (2007) 235–238.
[48] I. Ganesh, et al., Preparation and characterization of Fe-doped TiO2 powders for solar light response and photocatalytic applications, Process. Appl. Ceram. 6 (1) (2013) 21–36.
[49] Z. Sayyar, A. Akbar Babaluo, J.R. Shahrouzi, Kinetic study of formic acid degradation by Fe 3+ doped TiO 2 self-cleaning nanostructure surfaces prepared by cold spray, Appl. Surf. Sci. 335 (2015) 1–10.
[50] C.K.Y. Lau, K.D. Krewulak, H.J. Vogel, Bacterial ferrous iron transport: the Feo system, FEMS Microbiol. Rev. 40 (2) (2016) 273–298.
[51] J. Rodríguez-Chueca, M. Morales, R. Mosteo, M.P. Ormad, J.L. Ovelleiro, Inactivation of Enterococcus faecalis, Pseudomonas aeruginosa and Escherichia coli present in treated urban wastewater by coagulation-flocculation and photo-Fenton processes, Photochem. Photobiol. Sci. 12 (5) (2013) 864–871.
[52] G.P. Bienert, et al., Specific aquaporins facilitate the diffusion of hydrogen peroxide across membranes, J. Biol. Chem. 282 (2) (2007) 1183–1192.
[53] J.A. Imlay, The molecular mechanisms and physiological consequences of oxidative stress: lessons from a model bacterium, Nat. Rev. Microbiol. 11 (7) (2013) 443–454.
[54] Z. Hseu, Evaluating heavy metal contents in nine composts using four digestion methods, Bioresour. Technol. 95 (2004) 53–59.
[55] J.A. Imlay, Cellular defenses against superoxide and hydrogen peroxide, Annu. Rev. Biochem. 77 (1) (2008) 755–776.
[56] J.A. Imlay, Diagnosing oxidative stress in bacteria: not as easy as you might think, Curr. Opin. Microbiol. 24 (2015) 124–131.
[57] G. Discussion, APHA Standard Methods for the Examination of Water and Wastewater Part 3000 Standard Methods for the Examination of Water and Wastewater, (1999), pp. 1–184.
[58] E. Abdullah, A. Idris, A. Saparon, Addition of hydrogen peroxide to groundwater with natural Iron Induces water disinfection by Photo-Fenton at circumneutral pH and other photochemical events héctor, ARPN J. Eng. Appl. Sci. 12 (10) (2017) 3218–3221.
[59] M. Massoudinejad, S. Golmohammadi, M. Ghaderpoori, Use of ultraviolet and ultraviolet /peroxide hydrogen processes for degradation of humic substances from aqueous solutions, Biosci. Biotechnol. Res. Commun. 9 (4) (2016) 680–688.
[60] A. Takdastan, B. Kakavandi, M. Azizi, M. Golshan, Efficient activation of peroxymonosulfate by using ferroferric oxide supported on carbon/UV/US system: a new approach into catalytic degradation of bisphenol A, Chem. Eng. J. 331 (2018) 729–743.

Separation and Purification Technology 260 (2021) 118242

Contents lists available at ScienceDirect

Separation and Purification Technology

journal homepage: www.elsevier.com/locate/seppur

Mathematical modeling of *E. coli* inactivation in water using Fe-TiO_2 composite in a fixed bed reactor

Ina Thakur [a], Anoop Verma [a,*], Banu Örmeci [b]

[a] School of Energy and Environment, Thapar Institute of Engineering and Technology, Patiala 147004, India
[b] Civil and Environmental Department, Carleton University, Ottawa, ON KIS 5B6, Canada

ARTICLE INFO

Keywords:
Dual-technique
TiO_2-photocatalysis
Photo-Fenton
Synergy
Durability

ABSTRACT

An inexpensive Fe-TiO_2 composite fabricated via mixing clay with foundry sand (FS) and fly ash (FA), for the in-situ disinfection of *E. coli*. The continuous leaching of iron at acidic conditions into the solution through the composite and the TiO_2 photoactivity on the surface of Fe-TiO_2 composite beads exhibited an in-situ dual effect of photocatalysis and photo-Fenton in the treatment system. In this research work comparison of five different processes (UV irradiation; H_2O_2 with UV irradiation; TiO_2 assisted photocatalytic technique; photo-Fenton and dual-technique (photocatalysis + photo-Fenton) using three different kinetic models were done. Kinetic studies showed more than 2 times of increase in the reaction rate with a log reduction of 6.4 only in 90 min of treatment time, thus proves the faster rate of disinfection. 18% of synergy was observed with dual effect over photocatalysis and photo-Fenton. The composite beads were recycled 30 times and only 11% reduction in the photoactivity of the catalyst was observed. Thus the obtained results present a promising potential of the dual technology for the treatment of *E. coli* in water.

1. Introduction

The global concern of assuring reclaimed safe water free from microorganisms and chemical contaminants is increasing with an increase in population and uncertain climatic changes. The conventional methods for treating the effluents result in a high amount of micropollutants such as pharmaceuticals, pesticides, and pathogens such as viruses, bacteria, fungus, and parasites that may prompt harmful effects on human health when gets mixed with freshwater sources[1–4]. The consolidated tertiary treatments such as ozonation [2,5,6], UV radiation [7,8], and chlorination [9,10] have been used to treat micropollutants. Water disinfection through UV irradiation poses some drawbacks such as regrowth of microorganisms that is mainly because of the lack of residual disinfectant and self-repair mechanism of DNA. Other methods such as ozonation and chlorination also inactivate pathogens and degrade micropollutants, but also faces some drawbacks such as the generation of harmful disinfection by-products such as nitro sodimethylamine, organo-chlorine, and bromate[11]. Disinfection methods that do not require chemicals include membrane filtration[12], ultrasonication[13], hydrodynamic cavitation[14], and electrochemical oxidation[15] and have been used to remove microorganisms. However, these physical and electrochemical technologies have some common shortcomings including high operating cost, energy consumption along the need for sophisticated reactor design.

Advanced Oxidation Processes (AOPs) have been recommended as a prominent technique in disinfecting bacteria, and viruses when used after secondary treatment. The issue of removing bacteria from water has been subjected to investigations, stretching from UV only[16], UV + H_2O_2[17,18], TiO_2 assisted photocatalysis[19,20], and photo-Fenton [21,22] facilitated solutions. These techniques have been proven efficient in disinfecting pathogens in the laboratory as well as in pilot-scale studies. Therefore, the application of these techniques worth attention and is being employed in the upgrade of wastewater treatment plants [23].

From the aforementioned technologies, one of the prominent processes that have been used for the degradation of organic compounds and bacterial inactivation is TiO_2 photocatalysis. This technique works on the photoexcitation of electron (e^-) from the valence band to the conduction band creating a hole (h^+) in the valence band of the semiconductor leading to the redox reaction and ultimately production of oxidative Hydroxyl radicals. The first report on bacterial inactivation was done by Matsunaga et al. in 1985 [24]. In this study, the author used

* Corresponding author.
E-mail address: anoop.kumar@thapar.edu (A. Verma).

https://doi.org/10.1016/j.seppur.2020.118242
Received 26 September 2020; Received in revised form 13 December 2020; Accepted 17 December 2020
Available online 24 December 2020
1383-5866/© 2020 Elsevier B.V. All rights reserved.

powered TiO_2 as a semiconductor for the inactivation of *E. coli,* and 100% killing was observed after 120 min. Since then, many studies have focused on the utilization of TiO_2 in suspension and fixed form for bacterial inactivation. Attributable to its ability for scale-up studies, fixed-bed examines distinct supporting materials such as plates, cylindrical shapes, glass-ball, for disinfection studies. In one of the studies [25], a photoreactor having N-doped TiO_2 nanoparticles immobilized over glass beads was used to study the water disinfection and found a 3 log reduction of *E. coli* in 120 min of reaction time. In another study[26], a hybrid system of photocatalysis/microfiltration with immobilized TiO_2 over stainless steel was used for bacterial inactivation. A vast decrease in the bacterial concentration was observed due to the TiO_2 layer compression induced by transmembrane pressure. Although photocatalysis has shown efficient results in terms of water disinfection, still exhibited some shortcomings such as e^-h^+ recombination, catalyst separation from the solution, its durability and stability, increment in treatment time, and mass transfer limitation. These above-mentioned shortcomings question the capability of this technology in terms of commercialization and thus restrict its applications.

The other important advanced oxidation technique for water disinfection is photo-Fenton following a reaction of H_2O_2 with ferrous ion (Fe^{2+}) in the presence of artificial and natural sunlight has also been well reported[27–29] generating strong reactive oxygen species (ROS). The requirement of high H_2O_2 doses along with iron sludge formation is the main limitation of this technology. Many research studies in the literature showed the simultaneous use of TiO_2 and Fe in one system to increase the rate of bacterial inactivation. Zhang et al. [30] studied the effect of glass slides coated with ferric ion (Fe^{3+}) doped TiO_2 catalyst on *E. coli* inactivation and observed 95% of bacterial killing in 120 min of treatment time. Even though this hybrid technology helps in reducing the e^-h^+ recombination, still the catalyst stability is a major concern.

Keeping in view the previously mentioned drawbacks, the dual effect study of Fe-TiO_2 composite by combining photocatalysis and photo-Fenton was introduced[31]. In this study, spherical composite beads were made using iron in the form of foundry sand, and fly ash mixed with clay, and the outer surface was coated with TiO_2. This allows photocatalysis and photo-Fenton to occur in the same system at the same time. This approach resolves many issues faced by the aforementioned technologies while treating waste-water [32]. Iron leaching from the composite beads when pH is less than 6 (acidic condition) and H_2O_2 being there in the system leads to the photo-Fenton process. The systematic iron leaching in the system eliminates the iron sludge formation. Whereas, TiO_2 coating over the composite beads in the presence of light leads to a photocatalytic effect. The issue of electron-hole (e^-h^+) recombination occurring in photocatalytic technique can be eradicated by the reaction of e^- present in the conduction band with the ferric (Fe^{3+}) ion leaching out from the composite beads and form ferrous (Fe^{2+}) ion and led photo-Fenton to start again simultaneously as shown in Eqs. (1)–(8).

$$TiO_2 + uv \ \text{irradiation} \rightarrow e^-_{CB} + h^+_{VB} \quad (1)$$

$$e^-_{CB} + O_2 \rightarrow O_2^- \quad (2)$$

$$h^+_{VB} + H_2O \rightarrow OH^{\cdot} + H^+ \quad (3)$$

$$Fe^{2+}_{(leached)} + H_2O_2 \rightarrow Fe^{3+}_{(leached)} + OH^{\cdot} + OH^- \quad (4)$$

$$Fe^{3+}_{(leached)} + H_2O_2 \rightarrow Fe^{2+}_{(leached)} + H_3O^+ + HO_2^- \quad (5)$$

$$Fe^{3+}_{(leached)} + H_2O \xrightarrow{uv} Fe^{2+}_{(leached)} + OH^{\cdot} + H^+ \quad (6)$$

$$Fe^{3+}_{(leached)} + e^-_{CB} + H_2O \rightarrow Fe^{2+}_{(leached)} + OH^{\cdot} + H^+ \quad (7)$$

$$e^-_{CB} + H_2O_2 \rightarrow OH^{\cdot} + OH^- \quad (8)$$

With the advantage of continuous availability of Hydroxyl radicals and no sludge formation, the dual-technique has illustrated adequate outcomes in terms of synergy and efficacy for the treatment of wastewater[21,33]. But, a complete wastewater treatment technology includes both degradation and disinfection processes. There are no studies available on the disinfection of *E-coli* k12 with coupled photo-Fenton and photocatalytic technique, and the present study investigates the disinfection of *E. coli* using the in-situ dual technique.

The main objective of this research was to investigate and compare the *E. coli* inactivation efficiency of UV only, UV/H_2O_2, TiO_2-photocatalysis, photo-Fenton, and dual-technique (Fe-TiO_2 composite) in fixed mode. This was followed by the comparison between different kinetic disinfection models and the experimental data associating the results with the key operating parameters affecting the disinfection efficacy of the current system. The results of this study would provide useful information using the rate of inactivation, kinetic components, and fitting parameters: R^2 (regression distribution) and RMSD (root mean square deviation) to comprehend the disinfection mechanisms.

2. Mathematical models in *E. coli* inactivation

Three different mathematical models (log-linear, Weibull, and double Weibull) for inactivation were used in this study. The kinetic coefficients of these models were obtained by adjusting the experimental results to the corresponding equations by non-linear regression techniques. The fitting of the experimental values was done using Microsoft Excel: Solver and GInaFiT software [37] developed by Geeraerd et al 2005. R^2 and RMSD were used for the evaluation of the fitting of inactivation results. Also, to get some better information regarding the degree of fit of the models used, the experimental results obtained were compared with results obtained through mathematical models and represented graphically.

2.1. Log-linear model

The log-linear model is a moderation of the Chick's model. This model is used to govern the relationship between the No. of microorganisms inactivated and the number of molecules of disinfectant[28,38] as given in Eq. (9)

$$log\frac{A_t}{A_0} = -kCt \rightarrow log\frac{A_t}{A_0} = -k_{ap}t \quad (9)$$

Where the initial and final concentration is denoted by A_0 and A_t respectively. k is the first-order rate constant (min^{-1}), C indicates the disinfectant concentration; t is the reaction time. The integration of disinfectant concentration at an evident rate of constant can simplifies the model [39].

2.2. Weibull model

The Weibull model of inactivation is based on continuous probability distribution[34]. This model describes the degree of variability in the behavior of a system. In the case of first-order models, microbial populations are assumed to be homogeneous regarding resistance to external conditions. But the Weibull model describes the microbial population as heterogeneous. Also, the death of the cells depends on the time of exposure of cells to external stress conditions as well as the exposure time required by every cell to die or different. The dispersal resistance to the conditions bacterial cells are exhibited to is regulated by Weibull-type distribution. This model is a cumulative form of asymmetric probability density function for the heat resistance of individual bacterial cells. The Weibull distribution model is shown in Eq. (10) given below

$$log\frac{A_t}{A_0} = -\left(\frac{t}{\delta}\right)^p \quad (10)$$

The first decimal reduction time, i.e. time needed to complete the first decimal log decrease in the number of inhabitants in the *E. coli* cycle (for example, from A_0 to $A_0/10$) is denoted by δ. The equation's shape is denoted by p. The convex shape occurs when p is greater than 1, and the concave occurs when p is less than 1. The equation shows a linear first-order model when p is equal to 1.

2.3. Double Weibull model

The double Weibull kinetic distribution model is a moderation of the Weibull distribution model. This model is based on the theory that the resistance to the external stress condition of two different subpopulation groups of microbial populations is at different levels and follows the Weibull distribution as shown in Eq. (11)

$$A = \frac{A_0}{1+10^{\alpha}} \times \left(10^{-\left(\frac{t}{\delta_1}\right)^{p_1+\alpha}} + 10^{-\left(\frac{t}{\delta_2}\right)^{p_2}} \right) \quad (11)$$

where α is the Subpopulation fraction in the population, subscripts 1 and 2 describe different Subpopulations. Also, p indicates the shape parameter, t denotes time, δ denotes the first decimal decrease in the treatment time. Subpopulation 1 more sensitive to stress as compared to Subpopulation 2($\delta_1 < \delta_2$).

3. Material and methods

3.1. Chemical reagents

H_2O_2 30% was provided by Ranbaxy, India. P25-TiO_2 was provided by Evonik Industries, India. Waste foundry sand, fly ash, and clay were procured from a local supplier, Patiala, India. Reagent grade Sodium acetate and acetic acid were purchased from Tokyo Chemical Industry, India. The isotonic solution for the bacterial cell made from 99.5% NaCl was procured from Fisher Scientific, Mumbai, India. Agar-Agar Type I and Luria Bertani broth (LB) for cell growth were bought from HiMedia Laboratories Pvt Ltd, Mumbai, India. All the solutions were prepared using double-distilled water.

3.2. Bacterial strain and growth media

The bacterial strain used was *E. coli* (wild type K12) and was supplied by MTCC and Gene bank (Microbial Type Culture Collection) from Chandigarh (India). It is non-pathogenic and an indicator of bacteria for enteric pathogens. *E. coli* strains were prepared with 20% glycerol and kept at −20 °C in cryo-vials. The colony from the sample strain was streaked on the agar plate to prepare the pre-cultures for every experimental series. Afterward, the plates were incubated at 37 °C in an incubator for 24 h. After incubation, the grown colony was again plated on a new Agar plate and again kept for incubation at 37 °C for 24 h. For the experiments, the cell pellet was prepared by picking the colony from the pre-cultures with the help of a loop and inoculated in a 50 mL of sterile borosil Erlenmeyer flask having 5 mL of Luria-Bertani (LB) broth. Then the incubation of the flask was done at 37 °C and 180 rpm in an incubating shaker. After 8 h, 1% dilution of bacterial cells was made in a sterilized 250 mL Erlenmeyer flask having 50 mL of already autoclaved LB broth. In to achieve a physiological stationary phase the cells were incubated in aerobic conditions at 37 °C. The bacterial stationary and growth phase was observed by optical density (OD) at 600 nm. The LB broth having tryptone (10g), sodium chloride (10g), and yeast extract (5g) in 1L of distilled water is sterilized by autoclaving at 121 °C for 20 min. The bacterial cells were harvested by centrifuging for 15 min at 4 °C and 5000 rpm. The obtained bacterial pellet was washed with 0.8% NaCl saline solution (3 times washing). The final bacterial pellet was obtained then re-suspended in the saline solution having 50 mL of the initial volume. This method resulted in approximately 10^9 colony-forming units per milliliter ($CFUmL^{-1}$) of cell density. The bacterial solution (*E. coli*) was diluted in the sterilized distilled water and obtained a cell density of 10^6 $CFUmL^{-1}$. This cell density was then used in all the experiments done in this study. The concentration of the *E. coli* present in the water sample ($CFUmL^{-1}$) was calculated by plating on agar plates. During the experiments, a 1 mL sample was withdrawn, stored at 4 °C, and immediately plated on the agar plate using the standard plate count method. After plating, the plates were kept for incubation overnight at 37 °C and the counting of the colonies on the plates was done manually. Moreover, the plating was done by spreading 0.1 mL of the *E. coli* sample on Petteri dishes. To achieve the desired concentration of *E. coli*, serial dilutions were made for each water sample. The data points presented are the average of two replicates and the error bars represent the standard deviation from the mean. The above-mentioned methodology for determining *E. coli* concentration is the most efficient method applied for the testing of microorganisms present in the natural water with low error[35,36]. The inactivation efficiency was calculated using equation (Eq. (12)), where A_t is the concentration of *E. coli* (CFU/mL) at any time t, A_0 is the initial concentration of *E. coli* (CFU/mL)

$$L_r = \log(A_t/A_0) \quad (12)$$

3.3. Preparation of fixed bed support material

Clay as a supporting material used for composing the spherical beads consisting of FS (foundry sand) and FA (fly ash) in the ratio of 2:1:1, respectively, and then dried at room temperature. The size of the beads was kept 10 mm via measuring them from 4 different directions using a screw gauge. The beads were muffled at 800 °C for 1.5–2.0 h. The beads were cured by soaking them in the water for 48 h. This increases the durability and strength of the support material. These beads were then used for the *E. coli* inactivation in the photo-Fenton process. To study the photocatalytic process, the clay beads were made and muffled at 800 °C for 1.5–2.0 h. After this, a 1% (*w/v*) TiO_2 solution was sonicated for the dispersion of TiO_2 particles. The beads with and without FS and FA were then dipped in this sonicated solution and coated with the TiO_2 catalyst, known as the dip-coating method[33]. For the proper coverage, the beads were coated two times with the sonicated TiO_2 solution. The coated bead dried at room temperature and then muffled at 350 °C for 1.5 h for proper attachment of the TiO_2 over the surface of the composite bead. The thickness of the TiO_2 coating over the support was observed to be 71 μm as shown in our previous studies using scanning electron microscopy (SEM) analysis[31]. These Fe-TiO_2 composite beads were then used to study the dual effect in fixed mode.

3.4. Experimental set-up

The experiments were conducted in a rectangular closed wooden chamber having 36 W 7 Philips UV tubes with a wavelength of 365 nm were fixed parallel to each other on the roof of the wooden chamber. A 1000 mL glass Petri dish filled with 250 mL of working solution of 10^6 $CFUmL^{-1}$ was used to study the *E. coli* inactivation. For the bacterial acclimatization, the working solution was stirred for 25 min. Then the surface of the Petri dish was filled with the composite beads. The pH of the working solution was kept in acidic conditions (3.5) for leaching of iron from the beads. 0.3 gL^{-1} of H_2O_2 (0.25 mL) was added into the petri dish before the experiment starts for the photo-Fenton and dual-technique to take place. The value of the pH and the concentration of H_2O_2 was already quoted in our previous study [31]. Then the Petri dish was kept inside the UV chamber on a jack to maintain 24 Wm^{-2} of the intensity measured by a radiometer (Eppley, model no. 33013). The homogeneity of the reaction was maintained by providing aeration (3.0 $Lmin^{-1}$) to the Petri dish using two spargers placed at the same distance from the center. The concentration of H_2O_2, intensity of light, and pH of the solution was kept the same for each experiment done in this study.

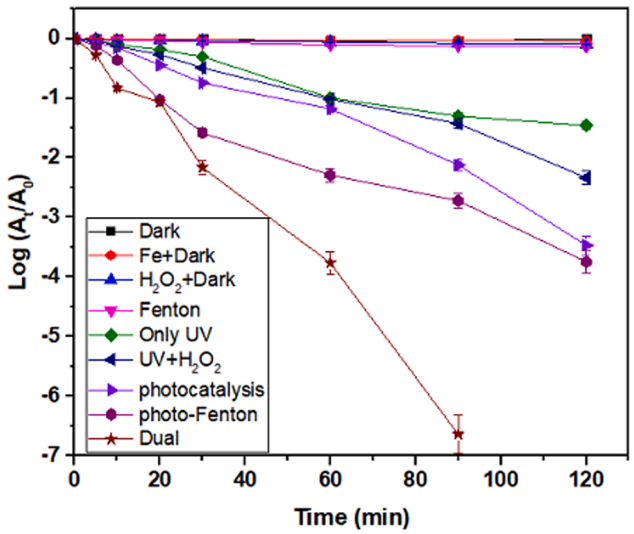

Fig. 1. *E. coli* inactivation in dark and UV under different conditions.

For disinfection studies, at regular intervals for 120 min, a 1 mL sample of treated water was taken out from the Petri dish and the reduction in the *E. coli* count was calculated using the plating counting method. All the Petri dishes and glassware used in the experiment were washed and autoclaved before each experiment.

3.5. Characterization of composite beads

PANalyticalXpert Pro was used for X-Ray diffraction analysis to determine the crystallinity of Fe-TiO_2 composite. The wavelength of Cu Kα (λ) was kept 1.5405 in between 2θ = 20–80°. For further analysis of the catalytic beads, Fourier–transform infrared spectroscopy (FTIR) between 4000 and 400 cm^{-1} infrared spectrum.

4. Results and discussion

4.1. Experimental findings

4.1.1. Dark study

The initial population of *E. coli* at the start of experiments was approximately 10^6 CFU/mL in the water sample. The dark control (without UV light) produced no bactericidal effects and did not show any reduction in the *E. coli* population. The viability of cells was not

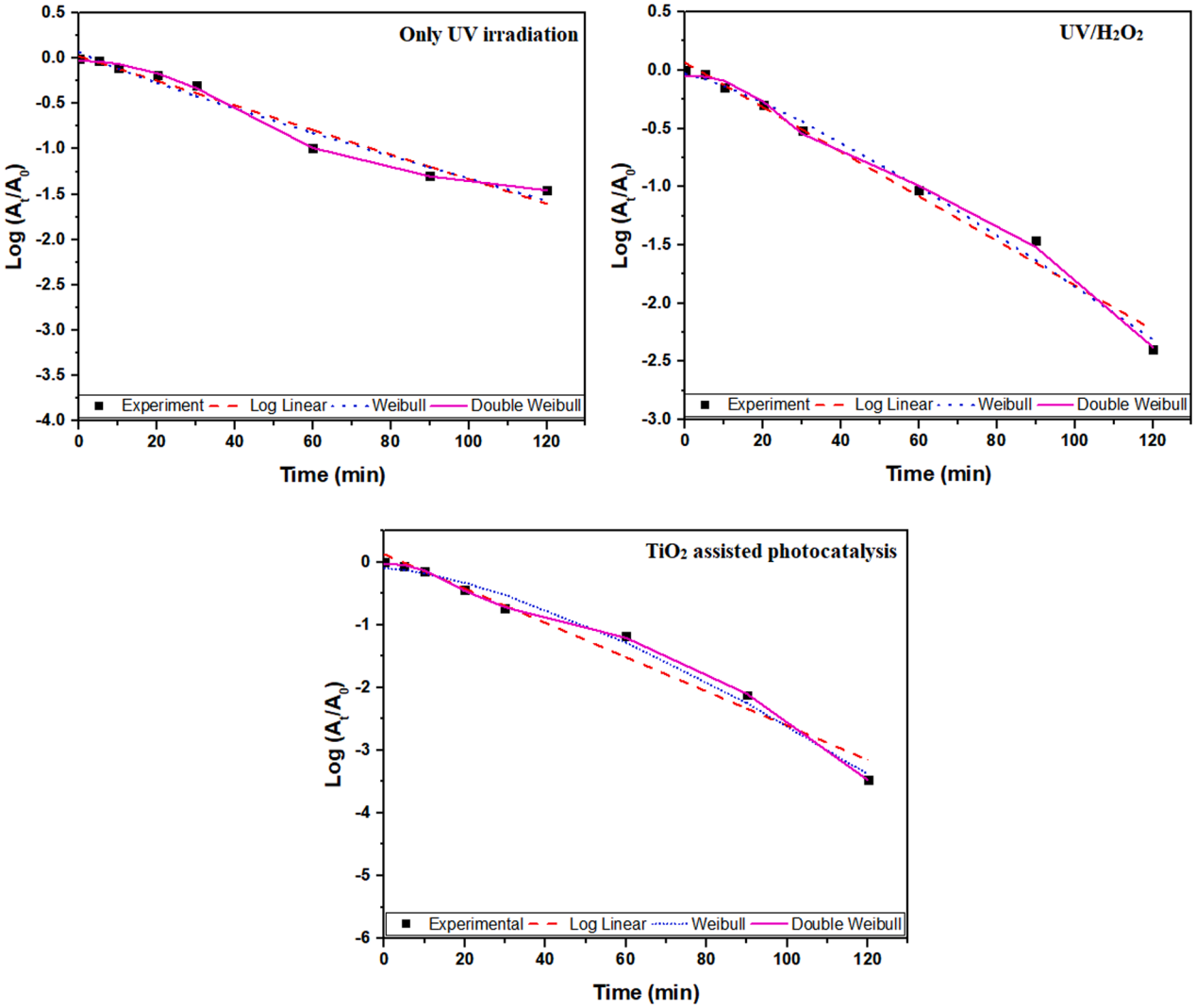

Fig. 2. **(a)** Fitting of different mathematical models with kinetic parameters used in the only UV disinfection process of *E. coli* **(b)** Fitting of different mathematical models with kinetic parameters used in the UV/H_2O_2 process of *E. coli* **(c)** Fitting of different mathematical models with kinetic parameters used in the TiO_2-photocatalytic process of *E. coli*.

Table 1
Different mathematical models with kinetic parameters used in the UV disinfection process of *E. coli.*

Treatment	Models	K (min^{-1})	δ_1 (min)	δ_2 (min)	$\frac{R^2}{RMSD}$
UV irradiation					
	Log linear	0.03	–	–	0.966/ 0.119
	Weibull	–	68.18	–	0.969/ 0.124
	Double Weibull	–	51.91	207.73	0.998/ 0.036

Table 2
Different mathematical models with kinetic parameters used in the H_2O_2/UV disinfection process of *E. coli.*

Treatment	Models	K (min^{-1})	δ_1 (min)	δ_2 (min)	$\frac{R^2}{RMSD}$
H_2O_2/UV					
	Log linear	0.04	–	–	0.985/ 0.107
	Weibull	–	62.67	–	0.991/ 0.090
	Double Weibull	–	34.05	100.95	0.997/ 0.051

affected by distilled water in 2 h of the reaction time, so any effect occurring in the cell's viability accredited to the die-off of the cell mainly due to the osmatic stress that occurred when *E. coli* were introduced to the water sample. Similar results were found in the literature even for a longer period and no bacterial reduction was observed[34,37]. *E. coli* generates H_2O_2 internally but doesn't affect cell viability as it is regulated by catalase and peroxidase[38]. Similar results were obtained when only H_2O_2 (0.25 mL) added into the petri dish under dark conditions and a negligible reduction in *E. coli* concentration was found as can be seen in Fig. 1. H_2O_2 has the same polarity as that of water, which allows H_2O_2 to diffuse into the cell very easily and undoubtedly damages the cell via internal photo-Fenton. However, the presence of KatE and alkyl hydroxide reductase (*aph*) causes fast decomposition of H_2O_2 resulting in a negligible reduction in *E. coli.*[39] As in our tests, the cells were in stationary phase so, likely katE protected cells against H_2O_2 production as *aph* works in a growing cell[40]. Fe^{2+} leaching out from the Fe-TiO_2 beads had shown very little (0.05 log) reduction in the *E. coli* population as observed in Fig. 1. This loss in the cell count might be due to the movement of Fe^{+2} using porins (present at cell membrane) into the periplasm of the cell[37] and can cause an interim disruption of Fe^{2+} stability inside the bacterial cell. Finally, the Fenton process by simultaneous addition of both reagents (Fe leached out from beads and 0.3 g L^{-1} of H_2O_2) inducing the Fenton process did not show any significant effect in 2 h of treatment. Fe^{3+} generated during the reaction of Fe^{2+} and H_2O_2 may form oxides and precipitate[41]. The oxidized iron could lead to a heterogeneous Fenton reaction, but in 120 min. The *E. coli* population didn't decrease, indicating a negligible contribution. The results obtained above shows that the disinfection efficiency depends upon the UV light (365 nm).

4.1.2. UV assisted study

In this study, UV only, UV + H_2O_2, TiO_2-photocatalyst, photo-Fenton, and a combination of the photo-Fenton and TiO_2-photocatalyst in a fixed bed using Fe-TiO_2 composite beads were studied to evaluate and compare the killing efficiency of the system. As clear from Fig. 1, the only UV irradiation and 0.3 gL^{-1} of H_2O_2/UV irradiation experiments showed 1.4 and 2.3 log reduction inactivation of *E. coli,* respectively. It can be seen in Fig. 2(a), that all three mathematical models showed good fitting when the only UV treatment for *E. coli* inactivation was applied. Though the double Weibull model showed the best fitting curve for inactivation considering the fitting of the average values of inactivating *E. coli* and attaining relatively good R^2 (0.99) and RMSD (0.03) values as given in Table 1. Because in the double Weibull model coefficient of determination (R^2) is much closer to 1 as compared to other models that indicate that the regression line completely fits the data. Another reason was RMSD, whose value is much closer to 0 in comparison to the other two models that indicate a perfect fit of estimated values with the real values[34]. When H_2O_2/UV technique was used (Fig. 2b), the Weibull and double Weibull model attained the best fit for the average of the *E. coli* inactivation results with R^2 value as 0.99 in both the cases, whereas RMSD is 0.05 for double Weibull and 0.09 for Weibull model. When both the treatment techniques were compared having disinfection rate constants (k) and reduction of the first decimal parameters (δ) showed minute variations among these treatments as observed in Table 1 and Table 2. By considering the double Weibull distribution, the reduction of first decimal parameters of the 2 subpopulations of *E. coli* in the only UV technique was $\delta_1 = 51.9$ min and $\delta_2 = 207.7$ min (Table1), whereas in the H_2O_2 with UV technique the δ_1 was 34.05 min and δ_2 was 100.95 min as shown in Table 2. While comparing the aforementioned techniques through the double Weibull distribution, the addition of oxidant (H_2O_2) with UV is insufficient in improving the *E. coli* inactivation for the selected exposure time. Thus achieving minute change in the rate of reaction and the inactivation level as compared to the only UV technique. Therefore, the results obtained through these techniques are perfectly fitted using the double Weibull model where it is assumed that the two distinct Subpopulation groups (Subpopulation 1, which are sensitive cells and inactivates at a short period (δ_1) and Subpopulation 2, more resistant and takes more to inactivate (δ_2)) are present with different levels of endurance to the disinfection treatment.

4.1.3. TiO_2 assisted photocatalysis in fixed mode

The TiO_2-photocatalysts coated over clay beads were evaluated for their potential to inactivate the *E. coli* in water under UVA radiation (24 Wm^{-2}) and the results obtained are shown in Fig. 1. Almost 3.27 log reduction in *E. coli* population was observed with TiO_2 coated beads upon irradiation for 120 min. These results are consistent with the previous results reported in the literature. For instance, Adan et. al. [42] studied the *E. coli* inactivation using TiO_2 coated glass raschings and obtained approximately similar log decrease in 120 min of treatment time. This low disinfection efficiency of the current study might be due to fast e^-h^+ recombination in the semiconductor leading to less production of reactive oxygen species, which ultimately reduces the efficiency of the system[43]. It can be seen from Fig. 1 that initially the rate of log reduction is slower and increases with an increase in the treatment time, thus confirming that the reaction time plays an important role in the bacterial reduction. The mechanism of the inactivation of cells using TiO_2 photocatalysis has not yet been elucidated. However, several studies have provided different mechanism patterns. The reactive oxygen species ($OH^{\cdot}$, $HO_2^{\cdot}$, $O_2^{\cdot-}$) generated on the surface of TiO_2 induces oxidative stress in the bacteria and led to its inactivation. Several studies reported that the lipid peroxidation reaction in the cell membrane occurs in the presence of TiO_2 that affects the respiratory activity of cells. Other studies proposed that [44] the first step in the photoinactivation of *E. coli* is the damage and disordering of the outer membrane serving as a barrier of the cells. The degradation of the outer membrane helps the reactive oxygen species penetrate the cytoplasmic membrane led to the loss of intracellular substances[45]. It has been reported that [46] Hydroxyl radicals are highly reactive as compared to the $O_2^{\cdot-}$ but has a short half-life in comparison to $O_2^{\cdot-}$. Yet, can't penetrate the cell membrane to damage DNA because of their charge. Therefore, the TiO_2 photocatalysis interacts immediately with the outer surface of an *E. coli* unless the TiO_2 particle has penetrated the cell.

It was observed from Fig. 4, that all the applied mathematical models showed a good fit when TiO_2 assisted photocatalytic technique in a fixed

Table 3
Different mathematical models with kinetic parameters used in the TiO_2-photocatalytic disinfection process of *E. coli*.

Treatment	Models	K (min^{-1})	δ_1 (min)	δ_2 (min)	$\frac{R^2}{RMSD}$
TiO_2-photocatalysis					
	Log linear	0.06	–	–	0.973/ 0.219
	Weibull	–	53.32	–	0.989/ 0.147
	Double Weibull	–	23.13	76.02	0.999/ 0.028

bed was employed. But the perfectly fitted curve was observed in the Weibull and double Weibull distribution, considering the R^2 values (0.99 and 0.98 respectively) and RMSD values (0.02 and 0.1, respectively). To understand the impact of different parameters on the kinetic rate of *E. coli* inactivation modeling is used. Therefore, the k and δ values showed in Table 3 in comparison to the values in Table 1 (only UV) and Table 2 (H_2O_2 with UV) indicate a higher inactivation rate of *E. coli* in the TiO_2 assisted photocatalytic. Therefore, comparing the k and δ values of the average fitted curve as observed in the log-linear and Weibull distribution showed that the TiO_2 assisted photocatalysis in fixed mode ($k = 0.06\ min^{-1}$; d = 53. 32 min) was significantly faster than the only UV ($k = 0.03\ min^{-1}$; d = 68.13 min) and H_2O_2 with UV technique ($k = 0.04\ min^{-1}$; d = 62.6 min).

4.1.4. Photo-Fenton in fixed mode

For executing the fixed bed photo-Fenton technique, the iron was made to leach from the composite beads by maintaining the acidic conditions (pH = 3.5), and Fig. 1 showed a demonstration of the corresponding inactivation values. Leaching of the iron from the clay always happens in acidic conditions because it helps in tearing the bond of iron with other organic compounds and causes the extraction of iron known as iron leaching[47]. 0.3 g L^{-1} of H_2O_2 concentration (0.25 mL) was added for the photo-Fenton to take place. It was observed that this treatment achieved a 3.79 log reduction in *E. coli* after 120 min of treatment. The addition of H_2O_2 and iron leaching from the beads imposes two important changes in the cell inactivation. First is a massive generation of Hydroxyl radicals into the system (reaction of H_2O_2 and iron), which led to the oxidation of the cells externally[48]. The second is the penetration of ferrous ion and H_2O_2 into the cell via porins. As the size of the Ferrous ion (<6 Å) and H_2O_2 ion (1.2–1.4 Å) is smaller in comparison to the size of bacteria (11 Å), thus destroys cells internally after the deactivation of catalases. As this process is happening in the presence of UV light, ferrous ion reacts with the internal reactive oxygen species (ROS), which results in damage to the cell. Whereas H_2O_2 will cause moderation in biosynthetic and catabolic function, which will further result in loss of iron from the iron/sulfur cluster and generates Hydroxyl radicals[36]. This H_2O_2 also affects cells externally via reacting with the cell wall. This increases the permeability of the cell due to the major influx of H_2O_2 leading to the oxidation of the cell wall. It happens because H_2O_2 oxidative activity (0.18) is higher than the oxidation potential of the membrane. The H_2O_2 present outside the cell will generate ROS via homolysis and when H_2O_2 reacts with iron this adds up to the external oxidation of the bacteria. It was observed from Fig. 3(a), that all the applied mathematical models showed a good fit when the photo-Fenton technique in a fixed bed was employed. But the perfectly fitted curve was observed in the Weibull and double Weibull distribution, considering the R^2 values (0.98 for both models) and RMSD values (0.2 for both models). While considering the double Weibull model as shown in Table 4, the first decimal reduction parameters were $\delta_1 = 17.66$ min and $\delta_2 = 33.53$ min of the 2 subpopulations of *E. coli* inactivation in the photo-Fenton process.

4.1.5. Dual-technique in fixed mode

The in-situ dual technique was executed using Fe-TiO_2 composite beads through subsequent leaching of iron and surface-active TiO_2 coating. This process was marked with parallel execution of both processes of photo-Fenton and TiO_2 assisted photocatalysis in a fixed mode. This dual technique yielded the highest log reduction of 6.4 as compared to the photo-Fenton and TiO_2 assisted photocatalysis individually. This might be due to its ability to restrict the e^- h^+ recombination occurring

Table 4
Different mathematical models with kinetic parameters used in the photo-Fenton disinfection process of *E. coli*.

Treatment	Models	K (min^{-1})	δ_1 (min)	δ_2 (min)	$\frac{R^2}{RSMD}$
Photo-Fenton					
	Log linear	0.07	–	–	0.9604/ 0.29
	Weibull	–	19.07	–	0.9814/ 0.218
	Double Weibull	–	17.66	33.53	0.9821/ 0.23

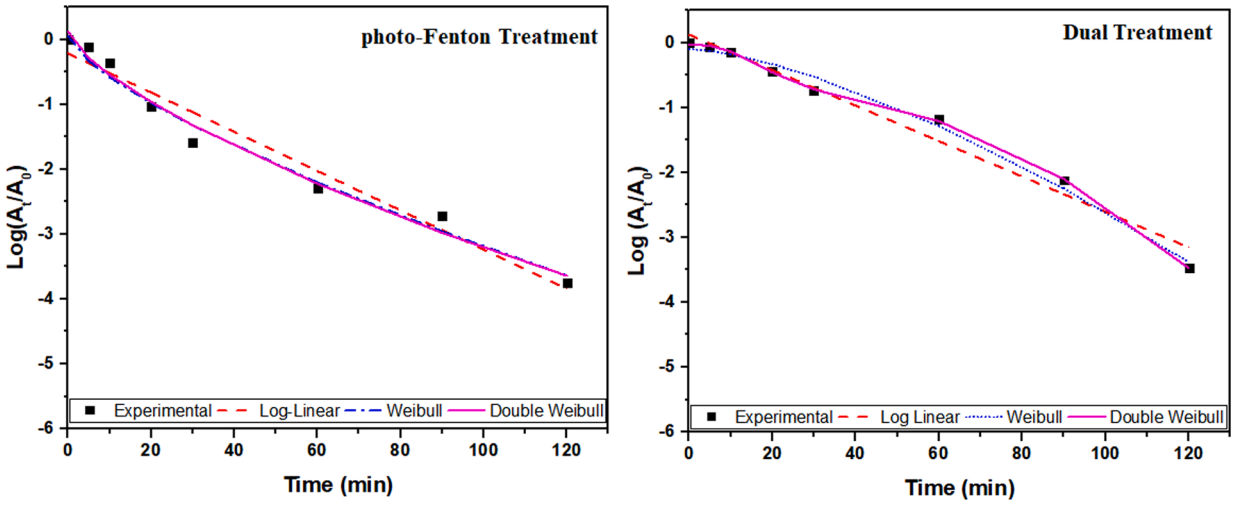

Fig. 3. (a) Fitting of mathematical models to the inactivation curve of *E. coli* through the photo-Fenton treatment **(b)** Fitting of mathematical models to the disinfection curve of *E. coli* through the dual process.

Table 5
Different mathematical models with kinetic parameters used in the dual disinfection process of *E. coli*.

Treatment	Models	K (min^{-1})	δ_1 (min)	δ_2 (min)	R^2 / RSMD
Dual					
	Log linear	0.16	–	–	0.985/ 0.287
	Weibull	–	18.56	–	0.991/ 0.270
	Double Weibull	–	8.63	27.77	0.994/ 0.257

in TiO_2 photocatalysis by combining the ferric ion produced from the photo-Fenton technique with e^- present the conduction band of TiO_2 to produce ferrous ion as shown in Eqs. (1)–(8). Hence, leading to the photo-Fenton process in recurring mode with no sludge formation. The addition of H_2O_2 in the system played a dual role and engaged in reaction with both TiO_2 and iron for the generation of more Hydroxyl radicals in the treatment system as shown in Eq. (3). This increased production of Hydroxyl radicals in the system was confirmed through fluorescence spectroscopy. The dual mechanism eventually led to an almost double reaction rate in comparison to the photo-Fenton and TiO_2 assisted photocatalysis in fixed mode. The proposed hypothesis has led to the concept of synergy that exists between these three processes as discussed in the next section. Leaching of the iron in the system in terms of total, ferrous and ferric ion was also determined to confirm the occurrence of the photo-Fenton process. The maximum average concentration of total iron, ferric ion, and ferrous ion was found to be (167 μgL^{-1}, 102.8 μgL^{-1}, and 62 μgL^{-1} respectively) as given in Fig. 6(a-b). The amount of iron present in the system is less as compared to the other studies [37,38], yet have shown better results in less treatment time. A higher concentration of iron in the system only hinders the bacterial inactivation due to light scattering and decreases direct UVA irradiations. The mechanism of killing *E. coli* will remain the same as discussed above.

The results obtained after inactivating *E. coli* in dual (photo-Fenton + photocatalysis) process in fixed mode, all employed mathematical models showed a good fit as given in Fig. 3(b). But, the best-fitted curve was observed in the Weibull and double Weibull distribution, considering the R^2 and RMSD values of 0.99 and 0.2 for both the models, respectively. On comparing the k and δ as given in Table 5, the disinfection rate of *E. coli* increased in the dual process in comparison to the TiO_2 assisted photocatalysis as shown in Table 3 and photo-Fenton treatments as shown in Table 4. Thus considering the kinetic parameters such as "k" of log-linear and "δ" of double Weibull for fitting the *E. coli* inactivation results and comparing the different techniques showed that the dual-technique in fixed mode (k = 0.16 min^{-1}; δ_1 =

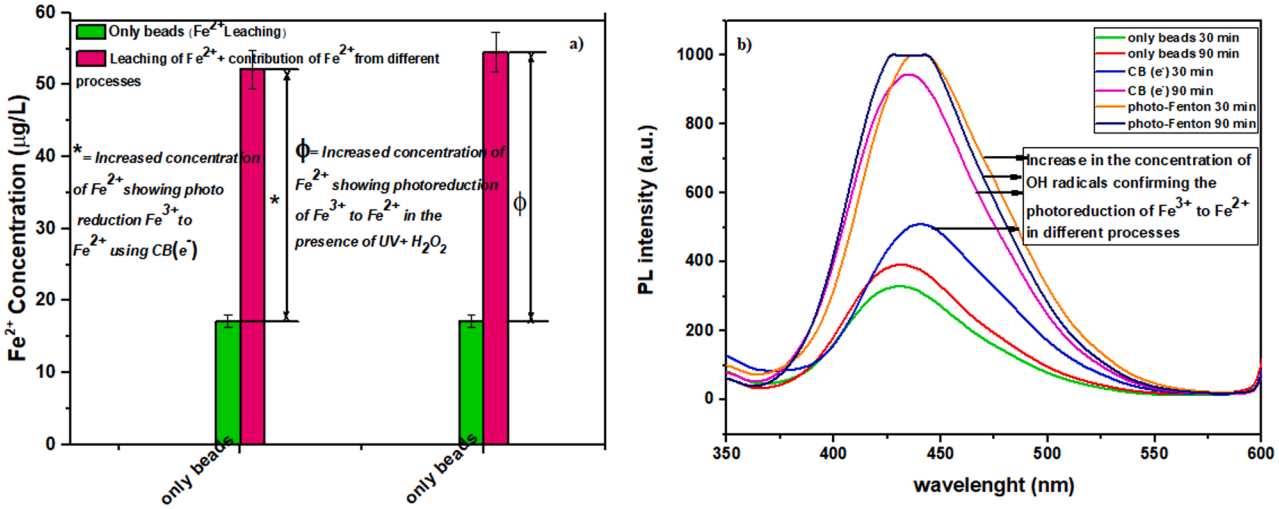

Fig. 4. **(a)** Photoreduction of Fe^{3+} to Fe^{2+} in different processes **(b)** OH radical spectra using fluorescence spectrophotometer.

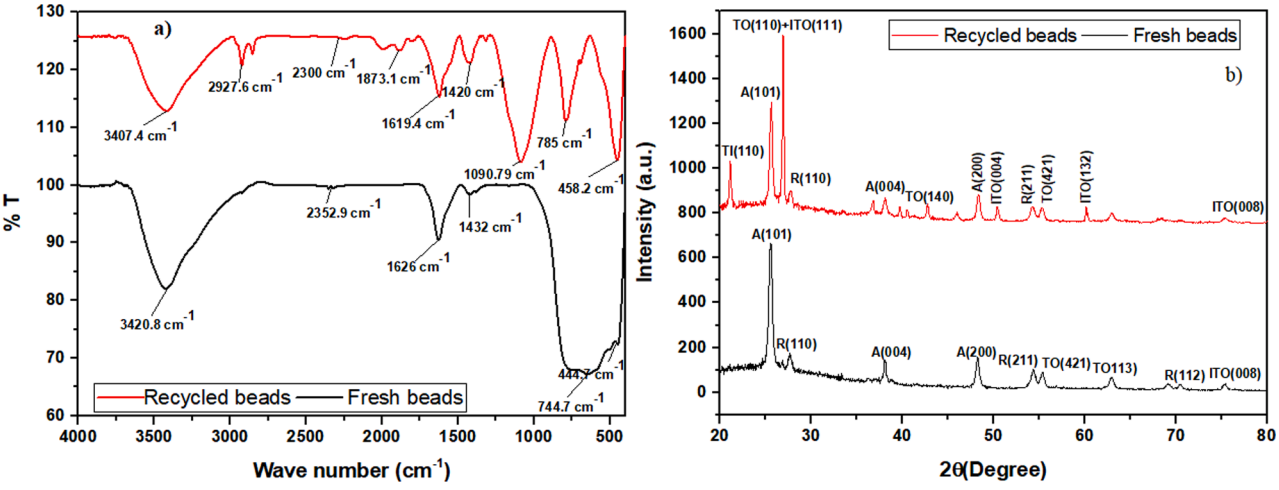

Fig. 5. **(a)** FTIR pattern of recycled and fresh beads **(b)** XRD pattern of recycled and fresh beads.

8.63 min, $\delta_2 = 27.7$ min) proved to be significantly faster in comparison to other techniques; TiO_2 assisted photocatalysis ($k = 0.06\ min^{-1}$; $\delta_1 = 23.1$ min, $\delta_2 = 76$ min); photo-Fenton ($k = 0.07\ min^{-1}$; $\delta_1 = 17.66$ min, $\delta_2 = 33.53$ min; H_2O_2 with UV ($k = 0.04\ min^{-1}$; $\delta_1 = 34.05$ min, $\delta_2 = 100.95$ min) and Only UV($k = 0.03\ min^{-1}$; $\delta_1 = 51.91$ min, $\delta_2 = 207.73$ min. Thus inactivation efficiency of *E. coli* using different oxidation processes on the bases of the rate constant can be ranked as:

Dual > photo-Fenton > photocatalysis > UV + H_2O_2 > UV only

5. Confirmation of Dual-technique

To confirm and verify the dual effect, a different set of experiments were performed. Firstly the photoreduction of Fe^{3+} to Fe^{2+} through e^-_{CB} (Eq. (7)) was cross-verified by performing the experiments at different time intervals and the average of them was quoted as given in Fig. 4 (a) and also to verify if Fe^{3+} can be photo-reduced in the presence of H_2O_2 under the influence UV wavelength photons, experiments were performed as given in Fig. 4(a) and it was found that there was an increase in the concentration of Fe^{2+} which might be du the photoreduction of Fe^{3+}. The hypothesis of extraction of e^- from the conduction band of TiO_2 and utilization of H_2O_2 for converting Fe^{3+} to Fe^{2+} during the in-situ dual process was justified with excess production of Hydroxyl radicals helping in inactivation of *E. coli* in water as shown in Fig. 4(b). Also, the composite beads used in this study have shown higher production of Hydroxyl radicals in comparison to the beads used for photo-Fenton and TiO_2 assisted photocatalysis. The composite beads have shown extended durability as beads used in our previous study [31] continued to give better results in this study also. The present study has observed *E. coli* log reduction of 6.4 ($k = 0.16\ min^{-1}$) in comparison to photocatalysis (3.27 log reduction and $k = 0.06\ min^{-1}$) and photo-Fenton (3.79 log reduction and $k = 0.07\ min^{-1}$). Thus higher log reduction of *E. coli* in the dual process confirms the continued jump in the production of Hydroxyl radicals in the system.

For further confirmation of dual-technique, characterization such as XRD and FTIR analysis of freshly coated and recycled composite beads was done to verify the presence of TiO_2 and iron in it. In the FTIR analysis (Fig. 5a), the wavenumber from 400 to 1200 cm^{-1} in both freshly coated and recycled Fe-TiO_2 beads showed Ti-O-Ti bond thus, validates the existence of TiO_2 lattice. The peaks at 458 cm^{-1} and 444 cm^{-1} wavenumbers represented the anatase phase in both freshly coated and recycled beads respectively. The Fe-O-Ti bond was also found in the spectrum of freshly coated and recycled catalyst at 2353 cm^{-1} and 2300 cm^{-1} peak, thus verify the existence of iron in it. Similar peaks were also observed in Bansal et al.[49]. For XRD analysis, the catalyst particles were scrapped off and analyzed. For TiO_2-P25 the biphasic nature was observed as peaks corresponding to anatase and rutile was there in the diffraction pattern. Fig. 5(b) showed the existence of anatase (A) and rutile phase (R) in the fresh as well as the beads obtained after 30 recycles. Other than this, the diffraction patterns also showed the existence of iron titanium oxide (ITO). Thus, eases the capturing of TiO_2 (e^-) by Fe^{3+} and proving the simultaneous working of photocatalysis and photo-Fenton process.

6. Synergistic effect

Another system to validate the dual effect is the justification of the synergy of the combined process over the individual processes of photocatalysis and photo-Fenton. The synergy of the dual-process over photocatalysis and photo-Fenton process means the combined effect of photocatalytic and photo-Fenton process over the individual process (photocatalysis and photo-Fenton) for inactivation of *E. coli*. The synergistic effect can be calculated using the first-order inactivation rate constants for all the processes. In this context, the synergy of the dual-technique was calculated and quantified accordingly. The combined effect of photo-Fenton and photocatalytic technique (dual process) was

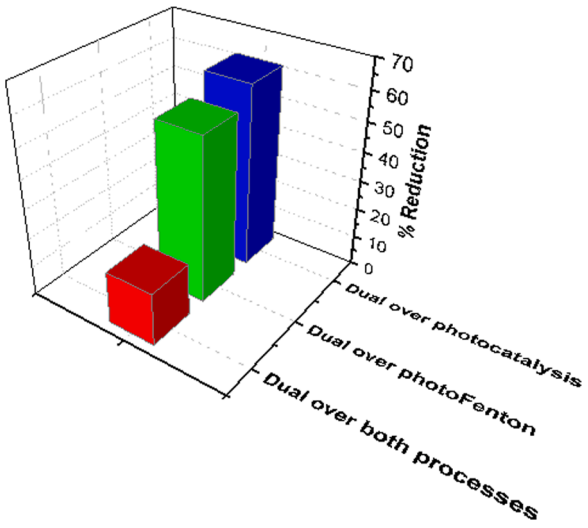

Fig. 6. Synergy of dual-technique over photocatalysis and photo-Fenton process.

significant as the rate constant for this process was greater than the sum of the reaction rate constants obtained individually in photo-Fenton and TiO_2 assisted photocatalytic process. The synergy of the dual-technique upon both the techniques in combination was found to be 18.7% (Fig. 6) and shown using the following Eqs. (12)–(14) [31].

The synergy of dual-technique upon photocatalytic process

$$\%synergy = 100 \times \{(k_{dual} - k_{photocatalysis})\}/k_{dual} \quad (12)$$

$$\%synergy = 100 \times \{(0.16 - 0.06)\}/0.16$$

$$\%synergy = 62\%$$

The synergy of dual-technique upon photo-Fenton process

$$\%synergy = 100 \times \{(k_{dual} - k_{photo-Fenton})\}/k_{dual} \quad (13)$$

$$\%synergy = 100 \times \{(0.16 - 0.07)\}/0.16$$

$$\%synergy = 56\%$$

The synergy of dual-technique upon photocatalytic and the photo-Fenton process together i.e Total synergy:

$$\%synergy = 100 \times \{(k_{dual} - (k_{photocatalysis} + k_{photo-Fenton})\}/k_{dual} \quad (14)$$

$$\%synergy = 100 \times \{(0.16 - (0.06 + 0.07)\}/0.16$$

$$\%synergy = 18\%$$

This high percent of synergy can be credited to the in-situ dual process which actually produce significant amount of Hydroxyl radicals Moreover, the reaction of ferric ion with conduction band e^- to perform the photo-Fenton process, thus along with preventing the e^-h^+ recombination in photocatalytic process, gives a significant boost to synergy as discussed earlier.

7. Durability

The durability/stability of the Fe-TiO_2 composite beads was the biggest challenge for this study as the system has to retain both the catalytic activities (photo-Fenton and photocatalysis) with subsequent recycles. It means that the composite beads have to sustain iron leaching as well as retain the activity of the TiO_2 layer with repeated cycles. For this study, the composite beads were recycled 30 times and the durability was studied in terms of unit log reduction of *E. coli*. The beads were durable enough as only 11% decrement in the photoactivity of the

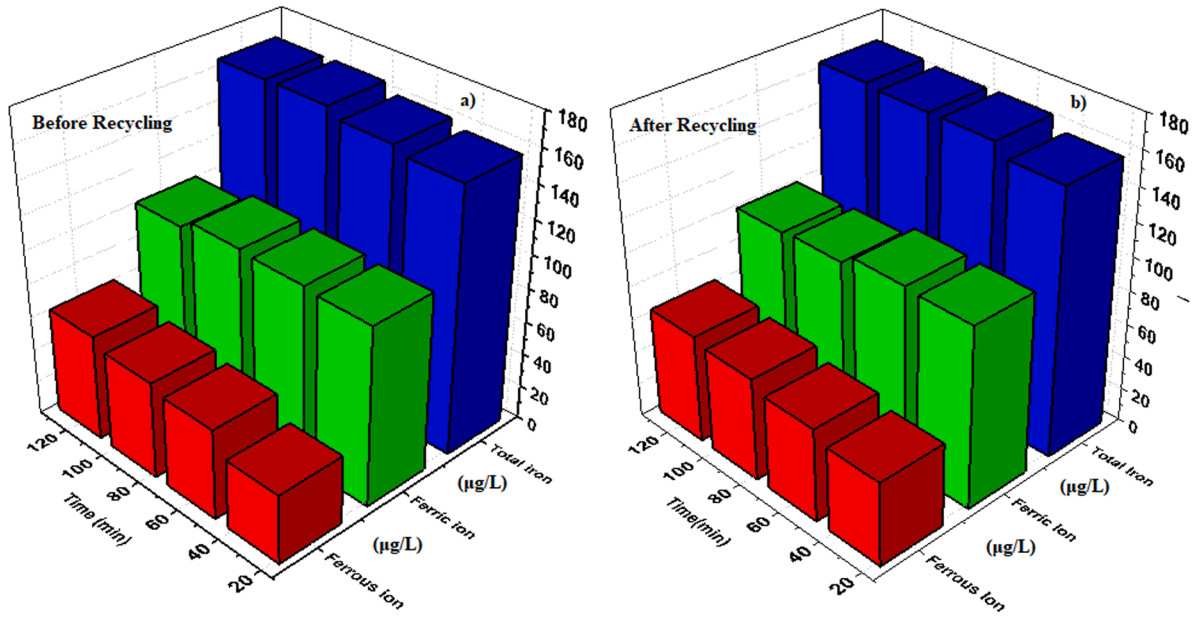

Fig. 7. (a-b) Iron concentration (µg/ L) present in the dual process before and after recycling.

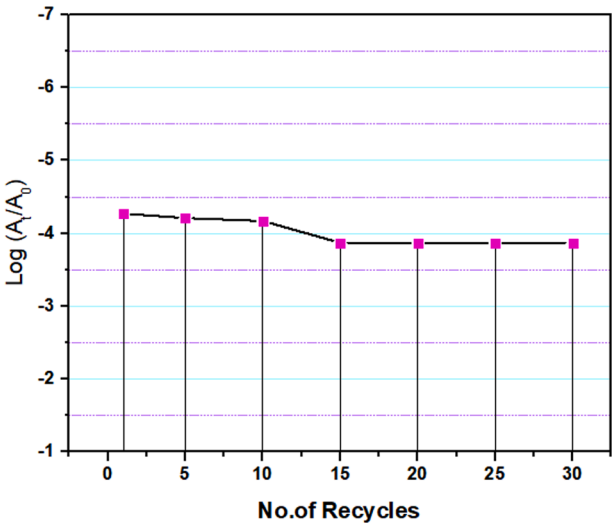

Fig. 8. Durability study of composite beads for 30 cycles.

photocatalytic beads was found after 30 recycles, as given in Fig. 8. Even the iron leaching was sustained with repeated cycles (Fig. 7(a-b), thus validating the durability of the dual effect. A small reduction in catalytic ability might be due to weathering off of the catalyst coating over the beads or a reduction in the specific surface area of the catalyst. This might be due to the blockage of some active sites and pores by degraded organic intermediates [50]. TiO_2 intactness over the composite beads and its stability were analyzed by different characterization techniques, as discussed in our previous section, and verified the existence of dual-technique in the system. The peak intensities and location even after 30 runs stayed almost the same and thus signifying that the structural framework of Fe-TiO_2 did not significantly change.

8. Conclusion

The inactivation of *E. coli* was studied using three different mathematical models wherein the double Weibull distributions accurately describe the *E. coli* reduction curve in all the treatment processes studied in this work. The first decimal deduction parameter (δ) and disinfecting rate parameter (k) proved that the dual-technique was the fastest treatment as compared to the other processes. The dual-technique in a combination of TiO_2 assisted photocatalysis and photo-Fenton in fixed mode showed the highest levels of *E. coli* inactivation with less contact time. The treatment time in the dual-technique was also reduced to 90 min with 6.4 log reduction as compared to the other techniques where treatment time was 120 min and log reduction was not even near to it. On the other hand, a negligible difference was found in photo-Fenton and TiO_2 assisted photocatalysis in terms of *E. coli* inactivation. The beads were durable enough as only 11% reduction in the photoactivity of the catalyst was found even after 30 runs. Thus proved its ability in terms of the potential use of waste materials as a promising concept for post-treatment of wastewater, which can find successful field-scale applications too.

Author contributions

Conception and design of the study: A. Verma, I. Thakur. Experimentation: I. Thakur. Analysis/Interpretation of Data: I. Thakur. Drafting the Manuscript: I. Thakur, A. Verma, B. Örmeci. Revising the manuscript critically for important intellectual content: A. Verma, B. Örmeci.

Declaration of Competing Interest

The authors declare that they have no known competing financial interests or personal relationships that could have appeared to influence the work reported in this paper.

Acknowledgment

The authors would like to thank the central instrumentation laboratory and sophisticated analytical instrumentation facility, Punjab University, Chandigarh, India for providing their facilities for the characterization of samples.

Funding

This research did not receive any specific grant from funding agencies in the public, commercial, or not-for-profit sectors.

References

[1] M.A.R. Cardenas, I. Ali, F.Y. Lai, L. Dawes, R. Thier, J. Rajapakse, Removal of micropollutants through a biological wastewater treatment plant in a subtropical climate, Queensland-Australia, J. Environ. Heal. Sci. Eng. 14 (2016) 1–10, https://doi.org/10.1186/s40201-016-0257-8.

[2] A.C. Mecha, M.S. Onyango, A. Ochieng, M.N.B. Momba, Evaluation of synergy and bacterial regrowth in photocatalytic ozonation disinfection of municipal wastewater, Sci. Total Environ. 601–602 (2017) 626–635, https://doi.org/10.1016/j.scitotenv.2017.05.204.

[3] P. Bansal, A. Verma, Novel Fe-TiO2composite driven dual effect for reduction in treatment time of pentoxifylline: Slurry to immobilized approach, Mater. Des. 125 (2017) 135–145, https://doi.org/10.1016/j.matdes.2017.03.083.

[4] X. Li, X. Jin, N. Zhao, I. Angelidaki, Y. Zhang, Novel bio-electro-Fenton technology for azo dye wastewater treatment using microbial reverse-electrodialysis electrolysis cell (2017) 322–329. https://doi.org/doi.org/10.1016/j.biortech.2016.12.114.

[5] L.T. Arayan, A.W.B. Reyes, H.T. Hop, H.T. Xuan, E.J. Baek, H.S. Yang, H.H. Chang, S. Kim, Antimicrobial effect of different concentrations of ozonated water in the sanitation of water experimentally inoculated with Escherichia coli, J. Prev. Vet. Med. 41 (2017) 84–87, https://doi.org/10.13041/jpvm.2017.41.2.84.

[6] A.B.V. Camel, The use of ozone and associated oxidation process in drinking water treatment, Water Res. 32 (1998) 3208–3222.

[7] A.C. Mecha, M.S. Onyango, A. Ochieng, M.N.B. Momba, UV and solar photocatalytic disinfection of municipal wastewater: inactivation, reactivation and regrowth of bacterial pathogens, Int. J. Environ. Sci. Technol. (2018), https://doi.org/10.1007/s13762-018-1950-1.

[8] G.Q. Li, W.L. Wang, Z.Y. Huo, Y. Lu, H.Y. Hu, Comparison of UV-LED and low pressure UV for water disinfection: Photoreactivation and dark repair of Escherichia coli, Water Res. 126 (2017) 134–143, https://doi.org/10.1016/j.watres.2017.09.030.

[9] Q. Shen, J. Zhu, L. Cheng, J. Zhang, Z. Zhang, X. Xu, Enhanced algae removal by drinking water treatment of chlorination coupled with coagulation, Desalination 271 (2011) 236–240, https://doi.org/10.1016/j.desal.2010.12.039.

[10] D. Ghernaout, Coagulation and Chlorination of NOM and Algae in Water Treatment: A Review, Int. J. Environ. Monit. Anal. 2 (2014) 23, https://doi.org/10.11648/j.ijema.s.2014020601.14.

[11] M. Koivusalo, T. Vartiainen, Drinking Water Chlorination By-Products And Cancer 12 (1997) 81–90.

[12] N. Daels, S. De Vrieze, I. Sampers, B. Decostere, P. Westbroek, A. Dumoulin, P. Dejans, K. De Clerck, S.W.H. Van Hulle, Potential of a functionalised nanofibre microfiltration membrane as an antibacterial water filter, Desalination 275 (2011) 285–290, https://doi.org/10.1016/j.desal.2011.03.012.

[13] S.D.R. Nithila, B. Anandkumar, S.C. Vanithakumari, R.P. George, U.K. Mudali, R. K. Dayal, Studies to control biofilm formation by coupling ultrasonication of natural waters and anodization of titanium, Ultrason. Sonochem. 21 (2014) 189–199, https://doi.org/10.1016/j.ultsonch.2013.06.010.

[14] Z. Dong, Z. Qin, Experimental Study of Pathogenic Microorganisms Inactivated by Venturi-Type Hydrodynamic Cavitation with Different Throat Lengths, J. Civ. Eng. Forum. 4 (2018) 209, https://doi.org/10.22146/jcef.38756.

[15] G. Cossali, E.J. Routledge, M.S. Ratcliffe, H. Blakes, J.E. Fielder, T.G. Karayiannis, Inactivation of *E. coli*, Legionella, and Pseudomonas in Tap Water Using Electrochemical Disinfection, J. Environ. Eng. 142 (2016) 04016063, https://doi.org/10.1061/(asce)ee.1943-7870.0001134.

[16] G. Rao, K.S. Brastad, Q. Zhang, R. Robinson, Z. He, Y. Li, Enhanced disinfection of Escherichia coli and bacteriophage MS2 in water using a copper and silver loaded titanium dioxide nanowire membrane, Front. Environ. Sci. Eng. 10 (2016), https://doi.org/10.1007/s11783-016-0854-x.

[17] H. Mamane, H. Shemer, K.G. Linden, Inactivation of E. coli, B. subtilis spores, and MS2, T4, and T7 phage using UV/H2O2 advanced oxidation, J. Hazard. Mater. 146 (2007) 479–486. https://doi.org/10.1016/j.jhazmat.2007.04.050.

[18] P. Sun, C. Tyree, C.H. Huang, Inactivation of Escherichia coli, Bacteriophage MS2, and Bacillus Spores under UV/H2O2 and UV/Peroxydisulfate Advanced Disinfection Conditions, Environ. Sci. Technol. 50 (2016) 4448–4458, https://doi.org/10.1021/acs.est.5b06097.

[19] A.C. Mecha, M.S. Onyango, A. Ochieng, M.N.B. Momba, UV and solar photocatalytic disinfection of municipal wastewater: inactivation, reactivation and regrowth of bacterial pathogens, Int. J. Environ. Sci. Technol. 16 (2018) 3687–3696, https://doi.org/10.1007/s13762-018-1950-1.

[20] C. Sordo, R. Van Grieken, J. Marugán, P. Fernández-Ibáñez, Solar photocatalytic disinfection with immobilised TiO2 at pilot-plant scale, Water Sci. Technol. 61 (2010) 507–512, https://doi.org/10.2166/wst.2010.876.

[21] P. Bansal, A. Verma, Pilot-scale single-step reactor combining photocatalysis and photo-Fenton aiming at faster removal of Cephalexin, J. Clean. Prod. 195 (2018) 540–551, https://doi.org/10.1016/j.jclepro.2018.05.219.

[22] D. Spuhler, J. Andrés Rengifo-Herrera, C. Pulgarin, The effect of Fe2+, Fe3+, H2O2 and the photo-Fenton reagent at near neutral pH on the solar disinfection (SODIS) at low temperatures of water containing Escherichia coli K12, Appl. Catal. B Environ. 96 (2010) 126–141, https://doi.org/10.1016/j.apcatb.2010.02.010.

[23] S. Giannakis, M. Voumard, D. Grandjean, A. Magnet, L.F. De Alencastro, C. Pulgarin, Micropollutant degradation, bacterial inactivation and regrowth risk in wastewater effluents: Influence of the secondary (pre)treatment on the efficiency of Advanced Oxidation Processes, Water Res. 102 (2016) 505–515, https://doi.org/10.1016/j.watres.2016.06.066.

[24] A. Chemistry, S. We, Photoelectrochemical sterilization of microbial cells by semiconductor powders 29 (1985) 211–214.

[25] S.K. Kassahun, Z. Kiflie, D.W. Shin, S.S. Park, Y.R. Chung, Novel multistage fixed-bed photoreactor for bacterial inactivation using N-doped TiO2 nanoparticles under vis-LEDs and sunlight illumination, Nanotechnol. Environ. Eng. 3 (2018), https://doi.org/10.1007/s41204-017-0032-9.

[26] C. Adán, J. Marugán, S. Mesones, C. Casado, R. van Grieken, Bacterial inactivation and degradation of organic molecules by titanium dioxide supported on porous stainless steel photocatalytic membranes, Chem. Eng. J. 318 (2017) 29–38, https://doi.org/10.1016/j.cej.2016.04.091.

[27] M.S. Lucas, J.A. Peres, Decolorization of the azo dye Reactive Black 5 by Fenton and photo-Fenton oxidation, Dye. Pigment. 71 (2006) 236–244, https://doi.org/10.1016/j.dyepig.2005.07.007.

[28] M.I. Polo-López, M. Castro-Alférez, I. Oller, P. Fernández-Ibáñez, Assessment of solar photo-Fenton, photocatalysis, and H2O2 for removal of phytopathogen fungi spores in synthetic and real effluents of urban wastewater, Chem. Eng. J. 257 (2014) 122–130, https://doi.org/10.1016/j.cej.2014.07.016.

[29] E.D.C. Severo, C.G. Anchieta, V.S. Foletto, R.C. Kuhn, G.C. Collazzo, M.A. Mazutti, E.L. Foletto, Degradation of Amaranth azo dye in water by heterogeneous photo-Fenton process using FeWO4 catalyst prepared by microwave irradiation, Water Sci. Technol. 73 (2016) 88–94, https://doi.org/10.2166/wst.2015.469.

[30] W. Zhang, Y. Chen, S. Yu, S. Chen, Y. Yin, Preparation and antibacterial behavior of Fe 3 + -doped nanostructured TiO 2 thin films, 516 (2008) 4690–4694. https://doi.org/10.1016/j.tsf.2007.08.053.

[31] I. Thakur, B. Örmeci, A. Verma, Inactivation of E. coli in water employing Fe-TiO2 composite incorporating in-situ dual process of photocatalysis and photo-Fenton in fixed-mode, J. Water Process Eng. 33 (2020) 101085. https://doi.org/10.1016/j.jwpe.2019.101085.

[32] S. Talwar, V.K. Sangal, A.K. Verma, In-situ dual effect of novel Fe-TiO2 composite for the degradation of phenazone, Sep. Purif. Technol. 211 (2019) 391–400, https://doi.org/10.1016/j.seppur.2018.10.007.

[33] P. Bansal, A. Verma, S. Talwar, Detoxification of real pharmaceutical wastewater by integrating photocatalysis and photo-Fenton in fixed-mode, Chem. Eng. J. 349 (2018) 838–848, https://doi.org/10.1016/j.cej.2018.05.140.

[34] J. Rodríguez-Chueca, M.P. Ormad, R. Mosteo, S. Canalis, J.L. Ovelleiro, Escherichia coli Inactivation in Fresh Water Through Photocatalysis with TiO2-Effect of H2O2 on Disinfection Kinetics, Clean - Soil, Air, Water. 44 (2016) 515–524, https://doi.org/10.1002/clen.201500083.

[35] P.V. Laxma Reddy, B. Kavitha, P.A. Kumar Reddy, K.H. Kim, TiO2-based photocatalytic disinfection of microbes in aqueous media: A review, Environ. Res. 154 (2017) 296–303, https://doi.org/10.1016/j.envres.2017.01.018.

[36] S. Giannakis, M. Voumard, S. Rtimi, C. Pulgarin, Bacterial disinfection by the photo-Fenton process: Extracellular oxidation or intracellular photo-catalysis? Appl. Catal. B Environ. 227 (2018) 285–295, https://doi.org/10.1016/j.apcatb.2018.01.044.

[37] R. Mosteo, A. Varon Lopez, D. Muzard, N. Benitez, S. Giannakis, C. Pulgarin, Visible light plays a significant role during bacterial inactivation by the photo-fenton process, even at sub-critical light intensities, Water Res. 174 (2020), 115636, https://doi.org/10.1016/j.watres.2020.115636.

[38] S. Shekoohiyan, S. Rtimi, G. Moussavi, S. Giannakis, C. Pulgarin, Enhancing solar disinfection of water in PET bottles by optimized in-situ formation of iron oxide films. From heterogeneous to homogeneous action modes with H2O2 vs. O2 – Part 1: Iron salts as oxide precursors, Chem. Eng. J. 358 (2019) 211–224, https://doi.org/10.1016/j.cej.2018.09.219.

[39] S. Giannakis, Analogies and differences among bacterial and viral disinfection by the photo-Fenton process at neutral pH: a mini review, Environ. Sci. Pollut. Res. 25 (2018) 27676–27692, https://doi.org/10.1007/s11356-017-0926-x.

[40] L.C. Seaver, J.A. Imlay, P. Loewen, Alkyl Hydroperoxide Reductase Is the Primary Scavenger of Endogenous Hydrogen Peroxide in Escherichia coli Downloaded from http://jb.asm.org/ on November 24, 2014 by Univ of California-Berkeley Biosci & Natural Res Lib, J Bacteriol. 183 (2001) 7173–7181. https://doi.org/10.1128/JB.183.24.7173.

[41] L. Demarchis, M. Minella, R. Nisticò, V. Maurino, C. Minero, D. Vione, Photo-Fenton reaction in the presence of morphologically controlled hematite as iron source, J. Photochem. Photobiol. A Chem. 307–308 (2015) 99–107, https://doi.org/10.1016/j.jphotochem.2015.04.009.

[42] C. Adán, A. Magnet, S. Fenoy, C. Pablos, C. del Águila, J. Marugán, Concomitant inactivation of Acanthamoeba spp. and Escherichia coli using suspended and immobilized TiO2, Water Res. 144 (2018) 512–521, https://doi.org/10.1016/j.watres.2018.07.060.

[43] X. Kang, S. Liu, Z. Dai, Y. He, X. Song, Z. Tan, Titanium dioxide: From engineering to applications, 2019. https://doi.org/10.3390/catal9020191.

[44] S. Pigeot-Rémy, F. Simonet, E. Errazuriz-Cerda, J.C. Lazzaroni, D. Atlan, C. Guillard, Photocatalysis and disinfection of water: Identification of potential bacterial targets, Appl. Catal. B Environ. 104 (2011) 390–398, https://doi.org/10.1016/j.apcatb.2011.03.001.

[45] Z.X. Lu, L. Zhou, Z.L. Zhang, W.L. Shi, Z.X. Xie, H.Y. Xie, D.W. Pang, P. Shen, Cell Damage Induced by Photocatalysis of TiO2 Thin Films, Langmuir 19 (2003) 8765–8768, https://doi.org/10.1021/la034807r.

[46] F. Collin, Chemical basis of reactive oxygen species reactivity and involvement in neurodegenerative diseases, Int. J. Mol. Sci. 20 (2019), https://doi.org/10.3390/ijms20102407.

[47] Z. Hseu, Evaluating heavy metal contents in nine composts using four digestion methods, 95 (2004) 53–59. https://doi.org/10.1016/j.biortech.2004.02.008.

[48] S. Giannakis, M. Inmaculada, P. López, D. Spuhler, J. Antonio, S. Pérez, P. Fernández, Applied Catalysis B: Environmental Solar disinfection is an augmentable, in situ -generated photo-Fenton reaction—Part 1: A review of the

mechanisms and the fundamental aspects of the process, 199 (2016) 199–223. https://doi.org/10.1016/j.apcatb.2016.06.009.

[49] P. Bansal, A. Verma, In-situ dual effect studies using novel Fe-TiO2 composite for the pilot-plant degradation of pentoxifylline, Chem. Eng. J. 332 (2018) 682–694, https://doi.org/10.1016/j.cej.2017.09.121.

[50] A.A. Isari, F. Hayati, B. Kakavandi, M. Rostami, M. Motevassel, E. Dehghanifard, N, Cu co-doped TiO2@functionalized SWCNT photocatalyst coupled with ultrasound and visible-light: An effective sono-photocatalysis process for pharmaceutical wastewaters treatment, Chem. Eng. J. 392 (2020), 123685, https://doi.org/10.1016/j.cej.2019.123685.

I&EC research
Industrial & Engineering Chemistry Research

pubs.acs.org/IECR

Article

Fe−TiO_2 Composite Mediated the Hybrid Effect of Photocatalysis and Photo-Fenton for the Inactivation of *Escherichia coli* Using a Continuous Flow Recirculation Reactor

Ina Thakur, Anoop Verma,* and Banu Örmeci

Cite This: https://doi.org/10.1021/acs.iecr.1c00628

Read Online

ACCESS | Metrics & More | Article Recommendations | Supporting Information

ABSTRACT: To reduce the harmful effects of bacteria, the low-cost and visibly active Fe−TiO_2 composite was prepared to remove *Escherichia coli* from water using a continuous recirculating reactor. The performance of the hybrid process (Fe−TiO_2) was evaluated in terms of reaction rate constant, quantum yield, and some other operating parameters. This hybrid process showed a significant increase in reaction rate constant and quantum yield (0.065 min^{-1} and 0.077 × 10^{-15} cells/photons, respectively) compared to photo-Fenton (0.029 min^{-1} and 7.57 × 10^{-15} cells/photons, respectively) and photocatalysis (0.025 min^{-1} and 11.96 × 10^{-15} cells/photons, respectively) in 150 min treatment time. The *p*-value was less than 0.0001, and the *F*-value was greater than 5 for each process. The optimized values of the operating parameters were found to be 3.4, 62 mg L^{-1}, 106 mL min^{-1} for the reaction pH, H_2O_2 concentration, and flow rate, respectively. With these optimum conditions, a percentage reduction of *E. coli* of 93% was observed. The Fe−TiO_2 composites exhibited high stability under continuous flow conditions, demonstrating their long-term durability. The results of this study demonstrate the potential of waste materials as a promising concept for the post-treatment of wastewater that can be successfully applied in real life.

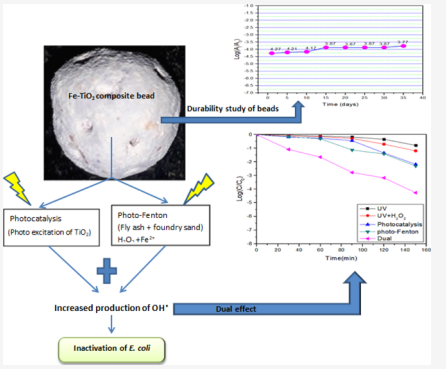

Downloaded via Anoop Verma on May 12, 2021 at 06:25:44 (UTC).
See https://pubs.acs.org/sharingguidelines for options on how to legitimately share published articles.

1. INTRODUCTION

Effective sanitation and availability of safe drinking water are serious concerns in developing countries. So far, various conventional and chemical methods such as chloramination and chlorination have both resulted in inadequacies and posed a serious threat to the receiving waters as these methods generate chlorine-substituted byproducts.[1,2] One of the studies[3] reported that prolonged consumption of even the small concentrations of such byproducts [haloacetic acid (60 ppb) and trihalomethanes (80 ppb)] can lead to chronic heart failure in the human body. Algal growth in water can occur due to poor handling of ammonia during chloramination by direct nitrification.[4] This has prompted scientists to look for some chemical-free technologies to avoid the formation of by-products.

Recent studies on the inactivation of *Escherichia coli* have been focused on the development of advanced technologies such as electrochemical oxidation,[5,6] ozonation,[7,8] ultra-sonication,[9,10] microfiltration,[11] OH radical-based advanced oxidation processes (AOPs) (chemical-free technology),[12,13] and so forth, which have certainly provided the desired results for the treatment of wastewater.[14] However, when it comes to the treatment of real wastewater, the advanced oxidation processes have proved to be incompetent due to their commercial viability. The main obstacles in the application of AOPs at the field scale are prolonged reaction time, the design of the reactor for scale-up studies, the increase in the energy costs, the separation of the catalyst after the completion of the reaction, and the light source.[15,16] Among the AOPs, the well-established photo-Fenton process (Fe^{2+}/Fe^{3+} + hydrogen peroxide)[17−19] and TiO_2 photocatalysis[20−23] have found their place in the literature for the treatment of a wide range of chemical contaminants and disinfection of pathogens. Matsunaga et al.[24] were the first to investigate the use of semiconductor powders in the presence of UV light for cell damage. Since then, various basic TiO_2-photocatalytic and photo-Fenton disinfection studies have been conducted to effectively inactivate different coliforms, fungi, viruses, algae, and bacteria[25−29] by increasing the external production of OH radicals and causing the internal imbalance of reactive oxygen species (ROS).[30,31] However, these processes have operational problems such as iron sludge formation in the photo-Fenton process and electron−hole recombination and catalyst separation in slurry photocatalysis.

Received: February 11, 2021
Revised: April 28, 2021
Accepted: May 2, 2021

© XXXX American Chemical Society

In recent years, research has focused on the treatment of water with fixed-bed reactors in which a catalyst is coated on the surface of a support material.[21,32−34] In one of the studies,[21] N-doped TiO_2 immobilized on glass beads was used to study the *E. coli* (*E. coli*) inactivation in a multistage fixed-bed reactor and the results showed that photocatalysis in the fixed mode is effective enough in reducing the concentration of bacteria present in water. In another study,[35] the photocatalytic-microfiltration technique with the TiO_2 catalyst coated over porous steel was used and showed good efficiency for *E. coli* inactivation. However, this technique in the fixed form still faces some challenges such as intactness of the catalyst over the support material, mass transfer limitation, and reduction in treatment efficiency. Moreover, in photocatalysis, electron−hole recombination remains a problem in improving the kinetic reaction rate. All these operational drawbacks have restricted the applications of AOPs for scale-up studies.

Recent studies have introduced the concept of the hybrid process, where two technologies are coupled to overcome the drawbacks of each processes.[36] However, cost efficiency and certain other inputs can be visualized before actual field scale-up. In the present study, a robust system is proposed using an in situ fixed-bed process for the disinfection of water contaminated with *E. coli*. This study uses foundry sand (FS) and fly ash (FA) (as the iron source) incorporated with clay (support material) and TiO_2 coating (over the support material), which facilitates the coupling of the two processes.[37] The FA and FS are a good mixture of unburned silica, carbon, and metal oxides with aluminum and iron, leading to the hypothesis that these waste materials can be used for wastewater treatment.[38] According to recent research, FA and FS can be used in advanced wastewater treatment technologies such as photo-Fenton as oxides of aluminum and iron can serve as the in situ Fenton system.[39] The surface-active TiO_2 layer contributes to photocatalysis, while iron lixiviation from the support leads to photo-Fenton in the presence of H_2O_2.[40] This process also solves the problem of e^-h^+ recombination in TiO_2 photocatalysis. Since the e^- in the conduction band (e_{CB}^-) performed during TiO_2 photocatalysis reacts with Fe^{3+} ions lixiviated from the composite beads and converts to Fe^{2+},[37] this Fe^{2+} ion now reacts with H_2O_2, leading to the photo-Fenton process. Thus, a hybrid effect is presented in the system.

The main innovation of this technology is that unlike other studies mentioned in the literature,[41,42] this study has a natural dopant. The waste iron that is used for the fabrication of composite beads (for the photo-Fenton process) acts as a natural dopant. The iron present on the surface of the composite reduces the band gap of the catalyst over time and also makes it active in the visible region, as explained in Section 3. This makes the present technology cost-effective as no investments have been made to dope the catalyst. Another innovative component of this technology is that one process supports the other by suppressing the disadvantages of the other. This hybrid process increases the efficiency of the reaction by increasing the rate of reaction, which in turn improves the treatment and disinfection performance. Moreover, the systematic lixiviation of the iron from the inert beads (photo-Fenton) does not lead to the formation of iron sludge. Also, the utilization of FS together with FA increases the compressive strength and binding capacity of supports apart from augmenting the concentration of iron.[43] At the same time, the use of waste materials confirms the economy of the process. With the advantage of no sludge formation and continuous availability of OH radicals, the coupled process has shown satisfactory results in terms of efficiency and synergy as reported in the literature for the treatment of wastewater.[44,45] However, an optimal wastewater treatment system includes both degradation and disinfection processes. Given the limited literature on disinfection of *E. coli* using a coupled photo-Fenton and TiO_2-photocatalytic process, the present study investigates the disinfection of water with *E. coli* using the in situ hybrid technique. The performance of the intended in situ hybrid process is evaluated in terms of increasing efficiency by reducing the treatment time. In addition, parametric evaluation for H_2O_2 concentration, flow rate, pH, and reaction time during treatment is studied. The optimization of these different parameters is also carried out using the techniques Box−Behnken design (BBD) and response surface methodology (RSM). Finally, the reusability and stability of the Fe−TiO_2 composite were further investigated to show the possibility of practical application. The results of this study indicate the potential use of waste materials as a promising concept for wastewater post-treatment that can be successfully applied in real life. To the best of the author's knowledge, this is the first study to report on a fixed-bed in situ hybrid process for inactivation of *E. coli* (*E. coli*) using a recirculating reactor.

2. MATERIALS AND METHODS

2.1. Reagents and Chemicals. The TiO_2 catalyst was supplied by Degussa, Frankfurt (Germany). Clay, FS, and FA were procured locally from a vendor, Patiala, Punjab (India). To control the pH of the reaction, acetate buffer solution was made from sodium acetate and acetic acid, which were obtained from Loba Chemical Pvt Ltd (India). 99.5% of NaCl was purchased from SD Fine-Chem, Ambala, Haryana (India). Agar−agar, type I, and Luria Bertani (LB) broth for the growth of *E. coli* were bought from Himedia Laboratories, Nasik, Maharashtra (India). The concentration of iron was determined by the colorimetry method by determining the colored complex of Fe^{2+} and 1,10-phenanthroline spectrophotometrically at 510 nm. All the solutions were prepared from double-distilled water. All the associated chemicals related to this study are bought from Ranbaxy, Gurugram (India).

2.2. Preparations of Iron Composite Beads Using Waste FS and FA and Catalyst Immobilization. The spherical composite beads were prepared from the inert support material using clay mixed with foundry waste sand FS and FA in a ratio of 2:1:1 and kept at room temperature for drying. The beads were then heated at 800 °C in a muffle furnace for 2 h. The strength and durability of the inert material were increased by immersion in water for 48 h, which is also known as curing. The average diameter of the beads was 10 mm, which was measured with a screw gauge by randomly selecting from 100 beads. Then, a 1% (w/v) TiO_2 solution was prepared in distilled water and sonicated to disperse the TiO_2 particles. The beads were coated with the TiO_2 catalyst using the dip-coating method,[46] and this process was repeated two times to get proper coverage of the beads with the TiO_2 solution. For proper bonding of the TiO_2 on the surface of the composite beads, they were heated at a high temperature of 350 °C for 1.5 h in a muffle furnace and then cooled to room temperature. The standard thickness of the coating over the beads was observed to be 71 μm as mentioned in our previous study.[47] These beads were referred to as Fe−TiO_2 composite beads.

https://doi.org/10.1021/acs.iecr.1c00628
Ind. Eng. Chem. Res. XXXX, XXX, XXX−XXX

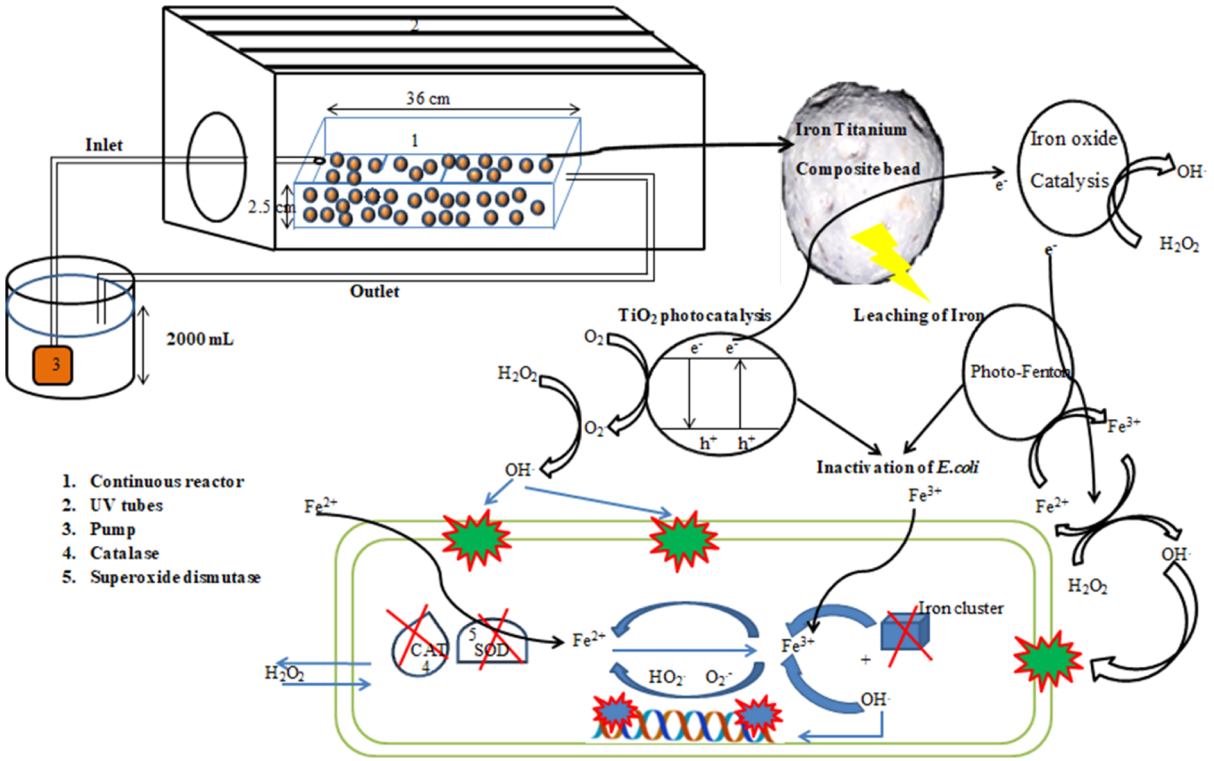

Figure 1. Schematic diagram of *E. coli* inactivation.

2.3. Preparation and Enumeration of *E. coli*. Wild-type *E. coli* K12 purchased from MTCC, no. 1302, Chandigarh, India, was used as an indicator organism to study the inactivation efficiency of the in situ hybrid process. LB broth was used for bacterial growth by dissolving it in distilled water after autoclaving and incubating at 37 °C with stirring at 180 rpm in a shaking incubator. Furthermore, a 1% v/v dilution was made in distilled water and again incubated at 37 °C at 180 rpm for 24 h. To obtain the pure bacterial palette, the cells were harvested by centrifugation at 5000 rpm for 15 min at 4 °C during the stationary phase. After centrifugation, the bacterial pellet was rinsed three times with a saline solution of 0.8% NaCl. This procedure resulted in a bacterial concentration of 10^9 cfu mL^{-1}. Bacterial colonies were enumerated by the pour plating method using 9 cm Petri plates into which LB and type I agar were poured. For each experiment, at least 1.5 mL of the treated aliquot was withdrawn from the glass reactor and stored in a refrigerator set at 4 °C until plating. A serial dilution of 10^{-1} to 10^{-5} was made, and 0.1 mL of the sample was plated onto the Petri dish. Then, these plates were incubated at 37 °C in an incubator. All samples were plated out in triplets. After 24 h of incubation, colonies were visually identified and counted. This initial concentration of *E. coli* was maintained throughout the study. The initial and final counts of *E. coli* in the working solution were determined by plating on the agar plate in the laminar flow chamber before the start and at the end of the experiment. The UV chamber and laminar chamber were fumigated once a week to maintain quality and sterile conditions in the chamber. The growth and sterility tests were performed before each experiment. Agar plates used for plating out *E. coli* were incubated at 37 °C for 24 h to ensure no growth or contamination. A standard plate counting method was used for this purpose. The inactivation efficiency of the dual process was calculated by a percentage reduction of *E. coli* (% *R*) as shown in eq 1.

$$R\ (\%) = \frac{C_0 - C}{C_0} \times 100 \tag{1}$$

2.4. Characterization. Fe−TiO_2 composite beads (fresh and recycled) were characterized using different technologies to confirm the existence of Fe and TiO_2 as catalysts. The elemental structure of the fresh and recycled beads was analyzed by energy-dispersive X-ray spectroscopy (EDS), Oxford Instruments INCAX-act (United Kingdom). Scanning electron microscopy (SEM), JSM-6510LV, JEOL (Japan), was used to study the surface morphology of the fresh and recycled beads. X-ray diffraction (XRD) analysis with a Cu Kα wavelength (λ) of 1.5405 in the range of 2θ = 20−80° was performed to identify and quantify the morphology of the crystalline phases of the composite beads. The UV-DRS spectrophotometer (UV-DRS) UV-2600 (Shimadzu, Asia Pacific) was used to determine the band gap energy of the composite beads in the range of 200−800 nm. Fourier transform infrared spectroscopy (FTIR) was also used to study the surface of the catalyst, and spectra were recorded using KBr pellets between 4000 and 200 cm^{-1} wavenumber.

2.5. Experimental Setup. A nonconcentrating flatbed reactor of rectangular shape (36 cm × 16 cm × 2.5 cm) made of glass was used to check the inactivation of *E. coli*. This reactor was provided with one inlet and one outlet and had removable baffles (6.5 cm × 2.5 cm × 0.6 cm), as shown in Figure 1. This reactor served as a recirculation chamber and was used to treat up to 2000 mL of the synthetic sample. This reactor was located in a rectangular wooden chamber with seven Philips UV tubes of 36 W and 365 nm wavelength placed under the UV chamber. The glass recirculating reactor was placed inside the chamber on an iron jack. The average

https://doi.org/10.1021/acs.iecr.1c00628
Ind. Eng. Chem. Res. XXXX, XXX, XXX−XXX

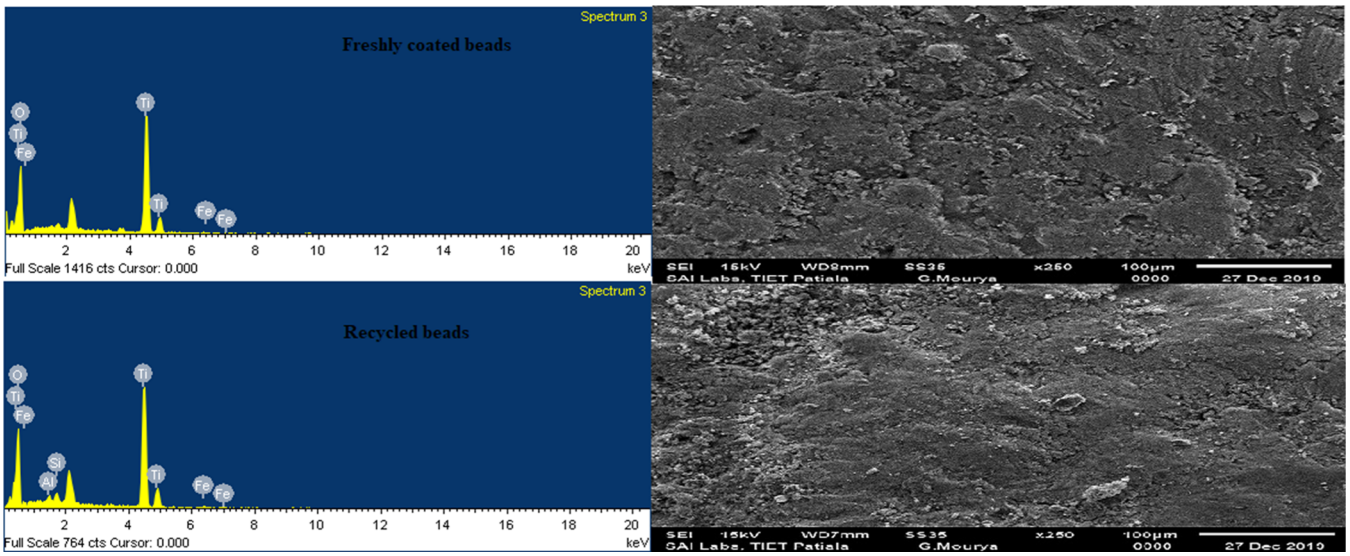

Figure 2. SEM/EDS images of fresh and recycled beads.

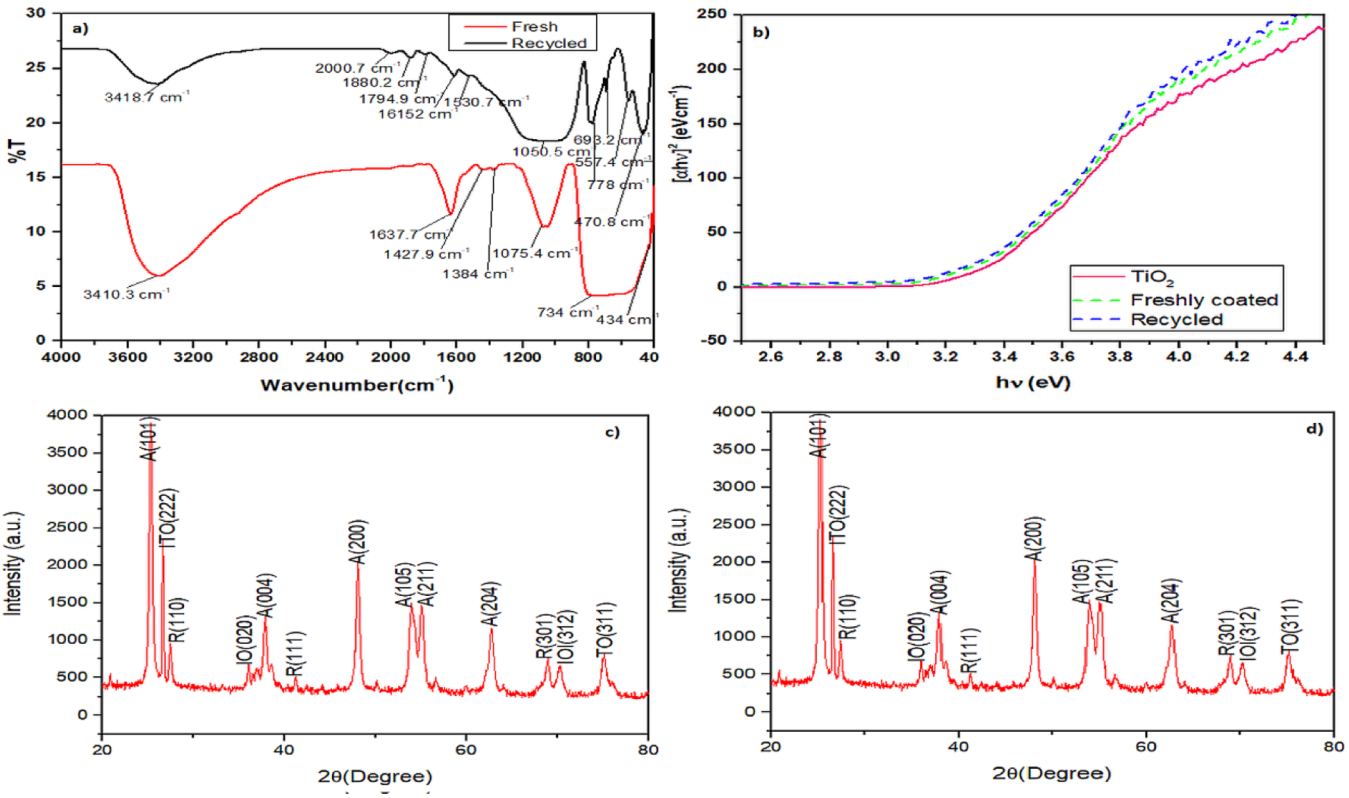

Figure 3. (a) FTIR pattern of fresh and recycled beads. (b) DRS images of fresh and recycled beads. (c,d) XRD peaks of fresh and recycled beads.

intensity supplied to the system was 25 W m^{-2}, and the intensity was recorded using a radiometer (Eppley, 33013). Distilled water (2000 mL) spiked with an *E. coli* concentration of 10^6 cfu mL^{-1} was stirred on a magnetic stirrer for 20 min for acclimation. The feed tank containing 2000 mL of the synthetic sample was connected to the inlet of the recirculating reactor, from where the sample was transferred to the glass reactor with the help of the pump. The reactor was aerated (3 L min^{-1}) with the help of two spargers kept at an equal distance from the center to maintain the homogeneity of the reaction. The pH of the reaction was maintained using an acetate buffer solution. In this study, the pH of the reaction was varied only in the acidic range, that is, 3−6. The reason is that the leaching (lixiviating) of iron occurs only under acidic conditions. Moreover, this study is a combination of TiO_2 photocatalysis and the photo-Fenton process (this photo-Fenton process needs iron to generate OH radicals). Then, the dual effect of this technology was studied as shown in the scheme in Figure 1.

In order to investigate the significance of the dual technique over the individual techniques (TiO_2-photocatalytic and photo-Fenton process), kinetic studies play a vital role to investigate the change in *E. coli* number before and after inactivation. The kinetics of water decontamination was

https://doi.org/10.1021/acs.iecr.1c00628
Ind. Eng. Chem. Res. XXXX, XXX, XXX−XXX

studied for the hybrid effect using a pseudo-first-order model (eq 2), which yields a first-order rate constant for bacterial inactivation, as shown in eq 3.

$$\frac{-\mathrm{d}C}{\mathrm{d}t} = k_1 C \tag{2}$$

$$\ln \frac{C}{C_0} = kt \tag{3}$$

where the initial *E. coli* concentration is denoted by C_0 at time $t = 0$, *E. coli* concentration at "t" time is denoted by "C", and "k" is the pseudo-first-order rate constant (min^{-1}).

2.6. Experimental Design. RSM involves statistical techniques for correlating responses and factors dependent on multiple process variables to assemble an experimental model.[48] This technique has many advantages, such as understanding the interactions between different parameters, rapid and reliable data collection, and the consequent significant reduction in experimental runs, cost, and time.[49,50] Therefore, RSM has been successfully used in the optimization of various parameters for microbial inactivation.[14,51−53] The response surface procedure (RSM) is a commonly used numerical and statistical strategy to represent and analyze a procedure in which the response of interest is determined by various parameters, and this technique guides the advancement of the response.[48,54] The parameters that affect the procedure are referred to as independent variables, while the responses are referred to as dependent variables.[55] In this study, BBD is used under RSM to optimize the process parameters. Statistics Design-Expert 6.0.8 (Stat-Ease Incorporated, East Hennepin Ave, Minneapolis, United States) was used for the experimental design. The response variables were fitted by a second-order nonlinear regression model in the form of a quadratic polynomial equation, represented by eq 4.

$$R = \beta_0 + \sum_{i=1}^{k} \beta_i x_i + \sum_{i=1}^{k} \beta_{ii} x_i^2 + \sum_{i,j=1} \sum_{i<j} \beta_{ij} x_i x_j \tag{4}$$

3. RESULTS AND DISCUSSION

3.1. Characterization of the Fe−TiO_2 Composite. *3.1.1. SEM−EDS Analysis.* The elemental composition of the composite beads (both freshly coated and recycled) and the surface morphology were determined using EDS together with SEM, as shown in Figure 2. The EDS image of the catalyst (fresh beads) and recycled beads showed the prominent peaks of iron (Fe) and titanium oxide (TiO_2); this proves the presence of both iron and TiO_2 as catalysts in the dual technique. The presence of the iron element could be related to the combination of waste FA, FS, and clay that form the composite beads. SEM images for both freshly coated and recycled composite beads showed relatively smooth surfaces, confirming the existence of TiO_2 and its intactness even after recycling.

3.1.2. FTIR Analysis. Freshly coated and recycled Fe−TiO_2 beads were analyzed by FTIR to determine the chemical bonds formed, as shown in Figure 3a. The stretching of the H−O−H bond can be seen between the wavenumbers of 3418.7 and 1637.7 cm^{-1}. The O−H group was found at the wavenumbers of 3418.7 and 3410.3 cm^{-1} for freshly coated and recycled Fe−TiO_2 beads, respectively, and the stretching vibrations are the main reason for the appearance of this group.[56] The Ti−O−Ti bond in the range of 400−1200 cm^{-1} was observed in both freshly coated and recycled Fe−TiO_2 beads, confirming the presence of a TiO_2 lattice. Peaks at 434.8 and 470 cm^{-1} indicate the anatase phase of freshly coated and recycled Fe−TiO_2 beads, respectively. Similar results were also observed in the previous literature,[37] showing the anatase phase in the range of 400−600 cm^{-1} wavenumber due to the presence of vibrations generated by Ti−O−Ti. The Fe−O−Ti bonding was observed at 2000.7 cm^{-1} wavenumbers, proving the presence of Fe in the recycled Fe−TiO_2 beads. A similar peak of the Fe−O−Ti bond was also reported by Bansal and Duta[37] in the Fe−TiO_2 beads.

3.1.3. UV-DRS Analysis. The band gap energy for the catalytic beads before (fresh beads) and after recycling was scanned in the visible range of 200−800 nm, using $BiSO_4$ as the base compound. A decrease in the band gap energy of the composite beads compared to TiO_2 was observed, which is due to the presence of iron, as shown in Figure 3b. This shows the light-absorbing ability of the catalytic beads in the visible region. The absorption range of titanium dioxide was found at 418 nm and then shifted toward 440 and 455 nm before (fresh beads) and after recycling the catalytic beads, respectively. The band gap energy for the prepared catalytic beads was calculated according to the Tauc relation described in eq 5[57]

$$(\alpha \upsilon h)^{1/n} = K(h\upsilon - E_g) \tag{5}$$

where E_g denotes the energy band gap (eV), υ denotes the photon frequency (Hz), h denotes Planck's constant, and K is the proportionality constant. The energy band gap of TiO_2 was 3.1 eV and reduced to 2.9 eV for freshly coated and 2.8 eV for recycled composite beads.

3.1.4. XRD Analysis. XRD analysis of the freshly coated and the recycled Fe−TiO_2 beads was carried out to confirm the intactness of TiO_2 crystalline planes even after 35 times of recycling, as shown in Figure 3c,d. The appearance of different phases such as anatase (A) and rutile (R) in freshly coated and recycled Fe−TiO_2 beads proved the intactness of TiO_2 and its activity after 35 cycles. In addition to these two phases of TiO_2, titanium iron oxide (TIO) and iron oxide (IO) also appeared in the diffraction pattern and verified the presence of TiO_2 with Fe in the same unit. In Figure 3c,d, iron oxide peaks are seen to allow the entrapment of photoexcited electrons from the TiO_2 photocatalytic process, regenerating Fe^{2+}. Therefore, both technologies, that is, photo-Fenton and photocatalysis, occur simultaneously in one unit.

3.2. Experimental Studies. *3.2.1. Hypothesis of the Hybrid Process.* The main objective of the current study was to pursue the real applications of in situ hybrid concepts of Fe−TiO_2 composites in a fully fixed mode for the treatment of *E. coli* in water. This novel concept of composite beads tended to lixiviate iron in wastewater under acidic conditions, contributing to the photo-Fenton reaction accompanied by TiO_2 photocatalysis. Moreover, systematic lixiviation of iron in the reactor helps in preventing iron sludge formation via photoreduction of Fe^{3+} to Fe^{2+}. The involvement of e_{CB}^- in the photoreduction of Fe^{3+} to Fe^{2+} and utilization of H_2O_2 and UV light for the photoreduction of Fe^{3+} to Fe^{2+}, leading to increased production of OH radicals (prominence of the hybrid effect), can be understood by the following hypothesis: TiO_2 photocatalysis is a well-established technique (eqs 6−8) involving the role of e_{CB}^- and h_{VB}^+ in the production of oxidative radicals. At the same time, lixiviation of iron from the catalytic beads after reaction with H_2O_2 resulted in photo-

https://doi.org/10.1021/acs.iecr.1c00628
Ind. Eng. Chem. Res. XXXX, XXX, XXX−XXX

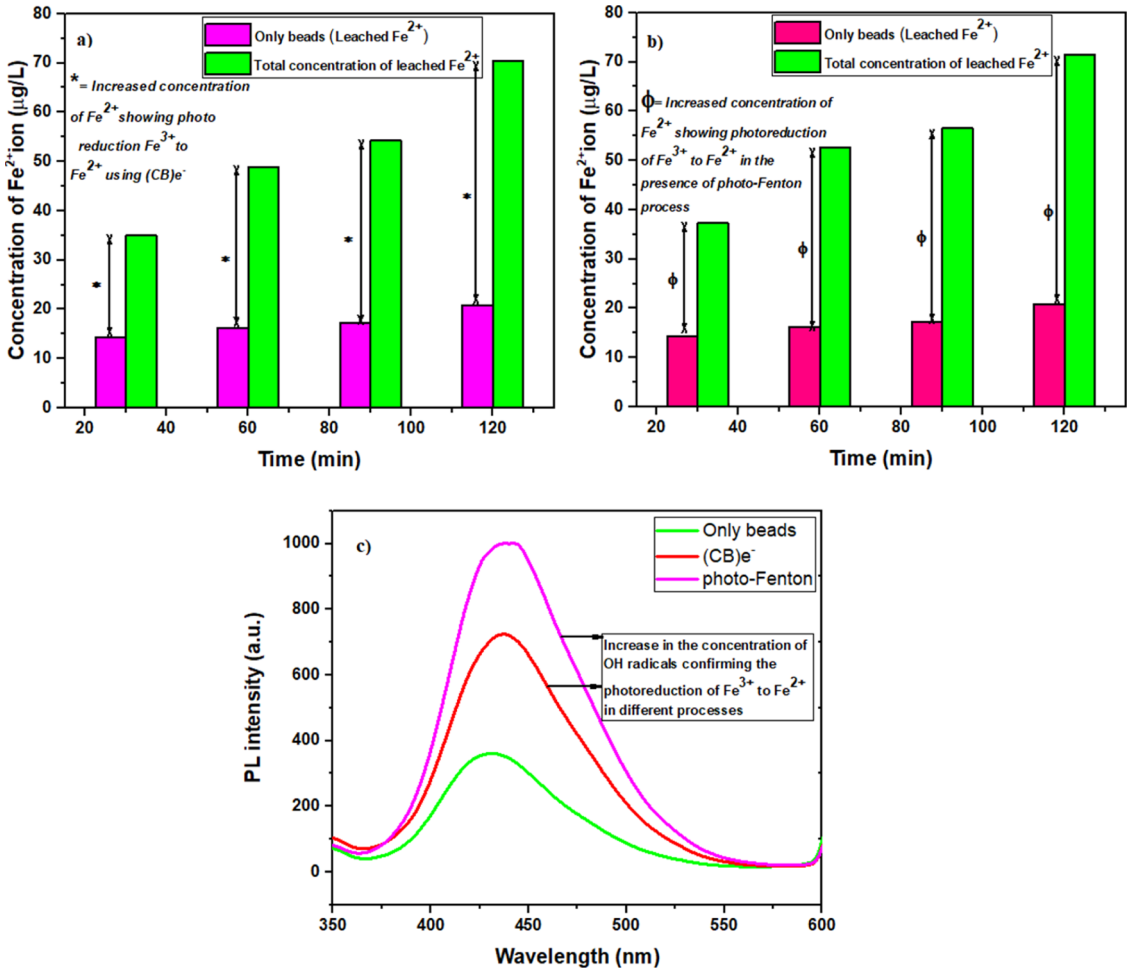

Figure 4. (a) Photoreduction of Fe^{3+} to Fe^{2+} using e_{CB}^-. (b) Photoreduction of Fe^{3+} to Fe^{2+} using the photo-Fenton process. (c) OH radical spectra using a fluorescence spectrophotometer.

Table 1. Estimated Quantum Yields of Different Processes for *E. coli* Inactivation in the Present Study

type of pollutant	volume (L)	initial count (cfu mL^{-1})	technique	light source	wavelength (nm)	time (min)	reaction rate constant (min−1)	log reduction	QY (cells/photons)
E. coli k-12	2	10^6	hybrid process	UV	365	150	0.065	>4 log	0.077×10^{-15}
E. coli k-12	2	10^6	photo-Fenton	UV	365	150	0.029	2.2	7.57×10^{-15}
E. coli k-12	2	10^6	photocatalysis	UV	365	150	0.025	2.3	11.96×10^{-15}

Fenton as shown in eqs 9−11 and showed a reduction of 4.3 log units (combined photocatalysis and photo-Fenton) in 150 min treatment time, as discussed in Section 3.2.2. The hybrid process reduces the e^-−h^+ recombination by combining the e_{CB}^- with Fe^{3+} to regenerate Fe^{2+}, as shown in eq 12. Moreover, the presence of H_2O_2 plays a dual role by reacting with the iron (photo-Fenton process, as mentioned above) and with the photocatalysis process, as shown in eq 13. Therefore, this process led to a higher production of OH radicals. Now, to verify the existence of a hybrid effect by the proposed mechanism, another set of tests was performed. First, the engagement of e_{CB}^- in the process of Fe^{3+} to Fe^{2+} photoreduction (eq 12) was cross-verified by performing the experiments with different time intervals, as shown in Figure 4a. Also, the effect of H_2O_2 and UV irradiation on the photoreduction of Fe^{3+} was verified by performing some experiments, as shown in Figure 4b. An increased concentration of Fe^{2+} was observed, which could be due to the photoreduction of Fe^{3+}. The theory of the extraction of e_{CB}^- from TiO_2 and the use of H_2O_2 for the reduction of Fe^{3+} to Fe^{2+} during the in situ hybrid process was verified with the excess amount of OH radicals produced (using the photoluminescence study), which helped in the disinfection of *E. coli* in water, as shown in Figure 4c. To quantify and verify the difference in inactivation kinetics between these three different processes (dual, photocatalysis, and photo-Fenton), we compared the constants of the inactivation rates of the three different processes; the results are shown in Table 1. The dual process showed a log reduction of 4.3 units with a rate constant of 0.065 min^{-1}. On the other hand, photo-Fenton and photocatalysis individually showed a reduction of 2.3 log units with a rate constant of 0.029 min^{-1} and a reduction of 2.2 log units with a rate constant of 0.025 min^{-1}, respectively. The rate constant for the dual process was found to be significantly higher than that of the photocatalytic and photo-Fenton processes. This is evident enough to prove the higher production of OH radicals in the hybrid process. As expected, the inactivation efficiency of the dual effect was about twice

https://doi.org/10.1021/acs.iecr.1c00628
Ind. Eng. Chem. Res. XXXX, XXX, XXX−XXX

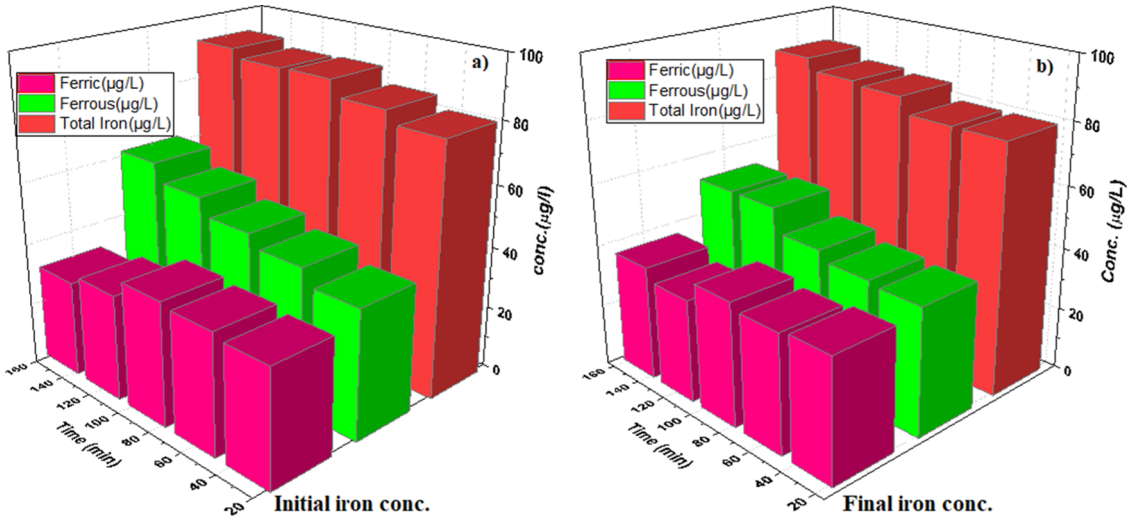

Figure 5. (a,b) Total iron concentration in the solution before and after recycling.

that of the photocatalytic and photo-Fenton processes individually. The presence of ferrous and ferric ions (required for the photo-Fenton process) lixiviated by the composite beads under acidic conditions was also estimated at regular intervals using the standard American Public Health Association (APHA) procedure (Discussion, 1999), as shown in Figure 5a,b, and SEM−EDS was performed to prove the integrity of the TiO_2 layer over the bead surface, as shown in Figure 2. Thus, these results proved the existence of an in situ dual effect, exhibiting both the active TiO_2 layer (led to photocatalysis) and iron lixiviation from the beads (led to photo-Fenton) with higher production of OH radicals. A one-sided ANOVA test was performed to determine the statistical significance of the means of the treated samples and found F values >5 and a p-value of <0.0001, making all results significant.

$$TiO_2 + \xrightarrow{uv} TiO_2(e^- + h^+) \quad (6)$$

$$e_{CB}^- + O_2 \rightarrow O_2^- \quad (7)$$

$$h_{(TiO_2)}^+ + H_2O_2 \rightarrow OH^\bullet + H^+ \quad (8)$$

$$Fe_{(aqueous)}^{2+} + H_2O_2 \rightarrow Fe_{(aqueous)}^{3+} + OH^\bullet + OH^- \quad (9)$$

$$Fe_{(aqueous)}^{3+} + H_2O_2 \rightarrow Fe_{(aqueous)}^{2+} + H_3O^+ + HO_2^- \quad (10)$$

$$Fe_{(aqueous)}^{3+} + H_2O \xrightarrow{uv} Fe_{(aqueous)}^{2+} + OH^\bullet + H^+ \quad (11)$$

$$Fe_{(aqueous)}^{3+} + e_{(CB)}^- + H_2O \rightarrow Fe_{(aqueous)}^{2+} + OH^\bullet + H^+ \quad (12)$$

$$e_{(CB)}^- + H_2O_2 \rightarrow OH^\bullet + OH^- \quad (13)$$

3.2.2. Performance Evaluation of the Catalyst. The main objective of this study was to determine the catalytic performance of the different processes (photo-Fenton, photocatalysis, and hybrid processes) in the fixed form in terms of light inactivation efficiency of *E. coli*. In order to compare the inactivation efficiency of the catalyst used in the three different methods, regardless of its appearance (shape and size) and irradiation conditions, the quantum yields (QY) were calculated according to eq 14. This yield illustrates the catalytic ability of these processes to inactivate *E. coli* when the same amount of UV irradiation was absorbed, and it can be measured as the ratio of the number of photo-inactivated cells divided by the number of absorbed photons.[58]

$$\text{quantum yield (QY)} = \frac{\text{decay rate (per second)}}{\text{photon flux (photon per second)}} \quad (14)$$

The QY of each of the processes used is shown in Table 1. The photon utilization efficiency of the applied photocatalysts was calculated. The QY values for the different processes used for the inactivation of *E. coli* in water varied from 0.077×10^{-15} to 11.96×10^{-15} cells/photons. Among all three photocatalytic processes, the highest QY value of 0.077×10^{-15} cells/photons was observed for the Fe−TiO_2 composite, as indicated in Table 1. The performance of these processes was also evaluated in terms of the difference in inactivation kinetics, the inactivation rate constant in the three different processes was compared, and the results are given in Table 1. The dual process showed a significantly higher rate constant of 0.065 min^{-1} compared to photo-Fenton and photocatalysis with 0.029 and 0.025 min^{-1} rate constants, respectively. This is evident enough to prove the effective performance of the hybrid process compared to others. As expected, the inactivation efficiency of the hybrid effect was about twice that of the individual photocatalytic and photo-Fenton processes.

The use of fixed-bed reactors or immobilization of the catalyst on a support material (as presented in the current study) eliminates the need for catalyst recovery after treatment. However, catalysts in suspension have been shown to be more efficient in terms of photocatalytic rate.[59] It is known that immobilized catalysts have less surface area compared to suspension systems, which reduces the treatment efficiency of the reactor. However, in the current study, the Fe−TiO_2 composite is spherical, which increases the surface area of the reactor and provides more surface area for bacterial inactivation. To evaluate the photon utilization efficiency of this study, the hybrid process was compared with previous literature, as shown in Table 2. The QY of the study was found

https://doi.org/10.1021/acs.iecr.1c00628
Ind. Eng. Chem. Res. XXXX, XXX, XXX−XXX

Table 2. Comparison of Estimated Quantum Yields of Different Processes for *E. coli* Inactivation

pollutant concentration (cfu mL^{-1})	volume (mL)	source of light	catalyst	type	wavelength (nm)	time (min)	reduction	QY (cells/photons)	refs
10^6	1000	Vis-LED and solar	N-TiO_2	fixed	395	120	>3 log	0.51×10^{-15}	21
10^6	7000	UV-A	TiO_2	fixed over CPC	365	300	complete reduction	6.6×10^{-15}	59
10^7	50	visible	g-C_3N_4/TiO_2	suspension	480	180	complete reduction	508.8×10^{-15}	60
10^7	460	UV	ZnO	suspension	365	40	complete reduction	0.00134×10^{-15}	61
10^6	2000	UV	Fe−TiO_2	fixed	365	150	>4 log	0.077×10^{-15}	present study

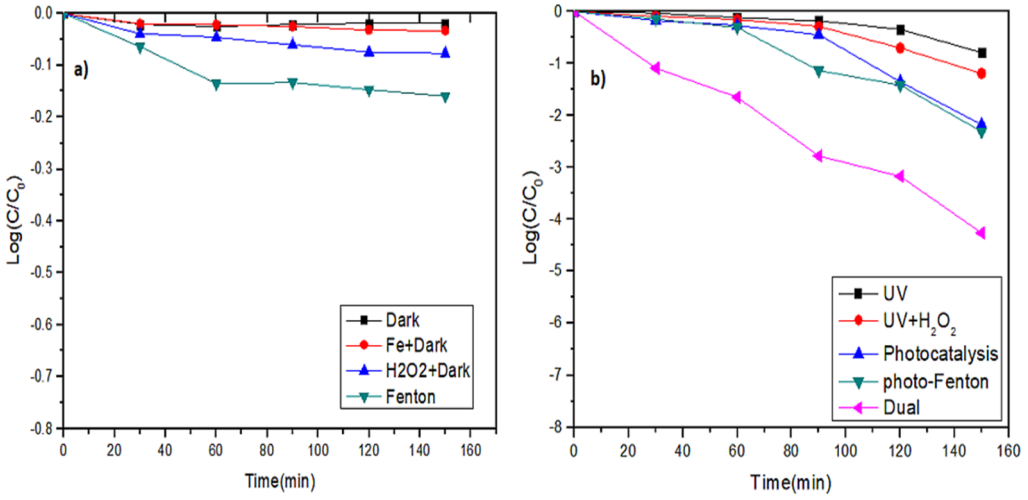

Figure 6. (a) *E. coli* inactivation with and without iron and oxidant doze in the dark. (b) *E. coli* inactivation with various technologies.

to be higher compared to the other fixed-bed studies in both UV and visible light, and the treatment time was also less. This could be due to the simultaneous functioning of photocatalysis and photo-Fenton in one system. This increases the OH radical production by reducing the e^-h^+ recombination and iron sludge formation in the system. The photon utilization efficiency of the catalyst in suspension is slightly higher side in comparison to fixed studies. However, post-treatment recovery of the catalyst in the suspension makes fixed-bed studies a more efficient technology for real application by increasing the simplicity in operation and design. Thus, the higher QY, fast kinetic rate constant, and use of waste iron in the form of FA and FA in the present study make Fe−TiO_2 an extremely attractive platform for real-life applications.

3.2.3. Preliminary Study and Efficiency of the Hybrid Process. In order to confirm the efficacy of the hybrid process and to establish the boundary conditions, the preliminary tests were carried out, the results of which are shown in Figure 6a. All these preliminary experiments (both in the dark and under UV light) were carried out using H_2O_2 = 100 mg L^{-1}, pH = 3−3.5, and flow rate = 110 mL min^{-1}. It can be seen from Figure 6a that during the dark process, the *E. coli* concentration (log C/C_0) showed minimal variation with time for the dark, Fe + dark, and H_2O_2 + dark cases. These results were in agreement with the results reported in previous studies.[18,59] However, Fenton in darkness shows the maximum log reduction of 0.1. This negligible decrease in *E. coli* concentration might be due to the death of bacteria due to osmotic shock.[18] Lixiviation of iron from the catalytic beads under acidic conditions in the dark showed a very little effect of 0.038 log units reduction in 150 min. This effect may be attributed to the imbalance in the cell of *E. coli* caused by Fe^{2+}. The Fe^{2+} ions are transported into the cytoplasm of *E. coli* by the nonspecific prions, resulting in an imbalance of concentration. The maximum unit log reduction due to H_2O_2 in the dark is found to be 0.07. The variation of H_2O_2 in the dark is determined by the diffusion of uncharged H_2O_2 molecules into the *E. coli* cell through its membrane. This initiates scavenging due to the presence of some primary enzymes such as KatG and alkyl hydro-peroxide reductase.[62] Another control experiment was performed by decreasing the pH at 3.5 and 4 and observed an insignificant log reduction of *E. coli* (<1 log).

After the baseline was established by preliminary experiments, the experiments were performed under UV light (365 nm) with an average intensity of 25 W m^{-2} to create a photocatalytic environment. All experiments were carried out under acidic conditions since acidic conditions are responsible for the lixiviating of iron from the catalytic beads. Thus, under the simulated photocatalysis environment, inactivation of *E. coli* was carried out using TiO_2-coated clay beads. In UV-A treatment without any catalyst for *E. coli* inactivation, it was observed that no reduction (less than 1) in log units of *E. coli* was achieved after 150 min of irradiation, as shown in Figure 6b. This was attributed to the minimal emission of the energetic portion of the UV spectrum of UV-A light (3.10−3.94 eV), which generally does not cause significant damage to the bacterial cell.[63] In refs 63 and 64, the authors reported that the UV-A-mediated inactivation should be facilitated by some catalyst to attain more cell damage.

https://doi.org/10.1021/acs.iecr.1c00628
Ind. Eng. Chem. Res. XXXX, XXX, XXX−XXX

During photocatalysis in a fixed bed, only a 2.2 log unit reduction of *E. coli* was observed, as shown in Figure 6b. The results showed a very low inactivation efficacy of the current system. This can be accredited to the faster e^-h^+ recombination on the TiO_2 semiconductor which led to less generation of ROS.[65] The mechanism of *E. coli* inactivation during photocatalysis states that the ROS generated on the surface of the TiO_2 semiconductor stimulate oxidative stress and cause cell damage. The photo-Fenton experiments (Figure 6b), consisting of coated composite beads (clay + FA + FS) and 100 mg L^{-1} H_2O_2, showed a unit log reduction of 2.3 in 150 min. The iron lixiviated from the composite beads has three different pathways in relation to bacterial inactivation: (1) Fe^{2+} has a low charge density and therefore can easily enter the cell (by diffusion).[18] After entering the cell, it causes internal oxidation of the cell in the presence of UV light. (2) Fe^{3+}, as the initial form or after oxidation of Fe^{2+}, enters the cell with the help of siderophore porins and forms photoactive ligands with the surface of bacteria after entering the cell.[62] When light falls on the cell, ligand-to-metal charge transfer can cause iron reduction with concomitant oxidation of the ligand, ultimately leading to inactivation of *E. coli*. (3) Photo-Fenton reaction, in which Fe^{2+} reacts with H_2O_2 to form OH radicals. This can lead to external oxidation of the cell wall and ultimately cell death. However, in a hybrid process where photo-Fenton and photocatalysis were used simultaneously in one system, it was found that the log unit reduction increased to 4.3. Thus, the inactivation efficiency of *E. coli* with different oxidation processes can be ranked as follows:

Dual > photo-Fenton > photocatalysis > UV + H_2O_2 > UV only.

3.3. Development and Evaluation of Prediction Study. To analyze the photocatalytic disinfection of water, four different operating parameters (Table 3), pH (3−6), H_2O_2 dose (30−120 mg L^{-1}), flow rate (100−400 mL min^{-1}), and time (30−150 min), were optimized under RSM using BBD. A total of 29 experiments were proposed by BBD and are shown in Table 4 with the percentage reduction of *E. coli*. By exploiting the sequential *F*-test, a quadratic model was proposed. For the response (percentage reduction), it was found that adequacy precision is 12.696. Adequacy precision estimates the signal to noise ratio, and a ratio greater than 4 is desirable. Therefore, this model can be used to navigate the design space.[66] The normal probability plot of the internally studentized residuals can be examined to assess the acceptability of the model. It can be seen from Figure S1 that all the residuals are well distributed along the straight lines, indicating that there is no significant departure from the assumptions underlying the analysis.[14] Statistical analysis of the percentage of *E. coli* in water was carried out using ANOVA, and the model was found to be significant with an *F*-value of 11.45. For % reduction of *E. coli*, time was found to be a highly significant variable, and flow rate, time^2, and interaction between time and flow rate were the significant variables, as shown in Table S1. This method provides a second-order statistical model for the *E. coli* inactivation rate in terms of coded factors, as shown in eq 15.

Table 3. Levels of the Factors Tested in the Box−Behnken Experimental Design

s. no.	variable	−1	0	−1
1	pH	3	4.5	6
2	H_2O_2 (mg L^{-1})	30	75	120
3	flow rate (mL min^{-1})	100	250	400
4	time (min)	30	90	150

Table 4. Full Factorial BBD Matrix with Four Independent Variables

experiment no.	x_1 pH	x_2 H_2O_2 (mg L^{-1})	x_3 flow rate (mL min^{-1})	x_4 time (min)	*R* % reduction of *E. coli*
1	3	75	400	90	97.6
2	4.5	75	250	90	98.17
3	3	75	100	90	99.48
4	4.5	30	100	90	96.39
5	3	75	250	150	99.8
6	4.5	120	250	30	81.68
7	4.5	75	250	90	90.10
8	4.5	75	250	90	89.01
9	4.5	30	400	90	95.9
10	4.5	75	400	30	46.6
11	4.5	120	400	90	98.1
12	4.5	75	100	30	82.7
13	6	75	250	150	99.45
14	4.5	75	100	150	99.88
15	4.5	120	250	150	99.88
16	4.5	120	100	90	99.85
17	6	75	250	30	58.07
18	3	120	250	90	99.30
19	4.5	75	250	90	98.1
20	6	120	250	90	95.6
21	6	75	100	90	99.39
22	3	30	250	90	97.27
23	4.5	75	400	150	99.46
24	4.5	30	250	150	99.7
25	4.5	30	250	30	71.49
26	4.5	75	250	90	98.05
27	6	75	400	90	91.8
28	6	30	250	90	93.7
29	3	75	250	30	69.28

$$R = 95.10 - 2.06x_1 + 1.67x_2 - 4.02x_3 + 15.70x_4 - 0.48x_1^2 + 3.05x_2^2 + 0.33x_3^2 - 12.07x_4^2 - 0.33x_1x_2 + 1.43x_1x_3 + 2.72x_1x_4 - 0.33x_2x_3 - 2.50x_2x_4 + 8.92x_3x_4 \quad (15)$$

where x_1 is pH, x_2 is H_2O_2 dose (mg L^{-1}), x_3 is the flow rate (mL min^{-1}), x_4 is time (min), and *R* is a percentage reduction of *E. coli* in water.

The positive and negative signs before the terms represent the encouraging and opposing effects of the parameters.

3.4. Optimization of Different Parameters. The effect of oxidant dose (H_2O_2), pH, and flow rate on percentage reduction of *E. coli* as a function of time was studied. The oxidant dose plays an important role in increasing the percent reduction of *E. coli* by adding additional OH radicals to the system. However, in the current study, H_2O_2 is consumed simultaneously in both the photocatalytic and photo-Fenton processes by reacting with the e_{CB}^- and preventing e^-−h^+ recombination, as shown in eq 12. In this study, the H_2O_2 concentration was varied from 30 to 120 mg L^{-1}. From Figure 7a, it can be seen that a marginal reduction was observed when the H_2O_2 concentration was less than 75 mg L^{-1}. However,

https://doi.org/10.1021/acs.iecr.1c00628
Ind. Eng. Chem. Res. XXXX, XXX, XXX−XXX

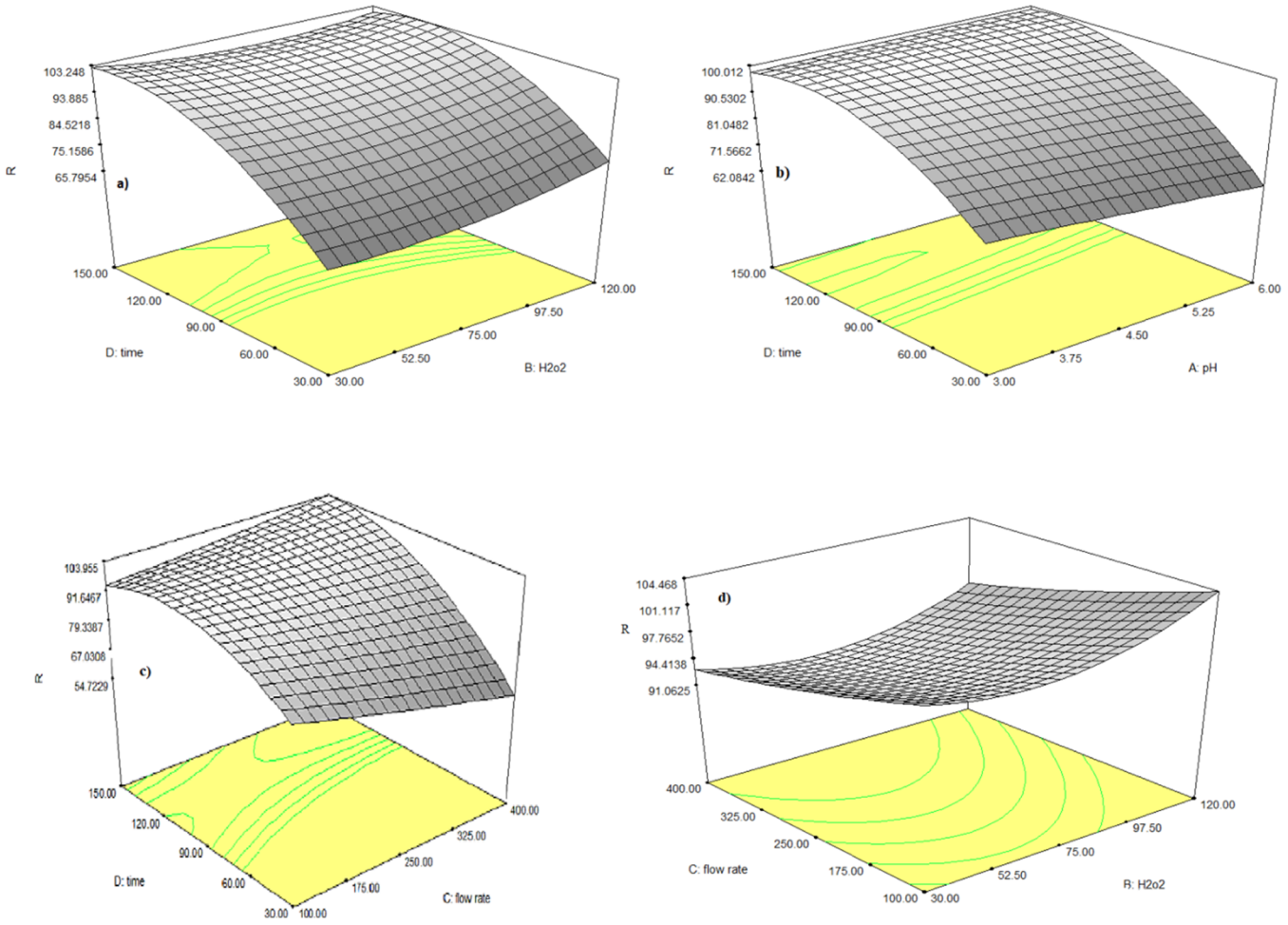

Figure 7. % reduction of *E. coli* 3D response surface graph: (a) % reduction 3D diagram of H_2O_2 dose with time, (b) % reduction 3D diagram of pH with time, (c) % reduction 3D diagram of H_2O_2 and flow rate w.r.t time, and (d) % reduction 3D diagram of flow rate with time.

when the H_2O_2 dose was increased from 75 to 120 mg L^{-1}, a high reduction of *E. coli* was observed with increasing treatment time. In Figure 7b, it was observed that at the lower H_2O_2 dose (30−75 mg L^{-1}) and pH (4.5), the percentage reduction increased with time.

As the pH increased from 4.5 to 6, the percentage reduction decreased and showed minimal changes in *E. coli* concentration with time. This could be due to the hydrolysis of Fe^{3+} and precipitation of the FeO(OH) complex, which eventually decreases the production of OH radicals and ultimately affects the *E. coli* reduction rate.[40] The effect of time and pH on the % reduction of *E. coli* with the change in H_2O_2 dose can be seen in Figure 7a. With increasing time at lower pH, the % reduction was observed to be high, but when pH increases from 4.5 to 6, it led to a decrease in the % reduction with time corresponding to a decrease in H_2O_2 dose.

In this study, the flow rate was also varied from 100 to 400 mL min^{-1}. From Figure 7c, it can be seen that when the flow rate of the reactor was increased from 250 to 400 mL min^{-1}, there was less change in the percentage reduction of *E. coli*. This can be attributed to the fact that as the flow rate increases, the contact time of *E. coli* with the catalytic particles decreases. It leaves the reactor without any significant contact with the catalytic particles, thus decreasing the inactivation efficiency. However, when the flow rate was reduced to 100 mL min^{-1}, the percentage reduction of *E. coli* increased with an increase in treatment time. From Figure 7d, it can be seen that the percentage reduction of *E. coli* was lower when the flow rate was high (400 mL min^{-1}), pH was high (4.5−6), and the oxidant dosage was low (H_2O_2 30−70 mg L^{-1}) than that when the flow rate was reduced to 100 mL min^{-1} under the same conditions. With increasing time at low pH (3.5), high H_2O_2 (120 mg L^{-1}), and lower flow rate, the percent reduction of *E. coli* increased. However, the percentage reduction decreased with time when the flow rate of the reactor was increased. In Table 4, as expected, low reduction values (46.6 and 58.0%) were obtained when the flow rate was higher and the contact time was correspondingly lower.

Based on the proposed model, Design-Expert software was used to reduce the final concentration of *E. coli*. The optimized values of the operating parameters were found to be 3.4, 62 mg L^{-1}, 106 mL min^{-1}, and 105 min for the reaction pH, H_2O_2 concentration, flow rate, and reaction time, respectively. With these optimal conditions, the percent reduction of *E. coli* was predicted to be 94.6%. The reason for selecting these particular values coincides with the rationale of minimal use of H_2O_2 dose, lower treatment time, and lower flow rate. To confirm the accuracy of the optimized results, experiments were conducted under the same conditions and a 93% reduction in *E. coli* concentration was observed. This slight change in the percentage reduction of *E. coli* shows good agreement between predicted and experimental values. It suggests that RSM is a

https://doi.org/10.1021/acs.iecr.1c00628
Ind. Eng. Chem. Res. XXXX, XXX, XXX−XXX

useful tool for optimizing dual (photo-Fenton and photocatalysis) disinfection processes.

3.5. Synergistic Effect. The synergy of the hybrid process was also calculated, and it was found that the inactivation rate constant obtained under the combined effect of photocatalysis and photo-Fenton (hybrid process) resulted in a reaction rate constant greater than the sum of the reaction rate constants of photocatalysis and photo-Fenton used separately. The synergistic effect of the dual technique when photocatalysis and photo-Fenton were used in combination was found to be 17%, which is represented by the following eqs 16−18.[47]

The synergy of the dual technique upon the photocatalytic technique

$$\% \text{ synergy} = 100 \times \{(k_{\text{dual}} - k_{\text{photocatalysis}})\}/k_{\text{dual}}$$

$$\% \text{ synergy} = 100 \times \{(0.0653 - 0.025)\}/0.0653$$

$$\% \text{ synergy} = 61\% \quad (16)$$

The synergy of the dual technique upon the photo-Fenton technique

$$\% \text{ synergy} = 100 \times \{(k_{\text{dual}} - k_{\text{photocatalysis}})\}/k_{\text{dual}}$$

$$\% \text{ synergy} = 100 \times \{(0.0653 - 0.029)\}/0.0653$$

$$\% \text{ synergy} = 55\% \quad (17)$$

The synergy of the dual technique over the photocatalytic and the photo-Fenton technique together, that is, total synergy

$$\% \text{ synergy} = 100 \times \{(k_{\text{dual}} - (k_{\text{photocatalysis}} + k_{\text{photo-Fenton}})\}/k_{\text{dual}}$$

$$\% \text{ synergy} = 100 \times \{(0.0653 - (0.025 + 0.029)\}/0.0653$$

$$\% \text{ synergy} = 17\% \quad (18)$$

The higher percentage of synergy can be ascribed to the combined effect of TiO_2-photocatalysis and photo-Fenton techniques; this led to the generation of a remarkable amount of OH radicals with greater inactivation, as shown in Figure 6b. Furthermore, the integration of e^- with the ferric ion to carry out photo-Fenton and prevention of e^-h^+ recombination in photocatalysis provide a significant boost to synergy.

3.6. Durability Study. The challenging task in this study was to obtain the durability of the composite in terms of both the intactness of the TiO_2 coating over the beads and the iron lixiviation from the beads. The durability of the beads was investigated by reusing the beads and then analyzing them in terms of reduction of *E. coli* in log units. The catalytic beads were reused 35 times, and only a 11% decrease in the photoactivity of the catalytic beads was observed, as shown in Figure 8. This decrease in the reduction unit can be attributed to the erosion of the catalyst from the catalytic beads.[36] The corresponding lixiviating of iron from the beads was also verified by measuring the concentration of iron in the solution at the beginning and the end of the study, as shown in Figure 5a,b. It was found that there was sufficient iron concentration in the system before and after recycling to perform the photo-Fenton reaction. The intactness and stability of TiO_2 on the composite beads were also verified by various characterization techniques, as described in Section 3.1, confirming the presence of photocatalysis in the system.

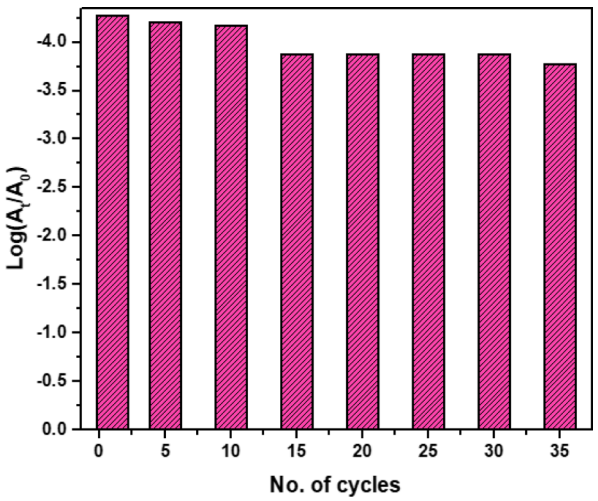

Figure 8. Recyclability study of composite beads for *E. coli* inactivation.

4. COST ANALYSIS OF THE LAB-SCALE IN SITU DUAL PROCESS

There are very few reported studies that consider the inactivation costs using the in situ hybrid effect with the recirculation batch reactor. The feasibility of the process has to be decided based on various expenses such as reagents, catalysts, UV sources, energy consumption, and fabrication of the reactor. The laboratory-scale cost analysis helps to get a rough idea of whether the photocatalytic reactor can be considered for larger-scale applications. Table S2 shows the total cost of the treatment technology in the current study. The total cost of the system was evaluated for 35 numbers of recycling and calculated to be US $16.01. More specifically, the total cost of treating 2 L of solution in a single run would be US $0.457 and US $0.228 per liter. Although there are no related studies to estimate the cost of bacterial deactivation, it still resulted in significantly lower costs than those reported in the literature[67] for degradation of priority pollutants.

5. CONCLUSIONS

In conclusion, the novel and cost-effective concept for the fabrication of Fe−TiO_2 composites using waste FS and FA has proved its potential in terms of strength, durability, and also excellent *E. coli* inactivation efficiency. The operating parameters were successfully optimized using the BBD model, and the optimum values for reaction time, pH, H_2O_2 concentration, and flow rate were found to be 105 min, 3.4, 62 mg L^{-1}, and 106 mL min^{-1}, respectively. Overall, a synergistic effect for disinfection of *E. coli* was found to be 17% over the single technologies of photo-Fenton and photocatalysis. Various characterizations (SEM−EDX, UV-DRS, FTIR, and XRD) confirmed the longevity and the stability of the Fe−TiO_2 composite even after 35 cycles. The total cost of killing *E. coli* in the solution was US $0.228 per liter, showing the potential for commercial application. The results of this study demonstrate the potential use of waste materials as a promising concept for wastewater post-treatment that can be successfully applied on a field scale.

https://doi.org/10.1021/acs.iecr.1c00628
Ind. Eng. Chem. Res. XXXX, XXX, XXX−XXX

■ ASSOCIATED CONTENT

Supporting Information

The Supporting Information is available free of charge at https://pubs.acs.org/doi/10.1021/acs.iecr.1c00628.

Analysis of variance for the response rate of E. coli elimination; plot of normal probability vs. internally studentized residuals of the response; and tentative cost evaluation of the treatment technique are available on the web at https://www.google.com/url?q=http://pubs.acs.org/&source=gmail-imap&ust=1616486382000000&usg=AOvVaw2AVAnE8hORIcF9dx08HGZL (PDF)

■ AUTHOR INFORMATION

Corresponding Author

Anoop Verma − *School of Energy and Environment, Thapar Institute of Engineering and Technology, Patiala 147004, India;* orcid.org/0000-0003-2818-6348; Phone: +91-7015396659; Email: anoop.kumar@thapar.edu

Authors

Ina Thakur − *School of Energy and Environment, Thapar Institute of Engineering and Technology, Patiala 147004, India*

Banu Örmeci − *Civil and Environmental Department, Carleton University, Ottawa ON K1S 5B6, Canada*

Complete contact information is available at: https://pubs.acs.org/10.1021/acs.iecr.1c00628

Funding

This research did not receive any specific grant from funding agencies in the public, commercial, or not-for-profit sectors.

Notes

The authors declare no competing financial interest.

■ ACKNOWLEDGMENTS

The authors would like to thank the central instrumentation laboratory and sophisticated analytical instrumentation facility, Punjab University, Chandigarh, India, for providing their facilities for the characterization of samples.

■ REFERENCES

(1) Yang, H.; Cheng, H. Controlling Nitrite Level in Drinking Water by Chlorination and Chloramination. *Sep. Purif. Technol.* **2007**, *56*, 392−396.

(2) Lu, J.; Zhang, T.; Ma, J.; Chen, Z. Evaluation of Disinfection By-Products Formation during Chlorination and Chloramination of Dissolved Natural Organic Matter Fractions Isolated from a Filtered River Water. *J. Hazard. Mater.* **2009**, *162*, 140−145.

(3) Coleman, H. M.; Vimonses, V.; Leslie, G.; Amal, R. Degradation of 1,4-Dioxane in Water Using TiO2 Based Photocatalytic and H2O2/UV Processes. *J. Hazard. Mater.* **2007**, *146*, 496−501.

(4) Sathasivan, A.; Fisher, I.; Tam, T. Onset of Severe Nitrification in Mildly Nitrifying Chloraminated Bulk Waters and Its Relation to Biostability. *Water Res.* **2008**, *42*, 3623−3632.

(5) Huang, E.; White, T.; Wang, B.; Shi, H.; Liu, J. Disinfection of Escherichia Coli by a Reactive Electrochemical Membrane System Involving Activated Carbon Fiber Cloth (ACFC). *Water* **2019**, *11*, 430.

(6) De Battisti, A.; Formaglio, P.; Ferro, S.; Al Aukidy, M.; Verlicchi, P. Electrochemical Disinfection of Groundwater for Civil Use − An Example of an Effective Endogenous Advanced Oxidation Process. *Chemosphere* **2018**, *207*, 101−109.

(7) Liu, T.; Wang, D.; Liu, H.; Zhao, W.; Wang, W.; Shao, L. Rotating Packed Bed as a Novel Disinfection Contactor for the Inactivation of E. Coli by Ozone. *Chemosphere* **2019**, *214*, 695−701.

(8) Kasler, D. R.; Pyatkovskyy, T.; Yousef, A. E.; Sastry, S. K. Effect of Moderate Electric Field Pretreatment in Combination with Ozonation on Inactivation of Escherichia Coli K12 in Intact Shell Eggs. *Food Sci. Technol.* **2020**, *127*, 109338.

(9) Hashim, K. S.; Ali, S. S. M.; AlRifaie, J. K.; Kot, P.; Shaw, A.; Al Khaddar, R.; Idowu, I.; Gkantou, M. Escherichia Coli Inactivation Using a Hybrid Ultrasonic−Electrocoagulation Reactor. *Chemosphere* **2020**, *247*, 125868.

(10) Lv, R.; Zou, M.; Chantapakul, T.; Chen, W.; Muhammad, A. I.; Zhou, J.; Ding, T.; Ye, X.; Liu, D. Effect of Ultrasonication and Thermal and Pressure Treatments, Individually and Combined, on Inactivation of Bacillus Cereus Spores. *Appl. Microbiol. Biotechnol.* **2019**, *103*, 2329−2338.

(11) Daels, N.; De Vrieze, S.; Sampers, I.; Decostere, B.; Westbroek, P.; Dumoulin, A.; Dejans, P.; De Clerck, K.; Van Hulle, S. W. H. Potential of a Functionalised Nanofibre Microfiltration Membrane as an Antibacterial Water Filter. *Desalination* **2011**, *275*, 285−290.

(12) Rodríguez-Chueca, J.; Ormad, M. P.; Mosteo, R.; Canalis, S.; Ovelleiro, J. L. Escherichia Coli Inactivation in Fresh Water Through Photocatalysis with TiO2-Effect of H2O2 on Disinfection Kinetics. *Clean: Soil, Air, Water* **2016**, *44*, 515−524.

(13) Shekoohiyan, S.; Rtimi, S.; Moussavi, G.; Giannakis, S.; Pulgarin, C. Enhancing Solar Disinfection of Water in PET Bottles by Optimized In-Situ Formation of Iron Oxide Films. From Heterogeneous to Homogeneous Action Modes with H2O2 vs. O2 − Part 1: Iron Salts as Oxide Precursors. *Chem. Eng. J.* **2019**, *358*, 211−224.

(14) Feilizadeh, M.; Alemzadeh, I.; Delparish, A.; Estahbanati, M. R. K.; Soleimani, M.; Jangjou, Y.; Vosoughi, A. Optimization of Operating Parameters for Efficient Photocatalytic Inactivation of Escherichia Coli Based on a Statistical Design of Experiments. *Water Sci. Technol.* **2015**, *71*, 823−831.

(15) Blanco, E.; González-Leal, J. M.; Ramírez-del Solar, M. Photocatalytic TiO2 Sol-Gel Thin Films: Optical and Morphological Characterization. *Sol. Energy* **2015**, *122*, 11−23.

(16) De Torres-Socías, E.; Prieto-Rodríguez, L.; Zapata, A.; Fernández-Calderero, I.; Oller, I.; Malato, S. Detailed Treatment Line for a Specific Landfill Leachate Remediation. Brief Economic Assessment. *Chem. Eng. J.* **2015**, *261*, 60−66.

(17) Rincón, A.-G.; Pulgarin, C. Fe3+ and TiO2 Solar-Light-Assisted Inactivation of E. Coli at Field Scale. Implications in Solar Disinfection at Low Temperature of Large Quantities of Water. *Catal. Today* **2007**, *122*, 128−136.

(18) Giannakis, S.; Voumard, M.; Rtimi, S.; Pulgarin, C. Bacterial Disinfection by the Photo-Fenton Process: Extracellular Oxidation or Intracellular Photo-Catalysis? *Appl. Catal., B* **2018**, *227*, 285−295.

(19) López, A. V.; López, K. H.; Giannakis, S.; Benítez, N. Effect of Reactor Material and Its Reuse on Photo-Fenton Process Efficiency at near-Neutral PH: Alterations in E. Coli Inactivation and Resorcinol Degradation Kinetics in Water. *J. Photochem. Photobiol., A* **2017**, *344*, 228−237.

(20) Makropoulou, T.; Panagiotopoulou, P.; Venieri, D. N-doped TiO2 Photocatalysts for Bacterial Inactivation in Water. *J. Chem. Technol. Biotechnol.* **2018**, *93*, 2518−2526.

(21) Kassahun, S. K.; Kiflie, Z.; Shin, D. W.; Park, S. S.; Chung, Y. R. Novel Multistage Fixed-Bed Photoreactor for Bacterial Inactivation Using N-Doped TiO2 Nanoparticles under Vis-LEDs and Sunlight Illumination. *Nanotechnol. Environ. Eng.* **2018**, *3*, 1−11.

(22) Lazar, M.; Varghese, S.; Nair, S. Photocatalytic Water Treatment by Titanium Dioxide: Recent Updates. *Catalysts* **2012**, *2*, 572−601.

(23) Cunha, D. L.; Kuznetsov, A.; Achete, C. A.; Machado, A. E. d. H.; Marques, M. Immobilized TiO2 on Glass Spheres Applied to Heterogeneous Photocatalysis: Photoactivity, Leaching and Regeneration Process. *PeerJ* **2018**, *6*, No. e4464.

(24) Matsunaga, T.; Tomoda, R.; Nakajima, T.; Wake, H. Photoelectrochemical Sterilization of Microbial Cells by Semiconductor Powders. *FEMS Microbiol. Lett.* **1985**, *29*, 211−214.
(25) Zhang, J.; Yuan, M.; Liu, X.; Wang, X.; Liu, S.; Han, B.; Liu, B.; Shi, H. Copper Modified Ti3+ Self-Doped TiO2 Photocatalyst for Highly Efficient Photodisinfection of Five Agricultural Pathogenic Fungus. *Chem. Eng. J.* **2020**, *387*, 124171.
(26) Wang, X.; Wang, X.; Zhao, J.; Song, J.; Su, C.; Wang, Z. Surface Modified TiO2 Floating Photocatalyst with PDDA for Efficient Adsorption and Photocatalytic Inactivation of Microcystis Aeruginosa. *Water Res.* **2018**, *131*, 320−333.
(27) Laxma Reddy, P. V.; Kavitha, B.; Kumar Reddy, P. A.; Kim, K.-H. TiO2-Based Photocatalytic Disinfection of Microbes in Aqueous Media: A Review. *Environ. Res.* **2017**, *154*, 296−303.
(28) García-Fernández, I.; Polo-López, M. I.; Oller, I.; Fernández-Ibáñez, P. Bacteria and Fungi Inactivation Using Fe 3+/Sunlight, H 2O 2/Sunlight and near Neutral Photo-Fenton: A Comparative Study. *Appl. Catal., B* **2012**, *121−122*, 20−29.
(29) Zhang, W.; Chen, Y.; Yu, S.; Chen, S.; Yin, Y. Preparation and Antibacterial Behavior of Fe 3 + -Doped Nanostructured TiO 2 Thin Films. *Thin Solid Films* **2008**, *516*, 4690−4694.
(30) Villegas- Guzman, P.; Giannakis, S.; Rtimi, S.; Grandjean, D.; Bensimon, M.; de Alencastro, L. F.; Pulgarin, C. A Green Solar Photo-Fenton Process for the Elimination of Bacteria and Micropollutants in Municipal Wastewater Treatment Using Mineral Iron and Natural Organic Acids. *Appl. Catal., B* **2017**, *219*, 538−549.
(31) Giannakis, S. Analogies and Differences among Bacterial and Viral Disinfection by the Photo-Fenton Process at Neutral PH: A Mini Review. *Environ. Sci. Pollut. Res.* **2018**, *25*, 27676−27692.
(32) Coutinho, C. A.; Gupta, V. K. Photocatalytic Degradation of Methyl Orange Using Polymer-Titania Microcomposites. *J. Colloid Interface Sci.* **2009**, *333*, 457−464.
(33) Ahmad, N.; Gondal, M. A.; Sheikh, A. K. Comparative Study of Different Solar-Based Photo Catalytic Reactors for Disinfection of Contaminated Water. *Desalin. Water Treat.* **2016**, *57*, 1−8.
(34) Sordo, C.; Van Grieken, R.; Marugán, J.; Fernández-Ibáñez, P. Solar Photocatalytic Disinfection with Immobilised TiO2 at Pilot-Plant Scale. *Water Sci. Technol.* **2010**, *61*, 507−512.
(35) Adán, C.; Marugán, J.; Mesones, S.; Casado, C.; van Grieken, R. Bacterial Inactivation and Degradation of Organic Molecules by Titanium Dioxide Supported on Porous Stainless Steel Photocatalytic Membranes. *Chem. Eng. J.* **2017**, *318*, 29−38.
(36) Talwar, S.; Sangal, V. K.; Verma, A. K. In-Situ Dual Effect of Novel Fe-TiO2 Composite for the Degradation of Phenazone. *Sep. Purif. Technol.* **2019**, *211*, 391−400.
(37) Bansal, P.; Verma, A. In-Situ Dual Effect Studies Using Novel Fe-TiO2 Composite for the Pilot-Plant Degradation of Pentoxifylline. *Chem. Eng. J.* **2018**, *332*, 682−694.
(38) Visa, M.; Duta, A. Methyl-Orange and Cadmium Simultaneous Removal Using Fly Ash and Photo-Fenton Systems. *J. Hazard. Mater.* **2013**, *244−245*, 773−779.
(39) Rajput, H.; Verma, A.; Kaur, M.; Kaur, T.; Toor, A. P. Heterogeneous Solar Photo-Fenton Degradation of Reactive Black 5 Using Foundry Sand and Fly Ash: Value Addition to Waste. *J. Environ. Eng. Landsc. Manag.* **2016**, *24*, 124−132.
(40) Bansal, P.; Verma, A. Novel Fe-TiO2composite Driven Dual Effect for Reduction in Treatment Time of Pentoxifylline: Slurry to Immobilized Approach. *Mater. Des.* **2017**, *125*, 135−145.
(41) Wang, X.; Lu, Y.; Hua, K.; Yang, D.; Yang, Y. Iodine-Doped Carbon Dots with Inherent Peroxidase Catalytic Activity for Photocatalytic Antibacterial and Wound Disinfection. *Anal. Bioanal. Chem.* **2021**, *413*, 1373−1382.
(42) Ren, Y.; Han, Y.; Li, Z.; Liu, X.; Zhu, S.; Liang, Y.; Yeung, K. W. K.; Wu, S. Ce and Er Co-Doped TiO2 for Rapid Bacteria- Killing Using Visible Light. *Bioact. Mater.* **2020**, *5*, 201−209.
(43) Naik, T. R.; Kraus, R. N.; Ramme, B. W.; Canpolat, F. Effects of Fly Ash and Foundry Sand on Performance of Architectural Precast Concrete. *J. Mater. Civ. Eng.* **2012**, *24*, 851−859.
(44) Bansal, P.; Verma, A.; Talwar, S. Detoxification of Real Pharmaceutical Wastewater by Integrating Photocatalysis and Photo-Fenton in Fixed-Mode. *Chem. Eng. J.* **2018**, *349*, 838−848.
(45) Bansal, P.; Verma, A. Pilot-Scale Single-Step Reactor Combining Photocatalysis and Photo-Fenton Aiming at Faster Removal of Cephalexin. *J. Cleaner Prod.* **2018**, *195*, 540−551.
(46) Verma, A.; Prakash, N. T.; Toor, A. P. Photocatalytic Degradation of Herbicide Isoproturon in TiO2 Aqueous Suspensions: Study of Reaction Intermediates and Degradation Pathways. *Environ. Prog. Sustainable Energy* **2014**, *33*, 402.
(47) Thakur, I.; Örmeci, B.; verma, A. Inactivation of E. Coli in Water Employing Fe-TiO2 Composite Incorporating in-Situ Dual Process of Photocatalysis and Photo-Fenton in Fixed-Mode. *J. Water Process. Eng.* **2020**, *33*, 101085.
(48) Yousefzadeh, S.; Matin, A. R.; Ahmadi, E.; Sabeti, Z.; Alimohammadi, M.; Aslani, H.; Nabizadeh, R. Response Surface Methodology as a Tool for Modeling and Optimization of Bacillus Subtilis Spores Inactivation by UV/ Nano-Fe0 Process for Safe Water Production. *Food Chem. Toxicol.* **2018**, *114*, 334−345.
(49) Khuri, A. I.; Mukhopadhyay, S. Response Surface Methodology. *Wiley Interdiscip. Rev. Comput. Stat.* **2010**, *2*, 128−149.
(50) Bezerra, M. A.; Santelli, R. E.; Oliveira, E. P.; Villar, L. S.; Escaleira, L. A. Response Surface Methodology (RSM) as a Tool for Optimization in Analytical Chemistry. *Talanta* **2008**, *76*, 965−977.
(51) Feilizadeh, M.; Mul, G.; Vossoughi, M. E. coli inactivation by visible light irradiation using a Fe-Cd/TiO 2 photocatalyst: Statistical analysis and optimization of operating parameters. *Appl. Catal., B* **2015**, *168−169*, 441−447.
(52) Asadi, S.; Moeinpour, F. Inactivation of Escherichia Coli in Water by Silver-Coated Ni0.5Zn0.5Fe2O4 Magnetic Nanocomposite: A Box−Behnken Design Optimization. *Appl. Water Sci.* **2019**, *9*, 1−9.
(53) Matin, A. R.; Yousefzadeh, S.; Ahmadi, E.; Mahvi, A.; Alimohammadi, M.; Aslani, H.; Nabizadeh, R. A Comparative Study of the Disinfection Efficacy of H2O2/Ferrate and UV/H2O2/Ferrate Processes on Inactivation of Bacillus Subtilis Spores by Response Surface Methodology for Modeling and Optimization. *Food Chem. Toxicol.* **2018**, *116*, 129−137.
(54) Braimah, M. N.; Anozie, A. N.; Odejobi, O. J. Utilization of Response Surface Methodology (RSM) in the Optimization of Crude Oil Refinery. *J. Multidiscip. Eng. Sci. Technol.* **2016**, *3*, 4361−4369.
(55) Khuri, A. I. Response Surface Methodology and Its Applications In Agricultural and Food Sciences. *Biom. Biostat. Int. J.* **2017**, *5*, 1−11.
(56) Sayyar, Z.; Akbar Babaluo, A.; Shahrouzi, J. R. Kinetic Study of Formic Acid Degradation by Fe 3+ Doped TiO 2 Self-Cleaning Nanostructure Surfaces Prepared by Cold Spray. *Appl. Surf. Sci.* **2015**, *335*, 1−10.
(57) Anil, T.; Naidu, K. L.; Raju, J. Band Gap Determination Using Tauc ' s Plot for LiNbO 3 Thin Films. *Int. J. ChemTech Res.* **2014**, *6*, 974.
(58) Raza, N.; Raza, W.; Gul, H.; Azam, M.; Lee, J.; Vikrant, K.; Kim, K.-H. Solar-Light-Active Silver Phosphate/Titanium Dioxide/Silica Heterostructures for Photocatalytic Removal of Organic Dye. *J. Cleaner Prod.* **2020**, *254*, 120031.
(59) Alrousan, D. M. A.; Polo-López, M. I.; Dunlop, P. S. M.; Fernández-Ibáñez, P.; Byrne, J. A. Solar Photocatalytic Disinfection of Water with Immobilised Titanium Dioxide in Re-Circulating Flow CPC Reactors. *Appl. Catal., B* **2012**, *128*, 126−134.
(60) Li, G.; Nie, X.; Chen, J.; Jiang, Q.; An, T.; Wong, P. K.; Zhang, H.; Zhao, H.; Yamashita, H. Enhanced Visible-Light-Driven Photocatalytic Inactivation of Escherichia Coli Using g-C3N4/TiO2 Hybrid Photocatalyst Synthesized Using a Hydrothermal-Calcination Approach. *Water Res.* **2015**, *86*, 17−24.
(61) Liu, H.-L.; Yang, T. C.-K. Photocatalytic Inactivation of Escherichia Coli and Lactobacillus Helveticus by ZnO and TiO2 Activated with Ultraviolet Light. *Process Biochem.* **2003**, *39*, 475−481.
(62) Giannakis, S.; López, M. I. P.; Spuhler, D.; Pérez, J. A. S.; Ibáñez, P. F.; Pulgarin, C. Solar Disinfection Is an Augmentable, in

https://doi.org/10.1021/acs.iecr.1c00628
Ind. Eng. Chem. Res. XXXX, XXX, XXX−XXX

Situ -Generated Photo-Fenton Reaction — Part 1: A Review of the Mechanisms and the Fundamental Aspects of the Process. *Appl. Catal., B* **2016**, *199*, 199−223.
(63) Rincón, A.-G.; Pulgarin, C. Comparative Evaluation of Fe3+ and TiO2 Photoassisted Processes in Solar Photocatalytic Disinfection of Water. *Appl. Catal., B* **2006**, *63*, 222−231.
(64) Chong, M. N.; Jin, B.; Saint, C. P. Bacterial Inactivation Kinetics of a Photo-Disinfection System Using Novel Titania-Impregnated Kaolinite Photocatalyst. *Chem. Eng. J.* **2011**, *171*, 16−23.
(65) Kang, X.; Liu, S.; Dai, Z.; He, Y.; Song, X.; Tan, Z. Titanium Dioxide: From Engineering to Applications. *Catalysts* **2019**, *9*, 191.
(66) Talwar, S.; Sangal, V. K.; Verma, A. Feasibility of Using Combined TiO2 Photocatalysis and RBC Process for the Treatment of Real Pharmaceutical Wastewater. *J. Photochem. Photobiol., A* **2018**, *353*, 263−270.
(67) Haranaka-Funai, D.; Didier, F.; Giménez, J.; Marco, P.; Esplugas, S.; Machulek-Junior, A. Photocatalytic Treatment of Valproic Acid Sodium Salt with TiO2 in Different Experimental Devices: An Economic and Energetic Comparison. *Chem. Eng. J.* **2017**, *327*, 656−665.

https://doi.org/10.1021/acs.iecr.1c00628
Ind. Eng. Chem. Res. XXXX, XXX, XXX−XXX

Journal of Environmental Chemical Engineering 9 (2021) 106322

Contents lists available at ScienceDirect

Journal of Environmental Chemical Engineering

journal homepage: www.elsevier.com/locate/jece

Visibly active Fe-TiO_2 composite: A stable and efficient catalyst for the catalytic disinfection of water using a once-through reactor

Ina Thakur [a], Anoop Verma [a,*], Banu Örmeci [b]

[a] School of Energy and Environment, Thapar Institute of Engineering and Technology, Patiala 147004, India
[b] Civil and Environmental Department, Carleton University, Ottawa, ON KIS 5B6, Canada

ARTICLE INFO

Editor: V. Victor

Keywords:
Disinfection
Once-through reactor, Plug flow
E. coli
Hybrid effect
Solar energy

ABSTRACT

This study presents a unique concept of fixed-bed in-situ once-through reactor approaching plug flow (PFR) employed for the disinfection of *E. coli*. This study discusses the potential applications of a low-cost composite composed of Foundry Sand (FS) and fly ash (FA) for combining hybrid effects. This composite has the intrinsic characteristic of containing iron, which lixiviates in acidic conditions (resulting in photo-Fenton), as well as surface-coated TiO_2, which results in photocatalysis, demonstrating a hybrid effect. The surface characteristic analysis of the catalyst (SEM/EDS, XRD, DRS, and FTIR) confirmed the presence of iron (acting as natural dopant) and TiO_2 making it visibly active. Therefore showed a significant reduction in the treatment time under solar irradiation with 10% synergy of in-situ hybrid-process over individual processes. The implementation of the in-situ hybrid effect in cascade reactor with three reactors in series helped the reactor approaching PFR with 45 min of retention time (Ţ) and 100% inactivation of *E. coli* cell count was observed with optimized operational parameters. The cell wall damage was confirmed by the increase in the K^+ concentration at regular intervals. No regrowth of cells after 24 and 48 h of treatment in the dark and sunlight was observed, in completely inactivated samples. Besides this, the Fe-TiO_2 composite portrayed an exceptional durability/recyclability efficacy (>100 recycles) under continuous flow conditions. To visualize the practical viability of the proposed high-performance once-through reactor system, the total cost of the treatment process was analyzed in detail.

1. Introduction

Biohazards arising from pathogenic microorganisms have long been considered a serious worldwide health issue, and millions of people suffered diseases and even death due to bacterial infection[1–4]. Therefore, pursuing cost-efficient, clean, sustainable, and reliable techniques for waterborne microorganisms' purification is urgently needed. Comparing to the several drawbacks (e.g. potential disinfection byproducts (DBPs) and costly-operation, etc) of the conventional methods (e.g. ultraviolet radiation, chlorination, ozonation, filtration technology, etc), the solar photocatalytic bactericidal possesses versatile advantages such as cost-efficient, recyclable, lower disinfection byproducts and used the clean solar energy[5–9].

The effective execution of these AOPs requires various engineering perspectives to be addressed. The mixed flow reactor (MFR) and plug flow reactor (PFR) have found a prominent space in literature for the treatment of different contaminants using different AOPs. Even though the MFR has established its mark in terms of efficacy and treatment time, yet poses various drawbacks such as intensive use of energy, back mixing, and less conversion of the reagents into products[10]. Therefore the largely preferred reactor with the advantage of providing high conversion is the PFR as compared to the MFR reactors[11,12]. The axial mixing in the PFR doesn't occur which makes the reactor more effective than MFR[13]. With so many reported applications of PFR and known credentials of AOP [4,14–16], their fusion has given less importance in the literature. Coupling both techniques can boost the real-time application of the PFR approach for treating wastewater via a continuous once-through AOP system. Moreover, the potential bottleneck to the scale-up studies of AOP could be answered by studying this fusion technique.

One of the most important attributes that need to be considered while examining the non-ideal behaviour of the reactor is residence time distribution (RTD)[17]. RTD is the primary method for determining the time for which the several reactants stayed in the reactor, the mixing of elements inside the reactor, several issues linked to the flow, the designing and scaling up of the reactor[18]. The most often used models

* Corresponding author.
E-mail address: anoop.kumar@thapar.edu (A. Verma).

https://doi.org/10.1016/j.jece.2021.106322
Received 7 July 2021; Received in revised form 1 August 2021; Accepted 2 September 2021
Available online 7 September 2021
2213-3437/© 2021 Elsevier Ltd. All rights reserved.

for such studies are tanks in series, axial dispersion, continuously stirred tank reactor alone or with the bypass, and dead zones. The axial dispersion model is frequently employed in tubular reactors that behave like PFR. Here, the Peclet number (Pe) plays a critical role in this case, indicating the particle dispersion in the axial direction[10]. With no axial mixing and total radial mixing, dispersion is critical. A high Pe value indicates negligible dispersion and behaviour similar to plug flow. However, low Pe (<10) values verify the axial dispersion and the model's behaviour as an MFR. For implementing the PFR in the actual-life application, the most frequently used reactor is the packed bed reactor[19], and the material supporting the immobilization of catalysts in these studies plays an important role. Scaling-up of a fixed bed PFR reactor usually faces various technical hitches such as durability/longevity of the support material, mass transfer limitation, increase in treatment time, and intactness of the catalyst, etc[15]. Moreover, most of the scaled-up reactor studies were found to be executed in recirculation mode[20,21] which increases the reaction time along with the pumping cost. Therefore to address the drawbacks of the fixed bed reactor, the main emphasis needs to be given to the development of a durable effective PFR induced photocatalytic reactor system.

The main objective of this study was to improve the efficacy of the fixed bed solar photocatalytic reactor in once-through mode to a degree that the reactor approaches plug-flow conditions. In the fixed-bed photocatalytic reactor, the plug flow conditions are difficult to approach, but the implementation of a novel in-situ hybrid effect in a once-through system has effectively led to the achievement of plug-flow conditions with a drastic reduction in the treatment time. The primary innovation of this approach is that, unlike other research, this one uses a natural dopant. Waste iron is a natural dopant that is utilized in the manufacturing of composite beads (by the photo-Fenton method). As mentioned in Section 3, the iron on the surface of the catalyst decreases the energy bandgap with time and also keeps it active in the visible region. As a result, the current method is cost-effective, as no investments in doping the catalyst have been undertaken. This makes the catalyst commercially viable in terms of durability, stability, and low cost. This system incorporates innovative composite beads implying two processes i.e. photo-Fenton and photocatalytic in a fixed-mode system. The stability and reusability of the Fe-TiO_2 composite were also investigated to confirm the probability of real-life application. To the best of the author's knowledge, this is the first study reporting a fixed-bed in-situ hybrid process in the once-through reactor approaching PFR for the inactivation of *Escherichia coli (E. coli)*.

2. Experimental analysis

2.1. Reagents and chemical

TiO_2 (Titanium dioxide) catalyst was purchased from Degussa, Frankfurt, Germany. Clay, FS, and FA (collected from local industry, Patiala, Punjab, India) were used to prepare spherical beads. To maintain the acidic pH conditions of the treatment reaction, acetate buffer was used (made from acetic acid, and sodium acetate) which were purchased from Loba Chemie Pvt Ltd, Maharashtra, India. To prepare the isotonic solutions for bacterial cells, 99.5% of NaCl was used. Luria Bertani (LB), Miller Agar-Agar, Type I, for cell growth were purchased from HiMedia Laboratories, Mumbai (India). Methylene blue used as a tracer for PFR studies was purchased from Loba Chemie Pvt Ltd, Maharashtra (India). BQ (1,4-benzoquinine), TEOA (triethanolamine), and IPA (isopropanol) were used as a special scavenger of superoxide radical ($O_2^{\bullet-}$), hole (h^+), and hydroxyl radical (HO°) species and were purchased from TCI Chemicals, India. All the solutions were prepared from double-distilled water.

2.2. Composite support material

The Fe-TiO_2 composite was prepared by appropriate mixing of FS, FA, and clay by keeping the mass ratio as 1:1:2 respectively to maintain the desired strength of the bead. Then the beads were air-dried and muffled at 800 C for 2 h to strengthen them. The curing of the beads was done by dipping them for 48 hin water. The diameter of the composite beads was found to be approximately 15 mm after measuring it with the screw gauge. The diameter of at least 100 beads was measured in all 4 different directions and the average value was quoted. The outer surface of the composite beads was coated with 2% TiO_2 using the dip-coating method for the photocatalytic process to take place[22]. The thickness of the coating was approximately 60–70 μm[23]. The treatment was executed in the acidic condition (4.0–4.5) so that leaching of iron from the beads could take place for the execution of the photo-Fenton reaction. The prepared composite of TiO_2 coated Fe-containing beads were used for the hybrid process to precede.

2.3. Characteristic analysis of the composite

In this study of the hybrid process, the spherical Fe-TiO_2 beads were analyzed to confirm the presence of both iron and TiO_2 in one system using different techniques such as UV-DRS, XRD, FT-IR, SEM-EDS. The chemical composition and morphology and uniformity of the catalyst were determined via a Scanning Electron Microscope (SEM) (JSM-6510LV, JEOL (Japan)) equipped with Energy-dispersive Spectroscopy (EDS) and Energy-Dispersive X-ray Analysis (EDX). The X-ray diffraction (XRD) using X'Pert high score in the scanning range of 20–80° was used to study the crystallography of the Fe-TiO_2 catalyst with radiation of Cu-Kα at $\lambda = 1.5418$ Å. The bandgap energy of the catalyst was recorded using UV–vis diffuse reflectance spectrometer (DRS), UV-2600, Shimadzu (Asia Pacific) equipped with barium sulphate ($BaSo_4$) as a standard reflectance. For the evaluation of compound bondings, linkages, and functionalized groups the Fourier TransformInfra-Red Spectrophotometer model RZX (Perkin Elmer) was used with KBr pellets and scanned in the range of 4000–200 cm^{-1}.

2.4. Bacterial quantification

The wild-type *E. coli,* K12 strain was originally purchased from Microbial Type Culture Collection and Gene bank, Chandigarh, India, and was immediately preserved at −20 °C in 20% glycerol solution. The detailed preparation method is already mentioned in our previous study [23,24]. Concisely, inoculation of a colony from an already prepared culture in 5 mL of sterilized Luria-Bertani (LB) broth was done. This solution was incubated for 8 h at 37 °C under 180 rpm. 1% of this culture was diluted in LB and incubated at least for 15 h under the same conditions. The obtained culture of *E. coli* was centrifuged for 15 min at 5000 rpm at 4 °C to separate the media from the cells. The cell pellet obtained after centrifuging was washed 3 times using an isotonic solution of 0.85% NaCl. This step was repeated 2 times and the final pellet was suspended in 25 mL of isotonic saline solution to obtained a bacterial cell count of 10^9 Colony Forming Units per mL (CFU mL^{-1}). Then the bacterial cell count was diluted to obtain an initial cell count of 10^6 CFU mL^{-1} and was used for every disinfection experiment. The result was calculated by the standard plate counting method manually after incubating at 37 °C for 24 h.

2.5. Experimentation in the pilot-scale once-through reactor system

For the inactivation of *E. coli*, the current system is comprised of 3 glass reactors connected in series having dimensions of 0.4 m × 0.2 m × 0.025 m each. The surface of the reactor is covered with the appropriate amount of Fe-TiO_2 composite beads and exposed to solar radiation. The complete solar irradiated reactor scheme was operated in once-through mode and provided with a cylindrical tank containing simulated *E. coli* solution. The exit point of the first reactor was attached to the inlet of the first glass reactor and so on to make it once through. An appropriate flow rate was maintained using a peristaltic pump. The schematic diagram of

the once-through reactor is shown in Fig. 1. Before the treatment process starts, the *E. coli* solution was kept at stirring for 30 min for the cells acclimatization. The inactivation of *E. coli* tests was carried out at Thapar Institute of Engineering and Technology, Patiala, India on sunny days of September and October (30.3564° N, 76.3647° E) from 12:00 PM to 2:00 PM. The fixed bed solar reactors were connected in series in such a way that the exit point of the first reactor becomes the inlet of the other and was placed in the sunlight for the reaction to start. The solar irradiation was monitored using a lux meter and the values were recorded at regular intervals, from which the average intensity was calculated and was found to be 590–600 W m^{-2}. The fundamental procedure followed for the experimentation comprises the adjustment of pH as (4–4.5) along with the addition of an appropriate amount of H_2O_2 and with subsequent pumping of the *E. coli* solution to the reactor. The *E. coli* solution is a simulated solution of *E. coli* and MilliQ water. The reactor was optimized by optimizing different parameters such as the number of the reactor (1–3), number of baffles (1–4), H_2O_2 (10 − 70 mg L^{-1}), flow rate (2–14 L h^{-1}), and the surface area covered (50–100%) in terms of number of beads. After regular intervals, 2 mL of samples were taken out from the inlet and exit from every reactor. The results were calculated using Eq. (1), where L_r is log unit reduction of *E. coli*, A_t is the reduction in *E. coli* at the time "t," where t is a regular interval of the treatment time at which treated samples were taken out of the reactor and A_0 is the initial cell count *E. coli* at t = 0 and t = 0 is the time at which initial sample was taken out.

$$L_r = log \frac{A_t}{A_0} \quad (1)$$

3. Results and discussion

3.1. Characterization of composite beads

The presence of Iron and TiO_2 in the composite was analyzed using different techniques as described below.

3.1.1. SEM-EDS analysis

The morphology and elemental composition of the uncoated and coated Fe-TiO_2 composite were confirmed using SEM-EDS analysis. The SEM image is shown in the supporting information file (Fig. S1) of TiO_2 coated composite beads that showed strongly bounded TiO_2 particles on the surface of the composite beads even after recycling. The peaks of Ti, O, and Fe in the EDS spectrum of catalysts (Fresh beads) and recycled beads are in good agreement with the recycled thus proved the existence of both iron (Fe) as well as TiO_2 catalyst in the hybrid technique.

3.1.2. XRD analysis

The XRD analysis of the prepared samples was done to see the changes occurring in the crystalline structure and phases of the catalyst after recycling and similar patterns of the XRD spectrum were observed as shown in the supporting information file (Fig. S2a). The anatase phase of the fresh and recycled catalyst was at 2θ = 25.26°, 37.79°, 48.04°, 53.9°, 54.9°, and 62.9 ° respectively and the rutile phase of the fresh and recycled catalyst was at 2θ = 27.552°, 36.6°, 39.6°, 41.4°, and 55.03° respectively. The anatase phase of the catalyst at different degrees responds to 101, 103, 200, 105, 211, and 204 planes. Similarly, the crystalline planes at 110, 101, 200, 111, and 211 represent the rutile phase. In Fig. S2a, iron oxide (IO) peaks at different planes at 101 and 034 can be seen, which enables the entrapment of photo-excited electrons from the TiO_2 photocatalytic process, which regenerates Fe^{2+}. Therefore, both the technologies i.e., photo-Fenton and photocatalysis, occur at the same time in one unit. The presence of these IO and ITO (iron titanium oxide) enhances the efficacy of the Fe-TiO_2 catalyst in visible light. This hypothesis was further confirmed through UV–visible absorption spectroscopy as explained in Section 3.1.3.

3.1.3. UV-Vis absorption spectra

The bandgap energy of the catalyst was measured in a visual spectrum of 200–800 nm before and after recycling, using BiSo4 as a baseline compound. The introduction of iron resulted in a reduction in composite beads' energy gap compared to TiO_2, as seen in the

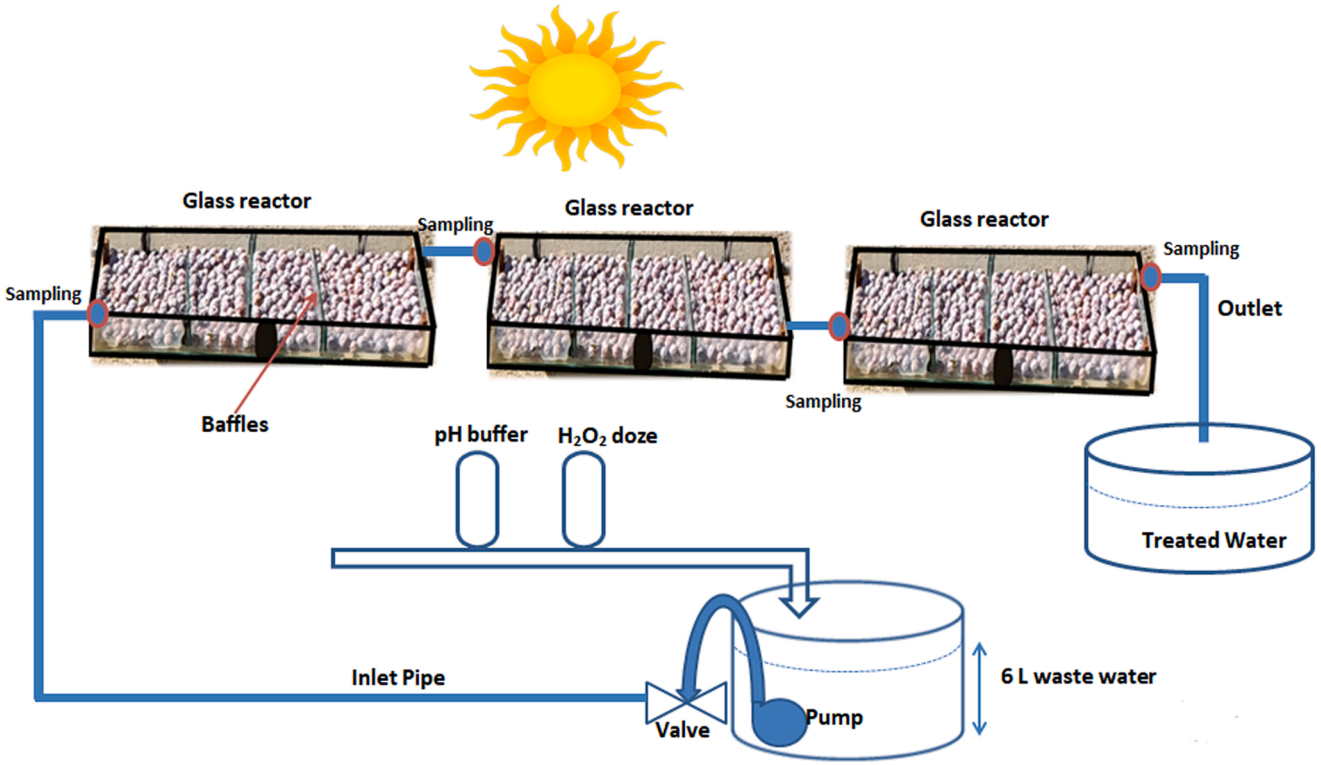

Fig. 1. Schematic diagram of the once-through reactor in series.

supporting information file (Fig. S2b). It demonstrates the catalytic beads' capacity to absorb light in the visible area. The absorbance range of TiO_2 was determined to be 450 nm and then changed to 470 nm and 490 nm before and following catalytic bead recycling. TiO_2 has a bandgap energy of 3.1 eV, which is lowered to 2.9 eV for newly coated composite and 2.8 eV for recycled composite beads. The bandgap energy of the synthesized catalyst was determined using Tauc's relation (Eq. (2) [1]):

$$(\alpha\vartheta h)^{\frac{1}{n}} = K(h\vartheta - Eg) \quad (2)$$

Where Eg is the energy bandgap (eV), h is Planck's constant (m-kg-sec), Hz is the photon frequency, and K is the proportionality constant.

3.1.4. FT-IR analysis

Freshly coated as well as recycled Fe-TiO_2 beads were analyzed using FTIR to determine the type of structural unit present in the system, as shown in the supporting information file (Fig. S2c). There are four bands present in the system having wavenumbers greater than 1500 cm^{-1}. This is because of the absorption of moisture by the crystalline material resulting in the stretching of the H-O-H bond between the wavenumber of 3398.8 cm^{-1}-1632.2 cm^{-1}. The O-H group was discovered at wavenumbers 3398.8 cm^{-1}, and 3413.1 cm^{-1} in fresh and recycled Fe-TiO_2 beads and stretching vibrations are the primary cause of this group's occurrence [25]. In both newly coated and recycled Fe-TiO_2 beads, a Ti-O-Ti bond in the range 400–1200 cm^{-1} was detected, indicated the presence of TiO_2 lattice. The spectra of fresh and recycled Fe-TiO_2 beads revealed the anatase phase at 472.0 cm^{-1} and 479 cm^{-1}, respectively. Similar findings have been obtained previously [26], indicating that the anatase phase exists in the 400–600 cm^{-1} wavenumber range due to the presence of Ti-O-Ti vibrations. The Fe-O-Ti bond was detected at a wavenumber of 2924.9 cm^{-1}, indicating iron in recycled Fe-TiO_2 beads. Bansal et al. [26] also observed a comparable peak of the Fe-O-Ti bond in Fe-TiO_2 beads.

3.1.5. Retention time distribution (RTD) study

To confirm the hydrodynamic behavior and flow pattern of the once-through reactor, an RTD approach was performed. RTD, the hallmark technique for examining the ideal reactor behavior, may also be used to scale up proposals for improved efficacy conditions. For implementing the RTD approach Exit age distribution (E (t)) was used. The E (t) distribution was calculated using Eq. (3) and the Peclet number (Pe) was also calculated and mentioned in Eq. (4):

$$E(t) = \frac{S(t)}{\int S(t)dt} \quad (3)$$

where S (t) denotes the tracer's concentration (mg L^{-1}) and t denotes the time (min).

$$Pe = \frac{\vartheta L}{D} \quad (4)$$

where ϑ designate the velocity of flow (m/s), L denotes the characteristics length (m), and D denotes the dispersion coefficient (m^2 /s).

The experimental and the theoretical retention time ought to have no distinction at the typical working conditions. If the theoretical retention time is less than the actual retention time, then it may be reasoned that either the particles of the tracer might have been held back or the flow rate calculations might be rechecked. Henceforth, for this reason, the dead volume (% Vd) was determined using Eq. (5).

$$\%Vd = 1 - \frac{T}{t} \times 100 \quad (5)$$

Methylene blue was used as a tracer for the RTD study. For modeling, the plug flow reactor model closed to diffusion was used. The average theoretical and actual resident time of 42 min and 45 min respectively was observed which are fairly similar to each other. The dispersion found in Fig. 2 is less as the 3 reactors were linked in series with less flow rate (6 L h^{-1}) prompted to the dispersal of the tracer when it moves from one reactor to the next. The estimation of the peclet number (Pe) was acquired as 78 and the dead volume was found to be very less i.e. 0.06, confirming the more contact time of the catalyst with the pollutant. The plug flow approach with the least dispersion is shown by this high Pe number.

3.1.6. Proposition of the hybrid-process

This study aims to illustrate practical applications of hybrid Fe-TiO_2 composites in the entirely fixed mode for the inactivation of *E. coli*. This unique idea of composite beads is designed so that lixiviation of iron takes place in the wastewater under acidic circumstances, hence facilitating photo-Fenton reactions followed by photocatalytic activity via surface-coated TiO_2. Additionally, the consistent iron lixiviation in the reactor aids in preventing the production of iron sludge through Fe^{3+} photoreduction. The following theory explains the role of e^-_{CB} in the reduction of Fe^{3+} and usage of H_2O_2 and sunlight in the photoreduction of Fe^{3+} to Fe^{2+}, resulting in the enhanced generation of OH° (predominance of hybrid effect):

TiO_2-photocatalysis is a well-established method (Eqs. (6–8)) that utilizes h^+_{VB} and e^-_{CB} to generate oxidant radicals. Furthermore, the addition of H_2O_2 and Iron lixiviating from the beads resulted in introducing the photo-Fenton process, as shown in Eqs. (9–11), and showed a 6.2 unit log reduction in just 45 min of inactivation time, as mentioned in section 3.3.5. As stated in Eq. (1), the hybrid process lowers e^--h^+ recombination by engaging the e^-_{CB} with Fe^{3+} to regenerate Fe^{2+} (Eq. (12)). Additionally, the presence of H_2O_2 serves a dual purpose by interacting with Iron (as discussed previously) and with TiO_2, as demonstrated in Eq. (13). As a result, this technique resulted in an increased OH° generation. A different series of tests was conducted to cross-verify the presence of a hybrid effect caused by the postulated mechanism. The involvement of e^-_{CB} to reduce Fe^{3+} to Fe^{2+} process (Eq. (12)) was cross-validated by conducting the experiments at different time intervals, as illustrated in Fig. 3a. Additionally, the effect of H_2O_2 and solar irradiation on Fe^{3+} photoreduction was verified by conducting some tests, as shown in Fig. 3b. A decrease in the concentration of Fe^{2+} was observed in Fig. 3b, which could be a result of Fe^{3+} photoreduction. The idea of TiO_2 e^-_{CB} extraction and usage of H_2O_2 for Fe^{3+} reduction in in-situ hybrid process was validated by the excess production of OH° (as determined by photo luminance analysis), which aided in the disinfection of *E. coli* in the manner shown in Fig. 3c.

To evaluate and confirm the differences in inactivation efficacy

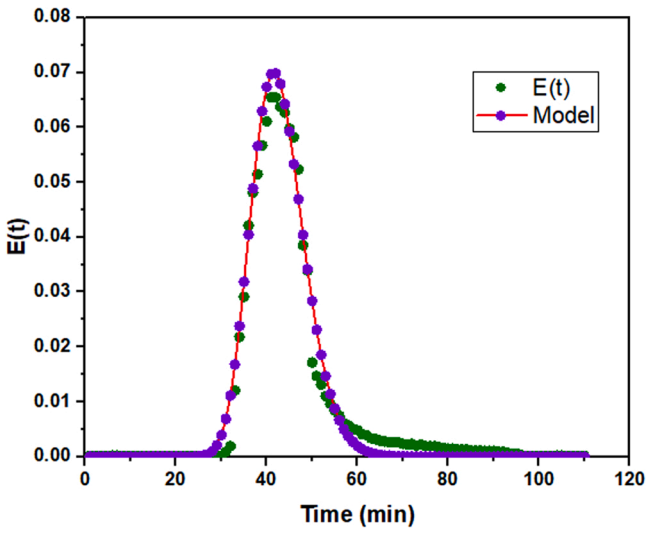

Fig. 2. RTD curve attained from the experimental analysis of the three reactors in series along with axial dispersion of fitted model.

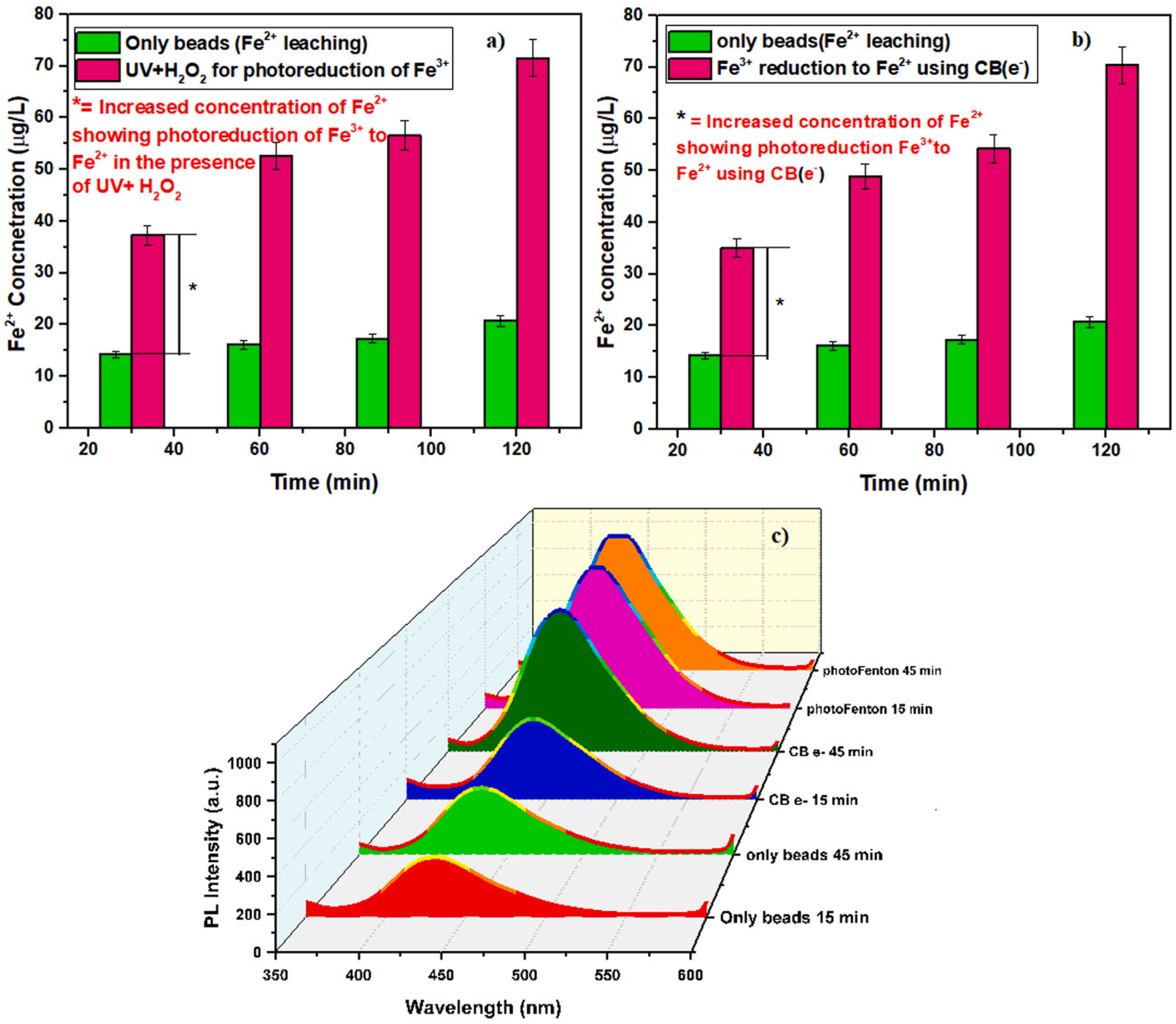

Fig. 3. (a) Photoreduction of Fe^{3+} to Fe^{2+} using e^-_{CB} (b) Photoreduction of Fe^{3+} to Fe^{2+} using photo-Fenton process (c) OH radical spectra using a fluorescence spectrophotometer.

among these three separate processes (hybrid, photocatalysis, and photo-Fenton), inactivation log reductions of *E. coli* are shown in Table 1. The hybrid method resulted in a log decrease of 6.2 units. On the other hand, photocatalysis and photo-Fenton demonstrated a reduction of 2.2 unit logs and 3.4 unit logs, respectively. The hybrid process's rate constant was much greater than that of the other two processes. This is sufficient evidence to demonstrate the hybrid process has increased OH° generation. As anticipated, the hybrid inactivation efficacy was nearly twice that of the photocatalyst and photo-Fenton processes alone. Thus, our results confirmed the role of an in-situ hybrid effect involving both the TiO_2 active layer (which resulted in photocatalysis) and for photo-Fenton, iron lixiviation from the beads, resulting in increased OH° production. Fig. 4 shows the schematic diagram of *E. coli* inactivation using this hybrid effect.

Table 1
Inactivation log reduction of different processes.

S. No	Different techniques	Log reduction
1	TiO_2-Photocatalysis	2.2
2	Photo-Fenton	3.4
3	Hybrid process	6.2

$$TiO_2 + \ uv \ \rightarrow TiO_2(e^- + h^+) \quad (6)$$

$$e^-_{CB} + O_2 \rightarrow O_2^- \quad (7)$$

$$h^+_{(TiO_2)} + \ H_2O_2 \rightarrow \ OH^\circ + \ H^+ \quad (8)$$

$$Fe^{2+}_{(aquous)} + \ H_2O_2 \rightarrow \ Fe^{3+}_{(aquous)} + \ OH^\circ + \ OH^- \quad (9)$$

$$Fe^{3+}_{(aquous)} + \ H_2O_2 \rightarrow Fe^{2+}_{(aquous)} + \ H_3O^+ + \ HO_2^- \quad (10)$$

$$Fe^{3+}_{(aquous)} + \ H_2O \ \xrightarrow{uv} \ Fe^{2+}_{(aquous)} + \ OH^\circ + \ H^+ \quad (11)$$

$$Fe^{3+}_{(aquous)} + e^-_{(CB\ )} + H_2O \rightarrow Fe^{2+}_{(aquous)} + OH^\circ + H^+ \quad (12)$$

$$e^-_{(CB)} + H_2O_2 \rightarrow OH^\circ + OH^- \quad (13)$$

3.2. Results obtained from experimental testing

To validate the prominence of the hybrid effect, the preliminary

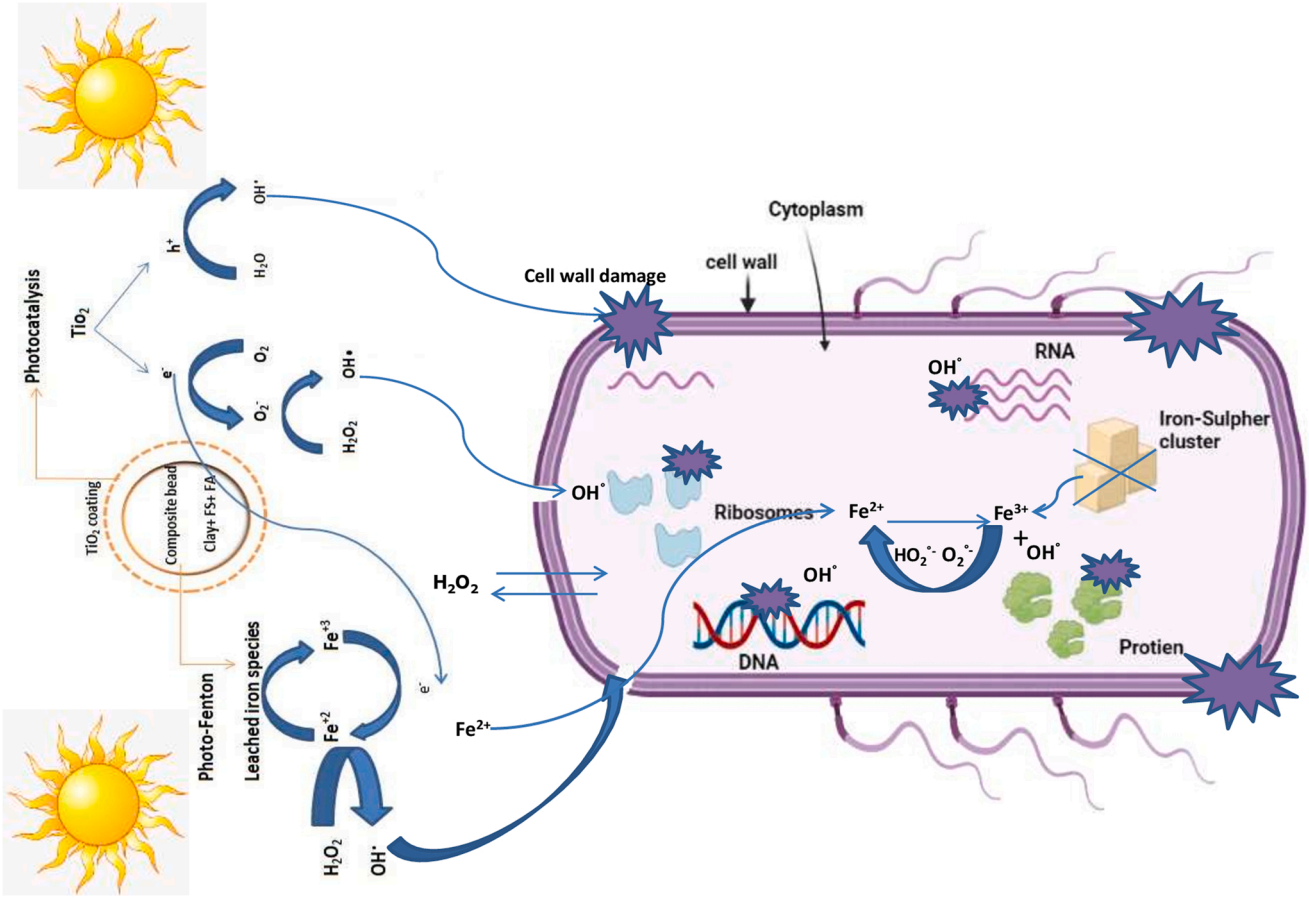

Fig. 4. Schematic diagram of *E. coli* inactivation using the hybrid process.

studies were executed using all the blank experiments (dark experiment, solar-light, solar-light/H_2O_2, TiO_2-assisted photocatalysis, and photo-Fenton process).

3.2.1. Dark and controlled experiments

The changes that occurred in the cell count of *E. coli* (log CFU mL^{-1}) in dark conditions are discussed in Fig. 5. The small change (<1 log reduction) could be attributable to the dying of sensitive cells, mostly because of the osmotic shock introduced in milli-Q water. Similar findings were observed with H_2O_2 (log reduction less than 1). The viability of the *E. coli* in dark conditions was also tested at pH 4–4.5 in the reactor and no significant decrease in the *E. coli* cell count was found as shown in Fig. 5. The same results were obtained when Rodríguez-Chueca et. al [14] studied the cell viability at the acidic condition and negligible reduction was observed. Concerning Fe^{2+} leaching, *E. coli* inactivation was close to 0.2 log reduction in 2 h. Therefore, showing no effect on the viability of the cells.

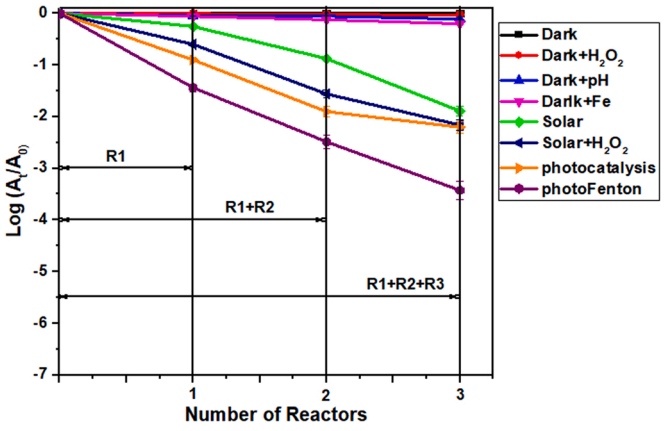

Fig. 5. Preliminary experiments of *E. coli* inactivation.

In this study, solar light only, solar+H_2O_2, TiO_2-photocatalyst, photo-Fenton in the once-through fixed-bed reactor were studied for analyzing and comparing the inactivation efficacy. It was observed from Fig. 5 that only solar irradiation and solar irradiation with 70 mg L^{-1} of H_2O_2 indicated 1.9 and 2.5 *E. coli* log reduction, respectively. In the TiO_2-photocatalysis, the reaction was carried out with composite beads coated at the neutral condition in the presence of solar light, and approximately 2.9 log reduction was observed on illumination for 2 h. Adan et. al. [27] reported the application of glass raschings coated with TiO_2 for inactivation of *E. coli* and found almost the same log reduction in 2 h of treatment time.

In the photo-Fenton process, the pH of the reaction was maintained a 4–4.5 for the iron lixiviation to start, and correspondingly *E. coli* inactivation was observed as given in Fig. 5. In acidic conditions, iron lixiviating from clay often occurs because it helps to tear the iron bond with other organic compounds and induces iron extraction, known as iron leaching [28]. In this process, 70 mg L^{-1} of H_2O_2 was added for the reaction to start and about 3.9 log reduction in *E. coli* was found in 2 h of reaction time. The iron lixiviation and H_2O_2 addition inflict two significant changes in the inactivation of bacteria.

After studying the control experiments, the prominence of the hybrid process was set by optimizing the following parameters.

3.2.2. Effect of number of reactors

In addition to raising concerns about the area needed, the number of

reactors in a series will affect the conversion rate of any pollutant. To study this, the number of reactors was varied to three (Fig. 6a) and efficiently measured the *E. coli* cell count after exiting from each reactor. In this series configuration of three reactors, 6 L of simulated wastewater was treated, with an H_2O_2 concentration of 50 mg L^{-1} and the flow rate of 10 L h^{-1}. To keep the entire experiment economically viable, the treatment of *E. coli* was done under natural solar light. The cell count of *E. coli* was found to decrease with the increasing number of reactors as shown in Fig. 6a. It was observed that only 0.9 log reduction in *E. coli* after the wastewater exited from the 1st reactor with RTD of approximately 10 min. The entire process was operated at the defined flow rate in once-through mode. It can be seen from Fig. 6a that there was a further decrease in the cell count of *E. coli* with the increase in the number of reactors in series. After the 2nd reactor, nearly 2.3 log reduction was observed. Also, by adding one more reactor, the efficacy of the treatment reactor was improved with the increase in the log reduction (3.4) of *E. coli*. The number of the reactor was not increased beyond this point because the decrease in the cell population was not the only aspect in the determination of the optimized number of reactors.

3.2.3. Effect of number of baffles

The addition of baffles to the reactor is intended to increase the residence time and thus improve the reactor's disinfection performance. In the current study, the number of baffles was varied from 1 to 4. It can be seen from Fig. 6b that with increasing the baffles from 1 to 3 the log reduction was also increased and reached 3.8 log. Later, the effectiveness of disinfection began to decrease, which may be accredited to the shading effect of the baffles. The prevalence of the shading effect of baffles caused an ineffective absorption of photons of solar light by the catalyst. A similar pattern was observed in a study done by Adishkumar et al. [29] where the decrease in the *E. coli* cell count was reduced with 3 baffles due to the shading effect.

3.2.4. Effect of the flow rate

In the current work, the flow rate of the reactor was changed from 2 ± 1 L h^{-1} to 14 ± 1 L h^{-1} with H_2O_2 concentration of 50 mg L^{-1} under natural solar irradiation using three glass reactors in series. From Fig. 6c, It was found that the inactivation of *E. coli* in the water started to decrease with an increase in the flow rate from 2 ± 1 L h^{-1} to 14 ± 1 L h^{-1}. This might be accredited to less time for the interaction of bacterial cells with the composite material. However, a further decrease in the flow rate would increase the efficacy of the reactor but would hinder its commercial viability by increasing the higher energy consumption. At a flow rate of 2 ± 1 L h^{-1}, the reaction time was 1 h 20 min

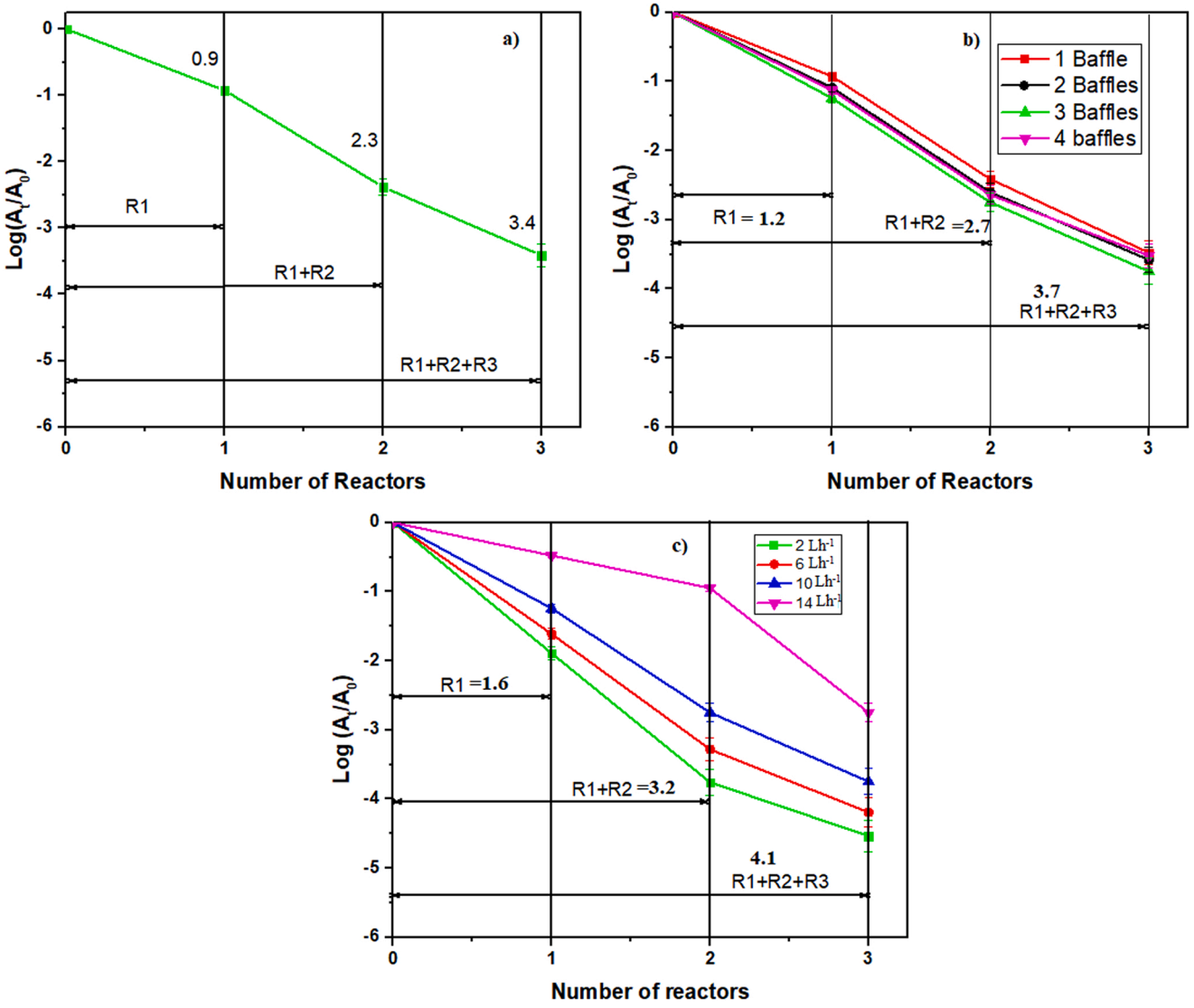

Fig. 6. Change in the cell count of *E. coli* with (a) variation in the number of reactors from 1 to 3 (b) variation in the number of baffles from 1 to 4 (c) variation in the flow rate of the reactor from 2 to 14 L h^{-1}.

with an overall log reduction of 4.5 at the outlet of the third reactor. In this study, with the increase in the flow rate to 14 ± 1 L h^{-1}, 2.7 log reduction of *E. coli* was found but the total reaction time was also decreased. Moreover, the log reduction of *E. coli* at 2 ± 1 L h^{-1} and 6 ± 1 L h^{-1} was almost the same at the end of the 3rd reactor. Therefore, from an economic point of view, 6 ± 1 L h^{-1} was preferred as the optimized flow rate for further experimentation.

3.2.5. Effect of surface area covered

In this study, the effect of surface area covered on the *E. coli* disinfection was evaluated by changing the number of composite beads according to the surface area available. This effect studies the optimum quantity of catalysts in terms of the number of beads needed for disinfection. The analysis was therefore depicted in terms of a percentage area covered, with changing the number of beads. The surface area was varied from 50% to 100% coverage and an increase in the log reduction of *E. coli* was observed as shown in Fig. 7a. The increased amount of catalysts improves the inactivation rate of *E. coli*. Simultaneously as the water is flowing from one reactor to another, the *E. coli* is coming in contact with the new fixed-bed composite catalyst placed in the reactor as seen from Fig. 7a thus increasing the active sites, leading to the production of more OH° and increase in the inactivation efficacy.

3.2.6. Effect of H_2O_2 concentration

The addition of H_2O_2 in the hybrid process is utilized simultaneously in both processes for the generation of OH°. This in-situ hybrid effect improves the reaction rate by using H_2O_2 as an electron acceptor. In this framework, the study was done using visibly active Fe-TiO_2 composite beads at acidic conditions (pH of 4–4.5) with varying H_2O_2 concentrations. As discussed earlier, the reactor was optimized with three glass reactors in series. In this case, the H_2O_2 concentration from 10 to 70 mg L^{-1} was used for the disinfection study. From Fig. 7b it was found that by increasing the H_2O_2 concentration, the rate of log reduction was increased up to 50 mg L^{-1}. This concentration of H_2O_2 has also shown some effective results (approximately 100% inactivation) in different studies found in the literature [30,31]. Further, with the increase in the concentration up to 70 mg L^{-1} no change in the cell count of *E. coli* was observed. This could be the scavenging effect of H_2O_2 at a high concentration. Therefore, 50 mg L^{-1} of H_2O_2 concentration was selected as the optimized concentration for the inactivation of *E. coli,* and approximately 6.2 log reduction was observed.

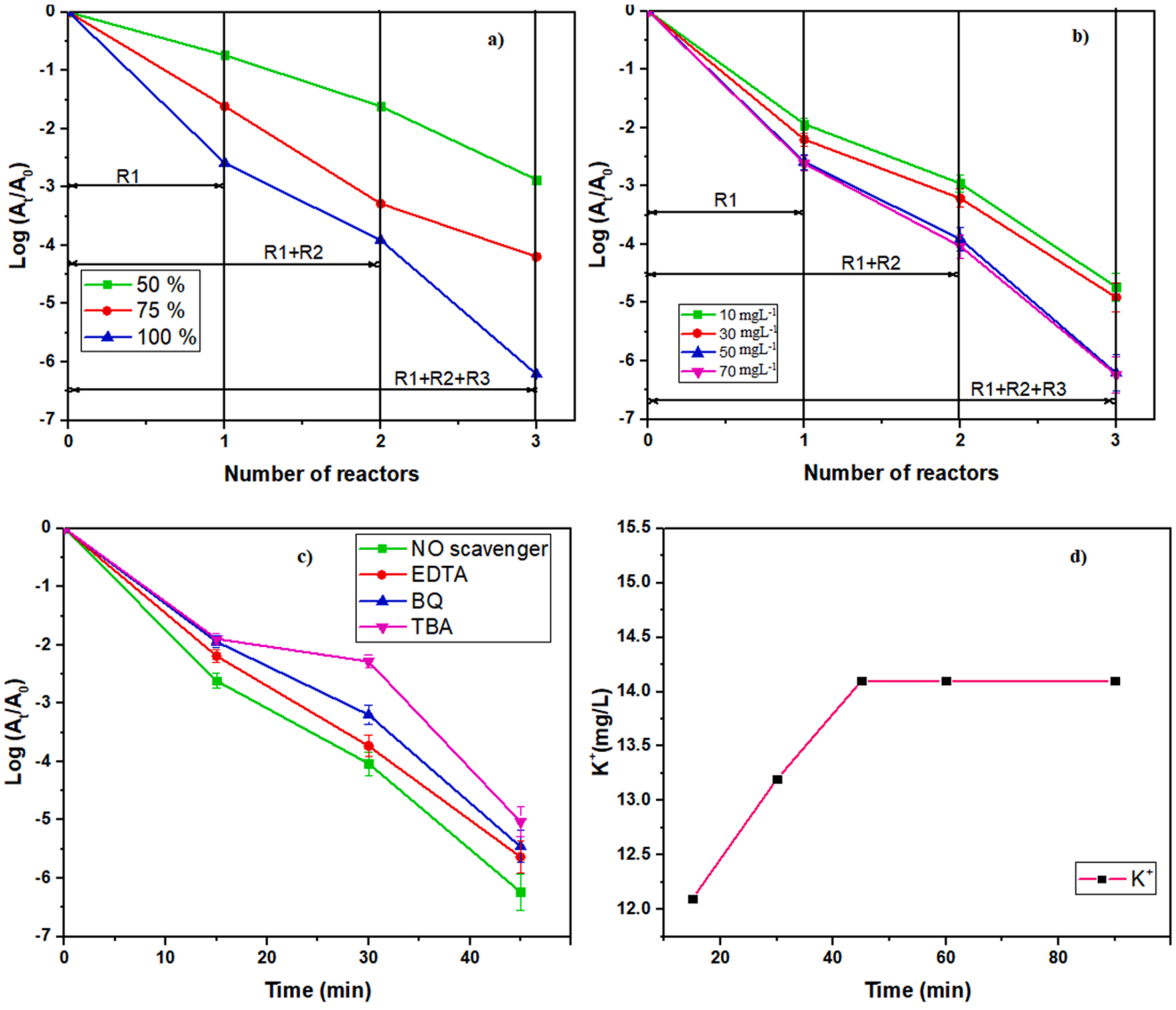

Fig. 7. Change in the cell count of *E. coli* with (a) variation in the % of surface area covered from 50% to 100% (b) variation in the concentration of H_2O_2 from 10 to 70 mg L^{-1} (c) Trapping study of different ROS (d) leakage of potassium ion from the cell damage.

3.2.7. Discussion of the experimental results

In this study, maximum log reduction was obtained in order: hybrid process > photo-Fenton > photocatalysis > solar+H_2O_2 >solar. No change in the bacterial cell count was found when the experiments were conducted in dark without adding any reagents. This showed that the bacterial count doesn't get affected by milli-Q water in 2 h of experimentation. When the bacterial cells were put in the milli-Q water they enter a "stationary" phase due to an acclimatization shock from the osmotic difference, they take in a lot of water and do pretty much nothing and similar results were observed in previous study mention in the literature [32] where no change in the cell count was observed in 2 h. Although *E. coli* produces H_2O_2 within the system when is regulated by some enzymes present inside the cell. This presence of an oxidant does not affect the viability of the cells until this equilibrium is disturbed [33]. Similar findings were observed with H_2O_2 as its polarity is the same as that of water which lets its diffusion into the cell and possibly damages the cell via internal Fenton reaction through oxidative stress, but the presence of catalases (kat) and alkyl hydroperoxide reductase (ahp) in the cytosol of stationary phase and in the growing cells respectively [33] results in the faster decomposition of H_2O_2. In our study mainly KatE protected the cell against H_2O_2 because the stationary phase cells were used for the entire experiment [34]. Previous work, however, showed that the concentration of intracellular H_2O_2 is 20% relative to the external addition (in scavenging-proficient cells) [33]. Hence, under the operating conditions studied, this mode of action is negligible.

SODIS settings demonstrated a modest potential for disinfection (0.25 Log decrease), but were more effective than dark-Fenton conditions. Now the efficacy of the solar disinfection is increased by using TiO_2 catalyst coated on the clay beads and also with the photo-Fenton process by using the composite beads (without TiO_2 coating). The current study's poor inactivation efficacy using TiO_2 photocatalysis may be attributable to the rapid recombination of charge carriers in the semiconductor, leading to less generation of ROS, which eventually decreases the system's efficacy [35]. The disinfection mechanism of TiO_2 photocatalysis has yet not been discovered. several studies, however, have revealed various mechanisms. The ROS such as $O_2^{-\bullet}$, OH°, and HO_2° produced on the TiO_2 surface gives rise to the oxidative stress inside the cell which causes the inactivation of the cell. From the previously reported studies, it was found that the presence of TiO_2 affects the respiratory system of cells by lipid peroxidation reaction. Other studies reported that [36] the *E. coli* inactivation occurs because of the disordering and damage of the outer cell membrane. This degraded outer membrane of the cell helps in the penetration of ROS into the cytoplasm which leads to the loss of intracellular materials [37]. The half-life time of highly reactive OH° is very short in comparison to the $O_2^{-\bullet}$ [38]. But still cannot damage the DNA of the cell because of their charge. Therefore, external cell damage is considered the first step of cell damage in TiO_2 photocatalysis until the TiO_2 particle enters the cell. Whereas in the case of the photo-Fenton process, the inactivation rate is higher in comparison to the other processes because of the intracellular and extracellular inactivation of *E. coli*. First is the oxidation of bacterial cells externally due to the excessive production of OH° in the system (reaction of iron with H_2O_2 [39]. The second is the internal oxidation of bacterial cells after the inactivation of catalases via diffusion of H_2O_2 and Fe^{2+} into the cell through porins. This is because of the small size of the H_2O_2 ion (1.2–1.4 Å) and the Fe^{2+} (<6 Å) as compared to bacterial size (11 Å). As this process takes place in the presence of sunlight, the internal ROS interacts with the Fe^{2+} ion, resulting in cell damage [32]. Whereas H_2O_2 can induce catabolic and biosynthetic function moderation, which will lead to Fe loss from the S/Fe cluster and produces OH°. The H_2O_2 also disrupts the cell wall externally, thus led to the degradation of the cell wall due to a major influx of H_2O_2. It occurs because the oxidative activity of H_2O_2(0.18) is higher than the membrane's oxidation potential. The external oxidation of the cell wall is happening due to the homolysis of H_2O_2 and the reaction of Fe with H_2O_2 generating an excessive amount of ROS.

After establishing the boundary conditions the prominence of the hybrid process was set doing parametric optimization of once-through fixed bed reactors. This hybrid process showed an aggressive reduction in *E. coli* cell count with 100% inactivation in water in 45 min of the treatment time. This effective result was obtained when the 3 reactors in series having a flow rate of 6 L h^{-1}, 100% surface area covered with beads, and 50 mg L^{-1} of H_2O_2 were used.

The optimum number of reactors determined is based on the system's maintenance and its control which further depends on the reactor's configuration, nature of pollutant, and conversion factor [15]. Miyawaki et al. [15] used slurry bubble column reactors in series for investigating the degradation of cyanide. It was found that for attaining 99% of degradation, 8 reactors in series were observed to be the optimal number. In these types of reactors, it is not possible to imagine a realistic solution as enormous loss in energy might occur due to photocatalysis in suspension. In the current study, while the disinfection efficacy of *E. coli* will be further improved by an additional number of reactors (>3), this could make the maintaining and regulation of the system difficult. In this framework, the number of reactors has not been increased further though attempts have been made to boost the disinfection efficacy of *E. coli* by optimizing other operational parameters by selecting 3 as the optimized number of reactors.

In the disinfection studies, especially in the plug flow reactor, the flow rate plays a significant role as it decides the amount of oxygen and turbulence level in the system. Variation in the flow rate changes the residence time of the reactor consequently affecting the disinfection efficacy. Wang et. al studied the flow-through reactor [16], where the inactivation of *E. coli* was observed under different flow rates using ultraviolet-C (UV-C) light-emitting diodes (LEDs) and found out that the *E. coli* log reduction started to decrease by increasing the flow rate beyond 2 ± 1 L h^{-1}. A higher flow rate decreases the interaction time between the catalyst and the pollutant. But on the other hand, the minimum flow rate would affect the economy of the operational system. Therefore, from an economic point of view, 6 ± 1 L h^{-1} was preferred as the optimized flow rate for further experimentation. After optimizing the different conditions the treatment time of this technology was found to be very less as compared to some other studies where approximately similar oxidant doze was used [30,31] for 100% killing of bacteria. This decrease in the treatment time can be attributed to the hybrid effect of the proposed technology where TiO_2 photocatalysis and photo Fenton process is working simultaneously for the higher production of OH°. Hence this technology has proved its competence in terms of the effective utilization of waste materials as a promising concept for the wastewater post-treatment, that could find successful real-life applications.

3.3. Trapping study

To determine the main oxidative holes or radicals (ie. OH°, $O_2^{\bullet-}$,and h^+) responsible for solar hybrid disinfection of *E. coli* through Fe-TiO_2 composite, several experiments were carried out at optimum experimental conditions over 60 min reaction employing different quencher compounds like tert-butyl alcohol (TBA) for OH°, disodium ethylene diamine tetraacetic acid (EDTA) for h^+, and p- benzoquinone (BQ) for $O_2^{\bullet-}$ at a concentration of 0.01 M (Fig. 7c). The results demonstrated a decrease in the log reduction in the presence of all trapping agents which revealed that all the mentioned oxidative species are responsible for the disinfection of *E. coli*. However, TBA showed a decrease in the log reduction from 6.2 to 5.0 which indicates that OH°are the most prominent agents in the *E. coli* inactivation process.

3.4. E. coli cell damage checked by K^+ leakage

The outer membrane of *E. coli* is made up of a lipopolysaccharide layer that plays an important role by acting as a barrier to the

permeability of the Gram-negative bacteria. The Fe-TiO_2 composite could damage the outer cell wall and the membrane by ROS and could lead to an increase in the permeability of the cell and subsequent seeping of intracellular substances such as K^+ [40,41]. Therefore, K^+ leakage from the inactivated *E. coli* under different time intervals was examined to study the permeability of the cell membrane (Fig. 7d). A gradual increase in the K^+ concentration was observed till 60 min of the treatment and then became steady with an increase in the treatment time. In this hybrid effect study, the K^+ ion instantly leaked out, and the concentration of leaked K^+ increased in parallel with the *E. coli* inactivation with irradiation time. The total K^+ concentration (15.1 ppm) from the tested *E. coli* was completely released when all the *E. coli* was completely killed at 60 min of irradiation. This result suggested that the cell membrane permeability had been disrupted with the inactivation of *E. coli.*

3.5. Photo-reactivation of E. coli

During many deactivation experiments, the bacteria tend to regrow by repairing their damaged DNA in the absence (dark condition) or in the presence (photo-reactivation) of light. Thus, the reactivation studies of *E. coli* in treated water were done in the dark and natural solar light. The photoreactivation capacity was assessed by taking out 100 mL of the treated water after each experiment. The treated sample was stored in a sterile conical flask and kept at continuous stirring for 3 h, 24 h, and 48 h under dark and natural solar light conditions as shown in Table 2. The viability of *E. coli* in the treated sample was analyzed using the same standard method implemented for inactivation experiments.

Nd*= Not detected.

4. Synergistic effect

The synergy of the hybrid process over the other two processes is mentioned in Supporting information in Section 4. Calculations were done using Eq. 14–16 mention in supporting information.

5. Reusability of the Fe-TiO_2 catalyst

The biggest challenge in fixed-bed catalytic reactors is the durability/longevity of the catalyst for repeated cycles. For this novel concept, things get more complex as this technology needs to handle two techniques at the same time and in the same place. For this technology to work smoothly the intactness of the photoactive TiO_2 layer over the surface and incessant iron lixiviating from the Fe-TiO_2 composite plays a very significant role. In this study, Fe-TiO_2 composite made from FS+FA were recycled for more than 100 cycles as shown in Fig. 8. Even after 100 cycles, the composite beads were found to be capable enough to perform both the process simultaneously in the system, thus further claim the novelty of the study. The concentration of iron in the system (lixiviating from the beads) was tested after 100 cycles also and the existence of the TiO_2 layer over the composite beads even after 100 cycles were confirmed by XRD and SEM-EDS analysis. It was found that the activity of the Fe-TiO_2 catalyst decreased by 5% only. The reactivation of composite beads after each recycling was done by keeping it in an oven at 80–90 °C overnight. This further strengthens the author's argument to visualize the real-life application of the hybrid process as it controls the economy of the technology.

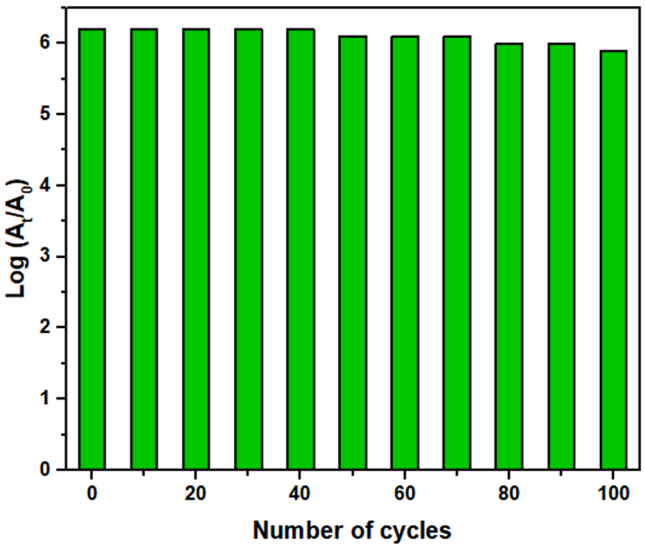

Fig. 8. Reusability/durability study of Fe-TiO_2 composite.

6. Scale-up studies and cost analysis

The scale-up studies are the significant part as they serve the interface between the prototype and the model which is performed using the scale-up factors. The commercial-scale applications of any process would certainly contemplate the economics of the process. The present research emphasizes the estimation of process economics by combining the tentative cost of raw materials and other process variables. The approximated cost involved in the treatment of wastewater is mentioned in Table S1. The anticipated cost can further be changed once the design components of the industrial-scale reactors were taken into consideration. To gauge the treatment cost of a modern scale reactor, let us think about the measure of wastewater being 6000 L. To assess this, the 0.6 rule was utilized for scaling up [42] and according to Eq. (17).

$$Cost_B = Cost_A\left(\frac{Size_B}{Size_A}\right)^N \quad (17)$$

The size exponnt is denoted by N, the dimensionless size factor is denoted by $Size_A/Size_B$. As discussed, we have considered scaling up the reactor by 6000 times. The values for various N were reported from [42].

The cost analysis showed the total cost of operation to be 0.00827 US $ for one reaction per cycle making it more feasible for the application in the industries as shown in Table S2. The expenditures indicated in the present research are much less than those found in earlier research on AOPs [43,44]. The majority of researches have assessed simply the cost of electricity consumed during the reactions or the cost analysis not taking into account the cost of fabrication of reactor [45,46]. Due to the remarkable reusability/durability of Fe-TiO_2 composite beads, the total cost of the present technique can be decreased further by using them for multiple cycles. As a result, a cascade reactor system equipped with extremely stable and durable Fe-TiO_2 composite beads would provide a

Table 2
Photoreactivation of *E. coli* under natural solar light and dark conditions, in solar light, inactivated water.

Technology	*E. coli cell count*	*Treatment time (min)*	*Treatment*	*E. coli Survival after 3 h inactivation*		*E. coli survival after 24 h of Inactivation*		*E. coli survival after 48 h of Inactivation*	
				light	*dark*	*light*	*dark*	*light*	*dark*
Phtotocataysis	10^6 CFU mL^{-1}	120 min	Solar irradiation	Nd*	Nd	Nd	Nd	Nd	Nd
Photo-Fenton	10^6 CFU mL^{-1}	100 min	Solar irradiation	Nd	Nd	Nd	Nd	Nd	Nd
Hybrid	10^6 CFU mL^{-1}	45 min	Solar irradiation	Nd	Nd	Nd	Nd	Nd	Nd

reduced-cost solution for wastewater treatment with a short treatment time.

7. Conclusion

The current research has documented the effective fusion of AOP with PFR and effectively used this technology for solar disinfection studies. For the execution of PFR, novel and visibly active Fe-TiO_2 composites were used that were capable of integrating in-situ dual effects with a significant reduction in treatment time. The reactor approached the plug flow condition (PFR) in 45 min of retention time (Ƭ) and a 100% inactivation of *E. coli* cells was observed with an H_2O_2 dose of 50 mg L^{-1}, 100% surface area covered, 6 L h^{-1} of flow rate, and three reactors in series. Furthermore, these Fe-TiO_2 composite showed exceptional durability even after 100 recycles that further claims the novelty of this technology. The total operating cost for treating water came out to be 0.00827 US$ for one reaction per cycle. No regrowth of bacterial cells in the solution even after 48 h of treatment, clearly indicated the commercial viability of the present reactor system. Also, the total cost of the process assessed in this study is substantially lower than other AOPs-related studies found in the literature. Therefore, the current fixed-bed once-through reactor under sunlight integrating in-situ dual effect with demonstrated validity of theoretical prediction might be efficiently used at a large-scale to handle the wastewater in lesser time.

Declaration of Competing Interest

The authors declare that they have no known competing financial interests or personal relationships that could have appeared to influence the work reported in this paper.

Acknowledgments

The authors would like to thank the central instrumentation laboratory and sophisticated analytical instrumentation facility, Punjab University, Chandigarh, India for providing their facilities for the characterization of samples.

Appendix A. Supporting information

Supplementary data associated with this article can be found in the online version at doi:10.1016/j.jece.2021.106322.

References

[1] T. Hu, Y. Yang, K. Dai, J. Zhang, C. Liang, A novel Z-scheme Bi 2 MoO 6 /BiOBr photocatalyst for enhanced photocatalytic activity under visible light irradiation, Appl. Surf. Sci. 456 (2018) 473–481, https://doi.org/10.1016/j.apsusc.2018.06.186.

[2] D. Xia, H. Liu, B. Xu, Y. Wang, Y. Liao, Y. Huang, L. Ye, C. He, P.K. Wong, R. Qiu, Single Ag atom engineered 3D-MnO2 porous hollow microspheres for rapid photothermocatalytic inactivation of E. coli under solar light, Appl. Catal. B Environ. 245 (2019) 177–189, https://doi.org/10.1016/j.apcatb.2018.12.056.

[3] X. Zeng, D.T. McCarthy, A. Deletic, X. Zhang, Silver/reduced graphene oxide hydrogel as novel bactericidal filter for point-of-use water disinfection, Adv. Funct. Mater. 25 (2015) 4344–4351, https://doi.org/10.1002/adfm.201501454.

[4] Y. Jia, S. Zhan, S. Ma, Q. Zhou, Fabrication of TiO2-Bi2WO6 binanosheet for enhanced solar photocatalytic disinfection of E. coli: insights on the mechanism, ACS Appl. Mater. Interfaces 8 (2016) 6841–6851, https://doi.org/10.1021/acsami.6b00004.

[5] P. Xia, B. Zhu, B. Cheng, J. Yu, J. Xu, 2D/2D g-C3N4/MnO2 nanocomposite as a direct Z-scheme photocatalyst for enhanced photocatalytic activity, ACS Sustain. Chem. Eng. 6 (2018) 965–973, https://doi.org/10.1021/acssuschemeng.7b03289.

[6] D. Xia, W. Xu, Y. Wang, J. Yang, Y. Huang, L. Hu, C. He, D. Shu, D.Y.C. Leung, Z. Pang, Enhanced performance and conversion pathway for catalytic ozonation of methyl mercaptan on single-atom Ag deposited three-dimensional ordered mesoporous MnO2, Environ. Sci. Technol. 52 (2018) 13399–13409, https://doi.org/10.1021/acs.est.8b03696.

[7] S. Weon, E. Choi, H. Kim, J.Y. Kim, H.J. Park, S.M. Kim, W. Kim, W. Choi, Active {001} facet exposed TiO2 nanotubes photocatalyst filter for volatile organic compounds removal: from material development to commercial indoor air cleaner application, Environ. Sci. Technol. 52 (2018) 9330–9340, https://doi.org/10.1021/acs.est.8b02282.

[8] D. Wang, L. Zhao, H. Ma, H. Zhang, L.H. Guo, Quantitative analysis of reactive oxygen species photogenerated on metal oxide nanoparticles and their bacteria toxicity: the role of superoxide radicals, Environ. Sci. Technol. 51 (2017) 10137–10145, https://doi.org/10.1021/acs.est.7b00473.

[9] Y. Choi, M.S. Koo, A.D. Bokare, D.H. Kim, D.W. Bahnemann, W. Choi, Sequential process combination of photocatalytic oxidation and dark reduction for the removal of organic pollutants and Cr(VI) using Ag/TiO2, Environ. Sci. Technol. 51 (2017) 3973–3981, https://doi.org/10.1021/acs.est.6b06303.

[10] S. Talwar, A.K. Verma, V.K. Sangal, Plug flow approaching novel reactor employing in-situ dual effect of photocatalysis and photo-Fenton for the degradation of metronidazole, Chem. Eng. J. 382 (2020), 122772, https://doi.org/10.1016/j.cej.2019.122772.

[11] O. Sacco, D. Sannino, V. Vaiano, Packed bed photoreactor for the removal of water pollutants using visible light emitting diodes, Appl. Sci. 9 (2019) 472, https://doi.org/10.3390/app9030472.

[12] T. Pérez, J.L. Nava, Simulations of a single-phase flow in a compound parabolic concentrator reactor, Int. J. Photo (2018 () (2018), https://doi.org/10.1155/2018/2569251.

[13] O. Levenspiel, Chemical reaction engineering, Chem. Eng. Sci. 19 (1964) 91–92.

[14] J. Rodríguez-Chueca, M.I. Polo-López, R. Mosteo, M.P. Ormad, P. Fernández-Ibáñez, Disinfection of real and simulated urban wastewater effluents using a mild solar photo-Fenton, Appl. Catal. B Environ. 150–151 (2014) 619–629, https://doi.org/10.1016/j.apcatb.2013.12.027.

[15] A. Miyawaki, S. Taira, F. Shiraishi, Performance of continuous stirred-tank reactors connected in series as a photocatalytic reactor system, Chem. Eng. J. 286 (2016) 594–601, https://doi.org/10.1016/j.cej.2015.11.007.

[16] C.P. Wang, C.S. Chang, W.C. Lin, Efficiency improvement of a flow-through water disinfection reactor using UV-C light emitting diodes, J. Water Process Eng. (2020), 101819, https://doi.org/10.1016/j.jwpe.2020.101819.

[17] D. Bošković, S. Loebbecke, Modelling of the residence time distribution in micromixers, Chem. Eng. J. 135 (2008) 138–146, https://doi.org/10.1016/j.cej.2007.07.058.

[18] D. Olivet, J. Valls, M.À. Gordillo, À. Freixó, A. Sánchez, Application of residence time distribution technique to the study of the hydrodynamic behaviour of a full-scale wastewater treatment plant plug-flow bioreactor, J. Chem. Technol. Biotechnol. 80 (2005) 425–432, https://doi.org/10.1002/jctb.1201.

[19] G. Towler, R. Sinnott, Des. React. Mixers (2013), https://doi.org/10.1016/b978-0-08-096659-5.00015-8.

[20] A. Gusmao, P.B. Moraes, E. Bidoia, Studies on the electrochemical disinfection of water containing Escherichia coli using a dimensionally stable anode article, Braz. Arch. Biol. Technol. 53 (2010) 1155–1160, https://doi.org/10.1590/S1516-89132010000500029.

[21] J. Marugán, R. van Grieken, A.E. Cassano, O.M. Alfano, Scaling-up of slurry reactors for the photocatalytic oxidation of cyanide with TiO2 and silica-supported TiO2 suspensions, Catal. Today 144 (2009) 87–93, https://doi.org/10.1016/j.cattod.2008.12.026.

[22] P. Bansal, A. Verma, Chemistry Synergistic effect of dual process (photocatalysis and photo-Fenton) for the degradation of Cephalexin using TiO 2 immobilized novel clay beads with waste fl y ash / foundry sand, J. Photochem. Photobiol. A Chem. 342 (2017) 131–142, https://doi.org/10.1016/j.jphotochem.2017.04.010.

[23] I. Thakur, B. Örmeci, A. verma, Inactivation of E. coli in water employing Fe-TiO2 composite incorporating in-situ dual process of photocatalysis and photo-Fenton in fixed-mode, J. Water Process Eng. 33 (2020), 101085, https://doi.org/10.1016/j.jwpe.2019.101085.

[24] I. Thakur, A. Verma, B. Ormeci, Mathematical modeling of E. coli inactivation in water using Fe-TiO 2 composite in a fixed bed reactor, Sep. Technol. 260 (2021), https://doi.org/10.1016/j.seppur.2020.118242.

[25] Z. Sayyar, A. Akbar Babaluo, J.R. Shahrouzi, Kinetic study of formic acid degradation by Fe 3+ doped TiO 2 self-cleaning nanostructure surfaces prepared by cold spray, Appl. Surf. Sci. 335 (2015) 1–10, https://doi.org/10.1016/j.apsusc.2015.01.014.

[26] P. Bansal, A. Verma, In-situ dual effect studies using novel Fe-TiO2 composite for the pilot-plant degradation of pentoxifylline, Chem. Eng. J. 332 (2018) 682–694, https://doi.org/10.1016/j.cej.2017.09.121.

[27] C. Adán, A. Magnet, S. Fenoy, C. Pablos, C. del Águila, J. Marugán, Concomitant inactivation of Acanthamoeba spp. and Escherichia coli using suspended and immobilized TiO2, Water Res. 144 (2018) 512–521, https://doi.org/10.1016/j.watres.2018.07.060.

[28] Z. Hseu, Evaluating heavy metal contents in nine composts using four digestion methods, Bioresour. Technol. 95 (2004) 53–59, https://doi.org/10.1016/j.biortech.2004.02.008.

[29] S. Adishkumar, S. Kanmani, J. Rajesh Banu, I. Tae Yeom, Evaluation of bench-scale solar photocatalytic reactors for degradation of phenolic wastewaters, Desalin. Water Treat. 57 (2016) 16862–16870, https://doi.org/10.1080/19443994.2015.1083481.

[30] E. Ortega-Gómez, B. Esteban García, M.M. Ballesteros Martín, P. Fernández Ibáñez, J.A.S.ánchez Pérez, Inactivation of Enterococcus faecalis in simulated wastewater treatment plant effluent by solar photo-Fenton at initial neutral pH, Catal. Today 209 (2013) 195–200, https://doi.org/10.1016/j.cattod.2013.03.001.

[31] E. Ortega-Gómez, B. Esteban García, M.M. Ballesteros Martín, P. Fernández Ibáñez, J.A.S.ánchez Pérez, Inactivation of natural enteric bacteria in real municipal wastewater by solar photo-Fenton at neutral pH, Water Res. 63 (2014) 316–324, https://doi.org/10.1016/j.watres.2014.05.034.

[32] S. Giannakis, M. Voumard, S. Rtimi, C. Pulgarin, Bacterial disinfection by the photo-Fenton process: Extracellular oxidation or intracellular photo-catalysis, Appl. Catal. B Environ. 227 (2018) 285–295, https://doi.org/10.1016/j.apcatb.2018.01.044.

[33] L.C. Seaver, J.A. Imlay, P. Loewen, Alkyl hydroperoxide reductase is the primary scavenger of endogenous hydrogen peroxide in Escherichia coli downloaded from http://jb.asm.org/ on November 24, 2014 by Univ of California-Berkeley Biosci & natural res lib, J. Bacteriol. 183 (2001) 7173–7181, https://doi.org/10.1128/JB.183.24.7173.

[34] K.L. Nelson, A.B. Boehm, R.J. Davies-Colley, M.C. Dodd, T. Kohn, K.G. Linden, Y. Liu, P.A. Maraccini, K. McNeill, W.A. Mitch, T.H. Nguyen, K.M. Parker, R. A. Rodriguez, L.M. Sassoubre, A.I. Silverman, K.R. Wigginton, R.G. Zepp, Sunlight-mediated inactivation of health-relevant microorganisms in water: a review of mechanisms and modeling approaches, Environ. Sci. Process. Impacts 20 (2018) 1089–1122, https://doi.org/10.1039/c8em00047f.

[35] X. Kang, S. Liu, Z. Dai, Y. He, X. Song, Z. Tan, Titan. Dioxide. Eng. Appl. (2019), https://doi.org/10.3390/catal9020191.

[36] S. Pigeot-Rémy, F. Simonet, E. Errazuriz-Cerda, J.C. Lazzaroni, D. Atlan, C. Guillard, Photocatalysis and disinfection of water: identification of potential bacterial targets, Appl. Catal. B Environ. 104 (2011) 390–398, https://doi.org/10.1016/j.apcatb.2011.03.001.

[37] Z.X. Lu, L. Zhou, Z.L. Zhang, W.L. Shi, Z.X. Xie, H.Y. Xie, D.W. Pang, P. Shen, Cell damage induced by photocatalysis of TiO2 thin films, Langmuir 19 (2003) 8765–8768, https://doi.org/10.1021/la034807r.

[38] F. Collin, Chemical basis of reactive oxygen species reactivity and involvement in neurodegenerative diseases, Int. J. Mol. Sci. 20 (2019), https://doi.org/10.3390/ijms20102407.

[39] S. Giannakis, M. Inmaculada, P. López, D. Spuhler, J. Antonio, S. Pérez, P. Fernández, Solar disinfection is an augmentable, in situ-generated photo-Fenton reaction – part 1: a review of the mechanisms and the fundamental aspects of the process, Appl. Catal. B Environ. 199 (2016) 199–223, https://doi.org/10.1016/j.apcatb.2016.06.009.

[40] C. Hu, J. Guo, J. Qu, X. Hu, Photocatalytic degradation of pathogenic bacteria with AgI/TiO2 under visible light irradiation, Langmuir 23 (2007) 4982–4987, https://doi.org/10.1021/la063626x.

[41] Q. Chang, H. He, Z. Ma, Efficient disinfection of Escherichia coli in water by silver loaded alumina, J. Inorg. Biochem. 102 (2008) 1736–1742, https://doi.org/10.1016/j.jinorgbio.2008.05.003.

[42] M.A. Tribe, R.L.W. Alpine, Scale economies and the “0.6 rule, Eng. Costs Prod. Econ. 10 (1986) 271–278, https://doi.org/10.1016/0167-188X(86)90053-4.

[43] C.B. Ozkal, A. Koruyucu, S. Meric, Heterogeneous photocatalytic degradation, mineralization and detoxification of ampicillin under varying pH and incident photon flux conditions, Desalin. Water Treat. 57 (2016) 18391–18397, https://doi.org/10.1080/19443994.2016.1155175.

[44] M.A. Vishnuganth, N. Remya, M. Kumar, N. Selvaraju, Photocatalytic degradation of carbofuran by TiO2-coated activated carbon: model for kinetic, electrical energy per order and economic analysis, J. Environ. Manag. 181 (2016) 201–207, https://doi.org/10.1016/j.jenvman.2016.06.016.

[45] M. Mehrjouei, S. Müller, D. Möller, Catalytic and photocatalytic ozonation of tert-butyl alcohol in water by means of falling film reactor: kinetic and cost-effectiveness study, Chem. Eng. J. 248 (2014) 184–190, https://doi.org/10.1016/j.cej.2014.03.047.

[46] D. Haranaka-Funai, F. Didier, J. Giménez, P. Marco, S. Esplugas, A. Machulek-Junior, Photocatalytic treatment of valproic acid sodium salt with TiO2 in different experimental devices: an economic and energetic comparison, Chem. Eng. J. 327 (2017) 656–665, https://doi.org/10.1016/j.cej.2017.06.148.

Environmental Science and Pollution Research
https://doi.org/10.1007/s11356-022-19202-1

Applications of waste-derived visibly active Fe-TiO_2 composite incorporating the hybrid process of photocatalysis and photo-Fenton for the inactivation of *E. coli*

Ina Thakur[1] · Anoop Verma[1] · Banu Örmeci[2] · Vikas Sangal[3]

Received: 17 August 2021 / Accepted: 9 February 2022
© The Author(s), under exclusive licence to Springer-Verlag GmbH Germany, part of Springer Nature 2022

Abstract
The study reports the applications of waste-derived visibly active Fe-TiO_2 composite for the inactivation of *E. coli* present in water. The Fe/TiO_2 catalyst holds remarkable properties of in situ hybrid effect via combining the TiO_2-photocatalytic and photo-Fenton process in one system causing increased production of OH°. The quantum yield (QY) and reaction rate constant of this hybrid process at 40 W m^{-2} (UV-A irradiation) were found to be significantly higher in less treatment time (45 min) of *E. coli* inactivation. 23% synergy of in situ hybrid process over single processes was also observed. The increase in the K^+ concentration at regular intervals confirmed the cell wall damage. In fully inactivated samples, no regrowth of cells was observed even after 24 and 48 h of dark study. Additionally, even after 100 recycles, the Fe/TiO_2 catalyst demonstrated an exceptional durability/recyclability efficacy. The findings of this study highlight the potential of the hybrid process as a viable idea for post-treatment of the wastewater that can be implemented effectively in practice.

Keywords UV-A irradiation · Hybrid effect · Photocatalysis · Photo-Fenton · Synergy · Regrowth

Introduction

Chlorine-based disinfection technologies have a long history of using chemicals in the degradation and disinfection of organic compounds and microorganisms in wastewater and drinking water. In comparison to this older technology, ultraviolet (UV) disinfection offers the advantages of not requiring chemical agents, broad-spectrum bactericidal action (Yu et al. 2016). As a result, it is commonly used in modern wastewater (Hassen et al. 2000) and drinking water (Barstow et al. 2014) disinfection systems. UV disinfection destroys the base pairs of genetic material in microorganisms by passing through their cell wall and plasma membrane, essentially reducing their reproductive ability. However, if the UV-inactivated bacteria are exposed to natural light for some time (Guo et al. 2012), their reproductive ability can be restored, posing environmental risks. In this regard, advanced oxidation processes such as photocatalysis (Carré et al. 2014; Kassahun et al. 2018; Kang et al. 2019) and photo-Fenton (Giannakis et al. 2016, 2018) disinfection have been extensively explored as one of the most promising and eco-friendly technologies. In this step, the photo-induced hole or OH° with a high strong oxidizing potential not just destroys the cellular wall and cytoplasm but also effectively degrades the intracellular substances leaking from the cell, resulting in the bacteria's death.

Nonetheless, its commercial uses have remained uncertain. Most of the techniques investigated have individual disadvantages, such as the difficulty of removing TiO_2 from the catalyst, the formation of iron sludge, the use of a high dose of H_2O_2, or process disadvantages, such as e^--h^+ recombination. Additionally, these systems are inherently inefficient when scaled up, resulting in significant issues such as increased reaction time, mass transfer constraints, compact design of the process, and a variety of other factors.

Responsible Editor: Sami Rtimi

✉ Anoop Verma
anoop.kumar@thapar.edu

Vikas Sangal
vksangal@gmail.com

[1] School of Energy and Environment, Thapar Institute of Engineering and Technology, Patiala 147004, India

[2] Civil and Environmental Department, Carleton University, Ottawa, ON KIS 5B6, Canada

[3] Department of Chemical Engineering, MNIT, Jaipur 302017, India

Published online: 17 February 2022

The focus of research has changed in recent years to fixed-bed photocatalysis (both homogeneous and heterogeneous), in which the coating of the catalyst is done over the substrate and then used to treat water (Adán et al. 2017; Cunha et al. 2018; De Vietro et al. 2019). However, apprehensions regarding the increase in the reaction time because of the limitations in mass transfer, the durability of catalyst, slow reaction rates, cost of support materials remained unresolved in fixed bed photocatalysis. As a result, the majority of research is still directed toward reducing treatment time and optimizing the process cost. In this context, the current study envisages the use of industrial iron-rich waste products to introduce the simultaneous effect of photocatalysis and photo-Fenton i.e. hybrid effect in fixed form for the killing of *E. coli*. Although the hybrid process is extremely efficient at disinfecting the bacteria, it has not been extensively investigated. The higher doses of chemicals and cost of the process can be considerably reduced by integrating the two separate processes in a single system, which also increases the disinfection rate. A few studies have recently proposed the idea of hybrid effect as a means of increasing disinfection efficiency. The increased efficiency was achieved by introducing the hybrid effect, which occurs when both ongoing processes generate an adequate number of OH° concurrently. The fundamental mechanism by which hybrid processes occur can be described as seen in Eqs. (1–8). This hybrid effect resolves the fundamental problem of e^{-}-h^{+} recombination by assisting in the conversion of Fe^{3+} to Fe^{2+}, as seen in Eqs. (7) and (8).

$$TiO_2 + uv\text{irradiation} \rightarrow e^{-}_{TiO_2} + h^{+}_{TiO_2} \quad (1)$$

$$e^{-}_{(TiO_2)} + O_2 \rightarrow O_2^{-} \quad (2)$$

$$h^{+}_{(TiO_2)} + H_2O \rightarrow OH^{\bullet} + H^{+} \quad (3)$$

$$Fe^{2+}_{(\text{leached})} + H_2O_2 \rightarrow Fe^{3+}_{(\text{leached})} + OH^{\bullet} + OH^{-} \quad (4)$$

$$Fe^{3+}_{(\text{leached})} + H_2O_2 \rightarrow Fe^{2+}_{(\text{leached})} + H_3O^{+} + HO_2^{-} \quad (5)$$

$$Fe^{3+}_{(\text{leached})} + H_2O \overset{uv}{\rightarrow} Fe^{2+}_{(\text{leached})} + OH^{\bullet} + H^{+} \quad (6)$$

$$Fe^{3+}_{(\text{leached})} + e^{-}_{(TiO_2)} + H_2O \rightarrow Fe^{2+}_{(\text{leached})} + OH^{\bullet} + H^{+} \quad (7)$$

$$e^{-}_{(TiO_2)} + H_2O_2 \rightarrow OH^{\bullet} + OH^{-} \quad (8)$$

For TiO_2 immobilization, the present study used a low-cost inert composite material, namely, foundry sand (FS) and fly ash (FA), both of which are rich in natural iron oxides. By using these waste materials as an iron source, this method becomes more economical from the application viewpoint. This has resulted in the development of a novel support material capable of combining two different processes; TiO_2-photocatalysis and photo-Fenton to generate the hybrid effect. The primary innovation of this technology is that, unlike previous experiments, this one makes use of naturally occurring dopants. Waste iron is a natural dopant used in composite beads production (via the photo-Fenton process). Incorporation of FS and FA would lead to the formation of Fe/TiO_2 complexes which is equivalent to iron doing to make it visibly active. As a result, the current technology is cost-efficient, as no investments in doping the catalyst have been made. Another novel aspect of this technology is that one method benefits the other by mitigating its disadvantages. With the increased reaction rate of the hybrid process, there is an improvement in the treatment and disinfection efficiency. Additionally, the combination of FS and FA improves the binding potential and compressive strength of supports.

This research aims to elucidate the impact of UV irradiation on photo-Fenton and photocatalysis on the disinfecting pathways leading to the inactivation of *E. coli*, either independently or in combination (hybrid). To accomplish these objectives, we investigate the Fenton process in the dark, light alone (UV-A light), UV-light/H_2O_2/Fe (photo-Fenton) processes with varying H_2O_2 concentrations, TiO_2-assisted photocatalysis, and their combination. The inactivation of *E. coli* is investigated in-depth kinetically in order to determine the relative significance of each of the aforementioned components, and mechanistic analysis was also done of the *E. coli* inactivation in order to comprehend our results.

Material and methods

Chemical reagents

Thirty percent w/v of H_2O_2 was obtained from Ranbaxy, Gurugram, India. TiO_2 catalyst (P-25 Degussa) was delivered by Evonik Industries, India. Waste FA, FS, and clay were acquired from a native dealer, Patiala, Punjab, India. To make acetate buffer, $C_2H_3NaO_2$ (sodium acetate) and CH_3COOH (acetic acid) of reagent grade were procured from TCI Chemicals, Chennai (India) Pvt. Ltd. To prepare the isotonic solution, 99.5% NaCl was bought from RFCL Limited, Okhla Industrial Area, New Delhi, India. Luria Bertani (LB) broth and Agar-Type I were purchased from HiMedia, Mumbai, India. For iron estimation, ammonium acetate ($NH_4CH_3CO_2$), hydroxylamine-hydrochloride ($HONH_2{\cdot}HCl$), 1,10-phenonthralein monohydrate, hydrochloric acid (HCl), potassium permanganate ($KMnO_4$), and ferrous ammonium sulfate ($(NH_4)_2Fe(SO_4)_2(H_2O)_6$) were

used. All these chemicals were of analytical grade (AR) and were obtained from Loba Chemie Pvt. Ltd. (India). All the solutions that are used in this study were made from Milli-Q water.

Bacterial strain

All experiments were conducted using *E. coli* K-12 wild type. The detailed procedure for preparing the bacterial inoculum was previously identified (Thakur et al. 2020). The resulting *E. coli* concentration was measured in colony-forming units per mL (CFU mL^{-1}), and the sample was prepared by 1000 times dilution of *E. coli* in the milli-Q water (i.e. 0.1% solution of *E. coli*), resulting in an initial concentration of 10^6 CFU mL^{-1} approx.

Microbiological methods

During assays, the cultivability of *E. coli* was determined by performing sufficient tenfold dilutions in sterilized brine solution and spreading 0.1 mL of solution on an Agar plate. For bacterial enumeration, the Petri plates were incubated for 24 h at 37 °C. After the experiments were completed, the *E. coli* solutions were preserved in the dark environment and the aforementioned technique was used to measure the post-irradiation cell survival after 6, 24, and 48 h. After every experiment, all glassware was dipped in acid and cleaned with milli-Q water and then autoclaved for 15 min at 121 °C, 15–20 psi before further usage.

The standard plating method was used to study the *E. coli* count in the solution under the Leminar flow chamber. To maintain the sterilized conditions inside the laminar and UV chamber, fumigation was done once a week. Growth of cells and sterility testing were done before every experiment. The agar plates were kept inside the chambers for 24 h to ascertain no growth and contamination.

Fabrication of composite beads

The clay was used to support the spherical beads, which were made of FS and FA in a ratio of 2:1:1, and then left to dry at normal temperature. The beads were held 10 mm in diameter by gauging them from four different directions with a vernier caliper. These beads were heated for 2 h at 800 °C, and subsequently cured for 48 h in water. This improves the support material's longevity and strength. The photo-Fenton method was then used to inactivate *E. coli* using these beads. More clay beads were made without adding any FS and FA and were heated at 800 °C for 1.5–2.0 h to study the photocatalytic inactivation of *E. coli*. Following that, sonication of 1% (w/v) TiO_2 mixture was done to disperse the TiO_2 particles uniformly. Then, TiO_2 catalyst coating was done over these beads (with or without an iron source) using the dip-coating technique (Dastan et al. 2016). To ensure sufficient coverage of the beads, their surface was coated 2 times with the TiO_2 catalyst. After drying the beads at the normal temperature, they were muffled at 350 °C for 1.5 h to ensure optimal adhesion of the TiO_2 to the composite bead's surface. Following that, the beads were rinsed with Milli-Q water to remove any remaining TiO_2 and dried in an oven set to 100 °C. As previously demonstrated using a scanning electron microscopy (SEM) study, the TiO_2 coating was found to be 71 µm thick over the support (Thakur et al. 2020). The fixed mode hybrid effect was then investigated using these Fe/TiO_2 composite beads.

Experimental set-up

The experiments were performed in a rectangular wooden enclosed chamber equipped with 7 Philips (36 W, 365 nm) UV tubes mounted to the chamber ceiling parallel to each other. To investigate *E. coli* inactivation, a 1000-mL glass reactor having 250 mL of solutions spiked with 10^6 CFUmL^{-1} stirred for 25 min to acclimate the bacteria. The reactor surface was then packed with composite beads. To allow iron leaching from the beads, the pH of the solution was kept low (4.5). The reaction was kept homogeneous by aerating it (3.0 L min^{-1}) with two spargers mounted at the very same distance from the middle. For disinfection tests, a 1-mL sample of treated water was removed from the reactor at regular intervals and the reduction in the *E. coli* count was measured using the plating technique. Five different experiments were conducted for their inactivation effect on *E. coli*: (i) dark, (ii) UV-A light, (iii) photo-Fenton process with three different H_2O_2 dozes (0.12, 0.18, and 0.3 mg L^{-1}), (iv) TiO_2-photocatalysis, (v) hybrid process. The inactivation efficacy was calculated using equation (Eq. 9):

$$L_r = \log\left(A_t / A_0\right) \tag{9}$$

Result and discussion

Dark study

The *E. coli* concentration in dark is depicted in Fig. 1. Without adding any reagents, the dark experiment did not affect the bacterial population for 6 h. This confirms that the distilled water does not have any impact on bacterial cell viability. Any changes that have occurred might be due to the osmotic shock introduced by distilled water. Additionally, although *E. coli* produces H_2O_2 intracellularly, its scavenging is successful in proficient cells and has no impact on the cell's viability, unless this balance is disrupted (López et al. 2017).

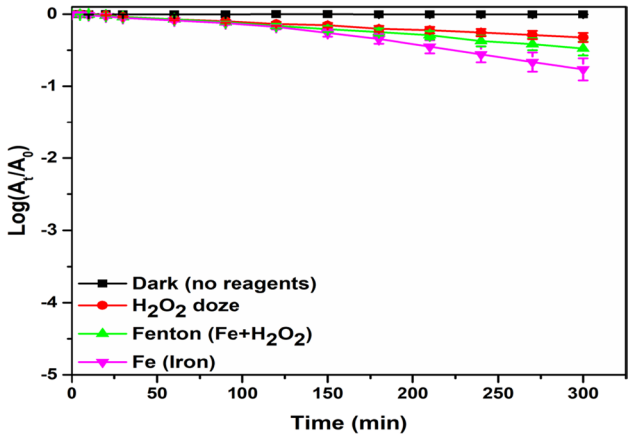

Fig. 1 Dark experiments: tests performed in the dark, with the addition of H_2O_2 (0.3 g L^{-1}), Leaching of Fe, both Fenton reagents

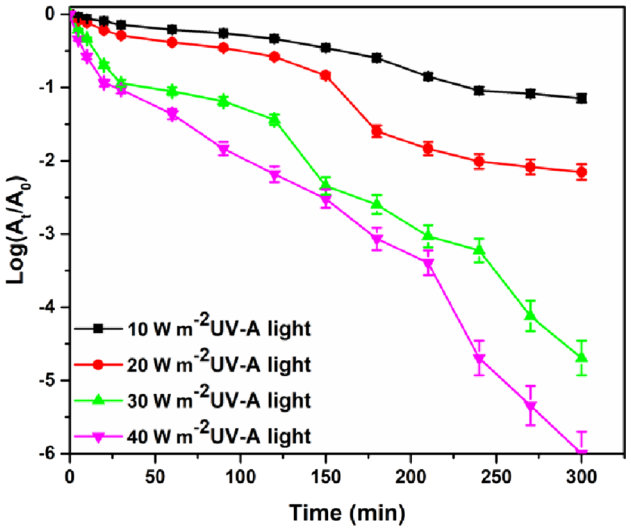

Fig. 2 Effect of UV-A light intensity on *E. coli* inactivation

The same findings were obtained when H_2O_2 was added in bulk. The water and H_2O_2 have the same polarity, which enables H_2O_2 to diffuse through bacteria and cause oxidative stress through the internal Fenton reaction (Mosteo et al. 2020). However, the existence of catalases (kat) and alkyl hydroperoxide reductase (ahp) during the stationary phase of *E. coli* cytosol results in rapid decay of H_2O_2. In stationary phase cells, such as those used in our experiments, katE acts as an effective buffer against this long-lasting ROS, thus showing an insignificant reduction in the *E. coli* concentration as shown in Fig. 1. When iron is introduced to the majority of the system, it is transported into the periplasm through the outer membrane's non-specific porins (Villegas- Guzman et al. 2017), accompanied by transportation into the cytoplasm by a variety of processes, as recently investigated. After iron undergoes normal oxidation by dissolved oxygen, the transportation process alters and is aided by new mechanisms, such as siderophores proteins that gather iron from precipitates or the surrounding environment and require specific receptors to enter the periplasm. Thus, any decrease of cultivability observed in the study will be due to Fe diffusion into the cell and a brief disruption of the Fe balance or aggregation produced by Fe_2^+ oxidation to Fe_3^+, and that is an efficient coagulant. Therefore, very little reduction in *E. coli* concentration was observed even after 6 h as shown in Fig. 1. Finally, in the presence of Fe and H_2O_2 in the reactor, the Fenton process starts but had no noticeable impact on the *E. coli* reduction. In theory, Fe^{2+} initiates the homogeneous Fenton reaction, which results in Fe^{2+} being oxidized to Fe^{3+} as seen in Eq. 10.

$$Fe^{2+} + H_2O_2 \rightarrow Fe^{3+} + OH^- + HO^{\circ} \quad (10)$$

$$Fe^{3+} + H_2O_2 \rightarrow Fe^{2+} + H^+ + HO_2^{\circ} \quad (11)$$

The kinetics of Eq. 11 is slower than those of Eq. 10, and thus, Eq. 11 is the rate-limiting step (Pignatello et al. 2006); eventually, the abundant iron species will be Fe^{3+}. In the iron speciation diagram, the prevailing species would be $Fe(OH)^{2+}$ and $Fe(OH)_3$. Fe^{3+} can precipitate as oxides (Demarchis et al. 2015). While the oxidized iron may have initiated a heterogeneous Fenton reaction, the *E. coli* concentration did not decrease even after 300 min, suggesting a marginal contribution relative to the homogeneous process. It is worth noting that comparing the addition of iron and Fenton reagents test revealed that the system Fe/dark significantly more effectively inactivates bacteria than the system Fe/H_2O_2/dark, where Fe^{2+} is quickly oxidized to Fe^{3+}. Furthermore, Spuhler et al. (2010) reported that the Fe^{2+}/dark process resulted in a higher degree of inactivation of *E. coli* in comparison to the Fenton technique.

Effect of the different intensities of light on E. coli inactivation pathways

From Fig. 2, it was observed that the *E. coli* experienced a minimum reduction of 1 log unit at the intensity of 10 W m^{-2}. However, when intensity was increased from 10 to 20 W m^{-2}, photoinactivation of *E. coli* was also increased and reached up to 2 log units, indicating that the defense mechanism is no longer efficient. After 6 h of UV-A light with an intensity of 40 W m^{-2}, total *E. coli* inactivation count was found. The initial shoulder of the inactivation graphs (Fig. 2) can be affected by a variety of factors, including improper mixing and the presence of bacteria clumps. However, under these operating conditions in irradiated UV-A systems, we hypothesize that the primary explanation

is bacteria's capacity to survive a certain degree of damage repair. Berney et al. (Berney et al. 2006) found that with an increase in the intensity of UV-A light, *E. coli* loses ATP synthesis and efflux pump activity, a loss of glucose uptake activity, and eventually, degradation of cytoplasm (Berney et al. 2006). The resulted removal of *E. coli* count is because of the absorption of UV-A light by photosensitizers such as tryptophan, flavin, cytochrome, and amino acids, which induce Type I and Type II photooxidation reactions that lead to the formation of ROS and transient species (Ravanat et al. 2001; Pfeifer et al. 2005). Exposure to radiations also disrupts the catalase enzymes, whose radical scavenging is hindered. Additionally, it was proposed that UV-A exposure induces an intracellular Fenton reaction, in which H_2O_2 is produced while flavoenzyme activation reacts with iron generated from siderophores, sulfur-iron clusters, etc. Consequently, the ROS produced throughout the Fenton reaction and photo-oxidation, such as OH° attacks on lipids, RNA, DNA, and proteins, destruction of cellular processes, mutations, and inhibition of DNA replication. Numerous studies show that oxidative species and their cumulative oxidative damage at the intracellular level play a critical role in water disinfection (Castro-Alférez et al. 2016). To support the oxidative process that occurred in the present study, post-irradiation experiments showed no regeneration of *E. coli* under any of the test conditions. In conclusion, though osmotic imbalance cannot be ruled out (Valero et al. 2017), DNA mutations under the influence of light would have been repairable and the regeneration of the *E. coli* would have happened; therefore, an oxidative process involving HO° and $^1O_2$ must occur.

Effect of the photo-Fenton process (UV-A/H_2O_2/Fe) on E. coli inactivation at different intensities

To execute the photo-Fenton fixed-bed technique, the working solution was kept in an acidic range (pH = 4.5) to cause the iron to leach from the composite beads. Iron leaching from clay occurs exclusively under the acidic range, as they aid in rupturing the chemical bonds between iron and other organic compounds, resulting in iron separation, often defined as iron leaching. As shown in Fig. 3, adding both Fenton reagents under UV-A light results in significant inactivation compared to UV-A only inactivation (Fig. 2). The addition of H_2O_2 and the leaching of iron reduce the *E. coli* concentration, even in reactions with very low irradiation (20 W m^{-2}). At 40 W m^{-2}, a 6-log reduction in UV-A/H_2O_2/Fe is observed at every oxidant doze, along with a simultaneous decrease in the treatment time required for inactivation. In comparison to the isolated UV-A method, the kinetics of UV-A/H_2O_2/Fe is found to be accelerated. This indicates that under UV-A light with both Fe^{2+} and H_2O_2, the predominant action is an intracellular reaction of the photo-Fenton process, instead of a photosensitization reaction. The inactivation pathways initiated by light alone are improved by adding H_2O_2 and Fe^{2+} in the process, and now, their transport inside the cytoplasm will enhance the current photo-Fenton mechanism in the presence of UVA-inactivated catalases. It has previously been demonstrated that the transportation of the Fenton reagents into the cell is critical photo-inactivation internally (Giannakis 2018), making it the prevalent mode of action in the photo-Fenton process for the *E. col* inactivation. Additionally, the H_2O_2 presence in the outer cell membrane can improve membrane permeability, promoting Fe^{2+} diffusion; thus demonstrating that bacterial inactivation by the Fenton process is a mixture of intracellular photocatalysis and extracellular oxidation, with a strong emphasis on the intracellular component, ultimately resulting in cellular dysfunction due to oxidative stress. The observed enhancement, however, is the product of the aforementioned hybrid behavior and the events that occur under UV light, as it is present in the radiated spectrum. Apart from the previously mentioned intracellular mechanisms, one should assume the simultaneous improvement of extracellular pathways, as a portion of Fe^{2+} and H_2O_2 react in the bulk. External ROS, mainly OH°, generated by the photo-Fenton reaction harms the bacterial membrane irreversibly.

Effect of the TiO_2-photocatalytic process on E. coli inactivation at different irradiance values

The TiO_2 catalyst coated over the clay beads was used for inactivating *E. coli* when exposed to UV-A irradiation. After 240 min of irradiation, complete inactivation of *E. coli* concentration at 40 W m^{-2} was observed using TiO_2-coated beads. As shown in Fig. 4, the rate of inactivation is slower initially, but as the UV irradiation intensity increases, the *E. coli* concentration decreases proportionately to the treatment period, indicating that treatment time plays a significant role in the *E. coli* reduction. The mechanism by which cells are inactivated using TiO_2 photocatalysis is uncertain. Several studies, however, have identified distinct mechanisms. The ROS (OH°, HO_2^-, and O_2^-) produced during TiO_2 photocatalysis cause oxidative stress in *E. coli*, which results in their inactivation. Numerous studies have shown that when TiO_2 is present in the cell membrane, the lipid peroxidation reaction occurs, impairing the cells' respiratory operation. Other researchers hypothesized that the very first stage in photo-inactivating *E. coli* is to disorder and disrupt the outer cellular membrane that serves as the cells' barrier (Pigeot-Rémy et al. 2011). The degradation of the outer membrane allows ROS to pass through to the plasma membrane, leading to the loss of internal cell constituents. It has been stated that (Collin 2019) OH° are more reactive than O_2^- but have a shorter half-life. However, their charge prevents them from penetrating the cell membrane and causing DNA damage.

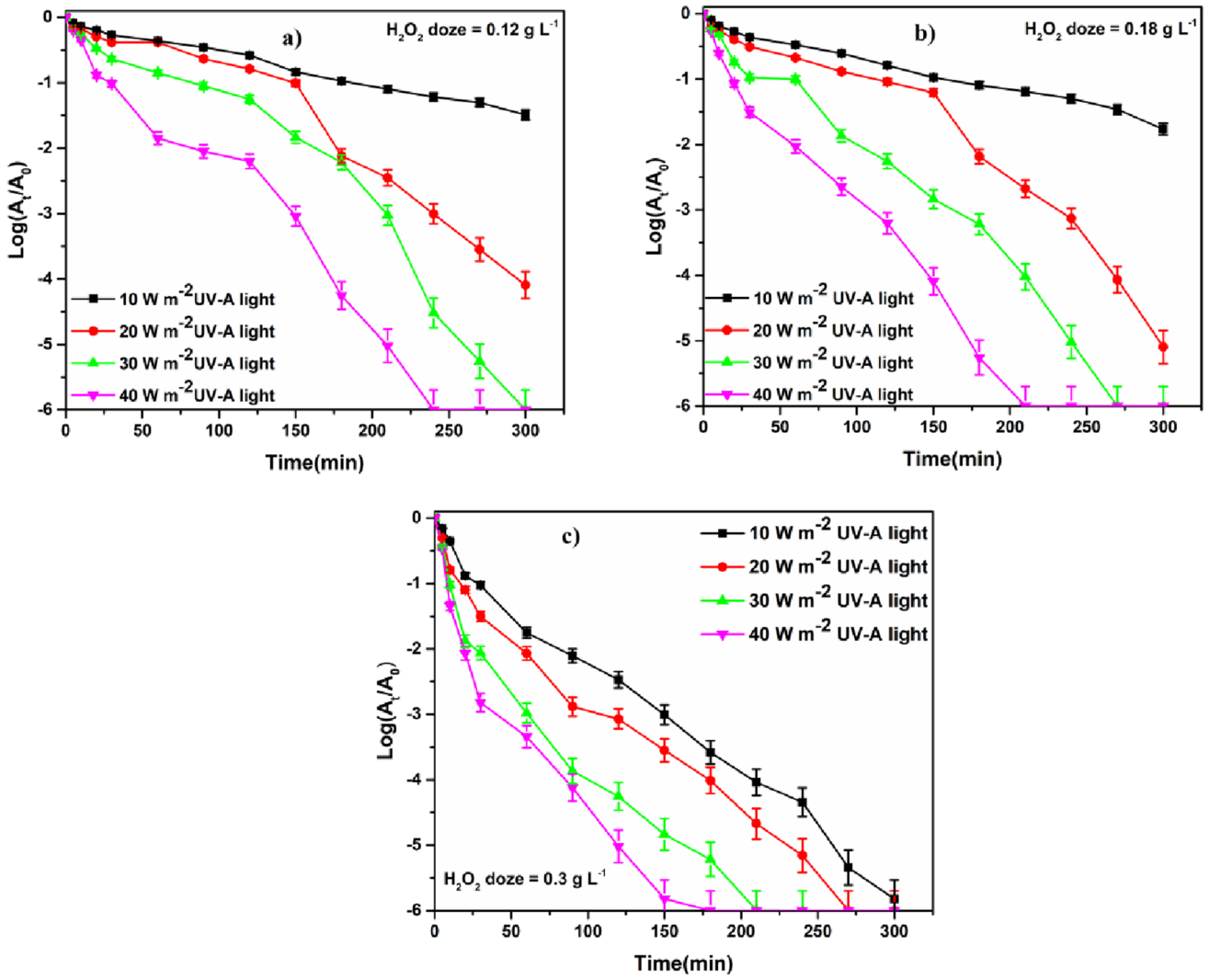

Fig. 3 Inactivation of *E. coli* in photo-Fenton process, grouped by different UV-A intensities and reagents addition. **a** Experiment under different UV-A intensity and 0.12 g L^{-1} H_2O_2. **b** Experiments under different UV-A intensities and 0.18 g L^{-1} H_2O_2. **c** Experiments under different UV-A intensities and 0.3 g L^{-1} H_2O_2

As a result, unless the TiO_2 catalyst penetrates the *E. coli* cell, and rapidly interacts with the *E. coli* external surface.

Effect of the hybrid process on E. coli inactivation at different irradiance values

The hybrid effect was carried out using Fe/TiO_2 catalyst via iron leakage and surface-active TiO_2 coating. The simultaneous execution of the aforementioned techniques in a fixed approach distinguished this technology. In comparison to individual photo-Fenton and photocatalysis, this hybrid technique achieved the complete log reduction in just 45 min (40 W m^{-2}) as shown in Fig. 5. This hybrid process also showed maximum log reduction at lower UV irradiation in comparison to the other two processes. This could be because it is capable of limiting the frequent recombination of electrons and holes that occur in TiO_2 photocatalytic activity by combining the Fe^{3+} formed by the photo-Fenton technique with the $CB_{(e-)}$ to form Fe^{2+}, given in Eqs. 1–8. As a result, the photo-Fenton process operates in a repeating mode without the creation of sludge. The addition of H_2O_2 to the system had a hybrid effect, as it reacted with both Fe and TiO_2, resulting in the production of additional OH° as shown in Eqs. 4 and 8. The hybrid mechanism ultimately resulted in a nearly doubled reaction rate compared to individual fixed mode photocatalysis. The amount of iron leached from the device was also measured in terms of total, ferrous, and ferric ions to verify the presence of the photo-Fenton process. As shown in Fig. 8a, the maximum concentrations of total iron, Fe^{3+} ion, and Fe^{2+} ion were (208 gL^{-1}, 138 gL^{-1}, and 70 gL^{-1}, respectively) (a). The mechanism of *E. coli* inactivation will remain the same as described previously.

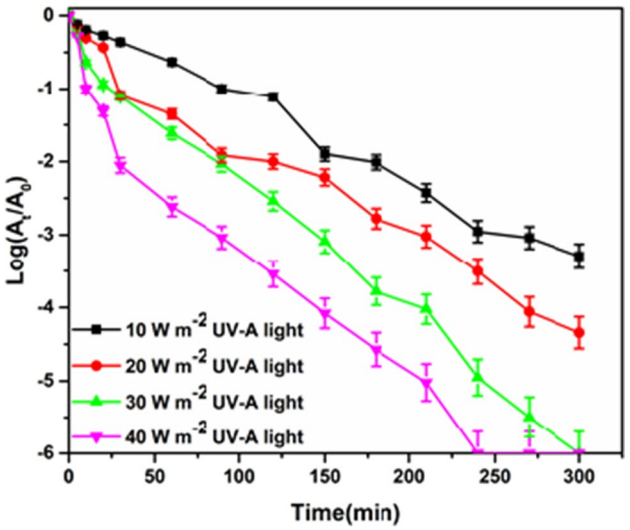

Fig. 4 Influence of UV-A light irradiance on *E. coli* inactivation under TiO_2 photocatalysis

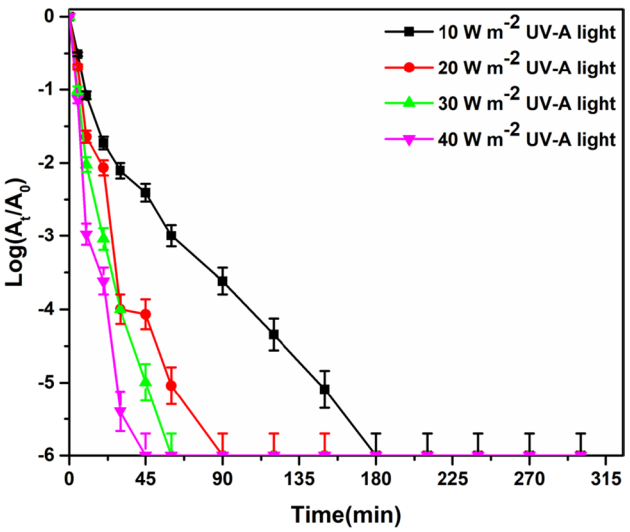

Fig. 5 Influence of UV-A light irradiance on *E. coli* inactivation under hybrid process

Performance evaluation of catalyst

The primary goal of this analysis was to evaluate the catalytic performance of the Fe/TiO_2 catalyst in comparison to the other processes mentioned in the literature in terms of *E.coli* inactivation efficacy. The inactivation efficacy of the catalyst used in these techniques, irrespective of its morphology and irradiation conditions was analyzed using quantum yields (QY) as shown in Eq. 12.

$$\text{Quantum yield(Qy)} = \frac{\text{Decay rate(per second)}}{\text{Photon flux(photon per second)}} \tag{12}$$

When the UV irradiation is consumed, this yield shows the catalytic potential of these approaches for *E. coli* inactivation, and it may be calculated as the ratio of decay rate to photons absorbed, as shown in Eq. 12, although catalysts in suspension are always more effective in terms of photocatalytic rate. The catalyst immobilization on the solid support (as shown in this study) removes the necessity of catalyst recovery post-treatment. It is well established that immobile catalysts have a smaller surface area than the catalyst in the suspension form and lowering the reactor's treatment efficiency. However, in the present research, the Fe/TiO_2 catalyst is spherical, raising the reactor's surface area and providing an additional area for microbial inactivation. To determine the hybrid technique's photon utilization efficacy, it was compared to earlier research, as can be seen in Table 2. The QY of the present research was observed to be higher (1×10^{-14} cells/photons) with lesser treatment time than that of other fixed bed studies stated in the earlier reports. Additionally, the efficacy of these systems was assessed by comparing their inactivation, and the findings are summarized in Table 1. This could be because of the higher reaction rate of the hybrid process. This led to the increase in the strong oxidant such as OH° with the reduction in e^--h^+ recombination and the formation of iron sludge in the system. The concentration of OH° in different processes was also studied using photoluminescence spectroscopy as shown in Fig. 6(a). In contrast to fixed experiments, in suspension, the efficacy of the catalyst in photon

Table 1 Estimation of QY for *E. coli* inactivation in the literature

Pollutant type (CFU mL^{-1})	Source of light	Catalyst	Type	Wavelength (nm)	Time (min)	Reduction	Quantum yield (QY) (cells/photons)	Ref
10^6	Vis-LED	N-TiO_2	Fixed	395	120	>3 log	51×10^{-16}	(Kassahun et al. 2018)
10^6	UV-A	TiO_2	CPC-fixed	365	300	CR*	6.6×10^{-15}	(Alrousan et al. 2012)
10^7	Visible	g-C_3N_4/ TiO_2	Suspension	480	180	CR	508.8×10^{-15}	(Li et al. 2015)
10^7	UV	ZnO	Suspension	365	40	CR	0.00134×10^{-15}	(Liu and Yang 2003)
10^6	UV	Fe/TiO_2	Fixed	365	45	CR	1×10^{-14}	Present study

*CR** complete reduction

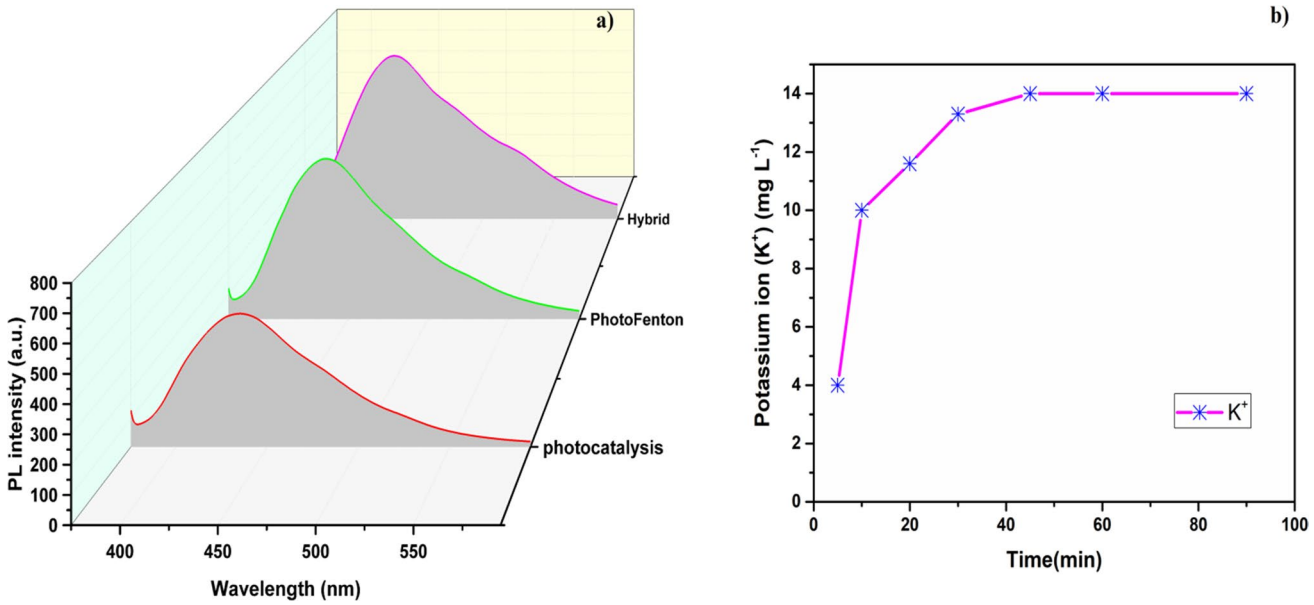

Fig. 6 **a** OH° estimation using photoluminescence spectroscopy. **b** Estimation of potassium ion leakage from the cell damage

utilization is marginally high. However, because catalysts in suspension require further recovery, fixed bed studies are a more productive and cost-effective approach for real-world application. Therefore, the higher QY, faster reaction rate constant, and use of FS and FA in the current research make Fe/TiO_2 an exceptional concept for real applications.

Also, the catalytic performance of the present research was studied using the synergy (Eqs. 13–15) of each of the processes. The hybrid process had a first-order rate constant of 0.3 min^{-1}, which was greater than that of photo-Fenton or photocatalysis, which had rate constants of 0.13 min^{-1} and 0.1 min^{-1}, respectively. The synergy of the process was studied using a first-order rate constant (Thakur et al. 2020). The synergistic effect of the hybrid technique over both techniques in combination was found to be 23% as given in Table 2. This high degree of synergy is due to the in situ hybrid process, which yields a significant amount of OH°. Additionally, the reaction of the Fe^{3+} ion with the $CB_{(e-)}$ to perform the photo-Fenton operation, in addition to reducing e^--h^+ recombination during the photocatalytic process, significantly increases synergy, as previously mentioned. This is sufficient evidence to demonstrate the hybrid process's superior efficiency to others. As predicted, the hybrid inactivation efficacy was roughly double that of the photocatalytic and photo-Fenton processes alone.

The synergistic effect of hybrid upon photocatalysis process

$$\%\ \text{Synergy} = 100 \times \frac{\left\{\left(k_{\text{dual}} - k_{\text{photocatalysis}}\right)\right\}}{k_{\text{dual}}} \tag{13}$$

The synergistic effect of hybrid upon the photo-Fenton process

$$\%\ \text{Synergy} = 100 \times \frac{\left\{\left(k_{\text{dual}} - k_{\text{photo-Fenton}}\right)\right\}}{k_{\text{dual}}} \tag{14}$$

The synergistic effect of hybrid upon both the processes

$$\%\ \text{Synergy} = 100 \times \frac{\left\{\left(k_{\text{dual}} - \left(k_{\text{photocatalysis}} + k_{\text{photo-Fenton}}\right)\right)\right\}}{k_{\text{dual}}} \tag{15}$$

Table 2 Quantum yields estimated for various processes of *E. coli* inactivation in the current study

Pollutant type	Concentration ($CFUmL^{-1}$)	Process	Source of light	Wavelength (nm)	Time (min)	Rate constant (min^{-1})	Log reduction	Synergy (%)
E. coli k- 12	10^6	Hybrid process	UV-A	365	45	0.3	Complete reduction	23%
E.coli k-12	10^6	Photo-Fenton	UV-A	365	45	0.13	3.3	57%
E. coli k-12	10^6	Photocatalysis	UV-A	365	45	0.1	2.6	67%

Table 3 Photoreactivation of *E. coli* in treated water sample under UV-light and dark conditions

Technology	*E.coli concentration*	*Treatment time (min)*	*Treatment*	*E. coli Survival after 6 h inactivation*		*E. coli survival after 24 h of inactivation*		*E. coli survival after 48 h of inactivation*	
				Light	***Dark***	***Light***	***Dark***	***Light***	***Dark***
Photocatalysis	10^6 CFU/mL	240 min	UV-A irradiation	Ab*	Ab	Ab	Ab	Ab	Ab
Photo-Fenton	10^6 CFU/mL	180 min	UV-A irradiation	Ab	Ab	Ab	Ab	Ab	Ab
Hybrid	10^6 CFU/mL	45 min	UV-A irradiation	Ab	Ab	Ab	Ab	Ab	Ab

*Ab*absent

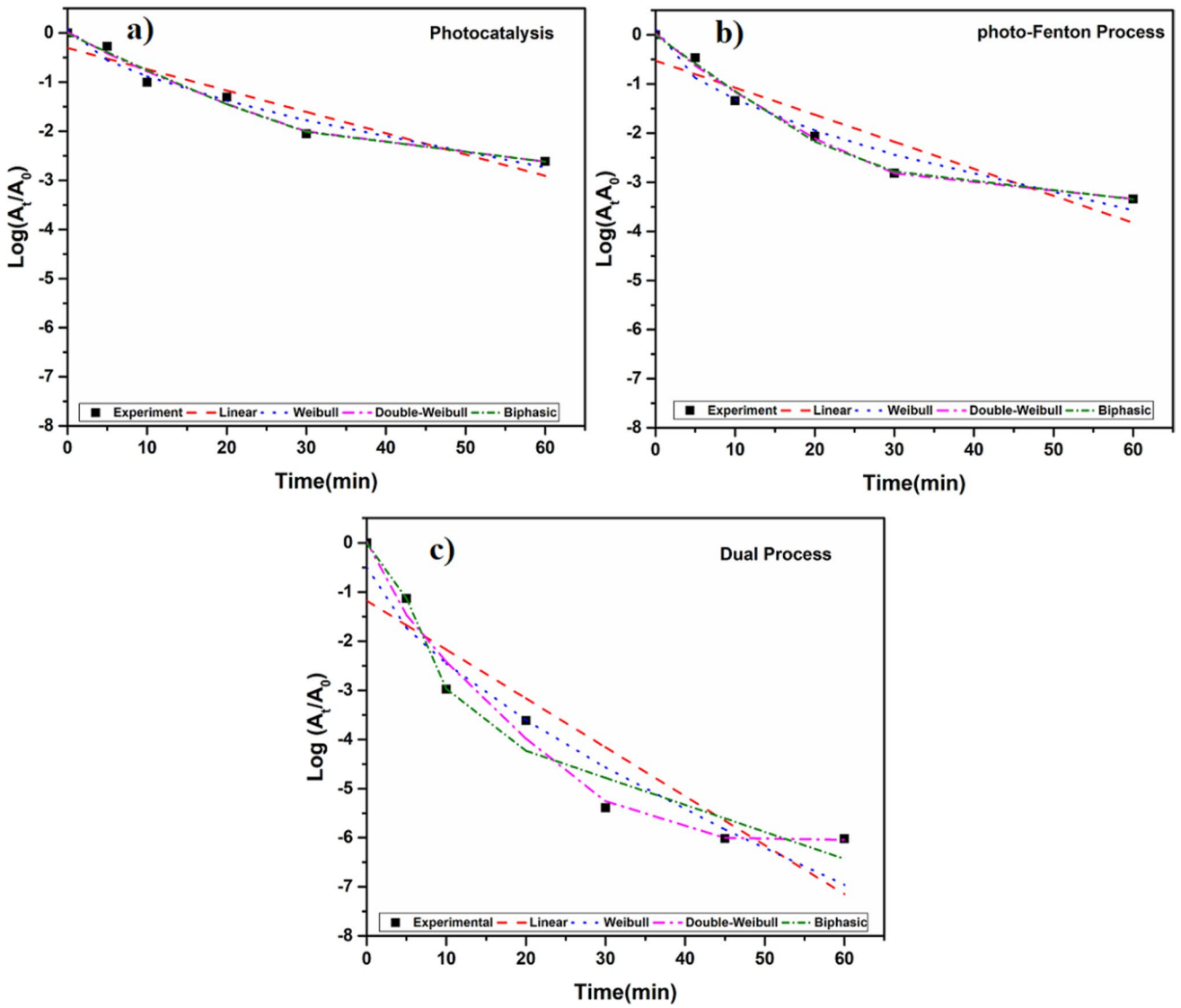

Fig. 7 Fitting mathematical models to the photocatalysis, photo-Fenton, and hybrid process inactivation curves of *E.coli*

Table 4 Kinetic parameters analysis for photocatalysis, photo-Fenton, and hybrid experiments

	K(min^{-1})	δ	R^2/RSM	Shoulder length (SL) (min)
10 W m^{-2}				
Photocatalysis	0.02	116.89	0.97/0.05	-
Photo-Fenton	0.07	27.27	0.98/0.1	7.13
Hybrid	0.11	8.39	0.98/0.01	1.87
20 W m^{-2}				
Photocatalysis	0.05	36.26	0.92/0.1	-
Photo-Fenton	0.08	16.01	0.98/0.1	4
Hybrid	0.19	4.67	0.96/0.4	-
30 W m^{-2}				
Photocatalysis	0.06	24.15	0.97/0.1	5.27
Photo-Fenton	0.11	8.06	097/0.2	3.43
Hybrid	0.22	4.80	0.99/0.2	0.4
40 W m^{-2}				
Photocatalysis	0.10	10.63	0.96/0.2	-
Photo-Fenton	0.13	5.09	0.95/0.3	-
Hybrid	0.3	3.61	0.95/0.6	3

Photo-reactivation of E.coli

Numerous deactivation studies have shown that bacteria have a proclivity for regrowth by restoring their damaged DNA in the absence (dark condition) or presence (photoreactivation) of light. As shown in Table 3, *E. coli* reactivation experiments in treated water were conducted in the dark and UV light. After each experiment, the photoreactivation ability was determined by removing 100 mL of the treated water. The treated sample was placed in a sterile conical flask and stirred continuously for 6 h, 24 h, and 48 h in the dark and under UV light. The viability of *E. coli* was determined in the treated sample using the same basic procedure used in inactivation experiments.

K^+ leakage activity

The outer membrane of *E. coli* is composed of a lipopolysaccharide layer that serves an essential function by serving as a barrier to the Gram-negative bacteria's permeability. ROS can cause damage to the outer cell wall and membrane of the Fe/TiO_2 composite, increasing the cell's permeability and subsequent seepage of intracellular substances such as K^+. As a result, K^+ leakage from inactivated *E.coli* was tested over a range of time intervals to determine the cell membrane's permeability (Fig. 6b). The K^+ concentration increased grahybridly until 45 min into the procedure and then remained constant as the treatment time increased. The K^+ ion immediately leaked out in this hybrid effect analysis, and the concentration of leaked K^+ increased in parallel with *E. coli* inactivation as irradiation time increased. When all *E. coli* was completely killed after 45 min of irradiation, the total K^+ concentration (4.3 ppm) was completely released. This finding indicated that the inactivation of *E. coli* disrupted the cell membrane's permeability.

Kinetic evaluation of the three different processes

A kinetic assessment of the results using three different models such as log-linear, Weibull, double Weibull, and biphasic as shown in Eqs. 16–19, respectively, was performed in order to evaluate and compare the three different processes (hybrid, photo-Fenton, and photocatalysis).

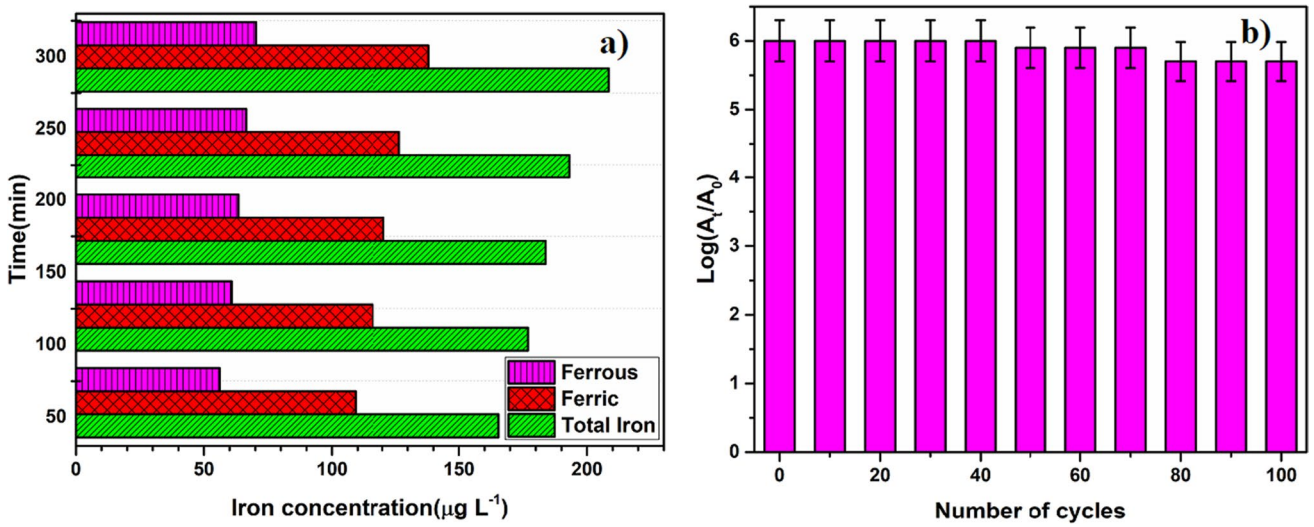

Fig. 8 **a** Iron concentration present in the hybrid process **b** durability studies for 100 cycles

The results achieved after *E. coli* inactivation in three different fixed-bed processes with 40 W m^{-2} of UV-A radiation the mathematical models used showed a good fit (Fig. 7). Considering the R^2 approaching 1 and RMSD values less than zero, the best-fitted curve was found with the Weibull distribution model. When the k and δ values of three different processes were compared (Table 4), the hybrid process showed a higher *E. coli* reduction rate. Thus, using log-linear and Weibull parameters to fit the *E. coli* inactivation results and comparing the different techniques revealed that the hybrid-technique in fixed mode at 40 W m^{-2} ($k = 0.3$ min^{-1}; $\delta = 3.6$ min) was considerably faster than the other technologies: photocatalysis ($k = 0.1$ min^{-1}; $\delta = 10.6$ min); and photo-Fenton ($k = 0.1$ min^{-1}; $\delta = 10.6$ min).

$$log\frac{A_t}{A_0} = -kCt \rightarrow log\frac{A_t}{A_0} = -k_{ap}t \tag{16}$$

where A_0 is the initial concentration of *E.coli* and A_t is the final concentration remaining after the reaction. The first-order rate constant is denoted by k (min^{-1}), the disinfectant concentration is denoted by C, and the treatment time is denoted by t.

$$log\frac{A_t}{A_0} = -\left(\frac{t}{\delta}\right)^p \tag{17}$$

The first decimal time reduction is denoted by δ. The equation's shape is represented by p. When $p > 1$, the shape is convex; when $p < 1$, the shape is concave. At $p = 1$, the equation denotes a first-order linear model.

$$A = \frac{A_0}{1 + 10^{\alpha}} \times \left(10^{-\left(\frac{1}{\delta_1}\right)^{p_1 + \alpha}} + 10^{-\left(\frac{1}{\delta_2}\right)^{p_2}}\right) \tag{18}$$

The sub-population fraction is denoted by α, α_1, and α_2 denote distinct sub-populations. time. Sub-population 1 exhibits greater susceptibility to stress than sub-population 2($\delta_1 < \delta_2$).

$$Log\frac{A_t}{A_0} = Log\left[P * e^{-k_1 * t} + (1 - P) * e^{-k_2 * t}\right] \tag{19}$$

where P denotes the fraction of microorganisms that survive in subpopulation group 1 and (1–P) denotes the fraction of microorganisms that survive in subpopulation group 2. Finally, $k_1$and k_2 represent the kinetic rate constant of the more susceptible population and more resistant population respectively.

Durability

The biggest challenge in fixed-bed catalytic reactors is the durability/longevity of the catalyst for repeated cycles. For this novel concept, things get more complex as this technology needs to handle two techniques at the same time and in the same place. For this technology to work smoothly, the intactness of the photoactive TiO_2 layer over the surface and incessant iron lixiviating from the Fe/TiO_2 composite plays a very significant role. In this study, Fe/TiO_2 composite made from FS + FA was recycled for more than 100 cycles as shown in Fig. 8b. Even after 100 cycles, the composite beads were found to be capable enough to perform both the process simultaneously in the system, thus further claim the novelty of the study. It was found that the activity of the Fe/TiO_2 catalyst decreased by 5% only. The reactivation of composite beads after each recycling was done by keeping it in an oven at 80–90 °C overnight. This further strengthens the author's argument to visualize the real-life application of the hybrid process as it controls the economy of the technology.

Conclusion

The current study demonstrates the effective application of an innovative Fe/TiO_2 composite for *E. coli* inactivation. Under the illumination of UV-A light(40 W m^{-2}), a 6-log reduction (complete inactivation) was achieved in just 45 min of treatment time which was much higher than the time required by photocatalysis (240 min) and photo Fenton (180 min) process for complete inactivation. Additionally, the kinetic parameters "k" of the log-linear and "δ" of the Weibull model was utilized to compare the different techniques and discovered that the hybrid technique in fixed mode was substantially faster than the other technologies. On the other hand, the beads were sufficiently robust, as only 5% of the catalyst's photoactivity was lost after 100 runs. One of the novel properties of this technology is that the catalyst is acting as natural dopant which makes this technology economically viable. Thus, the hybrid process revealed its potential for the use of waste products as a suitable strategy for wastewater post-treatment that can also be successfully implemented on the field scale.

Acknowledgements The authors would like to thank the sophisticated analytical instrumentation facility, Thapar Institute of Engineering and Technology, Punjab, India, for providing their facilities for the characterization of samples.

Author contribution All authors contributed to this study. Material preparation, data collection, and analysis were performed by Ina Thakur and Dr. Anoop Verma. The first draft of the manuscript was written by Ina Thakur. Final paper corrections were done by Dr. Anoop Verma, Dr. Banu Örmeci, and Dr. Vikas Sangal. All authors read and approved the final manuscript.

Data Availability All data generated or analyzed during this study are included in this published article.

Declarations

Ethics approval and consent to participate Not applicable.

Consent for publication Not applicable.

Competing interests The authors declare no competing interests.

References

Adán C, Marugán J, Mesones S et al (2017) Bacterial inactivation and degradation of organic molecules by titanium dioxide supported on porous stainless steel photocatalytic membranes. Chem Eng J 318:29–38. https://doi.org/10.1016/j.cej.2016.04.091

Alrousan DMA, Polo-López MI, Dunlop PSM et al (2012) Solar photocatalytic disinfection of water with immobilised titanium dioxide in re-circulating flow CPC reactors. Appl Catal B Environ 128:126–134. https://doi.org/10.1016/j.apcatb.2012.07.038

Barstow CK, Dotson AD, Linden KG (2014) Assessing point-of-use ultraviolet disinfection for safe water in urban developing communities. J Water Health 12:663–669. https://doi.org/10.2166/wh.2014.223

Berney M, Weilenmann HU, Egli T (2006) Flow-cytometric study of vital cellular functions in Escherichia coli during solar disinfection (SODIS). Microbiology 152:1719–1729. https://doi.org/10.1099/mic.0.28617-0

Carré G, Hamon E, Ennahar S et al (2014) TiO2 photocatalysis damages lipids and proteins in Escherichia coli. Appl Environ Microbiol 80:2573–2581. https://doi.org/10.1128/AEM.03995-13

Castro-Alférez M, Polo-López MI, Fernández-Ibáñez P (2016) Intracellular mechanisms of solar water disinfection. Sci Rep 6:1–10. https://doi.org/10.1038/srep38145

Collin F (2019) Chemical basis of reactive oxygen species reactivity and involvement in neurodegenerative diseases. Int J Mol Sci 20. https://doi.org/10.3390/ijms20102407

Cunha DL, Kuznetsov A, Achete CA, et al (2018) Immobilized TiO2 on glass spheres applied to heterogeneous photocatalysis: photoactivity, leaching and regeneration process. PeerJ 2018:1–19https://doi.org/10.7717/peerj.4464

Dastan D, Panahi SL, Chaure NB (2016) Characterization of titania thin films grown by dip-coating technique. J Mater Sci Mater Electron 27:12291–12296. https://doi.org/10.1007/s10854-016-4985-4

De Vietro N, Tursi A, Beneduci A et al (2019) Photocatalytic inactivation of Escherichia coli bacteria in water using low pressure plasma deposited TiO2 cellulose fabric. Photochem Photobiol Sci 18:2248–2258. https://doi.org/10.1039/c9pp00050j

Demarchis L, Minella M, Nisticò R et al (2015) Photo-Fenton reaction in the presence of morphologically controlled hematite as iron source. J Photochem Photobiol A Chem 307–308:99–107. https://doi.org/10.1016/j.jphotochem.2015.04.009

Giannakis S (2018) Analogies and differences among bacterial and viral disinfection by the photo-Fenton process at neutral pH: a mini review. Environ Sci Pollut Res 25:27676–27692. https://doi.org/10.1007/s11356-017-0926-x

Giannakis S, Voumard M, Grandjean D et al (2016) Micropollutant degradation, bacterial inactivation and regrowth risk in wastewater effluents: influence of the secondary (pre)treatment on the efficiency of Advanced Oxidation Processes. Water Res 102:505–515. https://doi.org/10.1016/j.watres.2016.06.066

Giannakis S, Voumard M, Rtimi S, Pulgarin C (2018) Bacterial disinfection by the photo-Fenton process: Extracellular oxidation or intracellular photo-catalysis? Appl Catal B Environ 227:285–295. https://doi.org/10.1016/j.apcatb.2018.01.044

Guo M, Huang J, Hu H et al (2012) UV inactivation and characteristics after photoreactivation of Escherichia coli with plasmid: health safety concern about UV disinfection. Water Res 46:4031–4036. https://doi.org/10.1016/j.watres.2012.05.005

Hassen A, Mahrouk M, Ouzari H et al (2000) UV disinfection of treated wastewater in a large-scale pilot plant and inactivation of selected bacteria in a laboratory UV device. Bioresour Technol 74:141–150. https://doi.org/10.1016/S0960-8524(99)00179-0

Kang X, Liu S, Dai Z et al (2019) Titanium dioxide: from engineering to applications. Catalysts 9:191. https://doi.org/10.3390/catal9020191

Kassahun SK, Kiflie Z, Shin DW et al (2018) Novel multistage fixed-bed photoreactor for bacterial inactivation using N-doped TiO2 nanoparticles under vis-LEDs and sunlight illumination. Nanotechnol Environ Eng 3:1–11. https://doi.org/10.1007/s41204-017-0032-9

Li G, Nie X, Chen J et al (2015) Enhanced visible-light-driven photocatalytic inactivation of Escherichia coli using g-C3N4/TiO2 hybrid photocatalyst synthesized using a hydrothermal-calcination approach. Water Res 86:17–24. https://doi.org/10.1016/j.watres.2015.05.053

Liu HL, Yang TCK (2003) Photocatalytic inactivation of Escherichia coli and Lactobacillus helveticus by ZnO and TiO2 activated with ultraviolet light. Process Biochem 39:475–481. https://doi.org/10.1016/S0032-9592(03)00084-0

López AV, López KH, Giannakis S, Benítez N (2017) Effect of reactor material and its reuse on photo-Fenton process efficiency at near-neutral pH: alterations in E. coli inactivation and resorcinol degradation kinetics in water. J Photochem Photobiol A Chem 344:228–237. https://doi.org/10.1016/j.jphotochem.2017.04.019

Mosteo R, Varon Lopez A, Muzard D et al (2020) Visible light plays a significant role during bacterial inactivation by the photo-fenton process, even at sub-critical light intensities. Water Res 174:115636. https://doi.org/10.1016/j.watres.2020.115636

Pfeifer GP, You YH, Besaratinia A (2005) Mutations induced by ultraviolet light. Mutat Res - Fundam Mol Mech Mutagen 571:19–31. https://doi.org/10.1016/j.mrfmmm.2004.06.057

Pigeot-Rémy S, Simonet F, Errazuriz-Cerda E et al (2011) Photocatalysis and disinfection of water: identification of potential bacterial targets. Appl Catal B Environ 104:390–398. https://doi.org/10.1016/j.apcatb.2011.03.001

Pignatello JJ, Oliveros E, MacKay A (2006) Advanced oxidation processes for organic contaminant destruction based on the fenton reaction and related chemistry. Crit Rev Environ Sci Technol 36:1–84. https://doi.org/10.1080/10643380500326564

Ravanat JL, Douki T, Cadet J (2001) Direct and indirect effects of UV radiation on DNA and its components. J Photochem Photobiol B Biol 63:88–102. https://doi.org/10.1016/S1011-1344(01)00206-8

Spuhler D, Andrés Rengifo-Herrera J, Pulgarin C (2010) The effect of Fe2+, Fe3+, H2O2 and the photo-Fenton reagent at near neutral pH on the solar disinfection (SODIS) at low temperatures of water containing Escherichia coli K12. Appl Catal B Environ 96:126–141. https://doi.org/10.1016/j.apcatb.2010.02.010

Thakur I, Örmeci B, Verma A (2020) Inactivation of E. coli in water employing Fe-TiO2 composite incorporating in-situ hybrid process of photocatalysis and photo-Fenton in fixed-mode. J Water Process Eng 33:101085. https://doi.org/10.1016/j.jwpe.2019.101085

Valero P, Giannakis S, Mosteo R et al (2017) Comparative effect of growth media on the monitoring of E. coli inactivation and regrowth after solar and photo-Fenton treatment. Chem Eng J 313:109–120. https://doi.org/10.1016/j.cej.2016.11.126

Villegas- Guzman P, Giannakis S, Rtimi S et al (2017) A green solar photo-Fenton process for the elimination of bacteria and micropollutants in municipal wastewater treatment using mineral iron and natural organic acids. Appl Catal B Environ 219:538–549. https://doi.org/10.1016/j.apcatb.2017.07.066

Yu H, Song L, Hao Y et al (2016) Fabrication of pilot-scale photocatalytic disinfection device by installing TiO2 coated helical support into UV annular reactor for strengthening sterilization. Chem Eng J 283:1506–1513. https://doi.org/10.1016/j.cej.2015.08.042

Publisher's note Springer Nature remains neutral with regard to jurisdictional claims in published maps and institutional affiliations.

Journal of Cleaner Production 352 (2022) 131575

Contents lists available at ScienceDirect

Journal of Cleaner Production

journal homepage: www.elsevier.com/locate/jclepro

Inactivation of bacteria present in secondary municipal wastewater effluent using the hybrid effect of Fe–TiO_2 catalyst

Ina Thakur [a], Anoop Verma [a,*], Banu Örmeci [b]

[a] School of Energy and Environment, Thapar Institute of Engineering and Technology, Patiala, 147004, India
[b] Civil and Environmental Department, Carleton University, Ottawa, ON KIS 5B6, Canada

ARTICLE INFO

Handling Editor: Bin Chen

Keywords:
Disinfection
Degradation
Municipal wastewater
Photocatalysis
Photo-FentonDisinfection

ABSTRACT

A low-cost waste-driven visible active iron-titanium oxide composite was fabricated for the treatment of real municipal wastewater. The structured composite was characterized using morphological and spectroscopic techniques such as FE-SEM, XRD, UV-DRS, indicating that the fabrication procedure could uniformly coat the TiO_2 particles over the clay-supported composite spheres. The iron-titanium oxide composite was efficient in introducing a hybrid effect of photocatalysis and photo-Fenton that is being facilitated by the use of waste foundry sand (WFS) and waste fly ash (WFA) (both natural sources of iron) with a TiO_2 layer on the outer surface. The main emphasis was given to the disinfection of bacteria along with the degradation of organic matter in terms of BOD and COD present in municipal wastewater. This hybrid technology showed 100% inactivation of bacteria with optimized parameters such as 0.9 g L^{-1} of H_2O_2 dose, 5.5 pH, and 100% surface area covered with the catalyst in 60 min of treatment time. 54% and 40% reduction in BOD and COD was also observed in 60 min. The kinetic rate constant was found to be 2 times higher in the hybrid process as compared to the individual process. The damage to the cell wall was confirmed by potassium ion leakage and FE-SEM analysis. Fe–TiO_2 composites demonstrated excellent stability even after recycling 35 times, indicating the lasting durability of the composites. The findings of this study demonstrate the possibility for waste materials to be used as a viable approach for the bacterial inactivation application with the potential of the field-scale application.

1. Introduction

Wastewater reclamation, or the reuse of treated wastewater, is the most effective strategy for meeting the ongoing and prospective needs of diverse water-using sectors, including agricultural, commercial, industrial, and human water requirements (EPA, 2012; WHO, 2006). Accessibility to freshwater is becoming extremely expensive due to climate change, environmental contamination, and increasing demand for water resources. To save freshwater, non-potable water can be derived from reclaimed wastewater. To reuse this water safely, microorganisms present must be eliminated from the majority of reuse applications (Almuktar et al., 2018). This cannot be achieved with traditional secondary treatment alone, additional tertiary and disinfection steps are required.

Advanced oxidation treatment processes (AOPs) such as ozonation (Arayan et al., 2017; Mecha et al., 2017), photocatalysis (Carré et al., 2014; Laxma Reddy et al., 2017), photo-Fenton (Giannakis et al., 2018; Rodríguez-Chueca et al., 2014) have been widely explored to study the wastewater disinfection. In this process, the photo-induced hole or OH° with a strong oxidizing potential destroys the cellular wall, cytoplasm and also effectively oxidizes the intracellular substances leaking from the cell resulting in cell death. Amidst the various AOPs, those operated under natural solar light have garnered considerable interest over the last decades, as they eliminate the need for expensive light sources and their maintenance costs. TiO_2 photocatalysis and the photo-Fenton process proved to be a highly effective method of wastewater treatment for wide variety of microorganism (Berney et al., 2006; Giannakis et al., 2018).

In TiO_2 photocatalysis, the first study of bacterial inactivation was studied using UVA-activated TiO_2 (Tadashi et al., 1985). They used TiO_2 as a catalyst in suspension form, and complete inactivation was reported in 120 min of treatment time. The main focus of the researchers is on utilizing TiO_2 in fixed form for bacterial inactivation. TiO_2 fixed over different support materials such as glass balls, glass plates, cylinders is highly desirable for field-scale disinfection investigation. TiO_2 coated glass plates in a thin-film fixed-bed reactor (TFFBR) were used to study

* Corresponding author.
E-mail address: anoop.kumar@thapar.edu (A. Verma).

https://doi.org/10.1016/j.jclepro.2022.131575
Received 31 October 2021; Received in revised form 23 March 2022; Accepted 27 March 2022
Available online 6 April 2022
0959-6526/© 2022 Elsevier Ltd. All rights reserved.

the inactivation of Aeromonas hydrophila and complete inactivation was observed with a flow rate of 4.8 L h^{-1} (Khan et al., 2012). N-doped TiO_2 immobilized over glass beads was also utilized to analyze the disinfection studies and observed a 3 log reduction in 120 min of treatment time (Kassahun et al., 2020). These described research achieved a reasonable level of disinfection efficacy, but certain disadvantages such as catalyst separation, frequent e^-/h^+ recombination; and high electricity prices are limiting their applicability for field-scale applications.

The photo-Fenton process (Polo-López et al., 2013) another advanced oxidation process has shown its ability to remove *Phytophthora capsici zoospores* from distilled water, achieving the maximum disinfection rate under 60 min with 10 mg L^{-1} of H_2O_2, 5.0 mg L^{-1} of Fe^{2+} or Fe^{3+} and 2.5 kJ L^{-1} of ultraviolet solar irradiations. The photo-Fenton effect is significantly dependent on the structure of the cell; hence, optimum dozes of iron, H_2O_2, and UV light, as well as exposure times, are target-specific characteristics for each microbe. The best results were observed with 5 mg L^{-1} of H_2O_2, 20 mg L^{-1} of H_2O_2, pH 5.0, and light intensity of 500 Wm^{-2}) (Rodríguez-Chueca et al., 2012). Even after having such efficient results this technology have some drawbacks such as higher treatment cost; inadequate regeneration of catalyst; high dose of H_2O_2; and a large volume generation of iron sludge.

The focus has changed in recent years to combinatorial hybrid systems, where research has demonstrated that combining two or more technologies such as photocatalysis-biodegradation (Collivignarelli et al., 2020), photo-Fenton-biological oxidation (Changotra et al., 2019; Pariente et al., 2008), photo-Fenton-coagulation, and flocculation (Gil-Pavas et al., 2017), electro-oxidation (Collivignarelli et al., 2020), photocatalytic-ozonation (Mecha et al., 2017; Yuan et al., 2018), and ultrasonic-photocatalysis (Hu et al., 2017) can be an efficient approach for significantly increasing pollutant removal efficacy. These systems have been shown to offer higher oxidation rates, faster kinetic rates, short mass transfer operation times, and are simpler to operate. These techniques also have many disadvantages, such as the use of a high dose of H_2O_2, electron-hole recombination, iron sludge formation (Chen et al., 2009; Jiménez et al., 2011). In photocatalytic-ozonation, the ozone disintegrates rapidly into oxygen and complicates residual removal methods (Mecha et al., 2017). The relatively expensive cost of system maintenance, and the significant energy consumption associated with the operation process, restrict the development of large-scale applications.

Considering the aforementioned disadvantages, the current work presents an efficient system for disinfecting water under natural solar light that utilizes an in-situ fixed-bed mode. This study utilizes the WFA and WFS binded with clay and coated with TiO_2. This composite system as a whole enables the coupling of two techniques: photo-Fenton and photocatalysis. The WFA and WFS are composed primarily of silica as well as iron and aluminum, and these waste products can be utilized to treat wastewater (Visa and Duta, 2013).

This technique eliminates the e^--h^+ recombination problem in TiO_2 photocatalysis. The $e^-_{(CB)}$ combines with the Fe^{3+} lixiviating from the iron-titanium oxide composite and converting them to Fe^{2+} during TiO_2 photocatalysis. The Fe^{2+} ion combines with H_2O_2 once more, initiating the photo-Fenton reaction. Equation (1) illustrates the dual effect in the system. The presence of H_2O_2 serves two purposes: 1) reaction with iron (as described above) and 2) with the photocatalysis process, as illustrated in Equation (2). As a result, this procedure results in increased generation of OH°.

$$Fe^{3+} + e^-(photoexcited\ electron) \rightarrow Fe^{2+} \quad (1)$$

$$e^-_{(CB)} + H_2O_2 \rightarrow OH^o + OH^- \quad (2)$$

One of the novel parts of this technology is that it is comprised of a natural dopant. The coating of the TiO_2 and iron particles present on the surface of the composite combined together to generate specific complexes such as iron titanium oxide (confirmed using XRD analysis in the following section), which reduces the bandgap of the catalyst over time and makes the inactivation efficacy of the composite prevalent it in the visible light also. Thus, this approach is very economic, as minimum expenses in catalyst doping were made. The purpose of this study was to compare the efficacy of various solar-powered AOPs for removing bacteria from municipal wastewater treatment plant (MWWTP) secondary effluent using solar-H_2O_2, TiO_2-photocatalysis, the photo-Fenton process, and a hybrid process in a fixed bed laboratory-scale reactor.

2. Materials and methods

2.1. Chemicals and reagents

TiO_2 (titanium dioxide) catalyst having 70:30 anatase and rutile phase, with BET surface area of 50 m^2 g^{-1} and 30 nm of particle size was purchased from Sigma Aldrich Chemicals Pvt Ltd, Delhi, India. Clay, WFS, and WFA were accumulated from native industry, Punjab, India. 30% w/v of hydrogen peroxide (H_2O_2) was used as an oxidant and was purchased from Ranbaxy, India. Sodium acetate buffer was used to maintain the acidic pH conditions prepared from >99.5% acetic acid and 98.5% sodium acetate, bought from Loba Chemie Pvt Ltd, Maharashtra, India.

For iron estimation, ammonium acetate ($NH_4CH_3CO_2$), hydroxylamine-hydrochloride ($HONH_2{\cdot}HCl$), 1,10-phenonthralein monohydrate, hydrochloric acid (HCl), potassium permanganate ($KMnO_4$), and ferrous ammonium sulfate ($(NH_4)_2Fe(SO_4)_2(H_2O)_6$) were used. All these chemicals were of analytical grade (AR) and were obtained from Loba Chemie Pvt. Ltd. (India).

Luria Bertani (LB) (10 g BactoTM Tryptone, 5 g Yeast extract, 10 g NaCl, per liter), Miller Agar-Agar, Type I, was bought from HiMedia Laboratories, Mumbai India. Washing and re-suspension of *E. coli* were done in sterilized isotonic saline solution, using 99.5% of sodium chloride (NaCl), and was purchased from SD Fines Chemicals Ltd, India.

2.2. Analytical methods

The Physico-chemical analysis of wastewater was conducted using Standard APHA methods (2017). Nitrate ions (APHA, 2017: Sec. 4500-NO_3), phosphate ions by stannous chloride method (APHA, 2017: Sec 4500 (P.D)), Biochemical oxygen demand (BOD) (APHA, 2017), Chemical oxygen demand (COD ((APHA, 2017: Sec. 5220 (B)), and for iron estimation ((APHA 2017: Sec. 3111(B)). The generation OH^o was confirmed by photo-Luminance spectrophotometry (LS-45, PerkinElmer) by the formation of a fluorescent compound (2-hydroxy terephthalic acid).

2.3. Characterization of Fe–TiO_2 beads

The investigation of spherical Fe–TiO_2 beads using multiple techniques such as EDS, XRD, UV-DRS, FE-SEM, FTIR, HRTEM, elemental mapping, and XPS was done to validate the existence of both TiO_2 and iron in this hybrid process study. An Energy-dispersive Spectroscopy (EDS) was used to investigate the chemical properties of WFS and WFA. The samples were coated with platinum using a fine auto coater (Model: JEC-3000FC). The crystalline phases of the Fe–TiO_2 composite between 20 and 80 °C of scanning range with Copper-K radiation at = 1.5418 were studied using X-ray diffraction (XRD). The catalyst's bandgap energy was evaluated using a Differential reflectance spectroscopy (DRS), Shimadzu, UV-600 by setting the wavelength range between 200 and 800 nm. The baseline was set with barium sulfate ($BaSO_4$). Field Emission Scanning Electron Microscopy (FESEM) with EDS analysis was done to study morphology and chemical properties of the catalyst. The

compound linkage and bonding were analyzed by Fourier TransformInfra-Red Spectrophotometer (FTIR) model RZX (PerkinElmer) in the scanning range of 4000 to 200 cm^{-1}. The FTIR spectra were obtained by mixing 0.5 mg of synthesized material with 20 mg of potassium bromide. To study the lattice spacing of the Fe–TiO_2 composite High-resolution transmission electron microscopy (HRTEM) was done. The XPS (X-ray photoelectron spectroscopy) analysis was performed with XPS, Omicron Nanotechnology, Oxford Instruments.

2.4. Wastewater samples

All experiments were conducted using secondary treated municipal wastewater from MWWTP located at Thapar Institute of Engineering and Technology (TIET), Patiala, Punjab, India. The treated wastewater was taken from downstream of secondary treated MWWTP and was stored at 4 °C. The wastewater was used within the next three days. Table 1 lists the key characteristics of the treated wastewater sample.

Table 1
Physico-chemical analysis of municipal wastewater.

Wastewater characteristics	Concentration
pH	7.72
Nitrates	13.63 ± 0.20 mg L^{-1}
Phosphates	4.1 ± 0.3 mg L^{-1}
BOD	118 ± 2.3 mg L^{-1}
COD	200 ± 4.2 mg L^{-1}
Total bacteria count	10^5 CFU mL^{-1}

2.5. Bacterial Enummeration

The total cell count of naturally occurring bacteria in wastewater was evaluated by plating the sample on agar plates. After every 10 min of treatment, a small amount of sample was taken out of the reactor and stored at 4 °C. After the complete treatment of the wastewater, 0.1 mL out of the 1 mL treated sample and spreading over the agar plate was done using the standard plating method. Serial dilution of 10^{-1} to 10^{-5} was made. The plates were stored at 37 °C overnight for incubation, and the colonies on the plates were manually counted.

2.6. Fabrication of composite beads

Iron–Titanium oxide composite beads were fabricated using 2 parts of clay mixed with 1 part of WFS, and WFA. Supplementary file Fig. S1 depicts the WFS and WFA characteristics using EDS analysis. A vernier caliper was used to measure the average size of the beads from four different directions, resulting in a diameter of 10 mm. These beads were calcined for 2 h in a muffle furnace at 800 °C. They were immersed in water for 48 h and then dried at room temperature to improve their longevity and strength.

Blank beads are those that do not have a TiO_2 coating. The presence of WFS and WFA in the acidic circumstances caused the iron to lixiviate from these beads. The photo-Fenton procedure was then started with these beads. More clay beads were manufactured without any WFS or WFA and heated at 800 °C for 1.5–2.0 h to explore the photocatalytic inactivation of bacteria. The TiO_2 particles were uniformly dispersed by sonication of a 1% (w/v) TiO_2 mixture. Using the dip-coating process, TiO_2 catalyst coating was applied to these beads (with or without an iron source). Fig. 1a-b shows photos of both blank and TiO_2 coated beads. To

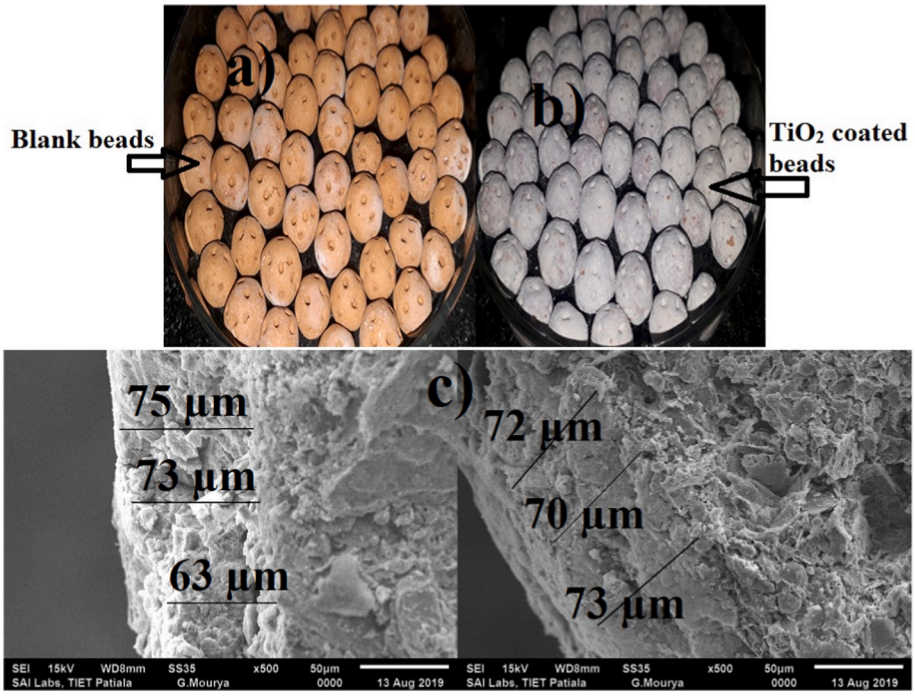

Fig. 1. Actual images of (a) blank and (b) TiO_2 immobilized composite beads (c) SEM image showing thickness of TiO_2 coating (Average thickness 71 µm) over composite beads.

ensure proper coverage, the exterior of the composite was covered twice with the TiO_2 solution.

To achieve excellent TiO_2 adherence to the composite bead's surface, they were heated at 350 °C for 1.5 h. The TiO_2 coating was determined to be 71 μm thick over the support, as illustrated in Fig. 1c, using a scanning electron microscopy (SEM) investigation. The supports were given the suffix 'composite' after TiO_2 immobilization to show that they contained both catalysts (iron (WFS and WFA) and TiO_2). These iron-titanium oxide composites were then utilized to explore the fixed mode hybrid effect.

2.7. Photocatalytic reactor set-up

A batch experiment was performed in a glass reactor (7.9 inches in diameter and 2.2 inches in height) under solar irradiation. The wastewater disinfection was carried out in the Thapar campus (30.3564° N, 76.3647° E) from August to October between 12:30 p.m. to 3:00 p.m. The average intensity of solar irradiation from the start to the end of experiments was observed to be between 590 and 600 W m^{-2}. TiO_2 coated composite beads were placed on the surface of the glass reactor. The disinfection performance of the hybrid method was tested using 200 mL of wastewater. Two air nozzles having a flow of (3 L min^{-1}) were held at an equal distance from the middle of the reactor to maintain the reaction uniformity. A sufficient amount of samples from the batch reactor was taken using a syringe at regular time intervals for the time-dependent analysis and then plated on an agar plate for bacterial cell count. The bacterial cells were counted using the standard Petri plate method in terms of CFU mL^{-1}. Parameters such as pH of the solution, H_2O_2 concentration, and the surface area covered using composite beads were used to optimize the batch reactor.

3. Results and discussion

3.1. Composite characterization

3.1.1. X-ray diffraction

The crystalline nature of the composite was confirmed using XRD analysis. Fig. 2a shows the results obtained from the fresh and recycled composite. The prominent peaks of the anatase phase at 25.4°, 37.8°, 48°, 55°, 62.6° and rutile phase at 26°, 36°, 55° was observed for P-25 TiO_2 (Kim et al., 2013; Zhou et al., 2006). The peaks of iron titanium oxide (ITO) were also observed (Sun et al., 2013). These peaks were still prominent in the recycled composite, indicating that there were no deformations in the catalyst even after >200 recycles. In Fig. 2a, the iron titanium oxide (IO) peaks at 70.3° and 75.28° planes indicated that photoexcited electrons from the TiO_2 photocatalytic process were trapped by Fe^{3+} for the redevelopment of Fe^{2+}. This confirmed the presence of photo-Fenton and photocatalysis in one unit. In visible light, these ITO particles increased the efficacy of the iron-titanium oxide catalyst. As stated in the following section, this theory was further validated using UV-DRS analysis.

3.1.2. UV–visible differential reflectance spectroscopy

Differential reflectance spectroscopy was done on the composite for the determination of the energy bandgap in the spectrum range of 200–800 nm. To set the baseline of the sample Barium sulfate ($BaSO_4$) was used as a reference compound. The bandgap energies were obtained from the linear intercept of the $(\varepsilon h\nu)^2$ vs. hν plots on hν axis using Tauq equation (Equation (3)) as shown in Fig. 2b. The energy band gaps were found to be 3.12 eV for P25–TiO_2 and then reduced to 2.9 eV for the composite as shown in Fig. 2b. This shift in the Fe–TiO_2 composite to the visible region is because of the presence of more valence electrons in Fe (III) than Ti (IV) which leads to the filling up of new energy levels (Talwar et al., 2019). The presence of iron in the crystal structure of Fe–TiO_2 leads to the change in the bandgap energies towards the visible range of light.

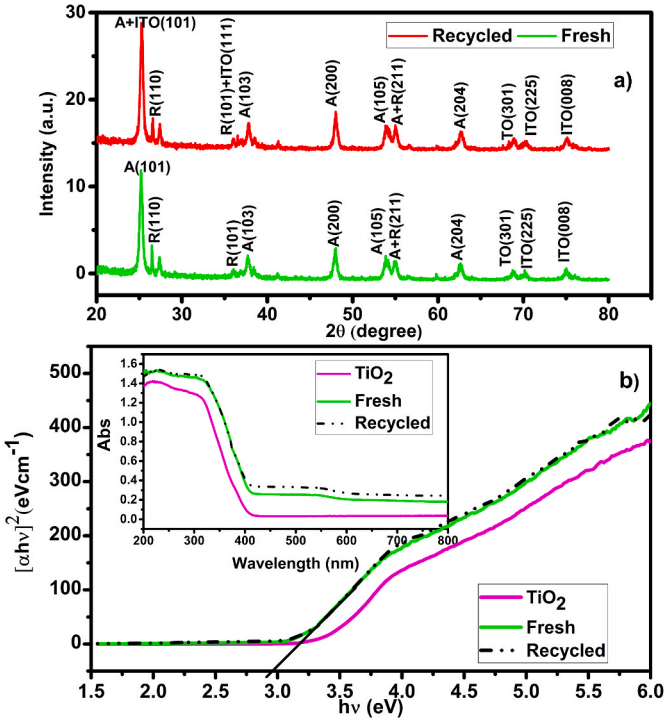

Fig. 2. (a) XRD analysis of fresh and recycled iron-titanium oxide composite (b) UV–visible DRS analysis of P-25 TiO_2 fresh and recycled composite.

$$(\alpha\vartheta h)^{\frac{1}{n}} = k\left(h\vartheta - E_g\right) \quad (3)$$

Where α represents the excitation coefficient, h represents Planck's constant, E_g denotes the bandgap of energy (eV), and k is constant.

3.1.3. Fourier transform infrared spectroscopy

Fig. 3 shows the types of structural units formed in freshly coated and recycled composite using FTIR spectra. In both the samples, the broad absorption in the lower wavenumber region (500-1200 cm^{-1}) corresponded to the presence of Ti bonds with O in the TiO_2 lattice and also the presence of Fe in the composite. The wavenumbers obtained between 3200 and 2000 cm^{-1} show the vibrations of water (H_2O) molecules, which get absorbed in the catalyst. The characteristic peaks of Si–O stretching vibrations were also observed at around 600-500 cm^{-1}

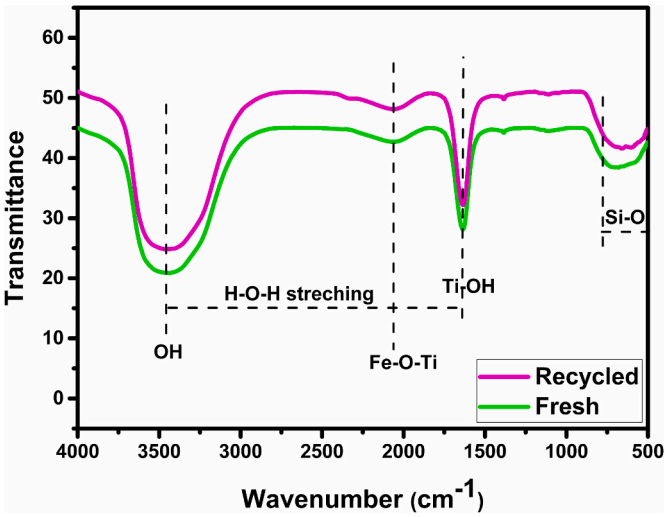

Fig. 3. FTIR analysis of fresh and recycled composite.

leading to the broadening of the bond between Ti–O–Si. The existence of iron is also confirmed by the peak at 1615 cm^{-1} showing the bond of Fe–O–Ti. Same peaks were also found in a previously done study (Bansal and Verma, 2018a).

3.1.4. Field Emission Scanning Electron Microscopy and energy-dispersive spectroscopy

For the surface morphology analysis of the composite beads, FESEM analysis was performed. The analysis of the fresh and recycled composite showed that the surface was evenly uniform without many cracks and also after recycling the coating did not wave off as the surface was still uniform (Bansal and Verma, 2018b). The EDS analysis validates the existence of Fe, Ti, O elements (Fig. 4). This confirms the dual nature of this hybrid system. Even the recycled composite elements including Ti, Fe, and O existed.

3.1.5. High-resolution transmission electron microscopy and elemental mapping

HRTEM images of fresh and recycled Fe–TiO_2 nanoparticles were analyzed to study their morphology and lattice spacing (Fig. S2). The lattice stripes of Fe–TiO_2 particles are shown in supplementary file Fig. S2, and lattice spacing of 0.35–0.36 was observed corresponding to the crystal plane of the TiO_2 anatase (101) phase. Elemental analysis was also done to determine the presence of iron and TiO_2 in the composite. From supplementary file Fig. S3 uniform dispersion of Ti, O, and Fe elements in the entire visual field was observed, showing that Fe has generated uniform doping in TiO_2 and confirms the uniform doping of Fe elements.

3.1.6. X-ray photoelectron spectroscopy

The Chemical composition of Fe–TiO_2 was also studied using X-ray photoelectron spectroscopy (XPS). The survey spectra of the Fe–TiO_2 composite are shown in supplementary file Fig. S4. This synthesized composite does not contain any carbon, but the carbon peak demonstrated in the survey scan comes from the background. The dominant peak at 458.6 eV is associated with Ti ions with a formal valence 4^+ (Ti^{4+}), while the peak at the lower binding energy of ~456.6 eV is associated with Ti ions with a reduced charge state (Ti^{3+}) shown in supplementary file Fig. S5a. The O 1s core level (Fig. S5b) is centered at 529.8 eV, corresponding to the metal oxide (TiO_2). The Spectra shown in supplementary file Fig. S5c are the weak peaks of iron. Similar results were observed in the previous study showing the dominant peaks of Ti (458.6 eV), O (529.8 eV), and Fe (724 eV) (Ismail et al., 2021). Thus confirming the presence of both iron and titanium in one system.

3.1.7. Control and dark experiments

The preliminary tests were conducted on all of the blank experiments to establish the dominance of the hybrid process. In Fig. 5, the changes in the cell count (CFU mL^{-1}) that occurred in the dark environment were addressed. The minor change of <1 log reduction might be due to sensitive cells dying, primarily as a result of the oxidative stress produced in double-distilled water (Giannakis et al., 2018). Similar results were obtained even for a much longer duration in the literature and no reduction in the bacterial concentration was observed (Rodríguez-Chueca et al., 2016; Venieri et al., 2018). Similar results were reported with H_2O_2 also. The polarity of H_2O_2 and water is the same, which helps H_2O_2 permeate inside the cell pretty quickly and destroys the cell internally. But, the regulators such as alkyl hydroxide reductase (aph) and katE cause a quick breakdown of H_2O_2, resulting in a minimal reduction in bacterial concentration (Giannakis, 2018). In the present study, the cells were in the stationary phase, making katE protect cells against H_2O_2 generation as aph works in a growing cell (Seaver et al., 2001).

After the characterization of the dark experiments, the solar

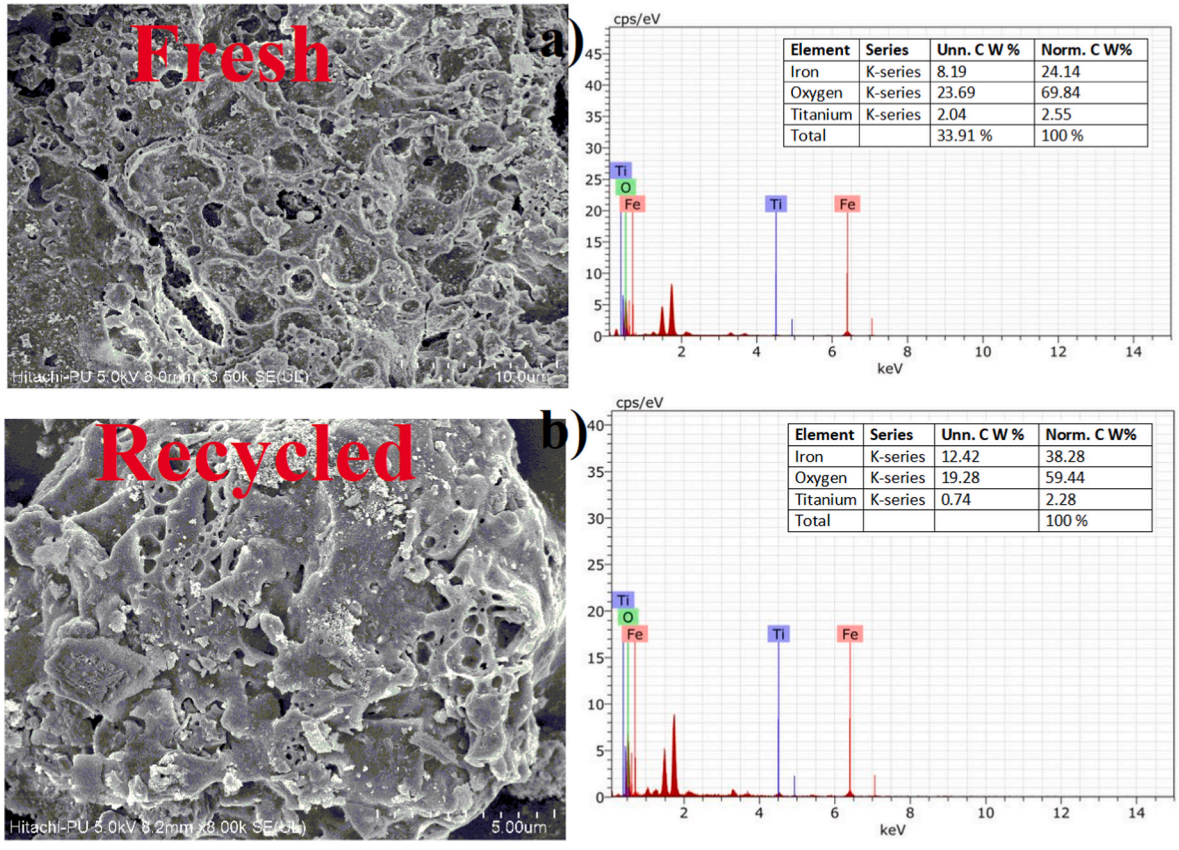

Fig. 4. FESEM-EDS images (a) freshly coated composite beads (b) recycled composite beads.

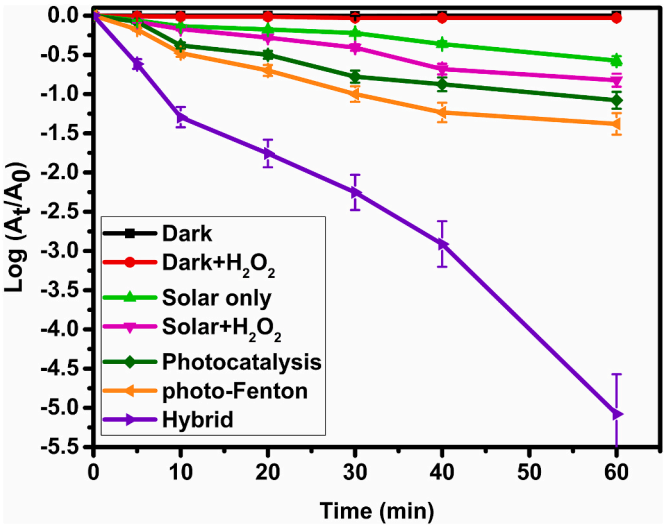

Fig. 5. Preliminary analysis of bacterial inactivation under dark and solar conditions.

processes are presented. Fig. 5 describes the solar-based tests (irradiance: 600 W m^{-2}), namely solar light alone, solar light/H_2O_2 (0.75 g L^{-1}), TiO_2-photocatalysis, and solar light/Fe/H_2O_2 (photo-Fenton) in municipal wastewater. For solar light alone and solar light with H_2O_2, the results were found with insignificant log reductions, as shown in Fig. 5. The TiO_2-photocatalysis reaction showed a 1 log reduction in the bacterial population after 60 min of illumination.

In the photo-Fenton process, for the iron lixiviating to begin, the pH of the reaction was kept at 4–4.5. In this method, 0.75 g L^{-1} of H_2O_2 was introduced to initiate the reaction, and after 60 min of reaction time, a 1.2 log decrease was detected as shown in Fig. 5. After evaluating the controlled experiments, parametric optimization of the hybrid process by varying concentrations of the following parameters (percent surface area covered, pH, and H_2O_2 concentration).

3.1.8. Study on surface area covered

The impact of surface area covered for wastewater disinfection was examined in this study by altering the amount of composite beads on the surface of the reactor. The optimum number of catalytic beads required for disinfection is investigated in this effect. The analysis was depicted as a percentage area covered, with a change in the number of beads. As shown in Fig. 6a, increased log reduction was observed when the coverage of the surface of the reactor was changed from 50% to 100%. The inactivation rate is improved by using more catalysts. The increased amount of catalyst increases the active sites, resulting in the inactivation efficiency with the production of more OH°. When the coverage of the reactor's surface was increased to 150%, a decrease in the bacterial log reduction was found. This could be due to excessive iron lixiviation from the beads obstructing the active surface area of the catalyst. This resulted in less reduction of the cell population through the formation of dead zones. These dead zones are created due to the overlapping of beads which effectively reduce the volume of wastewater to be treated. When the number of beads was increased beyond 100%, the concentration of both TiO_2 and iron increased, significantly boosting the generation of OH^o. This makes the scavenging action dominate in that circumstance (Djeffal et al., 2014).

3.1.9. Effect of pH change

pH is a critical parameter in the hybrid process because iron leaches from composite beads under acidic circumstances. The iron then performs the photo-Fenton reaction in the system with H_2O_2. To optimize the pH, studies were conducted at various pH values ranging from 4.5 to 6.5, as illustrated in Fig. 6b. The experiment was completed in 60 min at controlled pH with 0.75 g L^{-1} of H_2O_2 concentration. As illustrated in Fig. 6b, maximal bacterial inactivation (5 log unit) was achieved in 60 min at pH 4.5. At pH 5.5, a slight drop in log reduction (4.0) was seen after 60 min. The inactivation effectiveness reduces as the pH increases above 5.5 due to the generation of less effective HO_2^- at alkaline conditions. Then its reaction with non-dissociated H_2O_2, O_2, and H_2O are formed (Equation (4)), ultimately decreasing the process efficacy. The formation of OH^o slows down at high pH levels due to the hydrolysis of ferric ions and precipitation of ferric oxyhydroxide complex from the solution, which impacts the generation of OH^o (Herney-Ramirez et al., 2010). These findings make it evident that pH has a substantial effect on inactivation.

The results mentioned above showed that with the increase in the pH, the bacterial log reduction decreases. This is because of the de-

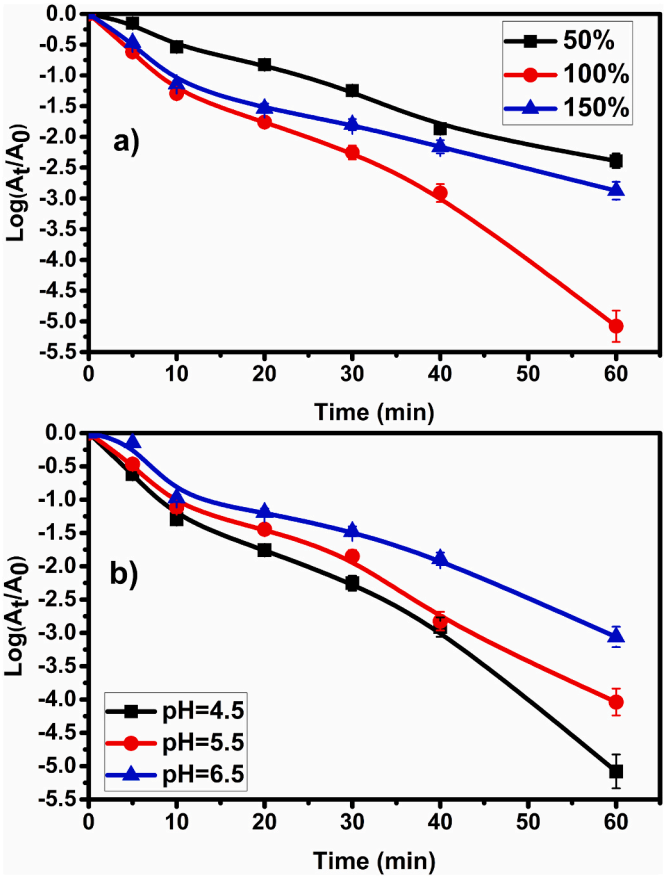

Fig. 6. (a) Effect of variation of percentage surface area covered on bacterial inactivation (b) Effect of variation of pH on bacterial inactivation.

Table 2
Concentration of iron species leaching out of composite beads at different pH.

Time (min)	Concentration of iron (μg L^{-1}) at pH 4.5		
	Ferrous ions	Ferric ions	Total Iron
10	51.53846	106.15385	157.69231
20	53.84615	107.69231	161.53846
30	57.69231	108.84615	166.53846
40	63.07692	103.07692	166.15385
50	68.84615	100	168.84615
Time (min)	**Concentration of iron (μg L^{-1}) at pH 5.5**		
	Ferrous ions	**Ferric ions**	**Total Iron**
10	48.46153846	78.46153846	126.9230769
20	50	92.30769231	142.3076923
30	55.76923077	93.84615385	149.6153846
40	61.53846154	98.07692308	159.6153846
50	65	97.30769231	162.3076923
Time (min)	**Concentration of iron (μg L^{-1}) at pH 6.5**		
	Ferrous ions	**Ferric ions**	**Total Iron**
10	38.46153846	52.69230769	91.15384615
20	39.23076923	58.84615385	98.07692308
30	40	60	100
40	41.15384615	69.23076923	110.3846154
50	41.92307692	73.46153846	115.3846154

pendency of iron leaching from the composite on the pH of the solution. As the pH of the solution decreases, the lixiviation of iron from the composite increases. In soil, iron is found in association with other components, and acid (pH < 6) aids in disrupting the binding between iron and an organic compound. Thus removing the iron from the clay, a process known as iron leaching (Hseu, 2004). This was confirmed by analyzing iron leaching from the Fe–TiO_2 beads under solar light at different time intervals and the results are shown in Table 2. The concentration of iron was found to be increased when pH was decreased from 6.5 to 4.5, subsequently showing the increase in the inactivation efficiency. The pH of the solution was not decreased beyond 4.5 because at lower pH the scavenging effect of OH^o predominates by H^+ (Yadav, 2010), as given in Equation 5

$$H_2O_2 \rightarrow HO_2^- + H^+ + H_2O + O_2 \quad (4)$$

$$OH^0 + H^+ + e^- \rightarrow H_2O \quad (5)$$

The iron concentration observed in the present system was much less than the previous trials (Mosteo et al., 2020; Shekoohiyan et al., 2019) yet showed significant inactivation in a shorter treatment time. The higher iron concentration in the system only inhibits the inactivation efficacy due to light scattering and diminishes direct irradiations.

3.1.10. *Effect of H_2O_2 concentration*

The influence of H_2O_2 on photo-Fenton and photocatalysis is a well-established method for increasing the amount of OH^o in the system. In the current case, the introduction of H_2O_2 serves a dual purpose because it is used concurrently in both processes, as demonstrated in Equations (6)–(8). In a photocatalytic reaction, oxidants are supplied to react with the conduction band electron preventing the recombining of electrons and holes together as shown in Equation (6). This hybrid process enhances the formation of ROS and OH^o. The concentration of H_2O_2 was tuned in this study by adjusting it between 0.3 and 0.9 g L^{-1}, with the best concentration observed to be 0.9 g L^{-1}. The complete inactivation of bacteria was observed within 60 min of reaction time at 0.9 g L^{-1} of H_2O_2 as illustrated in Fig. 7. This is due to the increased availability of H_2O_2 molecules to react with Fe^{2+} ions, increasing the amount of OH^o.

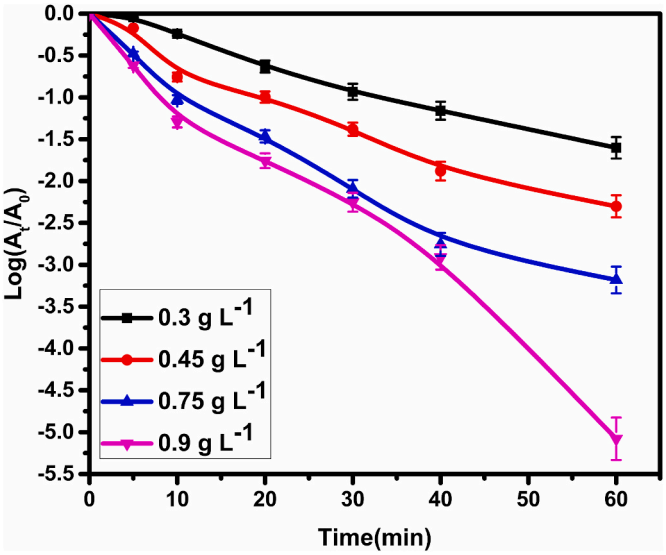

Fig. 7. Effect of variation of H_2O_2 doze on bacterial inactivation.

$$TiO_2(e^-) + H_2O_2 \rightarrow TiO_2 + OH^- + OH^o \quad (6)$$

$$Fe^{2+}_{(aquous)} + H_2O_2 \rightarrow Fe^{3+}_{(aquous)} + OH^\circ + OH^- \quad (7)$$

$$Fe^{3+}_{(aquous)} + H_2O_2 \rightarrow Fe^{2+}_{(aquous)} + H_3O^+ + HO_2^- \quad (8)$$

4. Mechanism of bacterial killing

The bacterial inactivation mechanism is presented according to the experimental findings. In this hybrid process, photo-Fenton and photocatalytic processes are taking place simultaneously in one unit. This hybrid process led to excessive generation of OH^o. The present technology imposes two important changes in the morphology of the bacteria. The first change is the degradation of the cell wall externally (Giannakis et al., 2016) due to the massive generation of OH^o. This massive generation is the result of the addition of the photo-Fenton reagent i.e. H_2O_2 and iron (leached out from the beads) into the system. Simultaneously the ROS species (OH^o, $HO_2^{-\circ}$, $O_2^{-\circ}$) produced during TiO_2 photocatalysis also gives rise to oxidative stress in the bacteria and led to its inactivation. This H_2O_2 also impacts cells externally via interacting with the cell's outer membrane. This allows the passage of the cell due to the massive input of H_2O_2, resulting in cell wall oxidation. It happens because the oxidative activity of H_2O_2 (0.18) is greater than the membrane oxidation potential.

The second is the degradation of the cell wall internally. The current study is working under solar light. This solar light helps in the inactivation of antioxidant enzymes such as catalase and peroxidase. These enzymes are the regulators of ROS (generating inside the cell) to oppose the imbalances created by them inside the cells by enzyme auto-oxidation. The Fenton reagents i.e. H_2O_2 and Fe^{2+} diffuse into the cytoplasm of the cell through porins. The size of the H_2O_2 ion (1.2–1.4 Å) and Fe^{2+} (<6 Å) is much smaller than the size of bacteria (11 Å), which helps in degrading the cells internally as no antioxidant enzymes are present inside the cell. This already present ROS reacts with Fe^{2+} resulting in damaging the cell. While H_2O_2 would induce modulation in

biosynthetic and catabolic activity, that will lead to Fe loss from the 4Fe–4S cluster and produce OH^o (Giannakis et al., 2018). This OH^o oxidizes the cytoplasmic proteins, DNA, and cell wall components.

5. Kinetic analysis

A kinetic assessment of the results using five different models such as Log-linear, Weibull, double Weibull, biphasic and biphasic shoulder as shown in Equations (9)–(13), was performed to evaluate and compare the three different processes (hybrid, photo-Fenton, and photocatalysis).

$$log\frac{A_t}{A_0} = -kCt \rightarrow log\frac{A_t}{A_0} = -k_{ap}t \tag{9}$$

Where A_0 is the initial bacterial concentration and A_t is the final concentration remaining after the reaction. The first-order rate constant is denoted by k (min^{-1}), the disinfectant concentration is represented by C, and the treatment time is denoted by t.

$$log\frac{A_t}{A_0} = -\left(\frac{t}{\delta}\right)^p \tag{10}$$

The first decimal time reduction is represented by δ. The equation is represented by p. When $p > 1$, the shape is convex; when $p < 1$, the shape is concave. At $p = 1$, the equation denotes a first-order linear model.

$$A = \frac{A_0}{1+10^{\propto}} \times \left(10^{-\left(\frac{1}{\delta_1}\right)^{p_1+\alpha}} + 10^{-\left(\frac{1}{\delta_2}\right)^{p_2}}\right) \tag{11}$$

The sub-population fraction is denoted by α, α_1 and α_2 denote distinct sub-populations. Sub-population 1 exhibits greater susceptibility to stress than sub-population 2($\delta_1 < \delta_2$).

$$Log\frac{A_t}{A_0} = Log\left[P * e^{-k_1 * t} + (1-P) * e^{-k_2 * t}\right] \tag{12}$$

where P represents the portion of bacteria that survive in subpopulation group 1 and (1–P) denotes the portion of bacteria that survive in subpopulation group 2. k_1 and k_2 represent the kinetic rate constant of the more susceptible population and more resistant population.

$$log\frac{A_t}{A_0} = Log\left[f*e^{-k_1 t}\frac{e^{k_1 s_1}}{1+(e^{k_1 s_1}-1)*e^{-k_1 t}} + (1-f)*e^{-k_2 t}*\left(\frac{e^{k_1 s_1}}{1+(e^{k_1 s_1}-1)*e^{-k_1 t}}\right)\right]^{\frac{k_1}{k_2}} \tag{13}$$

It is critical to establish suitable treatment conditions using a mathematical model that precisely depicts the disinfection kinetics. The parameters R^2 and RMSE were used to ascertain the model's accuracy. The findings of the statistical data of kinetic changes in resistance to treatment for all microorganisms used in this study incorporating various models are summarized in Table 3. The results obtained following bacterial inactivation in three different fixed-bed processes using solar irradiation demonstrated an excellent fit to the mathematical models used (Fig. 8a–c). With R^2 values reaching 1 and RMSD values reaching zero, the Weibull distribution and double Weibull distribution model provided a good fit. The δ value parameter in the Weibull model

Table 3
Kinetic analysis of photocatalysis, photo-Fenton and hybrid process using different models.

Technology	Different types of models	K (min^{-1})	k_{1max}	k_{2max}	δ_1 (min)	δ_2 (min)	$\frac{R^2}{RMSD}$
Dual							
	Biphasic-shoulder		0.18	0.0	–	–	0.98/0.106
	Biphasic	–	0.18	0.0		–	0.98/0.088
	Double-Weibull	–			15	62	0.98/0.085
	Weibull	–			3.01	–	0.911/0.464
	Log-linear	0.18			–	–	0.79/0.96
Photo-Fenton							
	Biphasic-shoulder		0.06	0.06	–	–	0.85/0.49
	Biphasic	–	0.06	0.06	96.48	–	0.84/0.42
	Double Weibull	–			29.7	122.06	0.98/0.047
	Weibull	–			96.48	–	0.90/0.23
	Log-linear	0.06			–	–	0.84/0.31
photocatalysis							
	Biphasic-shoulder		1.22	0.03	–	–	0.99/0.0126
	Biphasic	–	0.83	0.03		–	0.98/0.0127
	Double Weibull	–	–	–	53.91	53.91	0.98/0.0178
	Weibull	–			53.9	–	0.98/0.0153
	Log-linear	0.04			–	–	0.98/0.015

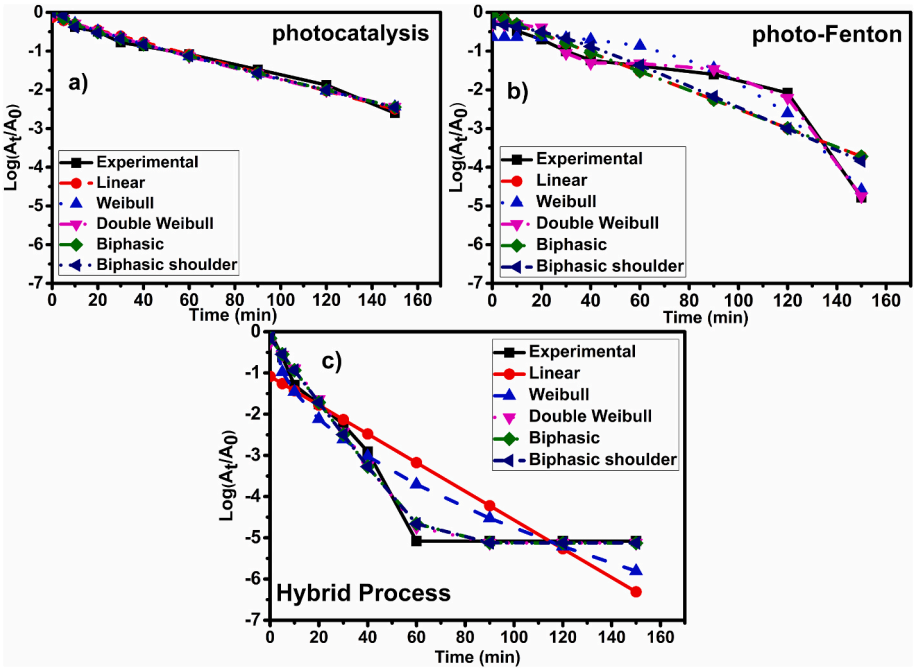

Fig. 8. Inactivation curves of bacteria using mathematical models on (a) TiO_2-photocatalysis (b) photo-Fenton process (c) hybrid-process.

represents the time required for the first decimal reduction of a cell colony or the inverse of the disinfection rate. This means if the δ value is higher, the bacterial inactivation rate is slower.

In this study, values (Table 3) for the hybrid process were more significant than those for the individual processes. The low δ values obtained demonstrated the hybrid process's effectiveness in inactivating bacteria. When the k and δ values of three different processes were compared (Table 3), it was discovered that the hybrid process reduced the bacterial count at a faster rate. Thus, using log-linear and Weibull parameters to fit the bacterial inactivation results and its comparison with the different techniques revealed that the hybrid-process ($k = 0.18$ min^{-1}, $\delta = 3.01$ min) was considerably faster than the other technologies: photocatalytic process ($k = 0.06$ min^{-1}, $\delta = 96.48$ min); and photo-Fenton process ($k = 0.04$ min^{-1}, $\delta = 53.9$ min). To confirm the prominence of the hybrid process, photoluminescence spectroscopy of three different processes (photo-Fenton, photocatalysis, and hybrid process) was also performed as shown in supplementary file Fig. S6. Fig. S6 showed the higher production of OH^{o} in hybrid process in comparison to the other two processes leading to complete inactivation of the bacteria present in wastewater.

6. FE-SEM analysis for E. coli inactivation

The FE-SEM technique was used to examine the structural changes in *E. coli* cells following treatment with Fe–TiO_2 catalysts in deionized water. In this study for microscopic analysis, *E. coli* in deionized water was tested with Fe–TiO_2 composite. The real wastewater was not used here to get clear images of damaged cells without any interference of other organic matter. Fig. 9a shows an FE-SEM image of the untreated *E. coli* cells. The cells are healthy and morphologically intact in Fig. 9a. There is clear cell disruption and morphological damage in Fig. 9b. In contrast, the *E. coli* cells treated with Fe–TiO_2 under the same conditions showed dramatic morphological changes during the process of cell death. For the cells treated in deionized water (shown in Fig. 9b), the whole cells were completely disrupted as shown in Fig. 9b. The cell fragments found in Fig. 9b were presumably caused by lysing bacterial cells, resulting in the leaking of broken DNA molecules. This indicates that more potent oxidizing agents were created to kill the cells completely.

7. Degradation of organic compounds

The organic matter present in the wastewater was also treated to study the complete treatment of the wastewater. The results are presented in terms of chemical oxygen demand (COD), biochemical oxygen demand (BOD), nitrate (NO_3^-), and phosphates (PO_4^{3-}). These parameters were detected throughout the treatment process using the hybrid process at its optimized conditions ($H_2O_2 = 0.9$ g L^{-1}, pH = 5.5, the surface area covered = 100%) (Fig. 10 a-d). In the present work, the concentration of nitrate and phosphates ions decreased from 13.3 mg L^{-1} to 5.6 mg L^{-1} and 4.1 mg L^{-1} to 3.5 mg L^{-1} respectively in 60 min of treatment time. There was almost a 40% and 54% reduction in both COD and BOD after 60 min of treatment. This significant decline in COD and BOD was credited to the leaching of iron enabling photo-Fenton reaction in conjunction with the TiO_2 layer, facilitating photocatalysis. With 100% coverage of the surface of the reactor with composite beads, the exposed catalyst active sites were increased and made readily available for effective pollutant binding, resulting in the elimination of pollutants contained in the wastewater.

8. Durability studies

The durability of the immobilized catalyst with retained activity is a critical challenge while visualizing the proposed concept of the hybrid process on a large scale. The primary aim of this study was to examine the in-situ hybrid effect in disinfection tests. The reported investigation should demonstrate both the sustainability of iron leaching and the stability of the catalyst (TiO_2) coating on the beads by subsequent recycling experiments. The recyclability/durability and activity of catalyst (Fe–TiO_2 composite) were examined through recycling experiments for the disinfection of bacteria present in wastewater. The beads were effectively employed for at least 35 trials without showing any

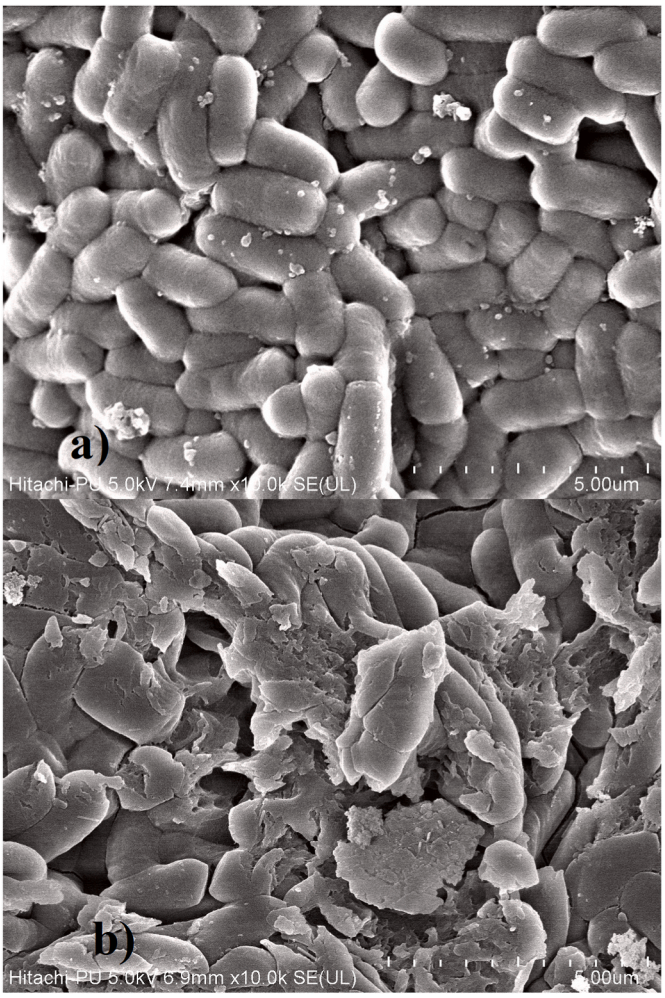

Fig. 9. (a) FESEM image of *E.coli* before treatment (b) FESEM image of inactivated *E. coli* after treatment.

significant decrease in bacterial log reduction activity as shown in Fig. 11. No significant variation in disinfection efficiency between subsequent runs ($P > 0.05$) was observed. The catalyst remained intact on the surface and was sufficiently active to exhibit effective disinfection even after 35 cycles of recycling. Effective disinfection by an in-situ hybrid approach utilizing recycled composite beads verifies the systematic lixiviation of iron from recycled beads, contributing to the photo-Fenton process occurring concurrently with photocatalysis. In recycled composite beads, the existence of TiO_2 and iron was established using the techniques described in the preceding sections for the characterization of composite beads.

9. Conclusion

The study presents the concept of circular economy through waste-driven value-added products for the treatment of secondary treated municipal wastewater. This article reports the synthesis and characterization of Fe–TiO_2 composites. This waste foundry sand and fly ash-derived composite with surface-active TiO_2 layer introduced the novel concept of the hybrid effect in one system. The prepared fixed bed catalyst was evaluated for the disinfection of secondary municipal wastewater. The results revealed that the natural doping of iron with TiO_2 significantly affects the optical properties which enhanced the bacterial disinfection. This hybrid technology showed 100% bacterial inactivation in 60 min of reaction time with 0.9 g L^{-1} of H_2O_2 dose at 5.5 pH and 100% surface area covered with composite. With the use of

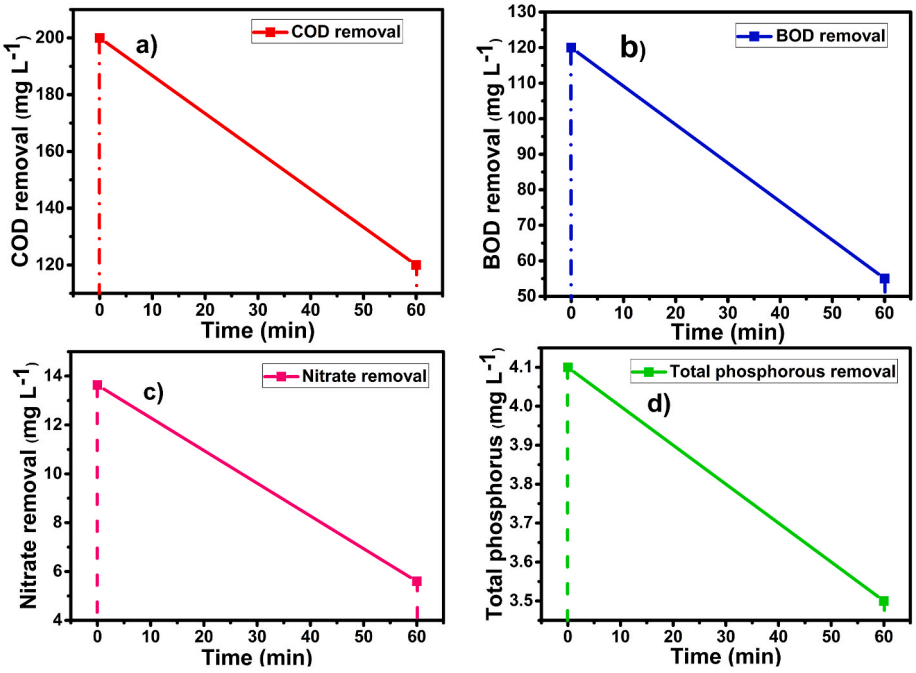

Fig. 10. Treatment of wastewater effluent using Fe–TiO_2 composite (a) COD removal (b) BOD removal (c) Nitrate removal (d) Phosphate removal.

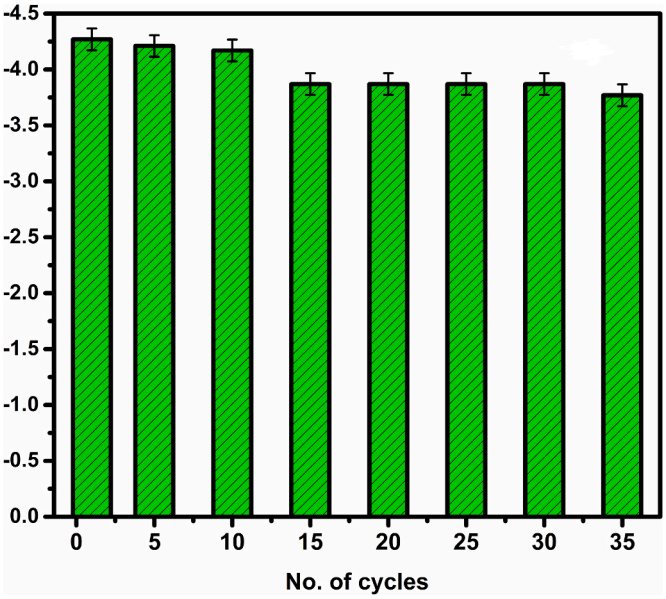

Fig. 11. Durability analysis of composite beads.

different kinetic models, the Weibull, double Weibull, and Biphasic models were the best models to represent the inactivation kinetics. To study the durability of the composite, they were recycled 35 times and the photoactivity of the catalyst was only reduced by 11%. Different characteristic analyses of composite beads also proved the durability and stability of the catalyst even after 35 cycles. The findings of this study demonstrate the possibility for waste materials to be used as a viable approach for the post-treatment of the effluent that can be implemented effectively on field size.

CRediT authorship contribution statement

Ina Thakur: Conception and design of the study, Experimentation, Analysis/Interpretation of Data, Drafting the Manuscript. **Anoop Verma:** Conception and design of the study, Drafting the Manuscript, Revising the manuscript critically for important intellectual content. **Banu Örmeci:** Drafting the Manuscript, Revising the manuscript critically for important intellectual content.

Funding

This research did not receive any specific grant from funding agencies in the public, commercial, or not-for-profit sectors.

Declaration of competing interest

The authors declare that they have no known competing financial interests or personal relationships that could have appeared to influence the work reported in this paper.

Appendix A. Supplementary data

Supplementary data to this article can be found online at https://doi.org/10.1016/j.jclepro.2022.131575.

References

Almuktar, S.A.A.A.N., Abed, S.N., Scholz, M., 2018. Wetlands for wastewater treatment and subsequent recycling of treated effluent: a review. Environ. Sci. Pollut. Res. 25, 23595–23623. https://doi.org/10.1007/s11356-018-2629-3.

Arayan, L.T., Reyes, A.W.B., Hop, H.T., Xuan, H.T., Baek, E.J., Yang, H.S., Chang, H.H., Kim, S., 2017. Antimicrobial effect of different concentrations of ozonated water in the sanitation of water experimentally inoculated with Escherichia coli. J. Prev. Vet. Med. 41, 84–87. https://doi.org/10.13041/jpvm.2017.41.2.84.

Bansal, P., Verma, A., 2018a. In-situ dual effect studies using novel Fe-TiO2 composite for the pilot-plant degradation of pentoxifylline. Chem. Eng. J. 332, 682–694. https://doi.org/10.1016/j.cej.2017.09.121.

Bansal, P., Verma, A., 2018b. N, Ag co-doped TiO2 mediated modified in-situ dual process (modified photocatalysis and photo-Fenton) in fixed-mode for the degradation of Cephalexin under solar irradiations. Chemosphere. https://doi.org/10.1016/j.chemosphere.2018.08.120.

Berney, M., Weilenmann, H.U., Egli, T., 2006. Flow-cytometric study of vital cellular functions in Escherichia coli during solar disinfection (SODIS). Microbiology 152, 1719–1729. https://doi.org/10.1099/mic.0.28617-0.

Carré, G., Hamon, E., Ennahar, S., Estner, M., Lett, M.C., Horvatovich, P., Gies, J.P., Keller, V., Keller, N., Andre, P., 2014. TiO2 photocatalysis damages lipids and proteins in Escherichia coli. Appl. Environ. Microbiol. 80, 2573–2581. https://doi.org/10.1128/AEM.03995-13.

Changotra, R., Rajput, H., Dhir, A., 2019. Treatment of real pharmaceutical wastewater using combined approach of Fenton applications and aerobic biological treatment. J. Photochem. Photobiol. Chem. 376, 175–184. https://doi.org/10.1016/j.jphotochem.2019.02.029.

Chen, Q., Wu, P., Li, Y., Zhu, N., Dang, Z., 2009. Heterogeneous photo-Fenton photodegradation of reactive brilliant orange X-GN over iron-pillared montmorillonite under visible irradiation. J. Hazard Mater. 168, 901–908. https://doi.org/10.1016/j.jhazmat.2009.02.107.

Collivignarelli, M.C., Abbà, A., Carnevale Miino, M., Arab, H., Bestetti, M., Franz, S., 2020. Decolorization and biodegradability of a real pharmaceutical wastewater treated by H2O2-assisted photoelectrocatalysis on TiO2 meshes. J. Hazard Mater. 387, 121668. https://doi.org/10.1016/j.jhazmat.2019.121668.

Djeffal, L., Abderrahmane, S., Benzina, M., Siffert, S., Fourmentin, S., 2014. Efficiency of natural clay as heterogeneous Fenton and photo-Fenton catalyst for phenol and tyrosol degradation. Desalination Water Treat. 52, 2225–2230. https://doi.org/10.1080/19443994.2013.799440.

EPA, 2012. EPA Guidlines for Water Reuse U.S. Environmental Protection Agency, Environmental Protection Agency.

Giannakis, S., 2018. Analogies and differences among bacterial and viral disinfection by the photo-Fenton process at neutral pH: a mini review. Environ. Sci. Pollut. Res. 25, 27676–27692. https://doi.org/10.1007/s11356-017-0926-x.

Giannakis, S., Inmaculada, M., López, P., Spuhler, D., Antonio, J., Pérez, S., Fernández, P., 2016. Solar disinfection is an augmentable , in situ -generated photo-Fenton reaction - Part 1 : a review of the mechanisms and the fundamental aspects of the process. Appl. Catal. B Environ. 199, 199–223. https://doi.org/10.1016/j.apcatb.2016.06.009.

Giannakis, S., Voumard, M., Rtimi, S., Pulgarin, C., 2018. Bacterial disinfection by the photo-Fenton process: extracellular oxidation or intracellular photo-catalysis? Appl. Catal. B Environ. 227, 285–295. https://doi.org/10.1016/j.apcatb.2018.01.044.

GilPavas, E., Dobrosz-Gómez, I., Gómez-García, M.Á., 2017. Coagulation-flocculation sequential with Fenton or Photo-Fenton processes as an alternative for the industrial textile wastewater treatment. J. Environ. Manag. 191, 189–197. https://doi.org/10.1016/j.jenvman.2017.01.015.

Herney-Ramirez, J., Vicente, M.A., Madeira, L.M., 2010. Heterogeneous photo-Fenton oxidation with pillared clay-based catalysts for wastewater treatment: a review. Appl. Catal. B Environ. 98, 10–26. https://doi.org/10.1016/j.apcatb.2010.05.004.

Hseu, Z., 2004. Evaluating heavy metal contents in nine composts using four digestion methods. Bioresour. Technol. 95, 53–59. https://doi.org/10.1016/j.biortech.2004.02.008.

Hu, X., Zhu, Q., Gu, Z., Zhang, N., Liu, N., Stanislaus, M.S., Li, D., Yang, Y., 2017. Wastewater treatment by sonophotocatalysis using PEG modified TiO2 film in a circular Photocatalytic-Ultrasonic system. Ultrason. Sonochem. 36, 301–308. https://doi.org/10.1016/j.ultsonch.2016.12.008.

Ismail, M.A., Hedhili, M.N., Anjum, D.H., Singaravelu, V., Chung, S.H., 2021. Synthesis and characterization of iron-doped tio2 nanoparticles using ferrocene from flame spray pyrolysis. Catalysts 11. https://doi.org/10.3390/catal11040438.

Jiménez, M., Oller, I., Maldonado, M.I., Malato, S., Hernández-Ramírez, A., Zapata, A., Peralta-Hernández, J.M., 2011. Solar photo-Fenton degradation of herbicides partially dissolved in water. Catal. Today 161, 214–220. https://doi.org/10.1016/j.cattod.2010.11.080.

Kassahun, S.K., Kiflie, Z., Kim, H., Gadisa, B.T., 2020. Effects of operational parameters on bacterial inactivation in Vis-LEDs illuminated N-doped TiO2 based photoreactor. J. Environ. Chem. Eng. 8 https://doi.org/10.1016/j.jece.2020.104374.

Khan, S.J., Reed, R.H., Rasul, M.G., 2012. Thin-film fixed-bed reactor for solar photocatalytic inactivation of Aeromonas hydrophila: influence of water quality. BMC Microbiol. 12 https://doi.org/10.1186/1471-2180-12-285.

Kim, T.H., Rodríguez-González, V., Gyawali, G., Cho, S.H., Sekino, T., Lee, S.W., 2013. Synthesis of solar light responsive Fe, N co-doped TiO2 photocatalyst by sonochemical method. Catal. Today 212, 75–80. https://doi.org/10.1016/j.cattod.2012.09.014.

Laxma Reddy, P.V., Kavitha, B., Kumar Reddy, P.A., Kim, K.H., 2017. TiO2-based photocatalytic disinfection of microbes in aqueous media: a review. Environ. Res. 154, 296–303. https://doi.org/10.1016/j.envres.2017.01.018.

Mecha, A.C., Onyango, M.S., Ochieng, A., Momba, M.N.B., 2017. Evaluation of synergy and bacterial regrowth in photocatalytic ozonation disinfection of municipal wastewater. Sci. Total Environ. 601– 602, 626–635. https://doi.org/10.1016/j.scitotenv.2017.05.204.

Mosteo, R., Varon Lopez, A., Muzard, D., Benitez, N., Giannakis, S., Pulgarin, C., 2020. Visible light plays a significant role during bacterial inactivation by the photo-fenton process, even at sub-critical light intensities. Water Res. 174, 115636. https://doi.org/10.1016/j.watres.2020.115636.

Pariente, M.I., Martínez, F., Melero, J.A., Botas, J.Á., Velegraki, T., Xekoukoulotakis, N. P., Mantzavinos, D., 2008. Heterogeneous photo-Fenton oxidation of benzoic acid in water: effect of operating conditions, reaction by-products and coupling with biological treatment. Appl. Catal. B Environ. 85, 24–32. https://doi.org/10.1016/j.apcatb.2008.06.019.

Polo-López, M.I., Oller, I., Fernández-Ibáñez, P., 2013. Benefits of photo-Fenton at low concentrations for solar disinfection of distilled water. A case study: Phytophthora capsici. Catal. Today 209, 181–187. https://doi.org/10.1016/j.cattod.2012.10.006.

Rodríguez-Chueca, J., Mosteo, R., Ormad, M.P., Ovelleiro, J.L., 2012. Factorial experimental design applied to Escherichia coli disinfection by Fenton and photo-Fenton processes. Sol. Energy 86, 3260–3267. https://doi.org/10.1016/j.solener.2012.08.015.

Rodríguez-Chueca, J., Ormad, M.P., Mosteo, R., Canalis, S., Ovelleiro, J.L., 2016. Escherichia coli inactivation in fresh water through photocatalysis with TiO2-effect of H2O2 on disinfection kinetics. Clean 44, 515–524. https://doi.org/10.1002/clen.201500083.

Rodríguez-Chueca, J., Polo-López, M.I., Mosteo, R., Ormad, M.P., Fernández-Ibáñez, P., 2014. Disinfection of real and simulated urban wastewater effluents using a mild solar photo-Fenton. Appl. Catal. B Environ. 150–151, 619–629. https://doi.org/10.1016/j.apcatb.2013.12.027.

Seaver, L.C., Imlay, J.A., Loewen, P., 2001. Alkyl hydroperoxide reductase is the primary scavenger of endogenous hydrogen peroxide in Escherichia coli. J. Bacteriol. 183, 7173–7181. https://doi.org/10.1128/JB.183.24.7173.

Shekoohiyan, S., Rtimi, S., Moussavi, G., Giannakis, S., Pulgarin, C., 2019. Enhancing solar disinfection of water in PET bottles by optimized in-situ formation of iron oxide films. From heterogeneous to homogeneous action modes with H2O2 vs. O2 – Part 1: iron salts as oxide precursors. Chem. Eng. J. 358, 211–224. https://doi.org/10.1016/j.cej.2018.09.219.

Sun, H., Zhou, G., Liu, S., Ang, H.M., Tadé, M.O., Wang, S., 2013. Visible light responsive titania photocatalysts codoped by nitrogen and metal (Fe, Ni, Ag, or Pt) for remediation of aqueous pollutants. Chem. Eng. J. https://doi.org/10.1016/j.cej.2013.07.019.

Tadashi, M., Ryozo, T., Toshiaki, N., Hitoshi, W., 1985. Photoelectrochemical sterilization of microbial cells by semiconductor powders. FEMS Microbiol. Lett. 29, 211–214.

Talwar, S., Verma, A.K., Sangal, V.K., 2019. Modeling and optimization of fixed mode dual effect (photocatalysis and photo-Fenton) assisted Metronidazole degradation using ANN coupled with genetic algorithm. J. Environ. Manag. 250 https://doi.org/10.1016/j.jenvman.2019.109428.

Venieri, D., Panagiotopoulou, P., Makropoulou, T., 2018. N-doped TiO2 Photocatalysts for Bacterial Inactivation in Water. https://doi.org/10.1002/jctb.5639.

Visa, M., Duta, A., 2013. Methyl-orange and cadmium simultaneous removal using fly ash and photo-Fenton systems. J. Hazard Mater. 244–245, 773–779. https://doi.org/10.1016/j.jhazmat.2012.11.013.

WHO, 2006. Guidelines for the Safe Use of Wastewater. Excreta and Greywater.

Yadav, P., 2010. Titanium dioxide mediated photocatalytic degradation of chlorpyrifos in aqueous phase. Int. J. Environ. Sci. s 3, 743–755. https://doi.org/10.6088/ijes.2012030132001.

Yuan, X., Duan, S., Wu, G., Sun, L., Cao, G., Li, D., Xu, H., Li, Q., Xia, D., 2018. Enhanced catalytic ozonation performance of highly stabilized mesoporous ZnO doped g-C3N4 composite for efficient water decontamination. Appl. Catal. Gen. 551, 129–138. https://doi.org/10.1016/j.apcata.2017.12.011.

Zhou, M., Yu, J., Cheng, B., 2006. Effects of Fe-doping on the photocatalytic activity of mesoporous TiO2 powders prepared by an ultrasonic method. J. Hazard Mater. https://doi.org/10.1016/j.jhazmat.2006.05.028.